CONF-890114--

SGP-TR--122

DE92 016026

PROCEEDINGS
FOURTEENTH WORKSHOP
GEOTHERMAL RESERVOIR ENGINEERING

January 24–26, 1989

Henry J. Ramey, Jr., Paul Kruger, Frank G. Miller,
Roland N. Horne, William E. Brigham,
Jean W. Cook
Stanford Geothermal Program
Workshop Report SGP-TR-122

MASTER

Library of Congress Catalog Card No. 89-51577

TABLE OF CONTENTS

GEOSCIENCE

GEOSCIENCE AND GEOCHEMISTRY

GEOCHEMISTY

REINJECTION/HOT DRY ROCK

HOT DRY ROCK

NUMERICAL MODELLING

NUMERICAL MODELLING - El Salvador

INNOVATIVE RESEARCH/FIELD PERFORMANCE

NOT PRESENTED

PREFACE

The Fourteenth Workshop on Geothermal Reservoir Engineering was held at Stanford University on January 24-26, 1989. Although the domestic geothermal industry continues to suffer from depressed crude oil prices, world-wide geothermal activities continue to grow, and it is becoming difficult to catalog them. This growth has placed burdens on consulting firms and increased demands for training of technical personnel. The Workshop Banquet speaker, Dr. Manfred Hockstein discussed worldwide geothermal training needs. Dr. Hockstein is Director of the Geothermal Institute at the University of Auckland. We deeply appreciate his contribution to the workshop.

Attendance continued to be high with 130 registered participants. Seven foreign countries were represented: England, Iceland, Italy, New Zealand, Japan, Mexico and San Salvador. There were forty-six technical presentations at the Workshop. Three technical papers not presented are also contained in this Proceedings. In addition to these technical presentations or papers, introductory addresses were given by John E. Mock, U.S. Department of Energy; Warren D. Noteware, California Energy Commission; Vasel W. Roberts, EPRI; and Stephen Pye, UNOCAL Geothermal. We appreciated their thoughts on the future prospects for geothermal energy and the importance of research in development of geothermal resources.

The chairmen of the technical sessions made an important contribution to the workshop. Other than Stanford faculty members they included: Bo Bodvarsson, Tom Box, John Counsil, Bob Fournier, Mohinder Gulati, Eduardo Iglesias, Jim Lovekin, Pat Muffler & Jeff Tester.

The Workshop was organized by the Stanford Geothermal Program faculty, staff and graduate students. We would like to thank Heather Jones, Pat Oto, Yasmin Gulamani, Phalguni Kikani, and Rosalee Benelli for their valued help with the meeting arrangements and preparing the Proceedings. We also owe a great deal of thanks to our students who arranged and operated the audio-visual equipment, and especially to Jitendra Kikani who coordinated the meeting arrangements.

Henry J. Ramey, Jr.
Paul Kruger
Roland N. Horne
Frank G. Miller
William E. Brigham
Jean W. Cook

PROCEEDINGS, Fourteenth Workshop on Geothermal Reservoir Engineering
Stanford University, Stanford, California, January 24-26, 1989
SGP-TR-122

ADVANCES IN GEOTHERMAL RESEARCH

John E. Mock
Director, Geothermal Technology Division
U.S. Department of Energy
Washington, D.C. 20585

Gene V. Beeland
Meridian Corporation
Alexandria, VA 22302

ABSTRACT

The accomplishments of the various elements of the geothermal research and development program of the Department of Energy during 1988 are outlined. It is noted that research advances will help to place the geothermal industry in a better technical position to meet the challenges of an increased energy demand in the 1990's, as predicted by DOE. Recent federal technology transfer initiatives are identified and preliminary results of an analysis of all energy sources in the U.S. vis-a-vis geothermal's ranking in the total energy resource base, the accessible resource base, and energy reserves are presented.

TECHNOLOGY TRANSFER

Thank you for inviting me to participate in the 14th Annual Stanford University Geothermal Reservoir Engineering Workshop. I know of no more effective technology transfer forum than this one. It provides splendid support both to the general technology transfer mission of the Department of Energy and the specific efforts of the Geothermal Technology Division.

Since your presence here indicates your interest in technology transfer, you may be interested in some of the government's initiatives to facilitate this function. Of note among these initiatives is the President's April 10, 1987, Executive Order No. 12591 on Facilitating Access to Science and Technology. The overall thrust of the Executive Order is to ensure that Federal agencies and laboratories assist universities and the private sector in broadening the technology base by moving new knowledge from the research laboratory into development of new products and processes. It has provisions for establishing consortia among laboratories, universities, and industry. DOE's new policies with respect to intellectual property and its continuing efforts to improve its procedures will carry out the mandate of Executive Order 12591. The Department strongly believes that research results and intellectual property rights should be transferred to the private sector in a manner which provides incentives for commercialization, provides the proper accountability for public funds, supports the missions of the national laboratories, assures that adequate rights are retained to accomplish government purposes, and assures that the laboratories serve as resources to industry rather than competitors.

Improvements have been made by the Department in recent years to reduce institutional barriers to the transfer of technology from the national laboratories; e.g., provisions have been made for more flexibility for laboratory staff to consult for industry, and for class waivers for patents originating from user facilities and work-for-others agreements. A computer software policy to allow contractors to copyright and license software has been completed, and the Assistant Secretary of Defense Programs is implementing, consistent with DOE's national security responsibilities, a program for identifying technology transfer mechanisms and incentives that accelerate commercialization of defense technologies. Undersecretary Donna Fitzpatrick recently stated: "The Department believes that defense programs are a prime source of valuable applied technology and a national asset in the management of industrial technologies whereby advances in new technologies in one field spur advances in another."

ENVIRONMENTAL ISSUES

In addressing the Department's policy on another issue of considerable significance, Secretary Herrington recently stated that the U.S. responses to environmental issues "will be most effective over the long term if they seek to stimulate technological innovation and to ensure that the marketplace has sufficient information to make appropriate choices." He indicated that such a response to the "greenhouse effect" is currently far from available: "Research on the causes and possible solutions is still incomplete and should be pursued expeditiously."

In a preliminary look at geothermal power plants vis-a-vis carbon dioxide emissions, GTD found that the CO_2 emissions of U.S. geothermal power plants for which data are available range from zero to 11 percent of those of a Western coal plant. Almost all of

them emit less than 5 percent of the CO_2 that would be emitted by a coal plant of the same capacity. Binary plants, of course, would release no gases into the atmosphere.

We are now pursuing a project to gather detailed CO_2 data from specific geothermal plants, develop a scenario for each Known Geothermal Resource Area (KGRA), project CO_2 emissions, and compare them with fossil emissions. The study will then determine what the technology options would be if CO_2 reductions were ever to be mandated at the state or federal level and whether R&D assistance would be needed to enhance available technologies or to develop new ones.

PROJECTED POWER DEMAND

If, as the Department now believes likely, power demand increases markedly in the 1990's, the geothermal industry does not need any environmental "hang-ups" to prevent it from participating to the fullest extent desirable. A new DOE report entitled "United States Energy Policy - 1980-1988" finds that if power demand grows just 2 percent annually, the nation will need about 100 GW of additional electric generating capacity by the year 2000 over that currently under construction. This increase would be the equivalent of 100 nuclear power plants and an increase of one-sixth of existing capacity. The figure may be conservative, however, since demand projections based on the first half of the 1980's suggest that during periods of economic growth, electricity demand grows at about the same rate as economic output. Thus, if annual GNP growth is greater than 2 percent, it is likely that electricity demand growth will be higher. In 1987, for example, GNP grew by 3.3 percent and electricity demand was up 4.7 percent. A finding of the report that may be of even more interest to the geothermal community is that it is likely that every region of the country will need new generating capacity by the early 1990's.

If GTD technology objectives -- arrived at with input from nearly all sectors of the geothermal community -- are achieved, the geothermal industry will be in a better technical position to meet the challenges of an increased power market in the next decade. To the extent that space permits, I would like to tell you about some of GTD's accomplishments of last year which keep us on the road to objective achievement.

HYDROTHERMAL RESEARCH

Reservoir Technology

Reservoir Analysis - The emphasis of this task in 1988 was on methods to replace costly drilling as the only means for providing evidence that a reservoir is adequate to support power generation for the expected life of a proposed plant -- i.e., to extend the information gained from one well to the field around it, thus reducing the number of wells needed for this purpose. Specific accomplishments included the discovery that borehole breakouts indicate varying stress directions in individual blocks of rock, inversion codes for interpretation of borehole-to-borehole and borehole-to-surface resistivity surveys, and the Medicine Lake Volcano teleseism experiment.

The Medicine Lake work in 1988 involved seismic tomographic data gathered at Medicine Lake in 1986 by the U.S. Geological Survey and the Lawrence Berkeley National Laboratory. Derived from eight explosions in a 50 km area from the caldera, these geophysical results provided one of the best data sets yet achieved. The 1986 studies focused on using the data to measure delay times in the rocks; in the 1988 studies, more sophisticated interpretation procedures were applied to the same data to try to determine the saturation of the rocks. The results to date are shown in Exhibit 1. In this geological cross section, the horizontal lines with angled hatchures represent the previous velocity model from the seismic refraction study; the high velocity core of the volcano is shown (5.7 km/s, subsolidus dike and intrusion complex); the suspected magma chamber with at least partial melt in the low-velocity, high attenuation body in the center of the caldera is identified; and the area where steam is believed to be present is indicated as "boiling water."

Exploration Technology - The exploration task is designed to develop techniques to locate and characterize geothermal resources in young siliceous volcanic environments, particularly in areas with deep circulation of groundwater. Gathering of the geological, geophysical, and geochemical field data, acquired by cost-sharing several deep heat flow holes with industry in the Cascades Range of the Pacific Northwest was completed in 1988. The data will be integrated in reservoir models which will serve as a tool for locating geothermal resources hidden by deep movement of groundwater in the Cascades Range.

Brine Injection - The injection task focuses on techniques to predict the intensity and timing of the thermal, chemical, and hydrologic effects of injection in order to provide methods to reduce temperature and pressure degradation in geothermal reservoirs. Accomplishments in 1988 included: 1) models for the interpretation of injection tests in fractured reservoirs, 2) techniques to use tracer test results to design optimal injection schemes, and 3) a dual permeability model to simulate flow in fractured rock with secondary porosity. These are all techniques for maintaining reservoir pressure while avoiding thermal breakthrough to the producing zone.

Geothermal Technology Organization - The GTO, the joint DOE/industry group that jointly funds technology development efforts that will provide immediate benefits to the geothermal industry in the areas of reservoir performance and energy conversion, began one project in FY 1988 -- a microseismic study of The Geysers geothermal field. GEO Operator Corp. and the Unocal Geothermal Division are the industry participants.

Salton Sea Scientific Drilling Task - The testing facility was reconditioned in 1988, and a successful 20-day production flow test was conducted, with flow rates up to 700,000 pounds/hour of hot 260°C (500°F) brine. Ancillary studies of brine chemistry, waste disposal, and microseismic detection also were carried out.

Hard Rock Penetration

Lost Circulation Control - R&D was undertaken to develop a basic understanding of the two-phase (solid/liquid) flow phenomenon that dictates fracture plugging mechanics for single-particle, high-temperature, and multiple constituent lost circulation materials. In addition, the plugging characteristics of high-temperature lost circulation materials were measured under a range of temperature and pressure conditions.

Rock Penetration Mechanics - Activities during 1988 included the development of a concept for a core drilling system for deep thermal regimes, and, working with industry suppliers, the completion of two designs for insulated drill pipe. Analysis of acoustical data telemetry through the drill string was completed, and testing of a laboratory scale model of the drill string transmission system showed excellent agreement between theory and lab data.

Instrumentation - A User Group was formed to promote the use and further development of a computer code to calculate the forces on a bit and bottom-hole assembly that will permit optimization of well design. In addition, a new lower power transmitter was fabricated and added to a prototype radar fracture mapping tool designed to locate fractures in a rock formation that do not intersect the wellbore. Field tests in 1988 showed that it can detect distinct targets in non-uniform geologic media.

Geothermal Drilling Organization - In 1988, a high-temperature borehole televiewer, being developed for casing inspection and fracture mapping in the open wellbore, was assembled and successfully demonstrated in a hot well owned by Unocal in Long Valley, California. A test of a tool for deploying an expanding foam in lost circulation zones at The Geysers showed insufficient expansion of one type of foam under field conditions. However, three field tests at The Geysers of a downhole air turbine for directionally drilling geothermal wells gave promising results, and led to design modifications of the transmission assembly. Temperature-resistant elastomer materials were screened for suitability for use in the fabrication of drill pipe protectors.

Conversion Technology

Heat Cycle Research - In 1988, supercritical tests of the Heat Cycle Research Facility with the condenser at the near vertical position with the propane family of working fluids was completed, as was Phase I of the relocation of the HCRF from the Geothermal Test Facility at East Mesa, California, to the property of the nearby B.C. McCabe binary plant. The second phase of the relocation was initiated, including installation of a two-dimensional expansion nozzle and a reaction turbine. The application of the new Kalina concept to geothermal power cycles was completed, and data from previous experiments with a near horizontal condenser were evaluated.

Materials Development - Major 1988 activities included downhole testing of advanced high-temperature 300°C (572°F) lightweight cements for well completions, which produced very promising results; initial steps for conducting tests of polymer-lined heat exchanger tubing; and completion of an analysis of high-temperature elastomers for use in geothermal sealing applications.

Advanced Brine Chemistry - In 1988, the interim brine equilibrium model for silica, calcite, and carbon dioxide was completed; the model will now be expanded to additional minerals in order to make it a more realistic simulator of the thermodynamic conditions under which problems will occur in geothermal power plants from scale deposition, corrosion, and suspended solids. In addition, laboratory tests of prototype particle meters were conducted using a high-temperature, high-pressure synthetic brine so that technical problems experienced in field tests could be corrected. An ultrasonic particle meter was tested at the Salton Sea Scientific Drilling Project to learn how the instrument would perform under actual field conditions; a report on its performance is forthcoming.

Other research conducted under the brine chemistry task is the series of experiments underway on the use of a biochemical technique to concentrate and remove toxic metals from wastes: the leaching of metals by micro-organisms from sludge-like residues that result from the precipitation of minerals from spent geothermal brines before injection.

GEOPRESSURED-GEOTHERMAL

Well Operations

The well operations project involves field activities to obtain information on reservoir performance under production conditions, surface handling systems, disposal well injection procedures, brine chemistry and scale inhibitor treatment, and automation. The Pleasant Bayou well, located in Brazoria County, Texas, near Houston, was placed back in production in May 1988, after being treated with a scale inhibitor, and has been flowing at about 20,000 barrels per day. The Gladys McCall well located in Cameron Parish, Louisiana, was subjected periodically to high rate flow tests at over 25,000 barrels per day of brine for over two years. It produced a total of over 27 million barrels of brine and nearly 676 million scf of methane, and was the subject of the breakthrough in geopressured scale inhibition treatment. It was shut in during October 1987, and is undergoing a long-term pressure build-up test to help in understanding the drive mechanisms of geopressured reservoirs. The Willis Hulin well was drilled in Vermilion Parish, Louisiana, as a commercial gas producer. It penetrated an unusually good geopressured zone at about 20,000 feet, and when it was no longer operable as a gas well, DOE agreed to assume ownership from the Superior Oil Co. Most of the physical parameters of the Hulin well differ from those of the experimental wells drilled specifically for geopressured brine production, and it thus provides the opportunity to facilitate determination of drive mechanisms under another set of downhole conditions. In addition, the higher expected temperature and gas content make fluid from the Hulin well substantially more valuable per unit volume than fluid from the design wells. Annular pressures at the wellhead were monitored on a regular basis in 1988, site facilities were upgraded in preparation for workover activities, and a safety evaluation of well pressure buildup was performed.

Geoscience and Engineering Support

The 1988 accomplishments of this project included: 1) refined mapping of Pleasant Bayou reservoir sandstone within the fault block; 2) development of simplified geologic models; 3) continued analysis and interpretation of the multirate flow tests of the Gladys McCall as well as shut-in data; and 4) the conclusion that environmental monitoring at the Gladys McCall has not shown any detrimental environmental effects attributable to the long-term testing (microseismic, water quality, and subsidence).

Energy Conversion

The construction of a "hybrid" power conversion system designed to utilize both geothermal heat and methane was begun in 1988 at the Pleasant Bayou well site, and a power generation experiment is scheduled to begin there early in 1989. Flow testing of the well has been resumed in preparation for the experiment.

HOT DRY ROCK

Fenton Hill Operations

The focus of the Fenton Hill Operations project in 1988 was preparing for the upcoming Long-Term Flow Test (LTFT) of the Phase II reservoir. This test is a significant milestone in hot dry rock research because of the information it will provide on reservoir impedance, thermal drawdown, energy output, and water consumption. The significant 1988 accomplishment was completion of the repair of the well used to produce heated water from the man-made reservoir. The repair was accomplished by redrilling into the existing reservoir and sidetracking the well around the damaged section. This work will enable optimum production during the LTFT of the reservoir scheduled to begin in 1990.

Scientific and Engineering Support

Accomplishments in 1988 included a re-analysis of the micro-earthquakes resulting from the massive hydraulic fracturing experiment of 1983 using improved mapping methods and initiation of a programming effort toward automation. A prototype borehole televiewer was also completed, and the injection borehole was surveyed.

MAGMA

Long Valley Operations

The key achievement of this project in 1988 was finalizing selection of an exploratory drill site in the Long Valley caldera in California which was approved by a DOE review panel. Permits for operation at the site were initiated, and preliminary site work completed. A science guide for supporting scientific measurements in the exploratory well was developed during a workshop attended by over sixty researchers.

Laboratory and Engineering Support

Research continued in 1988 on the energy extraction and geochemistry/ materials tasks. Advances were made in evaluating magma convection, overall energy extraction analysis, analysis of energy conversion systems, understanding thermal fracturing processes, examining the reaction of potential heat exchanger materials with magmatic fluids, evaluating mass transport near the heat exchanger, and collecting laboratory data related to potential hazards during drilling.

WHY CONTINUE GEOTHERMAL R&D?

A new study in preparation for the Deputy Assistant Secretary for Renewable Energy provides another indication of the importance of continuing geothermal R&D and achieving our objectives. In analyzing the energy sources in the U.S. and standardizing the definitions of all sources, the preliminary finding is that geothermal energy within six kilometers of the earth's surface -- seven for geopressured -- accounts for 42.7 percent of the U.S. total energy resource base, as shown in Exhibit 2. The total resource base is defined as the total physically available energy-- identified and undiscovered -- regardless of whether or not it can be practically or economically extracted. However, geothermal accounts for only 4.4 percent of the U.S. accessible resource base -- the portion of the resource base that can be exploited within known or developing technology -- and 3.8 percent of U.S. energy reserves -- those portions that are economically recoverable under current conditions. With improved technology we can greatly increase geothermal's portion of both the accessible resource base and the reserve category, making a significant contribution to the nation's energy supply.

EXHIBIT 1

CROSS SECTION OF MEDICINE LAKE VOLCANO
FROM SEISMIC TOMOGRAPHY

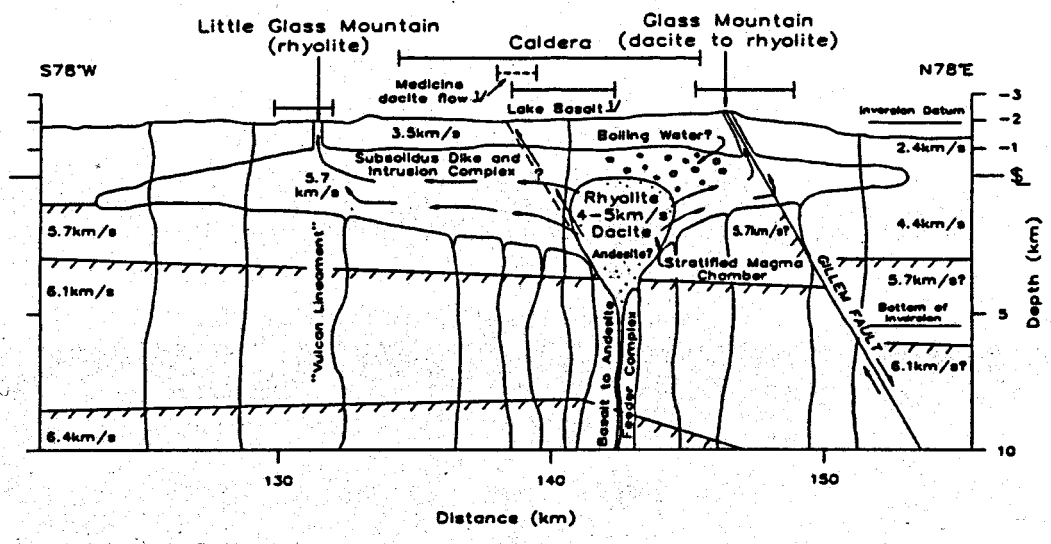

(Source: Three Dimensional Velocity and Attenuation Structure at Medicine Lake Volcano, California, from Seismic Tomography, J. S. Evans, U. S. Geological Survey, J. J. Zucca, Lawrence Livermore National Laboratory)

EXHIBIT 2*

U. S. GEOTHERMAL RESOURCES

TOTAL RESOURCE BASE[a]		U.S. ACCESSIBLE RESOURCE BASE[b]		U.S. RESERVES[c]	
Quads	BBOE[d]	Quads	BBOE[d]	Quads	BBOE[d]
1,505,408	255,910	22,588	3,840	247	42
(42.7% of Total U.S. Energy Resource Base)		(4.4% of Total U.S. Accessible Energy Resource Base)		(3.8% of Total U.S. Energy Reserves)	

* Still subject to review by the U.S. Geological Survey.

[a] The total resource as specified in USGS Circular 790, but modified by the National Academy of Sciences to include resources within 6 kilometers of the surface and with a heat value > 80°C (except for hydrothermal, which is > 40°C). Geopressured resources are included to a depth of 7 kilometers.

[b] The accessible resource as specified in USGS Circular 790, but modified by the National Academy of Sciences to include only accessible resources within 6 kilometers of the surface and > 80°C, except for hydrothermal resources which are > 40°C. Geopressured resources to a depth of 7 kilometers are also included.

[c] The reserve as specified in USGS Circular 790, but modified by the NAS. In addition, low temperature (>40°C) hydrothermal 30-year resources form USGS Circular 892 are added to the total.

[d] Billion barrels of oil equivalent.

PROCEEDINGS, Fourteenth Workshop on Geothermal Reservoir Engineering
Stanford University, Stanford, California, January 24-26, 1989
SGP-TR-122

FUTURE PROSPECTS FOR GEOTHERMAL ENERGY DEVELOPMENT IN CALIFORNIA

Warren D. Noteware, Commissioner

California Energy Commission

I want to thank Paul Kruger for the opportunity to address this workshop on the subject of geothermal energy development in California.

When I was invited to speak at this conference, I gladly accepted because I believe this type of interaction between all levels of government and industry organizations is important. It is the application of your collective skills and resources that makes the geothermal industry work. Therefore, any governmental or market action that affects the value or the contribution of geothermal energy to meeting the state's needs is of vital interest.

Foregoing any discussion of where the industry has been or what it has accomplished, I would like to focus on the present and mention some new opportunities that you may not have previously considered.

First, the present. The two state regulatory agencies that will largely influence the future of geothermal energy development in California are the Public Utilities Commission and the California Energy Commission.

As you are aware, the Public Utilities Commission suspended the signing of any new Interim Standard Offer 4 contracts back in 1985. The lucrative terms and prices offered in these contracts provided the impetus for the growth of the independent geothermal energy industry today. At the time of the suspension, independent geothermal developers had signed contracts totalling 1,055 MW.

Since then, contracts accounting for 156 MW have been terminated while projects totalling 334 MW have been developed, leaving 565 MW that have not yet been developed. Since most of these contracts will not expire until 1990, these remaining MWs represent the near-term market potential for geothermal development in California.

The Energy Commission is currently preparing its biennial Electricity Report. This report will include a forecast of the demand for electricity over the next 5-, 12-, and 20-year horizons. The report also will present a forecast of the supplies of electricity that will be available to meet this demand. One of the key issues in this, our seventh, Electricity Report, will be the forecast of generating capacity that will be developed between now and 1992 from the remaining standard offer contracts. The forecast in the draft final report shows that only 295 MW of geothermal energy are expected to come online between now and 1992.

Looking to the future, the Energy Commission's forecast will directly affect the determination of the need for additional generation resources by the investor-owned utilities and thus new potential market opportunities for the geothermal industry. The availability of future long-term power purchase contracts during the next eight years will be determined by a bidding process adopted by the Public Utilities Commission. Under this plan, the utilities will be allowed to build new facilities or to purchase capacity and energy from independent producers that can supply it at the least cost.

In a recently-completed report entitled the Energy Technology Status Report (ETSR), the Energy Commission conducted a detailed assessment of over 220 electric generation, nongeneration, and automotive transportation technologies. This report serves as the technical basis for the state's energy research and development policies and provides input to certain power plant siting case evaluations.

What the geothermal industry should learn from this report is that geothermal technologies, particularly flashed-steam and binary-cycle, presently cannot compete with technologies such as gas-fired

cogeneration on a cost basis. Therefore, the industry must find ways to reduce exploration and production costs, or the contribution of geothermal to future generation additions in California may be limited. Further limiting future opportunities is the recent revelations about the long-term productivity of The Geysers steam resource and the decision by PGandE to shelve plans for 3 new plants in The Geysers. Up to this point, electrical energy from The Geysers was one of California's least expensive sources.

The problem, though, with the PUC's bidding process is that the least-cost technologies, which may likely be fossil-fueled facilities, will only exacerbate California's air quality problems, and may adversely affect the long-term security and costs of energy supplies in the state.

However, it is California's inability to meet federal air quality attainment standards that is leading to ever-tightening constraints on the combustion of fossil-fuels. The most comprehensive are the proposals by the South Coast Air Quality Management District (SCAQMD). The most extreme provisions of the SCAQMD proposals may prohibit the combustion of fossil fuels within the basin, requiring complete electrification of all industrial, commercial, and transportation functions. This would have obvious implications regarding the need for new, nonpolluting generation sources. And, as the Energy Commission does not favor the export of pollution from nonattainment areas to attainment areas, greater preference would be given to clean sources.

In addition, both the Energy Commission and the Public Utilities Commission are now being urged to incorporate the effects of nonprice externalities in their need determination process. Recently, the California Legislature passed Assembly Concurrent Resolution No. 160 which requests both the Energy Commission and the Public Utilities Commission to take into account the benefits of nonprice factors when conducting our respective resource supply assessment and standard offer proceedings. This, of course, would place greater emphasis on noncombustion technologies such as geothermal energy. The resolution further requires the two commissions to inform the Legislature on or before December 1, 1989, on how these factors will be taken into account in our respective proceedings.

Although such regulatory actions would enhance the marketability of geothermal energy, your industry still may find strong competition from out-of-state power sources. All this points to an uncertain future for geothermally-produced electrical energy, and the need for a stronger partnership between the state and federal government and the geothermal industry to focus limited research and development dollars into those areas that will make geothermal energy more competitive in the market place. From a government perspective, however, this goal must also be balanced by the need to develop other new technologies that offer promise for the next century.

In the last few years, the Energy Commission has begun new programs that are intended to address near-term market and environmental issues as well as long-term research and development goals. We are strengthening our programs that provide energy end users with economic options to fossil fuels both for electric generation and thermal applications. We are providing cost sharing for projects that focus on longer-term research and development issues. We are providing assistance to California's advanced energy technology companies in both domestic and foreign markets. And, we will be stepping up our efforts to ensure that environmental factors are given stronger consideration in our regulatory actions.

Through our Geothermal Grant and Loan Program, the CEC is providing grants and loans as well as technical assistance to local governments for the exploration and development of the state's vast low- and moderate-temperature geothermal resources for direct-use applications. Given the uncertainties of the market for electrical energy in California, your industry must begin to consider this opportunity that, in the past, may not have been considered enough of a lucrative market for major private investment.

The energy potential from low- and moderate-temperature resources in California is substantial. And, despite the currently-depressed oil market, direct-use applications remain a reasonably good investment for many local governments and private developers. For example, many heating and air conditioning systems require electricity. The retail price for electricity has not been affected by the drop in oil prices as have natural gas and distillate oil prices. In fact, retail electricity prices have

increased, making the use of low- and moderate-temperature resources to displace electrical energy reasonably cost effective.

However, high exploration costs has kept many local governments and private investors out of the direct-use market. The role of the CEC's Geothermal Program, therefore, is to provide technical and financial assistance to overcome these impediments.

Perhaps the best example of this effort is the geothermal district heating system in the City of San Bernardino. Owned and operated by the San Bernardino Municipal Water Department, the system presently uses low-temperature geothermal water, about 135 °F, for space and water heating in twelve downtown buildings. This number should expand to 27 by the end of 1989, making this system the largest of its kind in the United States. The cost thus far for this project is $6.7 million, of which the Energy Commission has provided $4.7 million.

To date, the Energy Commission has provided more than $13 million for resource exploration and development projects throughout the state. Many of these projects have included geochemical, geophysical, and hydrological analyses as well as temperature gradient, production, and injection well drilling.

Our newest funding effort, the Energy Technologies Advancement Program (ETAP), is an energy research and development program that was begun by the Energy Commission three years ago. Through the ETAP, the Energy Commission provides research contracts and loans for projects to make a wide range of energy technologies more efficient and cost- effective in California. Unlike the Geothermal Grant and Loan Program, which does not fund technology research, through ETAP the CEC can provide funding for projects along the entire energy research and development spectrum, from basic laboratory research through final testing and demonstration of full-scale energy systems applications.

The ETAP is fully funded from State resources. We currently have twenty-six active research contract and loan projects costing over $35 million, and funded with $8.4 million from the Energy Commission.

Several of these projects demonstrate technologies near to commercialization, while others focus on laboratory or pilot-scale research and development of components of new technologies that have commercialization horizons of from five to fifteen years. For example, work is underway for the development of a new process to gasify high-ash, high-moisture biomass byproducts such as paper pulp residues. Under another contract, a family of low-cost catalysts are being developed to reduce NOx air emissions from electrical generating facilities. Another contractor is performing laboratory research and field testing of a proprietary process to directly generate steam for use in solar thermal power plants, a process which will eliminate the need for costly, and sometimes hazardous, heat transfer fluids. Still another is developing new low-cost semi-conductor materials for higher cell efficiencies in photovoltaic power generation systems.

Unfortunately, none of these are specifically related to geothermal technologies. We have received only a few applications out of more than 125 in the last three years relating to geothermal energy technologies. We strongly encourage applications from this industry that will lead to improved and more cost effective exploration techniques and electrical and thermal energy conversion processes. These types of improvements may be important to the future success of the geothermal industry in the California energy market.

Another program, the Energy Technologies Export Program, was established three years ago to assist California's energy industry in promoting their products in the international markets. This program complements the mission of the Department of Energy's Committee on Renewable Energy, Commerce and Trade (CORECT), which coordinates federal efforts to encourage exports of renewable energy products.

Through our Export Program, the Energy Commission acts as a broker to introduce foreign buyers to domestic equipment vendors, technical consultants, and other service contractors interested in expanding their business to foreign markets. We also conduct activities to evaluate international market opportunities, identify sources of financing and assistance available for both parties, and assist California firms to overcome export barriers.

Since the Export Program began, the Energy Commission has conducted two reverse trade missions in which representatives from 31 countries were brought to California to meet with representatives from domestic geothermal and wind energy companies. These missions have resulted in equipment sales of $3.4 million. An additional $70 million in power plant sales is under negotiation.

Another issue that may indirectly affect the geothermal industry is global warming. The CEC is presently involved in a comprehensive study to assess the implications of global warming on California. This multi-agency effort was initiated in response to the mounting scientific evidence pointing to global warming trends. The participants include other state agencies, the University of California as well as federal and private research groups. This work will culminate in a report to the California Legislature in June 1990. The report will focus on determining the potential magnitude of global warming impacts and provide recommendations that will help California prepare for any such eventuality. It also will recommend ways the state can participate in national and international efforts to slow global warming trends. The possibility of global warming could have implications in future power plant siting proceedings and strengthen the Energy Commission's policy actions regarding nonfossil-fuel technologies such as geothermal energy.

Already, the Energy Commission is incorporating global warming issues in its assessment of appropriate energy technologies. For example, many new alternative technologies which emit little or no carbon dioxide are being given priority in the Energy Commission's Energy Development Report. This represents the first steps towards addressing the implications of the greenhouse effect in public policy decision making.

In closing, it is clear that your industry has been quite successful in developing this state's geothermal energy resources. But, as we enter the 1990s, the industry is confronted with new challenges that may dictate its future. Today, I have briefly discussed some of the challenges facing the industry in California and some options available from the Energy Commission to assist you in meeting them. I look forward to working with you and to the continued development of this valuable energy resource.

PROCEEDINGS, Fourteenth Workshop on Geothermal Reservoir Engineering
Stanford University, Stanford, California, January 24-26, 1989
SGP-TR-122

GEOTHERMAL RESEARCH AT EPRI

Vasel W. Roberts

Electric Power Research Institute
Palo Alto, California, 94303

ABSTRACT

The rules by which the energy game is played have been changing since 1985 and may not firm for some time. This has affected the way in which geothermal is viewed within the utility industry. The net result has been to downgrade the relative importance of geothermal and geothermal R&D. Some of the reasons for the downgrade are reviewed and the content of EPRI's Geothermal Program discussed.

A DOWNWARD TREND

In 1982 many utilities with access to geothermal resources viewed themselves as eventually owning and operating geothermal power plants. Those who were not already involved in development at The Geysers contemplated participation in the development of hot water resources. As it happened, the course of events did not take the expected path. Only two hot water plants, Utah Power and Light's 20 MWe single stage flash unit at Roosevelt Hot Springs in Utah, and the 45 MWe binary cycle plant of San Diego Gas and Electric at Heber in California, were owned and operated by electric utilities. And only one of those is in operation at this time. All others are owned and operated by second or third parties as qualifying facilities. As a result, the number of utility players did not increase as originally expected but declined. In fact, most have now withdrawn to the sidelines either as power purchasers or with no particular interest, pending future developments relating to power demand, capacity need, alternative energy costs and deregulation.

The original expectation did not materialize for three basic reasons. These were related to low energy costs, revised estimates of when new generating capacity would be needed, and pending deregulation. It was also clear that geothermal would have difficulty competing with oil below $18 to $20/bbl. Since there was little need for new generating capacity the urgency for pursing geothermal, or any other resource for that matter, simply diminished. Furthermore, it was not clear how geothermal would fit in a deregulated industry. The sum of these factors was enough to cause many utilities to back off and re-examine their geothermal objectives, or to indefinitely postpone them. In the prevailing economic environment attention turned to other more pressing issues and R&D priorities shifted. Primary emphasis is being placed on coal and nuclear generation technologies, environmental issues, and storage system technologies. Priorities for renewable resources were lowered and technologies having regional limitations, such as geothermal were pushed to the bottom if not off the list entirely.

During this same time, federal emphasis on energy research slowly eroded. Some in the industry, under the circumstances, did not find it difficult to follow suit. It is now clear that the federal lead in geothermal research is crucial. For this reason, it is unlikely that the present trend will turn around unless signaled by federal energy policy. Unfortunately, one result is that advanced geothermal research is pushed farther into the future.

THE UPWARD TRENDS

Any upward trend that might be in the making is not yet in sight. However, in trying to discern future direction global issues are likely to play an important role. In the past it has served no purpose to prophesy gloom, and certainly that is not the intent here, but the truth is that oil supply is more out of our control than at any time in the past. It would be naive to think that this does not pose an unpredictable risk to the health of the economy. Externally, the world's appetite for energy can flare in any expanding world economy. The problem can be compounded if authoritative estimates are correct that the world's supply of oil is just over 30 years. Even if one takes the

optimistic view and assumes twice as much, we have reached a point in time where the end of the oil era is more or less predictable. As it approaches price gyrations could be severe.

Consumption pressures may be compounded by environmental factors such as acid rain and the greenhouse effect. If the greenhouse effect is taken to be real by the political establishment, it could accelerate the use of oil, the reason being that oil produces only 160lb of carbon dioxide per million BTU's while coal produces about 225lb and gas about 126lb. >This simply suggests that the time is approaching when it may become necessary to consider other options that might be available. For example, is it realistic to think that a nuclear-biomass-solar-geothermal energy economy might be practical in the long run, and dramatically reduce the greenhouse gases at the same time? Many obstacles lie in this path. Certainly, the resource base seems to be there, particularly if the hot dry rock and magma resources are as large as thought. On the other hand, the vested interest in coal technology is enormous and could not be rapidly changed. In any case, there is a need to develop a good understanding of the potential options and such considerations may drive the next upturn in geothermal development.

1988 IN PERSPECTIVE

In 1988 EPRI's geothermal budget was about $2.3 million. In 1989 it will be around $1.5 million. In order to fit within this 35 percent reduction the scope of some projects had to be reduced and others terminated. Before discussing the program content for this year I want to mention three projects that are being phased out.

The first is actually a group of four projects related to EPRI's efforts to develop technology for upstream hydrogen sulfide removal from geothermal steam. The approach is based on the reboiler concept. The primary effort in this area has been to scale the technology from a 1000lb/h experimental unit to a 200,000lb/h commercial type system designed for use with geothermal fluids having a noncondensable gas content of up to 8 percent. This was done in cooperation with the Philippine National Oil Company and Pacific Gas & Electric Company, who did the design studies. It was not possible to complete the detailed design, however, most of the engineering analyses were completed. The reason for calling your attention to it is that confidence was gained that the design would function as expected and that it could be cost effective depending on the gas content in the geothermal steam, in the range of 3 to 8 percent. One of the by-products of this effort has been the development of techniques for estimating heat transfer in condensers having high gas concentrations.

The second project that should be mentioned is the crystallizer effort. A number of tests were run at Cerro Prieto to investigate the feasibility of removing silica by precipitation and crystal growth in a flash crystallizer vessel. I must report that the results from this particular set of tests were not very encouraging.

The third effort being closed out is the Mobile Chemistry Lab project. The one thing that should be mentioned in relation to this project is that an effort is being made to preserve the data accumulated over the last several years and to prepare it for publication.

THE YEAR AHEAD

In 1989 the program will pursue four projects. Three are continuing and one is new. The three continuing projects are as follows:

Modular Binary Wellhead Power System Design
Geothermal Information Series
Trace Element Specification, Transport, and Distribution.

Modular Binary Wellhead Power System Design: The objective of this effort is to create a single design that will have the flexibility to perform over a wide range of geothermal fluid temperatures and flows. Because of the wide range, the capacity of the system will be in the range of 2 to 7MWe, depending on the exact conditions at the wellhead. The reasons for pursuing this effort is to fulfill a perceived need for a small modular power system that can satisfy the following applications:

- First unit in new fields
- Development of small fields
- Development of low temperature fields
- Staged development of larger fields, and
- Backfill in existing fields

The design effort is being done by the Pacific Gas & Electric Company. Most of the engineering analyses have been completed and detailed process, mechanical and civil design efforts are now under way. The present plan is to complete the

design around mid-year.

Geothermal Information Series: The goal here is to capture and preserve some of the more vital lessons learned about geothermal development over the past decade. Radian is the general contractor for this effort. The first document will be a set of guidelines for geothermal fluid chemical sampling and analyses. This document is in the final stages of preparation and should reach the publisher in about two months. The next document in this series, as presently planned, will be a set of guidelines for power cycle selection. A third document will be started this year although the final choice of the subject matter has not yet been made.

Trace Element Transport and Distribution: The approach used in this project is to develop analytical techniques for estimating the transport and distribution of arsenic, boron, mercury and other toxic trace elements in geothermal fluid flow streams, based on fundamentals. This includes considerations of the metallic ores most likely to be present in geothermal reservoir rock formations, the solubilities of such ores at reservoir temperatures depending on the presence of other mineral species, as applicable, and the speciation and bulk quantities as the temperatures and pressures change when the fluid passes through the power plant. The project is studying both the liquid and vapor streams with special emphasis on steam and condensate. The final report on arsenic is now available. At present an effortis underway to program the techniques used for arsenic on the personal computer to simplify their use. The effort on mercury will continue this year and is scheduled for completion early next year. This work is being done at San Diego State University.

As previously mentioned, the present plan calls for starting one new project in 1989. EPRI will participate with the Hawaiian Electric Company and the University of Hawaii at Manoa in the evaluation of the geothermal resource in Hawaii, one of the critical paths in Hawaii's deep sea cable program. Their plan for the basic assessment is to use a combination of data from existing wells, several new slim hole wells, and geological and geophysical surveys that have already been completed. It is hoped that large bore confirmation wells can be drilled later in the program. EPRI plans to cofund the analytical portion of the effort. Both the mobile chemistry laboratory and the crystallizer equipment will be transferred to the project to aid in geochemical analyses and to study silica removal.

CLOSURE

In closing three points should be kept in mind. First, the energy market, except for the remaining standard offer No.4's promises to be highly competitive. It will be a challenge but, geothermal can find a niche in that market. The second point is that federal energy policy sets the R&D pace and if the downtrend is to be reversed, it must start with policy. The final point is that much of the long-range research has been suffered in the pursuit of solutions to near-term problems. It may be time to adopt a more proactive approach to R&D.

PROCEEDINGS, Fourteenth Workshop on Geothermal Reservoir Engineering
Stanford University, Stanford, California, January 24-26, 1989
SGP-TR-122

RESEARCH CAN KEEP GEOTHERMAL COMPETITIVE

Stephen Pye

Unocal Geothermal Division
Unocal Corporation
Los Angeles, California, 90017

OUR PROBLEMS: EXCESS ENERGY SUPPLY AND LOW ENERGY PRICES

New geothermal projects face two problems, with the most serious being a low price for geothermal fuel. The other problem is an excess of electrical generating capacity in the Western United States, which makes any new generation plant difficult to promote. This should be a temporary problem, because it is the result of a supply/demand imbalance. However, since it affects our activities it is frustrating because we have no control. Hopefully this problem will decrease as a factor in our local market within the next decade.

Our most serious problem is the low fuel price for geothermal. The price for all fuels has declined because of the current oversupply of fossil fuels (oil, gas, and coal) which are the primary competitors for the electric generation market. Other alternatives, including hydro, nuclear, etc., all have problems. Domestic hydro is fully developed, nuclear is out of favor, and other alternatives too expensive. Consequently, in the near term (5-10 years) fossil fuels will remain the primary competition. We must compete in this market.

CAN WE CHANGE THE PRICE TO SOLVE OUR PROBLEMS?

When will oil prices rise?

Oil prices will rise, and fall, when the members of OPEC allow them to rise and fall. When oil prices rise, the geothermal price rises, but so do costs. The costs of pipe, valves, etc., will rise because the energy required to produce them will be more expensive. As prices rise, demand falls (remember our excess capacity?). I do not believe we can rely on an increase in fossil fuel prices to solve our problem.

Geothermal - The premium fuel/worth ?% more

Geothermal energy is a premium fuel that should be politically favored because it is a domestic energy source, it's clean, yields lower CO_2 emissions and has no radioactivity hazard. But, will the customer pay a big premium, a little premium, or no premium? How much will the consumer pay for a secure fuel supply with environmental advantages? In the absence of a legislated incentive for geothermal or disincentive for competing fuels (i.e. reduce CO_2 emissions by X%) I believe any premium will be too small to have a major influence on geothermal project economics.

Conclusion -- We Must Be Competitive At The Current Price.

RESEARCH - A METHOD OF REDUCING COSTS

Since we cannot significantly impact the price we are paid for the product, we must control costs if we are to compete in the current market. The geothermal industry may have an advantage over fossil fuel competitors with respect to reducing costs. Since the fossil fuel industry is quite mature relative to geothermal, it is much farther out on the learning curve. Consequently, research efforts in geothermal should increase efficiency proportionally more than similar efforts would in the fossil fuel industry. But, this can only occur if we do the research.

That will require an all-out effort by the industry. Unocal is committed to increasing efficiency through research which can be seen by our willingness to devote manpower and financing to research projects. While our major effort is still devoted to our own proprietary research programs, we have been increasing our participation in joint-funded research. We hope that all sectors of the industry will participate in the joint-funded research projects as well as pursuing proprietary research.

AREAS FOR RESEARCH

There are many areas for research in the geothermal industry, but to effect a reduction in cost and risk we need to focus on only a few areas. The major cost areas are in drilling, production systems, and the lag time between expenditures and the revenue stream. The major risk areas are reservoir performance, injection and chemical reactions. Research expenditures should be concentrated in these areas.

If capital expenditures (drilling and production system costs) and the time delay between investment and income could be reduced, we could sell geothermal fuel at a lower price. The need to reduce capital expenditures is well understood. Advancing the revenue stream closer to the investment reduces the interest cost, which may be substantial. Shortening the time delay requires that the development move rapidly. Inherent in an accelerated development program is the increased risk in relying on reservoir performance predictions, including the long term effect of injection.

One approach to accelerating income is to develop smaller increments of power over a longer time. This would be feasible if transmission is available or if we could develop an inexpensive, long distance electric transmission system that fits this same incremental growth pattern. However, this is an area of research that is outside our normal business.

RESEARCH IN PROGRESS

I am going to discuss some of the research areas on which Unocal is working. Where possible I will be specific, but in some cases the sensitivity will require that I just make general comments.

We usually divide costs into finding, development, and operations, but it is easier to discuss research by the particular discipline -- exploration, reservoir, drilling, design/construction, and production.

Research success accomplishes either a reduction in actual costs (a drill bit that increases penetration rate) or a reduction in risk (an improved blow-out preventer rubber that reduces the risk of having a blow-out). The first is easier to measure than the second, but both are important.

Exploration

Research is aimed at identification of those areas with the most potential, at discovery of hidden systems and at methods to map the reservoir configuration. The work involves developing new methods or tools, as well as improving existing techniques. An example would be to develop seismic methods that are effective in mapping geothermal systems which are typically poor data zones. This involves technique, equipment and processing improvements.

Reservoir

Research in reservoir engineering centers on improving the ability to predict reservoir and well performance. It includes better reservoir simulation, reservoir definition and well test models. Determining the effects of injection with models and tracers also falls into this area. We not only do proprietary research in this area, but we also do cooperative research through the Geothermal Technology Organization. GTO still needs other companies to join in the research effort.

Drilling

Drilling wells is one of the major costs in geothermal development. Research in drilling is aimed at reducing well costs, which also affects exploration since the drill bit is still the ultimate exploration tool. Unocal is currently participating in joint funded research in the Geothermal Drilling Organization on air turbines, high temperature elastomers, and televiewer logging. We have also worked with selected suppliers on drilling fluids, bits, stabilizers, alloy materials, and drilling tool maintenance. We are continuing our research in cement degradation from temperature and CO_2 attack.

Design and Construction

Facility construction is the other major cost area in geothermal development. Research in this area is aimed at reducing construction costs or reducing maintenance costs. Proper materials of construction (corrosion resistant) fall into both categories, while designing to control scale fits into the maintenance cost area.

Production

Scale control, waste handling, chemical scale removal, H_2S abatement, corrosion controls, and fluid injectability are some of the research projects in this area.

COOPERATIVE RESEARCH PROJECTS

Geothermal may be competitive with fossil fuels if we succeed in some key research efforts and are selective in the projects we choose to develop. As companies, we cannot individually solve all the problems. There are, however, areas of research and development that are more suitable for cooperative effort and funding than for competitive, proprietary research. In the drilling area, these projects are typified by the Geothermal Drilling Organization projects. These are primarily developments that would normally be undertaken by the service sector, but the significant investment

requfred cannot be justified by the small geothermal market.

In the production area, we need to work with the code committees to make sure we have realistic, safe design and operation standards. This will require doing the research necessary for any changes that would be specific to geothermal, and is particularly important as we work with non-conventional materials in an attempt to handle corrosive fluids.

In the reservoir area, we need to develop methods to characterize the reservoir geometry (i.e., fracture orientation, intensity, frequency, etc.), monitor thermal injection fronts, and predict the chemical behavior. Once chemical behavior can be predicted, research can concentrate on reducing the cost of solving these problems. The problems include precipitation/dissolution reactions during production and injection, including corrosion and problems related to gases.

CONCLUSION:

The geothermal industry has an abundance of talented people. If we support their ideas for solving our problems, and manage a successful research program, we can improve the competitive position of the industry.

PROCEEDINGS, Fourteenth Workshop on Geothermal Reservoir Engineering
Stanford University, Stanford, California, January 24-26, 1989
SGP-TR-122

Pressure-Dependent Water Loss From a Hydraulically Stimulated Region of Deep, Naturally Jointed Crystalline Rock

Donald W. Brown and Michael C. Fehler

Los Alamos National Laboratory
Los Alamos, NM 87544

ABSTRACT

The rate of water loss from a hydraulically stimulated region of naturally jointed crystalline rock is shown to be dependent on both the pressure and the pressure gradient. However, there is a threshold pressure above which the rate of water loss increases much more rapidly. Above this threshold pressure, further growth and extension of the previously stimulated region occurs due to additional dilation and shear displacement of peripheral joints, as evidenced by greatly increased microseismic activity at the boundaries of the region. Therefore, the increased water loss at pressures above this threshold pressure is primarily due to fluid storage within the newly stimulated region, rather than to increased permeability losses at the boundaries.

Introduction

In conjunction with the Los Alamos National Laboratory's Hot Dry Rock (HDR) Geothermal Energy Project, two flow tests recently have been conducted on the deeper Phase II HDR reservoir at the Fenton Hill test site in north-central New Mexico. These flow tests have been performed at injection pressures varying from 24 MPa to 31 MPa,* and at rates of from 6 l/s to 18.5 l/s. The first of these flow tests, referred to as the Initial Closed-Loop Flow Test (ICFT), was conducted during a 30-day period from 19 May - 18 June 1986. The second flow test, referred to as Experiment 2074, was conducted during a 7-day period from 2 to 9 December 1987. For each flow test, the transient water loss rate was measured as a function of pressure, and the pumping-induced seismicity was monitored.

These two flow tests were intended to provide essential information needed in designing the surface flow system and planning for the forthcoming one- to two-year circulation test of the deeper Phase II HDR reservoir at Fenton Hill, referred to as the Long-Term Flow Test (LTFT). Two of the most important parameters needed for designing the LTFT surface system are the maximum allowable surface injection pressure, and the anticipated reservoir water loss rate under long-term operating conditions. After reinflation, reservoir water loss results from two dominant mechanisms: (1) flow of water out of the stimulated region through the natural permeability of the surrounding rock, and (2) water storage within newly sti-mulated regions of rock at the boundaries of the reservoir. To aid in understanding tran-sient reservoir behavior, one of the primary requirements for the LTFT is that the reser-voir volume remain constant, to allow accurate measurements of reservoir water loss, fluid volume, impedance, heat extraction, and power production throughout the test.

Since one of these flow tests was essentially aseismic, while the other was highly seismic, it is apparent that there exists sufficient data to estimate the maximum surface injection pressure that would preclude reservoir growth. In this context, reservoir growth is defined as the stimulation, through hydraulic pressurization, of the joints bounding the previously created reservoir region, as determined from the occurrence of microseismic signals associated with the extension of the principal sets of shear joints which provide the primary interconnecting flow paths within the reservoir.

In order to predict the long-term water loss from the reservoir due to permeation at the boundaries, it is necessary to first model the pressure-dependent (i.e., effective-stress-dependent) permeability of the surrounding rock, and then determine the coefficients in this model from available reservoir water loss rate data. (An entire sequence of water-loss-rate measurements as a function of reservoir pressure is now planned for this spring.) A principal motivation for these field measurements and associated modeling is the assertion by some that reservoir water loss will be a major problem in developing and implementing the HDR Geothermal energy concept.

Selection of a Pressure-Dependent Permeability Model

Of the several available pressure-dependent permeability (or joint deformation) models, the one that has been found to best represent both the elastic moduli and permeability/porosity of microcracked and jointed crystalline rock is that of Gangi and Carlson (Gangi, 1978 and 1981; Carlson and Gangi, 1985). Unlike

* All pressures and stresses given in this paper are as measured at the surface (i.e., above hydrostatic).

the linear dependence of the modulus on pressure (i.e., stress) as determined from the joint deformation models of Goodman (1976), Greenwood and Williamson (1966), and Swan (1983), the deformation modulus of Gangi and Carlson asymptotes to a constant value at high confining stress. This limiting modulus behavior, where the modulus for the cracked rock approaches that of the linearly elastic unflawed rock at elevated stresses (of the order of 70 to 120 MPa), would be expected to better represent the in situ behavior of typically discontinuous deep crystalline rock masses, and is in agreement with numerous laboratory measurements (e.g. Brace, 1965; and Walsh and Brace, 1973). Limited field measurements in our Phase II HDR reservoir at Fenton Hill suggest that the Gangi "bed-of-nails" model adequately represents the pressure-dependent permeability of the microcracked and naturally jointed crystalline reservoir rock, at least for effective stresses in the range of 0 to 30 MPa. This permeability model is (Gangi, 1978)

$$k(P) = k_o[1-(P/P_1)^m]^3 \qquad (1)$$

where P is the effective normal stress (total stress minus pore fluid pressure) across the joint, k_o is the zero-pressure (i.e., zero-effective-stress) permeability, P_1 is the normal stress at which the joints or microcracks are essentially closed, and m is a constant ($0<m<1$) which characterizes the joint surface asperity height distribution function.

Other, more complicated models are available which allow the permeability to asymptote to a finite, but very small residual value at high stress. Although these models are possibly more appropriate over the full range of in situ stresses, they are not necessary for the anticipated stress conditions associated with an HDR reservoir, where the main objectives are to model the reservoir flow behavior and the far-field permeable outflow, under conditions of moderate to low effective confining stress.

The Gangi permeability model, Eq. 1, explicitly assumes the validity of the cubic law* relating the joint permeability to the joint porosity for constant planar area joints. Therefore

$$\phi(P) = \phi_o[1- (P/P_1)^m] \qquad (2)$$

where ϕ_o is the equivalent zero-stress porosity. Witherspoon et al. (1980) report extensive measurements on fluid flow through artificial tensile fractures in granite, basalt, and marble which confirm the validity of the cubic law for fracture apertures down to 4 μm, normal stresses up to 20 MPa, and a range of flow rates that typically spans about 5 decades.

As an example of the applicability of the Gangi model, the stress-displacement behavior of a natural joint in crystalline rock has been selected from the literature. Figure 1 shows the nonlinearly elastic deformation of a joint in a large block (0.3 m across) of Red granite as measured by Sun et al. (1985). Fitting the displacement form of Eq. 2

$$w(P) = w_o[1 - (P/P_1)^m] \qquad (3)$$

to the data shown in Fig. 1 for an assumed P_1 of 25 MPa gives

$$w(P) = 0.22[1 - (P/25)^{.364}] \qquad (4)$$

with a total joint closure of 0.22 mm at 25 MPa. Table I compares the smoothed data from Fig. 1 to the displacements as calculated from Eq. 4.

Table I

Comparison of Measured and Calculated Joint Widths as a Function of Normal Stress

Normal Stress MPa	Measured Joint Width, mm	Calculated Joint Width, mm (Eq.4)
0	0.220	0.220
2	0.132	0.131
6	0.086	0.088
10	0.062	0.062
25	(assumed zero)	0.000

Predicted Reservoir Peripheral Water Loss Rate vs. Pressure

For the long-term operation of a pressurized HDR Geothermal reservoir, a very important parameter is the rate of water loss due to permeation at the boundaries of the pressure-dilated (i.e., stimulated) region. This water loss to the lower-pressure far-field region will most probably be through the interconnected microcrack fabric in the surrounding unstimulated rock. The fluid will permeate outwards, generally in a direction parallel to the least principal earth stress, and normal to the longer axes of the ellipsoidal-shaped reservoir region. Therefore, the permeable outflow will be controlled primarily by the intermediate earth stress. However, the unopened extensions of the joints comprising the HDR reservoir, if not completely filled with secondary mineralization, may afford additional paths for water loss to the far field.

Figure 2 shows the measured matrix permeability (heavy lines) as a function of effective confining stress (or pressure) for three representative core samples obtained from the Fenton Hill test site (Duffy, 1980). Note that we do not presently know the relationship

* Based on the Reynolds equation for laminar flow between two parallel plates separated by a distance w, where the flow rate, for a given pressure gradient and fluid viscosity, is proportional to w^3.

between the stress-relieved core sample permeabilities (which are seen to vary by almost an order of magnitude) and the effective in situ permeability for the actual rock mass with included joints. For initial analysis, the permeability curves of Fig. 2 were averaged (the dashed curve) and then fitted with an equation of the form of Eq. 1

$$k(P) = 1.6 \times 10^{-18}[1 - (P/117)^{.285}]^3 \quad (5)$$

(The units of pressure and permeability for the above equation are MPa and m^2, not bars and nanodarcies as shown in Fig. 2.)

To illustrate the influence of the pressure-dependence of permeability on reservoir water loss, the Darcy flow equation in its steady-state form was used for ease of computation and clarity of comparison

$$\dot{Q} = \bar{k} \frac{A}{\mu} \frac{\Delta P}{\Delta L} \quad (6)$$

where $\bar{k}$ is the mean permeability over the pressure range, A is the reservoir perimeter area (about 2×10^6 m^2), μ is viscosity, and $\Delta P/\Delta L$ is the overall pressure gradient at the boundary of the reservoir.

Reasonable estimates for the mean peripheral reservoir permeability, for a range of HDR reservoir pressure levels, can be obtained from Eq. 5 by using the integral mean value theorem from calculus

$$\bar{k} = \int_{P_2}^{P_1} k(P)dp/(P_1 - P_2)$$

where P_1 and P_2 define the range of the effective stress variation at the boundary of the reservoir region. That is,

$$P_1 = \sigma_2$$

$$P_2 = \sigma_2 - P_r$$

where σ_2 is the far-field effective earth stress parallel to the strike of the reservoir region (and therefore normal to the permeating microcrack network off the "sides" of the reservoir), and P_r is the specified HDR reservoir pressure above hydrostatic. For the region surrounding the Phase II reservoir, σ_2 is assumed to be about 35 MPa above hydrostatic pressure based on several indirect measurements.

Figure 3 shows the calculated variation in reservoir water loss ($\dot{Q}$ in Eq. 6) as a function of reservoir pressure, normalized to the water loss for a pressure of 24 MPa -- the mean reservoir pressure level for Experiment 2074 as discussed in the next section. It is significant to note at this point that the predicted water loss at the higher reservoir pressure maintained for the last two weeks of the ICFT (31 MPa) is less than twice that for Experiment 2074 (at 24 MPa), as compared to the measured increase of over a factor of 4 (to 5 l/s during the last 6 days of the ICFT).

Measured Water Losses for the Phase II Reservoir

Since completing the engineering of the Phase II reservoir in 1985, two significant flow tests have been conducted: the 30-day ICFT in mid 1986, and the 7-day flow test in December of 1987 called Experiment 2074.

1. Experiment 2074. The damaged Phase II reservoir production wellbore EE-2 at the Fenton Hill Hot Dry Rock site was sidetracked and redrilled in October and November of 1987, resulting in the new wellbore, EE-2A. A 7-day flow test was conducted to determine the post-drilling condition of EE-2A; the proper depth for a cemented liner to be installed in the open hole; the effect of redrilling on the Phase II reservoir flow paths; production temperatures, impedance and water loss; and to assess the need for reservoir stimulation through this new wellbore.

Figure 4 shows both the injection flow rate and the measured water loss during this brief flow test. As shown, the water loss after only 7 days had declined to 1.4 l/s (22.5 gpm), and was still decreasing at a rate of about 0.13 l/s/day (2 gpm/day). By extrapolating the decline trend shown in Fig. 4, it appears probable that the reservoir water loss would have further declined to no more than 1.2 l/s (19 gpm) in 3 more days (10 days total).

During the last 3 days of Experiment 2074, the reservoir injection pressure was held constant at about 24 MPa (3480 psi) by slowly reducing the injection flow rate as shown in Fig. 4. Therefore, by using the above extrapolated water loss rate of 1.2 l/s at 24 MPa, one is able to apply a reasonable calibration factor to the normalized reservoir water loss rate curve shown in Fig. 3.

It should be noted that Experiment 2074 was essentially an aseismic flow test, with no events large enough to be located. However, numerous very small microseismic events were detected at the close-in geophone located at a depth of 2865 m in a nearby borehole. These very small events were particularly numerous during the last two to three days of pumping. Unfortunately, the absence of significant seismic activity during this flow test may be interpreted in two different ways: either the reservoir was not fully inflated after only 7 days of injection or, a pressure of 24 MPa is not sufficient to extend the reservoir by additional shear slippage on the peripheral joints. This flow test was just not long enough to differentiate between these two different hypotheses.

2. The Initial Closed-Loop Flow Test (ICFT). The 30-day ICFT (Dash et al., 1988) was essentially performed in two equal segments: an initial 15-day segment at an average injection rate of 11.5 l/s, and a final 15-day segment at an average injection rate of 17.8 l/s. During the first segment, the injection pressure stabilized at a level of about 27 MPa

(3900 psi) in 13 days, and during the second segment the injection pressure again stabilized at about 31 MPa (4500 psi) after an additional 12 days.*

Figure 5 shows both the injection pressure and water loss rate profiles during the ICFT. The water loss after 14 days (on 3 June) was 2.3 l/s (37 gpm) at a pressure of 27 MPa, and after 12 more days (on 14 June) was about 5 l/s (79 gpm) at a pressure of 31 MPa. As pointed out by Dash et al. (1988), the water loss near the end of the ICFT was excessive, and since it was accompanied by a significant amount of microseismic activity, suggested active reservoir growth at an injection pressure of 31 MPa. Based on a re-analysis of the relevant ICFT data, we further note that the Phase II reservoir was also actively growing at an injection pressure of only 27 MPa during the latter part of the initial lower-flow-rate segment. Table II compares the measured water losses for the ICFT with those predicted from Fig. 3, using the calibration factor determined from Experiment 2074: a water loss rate of 1.2 l/s at 24 MPa after 10 days. As shown in Table II, the ICFT water loss values do appear to be excessive, even at the lower 27 MPa pressure level.

* Note: After the reservoir has been reinflated, the pressure near the boundaries of the reservoir is assumed to be approximately equal to the injection pressure.

Table II
Comparison of the Measured and Predicted Water Loss During the ICFT

	First Segment	Second Segment
Date:	2 May	14 May
Injection Pressure, MPa (taken as the reservoir pressure)	27	31
Water loss rate, l/s	2.3	5.0
Ratio of water loss to that at 24 MPa (Experiment 2074):		
Observed, ICFT	1.9	4.2
Predicted, Fig. 3	1.3	1.9

Microseismic Activity During the ICFT

As noted previously, the Phase II reservoir was essentially aseismic during the 7-day Experiment 2074 flow test. In contrast, the reservoir was quite seismically active during the ICFT, even during the initial, lower-flow-rate segment. This activity is shown in Fig. 6, a plot of the cumulative number of locatable microseismic events during the ICFT. (Also shown in Fig. 6 is the injection pressure profile for correlation purposes.)

Through 4 June during the first (lower) flow rate segment, 41 microseismic events were recorded which were sufficiently large to be adequately received at all three downhole stations and therefore reliably located. Figures 7 and 8 are plan and section views showing the locations of these 41 events superimposed on maps of the microseismic event locations defining the previous Phase II reservoir region, as initially formed during the Massive Hydraulic Fracturing Test in December 1983, and extended in mid-1985 during the high-pressure injection of Experiment 2062. Even at an injection pressure of only 27 MPa, it is readily apparent from these two figures that the reservoir was expanding: generally to the east as shown in Fig. 8, and in two discrete regions as shown in the epicenter plot (Fig. 7). The obvious conclusion is that an injection pressure of 27 MPa (3900 psi) is above the threshold pressure for active reservoir extension.

When the surface injection pressure was increased to over 30 MPa on the afternoon of June 4 by increasing the pumping rate to 18 l/s (6.8 BPM), there was a resulting "burst" of microseismicity lasting for the next 37 hours (Fig. 6). The onset of this period of very active reservoir seismicity is coincident with a sudden and pronounced 7.9 l/s increase in the reservoir water loss rate as shown in Fig. 5 (from 2.3 l/s to 10.2 l/s). Again, it is clear that the reservoir was expanding -- and even more vigorously -- at this higher injection pressure. The subsequent peak in seismic activity on June 12 appears to represent an episodic extension of the Phase II reservoir. This additional period of very rapid reservoir expansion was probably the direct result of the sudden -- but short-lived -- 24% increase in the injection flow rate, from 17.8 to 22 l/s, which was accompanied by the observed pressure "spike" to 33.6 MPa (4870 psi) shown in Fig. 6.

Figures 9 and 10 show composite plan and section views of all the reliably located microseismic events during the entire 30-day ICFT. Again, it can be seen that there was continuing reservoir growth to the east in the general regions first stimulated at 27 MPa (refer to Figs. 7 and 8). However, in composite, there is also considerable downward growth to the south and east, and a pronounced shallower extension to the south -- almost 600 m away from the injection zone shown in Fig. 9 (solid line).

One further point can be made from the seismic data and injection pressure data recorded during the first 9 days of the ICFT. The two early pressure pulses above 30 MPa shown in Fig. 6, lasting for 28 hours on May 25 and 26, and 12 hours on May 27 and 28, produced very different microseismic responses from the reservoir. The first -- and longer -- pulse, resulting from an increase in the injection rate to 18 l/s, was aseismic, in marked

contrast to the reservoir behavior during the second flow rate segment. However, the second -- and shorter -- pulse, again resulting from a short period of increased flow, produced 16 microseismic events. That the first pressure pulse above 30 MPa was aseismic strongly suggests that the reservoir was not yet fully inflated at this time, even after 7 days of pumping. However, the onset of microseismic activity at 04:00 on May 28 (see Fig. 6) appears to mark the point where the reservoir first started to expand. By integrating the water loss profile of Fig. 5 through 04:00 on 28 May (5,520 m^3), and subtracting out an estimate for the far-field permeable flow loss during these 8.5 days (920 m^3), one can infer that it required approximately 4,600 m^3 (1.2×10^6 gal) of water to reinflate the Phase II reservoir to about 27 MPa, the mean injection pressure during the previous 30 hours (assumed to be approximately equal to the reservoir pressure after 8 days of inflation).

In reference to the lower-pressure Experiment 2074, the integral of the water loss profile shown in Fig. 4 is only 1,410 m^3 (372,000 gal), for the 7 days of pumping at 24 MPa. This is only 30% of the ICFT inflation volume of 4,600 m^3 at 27 MPa given above. This implies that the Phase II reservoir was not fully inflated by the end of this 7-day flow test, suggesting that the reservoir could have started to extend after several more weeks of pumping at 24 MPa.

Conclusions

1. The Gangi pressure-dependent permeability model has been proposed for predicting the peripheral water loss from a hydraulically stimulated region of naturally jointed, crystalline rock. This model has been shown to adequately represent the permeability of both jointed and microcracked crystalline rock as a function of effective stress.
2. Above a threshold pressure of less than 27 MPa (3900 psi), the deeper Phase II HDR reservoir at Fenton Hill is shown to expand due to additional joint stimulation at the boundaries of the previously stimulated region.
3. For long-term nonextensional flow testing, the Phase II HDR reservoir should be operated at a surface injection pressure less than 27 MPa (3900 psi), and more probably in the range of 24 MPa (3500 psi).

Acknowledgment

This work was done under the auspices of the US Department of Energy.

References

Brace, W.F., "Some New Measurements of Linear Compressibility of Rocks," J. Geophys. Res., 70, 391-398 (1965).

Carlson, R.L., and A.F. Gangi, "Effects of Cracks on the Pressure Dependence of P-Wave Velocities in Crystalline Rocks," J. Geophys. Res., 90, 8675-8684 (1985).

Dash, Z.V. (Ed.), R.G. Aguilar, B.R. Dennis, D.S. Dreesen, M.H. Fehler, R.H. Hendron, L.S. House, Hisao Ito. S.M. Kelkar, M.V. Malzahn, J.R. Miller, H.D. Murphy, V.S. Phillips, S.B. Restine, P.M. Roberts, B.A. Robinson, and W.R. Romero, Jr., "ICFT: An Initial Closed-loop Flow Test of the Fenton Hill Phase II HDR Reservoir," Los Alamos National Laboratory report LA-11498-HDR, Los Alamos, NM (1988).

Duffy, C.J., unpublished data, Los Alamos National Laboratory, Los Alamos, NM (1980).

Gangi, A.F., "Variation of Whole and Fractured Rock Permeability with Confining Pressure," Int. J. Rock Mech. Min. Sci., 15, 249-257 (1978).

Gangi, A.F., "The Variation of Mechanical and Transport Properties of Cracked Rock with Pressure," in Proceedings of the 22nd U.S. Symposium on Rock Mechanics, Pub. Massachusetts Institute of Technology, Cambridge, Mass., 85-89 (1981).

Goodman, R.E., Methods of Geological Engineering in Discontinuous Rocks, West Publishing Company, San Francisco, CA, 472 pp. (1976).

Greenwood, J.A, and J.B.P. Williamson, "Contact of Nominally Flat Surfaces," Proc. R. Soc., Comp. A, 295, 300-39 (1966).

Sun, Z., C. Gerrard, and O. Stephannson, "Rock Joint Compliance Tests for Compression and Shear Loads," Int. J. Rock Mech. Min. Sci., 22, 197-213 (1985).

Swan, G., "Determination of Stiffness and Other Joint Properties from Roughness Measurements," Rock Mechanics and Rock Engineering, 16, 19-38 (1983).

Walsh, J.B., and W.F. Brace, "Mechanics of Rock Deformation," in Rock Mechanics Symposium, The Winter Annual Meeting of the ASME, Detroit, Pub. ASME, New York, 1-24 (1973).

Witherspoon, P.A., J.S.Y. Wang, K. Iwai, and J.E. Gale, "Validity of Cubic Law for Fluid Flow in a Deformable Rock Fracture," Water Resources Res., 16:1016 (1980).

Page missing from original document

Page missing from original document

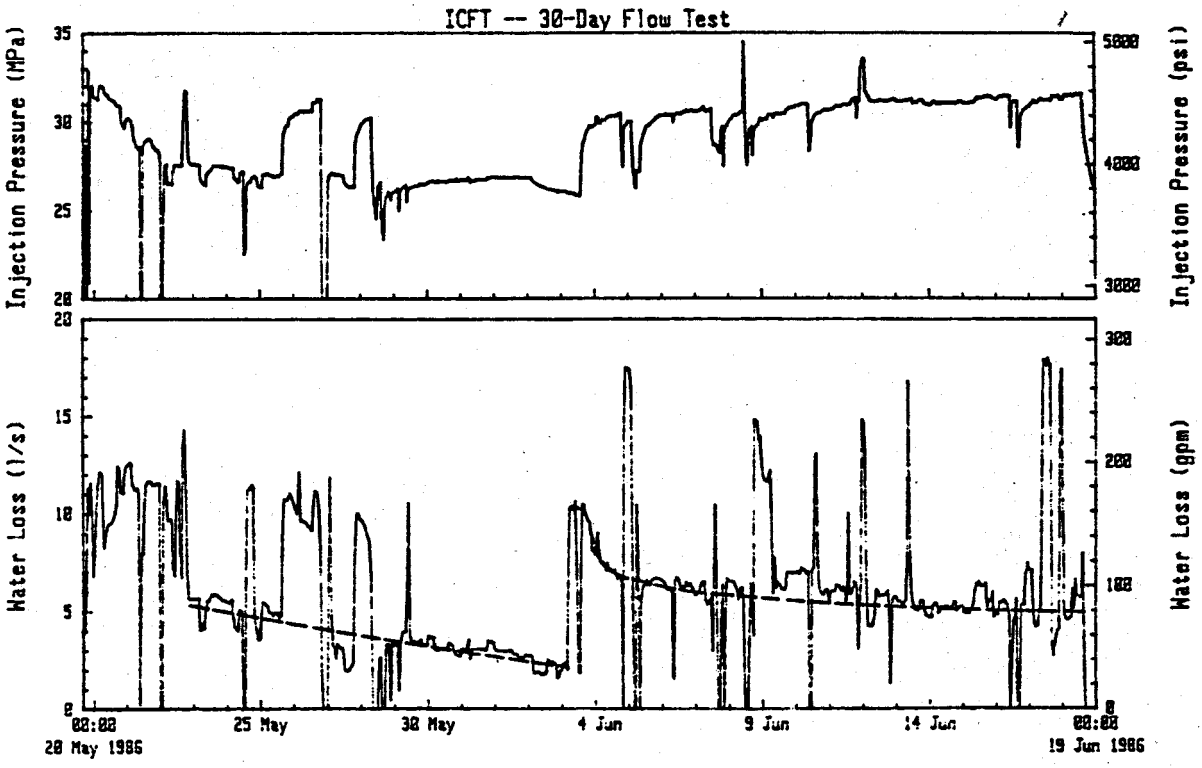

Fig. 5: ICFT injection pressure and water loss rate.

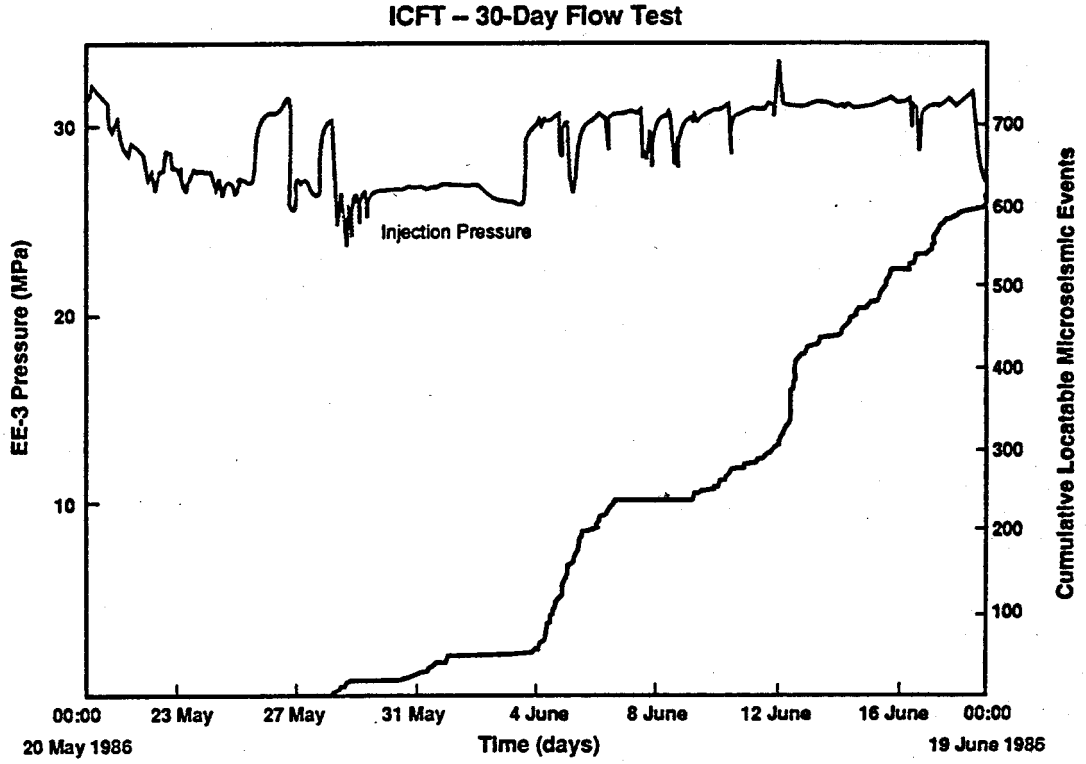

Fig. 6: Cumulative number of locatable microseismic events recorded during the 30-day ICFT.

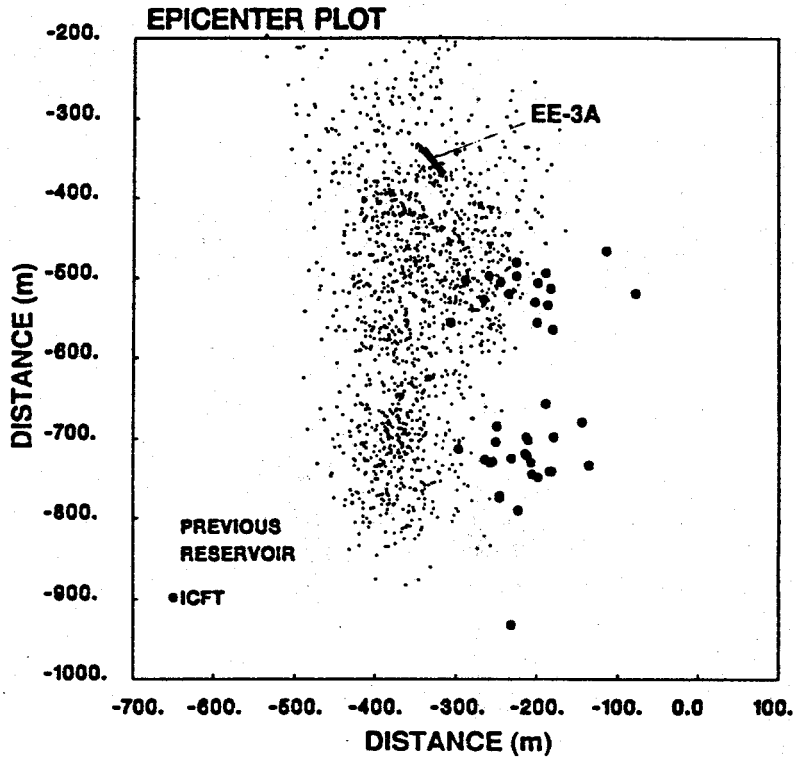

Fig. 7: Plan View: Locations of the 41 reliably located microseismic events recorded during the initial segment of the ICFT, at an injection pressure of 27 MPa.

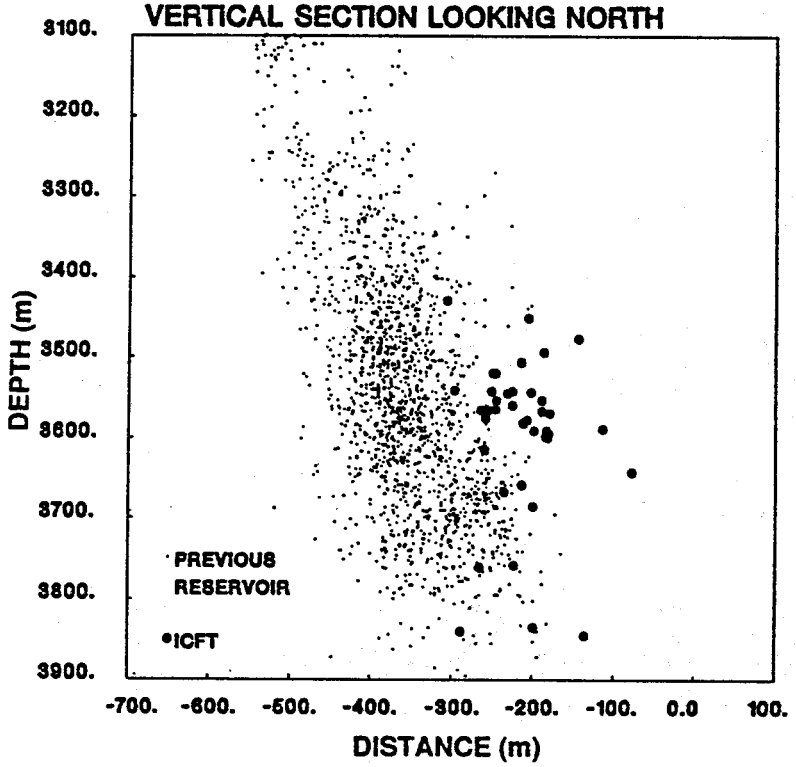

Fig. 8: Section View: Locations of the 41 reliably located microseismic events recorded during the initial segment of the ICFT, at an injection pressure of 27 MPa.

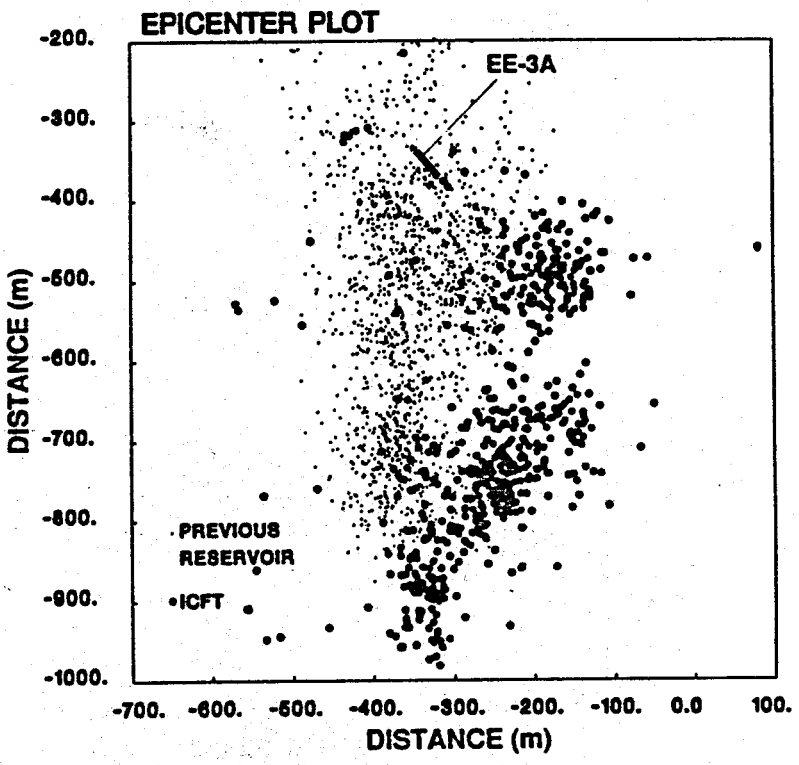

Fig. 9: Plan View: Locations of all the reliably located microseismic events recorded during the ICFT. (The solid line shows the position of the injection interval in wellbore EE-3A.)

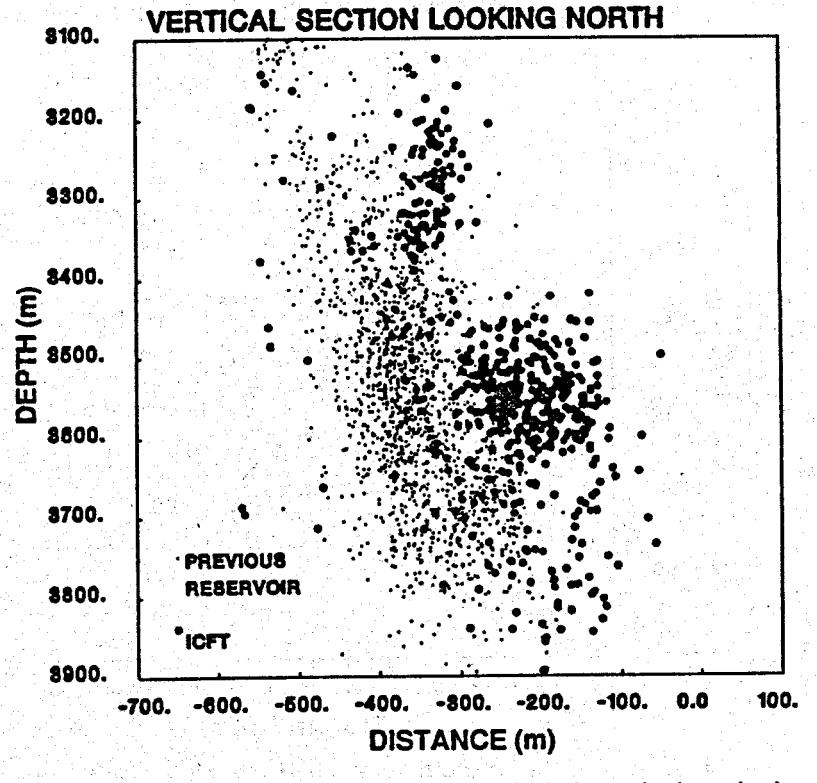

Fig. 10. Section View: Locations of all the reliably located microseismic events recorded during the ICFT.

PROCEEDINGS, Fourteenth Workshop on Geothermal Reservoir Engineering
Stanford University, Stanford, California, January 24-26, 1989
SGP-TR-122

AN INVESTIGATION OF THE INFLUENCE OF HIGH-VELOCITY FLOW ON THE TRANSIENT PRESSURE BEHAVIOR OF LIQUID-DOMINATED WELLS

Hiram Villalobos L*, Fernando Rodríguez* and
Fernando Samaniego V.**

Universidad Nacional Autónoma de
México, Facultad de Ingeniería,
04510 México, D.F.

ABSTRACT

The present study on the influence of high-velocity effects on the flow of hot-water through porous media was undertaken based upon the analysis of tests taken in the Cerro Prieto and East Mesa fields. These fields produce form a sedimentary formation of the "homogeneous" (non-fractured) type. The study is based on a numerical solution to the radial flow (isothermal) problem of hot-water considering high-velocity flow. An expression for the rate dependent pseudo-skin effect term is derived. It is demonstrated through an integration of the Forchheimer flow equation and the simulation of drawdown tests that consider no skin damage that this pseudo-skin is essentially equal to the product Dw, where D is the turbulent term coefficient defined as $\beta k/2\pi r_w h\mu$ It is also shown that the semilogarithmic slope of 1.1513 characteristic of radial flow is obtained once a stabilized high-velocity condition is reached. The start of this straight line was found to be dependent on the intensity of high-velocity flow effects. For practical producing conditions found in the field, it was found that the start of the semi-log straight line can be predicted by the correlation of Ramey et al.; provided that the apparent skin effect s' is used instead of the skin factor s. This study also considers the influence of high velocity flow on pressure buildup tests. The effects of a finite formation skin and isothermic wellbore storage are also included in this work.

INTRODUCTION

The subject of high-velocity flow through porous media was first discussed by Forchheimer (1901). After this work a number of studies have addressed this subject, particularly oriented toward the laboratory verification of this phenomenon (Fancher et al., 1933; Johnson and Taliaferro, 1938; Green and Duwez, 1951; Cornell and Katz, 1953; Firoozabadi and Katz, 1979).

The influence of high-velocity flow in the transient pressure behavior of gas well tests has been thoroughly reported in the literature (Ramey, 1965; Wattenbarger and Ramey, 1968; Energy Resources Conservation Board, 1975). This effect has also been considered in two phase flow of oil and gas (Kadi, 1980). With regard to the flow through perforations, it has also been studied for gas flow (Tarik, 1984) and for two phase flow of oil and gas (Perez and Kelkar, 1988).

Due to the high production rates commonly encountered in geothermal liquid-dominated wells, we suspected that conditions were proper for high-velocity effects to affect the transient pressure behavior of well tests. With this idea in mind, we analyzed testing conditions for the Cerro Prieto and East Mesa fields and found that this effect was present. These fields produce from a sedimentary formation of the "homogeneous" (non-fractured) type.

The purpose of this study is to present an analysis of the influence of high-velocity flow on the transient pressure behavior of liquid-dominated wells. Pressure drawdown and buildup tests are considered. The effects of skin damage and wellbore storage affecting the test simultaneously with high-velocity flow are also studied.

MATHEMATICAL DEVELOPMENT

Due to the fact that single-phase (steam or hot water) flow in geothermal reservoirs is essentially isothermal (Whiting and Ramey, 1969), transient pressure analysis techniques are ussually based on a strict analogy with the single-phase isothermal flow tecniques developed by petroleum engineers and hydrogeologists. The analysis techniques are based on solutions to the difussivity equation (Muskat, 1937; Matthews and Russell, 1967; Earlougher, 1977) which consider the following assumptions: a) flow of a constant compressibility fluid in a radial, horizontal, isotropic reservoir, b) applicability of Darcy's law, c) small pressure gradients, and d) rock and fluid properties are independent of pressure. For convenience, the solution to this reservoir fluid flow problem is ussually expressed in dimensionless form. The following groups have been defined by Ramey (1975) and

*The author also associated with Instituto Mexicano del Petróleo
**The author also associated with Pemex

Ramey and Gringarten (1975), where α_w and β_t are unit constants:

Dimensionless pressure for hot-water reservoir flow (p_D)

$$p_D(r_D,t_D)=\frac{kh(p_i-p(r,t))}{\alpha_w q_{sc} B\mu} \quad (1)$$

Dimensionless time (t_D)

$$t_D=\frac{\beta_t k t}{\phi\mu c_t r_w^2} \quad (2)$$

Dimensionless radial distance (r_D)

$$r_D=\frac{r}{r_w} \quad (3)$$

If a consistent set of units is used, then the constants will have a value equal to one. Table 1 (Samaniego and Cinco, 1982) shows some of the most used unit systems and the corresponding values for α_w and β_t.

Using the definitions of the dimensionless groups given by Eqs. 1-3, the equation that describes the flow of hot-water, considering the effect of high-velocity flow is given by Eq. 4:

$$\frac{1}{r_D}\frac{\partial}{\partial r_D}\left(r_D\delta\frac{\partial p_D}{\partial r_D}\right)=\frac{\partial p_D}{\partial t_D} \quad (4)$$

where δ is the L.I.T. (laminar, inertial and turbulence) correction factor. In the derivation of this equation and in all remaining equations of this section, a consistent set of units is assumed, resulting in values of the parameters α_w and β_t equal to $\frac{1}{2}\pi$ and unity, respectively. This is just for easiness in the derivations, but for field applications of the results of this study these unit conversion constants are very convenient.

The inner boundary condition considered in this study is of constant mass rate at the well, including the effects of skin damage and isothermic wellbore storage:

$$-\left(\delta\frac{\partial p_D}{\partial r_D}\right)_{r_D=1}=\frac{k}{k_s}-C_D\frac{k}{k_s}\left(\frac{\partial p_D}{\partial t_D}\right)_{r_D=1} \quad (5)$$

The external boundary condition is that of an infinite reservoir:

$$\lim_{r_D\to\infty} p_D(r_D,t_D)=0 \quad (6)$$

The initial condition is of uniform pressure at the reference time $t_D=0$:

$$\lim_{t_D\to 0} p_D(r_D,t_D)=0\ ,\ 1\le r_D<\infty \quad (7)$$

This completes the mathematical model solved numerically in this study.

Next we present some additional mathematical aspects related to the high-velocity flow effects. First, we will comment on the way we handled Forchheimer's equation given by Eq. 8:

$$-\frac{dp}{dr}=\frac{\mu}{k}v_r+\beta\delta v_r^2 \quad (8)$$

where β is the velocity coefficient. This equation can be written in dimensionless form by means of the parameters defined by Eqs. 1-3:

$$\frac{dp_D}{dr_D}=v_{rD}+\beta_D v_{rD}^2 \quad (9)$$

where v_{rD} and β_D are a dimensionless velocity and a dimensionless velocity coefficient defined by Eqs. 10 and 11, respectively:

$$v_{rD}=\frac{2\pi h r_w}{q_{sc}}v_r \quad (10)$$

$$\beta_D=\beta\frac{k}{\mu}\cdot\frac{w}{2\pi r_w h} \quad (11)$$

Eq. 9 is valid for flow in the formation outside the damaged region near the wellbore. Thus, for flow in the damaged region, Eq. 9 can be written:

$$\frac{dp_D}{dr_D}=\frac{1}{k_{sD}}v_{rD}+\beta_{sD}v_{rD}^2 \quad (12)$$

where β_{sD} is the dimensionless velocity coefficient for the damaged region, and k_{sD} is the permeability ratio given by Eq. 13:

$$k_{sD}=\frac{k_s}{k} \quad (13)$$

Last, we will present an expression for the extra pressure drop caused by high-velocity effects. This, in other words, is the rate dependent pseudo-skin due to high-velocity effects. From Eq. 9, the pressure gradient caused by high-velocity flow $(dp_D/dr_D)_{hv}$, is given as follows:

$$\left(\frac{dp_D}{dr_D}\right)_{hv}=\beta_D v_{rD}^2 \quad (14)$$

It can be demonstrated that for radial flow, the dimensionless velocity v_{rD} can be expressed as follows:

$$v_{rD}=\frac{1}{r_D} \quad (15)$$

Then, Eq. 14 can be written as:

$$\left(\frac{dp_D}{dr_D}\right)_{hv}=\frac{\beta_D}{r_D^2} \quad (16)$$

Integrating this equation:

$$(p_D)_{hv} = (1 - \frac{1}{r_{hvD}})\beta_D \quad (17)$$

If we want to express Eq. 17 in the conventional way used for gas flow (Ramey, 1965); Wattenbarger and Ramey, 1968), we can get:

$$(p_D)_{hv} = Dw \quad (18)$$

where D is the turbulent term coefficient defined as:

$$D = \frac{\beta k}{2\pi r_w h \mu}(1 - \frac{1}{r_{hvD}}) \quad (19)$$

If a damaged region near the wellbore is considered, Eq. 17 can be written as follows:

$$(p_D)_{hv} = \beta_D [\frac{\beta_s}{\beta}(1 - \frac{1}{r_{sD}}) + (\frac{1}{r_{sD}} - \frac{1}{r_{hvD}})] \quad (20)$$

where r_{sD} is the dimensionless outer radius of the damaged region.

In the simulation of transient pressure tests to be discussed later in this paper, the velocity coefficient was evaluated by means of the correlation of Firoozabadi and Katz (1979).

FIELD EVIDENCE OF HIGH-VELOCITY FLOW

It has been shown that the extra dimensionless pressure drop caused by high-velocity effects, in the absence of formation damage, is given by Eq. 17. The results of our numerical simulations, to be discussed in the next section, indicate that the high-velocity radius r_{hvD} ranges between 33 and 110 for β_D values of 0.3 and 1, respectively; consequently for practical purposes the $1/r_{hvD}$ term may be neglected in the estimation of the rate dependent pseudo-skin due to high-velocity effects. Thus, in light of the foregoing conclusion we can write:

$$(p_D)_{hv} = \beta_D = Dw \quad (21)$$

where D is the turbulent term coefficient defined as:

$$D = \frac{\beta k}{2\pi r_w h \mu} \quad (22)$$

Next we present estimations of the rate dependent pseudo-skin Dw for wells of Cerro Prieto and East Mesa fields. As mentioned, these fields produce from a sedimentary formation of the "homogeneous" (non-fractured) type (Grant et al., 1984; Lyons and van de Kamps, 1974; Witherspoon et al., 1978).

For units of the hybrid system (Table 1), the parameter β_D(=Dw) given by Eq. 21 can be expressed as follows:

$$Dw = 1.54084 \times 10^{-12} \frac{\beta k w}{r_w h \mu} \quad (23)$$

First we evaluate this parameter for the data of well M-21A of Cerro Prieto taken from Rivera and Ramey (1977). The values of the parameters that enter into Eq. 23 are presented in Table 2. Evaluating Dw we obtain:

Dw = 0.405

Next calculations are shown for well M-109 of Cerro Prieto. This well was chosen because its characteristic curve shown by Iglesias et al. (1983) (their Fig. 5.6) shows a non-linear relationship of mass flow rate (w) vs bottom-hole pressure (p_{wf}), indicating that high-velocity effects may be influencing the performance of the well. The values of the parameters that enter into Eq. 23 are presented in Table 2. We obtain the following value for Dw:

Dw = 0.25

Last we show calculations for a well of the East Mesa field (Witherspoon et al., 1978). Again, the values of the parameters that enter into Eq. 22 are shown in Table 2. Evaluating the pseudo-skin Dw we get:

Dw = 0.14

The motivation for this last calculation came from reviewing the results of Morris et at. (1987) (their Fig. 9) for well E.M. 87-6, regarding a graph of pressure drawdown vs flow rate which shows slight curvature and Reynolds numbers (their Table 7) that are higher than unity, which is the ussually agreed upon upper limit for the validity of Darcy's law (Muskat, 1937).

Based on the above shown calculations and discussion, we felt that high-velocity flow may influence the transient pressure behavior of liquid-dominated wells and started the research reported in this paper.

VALIDATION OF THE NUMERICAL MODEL

Basically we checked our numerical model by considering Darcy flow (δ=1) conditions for which an analytical or a numerical solution are already available in the literature. A sensitivity analysis of results to different time and space discretizations was first undartaken. For cases of no skin damage and no wellbore storage, the numerical solution of this study were compared to that of van Everdingen and Hurst (1949), and a difference of less than 0.2% was obtained. For cases that included the skin damage and wellbore storage, the comparison was with the numerical solutions presented by Wattenbarger and Ramey (1970), and essentially we obtained

identical results. The above mentioned comparison with available results in the literature was acquired with a 40 nodes space discretization for $r_{eD}=2x10^4$; this reservoir external radius was large enough to have infinite acting behavior during the test time. With regard to the time discretization, 45 time steps per log cycle of time were needed to obtain this comparison. For more details of the numerical model the reader is referred to the report of Villalobos (1989).

DISCUSSION OF RESULTS

Based upon our discussion of the mathematical development section, it was found that high-velocity flow effects are strictly related to the dimensionless velocity coefficient β_D (Eqs. 9 and 11). The evaluation of this parameter for maximum producing conditions of a well gives an upper limit for β_D of one.

We first simulated drawdown tests for different values of the dimensionless velocity coefficient β_D. The results for values of β_D of 0.3, 0.6 and 1 are shown in the semilogarithmic graph of p_{wD} vs t_D of Fig. 1. We observe from these results that after the high-velocity flow region is stabilized, a straight line is reached of slope equal to the conventional value of liquid flow of 1.1513. This means, as already mentioned, that after stabilization occurs, the pressure drop due to high-velocity can be expressed as a rate-dependent pseudo-skin Dw. Thus, the dimensionless pressure drop may be expressed as follows:

$$p_{wD} = \tfrac{1}{2}(\ln t_D+0.80907)+Dw \qquad (23)$$

From the above discussion, it can be concluded that the formation conductivity kh can be accurately estimated even if the test is under the influence of high-velocity flow.

Next we consider the combined effects of formation damage and high-velocity flow. Constant flow rate cases were run for values of β_D of 1 that corresponds to maximum conditions and values of the skin factor s of -2, 0, 5, 10 and 20. Fig. 2 shows the results of these simulations. These data indicate that high-velocity flow in a composite reservoir does not affect the transient behavior more than in a homogeneous reservoir. The early transient flow is dominated by the region of altered permeability near the well. After a transition period, a straight line occurs whose slope is equal to the conventional value of liquid flow of 1.1513. This second straight line is parallel to $p_D(\beta_D=0)$ solution of van Everdingen and Hurst (1949), but is displaced by an amount equal to the apparent skin effect s'(Ramey, 1965) defined by

$$s' = s + Dw \qquad (24)$$

We checked the results of our simulations with regard to the rate dependent pseudo-skin factor Dw that resulted from the computer runs and that calculated from Eq. 20 and found an excellent agreement.

The factor that the straight line portion of the drawdown curve is parallel to $p_D(\beta_D=0)$ is important. This means that the conductivity kh of the outer portion of the formation can be determined accurately from a drawdown test. Thus, Eq. 23 can be extended to

$$p_{wD} = \tfrac{1}{2}(\ln t_D+0.80907)+s+Dw \qquad (25)$$

To calculate the skin factor s and the turbulent term coefficient D, the method of Ramey (1965) can be used.

To complete the study we included in our simulations the effect of isothermic wellbore storage. Constant flow rate cases were run at values of β_D of 1 and of c_D of 10, 10^2, 10^3 and 10^4. Fig. 3 shows a semilog graph of p_{wD} vs t_D. We observe from these results that the hot-water solutions that consider high-velocity flow essentially follow a parallel behavior with the liquid solution $p_D(\beta_D=0)$.

The wellbore storage effect was found to behave like liquid case solutions (van Everdingen and Hurst, 1949; Wattenbarger and Ramey, 1970). Wellbore storage has only a short-time effect on the transient pressure behavior and has no effect on the ultimate slope of the semilogarithmic drawdown curve.

The last case considered with regard to drawdown tests was one that includes simultaneously the effects of high-velocity flow, formation damage and wellbore storage. Constant flow rate cases were run for values of s=5 and $C_D=10^2$, and values of β_D of 0.3 0.6 and 1. Fig. 4 shows the results of these simulations. The conclusions reached from these results are essentially those already made for the cases of high-velocity flow affected either by formation damage (Fig. 2) or wellbore storage (Fig. 3). In short, the formation conductivity can be estimated from the drawdown test. In addition the skin factor s and the turbulent term coefficient D can be estimated by means of the method of Ramey (1965).

We also investigated what effects high-velocity flow would have on an analysis using the derivative type curve of Bourdet et al. (1983). We found that as the intensity of high-velocity flow increases, the error in the estimation of the formation parameters from the match point data also increases. As expected, the maximum error is found in the estimation of the skin factor, in some cases off by 200 per cent. A similar finding for real gas flow has been reported by Berumen et al.(1989). Fig. 5 shows an example of derivative type curves for the case of $C_D=100$,

s=5 and different values of β_D. Thus, in cases where high-velocity flow affects a test, results of type curve analysis are to be taken with caution.

We looked carefully to the effects of high-velocity flow on the beginning of the semi-log straight line. As expected, it was found that it was affected by the intensity of high-velocity flow represented by the parameter β_D. For practical producing conditions found in the field, it was found that the start of the semi-log straight line can be predicted by the correlation of Ramey et al. (1973), provided that the apparent skin effect s' is used instead of the skin factor s. This time for the start of the semi-log straight line is:

$$t_{Dbsl} = C_D(60+3.5s') \qquad (26.a)$$

or in term of real variables (Table 1):

$$t_{bsl} = \frac{\varepsilon}{\beta} \cdot \frac{CB\,\nu_{sc}}{kh}(60+3.5\ s') \qquad (26.b)$$

This study also considered the simulation of buildup tests under the influence of high-velocity flow. Fig. 6 presents a semi-logarithmic graph of simulated buildup curves for values of the parameter β_D of 0.3, 0.6 and 1. We see from these results that after the high-velocity flow effects vanish in a short time, the buildup curve joins the buildup solution for β_D=0. The shut-in time required to reach the straight line portion is approximately $\Delta t_D = 10^2$. For practical purposes, the determination of the formation conductivity kh from buildup test under the influence of high-velocity flow appears to be very accurate.

After having checked the influence of high-velocity flow on buildup tests, simulations then were made to investigate the effect of formation damage and wellbore storage on buildup tests under the influence of high-velocity flow. The main aim was to determine whether any of these two effects or both, in combination with high-velocity flow alter the straight line portion of the semilog buildup curve.

Results of simulated buildup curves under the influence of combined effects of high-velocity flow and formation damage are shown in Fig. 7. The values of the β_D and s parameters were the same as those of the corresponding drawdown tests already discussed (Fig. 2). It is concluded from these graphical results that after a period of influence from the formation damage, the buildup solutions become straight lines with the proper slope. Thus, the formation conductivity kh can be determined accurately from a build-up curve. As previously discussed for drawdown tests, the method of Ramey (1965) can be used to calculated the skin factor s and the turbulent term coefficient D.

Results of simulated buildup curves under the influence of combined effects of high-velocity flow and isothermic wellbore storage are shown in Fig. 8. The values of the β_D and C_D parameters were the same as those of the corresponding drawdown tests already discussed (Fig. 3). The family of curves of this figure is similar to buildup curves that consider β_D=0. After the effect of wellbore storage dies out, the buildup solutions joins the solution for C_D=0. Thus, the slope of the straight line portion is accurate provided the correct straight line portion is chosen.

Finally, the last case considered with regard to buildup tests is one that includes simultaneously the effects of high-velocity flow, formation damage and wellbore storage. The values of the β_D, s and C_D parameters were the same as those of the corresponding drawdown tests already discussed (Fig. 4). Fig. 9 shows results of these tests. The conclusions reached from these results are essentially those already made for the cases of high-velocity flow affected either by formation damage (Fig. 7) or wellbore storage (Fig. 8). In short, the formation conductivity can be estimated from the buildup test. The skin factor s and the turbulent term coefficient D can be estimated from results of buildup analysis by means of the method of Ramey (1965).

CONCLUSIONS

The main purpose of this work was to present a systematic study of transient pressure analysis of liquid dominated wells producing at constant mass rate under the influence of high-velocity flow. The motivation for the research subject of this study came from the analysis of testing conditions for the Cerro Prieto and East Mesa fields, that indicated the presence of this effect.

Based on the material presented in this paper, the following conclusions are pertinent:

1. The formation conductivity can be determined accurately from the analysis of pressure drawdown or buildup tests under the influence of high-velocity flow and the effects of formation damage and wellbore storage.
2. An easy to use expression is presented for approximate determination of the rate dependent pseudo-skin Dw.
3. The method of Ramey (1965) can be used for an accurate determination of the skin factor s and the turbulent term coefficient D.
4. If high-velocity flow affects a test, results of type curve analysis by means of the derivative type curves of Bourdet et al. (1983) are to be taken with caution.

5. It was found that the start of the semi-log straight line can be predicted by the correlation of Ramey et al.(1973), provided that the apparent skin effect s' is used instead of the skin factor s.

NOMENCLATURE

B= formation volume factor
c_t= system total compressibility
C^t= wellbore storage constant for hot water
C_D= Dimensionless wellbore storage constant $= \frac{\varepsilon C B \nu_{sc}}{\phi h r_w^2 c_t}$
h= thickness
k= permeability
p= pressure
r= radial distance
s= van Everdingen and Hurst skin factor
s'= apparent skin factor, Eq. 24
t= time
v_r= radial velocity
w= mass flow rate
β= velocity coefficient
δ= L.I.T. (laminar, inertial, and turbulent) correction factor
φ= porosity
μ= viscosity
ρ= density

Subscripts
D= dimensionless
hv= high-velocity
s= damaged region
t= total or time
sc= standard conditions
w= wellbore

ACKNOWLEDGMENTS

The authors are grateful to Dr. Jesus Rivera R. for his valuable comments regarding some field aspects of the research subject of this study.

REFERENCES

Berumen C., S., Samaniego V.F., and Cinco Ley, H., 1989. Transient Pressure Analysis and Performance of Gas Wells Producing Under Constant Pressure Conditions. Paper SPE 19098. Presented at 1989 SPE Gas Technology Symposium, Dallas, Tex., 7-9 June.

Bourdet, D., Whittle, T.M., Douglas, A.A., and Pirard, V.M., 1983. A New Set of Type-Curves Simplifies Well Test Analysis, World Oil, (May), pp. 95-106.

Cornell, D. and Katz, D.L. 1953. Flow of Gases Thorough Consolidated Porous Media. Ind. and Eng. Chem.(Oct.) 45, 2145.

Earlougher, R.C., Jr., 1977. Advances in Well Test Analysis. SPE monograph No. 5, Richardson, Tex.

Energy Resources Conservation Board, 1975. Theory and Practice of the Testing of Gas Wells, Calgary, Alberta.

Fancher, G.H., Lewis, J.A., and Barnes, K.B., 1933. Some Physical Characteristics of Oil Sands. Bull. 12, Pennsylvania State C., Mineral Industries Experiment Station, University Park.

Firoozabadi, A. and Katz, D.L., 1979. An Analysis of High-Velocity Gas Flow Through Porous Media. J. Pet. Tech. (February),pp. 211-216.

Forchheimer, P., 1901. Wasserbewegung durch Boden. Zeitz ver deutsch Ing. (1901) 45, 1731.

Green,L. and Orwez, P., 1951. Fluid Flow Through Porous Metals. J. Appl. Mech. (March) 18,39.

Grant, M.A., Truesdell, A.H., and Mañon, M., A., 1984. Production Induced Boiling and Cold Water Entry in the Cerro Prieto Geothermal Reservoir Indicated by Chemical and Physical Measurements, Geothermics, Vol. 13, No. 1/2, pp. 117-148.

Halfman, S.E., Lippmann, M.J. and Gilreath, J.A., 1985. Cerro Prieto Case History: Use of Wireline Logs to Characterize a Geothermal Reservoir, Soc. Pet. Eng. J. (December) pp. 793-803.

Iglesias, E., Arellano, V., and Molinar, R., 1983. A Method to Recover Useful Geothermal Reservoir Parameters from Production Characteristic Curves. (2) Hot Water Reservoirs, Proceedings Ninth Workshop Geothermal Reservoir Engineering, Stanford University, pp. 291-297.

Johnson, T.W. and Taliaferro, D.B., 1938. Flow of Air and Natural Gas Through Porous Media Technical Paper 592, USBM.

Kadi , K.S., 1980. Non-Darcy Flow in Dissolved Gas-Drive Reservoirs. Paper SPE 9301. Presented at 55th Annual Fall Technical Conference and Exhibition of SPE, Dallas, Tex., 21-24 September.

Lyons, D.J. and van de Kamp, P.C., 1979. Subsurface Geological and Geophysical Study of the Cerro Prieto Geothermal Field. Proc. Second Symp. Cerro Prieto Geothermal Field, Mexicali, October, 173-195.

Matthews, C.S. and Russell, D.G., 1967. Pressure Buildup and Flow Tests in Wells. SPE monograph No. 1, Richardson Tex.

Morris, C.W., Campbell, D.A., and Petty, S., 1987. Analysis of Geothermal Wells in Naturally Fractured Formations with Rate-Sensitive Flow. SPE Formation Evaluation (December), pp. 567-572.

Muskat, M., 1937. The Flow of Homogeneous

Fluids Through Porous Media. McGraw-Hill, New York.

Perez, G. and Kelkar, B.G., 1988. A New Method to Predict Two-Phase Pressure Drop Across Perforation. Paper SPE 18248. Presented at 63rd Annual Technical Conference and Exhibition of SPE, Houston, Tex., 2-5 October.

Ramey, H.J., Jr. 1965. Non-Darcy Flow and Wellbore Storage Effects in Pressure Buildup and Drawdown of Gas Wells. J. Pet. Tech. (February), pp. 223-233.

Ramey, H.J., Jr., Kumar, A., and Gulati, M.S., 1983. Gas Well Test Analysis Under Water-Drive Conditions, AGA, Arlington, Va.

Ramey, H.J., Jr. 1975. Pressure Transient Analysis for Geothermal Wells, Proc. 2nd U.N. Symposium on the Development and use of Geothermal Resources, San Francisco, 3, 1749-1757.

Ramey, H.J., Jr. and Gringarten, A.G., 1975 Effect of High-Volume Vertical Fractures on Geothermal Steam Well Behavior. Proc. 2nd U.N. Symposium on the Development and Use of Geothermal Resources, San Francisco 3, 1759-1762.

Rivera, R.J., and Ramey, H.J., Jr. 1977 Application of Two-Rate Flow Tests to the Determination of Geothermal Reservoir Parameters. Paper SPE 6887. Presented at the 52nd Annual Fall Technical Conference and Exhibition of SPE, Denver, Co., 9-12 October.

Samaniego, V.F. and Cinco-Ley, H., 1982. Reservoir Engineering Concepts. In L.M. Edwards, G.V. Chilingar, H.H. Rieke III and W.H. Fertl (eds), Handbook of Geothermal Energy, Gulf Publishing Co., Houston, Texas, pp. 426-470.

Tariq, S.M., 1984. Evaluation of Flow Characteristics of Perforations Including Nonlinear Effects Using Finite-Element Method. Paper SPE 12781. Presented at the 1984 SPE California Regional Meeting.

van Everdingen, A.F. and Hurst, W., 1949. The Application of the Laplace Transformation to Flow Problems in Reservoirs. Trans., AIME (1949) 186, pp. 305-324.

Villalobos L.H., 1989, Análisis de Pruebas de Presión en Yacimientos Naturalmente Fracturados Considerando el Efecto de Flujo de Alta Velocidad, M. Sc. report, Graduate School of Engineering, U. of Mexico.

Wattenbarger, R.A. and Ramey, H.J. Jr., 1968. Gas Well Testing with Turbulence, Damage and Wellbore Storage J.Pet.Tech. (August), pp. 99-109.

Wattenbarger, R.A. and Ramey, H.J., Jr., 1970 An Investigation of Wellbore Storage and Skin Effect in Unsteady Liquid Flow: II Finite Difference Treatment Soc. Pet. Eng. J.(Sept.) pp. 291-297.

Whiting, R.L. and Ramey, H.J., Jr., 1969 Applications of Material and Energy Balances to Geothermal Steam Production. J. Pet. Tech. (July), pp. 893-900.

Witherspoon, P.A., Narasihmham, T.N. and McEdwards, D.G., 1978. Results of Interference Tests from Two Geothermal Reservoirs. J. Pet. Tech. 30 pp. 10-16.

TABLE I.- ABSOLUTE AND HYBRID SYSTEM OF UNITS USED IN GEOTHERMAL RESERVOIR ENGINEERING (After Samaniego and Cinco-Ley, 1982).

Variable	SI system*	Hybrid-system
k	$metre^2$	md
h	m	m
p	$Newton/metre^2$=pascal	kg_f/cm^2
w	kg/sec	ton/hr
v_{sc}	$metre^3/kg$	cm^3/gm
B	$metre^3_{rc}/metre^3_{sc}$**	$metre^3_{rc}/metre^3_{sc}$
μ	$kg/metre.sec$	cp_{rc}
t	sec	hours
ϕ	fraction	fraction
c_t	$(Newton/metre^2)^{-1}$	$(kg_f/cm^2)^{-1}$
r	metre	$metre_f$
B_t	1	0.000348
α^{ω}	$1/2\pi$	456.7869
ϵ^{ω}	$1/2\pi$	$1/2\pi$

*SI is the abbreviation for International System of Units

**rc stands for reservoir conditions and sc for standard conditions

TABLE 2.- DATA ON TWO WELLS OF CERRO PRIETO AND A WELL OF EAST MESA FOR CALCULATION OF THE PARAMETER Dw

	Well M-21A (Cerro Prieto)	Well M-109 (Cerro Prieto)	Well 6-2 (East Mesa)
k(md)	36	36(2)	46
h(ft)	177.3	984(3)	500
w(ton/hr)	111	380	-
q(STB/D)	-	-	30000(4)
B(STB/RB)	-	-	1.13(4)
μ(cp)	0.1017	0.1017	0.18(4)
r_w(ft)	0.27	0.27	0.27(4)
$\beta^{w(1)}(ft^{-1})$	3.2×10^8	3.2×10^8	2.5×10^8

(1) Estimated from Firoozabadi and Katz's correlation (1979)
(2) Assumed value equal to the permeability of the Cerro Prieto I area
(3) Assumed value similar to the thickness of nearby well M-117 (Fig. 5.A of Halfman et al., 1985)
(4) Assumed values because they are not shown in the paper of Witherspoon et al. (1978)

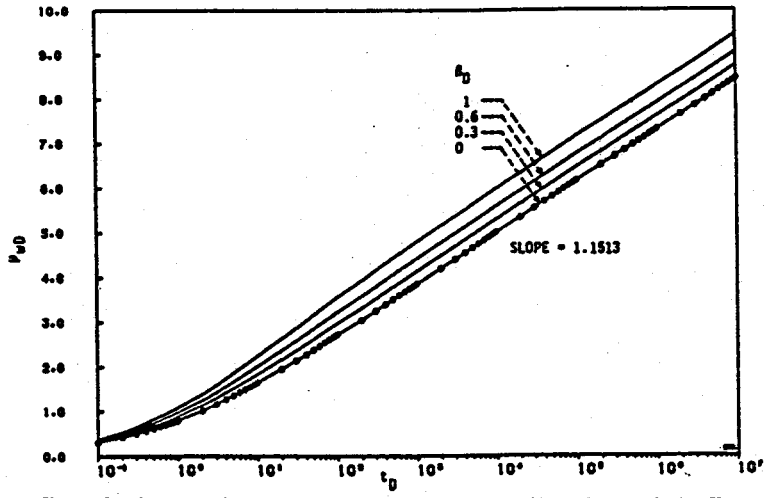

Fig. 1 Drawdown tests in a radial reservoir considering the effect of high-velocity flow.

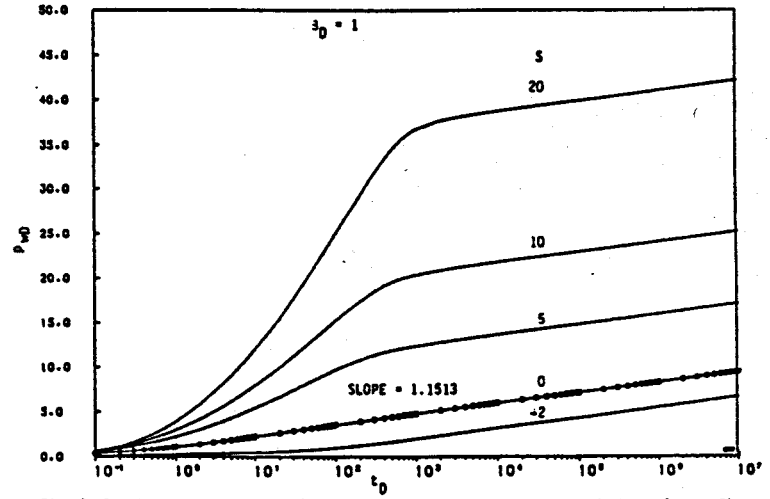

Fig. 2 Drawdown tests in a radial reservoir considering the effects of high velocity flow and formation damage

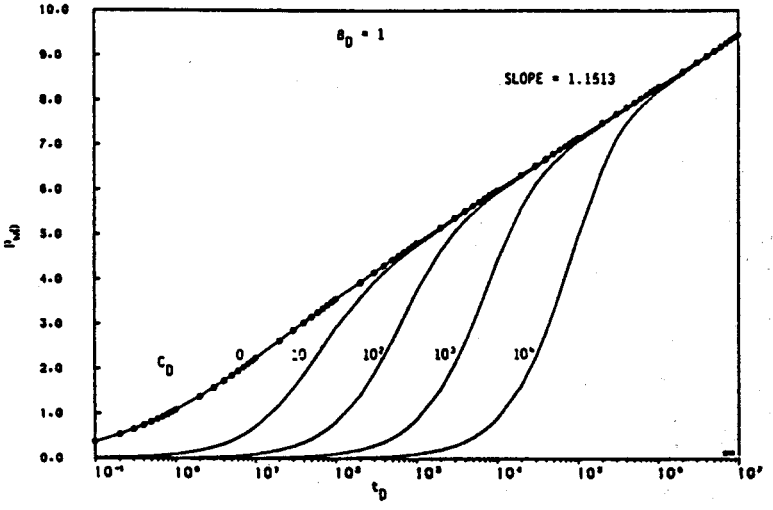

Fig. 3 Drawdown tests in a radial reservoir considering the effects of high-velocity flow and wellbore storage

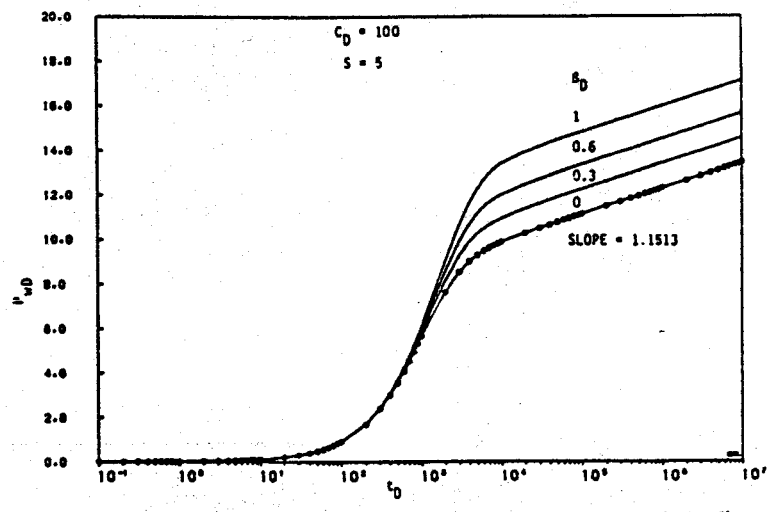

Fig.4 Drawdown tests in a radial reservoir considering the effects of high-velocity flow, formation damage and wellbore storage

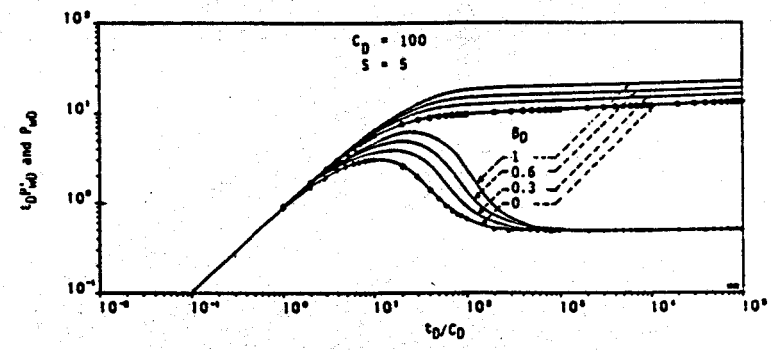

Fig. 5 Pressure derivative type curve results for a drawdown test in a radial reservoir, considering the effects of high-velocity flow, formation damage and wellbore storage

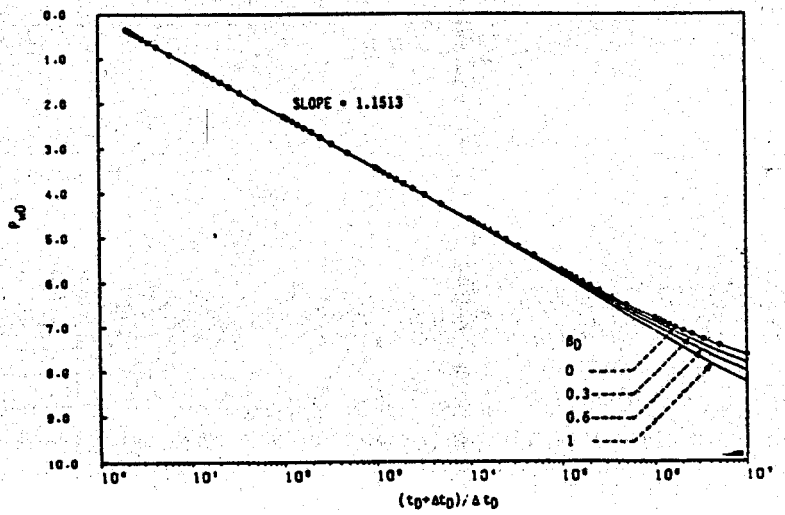

Fig. 6 Buildup tests in a radial reservoir considering the effect of high-velocity flow.

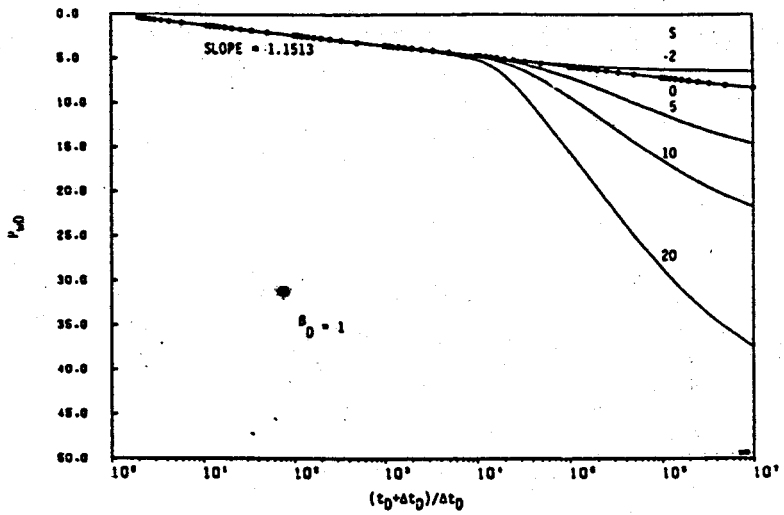

Fig. 7 Buildup tests in a radial reservoir considering the effects of high-velocity flow and formation damage.

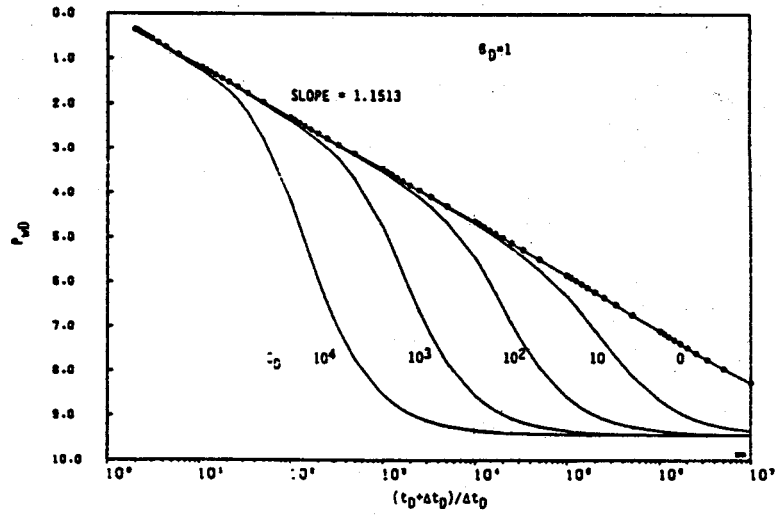

Fig. 8 Buildup tests in a radial reservoir considering the efects of high-velocity flow and wellbore storage.

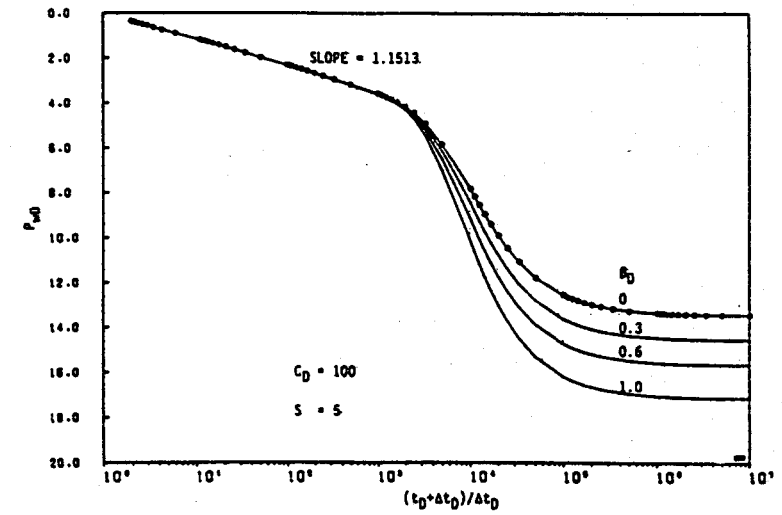

Fig. 9 Buildup test in a radial reservoir considering the effects of high-velocity flow, formation damage and wellbore storage.

PROCEEDINGS, Fourteenth Workshop on Geothermal Reservoir Engineering
Stanford University, Stanford, California, January 24-26, 1989
SGP-TR-122

COMPARISON OF PRESSURE TRANSIENT RESPONSE IN INTENSELY AND SPARSELY FRACTURED RESERVOIRS

Johns, R.T. and Jalali-Yazdi, Y.

Stanford University

ABSTRACT

A comprehensive analytical model is presented to study the pressure transient behavior of a naturally fractured reservoir with a continuous matrix block size distribution. Geologically realistic probability density functions of matrix block size are used to represent reservoirs of varying fracture intensity and varying degrees of fracture uniformity. Transient interporosity flow is assumed and interporosity skin is incorporated.

Drawdown and interference pressure transient tests are investigated. The results show distinctions in the pressure response from intensely and sparsely fractured reservoirs in the absence of interporosity skin. The pressure response in a nonuniformly fractured reservoir approaches that of a nonfractured (homogeneous) reservoir for the case of large matrix block size variability. Type curves are developed to estimate matrix block size variability and the degree of fracture intensity for drawdown and interference well tests.

INTRODUCTION

Currently, matrix block size distribution is not considered a determinable parameter from pressure transient tests. Yet, the utility of determining matrix block size distributions is paramount since block size is one of the main parameters of a fractured reservoir that governs producibility. In one phase flow, it controls the transition from early production from the fractures to late production from the total reservoir (matrix and fractures). In two phase flow, it controls the rate of imbibition (or displacement) and ultimately the recovery efficiency of the reservoir[11].

The Warren and Root model [19] and other pressure transient models of naturally fractured reservoirs assume fracture intensity is constant throughout the reservoir, i.e., they assume fracturing is uniform and matrix block size is constant. Geological and geomechanical studies of fractured reservoirs and outcrops, however, commonly report occurrences of nonuniform fracture patterns due to variability in lithology, bed thickness, degree of diagenesis, and stress environment [1,3,8,16,18,12,9]. For reservoir engineering purposes, fracture patterns can be represented by simple geometric shapes or designs shown in Figure 1. Skewed fracture patterns can also result due to variability in matrix block size and intersection angle.

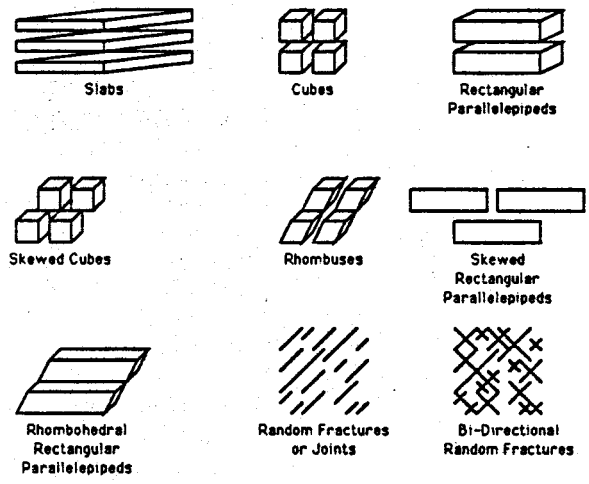

Figure 1: Idealizations of Typical Fracture Patterns seen in Nature.

Some fractures are calcite cemented or mineral filled which can restrict flow from the matrix blocks to the fractures. This phenomenon can be included as interporosity skin.

The distribution of fracture lengths commonly observed in outcrops are exponentially decaying (i.e. there are many short joint lengths and few large joint lengths). Figure 2 illustrates a probability density function constructed from an outcrop in the Mt. Abott quadrangle of the central Sierra Nevadas [18].

In well testing literature, the variability of matrix block size is generally not considered and a pseudosteady state (PSS) interporosity flow assumption is commonly used. Cinco-Ley *et al* [5], however, used a discrete model of up to five different block sizes and demonstrated the transition zone is affected significantly while the late and early time responses are not. Both Cinco-Ley *et al* , and Moench [13] presented a realistic explanation for the observance of the PSS behavior by introducing an interporosity skin factor. Belani and Jalali-Yazdi [2] extended the discrete formulation of Cinco-Ley *et al* to continuous probability density functions of matrix block size. They considered three probability density functions: Dirac delta, uniform, and bimodal. With an increase in the variance of the matrix block size distribution, they found features of a fractured reservoir response become less pronounced.

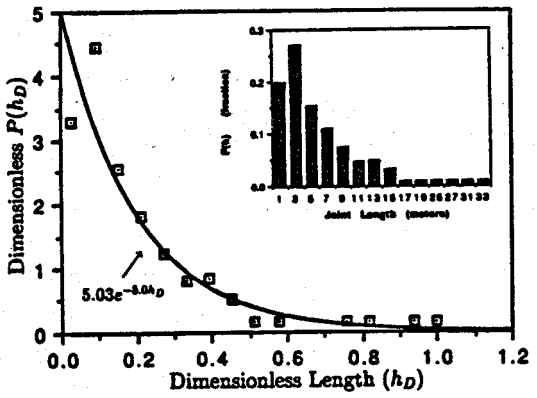

Figure 2: Construction of Probability Density Function from Outcrop, Central Sierra Nevadas.

In this paper, a continuous probability density function of matrix block sizes will be used. The objective is to show that drawdown and interference well testing can provide an indication of the degree of fracture intensity and the degree of uniformity of fracturing.

THEORY AND SOLUTION

The diffusivity equation for a double porosity reservoir can be modified to include a random distribution of matrix block size by adding a source integral [2]:

$$\frac{k_f}{\mu}\nabla^2 P_f = \phi_f c_f \frac{\partial P_f}{\partial t} + \int_{h_{min}}^{h_{max}} Q(h)P(h)\,dh. \quad (1)$$

The source integral in Equation 1 accounts for the flow contribution of the matrix to the fracture. It is assumed that fluid travels from the matrix to the fractures and to the wellbore. P(h) is the probability density function (PDF)describing the likelihood of a certain matrix block size to exist and Q(h) is the flow contribution from that matrix block to the fracture. For transient interporosity flow and slab geometry:

$$Q(h) = -\frac{k_m}{\mu h}\nabla p_m\,|_{interface}\,. \quad (2)$$

Q(h), therefore, takes into consideration the mode of interporosity flow and also the geometry of the matrix blocks.

For a well producing at constant rate in an infinite reservoir, the interference solution in Laplace space is:

$$\overline{P}_{D_f} = \frac{K_0(x r_D)}{s[C_D s(K_0(x) + S_D x K_1(x)) + x K_1(x)]}, \quad (3)$$

and for drawdown:

$$\overline{P}_{D_w} = \frac{K_0(x) + S_D x K_1(x)}{s[C_D s(K_0(x) + S_D x K_1(x)) + x K_1(x)]}. \quad (4)$$

Parameter s is the Laplace variable related to dimensionless time (t_D) and the Bessel function argument is:

$$x = \sqrt{sf(s)}. \quad (5)$$

The function f(s) embodies the reservoir parameters including the matrix block size distribution. For transient interporosity flow in the presence of interporosity skin:

$$f(s) = \omega_f + \omega_m \int_{h_{ratio}}^{1} \frac{\sqrt{\frac{\lambda}{\omega_m s}}\tanh(\sqrt{\frac{\omega_m s}{\lambda}})P(h_D)}{1 + S_{ID}\sqrt{\frac{\omega_m s}{\lambda}}tanh(\sqrt{\frac{\omega_m s}{\lambda}})}dh_D, \quad (6)$$

where,

$$h_{ratio} = \frac{h_{min}}{h_{max}}, \quad (7)$$

$$S_{ID} = \frac{k_m h_s}{k_s h}. \quad (8)$$

The interporosity skin factor (S_{ID}) is a function of matrix block size distribution and, hence is only constant when $\frac{h_s}{\lambda}$ is constant. A more realistic assumption is that the depth of skin damage (h_s) is constant for all matrix blocks, and hence, S_{ID} can be defined as:

$$S_{ID} = S_{ID_{min}}\sqrt{\frac{\lambda}{\lambda_{min}}}, \quad (9)$$

where,

$$S_{ID_{min}} = \frac{k_m h_s}{k_s h_{max}}. \quad (10)$$

and now:

$$f(s) = \omega_f + \omega_m \int_{h_{ratio}}^{1} \frac{\sqrt{\frac{\lambda}{\omega_m s}}\tanh(\sqrt{\frac{\omega_m s}{\lambda}})P(h_D)}{1 + S_{ID_{min}}\sqrt{\frac{\omega_m s}{\lambda_{max}}}tanh(\sqrt{\frac{\omega_m s}{\lambda}})}dh_D. \quad (11)$$

PROBABILITY DENSITY FUNCTIONS

Prediction of the pressure response requires the type of matrix block size distribution be known or assumed. Once the PDF is selected, fracture intensity can then be inferred from pressure transient data. Two types of probability density functions are used to represent the variability of matrix block sizes. These types, exponential and linear (Figure 3), occur most often as indicated in the geological literature. The Dirac delta (or uniform block size) and rectangular distribution are each subsets of the exponential and linear distributions. As fracture intensity increases, mean block size decreases and P(h) becomes skewed to the smaller block sizes. As fracture intensity decreases, the reverse is true.

The exponential PDF is given by:

$$P(h_D) = \frac{a(exp^{-ah_D})}{exp^{-(ah_{ratio})} - exp^{-a}}, \quad (12)$$

where 'a' is the exponential constant. The linear distribution function is:

$$P(h_D) = \frac{mh_D + b}{.5m(1 - h_{ratio}^2) + b(1 - h_{ratio})}, \quad (13)$$

where 'm' is the slope and 'b' is the vertical intercept of the cartesian plot of $P(h_D)$ versus h_D. Because a probability function must be positive, the slope must be in the range:

$$\frac{-2}{(1 - h_{ratio})^2} \leq m \leq \frac{2}{(1 - h_{ratio})^2}. \quad (14)$$

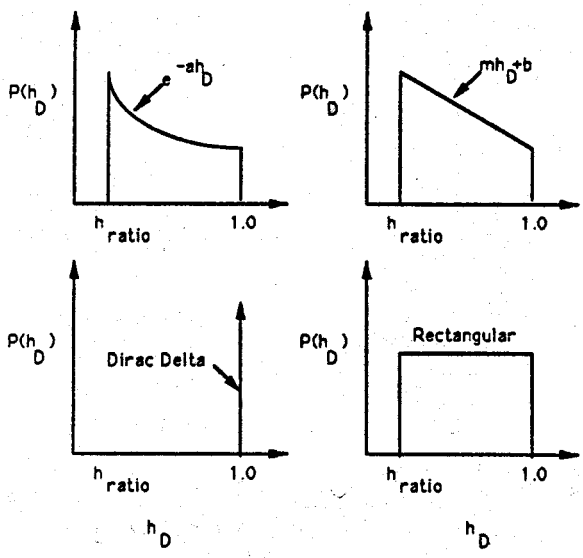

Figure 3: Probability Density Functions.

The intercept 'b' is given by:

$$b = \frac{1 - .5m + .5h_{ratio}^2}{1 - h_{ratio}}. \tag{15}$$

When 'm' is zero (linear) or 'a' is zero (exponential), both probability density functions reduce to the rectangular distribution:

$$P(h_D) = \frac{1}{1 - h_{ratio}}, \tag{16}$$

and when 'm' or 'a' approach infinity, the solutions reduce to the Dirac delta function:

$$P(h_D) = \delta(h - H). \tag{17}$$

The Dirac delta function is zero when $h \neq H$ and infinite when $h = H$ where H is the characteristic length of all matrix blocks. The Dirac delta distribution describes fractures that are perfectly ordered as in the Warren and Root model. The rectangular distribution, however, represents a continuum of block sizes that are equally probable from the smallest (h_{min}) to the largest (h_{max}). In general, the rectangular distribution should be used if the distribution type is unknown.

Once the type of PDF is determined, Equation 11 can be solved for f(s). Table 1 lists the solutions of f(s) for the various PDF's.

DISCUSSION-DRAWDOWN TESTING

Equation 4 in the absence of wellbore storage and skin reduces to:

$$\bar{P}_{D_w} = \frac{K_0(\sqrt{sf(s)})}{s^{3/2}\sqrt{f(s)}K_1(\sqrt{sf(s)})}. \tag{18}$$

Equation 18 is evaluated for the exponential PDF listed in Table 1. Figure 4 illustrates the response for varying values of 'a' holding h_{ratio} constant. For positively increasing

PDF	f(s), where $\xi = \sqrt{\frac{sm_f L^2}{\lambda_{max}}}$
Exponential	$\omega_f + \frac{a\omega_m}{\xi(e^{-ah_{ratio}} - e^{-a})} \int_{(h_{ratio})}^{\xi} \frac{e^{\frac{-ay}{\xi}} tanh(y)}{y[1 + S_{ID_{max}} \xi\, tanh(y)]} dy$
Linear	$\omega_f + \frac{\omega_m}{\xi[.5m(1 - h_{ratio}^2) + b(1 - h_{ratio})]} \int_{(h_{ratio})}^{\xi} \frac{[\frac{m}{\xi} + \frac{b}{y}] tanh(y)}{1 + S_{ID_{max}} \xi\, tanh(y)} dy$
Rectangular	$\omega_f + \frac{\omega_m}{\xi(1 - h_{ratio})} \int_{(h_{ratio})}^{\xi} \frac{tanh(y)}{y[1 + S_{ID_{max}} \xi\, tanh(y)]} dy$
Dirac delta	$\omega_f + \frac{\omega_m tanh(\xi)}{\xi[1 + S_{ID} \xi tanh(\xi)]}$, where $\lambda_{min} = \lambda_{max} = \lambda$

Table 1: Functions f(s) for various PDF's.

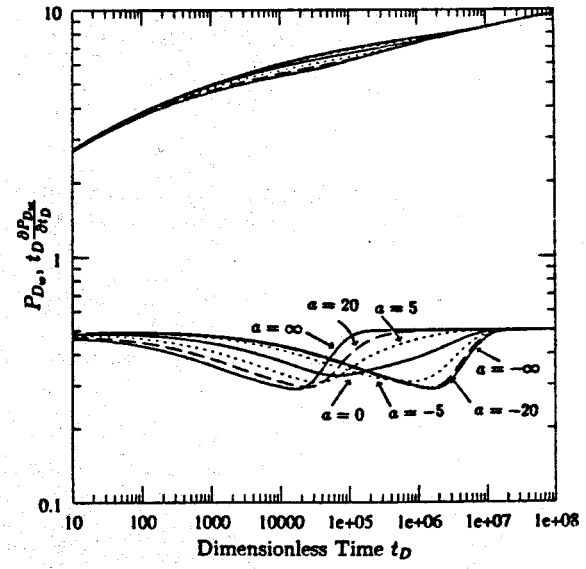

Figure 4: Exponential PDF: Varying 'a' with $h_{ratio} = .1$, $\lambda_{min} = 10^{-7}$, $\omega_m = .9$.

values of 'a', fracture intensity decreases and the response approaches the Dirac delta response for a uniform matrix block size h_{max}. For negatively increasing values of 'a', fracture intensity increases and the response approaches the Dirac delta response for a uniform matrix block size h_{min}.

For 'a' = 0, the response is that of a rectangular distribution of matrix block sizes. Also, it is evident the derivative profile shows a substantial degree of asymmetry with respect to the time axis as 'a' increases or decreases to large values. The response for the rectangular matrix block size distribution, however, is nearly symmetric. Asymmetry increases as fracturing becomes more uniform. Therefore, the shape of the derivative profile can be used as a qualitative indicator of the degree of matrix block size variability or nonuniformity. In addition, the parameter h_{ratio} is important in estimating matrix block size variability. An h_{ratio} approaching one indicates perfectly uniform fracturing, while h_{ratio} approaching zero indicates perfectly nonuniform fracturing.

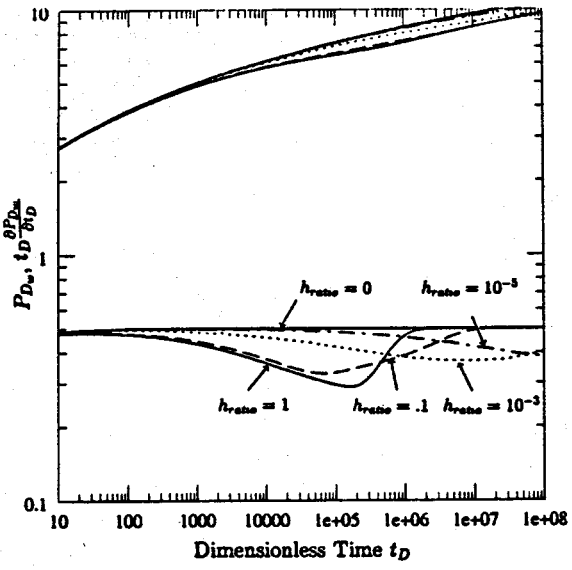

Figure 5: Rectangular PDF: Varying h_{ratio} for Geometric Mean $\lambda = 10^{-6}$, $\omega_m = .9$.

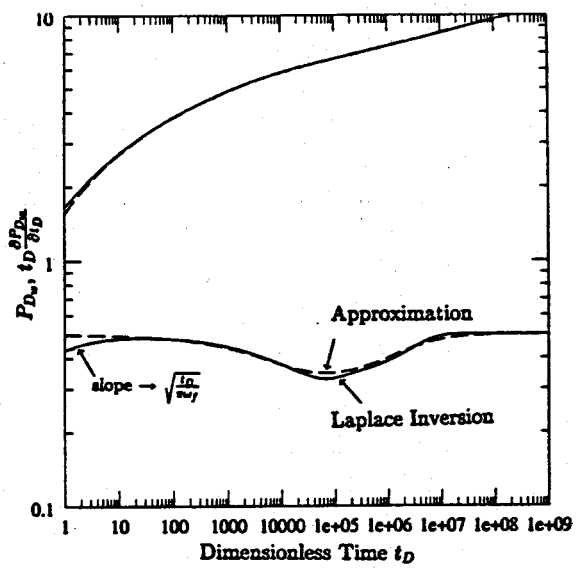

Figure 6: Rectangular PDF: Solution by Stehfest Inversion versus Time Domain Approximation, $h_{ratio} = .1$, $\lambda_{min} = 10^{-7}$, $\omega_m = .9$.

Figure 5 illustrates the pressure response for varying values of h_{ratio} with 'a' held constant. For h_{ratio} equal to zero, the response is similar to that of a homogenous reservoir. This occurs because there is an incessant gradual contribution from the matrix to the fractures. As long as fracturing is extremely nonuniform, the response will not exhibit the classical profile of a distinct transition zone separating early and late time response. For the rectangular PDF, a type curve can be developed for estimation of ω_m, λ_{min}, and h_{ratio}. The type curve is generated using the following time domain solution of the wellbore pressure response:

$$P_{D_w} = \frac{1}{2}[ln(\frac{t_D}{F(t_D)r_D^2}) + .80907], \qquad (19)$$

where $F(t_D)$ is the time-dependent reservoir storativity:

$$F(t_D) = \omega_f + \omega_m \int_{h_{ratio}}^{1} \sqrt{\frac{\lambda\gamma t_D}{\omega_m}} tanh(\sqrt{\frac{\omega_m}{\lambda\gamma t_D}}) P(h_D)\, dh_D . \qquad (20)$$

Equations 19 and 20 are obtained by applying the inversion technique of Najurieta and Schapery [17,15,14]. For the rectangular PDF, Equation 20 becomes:

$$F(\frac{t_D}{\tau_{max}}) = \omega_f + \frac{\omega_m}{(1-h_{ratio})}\sqrt{\frac{t_D}{\tau_{max}}} \times \int_{h_{ratio}\sqrt{\frac{\tau_{max}}{t_D}}}^{\sqrt{\frac{\tau_{max}}{t_D}}} \frac{tanh(y)}{y}\, dy, \qquad (21)$$

where y is the variable of integration and τ is the matrix response time coefficient:

$$\tau = \frac{\omega_m}{\gamma\lambda}, \qquad (22)$$

and τ_{max} is the response time coefficient of the most dormant or largest matrix block:

$$\tau_{max} = \frac{\omega_m}{\gamma\lambda_{min}}. \qquad (23)$$

In general, the time domain approximation gives remarkably good results (Figure 6). Using the difference between the extrapolated late time pressure response and the observed pressure, one obtains:

$$\Delta P = P_{D_w} - P_{D_{w_{late}}} = -\frac{1}{2} ln F(\frac{t_D}{\tau_{max}}). \qquad (24)$$

The type curve (Figure 7) is then generated by plotting the pressure difference ΔP versus $\frac{t_D}{\tau_{max}}$ for a range of h_{ratio} and ω_m values.

The type curve demonstrates several key ideas. As matrix storativity predominates (increasing ω_m), h_{ratio} affects the pressure response more significantly. The effect of an increasing h_{ratio} on the pressure response is greatest for lower values of h_{ratio} (e.g. the pressure response changes more significantly for h_{ratio} values from 0.1 to 0.5 than from 0.5 to 1.0). Therefore, the larger the matrix block size variability, the more significantly the pressure response is affected. For h_{ratio} approaching one, the response reverts to the uniformly fractured (uniform block size) case.

An example of the effect of interporosity skin ($S_{ID_{min}}$) on the pressure transient response is shown in Figure 8. For small interporosity skin factors, a significant change in the pressure derivative is seen, and thus, the effect of the matrix block size distribution is masked. The derivative profile becomes symmetric which is typical of the PSS response demonstrated by Warren and Root. As interporosity skin increases, the derivative profile shifts in time, giving apparent λ values that are too small (more dormant). Thus, interpreting pressure transient tests via Warren and Root may give systematically lower estimates of λ than actually exists in the reservoir. The fracture intensity will then be underestimated.

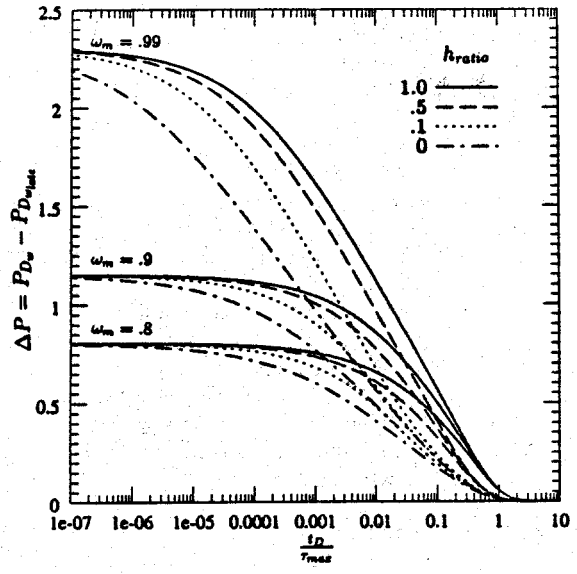

Figure 7: Rectangular PDF: Drawdown Type Curve for $t_D > 100$ and $\lambda_{min} < 10^{-4}$ for Varying h_{ratio}, λ_{min}, ω_m.

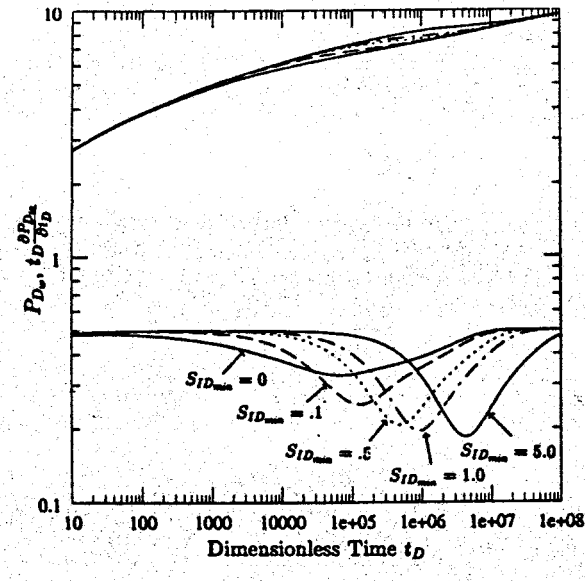

Figure 8: Rectangular PDF: Effect of Interporosity Skin, $h_{ratio} = .1$, $\lambda_{min} = 10^{-7}$, $\omega_m = .9$.

DISCUSSION-INTERFERENCE TESTING

Braester[4] demonstrated that drawdown (or buildup) testing in naturally fractured reservoirs may not be influenced by matrix blocks significantly away from the wellbore. Interference testing, therefore, is preferred because the response is affected by matrix blocks between the active and observation wells. A simplified solution for interference testing in the absence of storage and wellbore skin is the line source solution:

$$\overline{P}_{D_f} = \frac{K_0(r_D\sqrt{sf(s)})}{s}. \tag{25}$$

For any PDF distribution, it can be shown that $\theta = \lambda_{min} r_D^2$ is a correlating parameter [6,7]. For instance, using the linear PDF:

$$f(sr_D^2) = \omega_f + \frac{\omega_m}{.5m(1-h_{ratio}^2)+b(1-h_{ratio})}\sqrt{\frac{\theta}{\omega_m sr_D^2}} \times \int_{h_{ratio}\sqrt{\frac{\omega_m sr_D^2}{s}}}^{\sqrt{\frac{\omega_m sr_D^2}{s}}} [m\sqrt{\frac{\theta}{\omega_m sr_D^2}} + \frac{b}{y}]tanh(y)\,dy. \tag{26}$$

Equation 25 can then be evaluated using the inverse Laplace transform relation:

$$\mathcal{L}^{-1}[\overline{P}_{D_f}(sr_D^2)] = \frac{1}{r_D^2} P_{D_f}(\frac{t_D}{r_D^2}). \tag{27}$$

A type curve (Figure 9) is prepared using the uniform PDF case for a given ω_m. For each value of θ, h_{ratio} is varied from zero to one. If h_{ratio} determined from the type curve is equal to one, the PDF type is Dirac delta and the type curve is similar to that presented by Deruyck *et al* [6,7]. For large values of θ, the matrix block size variability becomes increasingly important and h_{ratio} can be better estimated. Thus, if the dimensionless distance (r_D) between the active and observation wells becomes large, or if λ_{min} becomes large, the matrix block size variability becomes one of the key parameters in interpretating the interference pressure transient test. For extremely large values of θ, however, the fracture response may not be detected and the response will be the same as the line source solution. Also, for large values of ω_m, the parameter h_{ratio} increasingly dominates the pressure response.

CONCLUSIONS

- A formulation incorporating transient interporosity flow and interporosity skin is presented for fractured reservoirs with variable matrix block size. Geologically realistic PDF's have been used to represent intensely or sparsely fractured reservoirs.
- Type curves have been generated for both drawdown and interference well tests based on the rectangular PDF and slab matrix block geometry. Type curves yield estimates of the parameter h_{ratio} which

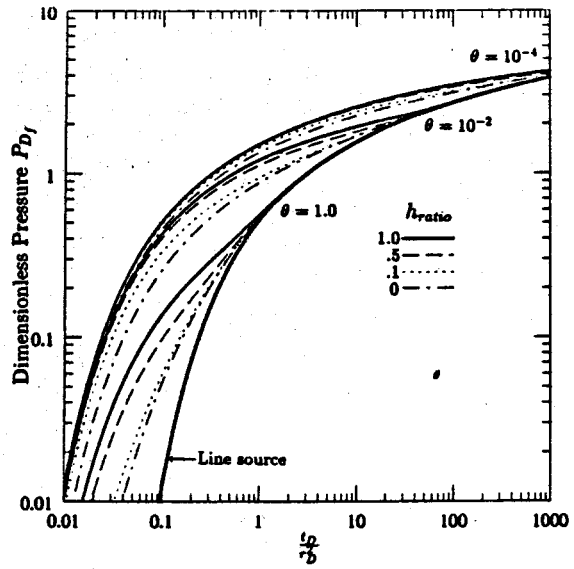

Figure 9: Rectangular PDF: Interference Type Curve for Varying h_{ratio}, θ, with $\omega_m = .9$.

describes the matrix block size variability or the degree of uniformity of fracturing. For h_{ratio} approaching unity, the response approaches that of a uniformly fractured reservoir, while for h_{ratio} approaching zero, the response resembles that of a homogeneous reservoir.

- For naturally fractured reservoirs with interporosity skin, the matrix block size variability is not estimatable. Fracture intensity may be underestimated if the Warren and Root interpretation is employed.

NOMENCLATURE

a	= exponential PDF constant
b	= intercept of linear PDF
c_f	= fracture total compressibility
c_m	= matrix total compressibility
C_D	= dimensionless wellbore storage
P(h)	= block size distribution function
$P(h_D)$	= dimensionless block size distribution function
f(s)	= Laplace space function
h	= matrix block size characteristic length (Volume/Area)
h_D	= dimensionless matrix block size length
h_f	= fracture thickness
h_{min}	= minimum block size length
h_{max}	= maximum block size length
h_{ratio}	= ratio of h_{min} to h_{max}
h_s	= interporosity damaged zone thickness
H	= constant matrix block size
k_f	= fracture permeability
k_m	= matrix permeability
k_s	= interporosity damaged zone permeability
$K_0(x)$	= modified Bessel function, second kind, zero order
$K_1(x)$	= modified Bessel function, second kind, first order
m	= slope of linear PDF
P_{D_f}	= dimensionless fracture pressure
P_{D_m}	= dimensionless matrix pressure
P_{D_w}	= dimensionless wellbore pressure
P_f	= fracture fluid pressure
P_i	= initial reservoir pressure
P_m	= matrix fluid pressure
P_w	= wellbore fluid pressure
Q(h)	= flow contribution from matrix size
r	= radial coordinate
r_D	= dimensionless radial coordinate
r_w	= wellbore radius
s	= Laplace parameter
S_D	= dimensionless wellbore skin factor
S_{ID}	= dimensionless interporosity skin factor
$S_{ID_{min}}$	= minimum dimensionless interporosity skin factor
t	= time
t_D	= dimensionless time
γ	= 1.781, exponential of Euler's constant
λ	= dimensionless interporosity flow coefficient
λ_{max}	= maximum dimensionless interporosity flow coefficient
λ_{min}	= minimum dimensionless interporosity flow coefficient
τ	= dimensionless matrix response time coefficient
τ_{max}	= maximum dimensionless matrix response time coefficient
μ	= viscosity
ϵ	= coordinate normal to fracture-matrix interface
ϵ_D	= dimensionless coordinate normal to fracture-matrix interface
ϕ_f	= dimensionless fracture porosity
ϕ_m	= dimensionless matrix porosity
ω_f	= dimensionless fracture storativity ratio
ω_m	= dimensionless matrix storativity ratio
θ	= dimensionless correlation parameter

APPENDIX

The dimensionless boundary conditions and flow equations are:

$$\frac{\partial^2 P_{D_f}}{\partial r_D^2} + \frac{1}{r_D}\frac{\partial P_{D_f}}{\partial r_D} = \omega_f \frac{\partial P_{D_f}}{\partial t_D} - \int_{h_{ratio}}^{1} \lambda \frac{\partial P_{D_m}}{\partial \epsilon_D}\Big|_{\epsilon_D=0} P(h_D)\, dh_D, \tag{28}$$

$$\frac{\partial^2 P_{D_m}}{\partial \epsilon_D^2} = \frac{\omega_m}{\lambda}\frac{\partial P_{D_m}}{\partial t_D}. \tag{29}$$

- $P_{D_f} = P_{D_m} = 0$ at $t_D = 0$
- $P_{D_f} = P_{D_m} = 0$ at $r_D \to \infty$
- $C_D \frac{\partial P_{D_w}}{\partial t_D} - \frac{\partial P_{D_f}}{\partial r_D}\Big|_{r_D=1} = 1$
- $P_{D_w} = [P_{D_f} - S_D \frac{\partial P_{D_f}}{\partial r_D}]\Big|_{r_D=1}$

- $P_{D_f} = [P_{D_m} - S_{ID}\frac{\partial P_{D_m}}{\partial \epsilon_D}]\,|_{\epsilon_D \approx 0 \text{ for slabs}}$
- $\frac{\partial P_{D_m}}{\partial \epsilon_D}\,|_{\epsilon_D \approx 1 \text{ for slabs}} = 0$ at no flow boundaries

where:

$$P_{D_f} = \frac{2\pi k_f h_f (P_i - P_f)}{q\mu} \tag{30}$$

$$P_{D_m} = \frac{2\pi k_f h_f (P_i - P_m)}{q\mu} \tag{31}$$

$$P_{D_w} = \frac{2\pi k_f h_f (P_i - P_w)}{q\mu} \tag{32}$$

$$t_D = \frac{k_f t}{(\phi_f c_f + \phi_m c_m)\mu r_w^2} \tag{33}$$

$$r_D = \frac{r}{r_w} \tag{34}$$

$$C_D = \frac{C}{2\pi h_f c_t r_w^2} \tag{35}$$

$$\lambda = \frac{k_m r_w^2}{k_f h^2} \tag{36}$$

$$\lambda_{min} = \frac{k_m r_w^2}{k_f h_{max}^2} \tag{37}$$

$$\lambda_{max} = \frac{k_m r_w^2}{k_f h_{min}^2} \tag{38}$$

$$\omega_m = \frac{\phi_m c_m}{\phi_f c_f + \phi_m c_m} \tag{39}$$

$$\omega_f = 1 - \omega_m \tag{40}$$

$$h_D = \frac{h}{h_{max}} \tag{41}$$

$$\epsilon_D = \frac{\epsilon}{h} \tag{42}$$

$$P(h_D) = h_{max} P(h)\,. \tag{43}$$

Other matrix block geometries can be included in the solution by changing the interporosity boundary conditions. After applying Laplace transforms to the flow equations and boundary conditions one obtains the solutions of Equations 3 and 4.

References

[1] Aguilera, R.:, *Naturally Fractured Reservoirs*, Petroleum Publishing Co. Tulsa, OK, (1980).

[2] Belani, A.K. and Jalali-Yazdi, Y.:, *"Estimation of Matrix Block Size Distribution in Naturally Fractured Reservoirs"*, SPE 18171, presented at the 63rd Fall Technical Conference held in, Houston, TX, Oct., 1988.

[3] Bles, J.L. and Feuga, B.:, *The Fracture of Rocks*, North Oxford Academic Publishers, (1986).

[4] Braester, C.:, *"Influence of Block Size on the Transition Curve for a Drawdown Test in a Naturally Fractured Reservoir"*, *Soc. Pet. Eng. J.*, 498–504, (1984).

[5] Cinco-Ley, H., et al.:, *"The Pressure Transient Behavior for Naturally Fractured Reservoirs with Multiple Block Size"*, SPE 14168, presented at the 60th Fall Technical Conference held in, Las Vegas, NV, Sept., 1985.

[6] Deruyck, B.G.:, *Interference Well Test Analysis For A Naturally Fractured Reservoir*, Master's thesis, Stanford Univ., (June 1980).

[7] Deruyck, B.G., et al.:, *"Interpretation of Interference Tests in Reservoirs with Double Porosity Behavior-Theory and Field Examples"*, SPE 11025, presented at the 57th Fall Technical Conference held in, New Orleans, LA, Sept., 1982.

[8] Dyer, J.R.:, *Jointing in Sandstones, Arches National Park, Utah*, PhD thesis, Stanford Univ., (August 1983).

[9] Isaacs, C.M.:, *"Geology and Physical Properties of the Monterey Formation, California"*, SPE 12733, presented at the California Regional Meeting held in, Long Beach, April, 1984.

[10] Johns, R.T. and Jalali-Yazdi, Y.:, *"Comparison of Pressure Transient Response in Intensely and Sparsely Fractured Reservoirs"*, SPE 18800, presented at the Calif. Reg. Mtg. held in, Bakersfield, CA, April, 1989.

[11] Mattax, C.C. and Kyte, J.R.:, *"Imbibition Oil Recovery from Fractured, Water-Drive Reservoir"*, *Soc. Pet. Eng.*, 177–184, (June 1962).

[12] McQuillan, H.:, *"Small Scale Fracture Density in Asmari Formation of Southwest Iran and its Relation to Bed Thickness"*, *AAPG Bulletin*, 57(12):2367–2385, (Dec. 1973).

[13] Moench, A.F.:, *"Double-Porosity Models for a Fissured Groundwater Reservoir with Fracture Skin"*, *J. Water Resources*, 20(7):831–846, (July 1984).

[14] Najurieta, H.L.:, *"Interference and Pulse Testing in Uniformly Fractured Reservoirs"*, SPE 8283, presented at the 54th Fall Technical Conference held in, Las Vegas, NV, Sept., 1979.

[15] Najurieta, H.L.:, *"A Theory for Pressure Transient Analysis in Naturally Fractured Reservoirs"*, *J. Pet. Tech.*, 1241–1250, (July 1980).

[16] Pollard, D.D. and Aydin, A.:, *"Progress in Understanding Jointing Over the Past Century"*, *Geol. Soc. Amer. Bull.-Centennial Vol.*, (March 1988).

[17] Schapery, A.:, *Approximate Methods of Transform Inversion for Viscoelastic Stress Analysis*, Technical Report, 4th U.S. National Congress Appl. Math., (1961).

[18] Segall, P.:, *The Development of Joints and Faults*, PhD thesis, Stanford Univ., (July 1981).

[19] Warren, J.E. and Root, P.J.:, *"The Behavior of Naturally Fractured Reservoirs"*, *Soc. Pet. Eng. J.*, 245–55, (Sept. 1963).

PROCEEDINGS, Fourteenth Workshop on Geothermal Reservoir Engineering
Stanford University, Stanford, California, January 24-26, 1989
SGP-TR-122

The Use of Computers in Well Test Analysis

Roland N. Horne *, *Pedro Sanchez-U.* **

* *Stanford University*
** *Comision Federal de Electricidad*

ABSTRACT

The advent of small and portable microcomputers provides interesting new possibilities for the acquisition and analysis of well test data. In particular, there is a considerable saving in time if the data is transferred directly (or remotely using a modem link) to the computer for scaling, filtering and plotting. In addition, since present day microcomputers have considerable processing power, it is possible to perform all of the interpretation using the same portable microcomputer.

The advantages of doing this are several. Computerized analysis using automated techniques can provide good estimates from much shorter test data than is required for standard graphical analysis. Thus it is possible to analyze the test at the same time data is being collected, and to terminate the test when the data are sufficient for interpretation. Examples given in the paper demonstrate that the well test can sometimes be shortened by an order of magnitude in this way. The cost saving could therefore easily pay for the computer itself.

The advents of compact and powerful microcomputers, of computerized data acquisition and control, and of automated interpretation software represent major advances in the field of well test analysis.

1. INTRODUCTION

The power and portability of microcomputers makes possible many engineering applications at the wellsite. One of these applications is associated with pressure transient testing. In the past, well testing has required the running of a downhole tool that measured pressure as a function of time, invisible to the operator until the tool was recovered. The pressure record was then taken back to the office, and analyzed by hand. In more recent times, surface recording pressure gauges have enabled the test operator to monitor the test while it is in progress, and make decisions as to the continuation of the test. The analysis was still done back at the office. Now, with high powered microcomputers at the wellsite during a well test, it is possible to simultaneously control and analyze the test, using the same or a pair of computers.

Another advance in this area has come with computer-aided interpretation. The standard methods of well test analysis can now be mechanized on a small portable computer, and performed during the test. In addition, automated analysis makes it possible to interpret much shorter tests than can be analyzed by hand, and also provide reliability estimates for the answers.

Thus, the use of wellsite and portable microcomputers makes it possible for a well test operator to simultaneously perform, monitor and interpret the well test, and to truncate the test when the desired degree of reliability has been obtained. The results of such an approach can be obtained with smaller expenditure on tool time and on personnel, and can achieve more reliable results with fewer errors, fewer misinterpretations and fewer "no result" tests.

This paper describes the use of a microcomputer based automated interpretation program. The use of the computer permits much faster and more reliable well test results than have formerly been possible.

The next section of this paper describes the approach of the automated interpretation system. The remaining sections describe field applications using it.

2. AUTOMATED INTERPRETATION

Computerized analysis of well tests has been around for some time, since early work by Earlougher [1], Padmanabhan and Woo [2], Tsang et al [3], Padmanabhan [4], and McEdwards [5]. The basic principle of an automated match is the same as that of a manual analysis, in that data are matched to a "reservoir model" which is a forecast of the pressure change during the test. The reservoir model assumes a particular reservoir configuration, and its pressure response is a function of one or more unknown reservoir parameters, such as permeability, wellbore skin effect and distance to a reservoir boundary. In most traditional analysis methods, the matching of the model depends on the recognition of graphical "signatures" of the model, such as the semilog straight line characteristic of infinite-acting reservoir response, or the unit slope log-log straight line characteristic of wellbore storage.

The difference between automated and traditional methods is that the automated method performs the match between the measured data and the reservoir model response in a mathematical sense. This is usually done with a non-linear regression algorithm that adjusts the values of the unknown reservoir parameters in such a way as to minimize the sum of the squares of the differences between the measured pressures and the calculated reservoir model response pressures at the same instant in time. As a result of this procedure, the automated method has the capability of matching the entire range of the measured data, without being restricted to specific "signature" regions of the response. Thus the automated match can provide more reliable and self-consistent results.

The work of Rosa and Horne [6] opened up several new possibilities in automated well test analysis. By calculating the reservoir model parameter gradients in Laplace space, Rosa and Horne [6] showed how it is possible to automate the matching of almost any standard reservoir model - many of which do not have solutions that are easily determinable in real space yet have readily differentiable forms when expressed in Laplace space. In

addition Rosa and Horne [6] demonstrated the estimation and use of confidence intervals as indicators of the reliability of the estimated parameter values. The confidence intervals are able to indicate whether the results are non-unique, whether the chosen reservoir model is consistent with the observed data, and whether there are sufficient data to adequately estimate a given parameter. As an example, since permeability only governs the reservoir response after wellbore storage effects have died away, an attempt to estimate permeability by matching data that lies only in the wellbore storage response region of the data will result in a very wide confidence interval. That is, the estimated result may be calculated as 15md, with a plus or minus confidence interval of 20md. This warns the operator that the result is not significant (normally, a confidence interval of less than 10% of the parameter value is required for statistical significance).

The work of Rosa and Horne [6] was extended by Guillot and Horne [7] to encompass cases in which flow rates during the test were not constant. This work demonstrated how the use of automated analysis can relax some of the restrictions placed on well test design by the traditional methods of analysis. Meunier, Kabir and Witmann [8] and Kucuk and Ayestaran [9] had formerly shown that the incorporation of the flow rate data gives rise to more precise interpretation in that more information is included in the analysis, and complications such as variable wellbore storage effect can be easily circumvented. Barua and Horne [10] and Horne and Kucuk [11] demonstrated how these approaches could be used in very practical applications (thermal falloff and gas well tests, respectively).

Finally, recent work in the same series by Barua, Horne, Greenstadt and Lopez [12] studied how the non-linear regression algorithms operate with the specific response functions characteristic of well test analysis. They were able to outline design criteria for the most solution efficient algorithm, and concluded that the Gauss-Marquardt [13] method was the most reliable except in instances when more than one reservoir parameter only weakly influenced the model response. In such cases it was shown that a variant of the Newton-Greenstadt method (Greenstadt [14]) was the best one to use.

Other than the speed of obtaining an answer, and the quantitative determination of confidence intervals, automated analysis has other advantages over traditional methods. Rosa and Horne [6] showed that it is possible to obtain reliable estimates of reservoir parameters with much shorter tests. This is because the automated matching procedure is able to estimate permeability and skin from the shape of the transition region that lies between the storage-influenced region and the infinite-acting region. The traditional approach using semilog analysis requires at least one and a half log cycles of data beyond the end of the storage-influenced region in order to identify the semilog straight line that is truly characteristic of the permeability and skin. Since the automated procedure is able to obtain the *same* answer without any semilog straight line at all, the test can be as much as ten times shorter than is necessary for standard analysis. This startling result is confirmed in the field example illustrated in the next section.

Automated analysis is not without its disadvantages however, and these must be handled carefully if the method is to become widely useful. The principle difficulty of the approach is that it is an iterative method, and must converge on a solution from an initial guess at the answer. Although it has been found by earlier authors that automated analysis will converge even from estimates that are one or even two orders of magnitude distant from the true values, the convergence is successful only about 90% of the time, depending on the quality of the data and the appropriateness of the reservoir model chosen by the engineer performing the analysis. Even though this sounds a reasonable success rate, it is not good enough for a program that is to be used confidently in everyday interpretation by users of varying experience and skill. There has to be a means by which the analysis software will *always* converge on the best possible answer. The most suitable way to do this would be to provide an on-screen graphical analysis of the data prior to the automated analysis, so that the interpretation engineer can provide the algorithm with a reasonably good initial estimate of the unknown reservoir parameters. This has the added advantage that it allows the engineer to have a close look at the data in displays with which he or she is familiar, and facilitates the selection of an appropriate reservoir model.

In the automated procedure, the program performs a non-linear regression match to the data, using the reservoir model selected by the user out of a menu of possible reservoir configurations. Most importantly, the automated match provides an answer that is free from subjective errors, bias or plain old human error. In addition, the program calculates approximate confidence intervals on the estimated answers, providing a quantitative impression of the validity of the values. Confidence intervals are made wider by noisy data, poor match, or inappropriate choice of reservoir model.

The algorithm used for the automated match is the Gauss-Marquardt [13] procedure, with added penalty functions as described by Bard [15]. This algorithm is similar to the one used by Rosa and Horne [6], with a revised line search procedure based on the one proposed by Bard [15]. In most cases it converges in six or seven iterations. Depending on the reservoir model, the required reservoir response function and its gradients with respect to the unknowns are calculated either directly (where they exist in real space) or in Laplace space.

3. FIELD EXAMPLE

The field example illustrated here is based on an actual test performed in an oil reservoir. It has been chosen here as an example since it shows a more extensive data set than is usually available in a geothermal well test. The actual test was performed continuously, not in two periods as is described here. In this discussion, the advantages of on-site microcomputer analysis (or remote analysis with modem transfer of the data) are emphasized by describing the test as if it had actually been given a preliminary interpretation while the test was still in progress. This was not actually done during the real test; even though the analysis shown here proves that the test was unnecessarily long as a result, the benefit of the on-site analysis was not available at the time the test was performed.

The test was a buildup after a long period of production, and is treated as if it were simply a drawdown (with the flow rate reversed). This is standard practice when the drawdown period is long (or unknown) compared to the buildup period.

Data measured for the well test are listed in Table 1.

Analysis after 15 hours:

After 15 hours of measurements, the pressure transient was as shown in Figures 1 (semilog) and 2 (log-log).

Table 1: Example Test Information

Compressibility (/psi):	.000005
Porosity (fraction):	.3
Viscosity (cp):	5.0
Formation volume factor (RB/STB):	1.1
Wellbore radius (feet):	0.2
Formation thickness (feet):	17
Initial reservoir pressure (psia):	2063
Flow rate before shut-in (STB/day):	100
Producing time (hours):	(long)

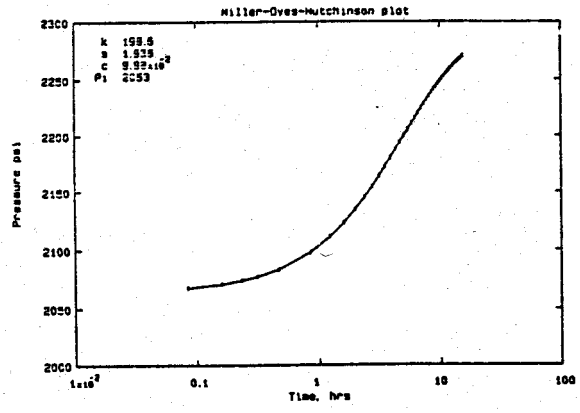

Figure 1: Semilog plot of 15-hour data (including match to data).

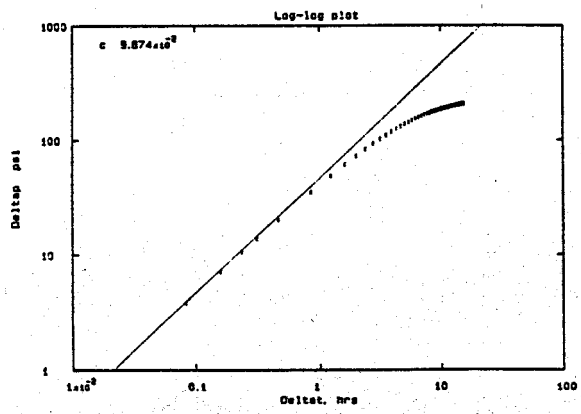

Figure 2: Log-log plot of 15-hour data.

It can be seen that the data has not yet reached infinite-acting behavior, in that no semilog straight line has appeared and the log-log plot shows that the end of the storage period (unit slope straight line) is less than one-and-a-half log cycles from the end of the test. Thus there was not yet sufficient data for traditional semilog analysis of the test. Figures 3 and 4 confirm that all of the data lay in the storage or in the transition region of the type curve and derivative type curve.

Based on traditional well test analysis criteria, it could be concluded that the test had insufficient data. Therefore the measurements were continued for a longer period, totaling 200 hours in all.

However, automated analysis has been shown to be capable of matching reliably even in transition data, and Figure 1 shows a good match to the data plotted as a full line overlaying the data (which are plotted as crosses). Table 2 lists the results inferred by the software for this match, and the confidence intervals that are to be placed on the estimates. Experience has shown us that confidence intervals of less than 10% of the estimated values represent an acceptable matched solution. Thus the estimates obtained from this first 15 hours of data are all within acceptable limits.

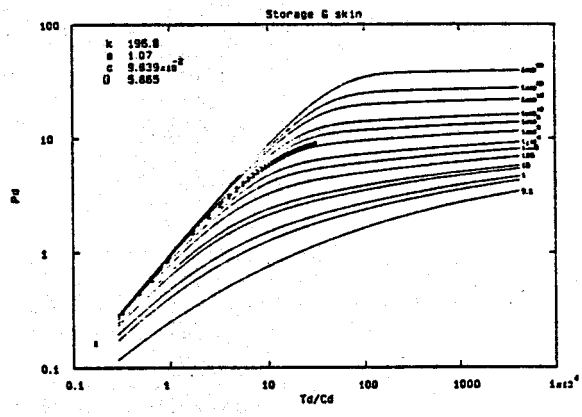

Figure 3: Type-curve match of 15-hour data.

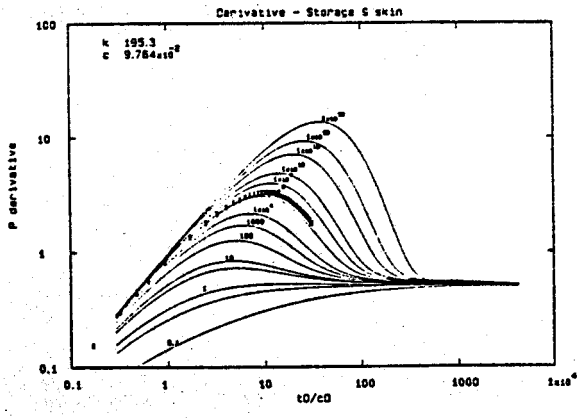

Figure 4: Derivative plot of 15-hour data.

Table 2: Estimated Results for 15 hours of Data

Variable	Estimate	±	± %
Permeability (md)	198.6	3.76	1.89%
Skin	1.94	0.168	8.67%
Storage (RB/psi)	0.100	0.00021	0.21%
Initial Pressure (psia)	2062.9	0.059	0.00%

An absolutely definitive test of the validity of the solution can be obtained by comparing the result with the answers derived from the subsequent interpretation of the full 200 hours of data.

Analysis after 200 hours:

The remainder of the test data are illustrated in Figure 5.

A good semilog straight line appears after about 60 hours. The steps of the interpretation using the automated well test analysis software are as follows:

1. Using a graphical plot of the data, a straight line is aligned through the apparent semilog straight line region of the data, as in Figure 5. The slope and position of this line allows the calculation of estimates for the permeability and the skin factor for the test.
2. Another straight line is aligned with the unit slope straight line on the log-log plot, as in Figure 2. The position of this line allows the calculation of an estimate for the wellbore storage coefficient.
3. Alternatively (or in addition), the data can be plotted over the appropriate type curve, such as the Gringarten et al [16] type curve shown in Figure 6 or the derivative type curve (Bourdet et al [17]) as in Figure 7. Moving the data with respect to the type curve allows for another calculation of the estimates for the reservoir parameters based on the pressure and time match points.
4. The computer program is then used to perform the automated match, using the estimated parameter values as starting guesses. The automated procedure calculates the best possible match to the chosen reservoir model (in a least squares sense) and estimates the approximate confidence intervals to be associated with the answers. The final match can be compared to the original data as in Figures 8, 9 and also in Figure 1.

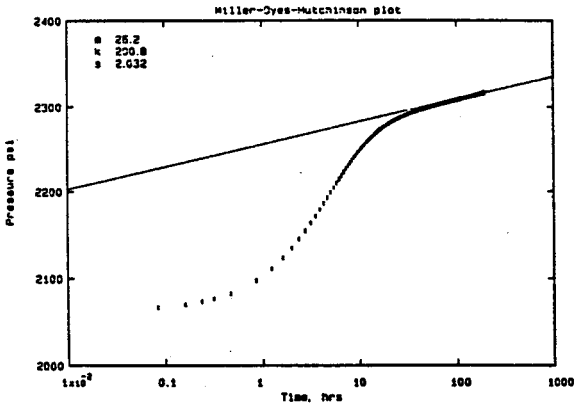

Figure 5: Semilog plot of 200-hour data (with correct straight line shown).

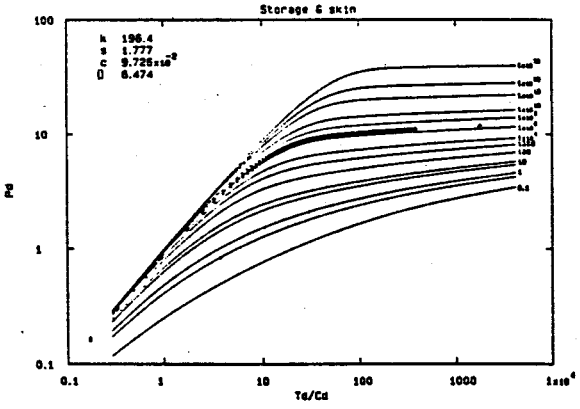

Figure 6: Type-curve match of 200-hour data.

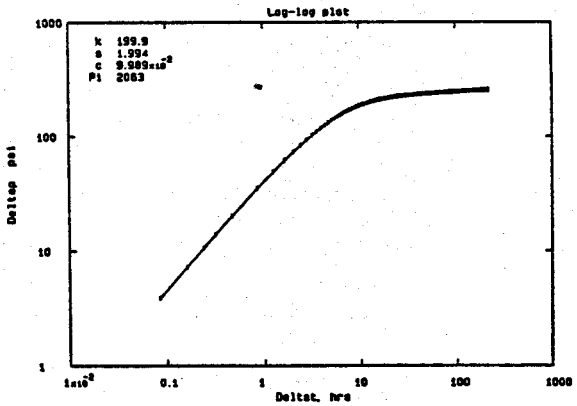

Figure 7: Derivative plot of 200-hour data.

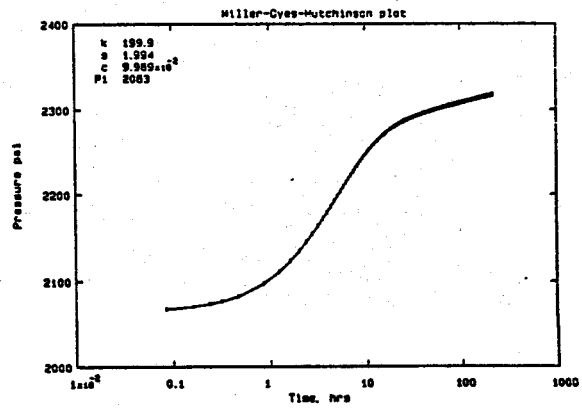

Figure 8: Best fit match to 200-hour data (semilog plot).

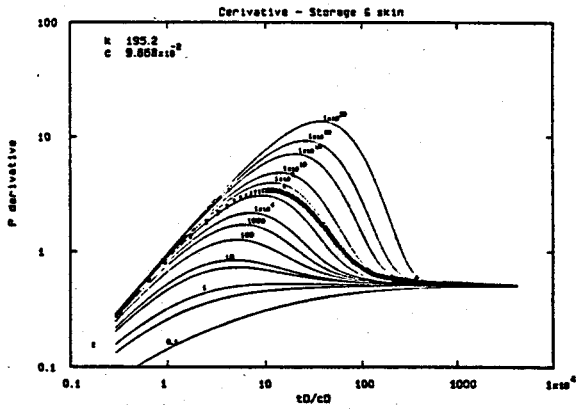

Figure 9: Best fit match to 200-hour data (log-log plot).

The results of the match to the full 200 hours of data are summarized in Table 3.

Table 3: Estimated Results for 200 hours of Data

Variable	Estimate	±	± %
Permeability (md)	199.9	0.140	0.07%
Skin	1.99	0.007	0.34%
Storage (RB/psi)	0.100	0.00005	0.05%
Initial Pressure (psia)	2062.9	0.033	0.00%

Comparison of the two solutions:

Comparison of Table 2 with Table 3 reveals that the automated procedure obtains the same answer using only the first 15 hours of the data, even though this data cannot be interpreted using traditional graphical methods. The shorter test time results in wider confidence intervals, but these are still within acceptable limits. This demonstrates that the computerized analysis procedure has been able to accurately interpret the test, using less than one tenth of the data collected. Figure 10 shows the position of the semilog straight line relative to the 15 hour test data; clearly it would be impossible to have inferred the position and slope of this line using traditional methods.

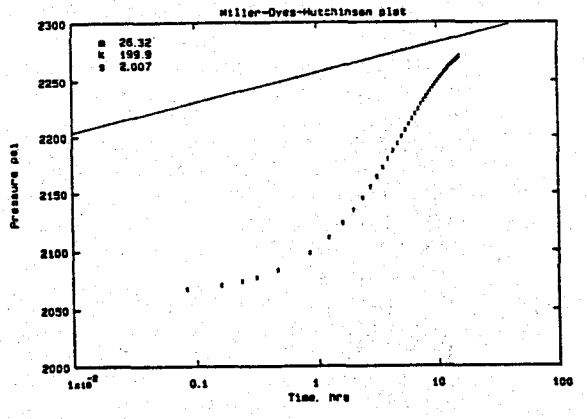

Figure 10: Semilog plot showing position of correct straight line in relation to 15-hour data.

4. APPLICATION TO MEXICAN GEOTHERMAL WELLS

During this study, several field examples from Mexican geothermal fields were analyzed by this technique.

Figure 11 shows an example of a test at Cerro Prieto M-113 that is missing the early time data, and only barely reaches the infinite acting region of the response (semi-log straight line region).

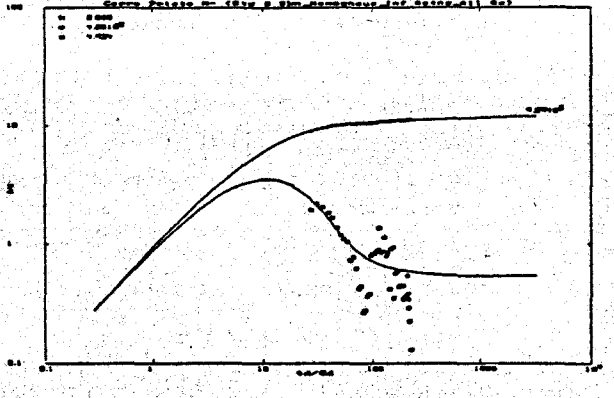

Figure 11: Well test data from Cerro Prieto M-113.

This data lies more or less entirely within the "transition" region between wellbore storage and infinite acting response regions, and is therefore particularly difficult to interpret by normal graphical methods. Table 4 shows the estimates of reservoir parameters obtained by automated analysis - even though acceptable estimates for the storage coefficient and skin factor cannot be obtained (since the early time data is all missing), it still possible to obtain the reservoir permeability within the criterion of acceptable confidence intervals. This is an example of the recovery of an interpretation from a set of welltest data that would be unlikely to be correctly analyzed by normal graphical "hand" methods.

Table 4: Estimated Results for Cerro Prieto M-113

Variable	Estimate	±	± %
Permeability (md)	2.82	0.24	8.63%
Skin	5.90	2.88	48.84%
Storage (RB/psi)	0.036	0.016	45.04%
Initial Pressure (psia)	2674.4	176.56	6.60%

In a second example, Figures 12 and 13 show two different interpretations for the same set of welltest data from well Los Azufres Az-17. (Details concerning the test are described in the Appendix). Figure 12 indicates a good match to the finite conductivity fracture type curve, and Figure 13 shows another good match (on a semilog plot) to a normal infinite acting reservoir response with the late time interception of a boundary effect at a an inferred boundary distance of 100 feet.

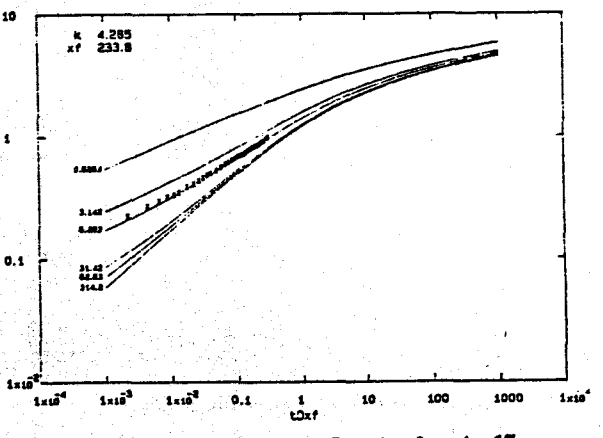

Figure 12: Well test data from Los Azufres Az-17.

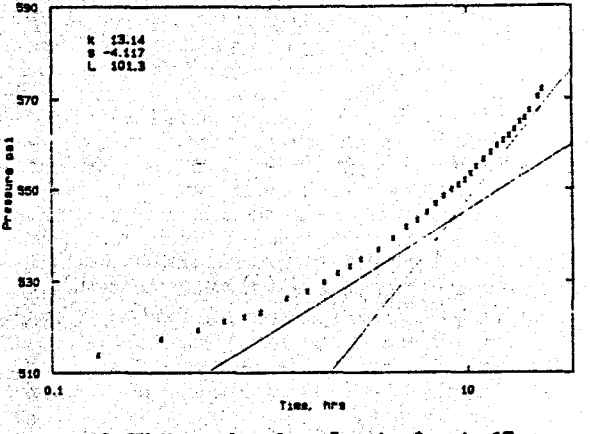

Figure 13: Well test data from Los Azufres Az-17.

Table 5: Estimated Results for Los Azufres Az-17 (model 1)

Variable	Estimate	±	± %
Permeability (md)	7.306	0.811	11.1%
Fracture length (ft)	108.70	14.30	13.16%
Fracture conductivity	18.11	4.64	25.61%

Table 6: Estimated Results for Los Azufres Az-17 (model 2)

Variable	Estimate	±	± %
Permeability (md)	12.99	2.48	19.11%
Skin	-4.10	0.12	2.90%
Storage (RB/psi)	0.00013	0.000005	3.79%
Boundary distance (ft)	101.25	0.47	0.46%

Examination of the confidence intervals for the two cases (Table 5 and 6) reveals that the apparent "boundary" interpretation is entirely unreasonable. This is because the apparent "infinite acting" semilog straight line is in fact part of the early time data, and it is the *second* straight line that is correctly representative of the reservoir permeability. In the absence of a unit slope straight line to recognize the end of the early time data region, this would have been difficult to realize in a normal manual analysis.

This second example underlines one of the principle advantages of the automated technique. Confronted with two very reasonable looking graphical matches, there is no independent way to distinguish one interpretation from the other by eye. Examination of the confidence intervals immediately shows that there is a definite difference between them. It should be noted that the estimates of the permeability in the two cases differ by almost an order of magnitude.

It is worth noting here that the resolution of the ambiguity as to which model to choose really lies in consideration of the geological structure of the reservoir. For formations such as those found at Los Azufres, a fracture intersecting the well is a much more probable explanation than an impermeable boundary 100 feet away. So in this case, a decision based on the consideration of the confidence intervals gives the same conclusion as consideration of the local reservoir geology.

5. CONCLUSIONS

The use of microcomputers in well test analysis has resulted in considerable improvements both in the acquisition and in the interpretation of data. These improvements can result in much less expensive tests, since the computer can perform data collection and test control much faster and with fewer people than manual recording. Measurements of multiple wells can be made as easily as measurements at a single well. In addition, the test can be analyzed by microcomputer, either at the site or at the home office if the data are telemetered from the measurements computer. Advances in interpretation made possible by the computerized automated analysis mean that the test need not be as long as is necessary for manual analysis.

Microcomputers can also greatly improve the analysis of tests that have already been performed under existing practise. The new capabilities of automated analysis make it possible to obtain a result from a test that was previously too short for analysis. The automated interpretation of such a test saves the execution of a new replacement test.

REFERENCES

1. Earlougher, R.C., Jr., "Advances in Well Test Analysis", SPE Monograph, Vol. 5, Chapter 12, 1977.
2. Padmanabhan, L., and P.T. Woo, "A New Approach to Parameter Estimation in Well Testing", Proceeding of the Fourth SPE Symposium on Reservoir Simulation, paper SPE 5741, Los Angeles, February 1976.
3. Tsang, C.F., McEdwards, D.G., Narasimhan, T.N. and Witherspoon, P.A., "Variable Flow Well Test Analysis by a Computer Assisted Matching Procedure, paper SPE 6547, 47th Annual California Regional Meeting of the Society of Petroleum Engineers of AIME, held in Bakersfield, California, April 13-15, 1977.
4. Padmanabhan, L., "Welltest - A Program for Computer-Aided Analysis of Pressure Transients Data from Well Tests", paper SPE 8391, presented at the 54th Annual Fall Meeting of the Society of Petroleum Engineers of AIME, Las Vegas, Nevada, September 23-26, 1979.
5. McEdwards, D.G., "Multiwell Variable-Rate Well Test Analysis, SPEJ, 21 p. 444 - 446, (1981), SPE Transactions 271.
6. Rosa, A.J. and Horne, R.N., "Automated Type-Curve Matching in Well Test Analysis Using Laplace Space Determination of Parameter Gradients", paper SPE 12131, presented at the 58th Annual Technical Conference and Exhibition, Society of Petroleum Engineers of AIME, San Francisco, California, October 5-8, 1983.
7. Guillot, A.Y., and Horne, R.N.: "Using Simultaneous Downhole Flow Rate and Pressure Measurements to Improve Analysis of Well Tests," SPE Formation Evaluation, June 1986, 217-226.
8. Meunier, D., Kabir, C.S. and Wittman, M.J.: "Gas Well Test Analysis: Use of Normalized Pressures and Time Functions", paper SPE 13082, presented at the 1984 SPE Annual Technical Conference and Exhibition, Houston, TX, September 16-19, 1984.
9. Kucuk, F. and Ayestaran, L.: "Analysis of Simultaneously Measured Pressure and Sandface Flow Rate in Transient Well Testing", J. Pet. Tech. (February 1985), 322-330.
10. Barua, J., and Horne, R.N.: "Computerized Analysis of Thermal Recovery Well Test Data," SPE Formation Evaluation, December 1987, 560-566; Transactions, AIME, 290.
11. Horne, R.N., and Kuchuk, F.: "The Use of Simultaneous Spinner and Pressure Measurements to Replace Isochronal Gas Well Tests", SPE Formation Evaluation, (June 1988), p. 467-470
12. Barua, J., Horne, R.N., Greenstadt, J.L., and Lopez, L.: "Improved Estimation Algorithms for Automated Type Curve Analysis of Well Tests", SPE Formation Evaluation, March 1988, 186-196
13. Marquardt, D.W., "An Algorithm for Least-Squares Estimation of Nonlinear Parameters", J. Soc. Indust. App. Math. (June 1963) 11, No. 2.
14. Greenstadt, J.L., "On the Relative Efficiencies of Gradient Methods", Mathematics of Computation, 21, p. 360-367, 1967.
15. Bard, Y., Nonlinear Parameter Estimation, Academic Press, Inc. Ltd., New York, 1974.

16. Gringarten, A.C., Bourdet, D.P., Landel, P.A. and Kniazeff, V.J., "A Comparison Between Different Skin and Wellbore Storage Type-Curves for Early-Time Transient Analysis", paper SPE 8205, presented at the SPE-AIME 54th Annual Technical Conference and Exhibition, Las Vegas, Nevada, September, 23-26, 1979.

17. Bourdet, D., Whittle, T.M., Douglas, A.A., and Pirard: "A New Set of Type Curves Simplifies Well Test Analysis", World Oil, May 1983

18. Venegas, S. S., and Huitron, R. : " Propuesta de Pozos para el Desarrollo de la Zona Norte de Los Azufres, Mich. ", Comunicacion 9/88, CFE Internal Report, 1988.

Appendix - Los Azufres Az-17 Test

Well Az-17 is located in the south zone of the Los Azufres Geothermal Field, Michoacan, Mexico, and was completed in February 1980 at a depth of 627 m . The circulation losses during the drilling process were registered between 613 and 627 m depth, at which depth it is presumed that the well intersected the Puentecillas Fault. Another important geological structure nearby the well is the Agua Ceniza Fault, located at the surface at a distance 140 m east. These geological structures have slopes with respect to surface of 82 and 84 degrees (Venegas et al.[18]), respectively. The well was completed with a casing pipe of 0.2245 m in diameter from 0 to 560 m depth, and with a liner of 0.1778 m in diameter from 450 to 622 m depth. The slotted part of the liner goes from 561 to 622 m depth.In December 1980 the well produced a maximum steam flow rate kg/s. At that time, the produced steam had a little humidity, however it was gradually coming into the superheated region. Up to date, the mean specific enthalpy of the produced fluid is around 2800 kJ/kg at any wellhead pressure. Based on the characteristics of this well, it was connected to a 5 MW turbogenerator unit in the second semester of 1982. Some scaling problems were detected in the turbine during the initial period of generation, however those were corrected.

February 22, 1987 well Az-17 was taken out of the generation system in order to give maintenance to the turbogenerator Unit Number 2 which was supported by this well almost without interruption since the second semester of 1982. In March of the same year, two tests were realized on this well: a production test to obtain the production output curve; and a pressure buildup test to determine the formation parameters. A little before the buildup test had started, simultaneous pressure and temperature Kuster logs were run to know the thermodynamic states of the fluid throughout the well. This information was also used to test the superheated steam well simulator developed by Upton in 1985. The pressure buildup test was carried out after that producing at a constant steam flow rate of 9.81 kg/s during 144 h. This condition was achieved by using an orifice plate of 0.0508 m. The recuperation period used was 23 h and the pressure Kuster element was located at 610 m depth.

PROCEEDINGS, Fourteenth Workshop on Geothermal Reservoir Engineering
Stanford University, Stanford, California, January 24-26, 1989
SGP-TR-122

NEDO'S PROJECT ON GEOTHERMAL RESERVOIR ENGINEERING: A RESERVOIR ENGINEERING STUDY OF THE SUMIKAWA GEOTHERMAL FIELD, JAPAN

Y. Kawano and H. Maki
New Energy and Industrial Technology
Development Organization
Tokyo, Japan

T. Ishido
Geological Survey of Japan
Tsukuba, Japan

Y. Kubota
Mitsubishi Metal Corporation
Kazuno, Japan

INTRODUCTION

In order to promote the development of geothermal energy resources, it is important to understand how to estimate reservoir capacity and to minimize the risks associated with various development schemes prior to full-scale commitment so that power plant design may be formulated. The New Energy and Industrial Technology Development Organization (NEDO) has been developing technology suitable for the evaluation of geothermal reservoirs since FY 1984. Phase I of this program was completed during FY 1987; the results of these studies are being published during FY 1988. Then, beginning in FY 1988, NEDO undertook Phase II of the program, of which the major purpose is to devise techniques to deal with more complex reservoir behavior. This includes reservoirs in which the effects of fractures must be specifically treated and/or in which the fluid mixture contains important constituents in addition to H_2O (such as carbon dioxide gas).

STRUCTURE OF NEDO'S PROJECT

Figure 1 indicates the overall NEDO project schedule. The project has three major components: (1) the development of numerical reservoir simulators, (2) the acquisition of data from real geothermal fields, and (3) modeling and simulation studies.

F.Y. / CONTENT		Phase I				Phase II				
		1984	1985	1986	1987	1988	1989	1990	1991	1992
1. Development of Simulators and Simulation Works										
2. Drilling of Observation Wells 1500m class x 2 in each field	Kirishima Sumikawa Mori Another	1x1500	1x1500 1x1600	1x1700		1000&1500				
3. Well Tests Pressure Interference Test, Discharge test etc	Kirishima Sumikawa Mori Another									
4. Interpretation and Evaluation of Simulator, Simulation and Methodology										

Figure 1. NEDO project schedule.

Simulator Development

So far, NEDO has developed three simulators suitable for geothermal reservoir engineering studies. The "SING-1" code is restricted to incompressible single-phase-liquid reservoirs using the Boussinesq approximation in either three-dimensional (Cartesian) or axisymmetric geometries. The more general "SING-2" simulator treats two-phase (water/steam) systems, including compressibility effects, and incorporates a representation for fracture/matrix phenomena. The generality of the SING-2 simulator is offset by computing cost; execution times are typically forty times greater for SING-2 than for SING-1. Hence, for preliminary studies SING-1 will be used wherever possible.

The "WENG" simulator is in a somewhat different category; it consists of an unsteady one-dimensional radial-flow single-phase-liquid heterothermal reservoir model coupled to a steady-state two-phase model of flow up a geothermal production well. Heat transfer through the casing is treated using a user-prescribed heat transfer coefficient in connection with a prescribed formation temperature profile. Frictional pressure drop and liquid-holdup effects are treated using empirical correlations.

The various NEDO simulators have been tested against analytical solutions and also against computed results obtained using older proven simulators. The results of the various test calculations have verified the reliability of the NEDO codes.

Field Studies

To apply the technology developed under this program to actual field situations, NEDO chose particular Japanese "model" geothermal fields for study: the Sumikawa and Kirishima fields (Phase I) and the Mori field (Phase II), as indicated in Figure 2. Several field surveys were conducted including long-term reservoir pressure observations, well logging, and discharge testing.

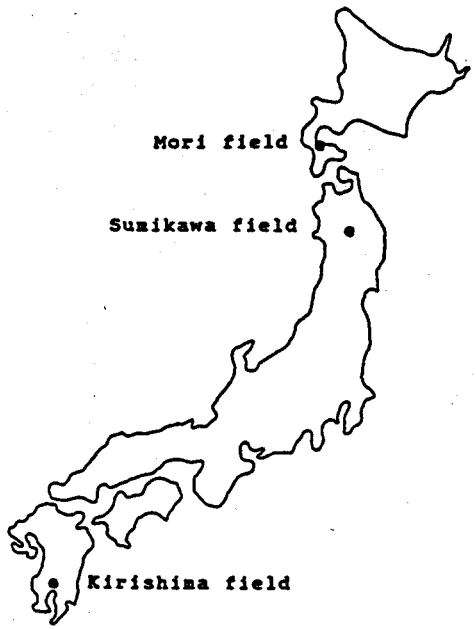

Figure 2. Locations of model geothermal fields.

The Kirishima study began in 1984 with the completion by NEDO of two deep observation wells in the field. Pressure observations have been made using these wells as well as six other preexisting wells drilled by the field developer. Results obtained from the Kirishima study have been summarized by Kitamura, *et al.* (1988) and Maki, *et al.* (1988a). The Sumikawa study started in 1985; as at Kirishima, two deep wells were first drilled for the purpose of pressure observations. Long-term pressure observations have been found to be very useful; at Kirishima, a total of eight observation wells have been instrumented and have recorded the response to a multi-year history of production and injection operations at the field on a year-round basis. The locations of the various Kirishima wells are shown in Figure 3 and the character of the discharge/injection/observation history is indicated in Figure 4. Results of pressure monitoring experiments at Sumikawa are discussed below.

Modeling and Simulation

Numerical reservoir simulation studies have been carried out to try to understand the reservoir mechanics in the selected geothermal fields (see, for example, Maki, *et al.*, 1988a; 1988b). These

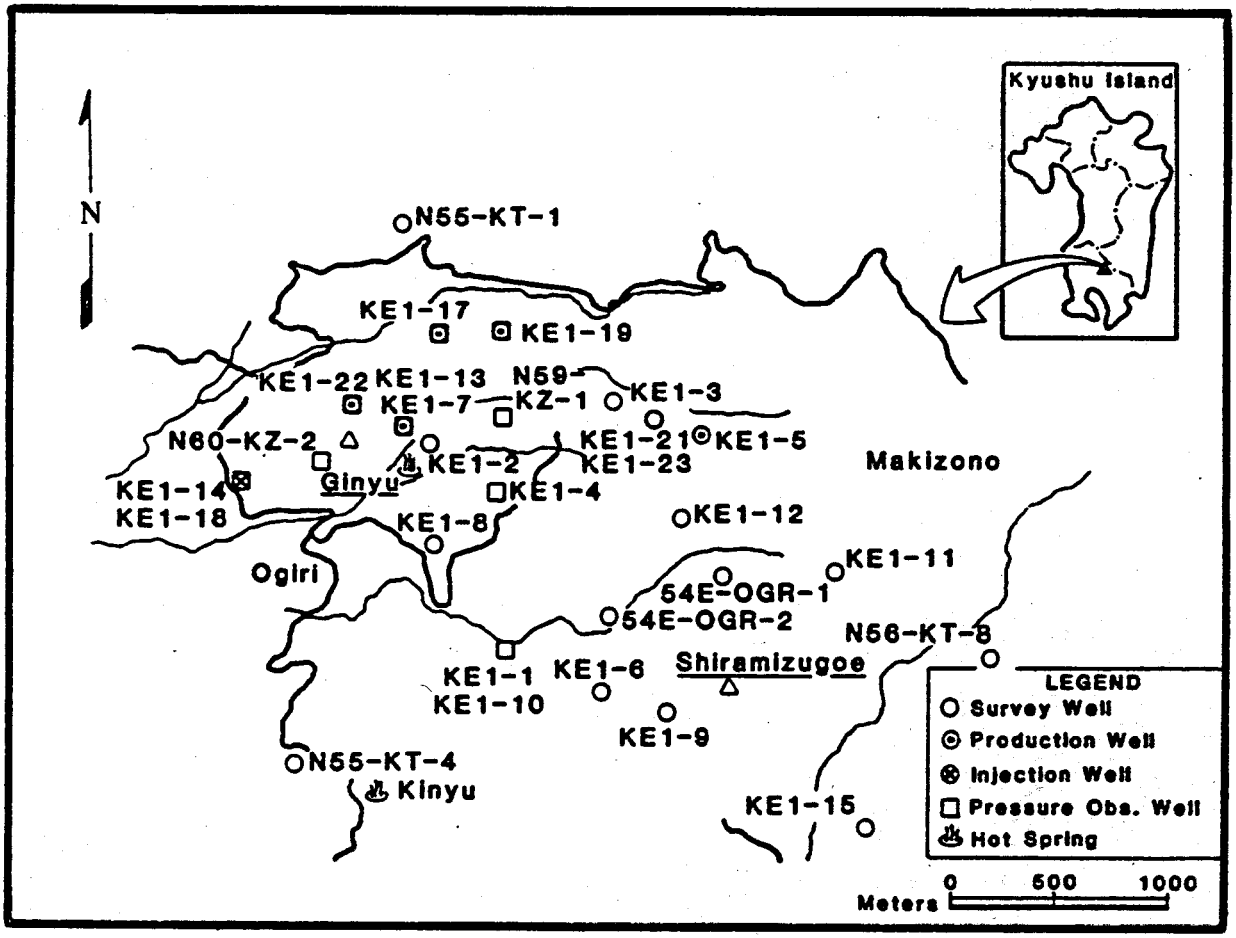

Figure 3. Map of the Kirishima geothermal field.

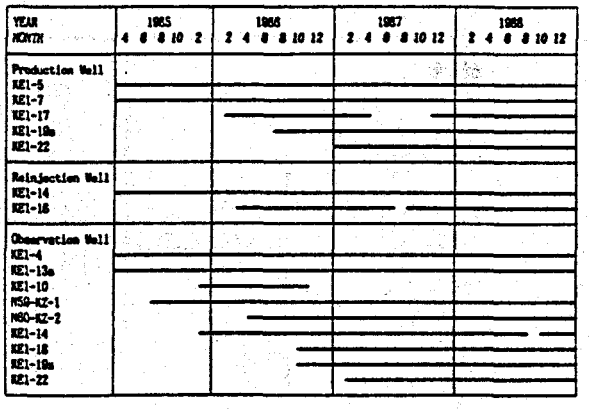

Figure 4. Kirishima pressure interference test schedule.

studies were based upon available analyses of well-test measurements, geological data, geophysical survey results and other pertinent information. Simulations of this type are carried out in an iterative manner, varying the values of the various unknown parameters in the mathematical model to maximize agreement between measurements and calculated results. These calculations are time-dependent in character but are carried forward for long periods of time so that a nearly steady natural-state representation is obtained. Adequate matches both for the (essentially steady) natural state of the system and for any documented transient behavior (such as long-term pressure transient testing and/or production history) are sought in this iterative procedure.

Once an internally consistent model of the reservoir in its natural state has been obtained which represents the known facts about the reservoir, a series of calculations may be performed to estimate the response of the reservoir to a variety of alternative development strategies. Sensitivity studies are also performed to evaluate the reliability of the resulting predictions, and an optimum reservoir development plan is devised.

THE SUMIKAWA GEOTHERMAL FIELD

The Sumikawa field is located on the northern slope of Mount Yake in Akita prefecture in northeastern Japan. Mitsubishi Metal Corporation (MMC) has been carrying out field exploration studies in the general vicinity since 1965. This early exploration program involved drilling five wells and the performance of a variety of surveys (resistivity, gravity, geochemistry, etc.). In 1973, MMC commissioned the Ohnuma geothermal power station, located about two kilometers east of Sumikawa.

In 1974-75, the Japanese government carried out further investigations in the Sumikawa area, including the completion of five additional wells and a resistivity survey. The results of these surveys made it clear that Sumikawa was a promising field. At this point, MMC (in collaboration with MGC - Mitsubishi Gas Chemical Corporation) initiated a new exploration program which focused specifically on the Sumikawa field, and drilled the four deep "S-series" (S-1, S-2, S-3 and S-4) wells between 1980 and 1984. Results of this drilling program indicated the presence of a substantial underground two-phase flow region in the southern part of the field.

As discussed above, Sumikawa was selected by NEDO as one of its "model" fields in 1985. NEDO drilled two additional wells in the area in 1985-1986. Meanwhile, another related NEDO project was carried out at Sumikawa which involved the completion of the deepest well in the field (well SN-7D; 2486 meters) in 1987. As a consequence of these exploratory programs, a reasonably self-consistent picture of the geology and hydrology of the reservoir at Sumikawa is emerging. The present understanding of the system has been summarized by Kubota (1988) and also by Pritchett, *et al.* (1989) at this Workshop.

PRESSURE INTERFERENCE MEASUREMENTS AT SUMIKAWA

As Figure 5 shows, extensive discharge tests were performed at Sumikawa in 1986 and again in 1988. Although these tests were significantly shorter in duration than those at Kirishima, several interesting signals were recorded. Figure 6 indicates the locations of the wells involved. The first test entailed the three-month discharge of deep well S-4 in the autumn of 1986; the separated liquid component was reinjected into nearby (relatively shallow) well S-2. Four shut-in observation wells (KY-1, KY-2, S-3 and O-5T) were equipped with downhole capillary-tube pressure gauges. No signals attributable to the discharge test were observed in wells KY-2, S-3 or O-5T, but a substantial response was detected in deep well KY-1, which lies about one kilometer north of S-4 (see Figure 7). Analyses of this interference signal (Maki, *et al.*, 1988c; Pritchett, *et al.*, 1989) suggest the presence of a deep permeable channel oriented north-south at Sumikawa.

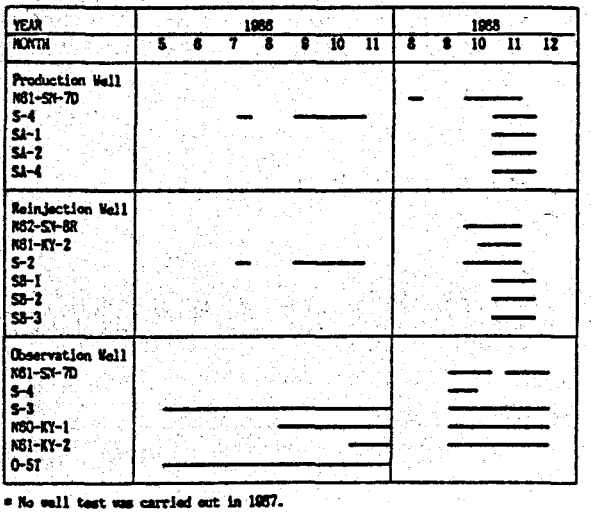

* No well test was carried out in 1987.

Figure 5. Sumikawa pressure interference test schedule.

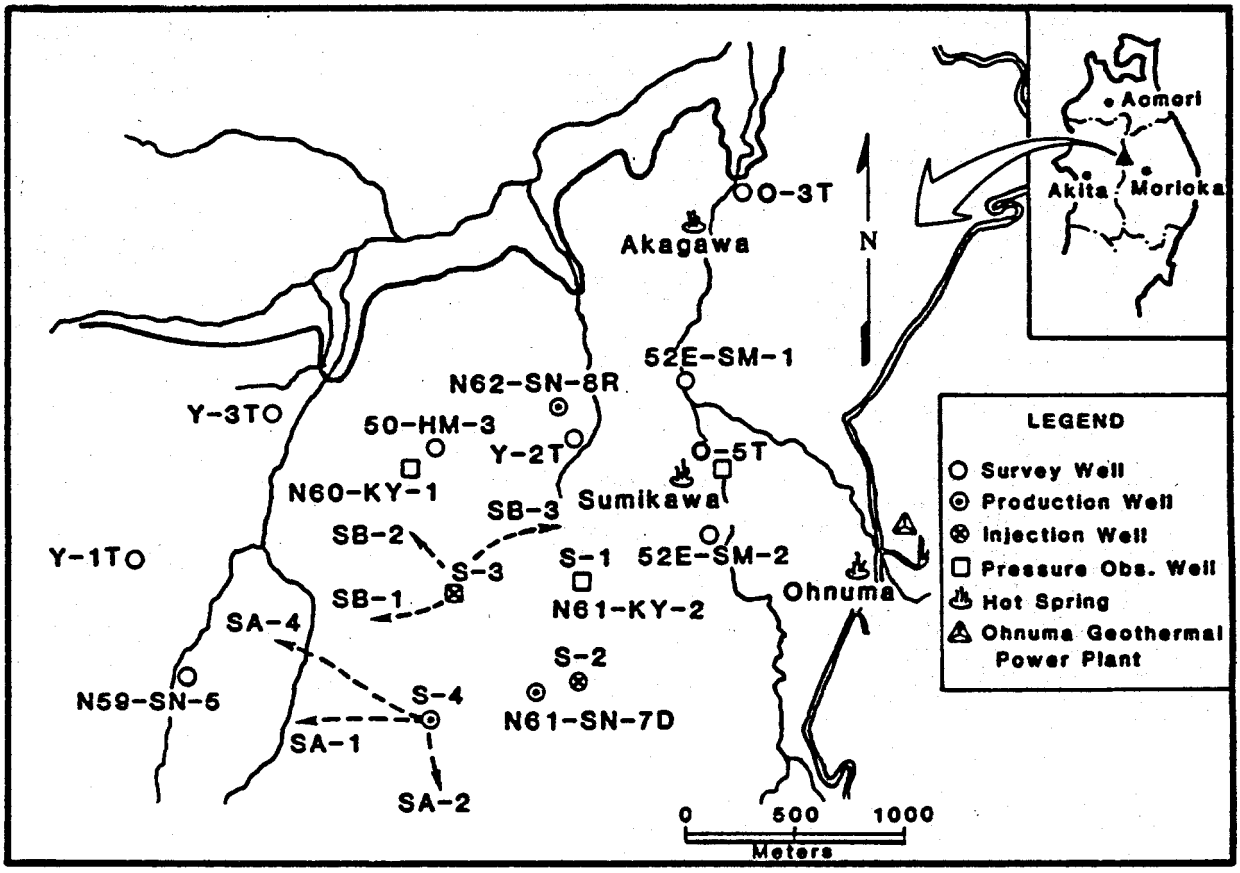

Figure 6. Map of the Sumikawa geothermal area.

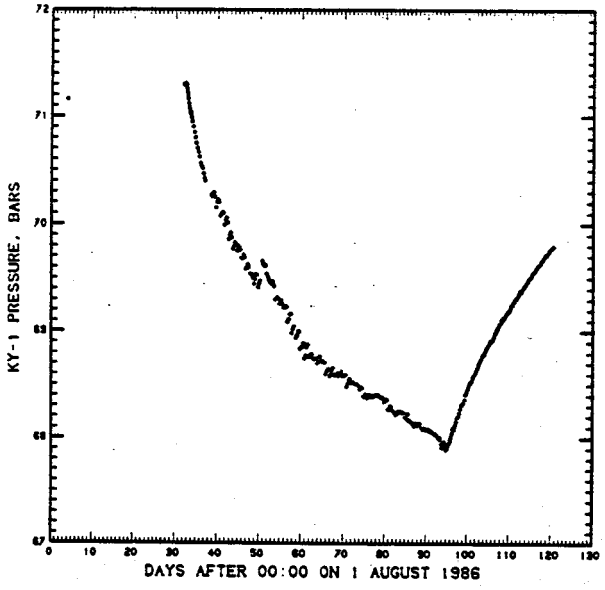

Figure 7. 1986 pressure interference signal in observation well KY-1.

Recently, additional pressure transient experiments have been performed. In autumn 1988, five wells (SA-1, SA-2, SA-4, S-4 and SN-7D) were discharged at various times and six wells (SB-1, SB-2, SB-3, S-2, SN-8R and KY-2) were used for reinjection at one time or another. Downhole pressure observations were made in wells SN-7D, S-4, S-3, KY-1 and KY-2. Analyses of the most recent tests are not yet complete; the results will be published in the near future.

MODELING STUDIES OF THE SUMIKAWA FIELD

An extensive computational effort using the "SING-2" numerical reservoir simulator is being carried out to try to understand the Sumikawa field in the natural state. Preliminary work was restricted to a two-dimensional vertical-section representation of the field to provide tentative estimates of the appropriate permeability distribution, boundary condition parameters, and so on. Then, the model was extended to three space dimensions and further refined. As new data is acquired, the model requires revision and upgrading. As discussed above, the development

of each model involved an extensive series of calculations to attain adequate agreement between computational results and field measurements. Sensitivity studies have been carried out to try to estimate the reliability of the computational model. The best model developed so far reproduces observed temperatures and pressures reasonably well; Figure 8 compares computed and measured pressures in the central area of the field. The computational model will be further refined in the future as more field data become available.

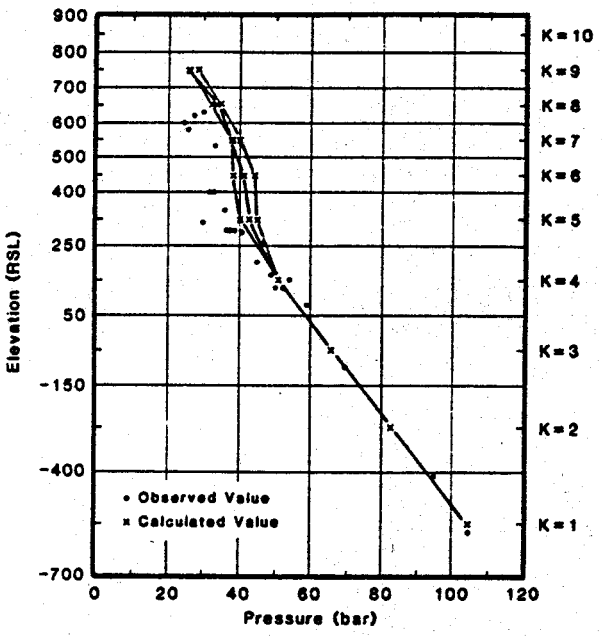

Figure 8. Observed and calculated pressure profiles in the Sumikawa field.

FUTURE PLANS

As discussed above, NEDO completed Phase I of the project in FY 1987 (ending March 1988) and initiated Phase II in FY 1988; the purpose of Phase II is to further examine a number of key issues raised during the Phase I effort. These include appropriate ways of dealing with fractured systems and the influence of incondensable gasses in the reservoir. Also, NEDO selected the Mori field in northern Japan as a new "model" field in 1988. The Mori system appears to be dominated by three major fault zones, and the fluid contains substantial amounts of CO_2 gas which has caused calcite scaling problems. Furthermore, a six-year production history is available for Mori, which permits reservoir studies to proceed beyond calculations of the natural state; history-matching calculations of the production phase will also be attempted. These calculations will incorporate representations for the effects of the fault zones and of the CO_2 gas in the system.

ACKNOWLEDGEMENTS

This research was performed as a part of NEDO's "Geothermal Development Promotion Survey Project" which has been in progress since 1980. The project is also subsidized by the Electric Power Generation Division of the Agency of Natural Resources and Energy, Ministry of International Trade and Industry.

REFERENCES

Kitamura, H., T. Ishido, S. Miyazaki, I. Abe and R. Nobumoto (1988), "NEDO's Project on Geothermal Reservoir Engineering – A Reservoir Engineering Study of the Kirishima Field, Japan," Proceedings of the Thirteenth Workshop on Geothermal Reservoir Engineering, Stanford University.

Kubota, Y. (1988), "Natural Convection System at the Ohnuma-Sumikawa Geothermal Field, Northeast Japan," Proceedings of the Tenth New Zealand Geothermal Workshop, University of Auckland, pp. 73-78.

Maki, H., T. Ishido, I. Abe, R. Nobumoto and Y. Oikawa (1988a), "A Modeling Study of the Natural State of the Kirishima Field," Proceedings of the International Symposium on Geothermal Energy 1988, Kumamoto/Beppu, Geothermal Research Society of Japan, pp. 144-147.

Maki, H., T. Ishido, Y. Kubota, T. Maeda, K. Ariki and T. Nakai (1988b), "A Modeling Study of the Natural State of the Sumikawa Field," Proceedings of the International Symposium on Geothermal Energy 1988, Kumamoto/Beppu, Geothermal Research Society of Japan, pp. 148-151.

Maki, H., J. W. Pritchett and S. K. Garg (1988c), "Interpretation of a Pressure Interference Test of the Sumikawa Geothermal Field," Proceedings of the International Symposium on Geothermal Energy 1988, Kumamoto/Beppu, Geothermal Research Society of Japan, pp. 557-560.

Pritchett, J. W., S. K. Garg, H. Maki and Y. Kubota (1989), "Hydrology of the Sumikawa Geothermal Prospect, Japan," Proceedings of the Fourteenth Workshop on Geothermal Reservoir Engineering, Stanford University (present volume).

PROCEEDINGS, Fourteenth Workshop on Geothermal Reservoir Engineering
Stanford University, Stanford, California, January 24-26, 1989
SGP-TR-122

HYDROLOGY OF THE SUMIKAWA GEOTHERMAL PROSPECT, JAPAN

J. W. Pritchett and S. K. Garg
S-CUBED
La Jolla, California 92038-1620

H. Maki
New Energy and Industrial Technology Development Organization
Tokyo, Japan

Y. Kubota
Mitsubishi Metal Corporation
Kazuno, Japan

INTRODUCTION

The Sumikawa geothermal field is located in the Hachimantai volcanic area in northern Honshu, Japan. Various investigations have been carried out in the area in recent years to assess the suitability of the field for electrical power production. This paper summarizes the principal characteristics of the natural fluid circulation system at Sumikawa and relates them to local geological structure. These features are deduced primarily from static (shut-in) pressure determinations in wells in the field and from a limited amount of pressure-transient testing. It is concluded that extensive natural two-phase flow prevails at intermediate depths at Sumikawa, and that a very high permeability zone is present below ~ 1 km depth containing fluids with temperatures exceeding 300°C. This zone is a suitable target for further study and possible future development.

GEOLOGICAL SETTING

Figure 1 shows the region of particular interest. The area depicted is about 28 square kilometers; the Sumikawa geothermal field lies in the western part of the area. To the east, the Ohnuma geothermal power station has been producing about 10 MW of electrical power for several years using a small borefield immediately surrounding the power station. The terrain is extremely irregular; Mt. Yake lies just to the southwest of the illustrated area and Mt. Hachimantai is just to the southeast. To the north of these volcanic peaks, the terrain drops away rapidly. Between the Sumikawa prospect (which may be regarded as centered in the neighborhood of the S-series wells: S-1, S-2, S-3 and S-4) and the Ohnuma borefield is a north-south region of relatively low ground surface elevation where natural hot-springs and fumaroles are found.

As discussed at length by Kubota (1985), the Sumikawa/Ohnuma area lies within a north-south oriented regional graben structure which extends many kilometers both north and south of the area shown in Figure 1. Indeed, the Sumikawa field itself appears to be located along the western edge of the graben. Figure 2 shows an east-west cross-section corresponding to line A-A′ in Figure 1. Figure 3 shows a similar north-south section (B-B′). These structural interpretations are based almost exclusively upon drilling experience – the only available seismic survey was far too regional in scope to be useful for local structural interpretation, and the results of a gravity survey are difficult to interpret owing to a lack of density contrast among the various deep formations in the area.

Extensive faulting has rendered the detailed geological structure at Sumikawa somewhat obscure, but the abundance of drilling logs from the various wells in the area has revealed an underlying geological sequence which applies to most of the area illustrated in Figure 1. In order of increasing depth, these are:

"ST" Formation:	Surficial andesitic tuffs, lavas and pyroclastics of Recent origin (from Mt. Yake).
"LS" Formation:	Lake sediments; Pleistocene tuffs, sandstones, siltstones and mudstones.
"DA" Formation:	Pliocene dacites, dacitic tuffs and breccias.
"MV" Formation:	"Marine/Volcanic Complex"; interbedded Miocene dacitic volcanic rocks and "black-shale" oxygen-poor marine shales and sediments.
"AA" Formation:	Altered andesitic rocks which are apparently extensively fractured.
"BA" Formation:	Crystalline intrusive rocks (mainly granodiorite and diorite).

As pointed out by Kubota (1988), the "BA" formation is the deepest so far encountered by drilling (well SN-7D bottomed in this formation at 2486 meters depth), but the pre-Tertiary basement which presumably underlies the above sequence has not yet been reached. Little

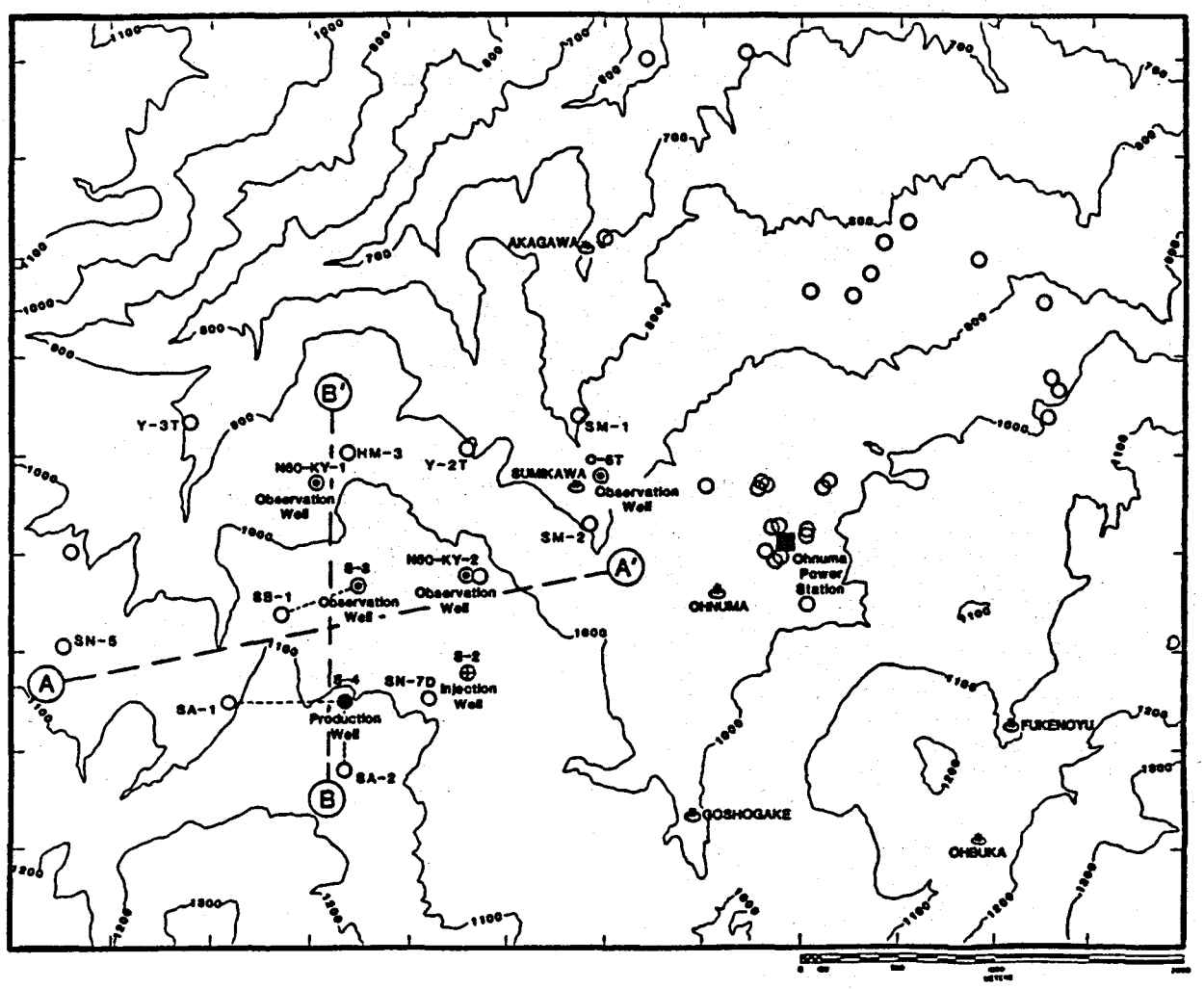

Figure 1. The Sumikawa/Ohnuma area, showing locations of wells, the Ohnuma power station, and cross-sections A-A' and B-B'.

evidence exists for significant permeability deep within the "BA" formation, however, so that it may be permissible to regard this layer as the "basement" from a hydrological standpoint. Further investigation is clearly needed to reveal the structure of the deepest parts of the field.

UNDERGROUND TEMPERATURES

At Sumikawa, underground temperatures are highest to the south and decline to the north and northwest. Figure 4 shows the estimated temperatures at sea level (~ 700 - 1100 m depth) in the area, based mainly on temperature surveys in shut-in wells. The area depicted in Figure 4 is the same as in Figure 1. The highest temperature so far measured in the field is at the bottom of well SA-2 (317°C at 840 meters below sea level); this is also the southernmost deep well at Sumikawa.

Temperatures are significantly higher at Sumikawa (near the S-series wells) than at the nearby operating Ohnuma borefield. On the whole, temperatures appear to increase monotonically with depth; large-scale temperature inversions are not observed. Ishido, *et al.* (1987) report the results of a self-potential survey in the area which shows a major positive anomaly in the neighborhood of the S-series wells, which is indicative of the presence of upwelling deep hot water in this vicinity. On the other hand, the relatively low temperatures encountered to the north and west of the Sumikawa field are consistent with interpretations by Kubota (1988) and by Maki, *et al.* (1988a) that these are areas in which cold water is flowing downward into the reservoir. Observed surface manifestations of hot-water upflow (hot springs) are generally located along a north-south axis lying between Sumikawa and Ohnuma – additional hot spring areas are located farther north of the area illustrated in Figure 4 along the same axis.

STATIC PRESSURE DISTRIBUTION

Maki, *et al.* (1988b) have examined the various downhole feedpoint pressure determinations available from wells in the Sumikawa/Ohnuma area in detail. Evidence from a series of 32 shallow (80 meters) heat-flow holes drilled throughout the area (but not shown in Figure 1)

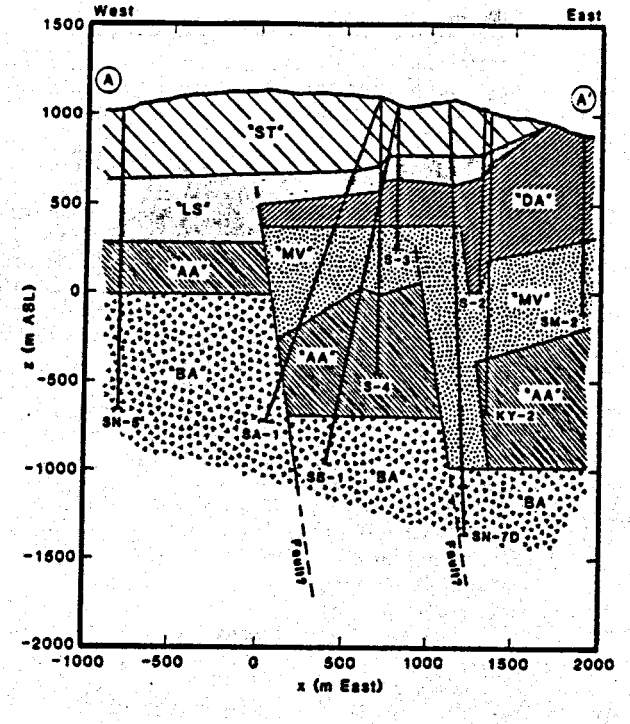

Figure 2. East-west A-A′ geological cross-section through the Sumikawa area.

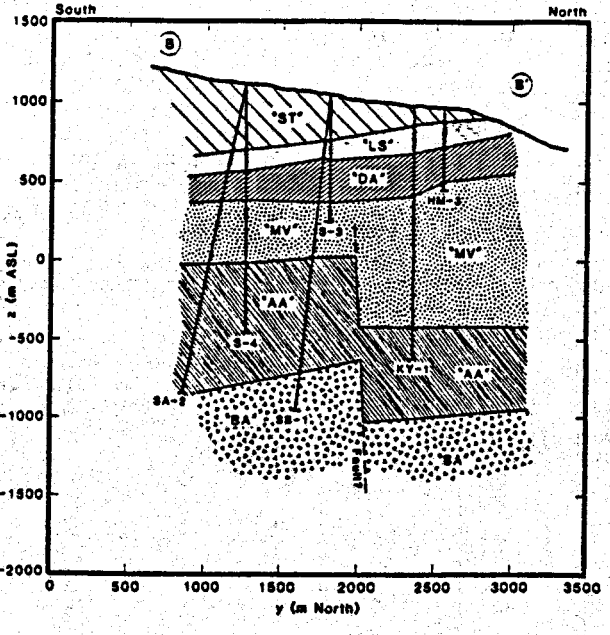

Figure 3. North-south B-B′ geological cross-section through the Sumikawa area.

indicates that near-surface pressures are cold-water hydrostatic relative to a water table depth which follows the local surface very closely; the water table is approximately 45 (± 21) meters below ground. At great depth, however, pressures are surprisingly uniform throughout the area; apart from a small region immediately adjacent to the Ohnuma power station, deep shut-in pressures may be correlated by:

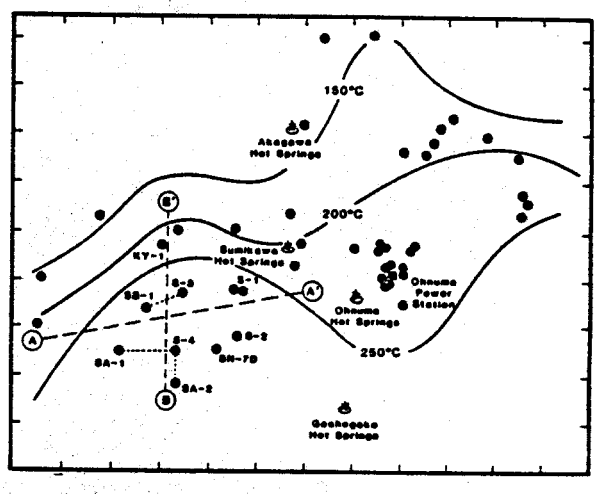

Figure 4. Temperatures at sea-level elevation in the Sumikawa/Ohnuma area (adapted from Kubota, 1988).

$$P \text{ (bars)} = 62 - 0.0776\ Z$$

where Z is elevation, measured in meters with respect to sea level (meters ASL). The standard deviation of this correlation from the measurements is only 1.4 bars (comparable to the reliability of the pressure determinations themselves). This pressure correlation was developed for wells in the southern part of the area (south of the 800 m ASL ground surface elevation contour).

This expression yields one atmosphere pressure at Z = + 786 meters ASL; it follows that in regions with lower ground surface elevation underground pressures must be lower than the above. Indeed, measured pressures in wells in the extreme northern part of the area are less than the above correlation, by an amount comparable to the difference in hydrostatic head between the local ground surface and + 786 m ASL. The clear implication is that a deep reservoir boundary must be present, oriented roughly east-west, at about the location of the 800 m ASL ground surface elevation contour (that is, passing approximately through the Akagawa hot spring area).

In graphical form, underground shut-in pressures at Sumikawa appear to be distributed with elevation as indicated in Figure 5, which is based exclusively on measured pressures in the area. So long as the ground surface elevation is above 800 m ASL, pressures below ~ 350 m ASL all lie on the same line. In areas of high ground surface elevation, however, a transition region characterized by pressures in the 25 to 30 bar range and pressure gradients which are significantly subhydrostatic is present, above which a shallow cold-water hydrostatic zone extends upwards to the ground surface. This transition zone corresponds spatially to the location of the "LS" formation (~ 600 m ASL), which appears to serve as a caprock. The

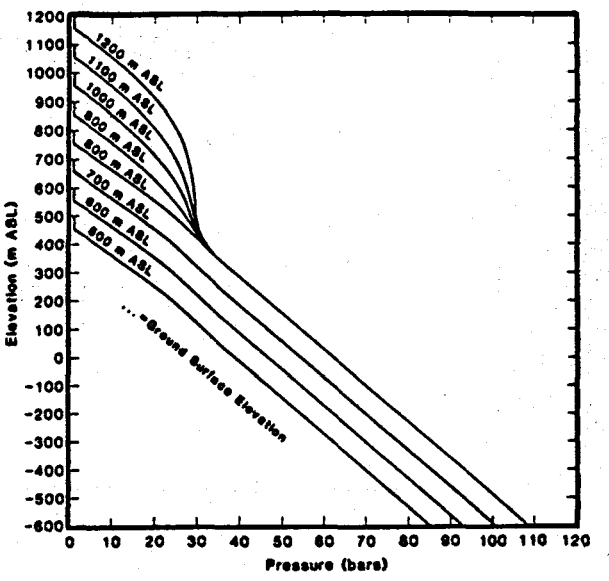

Figure 5. Static underground pressures in Sumikawa/Ohnuma area; influence of elevation and topography.

underlying subhydrostatic region is clearly associated with two-phase flow.

Below the "LS" caprock in the southern part of the system the two-phase (water-steam) flow zone extends at least as deep as + 350 m ASL. Note that the two-phase region could extend much deeper than this, since the presence of a hydrostatic gradient does not preclude two-phase behavior, but only indicates that liquid water is the dominant mobile phase. Closer to the caprock, however, the sub-hydrostatic gradient is indicative of high steam saturations. Confirmation is provided by drilling experience: well S-1 struck a permeable zone during drilling at ~ 450 meters depth (below the "LS" formation) which discharged dry steam. Since temperatures increase to the south toward Mt. Yake, it is likely that the depth reached by the two-phase zone increases to the south. North of the S-series wells, however, the two-phase zone apparently disappears, as evidenced by lower temperatures. It is noteworthy that the "LS" caprock formation peters out to the north and east of the S-series wells.

The substantial horizontal pressure gradients found in the "ST" formation above the lake sediments imply that the average permeability of these shallow volcanic rocks is relatively low. Furthermore, the permeability of the lake sediment ("LS") formation itself which separates the cold groundwater above from the hot two-phase zone below must be exceedingly low; a simple calculation shows that the vertical permeability of this layer must be a great deal less than 0.05 millidarcy. On the other hand, the remarkable homogeneity of the deep pressure distribution is indicative of substantial horizontal communication at depth in the area south of the 800 m ASL ground surface elevation contour. Laboratory tests have been carried out on cores from all the major formations; these indicate that the small-scale matrix permeabilities of these formations are all essentially zero, so that any large-scale permeability must be due to the presence of fractures.

PRESSURE-TRANSIENT RESULTS

In 1986, a large-scale pressure-interference experiment was carried out at Sumikawa. Deep well S-4 was discharged starting on September 2 and subsequently was shut in on 16:30 on November 3; the liquid fraction of the discharge was simultaneously reinjected into nearby shallow well S-2. Four shut-in observation wells (O-5T, S-3, KY-1 and KY-2) were equipped with downhole pressure gauges of the capillary-tube type (the flowing wells were not instrumented, however). No signals attributable to the S-4 discharge were recorded in O-5T, KY-2 or S-3, but a clear and immediate response was observed in deep well KY-1, located 1.1 km north of S-4. The principal feedpoints for wells KY-1 and S-4 both lie within the deep "AA" (altered andesite) formation, below the "black shale" marine/volcanic complex and above the granodiorite "BA" formation (see Figure 3).

Maki, *et al.* (1988c) have analyzed the pressure response of well KY-1 to the S-4 discharge. These studies all involved using the linear pressure-diffusivity equation; fluid properties assumed were those of water at 250°C, and measured rock porosities and compressibilities were employed. Figure 6 shows the measured response in KY-1 to the discharge/shutin of S-4. The first step in the analysis was to try to match the measured signal using the classical line-source technique. Optimizing the line-source ("radial flow") solution yielded, for the free parameters in the analysis:

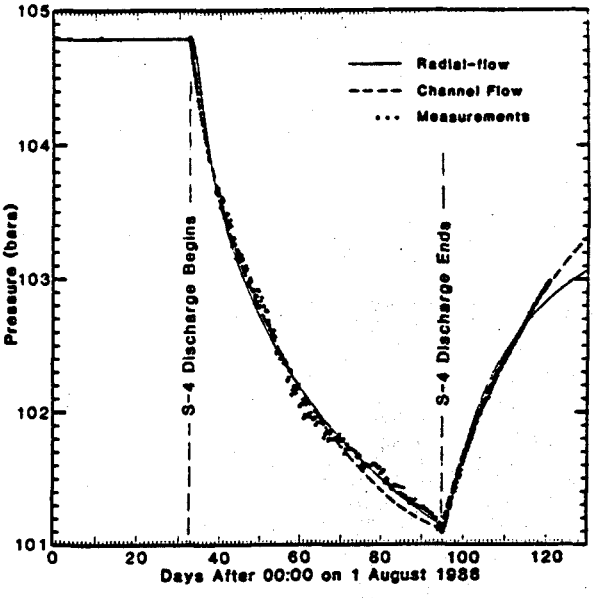

Figure 6. Pressure interference in well KY-1 due to discharge test of well S-4.

H (formation thickness) = 220 meters
kH (permeability-thickness) = 2.4 darcy-meters

providing a formation permeability of 11 millidarcies (presumably of the "AA" formation). The match of this solution to the measured response was superficially good (solid line in Figure 6), but it should be noted that the computed buildup response is in relatively poor agreement. An even more serious problem is illustrated in Figure 7 which shows only the first few days of the drawdown portion of the response on an expanded scale: clearly, the line-source radial-flow solution fails to explain the extremely rapid response to S-4 discharge observed in well KY-1.

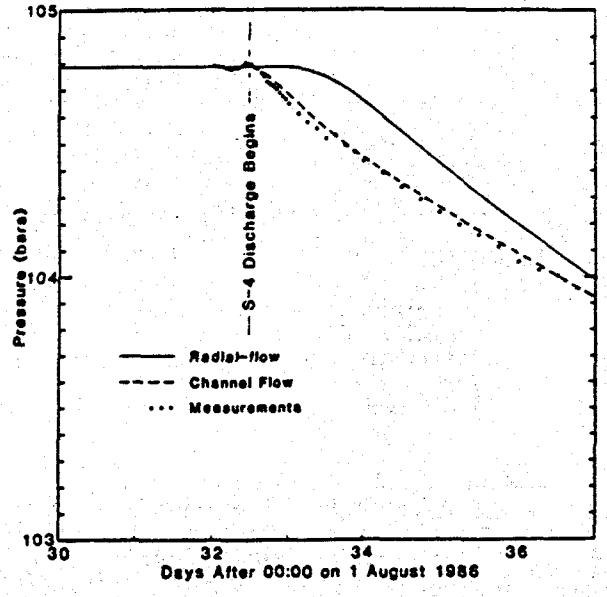

Figure 7. Early portion of response to S-4 discharge as measured in well KY-1.

Several other flow models were then employed in search of a better match with measurements – see Maki, *et al.* (1988c) for details. Finally, the following "channel-flow" representation was found. It was assumed that a permeable horizontal "channel" of constant cross-section area and constant permeability is present, oriented north-south, which contains the feedpoints of both wells (S-4 and KY-1). The east, west, upper and lower boundaries of the channel are impermeable. To the north, the channel terminates at an impermeable northern barrier; to the south, it ends at a constant-pressure boundary (representing the influence of a two-phase region). The free parameters in the model are (1) the channel cross-section area, (2) the channel permeability, (3) the distance to the northern (impermeable) boundary, and (4) the distance to the southern (constant-pressure) boundary. Minimization of the deviations between measurements and computed pressures yielded:

Cross-section	= 0.51 square kilometers
Permeability	= 195 millidarcies
Impermeable boundary position:	1.44 km north of well KY-1
Constant-pressure boundary position:	9.86 km south of S-4

Results from this model are shown in Figures 6 and 7 as the broken lines. The fit is essentially exact, in view of the noise level in the measured signal. The above parameter values, moreover, are supported by independently-obtained information. In particular, the above model suggests the presence of a reservoir boundary about 1.4 km north of well KY-1. This essentially corresponds to the location of the 800 m ASL ground elevation contour which appears to represent a reservoir boundary based on static pressure evidence (see above). Figure 3 shows a longitudinal (north-south) section through the channel, which presumably consists of the altered andesite ("AA") formation. Evidently, the "MV" black-shale layer above and the "BA" granodiorites below serve as aquitards. In the neighborhood of well S-4, the channel appears to have a vertical thickness of about 0.7 – 0.8 km, but thins somewhat to the north.

Figure 2 also shows the lateral channel boundaries. To the west, the channel is bounded by "BA" granodiorite owing to the presence of a fault (downthrown to the east) associated with the graben boundary. To the east, the boundary consists of "MV" black shale, as evidenced by drilling logs from well SN-7D. Indeed, the cross-section area of the "AA" body containing well S-4 appears to be approximately 0.5 square kilometers, in good agreement with the value obtained from the model. The only troubling implication of the model is that the southern constant-pressure boundary is located almost 10 km south of well S-4. It is very unlikely that the channel extends this far. Recall, however, that the analysis employed assumed linear single-phase fluid behavior in the channel. In reality, as noted above, it is likely that a two-phase mixture is present at depth to the south of well S-4. The resulting increase in compressibility would slow the transmission of pressure signals to the south. Approximate calculations indicate that, under these circumstances, the probable true position of the southern constant-pressure boundary (corresponding to a channel full of two-phase fluid) is only a few hundred meters south of well S-4.

The very high north-south permeability inferred for the "AA" formation (200 millidarcies) would tend to explain the apparent uniformity of pressures at depth in the Sumikawa area, and also accounts for the extremely rapid response of well KY-1 to the S-4 discharge. One proposed hypothesis is that the permeable zone really consists of a single north-south fracture which is intersected by both wells. This is unlikely, however, for two reasons. First, it is difficult to understand how the large fluid storage capacity implied by an effective channel cross section of 0.5 km^2 could be provided by a single fracture.

Furthermore, both wells were subjected to short-term cold-water injection testing after drilling. While these tests implied good permeability for well S-4, the apparent permeability for KY-1 is very low. If KY-1 intersects a large fracture (responsible for the observed pressure response), the cold-water injectivity should be good.

We believe that a different interpretation is more likely. The observed high regional permeability is probably due to a series of large parallel north-south fractures in the "AA" formation. Superimposed upon this major fracture network is a second fracture network consisting of a very large number of relatively low-permeability minor fractures which are oriented in a more or less isotropic fashion. The major fractures serve to transmit pressure signals over long distances, but the minor fractures provide pressure communication among the major fractures and between the major fractures and the wells. Evidently, while well S-4 is well-connected to the major fracture network, the coupling with KY-1 is poor – sufficient to transmit pressure signals quickly from a nearby major fracture, but insufficient to permit high fluid injection rates. Kubota (1988) notes that numerous regions of lost-circulation were encountered while drilling the southern (S-series) wells, but that farther north (where temperatures are lower) the fractures frequently appear to be sealed with vein materials. Such self-sealing would presumably act mainly to inhibit flow in the minor fracture network, and may be responsible for the poor injectivity of well KY-1.

CONCLUSIONS

The Sumikawa field is a very promising prospect for future development for electrical power generation. Consideration is now being given to the construction of a power station of ~ 50 MW capacity. In view of the large deep volume within the "AA" formation characterized by both high permeabilities and high temperatures, such a development would appear to be well within the capacity of the reservoir. Additional exploration and testing is currently being carried out at Sumikawa to further delineate the characteristics and capacity of the reservoir.

REFERENCES

Ishido, T., T. Kikuchi and M. Sugihara (1987), "The Electrokinetic Mechanism of Hydrothermal-Circulation-Related and Production-Induced Self-Potentials", *Proc. Twelfth Workshop Geothermal Reservoir Engineering*, Stanford University, pp. 285-290.

Kubota, Y. (1985), "Conceptual Model of the Northern Hachimantai-Yakeyama Area", *J. Geothermal Research Society of Japan, v. 7*, pp. 231-245 (in Japanese with English abstract).

Kubota, Y. (1988), "Natural Convection System at the Ohnuma-Sumikawa Geothermal Field, Northeast Japan", *Proc. Tenth New Zealand Geothermal Workshop* (in press).

Maki, H., T. Ishido, Y. Kubota, T. Maeda, K. Ariki and T. Nakai (1988a), "A modeling Study of the Natural State of the Sumikawa field", *Proc. International Symposium on Geothermal Energy 1988: Exploration and Development of Geothermal Resources, Kumamoto/Beppu, Japan*, pp. 148-151.

Maki, H., J. W. Pritchett, S. K. Garg and Y. Kubota (1988b), "Subsurface Pressure Distribution and the Hydrology of the Sumikawa Geothermal Field", *Proc. International Symposium on Geothermal Energy 1988: Exploration and Development of Geothermal Resources, Kumamoto/Beppu, Japan*, pp. 152-155.

Maki, H., J. W. Pritchett and S. K. Garg, (1988c), "Interpretation of a Pressure Interference Test of the Sumikawa Geothermal Field", *Proc. International Symposium on Geothermal Energy 1988: Exploration and Development of Geothermal Resources, Kumamoto/Beppu, Japan*, pp. 557-560.

PROCEEDINGS, Fourteenth Workshop on Geothermal Reservoir Engineering
Stanford University, Stanford, California, January 24-26, 1989
SGP-TR-122

THE FUZHOU GEOTHERMAL SYSTEM (P.R. CHINA): NATURAL STATE AND EXPLOITATION MODELLING STUDY OF A LOW TEMPERATURE, FRACTURE ZONE SYSTEM

M.P. Hochstein[1], S. Ehara[2], Yang Zhongke[1]

1) Geothermal Institute, University of Auckland, New Zealand
2) Dept of Mining, School of Engineering, Kyushu University, Fukuoka, Japan

ABSTRACT

A conceptual model is presented which explains the likely heat and mass transfer of the Fuzhou system in the natural and exploited state. The model was extended to 7 km depth to simulate a deep heat sweep of naturally convecting meteoric waters in a granitic crust. Convection is controlled by the high permeability (order of E-13m^2) of the fracture zone, the heatflow at the sweep base, as well as width and axial extent of the fracture zone. Recharge is controlled by a shallow, confined, highly permeable, Quaternary aquifer.

INTRODUCTION

The Fuzhou system (Fujian Province, China) has been described by *Huang and Goff (1986);* the study is based on an earlier report by *Huang (1983)*. The Fuzhou prospect is a low temperature, fracture zone system where heat is transferred by convection, involving deeply penetrating meteoric waters, from a resource base in the granitic upper crust to the surface. Thermal fluids ascend in a narrow, 100m wide, steeply dipping fracture zone in granites over a length of about 5-6 km (T ≤ 100°C at 500m depth in the fracture); the fluids are discharged into a thin (15m), extensive Quaternary (Q) aquifer at 50m depth. A vertical permeability barrier divides the system into a N- and a S-half sector. The terrain is rather flat (mean elevation 4m asl) except for higher terrain 5 to 10 km away in the N and E. A map of the prospect is shown in Fig. 1.

Little is known about fracture zone systems although they are common in SE Asia, often associated with extensive granites. The summary term "geothermal fracture zone system" has been used by *Hochstein (1988)* to classify these systems. They have some affinity with the theoretical models of *Sorey (1975)* and *Kassoy and Zebib (1978)* which demonstrate that fluid convection can occur in a narrow fracture zone which stands in a normal temperature, crustal setting.

The Fuzhou system has been exploited since about 1970 by shallow wells (Q-aquifer) and deep wells (within the fracture zone); abstraction increased continuously, reaching about 200 kg/s by 1982. Recently we obtained selected data from a report by the *Fujian Hydrogeological Team (1985)* which contains information describing the average pressure response in the Q-aquifer and average changes in temperature of produced fluids. Since the Fuzhou prospect is one of the few fracture zone systems exploited on a large scale, we used the available data to simulate likely heat and mass transfer for such a fracture zone system. Another aim of this study was to investigate the conditions under which such a system can develop.

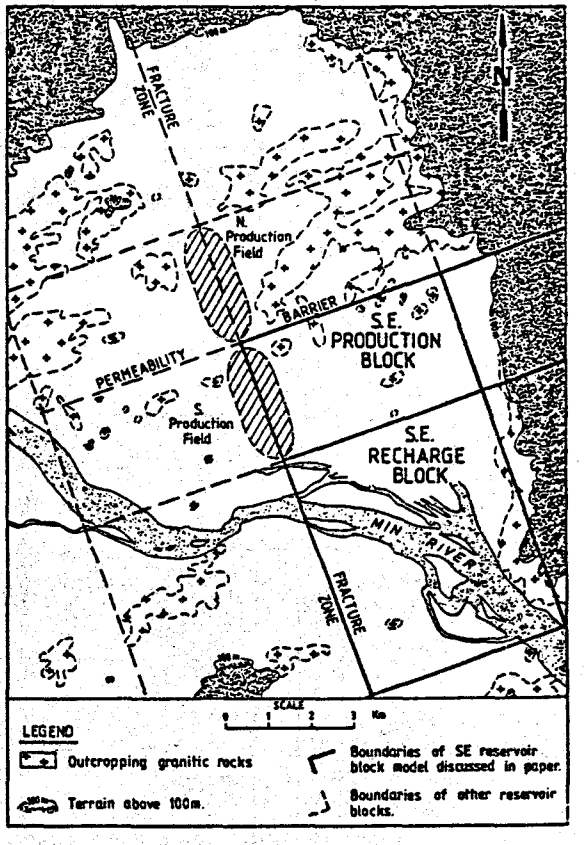

Fig. 1: Map of Fuzhou geothermal prospect. The location of the fracture zone and the ENE-trending, central, low permeability barrier are shown which were used to define quarter blocks of the model discussed in the text. Also shown is part of the SE quarter block and the SE adjacent recharge blocks (see Fig. 6).

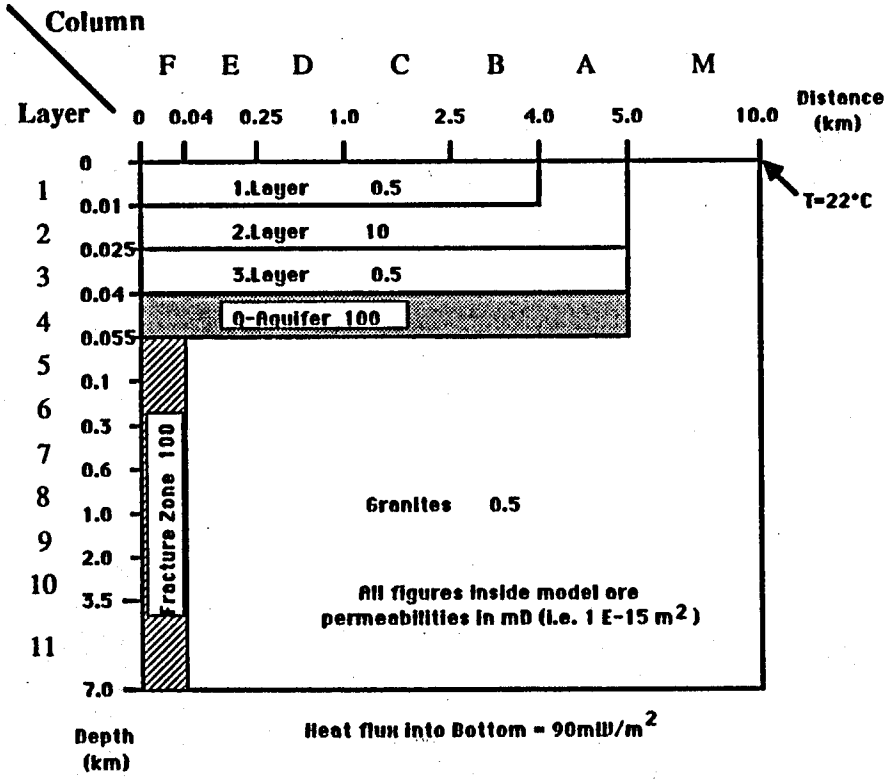

Layer	Sat.Density (10^3 kg/m^3)	Porosity	Therm.Conductivity (W/ °C m)
Surface	2.2	0.03	1
2nd Layer	2.2	0.2	1
3rd Layer	2.2	0.03	1
Q-Aquifer	2.2	0.2	1
Fracture Zone	2.6	0.1	2.5
Granites	2.6	0.01	2.5

TABLE 1: Diagram summarizing all parameters used for simulation of the natural state model described in the text.

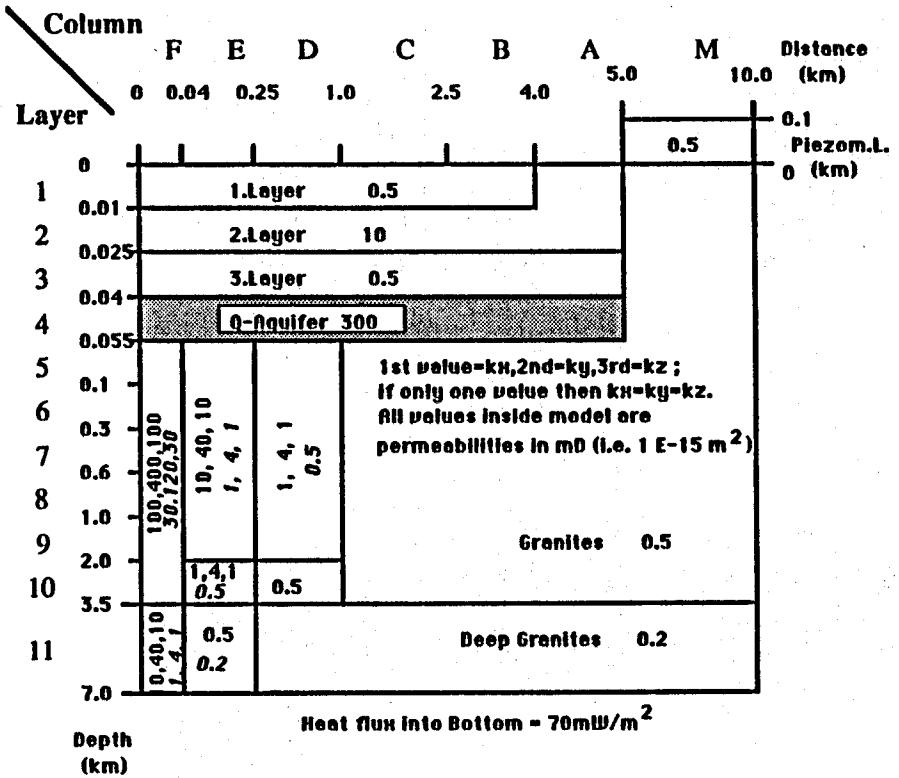

Layer	Sat.Density (10^3 kg/m^3)	Porosity	Therm.Conductivity (W/ °C m)
Surface	2.2	0.15	1.2
2nd Layer	2.2	0.2	1.3
3rd Layer	2.2	0.15	1.2
Q-Aquifer	2.2	0.2	1.3
F.Zone(F11-E9)	2.6	0.1 *(0.02, F11)*	2.5
E5-E9 (E10-D9)	2.6	0.05 *(0.02,E5-9)*	2.5
D5-D9 (D10-C10)	2.6	0.02 *(0.01,D5-11)*	2.5
Granites	2.6	0.01	2.5

TABLE 2: Diagram summarizing parameters used for simulation of the production state model described in the text. Values and comments in italics refer to the end-on recharge blocks (covering the extended fracture zone); all other values are common to recharge and production quarter block model.

NATURAL STATE MODEL (RESTRAINTS)

If one plots the temperature in the Q-aquifer versus distance from the fault trace, one finds that temperatures decrease almost exponentially (Fig. 2). The plot shows no systematic difference between data from the N and the S sector. Chloride data cited in *Huang and Goff (1986)* indicate an almost constant concentration of this constituent in the fracture zone and the Q-aquifer in each sector. This, in turn, implies that the shallow aquifer is overlain by rather impermeable sediments. As will be shown later, the T-data plotted in Fig. 2 (based on measurements in 1977) have already been affected by the production of fluids prior to 1977. Since only a small amount (a few kg/s) of hot water was discharged by springs before 1970, it can be inferred that most of the heat was lost by conduction through the shallow overburden and through the walls of the fracture zone. Using data shown in Figs. 2 and 3, these losses were estimated to be at least 5 MW, pointing to an upflow rate of $\geq$ 15 kg/s of fluids at 100 °C (at 500m depth). The mean annual temperature is about 22°C.

A plot of the temperatures in deep wells at 450m depth versus distance from the fracture zone is shown in Fig. 3; again, an exponential decrease is indicated. The effect of the dip (about 75° to the E) of the fracture zone has been eliminated by using reduced horizontal distances. For simulation, the effect of the dip was also neglected and a vertical fracture zone of equivalent width was used instead. The model was therefore reduced to one with axial symmetry, i.e. with respect to the axial plane of the fracture zone (half width model). The presence of the vertical permeability barrier perpendicular to the fracture zone (see Fig. 1), which prevents mixing of fluids across the barrier, as indicated by different mean chloride values in each sector *(Huang, 1983)*, allowed us to reduce the model further to a quarter block model.

Although the dimension of the outer part of any natural state model is not critical because of equivalence, we tried to use a realistic length for the block model. Heatflow measure-ments in granites about 10 km S of the prospect had shown anomalously low flux values (of the order of <50 mW/m^2; *Huang Shaopeng, pers. comm.)* whereas the average heatflow of the greater Fuzhou region appears to be about 80 mW/m^2 *(Wang Tianfeng et al., 1986)*. A length of 10 km and a width of 3 km was therefore adopted for the quarter block model. The thermodynamic Na/K geo-thermometer *(Giggenbach, 1986)* indicates deep equilibrium temperatures of about 150°C which prevail at the resource base. Using the observed reduced heat flow directly outside the system, the Na/K equilibrium temperature points to depths of the order of 7 km for the deepest sweep. Thus the dimensions of the quarter block model were defined.

There were some limited data which restrained the permeability structure of the natural state model. Specific yield tests of wells producing from the Q-aquifer (N sector) pointed to permeabilities of the order of 100 to 300 millidarcy (mD); the very small specific capacities of wells in granites away from the fracture zone indicated permeabilities of the order of a few mD. Although fracture permeability will be dominant in the fracture zone, data were insufficient to assess this parameter. Instead, we used an anisotropic structure limiting the vertical permeability to 100 mD since this value had been used in the theoretical study of a fracture zone by *Kassoy and Zebib (1978)*. In their model they had used a 100m wide fracture which transferred about 4.5 kg/s of fluids per km with T = 67°C at the surface in the steady state model, values similar to those observed at Fuzhou.

For simulation, a modified SHAFT 79 program *(O'Sullivan et al., 1983; Preuss and Schroeder, 1979)* was used; recharge was controlled by the vertical permeability of the top layers and by maintaining constant T and p at the free surface. To allow for granites outcropping in some inner blocks (see Fig. 1), the same low permeability (0.5 mD) was assigned to the surface layer and outcropping granites and metamorphics, which implies homogenous infiltration for the whole area.

NATURAL STATE MODEL (RESULTS)

The approximate structure of the steady state model is shown in Fig. 4. A trial and error method was used to refine the gross permeability structure of the initial model. For the simulation it was assumed that the fracture zone had been created at time t = 0, and that the temperature and pressure field was that given by an inferred undisturbed terrestrial heat flow (initially 80 mW/m^2), neglecting the heat-generating capacity of the granites between resource base and surface. The models were run until steady state conditions were reached; observed temperatures in wells and natural heat loss were used as matching parameters.

Parameters of one of the best fit models which reproduces approximately the observed data are listed in Table l; the steady state temperatures of this model are shown in Figs. 2 and 3. For this model, steady state conditions were reached after about t = 2 x 10^6 yrs. The significant cooling effects at the resource base (layer 11 in Table 1) have been described recently elsewhere *(Ehara et al., 1988)*.

Although the model listed in Table 1 reproduces the gross temperature structure of the Fuzhou Field, it is a very simple model which has various unrealistic features, namely:

1. too high heatflow at the bottom (90 mW/m^2); such high value was necessary to match the observed high temperatures in the fracture zone;
2. horizontal permeabilities are not restrained; the model does not allow for "cross-flow";
3. likely changes in permeability with depth were neglected;
4. significant permeability is not only confined to the fracture zone, but extends also outside as indicated by structural data *(Huang, 1983)* and minor productivity of deep wells standing close to the fracture zone.

Despite these limitations, simulation of steady state conditions has shown that:

natural convection in a thick crustal section of granites with an overall low permeability can be set up by the creation of a deep-reaching fracture zone; for this convection to occur, the dimensions of the block model must be finite.

REVISED MODEL ALLOWING FOR EFFECTS OF PRODUCTION

Production of hot water from the Q-aquifer in the N sector started in the mid 1960s using shallow wells (av. yield 0.5 to 2 kg/s); deep wells were drilled to intersect the fracture zone from 1970 onwards (10 of these wells have yields between 5-15 kg/s). No detailed production history is known, and flow meters were only installed in 1984; no systematic monitoring of well pressures has been undertaken except for sporadic measurement of water levels in presumably low productivity wells. From interviews and sparse data in the 1985 report of the Fujian Team we constructed idealized abstraction scenarios for equivalent quarter blocks in the N and S sector which are shown in Fig. 5; plotted also are average pressure drops in the Q-aquifer for the period 1977-1983. Only abstraction rates after 1984 are well documented.

It is obvious that, with the sparse data shown in Fig. 5, the pressure response of any realistic model cannot be fully tested, but the data provide some restraints which allowed revision of the natural state model. For this, it was assumed that the observed average pressure drop in the Q-aquifer is the mean of most of the wells shown in Fig. 2 which lie between 150 to 600m away from the fracture zone. Simulation of the pressure response was limited initially to the S sector where production comes almost entirely from the fracture zone.

Using the inferred abstraction scenario for the S sector it was found that the natural state model responded with too large pressure drops, amounting, for example, to -1.5 to -5 bars in the Q-aquifer after only 8 years production (i.e. 1970 to 1978) whereas the reported average drop in pressure was no more than about 2 bars after 13 yrs production in the S sector (about half as high as that in the N sector). Obviously, the natural state model did not allow for sufficient recharge.

A sensitivity analysis of various model parameters showed that each of the following reduced somewhat the pressure drop (in comparison with that of the natural state model):

(a) increase in permeability of Q-aquifer to about 300 mD and moderate increase in thickness of Q-aquifer;

(b) increase in permeability of granites in the blocks adjacent to the fracture zone by up to one order of magnitude;

(c) addition of two end-on recharge blocks (dimension 3 x 10 x 7 km each) allowing for some crossflow and for higher piezo-metric levels in the outermost blocks to simulate gross terrain effects.

Inclusion of (c) produced the interesting result that, by increasing the vertical permeability in the fracture zone of the outer block above a critical value, the fluid flow in the fracture zone in the "production" block (see Fig. 6) could be reversed (critical value in our case was 30 mD). The high permeability of fracture zones associated with natural convection must therefore be confined in axial direction.

None of the three changes listed above was sufficient to produce a pressure response similar to that shown in Fig. 5. All three modifications were then incorporated in the revised model shown in Fig. 6, with the additional modifications:

(d) reduction of heatflow at the bottom from 90 to 70 mW/m^2 to reduce the rather high temperatures in the fracture zone caused by (c);

(e) reduction of permeability with depth for the granites by up to half an order of magnitude; for the same reason as described in (d).

(f) slight increase in thermal conductivity of the sedimentary cover; to reduce too high temperatures in the Q-aquifer caused by (c).

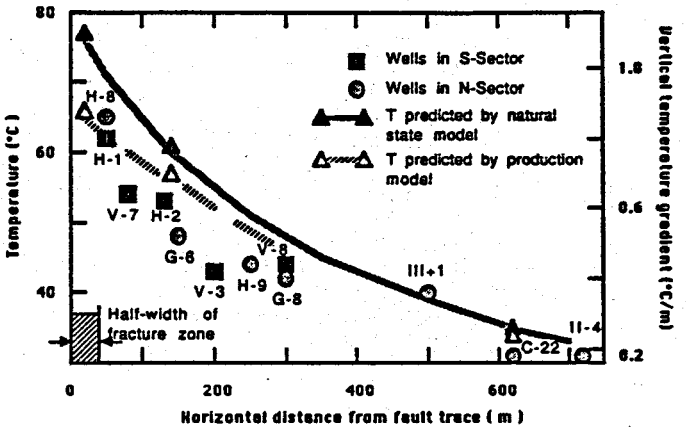

Fig. 2: Temperature in Q-aquifer (50m depth) plotted versus distance from median fault trace. Distances and temperatures were taken from *Huang (1983)*. All temperatures were measured in 1977. Also shown are theoretical temperatures of the natural state model (Table 1) and temperatures of the production model (Table 2) after 10 years production (1980) in the S sector.

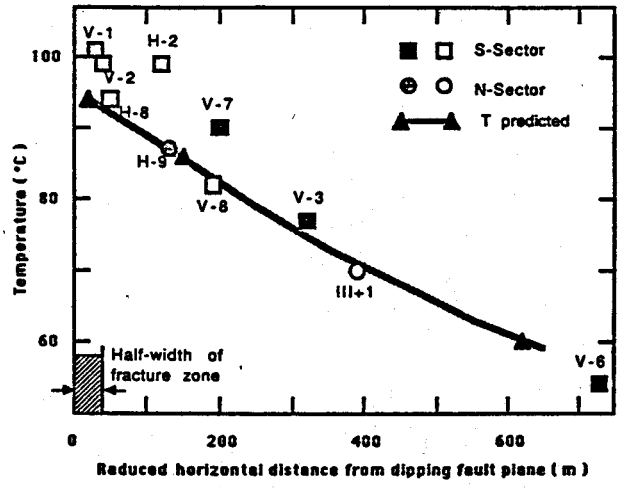

Fig. 3: Temperature at 450m depth plotted versus reduced horizontal distance (i.e. horizontal distance between well and median fault plane for a 75° E-dipping plane at 450m depth). Shown also are the temperatures predicted by the natural state and the production model which are almost the same.

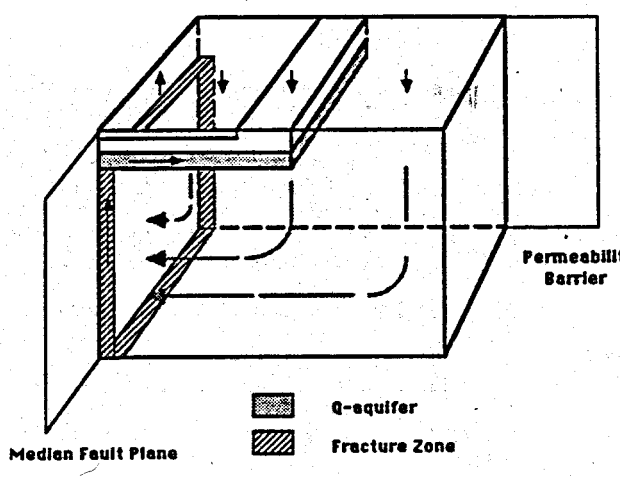

Fig. 4: Schematic diagram of natural state, quarter block model (for details, see Table 1).

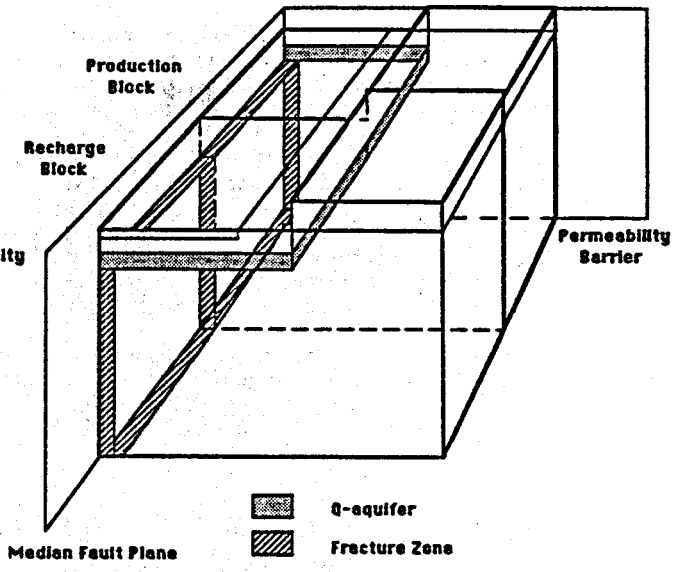

Fig. 6: Schematic diagram of production stage, quarter block model (for details, see Table 2).

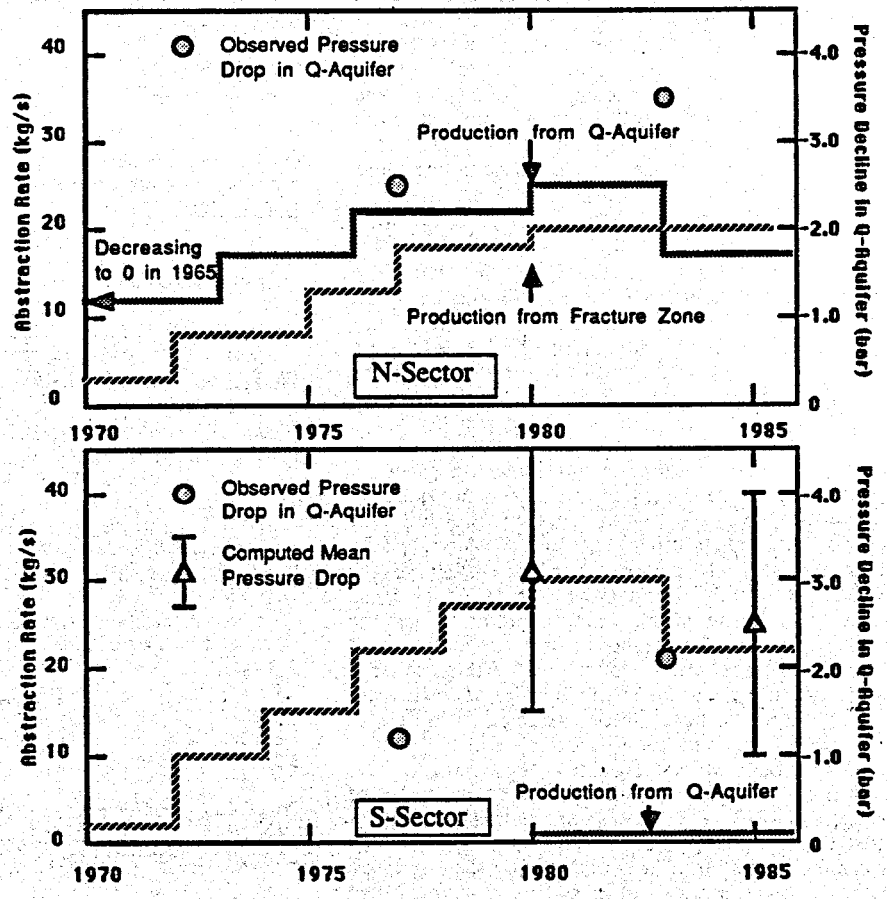

Fig. 5: Inferred production scenario (1970-1985) for quarter block models in the N and S sector of the Fuzhou field; only abstraction rates from 1984 onwards are based on measured flow rates. Also shown are observed average pressure drop in Q-aquifer between 1977 and 1983 (presumably from wells which lie between 100 and 600m away from the fracture zone) and computed mean pressure drop for 1980 and 1985 (error bars give Δp in D4 and E4 blocks).

With these modifications we obtained a production model shown in Fig. 6 (parameters listed in Table 2) which, for distances between 200 and 600m away from the fracture zone, produces pressure drops (-2.5 to -3 bars) in the Q-aquifer which are of the same order of magnitude as the observed mean value (about -2 bar). In addition, temperatures in the Q-aquifer were obtained for 1977 which are somewhat closer to the observed data than those given by the steady state model (see Fig. 2). Using the abstraction scenario of the N sector, the model also reproduces higher pressure drops as observed in Q-aquifer wells in the N sector but the computed values are significantly higher (up to 50%). Since the locality of wells for which piezometric level changes were observed are not known, further refinement of the "production" model is not justified. An interesting finding is that the temperature at the bottom of the fracture zone (block F11 in Fig. 6) is about 154°C, close to that indicated by the Na/K geothermometer.

SUMMARY

Simulation of the Fuzhou geothermal system has shown that in the presence of a deep-reaching, highly permeable fracture zone, natural convection can be established, even within rocks with low overall permeability, such as granites. For a steady state system to develop, the size of the convection cell must be finite, and the axial extent of the highly permeable fracture zone must be limited (about 3 km in the case of the Fuzhou system). High temperatures in the fracture zone can be the result of the combination of any of the following parameters: high permeability and extended width of the fracture zone, higher heatflow at the resource base, significant horizontal pressure gradient between recharge blocks and fracture zone (i.e. higher piezometric levels in the outer recharge blocks). By combining all three, we could simulate boiling point temperatures in the Q-aquifer using the "production" model shown in Table 2. This might explain why some wide fracture zone systems, like that of San Kamphaeng in Thailand *(Hochstein et al., 1987)*, can discharge hot water at boiling point at the surface in the natural state.

The study has also shown that, with respect to recharge characteristics under exploitation, the Fuzhou prospect is rather anomalous since dominant recharge is provided by a highly permeable, shallow aquifer. Analysis of the fluid flow of the "production" model indicates that about 98% of all produced fluids are recharged after 10 years of production (about 55% from Q-aquifer and 43% from upflow in the fracture zone), which explains in part the rather small pressure drop resulting from the exploitation of such a small reservoir. Since most of this recharge enters the fracture zone at the top (i.e. by downflow), a significant amount of heat can be extracted from the hot rocks inside the fracture zone. In this case, the energy potential can be obtained from a simple stored heat calculation or by using the planar fracture assessment of *Bodvarsson (1974)*. This assessment cannot be used for fracture zone systems which are not associated with a recharging shallow aquifer and which would exhibit significantly lower energy and mass flow potentials than the Fuzhou system.

ACKNOWLEDGEMENT

We would like to acknowledge the assistance of Mr Zhang Zhenguo (Ministry of Geology, Beijing) who provided selected data of the report compiled by the Fujian Hydrogeological Team. A/Prof. M.J. O'Sullivan assisted with simulation of the initial models. A/Prof. S. Ehara received the Mitsubishi New Zealand Ltd. 1987 Fellowship to undertake part of this study at the Geothermal Institute, University of Auckland.

At the proof stage we found that a map used originally for defining the width of the quarter block models contained a small scale error; the actual width is about 2.5 km instead of 3 km used here. The scale of Fig. 1, however, is correct. By proportional increase of permeability of all blocks, the same heat and mass transfer pattern can be obtained as presented in this paper.

REFERENCES

Bodvarsson , G. (1974). "Geothermal Resource energetics." Geothermics 3, 83-92.

Ehara, S., Hochstein, M.P., O'Sullivan, M.J. (1988). "Redistribution of terrestrial heat flow by deep circulating meteoric waters recharging low T geothermal systems." Proc. of Int. Symposium on Geothermal Energy, 1988, Kumamotu and Beppu (Japan), 618-621.

Fujian Hydrogeological Team (1985). "Studies of Fuzhou geothermal prospect." (Unpublished report), Fuzhou (in Chinese).

Giggenbach, W.F. (1986). "Graphical techniques for the evaluation of water/rock equilibration conditions by use of Na, K, Mg and Ca contents of discharged waters." Proc. 8th NZ Geothermal Workshop 1986 (Auckland), 37-43.

Hochstein, M.P. (1988). "Assessment and modelling of geothermal reservoirs (small utilization schemes)." Geothermics 17, 15-49.

Hochstein, M.P., O'Sullivan, M.J., Bhaddee, S. (1987). "Modelling of San Kamphaeng geothermal reservoir. Proc. 9th NZ Geothermal Workshop 1987 (Auckland), 159-162.

Huang, H.F. (1983). "Characteristics and reservoir model of the Fuzhou geothermal field, China". Geoth. Institute Report 83.08, University of Auckland (NZ), 52 pp.

Huang, H.F., Goff, F. (1986). "Hydro-geochemistry and reservoir model of Fuzhou geothermal field, China". Journal Volcanology and Geothermal Research 27, 203-227.

Kassoy, D.R., Sebib, A. (1978). "Convection fluid dynamics in a model of a fault zone in the Earth's crust." J. Fluid Mechanics 88, 769-792.

O'Sullivan, M.J., Zyvoloski, G., Blakeley, M.R. (1983). "Computer modelling of geothermal reservoirs." School of Engineering report 318, Univ. of Auckland (NZ).

Preuss, K., Schroeder, R.C. (1979). "Geothermal reservoir simulation with SHAFT 79." Proc. 5th Workshop on Geothermal Reservoir Engineering (Stanford), 183-188.

Sorey, M.L. (1975). "Numerical modelling of liquid geothermal systems." U.S. Geological Survey, Menlo Park (Calif.), Open File Report 75-613.

Wan Tianfeng, Tong, Y., Lin, S., Zheng, W. (1986). "Silica geothermometry estimates of heatflow in the Fujian Province (P.R. China)". Proc. 8th NZ Workshop 1986 (Auckland), 195-197.

PROCEEDINGS, Fourteenth Workshop on Geothermal Reservoir Engineering
Stanford University, Stanford, California, January 24-26, 1989
SGP-TR-122

MULTIDISCIPLINARY DATA SUBSTANTIATE VAPLIQ MODEL OF THE LOS AZUFRES GEOTHERMAL SYSTEM

E.R. Iglesias, V.M. Arellano, D. Nieva

Instituto de Investigaciones Eléctricas
Apartado Postal 475
Cuernavaca, Morelos 62000, México

ABSTRACT

We revise and expand our previous vapliq model of the Los Azufres hydrothermal system. We present data that delineate the vertical distributions of the formation's thermal conductivity and bulk density. Both distributions disclose a sharp change of formation properties at the boundary between the liquid-dominated layer and the steam cap. This supports the inference of our previous work that a substantial permeability contrast must exist between the liquid- and vapor-dominated layers of the system. We present the observed vertical distribution of liquid saturation in the system as inferred from the chemical composition of reservoir fluids and well logs; we use it, in addition to the pressure profile, to calibrate the model's thermophysical parameters. Calibration against both observed profiles greatly improves the reliability of the model. The new model predicts vertical permeability values of about 0.1×10^{-18} m^2 for the liquid-dominated layer and of about 80×10^{-18} m^2 for the steam cap. The low permeability of the liquid-dominated layer and the permeability contrast appear as the main reasons for the vapliq characteristic displayed by this geothermal system. In addition to the distribution of vertical permeability, the model provides estimates of the heat and mass fluxes and of the relative permeability functions of the system. The present model consistently represents a large body of multidisciplinary data.

INTRODUCTION

In previous work (Iglesias and Arellano 1988a, 1988b) we discussed vapliq hydrothermal systems and the thermohydrological conditions for their existence. (The central, upflowing part of vapliq systems is a stack with a compressed-liquid layer at the base, a liquid-dominated zone in the middle, and a vapor-dominated cap). We also presented a vapliq model of the Los Azufres system (natural state), and on its basis concluded that a substantial vertical permeability contrast must exist between the vapor- and the liquid-dominated layer, the smaller permeability corresponding to the later. Assuming a homogeneous vertical distribution of thermal conductivity we estimated permeability values and other thermohydrological parameters of the system.

Though this model was consistent with a number of observations (downhole pressures, stabilized temperatures, geothermometrical estimates, hydrother-mal alteration as deduced from drill cuttings, and the ranges of permeabi-lity and thermal conductivity found in laboratory measurements of drill cores), the reliability of the estimates remained somewhat questionable because: (a) only the observed vertical pressure profile was fitted in detail, and it is known that pressure fitting alone may be misleading if applied to standard-quality observations; (b) we knew, from theoretical calculations, that non-homogeneous thermal conductivity distributions, if applicable to Los Azufres, could require significant revisions of our estimates; and (c) no direct evidence substantiating a sudden change of formation properties at the boundary between the vapor- and liquid-dominated layers had been found at the time of our previous work.

THE MODEL

We consider a 1-D vertical, steady-state scenario, based on generally accepted conceptual models of the natural states of liquid- and vapor-dominated geothermal systems. We model only the central portion of the system where there is a net mass upflow, and where mass and heat transfer have only vertical components.

Based on our earlier results (Iglesias and Arellano 1988a, 1988b) we assume a step distribution of vertical permeabi-

lity, with the lower value corresponding to the liquid-dominated layer. At the base of the system there is hot compressed liquid that ascends isoentalpically (e.g., White, 1967). Eventually the compressed liquid reaches its boiling point and a 2-phase, liquid-dominated layer develops. This layer extends upwards until it is replaced by a vapor-dominated cap, starting at the permeability discontinuity.

The model equations are given in Iglesias and Arellano (1988a). They represent 2-phase, steady-state conservation of mass, momentum and energy, and are complemented by appropriate constitutive equations. Heat flux Q and mass flux F are constants of the system. This set of equations is numerically solved. The present numerical code allows arbitrarily varying distributions of thermal conductivity.

LIQUID SATURATION PROFILE

In-situ liquid saturations for 15 wells representative of ascending flow in the system were derived from 63 fluid samples (Table 1). A subset of these results appeared in Nieva et al. (1987).

Table 1. Sampling for liquid saturation

Well	Samples	Well	Samples
Az-5	9	Az-32	1
Az-6	8	Az-33	1
Az-9	3	Az-34	1
Az-16AD	8	Az-35	1
Az-17	9	Az-36	3
Az-19	4	Az-37	1
Az-22	5	Az-38	3
Az-28	6		

Liquid saturations were computed with a method originally devised by Giggenbach (1980) and modified by Nieva et al. (1985). This modification was necessary to apply the method to wells with high concentrations of non-condensable gases in their total discharges. Briefly, liquid saturation is computed from the seeming distortion of the relative proportions of chemical species participating in the Fischer-Tropsch reaction in the reservoir.

The method requires estimates of reservoir temperature for each well (feed zone). The required temperature estimates were obtained from cation geothermometers, temperature logs, pressure logs and 2-phase assumption, and extrapolation to zero flowrate at computed bottomhole conditions. These temperature estimates were independent from the results generated by the vapliq model described in the preceding section. This prevents circular bias. The sensitivity of the computed liquid saturation to the assumed reservoir temperature is relatively mild, e.g., a temperature error of ±5°C typically results in a 5% variation in liquid saturation.

The locations of the feed zones were obtained from records of drilling fluid losses, temperature logs, pressure logs, well completions and lithologic column records.

Figure 1 represents the resulting liquid saturation profile, and the associated uncertainties.

FORMATION PROPERTIES

As stated, previous work indicated that the vertical permeability distribution may be approximated by a step function with its discontinuity marking the location of the boundary between the liquid-dominated layer and the vapor-dominated cap. The corresponding permeability values were estimated in this work by fitting model-generated profiles to the observed pressure and liquid saturation profiles (see following section).

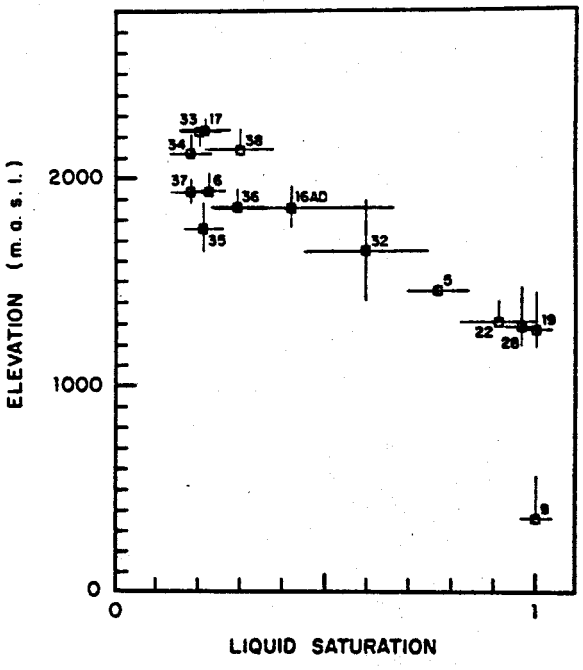

Fig. 1. Observed distribution of liquid saturation in the central, upflowing part of the system. Numbers identify wells.

Thermal conductivity was recently measured in 16 drill cores from Los Azufres (Iglesias et al., 1987; García et al., 1988). Figure 2 presents these results in terms of elevation. We discern two distinct trends in the data. The elevation of the boundary between both trends is strikingly coincident with that at which the liquid-dominated layer turns into the vapor-dominated cap, as attested by the observed pressure profile (Fig. 3). The upper trend of Fig.2 has a linear correlation coefficient r=-0.7988, with a confidence level (CL) greater than 99.5%. For the lower trend the corresponding figures are r=-0.8617, CL>99.5%. Note that the discontinuity in thermal conductivity is clearly observable in well Az-3 (cores 3-1, 3-4 and 3-5) and in well Az-26 (cores 26-2 and 26-3).

The percentage of total hydrothermal alteration of 20 drill cores from Los Azufres, which include the cores of the preceding paragraph, were also determined recently (Iglesias et al., 1987). The hydrothermal alteration of the cores lying in the vapor-dominated layer correlates well (r=-0.8075, CL>99.5%) with elevation, as illustrated in Fig. 4. No significant correlation of total alteration with elevation was found for the cores in the liquid-dominated zone.

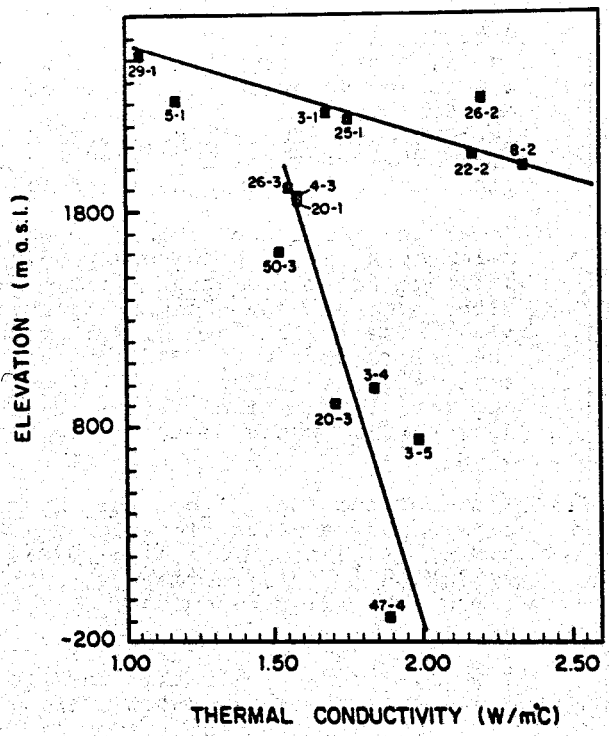

Fig. 2. Vertical distribution of thermal conductivity, from drill cores.

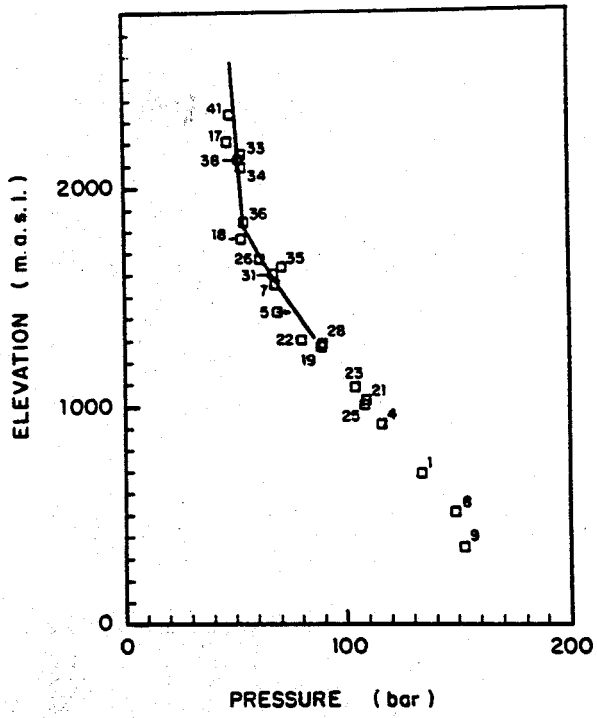

Fig. 3. Fit to the observed distribution of pressure in the central, upflowing part of the system. Numbers identify wells.

Coincidently, thermal conductivity correlates well (r=0.9917, CL>99.5%) with total hydrothermal alteration in the vapor-dominated cap (Fig. 5), and no significant correlation was found between these variables in the liquid-dominated layer.

Bulk density was measured in the same 20 drill cores (Iglesias et al., 1987). The corresponding results are plotted against elevation in Fig. 6. Two trends are also discernible in these data. In the vapor-dominated layer, bulk density correlates linearly with elevation (r=-0.6452) with a CL>98.64%. A stronger correlation (r=-0.8654, CL>99.98%) between these variables is found in the liquid-dominated zone.

These results clearly substantiate the notion that a sharp change in formation properties exists at the boundary between the liquid- and the vapor-dominated layers in Los Azufres, whatever its cause. The postulated vertical permeability contrast is consistent with such change.

MODEL RESULTS AND DISCUSSION

The thermohydrological conditions of the system were obtained by trial and error (e.g., Iglesias and Arellano,

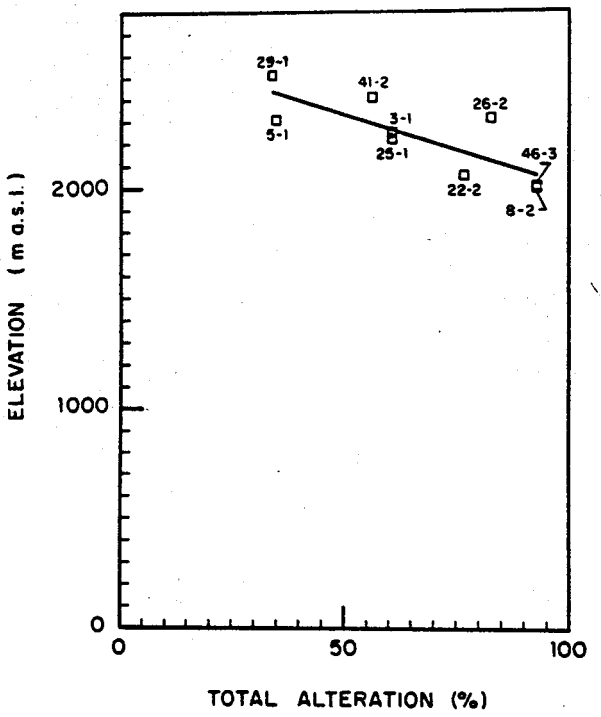

Fig. 4. Total hydrothermal alteration in the vapor-dominated layer. Numbers identify (well)-(core number).

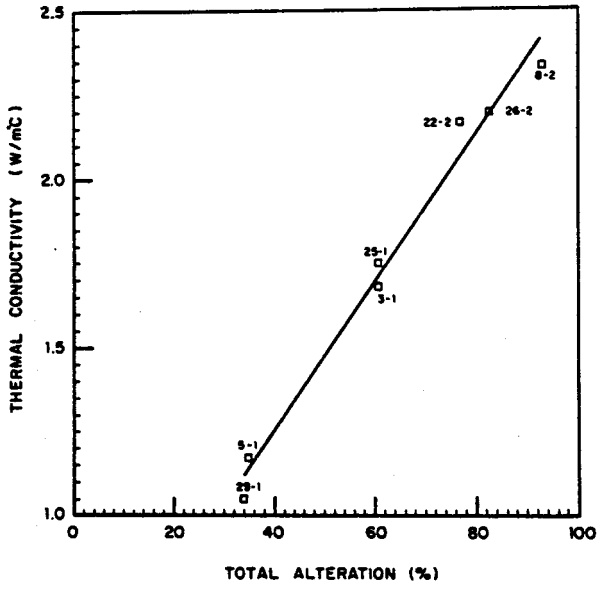

Fig. 5. Correlation between thermal conductivity and total hydrothermal alteration in the vapor-dominated layer. Numbers identify (well)-(core number).

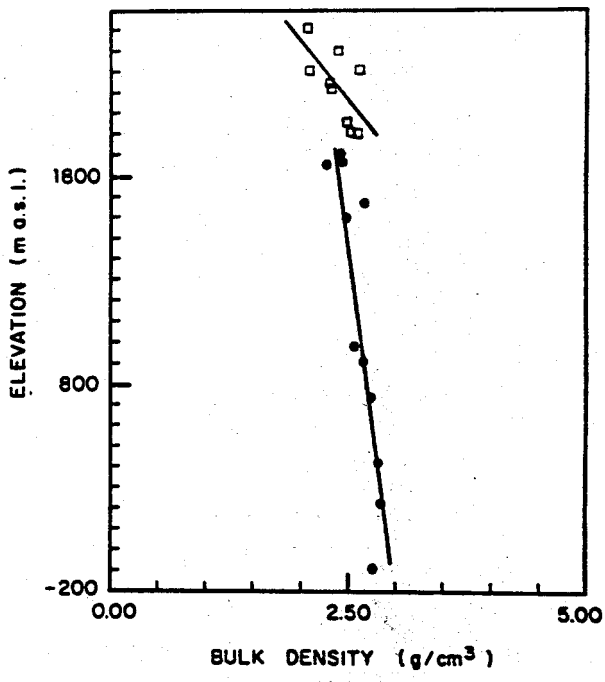

Fig. 6. Vertical distribution of bulk density, from dill cores.

1988a, 1988b), by matching model profiles to the observed pressure (Fig. 3) and liquid saturation (Fig. 1) profiles. The main parameters thus estimated are Q, the net (vertical) heat flux; F, the net (vertical) mass flux; k(z), the distribution of vertical permeability in terms of altitude z; k_L and k_V, the liquid and vapor relative permeabilities; S_{LR} and S_{VR}, the liquid and vapor irreducible saturations; and p(z) and S(z), the pressure and liquid saturation vertical profiles, respectively.

In this model we take as known input parameters p_B, the pressure at the boiling point of the system; z_B, the elevation of the boiling point; and K(z), the vertical distribution of thermal conductivity. The input parameters also include trial values of Q, and trial functions k(z), and $k_L(S)$ and $k_V(S)$, where S is liquid saturation.

The boiling point of the system is p_B=8.6 MPa, and its elevation z_B=1300 m a.s.l. (Iglesias et al., 1985). The variation of thermal conductivity along the liquid-dominated layer is small (Fig. 2). Thus a simple model is to set K=constant in the liquid-dominated layer, and K linearly varying with z, in the vapor-dominated cap, as in Fig. 2. Trial values for Q, k_{down} and k_{up} (the values of k(z) in the liquid- and vapor-dominated layers respective-

ly) were suggested by our previous work (Iglesias and Arellano, 1988a; 1988b). For the relative permeability functions we tried Corey- and X-type curves; only X-type curves resulted in reasonable matches of the observed pressure and liquid saturation profiles.

Our best match for the model of the preceding paragraph is shown in Figs. 3 and 7. The corresponding model parameters are $Q=0.1$ Wm^{-2}, $F=0.4$ kgm^{-2}s^{-1}, $k_{down}=1.0\times10^{-19}$ m^2, $k_{up}=0.8\times10^{-16}$ m^2, $K_{down}=1.6$ Wm^{-1}°C^{-1}, K_{up}=variable, $S_{LR}=0.20$, $S_{VR}=0.00$. The match to the pressure profile is excellent. The match to the liquid saturation profile looks promising but not quite satisfactory: the synthetic profile seems too low in the liquid-dominated layer. Despite this, it is interesting to note that the position of the nearly vertical line matching the liquid saturation of the vapor-dominated layer is totally determined by the value assigned to S_{LR}: lower (higher) values of this parameter shift the nearly vertical line to the left (right). Thus, we interpret the approximately constant observed liquid saturation of the steam cap as resulting mainly from the formation's irreducible liquid saturation. The value indicated for Q is consistent with that inferred from stabilized temperatures in the caprock (Iglesias et al., 1988a, 1988b). The small value obtained for F is qualitatively consistent with the mild (as compared with other geothermal fields) surface manifestations, which consist exclusively of fumaroles.

An improved match to the liquid saturation profile is presented in Fig. 8; the corresponding pressure results are indistinguishable from those of Fig. 3. This match was obtained using the same model parameters as before, except that K_{down} was allowed to vary as in Fig. 2. The reason for the improvement can be understood with the help of Fig. 9. The (constant) heat flux is the sum of a conductive and a convective component. Heat flow is overwhelmingly conductive in the liquid-dominated layer, due to its small permeability. Thus, even small variations of thermal conductivity (and therefore of the conductive flux) in this layer, translate in greater relative changes of the convective flux, which is mediated by liquid saturation via the relative permeability functions.

The present results confirm, refine and enlarge those of our previous work. The present model is consistent with a large body of multidisciplinary evidence, including pressure, temperature and

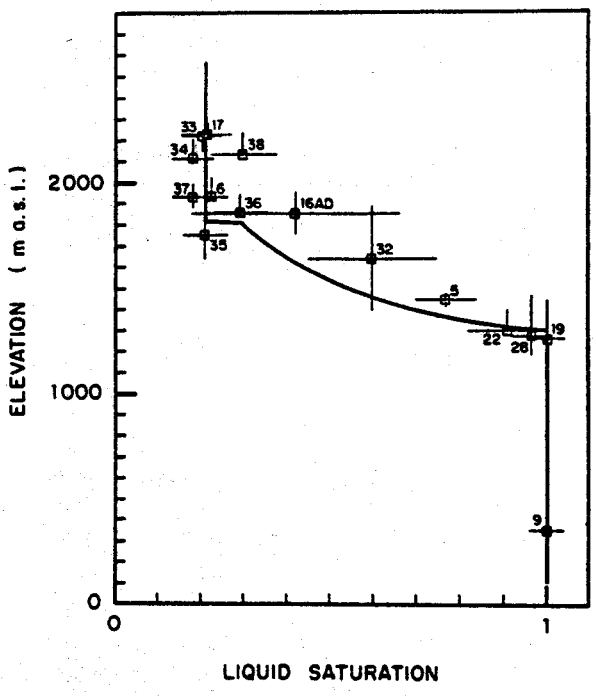

Fig. 7. Fit to the observed distribution of liquid saturation, taking $K_{down}=1.6$ Wm^{-1}°C^{-1}.

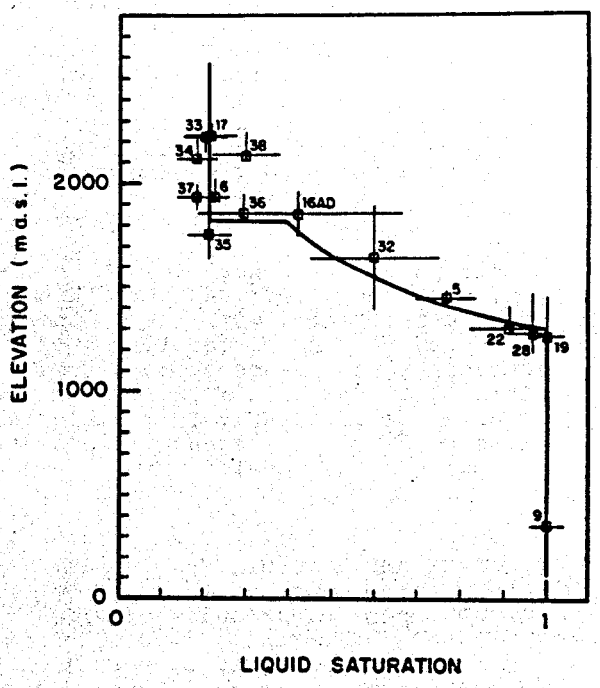

Fig. 8. Improved fit to S_L; K_{down} was allowed to vary as in Fig. 2.

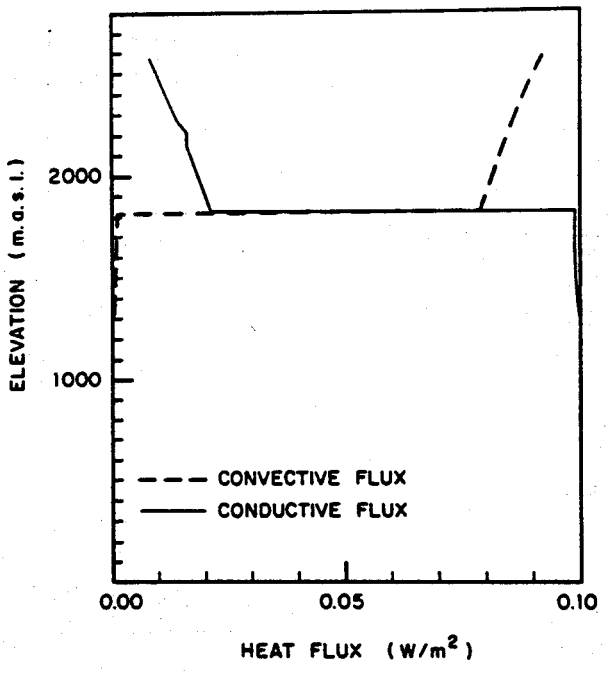

Fig. 9. Conductive and convective components of the heat flux.

drilling logs (used to define the observed pressure and liquid saturation profiles), stabilized temperatures, discharge enthalpies, chemical composition of total discharges (via the inferred liquid saturations), cation geothermometers, hydrothermal alteration as deduced from drill cuttings and cores [e.g., correlations of total hydrothermal alteration with thermal conductivity and with elevation; consistency of the 3-D distribution of calcite deposition with the inferred 2-phase layers (Iglesias et al., 1986a)], and measurements of formation density and thermal conductivity in drill cores (this paper). Furthermore, the permeability values predicted by this model are consistent with the laboratory measured matrix permeability of drill cores which ranges from less than 2×10^{-18} m^2 to about 400×10^{-18} m^2 (Iglesias et al., 1986b). This ample multidisciplinary consistency lends strong support to the model.

SUMMARY AND CONCLUSIONS

This paper contributes previously unpublished vertical distributions of thermal conductivity, formation bulk density, and observed liquid saturation, for the central, upwelling zone of the Los Azufres geothermal system. These contributions were used to refine a previous model of the system.

The present model is strongly supported by ample multidisciplinary evidence.

The observed vertical distributions of formation properties, pressure and liquid saturation, and the model results, consistently indicate the existence of a sharp change in formation properties at the boundary between the liquid-dominated layer and the vapor-dominated cap. Our model predicts vertical permeability values of about 0.1×10^{-18} m^2 for the liquid-dominated layer and of about 80×10^{-18} m^2 for the steam cap. The low permeability of the liquid-dominated layer and the existence of the inferred permeability contrast appear as the main reasons for the vapliq characteristic displayed by this geothermal system.

The model also indicates that the observed liquid saturation in the steam cap, S_L~0.2, reflects the formation's irreducible liquid saturation S_{LR}. The model furthermore indicates X-type relative permeability functions and S_{VR}~0.

REFERENCES

García A., Contreras E., Iglesias E.R., Domínguez B. (1988) Developments in geothermal energy in Mexico - Part Seventeen. Thermal conductivity of drill cores from the Los Azufres geothermal field: Experimental results and accurate prediction method, Heat Recovery Systems & CHP, vol. 8, No.4, pp.289-297.

Giggenbach W.F. (1980) Geothermal gas equilibria, Geochim. Cosmochim. Acta vol. 44, pp. 2021-2032.

Iglesias E.R., Arellano V.M., Garfias A., Miranda C., Aragón A. (1985) A one-dimensional vertical model of the Los Azufres, México, geothermal reservoir in its natural state, Geothermal Resources Council Transactions vol. 9, part II, pp. 331-336.

Iglesias E.R., Arellano V.M., Ortiz-Ramírez J. (1986a) Natural vertical flow in the Los Azufres, México, geothermal reservoir, Proc. 11th Stanford Workshop on Geothermal Reservoir Engineering, pp. 237-243.

Iglesias E.R., Contreras E. and García A. (1986b), Caracterización de propiedades físicas índice de 20 núcleos de perforación del campo geotérmico de Los Azufres, Report IIE/11/2014/I 02/P, Instituto de Investigaciones Eléctricas.

Iglesias E.R., Contreras E. and García A. (1987) Propiedades físicas de andesitas del campo geotérmico de Los Azufres, Report IIE/11/2014/I 03/F, Instituto de Investigaciones Eléctricas.

Iglesias E.R. and Arellano V.M. (1988-a), Vapliq hydrothermal systems, and the vertical permeability of Los Azufres, México, geothermal reservoir, Proc. 13th Stanford Workshop Geothermal Reservoir Engineering, pp.125-131.

Iglesias E.R. and Arellano V.M. (1988-b), Los Azufres, México, the prototype "vapliq" geothermal system, Proc. JIGASTOCK 88, Vol. 2 pp. 805-812.

Nieva D., González J., Garfias A. (1985), Evidence of two extreme flow regimes operating in the production zone of different wells from Los Azufres, Proc. 10th Stanford Workshop Geothermal Reservoir Engineering, pp.233-240.

Nieva D., Verma M.P., Santoyo E., Barragán R.M., Portugal E., Ortiz J., Quijano J.L. (1987), Estructura hidrológica del Yacimiento de Los Azufres, Proc. International Symposium on Development and Exploitation of Geothermal Resources, pp. 202-213, Instituto de Investigaciones Eléctricas/Commission of European Communities.

White D.E. (1967), Some principles of geyser activity, mainly from Steamboat Springs, Nevada, Am. J. Sci. vol 265, pp. 641-684.

PROCEEDINGS, Fourteenth Workshop on Geothermal Reservoir Engineering
Stanford University, Stanford, California, January 24-26, 1989
SGP-TR-122

FLUID CHEMISTRY AND HYDROLOGY OF THE HEBER GEOTHERMAL SYSTEM, CALIFORNIA

M.C. Adams(1), M. Lemieux(1), J.N. Moore(1), and S.D. Johnson(2)

1 University of Utah Research Institute, Salt Lake City, UT
2 Chevron Resources Company, San Ramon, CA

ABSTRACT

This paper presents the results of chemical and isotopic analyses of geothermal fluids and microthermometric measurements on fluid inclusions from the Heber geothermal system. The chemical analyses indicate that the reservoir fluids have salinities near 15000 ppm total dissolved solids and low gas contents. Small but consistent differences in the concentrations of total CO_2, B, Li, O-18, and deuterium are found between the fluids that feed the two power plants. These differences may be due to divergent paths of the thermal fluids as they flow from the south.

Fluid inclusion homogenization temperatures are similar to the present temperatures in a gradient well near the zone of upflow but are generally lower in the other two wells studied. Salinities determined from the freezing measurements suggest that the fluids contained within the inclusions are mixtures of the production fluids and other lower-salinity waters.

INTRODUCTION

The Salton Trough of southern California and Mexico is a major geothermal province hosting over a dozen separate thermal systems. With the exception of the geothermal system at Cerro Prieto (see, for example, Truesdell et al., 1981) few data have been published on the chemistry of the reservoir fluids that characterize this province. In this paper we present chemical and thermal data from the Heber geothermal system. These data were obtained from chemical analyses collected from production wells during 1987 and from microthermometric measurements on fluid inclusions contained within secondary calcite.

The Heber geothermal system is located 7 km north of the Mexico-U.S. border. The field currently has an installed capacity of 119 MW from a 52 MW dual flash plant (eastern production island) and a 67 MW binary plant (western production island). The location of the wells sampled in this study and the temperatures at a depth of 1830 m are shown in Figure 1. Based on the thermal data, James et al. (1987) concluded that an upwelling center is located near GTW 6, which has a bottom hole temperature of 199°C. They also concluded that fluid flow is to the north, towards the producing wells.

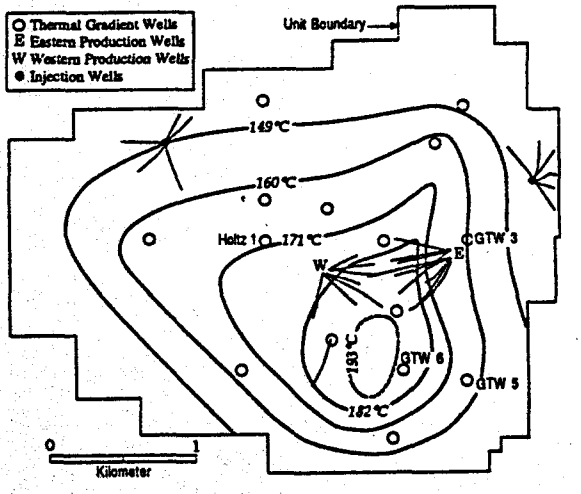

Figure 1. Location map of production, injection, and thermal gradient wells in the Heber geothermal field. Isotherms at a depth of 1830 m are also shown. Figure modified from James et al. (1987).

The geology and reservoir characteristics of the field have been described by Tansev and Wasserman (1978), Lippmann and Bovardsson (1985), and James et al. (1987). According to James et al. (1987), the geothermal system can be divided into three permeability units. These include the capping clays from 150 to 550 m, high matrix permeability sandstones from 550 to 1700 m, and permeable northwest- and northeast-trending fracture zones below 1700 m.

FLUID CHEMISTRY

Fluids from the eastern wells were sampled during August and December, 1987. The fluids were sampled primarily from sample ports on top of

the flow-lines within ten feet of the wellhead. Although flow in these wells is two-phase, the phases were found to be stratified at the position of the ports. Stratification was confirmed by the chloride content and pH of fluids taken during vertical traverses through the pipe with a sampling probe. The liquid samples were taken with the vertical probe near the bottom of horizontal flowlines, where the chloride contents and pH were highest. The gas samples were taken directly from the top port using a mini-cyclone separator. Chemical analyses of the steam condensates consistently showed less than a few ppm of Cl, indicating that good separations of brine and steam were achieved.

Fluids from the western production island were sampled during eight-hour flow tests in December, 1987. Samples were taken every two hours from the weirbox and also at the end of each test period using a mini-cyclone separator.

The chemical compositions of the fluids prior to boiling were reconstructed from the gas and liquid analyses using steam fraction values derived from measured downhole temperatures (eastern wells) or wellhead temperatures (western wells). The recombined analyses are shown in Table 1. Examination of Table 1 shows that while the concentrations of Na, K, and Cl in all of the fluids sampled are very similar, concentrations of SO_4, the minor elements, total CO_2, O-18, and deuterium display small but consistent differences between the two production islands.

The differences in the concentrations of the minor elements between the two production islands, particularly with respect to B, Li, and the stable isotopes, indicate that the western fluid has mixed with a small amount of lower-temperature fluid (see Table 1 and Fig. 2). In general, low temperature fluids exhibit lower B and Li, and lower isotope values.

Figures 3a and 3b show the variation of SO_4 and total CO_2 with respect to Ca. Because calcite scaling results in a loss of one mole of total CO_2 per mole of Ca, total CO_2 is plotted to preserve the relationship between these components. It can be seen that Ca varies directly with SO_4, but inversely with total CO_2. For a fluid in equilibrium with anhydrite and calcite, Ca, SO_4, and total CO_2 will increase as the temperature of the fluid decreases. The positive correlation of Ca with SO_4 and the higher concentrations of these elements in the western fluids suggest that the western fluids have equilibrated with anhydrite at a slightly lower temperature than the eastern fluids.

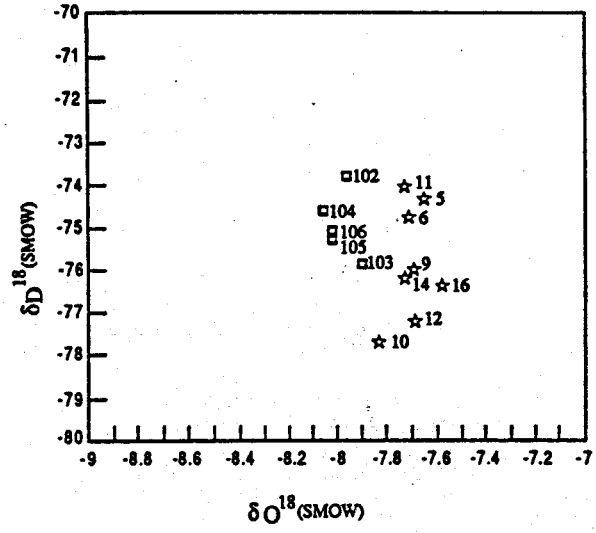

Figure 2. Isotopic compositions of the Heber geothermal fluids. The compositions are corrected for steam loss. The meteoric water line is to the left of the Heber compositions. Wells feeding the eastern production island are shown with stars and those feeding the western production island are shown with squares.

The inverse correlation between Ca and total CO_2 implies a mass-action relationship, where an increase in total CO_2 results in a decrease in Ca. As shown in Figure 3b, this relationship is well defined for the eastern fluids. The inverse correlation between these species thus implies that the elevated levels of CO_2 found in the eastern fluids resulted from either the addition of CO_2 or mixing with a CO_2-enriched fluid.

The differences in chemistry between the eastern and western fluids cannot be attributed to the depth of production because the wells all draw from similar depths. However, the wells do produce from different portions of the field. Figure 1 shows that the thermal contours at 1829 m are elongated along the fault that intersects the eastern wells. Thus the thermal fluid traveling northward from the vicinity of GTW 6 may diverge physically and chemically prior to reaching the western and eastern wells.

TABLE 1. Preflash chemical compositions of fluids from the Heber geothermal field. Chemical concentrations are in parts per million, isotopic concentrations are in per mil, and geothermometer temperatures (Fournier and Truesdell,1973; Fournier, 1981) are in degrees C. NA = not analyzed and AC = air contamination. Gas analyses were performed by Thermochem, Inc., chemical analyses by UURI, and isotopic analyses by SMU. Alk. = total alkalinity as HCO3.

WELL	DATE	Na	K	Ca	Mg	SiO2	B	Li	Sr	Ba
5	Dec-87	4019	333	750	1.76	237	4.12	6.64	40.6	4.39
6	Dec-87	4034	340	747	2.12	224	4.12	6.62	40.3	4.19
9	Dec-87	4060	332	717	2.05	243	4.17	6.75	41.1	4.64
10	Aug-87	4012	342	686	1.96	230	4.02	6.57	39.8	4.05
11	Dec-87	4242	354	655	2.81	221	4.25	6.92	45.4	4.22
12	Dec-87	4261	349	736	2.42	232	4.35	7.17	42.7	4.42
13	Aug-87	4140	324	565	2.31	275	4.83	7.89	45.2	4.98
14	Dec-87	4091	327	687	2.72	210	4.30	6.91	42.6	4.20
16	Dec-87	4147	317	617	3.42	207	4.82	7.90	46.0	4.73
101	Dec-87	3967	366	836	2.72	207	3.75	6.04	36.9	4.16
102	Dec-87	3925	347	816	1.83	208	3.64	5.67	35.7	3.83
103	Dec-87	3766	303	843	1.77	220	3.41	5.30	37.7	3.55
104	Dec-87	3840	338	810	1.79	206	3.60	5.53	35.5	3.78
105	Dec-87	3683	333	830	1.88	212	3.47	5.38	34.0	3.77
106	Dec-87	3907	359	794	1.60	212	3.67	5.84	35.3	3.95
107	Dec-87	3746	281	985	1.54	233	3.15	4.31	35.1	3.55
108	Dec-87	3908	329	839	1.19	249	3.59	5.47	36.6	4.30
110	Aug-87	3792	318	709	2.28	248	3.56	5.21	32.3	4.04

WELL	NH4	ALK.	Cl	F	SO4	TDS	Qtz Geoth.	Na-K-Ca Geoth.	Liq. Fract.	Steam Fract.
5	5.66	30.6	7758	2.04	65.9	13243	192	195	0.93	0.07
6	5.67	31.6	7738	2.79	63.2	13226	188	196	0.93	0.07
9	5.67	30.2	7815	2.01	64.0	13312	194	195	0.91	0.09
10	5.53	30.4	7746	2.30	73.7	13136	179	198	0.92	0.08
11	6.10	30.1	7835	1.82	62.9	13410	187	198	0.91	0.09
12	5.70	30.4	7866	2.02	64.4	13591	190	196	0.92	0.08
13	6.98	30.0	7625	3.49	59.7	13299	203	196	0.92	0.08
14	5.89	31.3	7801	2.03	59.9	13260	183	194	0.92	0.08
16	7.15	33.9	7758	2.20	55.0	13195	182	193	0.92	0.08
101	3.51	28.2	8105	2.22	77.8	13632	182	200	0.86	0.10
102	4.78	31.6	7667	2.16	74.0	13111	183	198	0.90	0.10
103	4.35	29.9	7429	2.17	83.4	12717	186	191	0.91	0.11
104	4.66	29.6	7571	2.15	74.5	12911	182	197	0.90	0.10
105	4.39	29.6	7598	2.06	71.7	12796	184	198	0.90	0.11
106	4.99	28.1	7673	2.63	66.2	13083	184	200	0.91	0.09
107	3.61	20.9	7318	4.10	100.0	12727	191	186	0.86	0.09
108	3.11	22.7	7871	2.69	73.9	13338	195	195	0.84	NA
110	3.78	57.1	7727	2.52	84.7	12960	193	197	0.84	NA

WELL	Delta O-18	Delta D	CO2	H2S	NH3	Ar	N2	CH4	H2
5	-7.65	-74.3	186	1.35	2.65	0.364	15.3	3.00	0.01368
6	-7.71	-74.7	197	1.47	2.76	0.381	14.1	2.72	0.00749
9	-7.69	-76.0	217	1.50	3.25	0.360	15.9	3.10	0.01677
10	-7.83	-77.7	207	1.70	2.92	0.359	14.9	2.80	0.01066
11	-7.73	-74.1	251	1.33	3.65	AC	AC	3.47	0.03213
12	-7.69	-77.2	212	1.30	3.16	AC	AC	3.33	0.01040
13	-7.69	-75.5	189	0.84	4.15	AC	AC	2.44	0.01911
14	-7.72	-76.2	238	1.11	3.16	0.453	17.4	3.65	0.02007
16	-7.59	-76.4	304	0.86	4.02	0.514	19.8	5.22	0.01992
101	NA	NA	230	2.27	2.63	0.576	21.6	3.31	0.06540
102	-7.96	-73.8	163	1.75	2.39	0.447	17.9	2.52	0.06311
103	-7.90	-75.7	127	1.11	2.14	0.369	14.6	2.23	0.03647
104	-8.06	-74.6	179	1.91	2.39	0.284	20.9	2.79	0.08621
105	-8.02	-75.3	163	1.34	2.63	AC	AC	2.82	0.02340
106	-8.02	-75.1	167	1.70	2.54	0.416	16.4	2.33	0.03301
107	NA	NA	145	1.35	1.81	0.497	19.2	2.05	0.10656

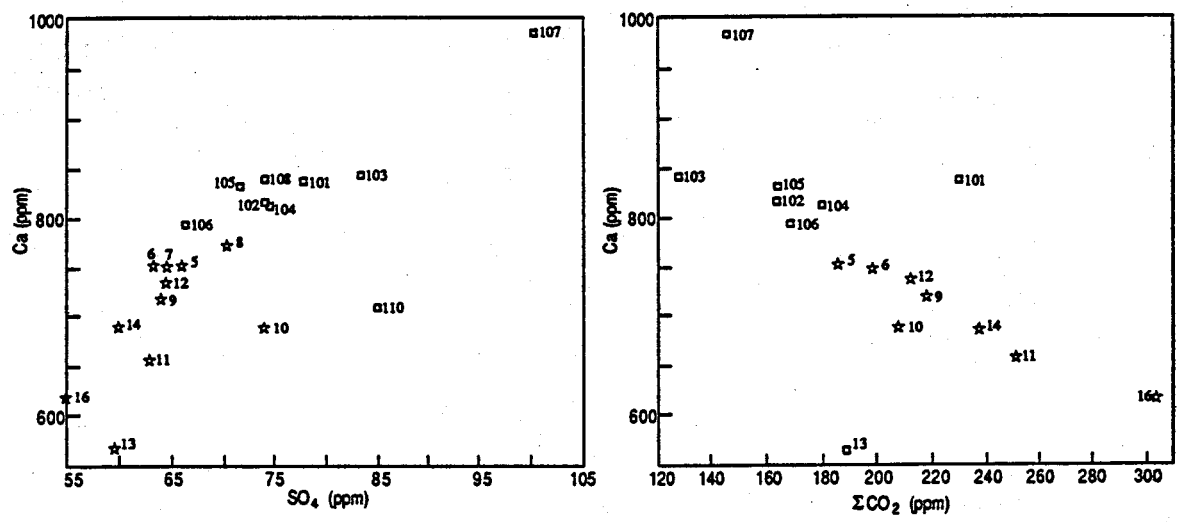

Figure 3. Variation of SO_4 and total CO_2 (HCO_3 + CO_2 in Table 1) with Ca in the Heber geothermal fluids. Note that the eastern production wells precipitate calcite in the wellbore. For an explanation of symbols see figure 2.

FLUID INCLUSION RESULTS

Calcite veins were sampled for fluid inclusions from wells GTW 3, GTW 5, and GTW 6 (Fig. 1). Veins ranging up to 2 mm in thickness are common within the shales below depths of 760 m in these wells.

All the fluid inclusions examined in this study were liquid-rich and contained a small vapor bubble that occupied about 15% of the inclusion volume at room temperature. Most of the inclusions studied are secondary or psuedosecondary, occurring along short, healed fractures within the interiors of the crystals.

Fluid inclusion heating and freezing measurements were made using a Fluid Inc. heating/freezing system. All measurements were made in duplicate. Replicate measurements were within 0.2°C. Most of the inclusions had maximum dimensions in the range of 2 to 15 microns. No evidence of a gas phase other than water or of daughter minerals were found in any of the inclusions.

The homogenization temperatures of the fluid inclusions from the three wells are plotted against depth in Figures 4a through 4c. For comparison, the measured downhole temperatures are also shown. Figures 4b and 4c show that the homogenization temperatures of inclusions in wells GTW 5 and 6 are similar and range from 130° to 202°C. Higher temperatures, reaching 244°C are recorded in fluid inclusions from GTW 3.

In many of the calcite crystals examined, two or three distinct generations of inclusions can be distinguished on the basis of their homogenization temperatures. For example, at 1820 m in GTW 5, three distinct generations are present. These are defined by homogenization temperatures ranging from 135°-140°C, 160°-165°C and 180°C. However, no cross-cutting relationships were observed which could be used to establish the relative ages of the different sets of inclusions. Browne (1977) also recognized two distinct thermal episodes in his study of Holtz 1 (refer to Fig. 1 for location).

Ice-melting temperatures range from -0.3° to -0.7°C in GTW 3, 0.0° to -0.8°C in GTW 5, and 0.0° to-0.6°C in GTW 6. For reference a freezing point depression of 0.8°C corresponds to a salinity of 1.4 equivalent weight percent NaCl (Potter et. al., 1978). No systematic differences in ice-melting temperatures were apparent with respect to depth or homogenization temperature.

Evidence for the formation of CO_2 clathrate during freezing was observed in inclusions from a depth of 1072 m in GTW 3. These inclusions displayed melting temperatures of +0.6°C, and initial freezing temperatures near -30°C. No other examples of CO_2-enriched fluids were observed.

DISCUSSION

The results of our chemical and fluid inclusion studies can be combined with the geologic studies of James et al. (1987) and the modeling study of Lippmann and Bovardsson

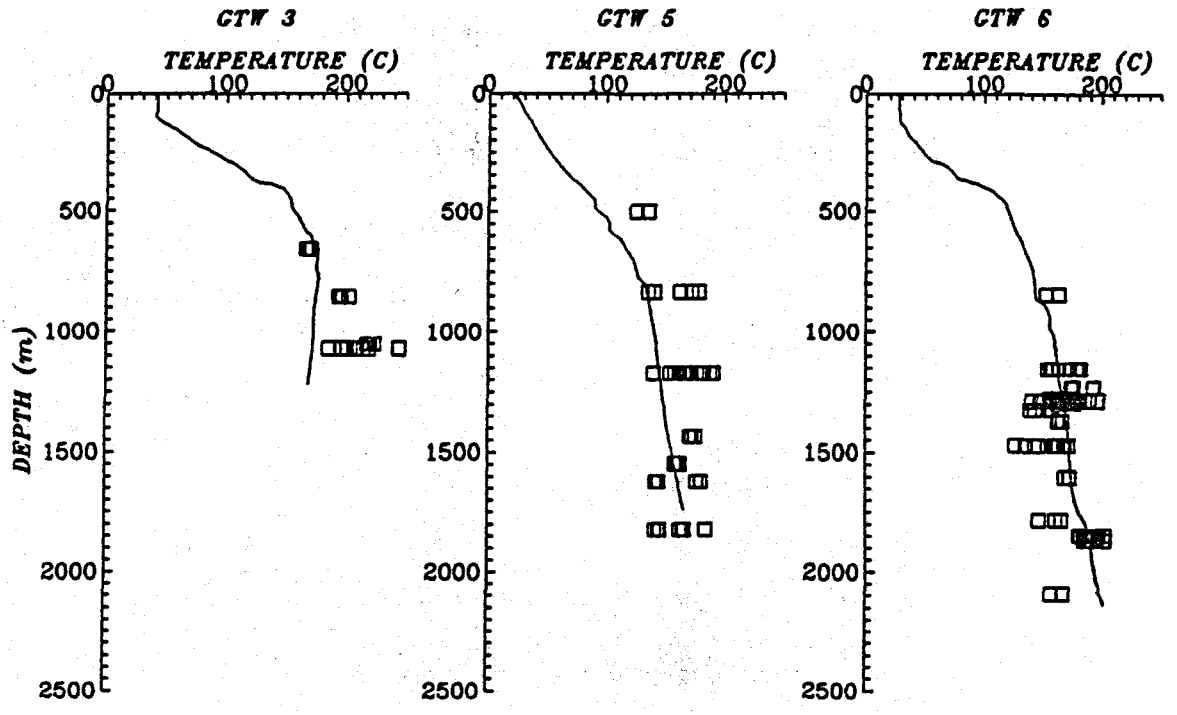

Figure 4. Fluid inclusion homogenization temperatures and measured temperatures in thermal gradient wells GTW 3, 5, and 6. The fluid inclusion temperatures are shown by squares and the measured temperatures by solid lines.

(1985) to refine the existing hydrogeochemical model of the geothermal system. The primary features of these previous studies are the presence of an upflow zone located to the south of GTW 6, a northward-trending thermal plume that feeds the production wells, and some recharge through the capping clays.

Our fluid inclusion studies of the wells near the upflow zone, GTW 5 and 6, suggest a complex pattern of heating and cooling within this region of the field. Comparison of Figures 4b and 4c shows that downhole measured temperatures are most similar to the lower limit of the fluid inclusion homogenization temperatures in GTW 5, but near the upper end of the homogenization temperatures in GTW 6. These relationships indicate that the rocks in GTW 5 are cooling whereas those in GTW 6 are being heated. Furthermore, maximum measured fluid inclusion temperatures in GTW 6 are approximately 20°C hotter than those in GTW 5 at similar depths. We infer from these observations that GTW 6 is closer to the source of the thermal plume than GTW 5, and that permeabilities in GTW 5 have been reduced since the inclusions formed.

The salinities of the fluid inclusions demonstrate that the upwelling fluids were diluted by lower-salinity waters. The maximum salinities of the fluid inclusions are similar to the 15000 ppm TDS contents of the produced fluids. However, the fluid inclusions also record salinities that range downward to less than 1700 ppm, indicating that significant mixing has occurred. The low-salinity fluids may in part represent meteoric water that has percolated through the clay cap, as proposed by Lippmann and Bovardsson (1985).

A small amount of mixing is also apparent in the chemistry of the fluids produced at the power plants, approximately 1.5 km north of GTW 6. Fluids that feed the western binary plant, which is slightly off-center of the thermal anomaly, display a minor amount of mixing and cooling. Fluids that feed the eastern dual flash plant have more CO_2 than the western fluids, indicating either an addition of CO_2 or mixing with CO_2-bearing fluids. CO_2-enriched fluids were also found in fluid inclusions at 1072 m in GTW 3, a thermal gradient well adjacent to the eastern production wells.

CONCLUSIONS

The fluids produced at the two production islands are slightly different in chemistry. The chemical compositions indicate that the fluids which feed the western binary plant may have mixed with another fluid and cooled slightly with respect to those that feed the eastern dual flash plant.

Our fluid inclusion studies are consistent with the geologic model of James et al. (1987), which indicates that the upwelling center is located in the southern part of the field. A comparison of the measured and fluid inclusion temperatures suggests that the rocks in GTW 5 are cooling. In contrast, the measured temperatures in GTW 6 are near the highest temperatures recorded by the fluid inclusions.

Chemical analyses of the eastern production fluids indicate that they are enriched in CO_2 relative to the western fluids. CO_2-enriched fluids are also preserved in fluid inclusions in GTW 3, but were not observed in GTW 5 or 6. These relationships suggest that the excess CO_2 is locally derived.

ACKNOWLEDGEMENTS

The authors would like to thank the management of Chevron Resources for enabling us to conduct this study and for providing the samples and well logs. We would also like to thank Bob Murray of Chevron Resources and the operations personnel at Heber. This research was supported by DOE contract DE-AC07-85ID12489.

REFERENCES

Browne, P. R. L., 1977, Occurrence and hydrothermal alteration of diabase, Heber geothermal field, Imperial Valley, California: Univ. Cal. Riverside, UCR/IGPP-77/9, 61 pp.

Fournier, R. O., 1981, Application of water geochemistry to geothermal exploration and reservoir engineering, in Rybach, L., and Muffler, L. J. P., eds., Geothermal Systems: Principles and Case Histories: John Wiley & Sons, New York, p. 109-143.

Fournier, R. O., and Truesdell, A. H., 1973, An empirical Na-K-Ca geothermometer for natural waters: Geochim. et Cosmochim. Acta, v. 37, p. 1255-1275.

James, E. D., Hoang, V. T., and Epperson, I. J., 1987, Structure, permeability and production characteristics of the Heber, California geothermal field: Proc. 12th Workshop on Geoth. Res. Eng., Stanford Univ., v. 12, p. 267-271.

Lippmann, M. J., and Bodvarsson, G. S., 1985, The Heber geothermal field, Califonia: natural state and exploitation modeling studies: Jour. Geophys. Research, v. 90, p. 745-758.

Potter, R. W., II, Clynne, M. A., and Brown, D. L., 1978, Freezing point depression of aqueous sodium chloride solutions: Econ. Geol., v. 73. p. 284-285.

Truesdell, A. H., Thompson, J. M., Coplen, T. B., Nehring, N. L., and Janik, C. J., 1981, The origin of the Cerro Prieto geothermal brine: Geothermics, v. 10, p. 225-238.

Tansev, E. O., and Wasserman, M. L., 1978, Modeling the Heber geothermal reservoir: Trans. Geotherm. Resour. Council, v. 2, p. 645-648.

PROCEEDINGS, Fourteenth Workshop on Geothermal Reservoir Engineering
Stanford University, Stanford, California, January 24-26, 1989
SGP-TR-122

Two-dimensional Simulation of the Krafla-Hvíthólar Geothermal Field, Iceland.

Helga Tulinius and Ómar Sigurðsson

Orkustofnun, National Energy Authority, Geothermal Division
Grensásvegur 9, 108 Reykjavík, Iceland

ABSTRACT

The Hvíthólar geothermal field is a part of the Krafla geothermal area in north-eastern Iceland. It has been exploited since 1984 for electrical production. Three wells have been drilled in the field to depths of 1200 – 1968 m. The two producers (KJ-21 and KJ-22) have a total flow capacity of 60 kg/s, sufficient for generation of 14 MW_e. The reservoir pressure in the field has declined by about 15 bar since 1982.

A two-dimensional model of the natural state of the reservoir has been developed. The model is a vertical cross section. The physical processes considered include mass transport, conductive and convective heat transfer, boiling, and condensation. The model adequately matches all relevant data from the field. The natural flow of hot fluids through the reservoir is estimated to be somewhat less than 10 kg/s. The natural state model was calibrated against the production history of the field, and three different future production schemes were evaluated. At current production rates, the field is expected to last no more than another decade.

INTRODUCTION

The Krafla geothermal area is located in the Neovolcanic zone in north-eastern Iceland (figure 1). Three geothermal fields, i.e. Hvíthólar, Leirbotnar, and Suðurhlíðar, within the Krafla area are under exploitation (Ármannsson et al., 1987). At Hvíthólar three wells, KJ-21, KJ-22, and KJ-23 were drilled in 1982 and 1983 (Guðmundsson et al., 1982, 1983; Steingrímsson et al., 1983, 1984; Ármannsson and Steingrímsson, 1984). Well KJ-21 was drilled to a depth of 1200 m; its main aquifers are at depths of around 975 m and at 630 m. This well yielded a total of about 40 kg/s, with 60% coming from the upper aquifer and 40% from the lower. Well KJ-22 was directionally drilled to 1877 m, corresponding to 1740 m in vertical depth. The bottom of the well is 540 m to the west of the wellhead (figure 1). The well intersects several aquifers, the principal ones at 600 m, 960 m, and 1270 m depth, and yields a total discharge of 20 kg/s, 40% of which comes from the upper aquifers and 60% from the lowest. Well KJ-23, which was drilled to a depth of 1968 m, intersected few aquifers, all of them small, the biggest at 600 m and 700 m depth. This well has never been put into production.

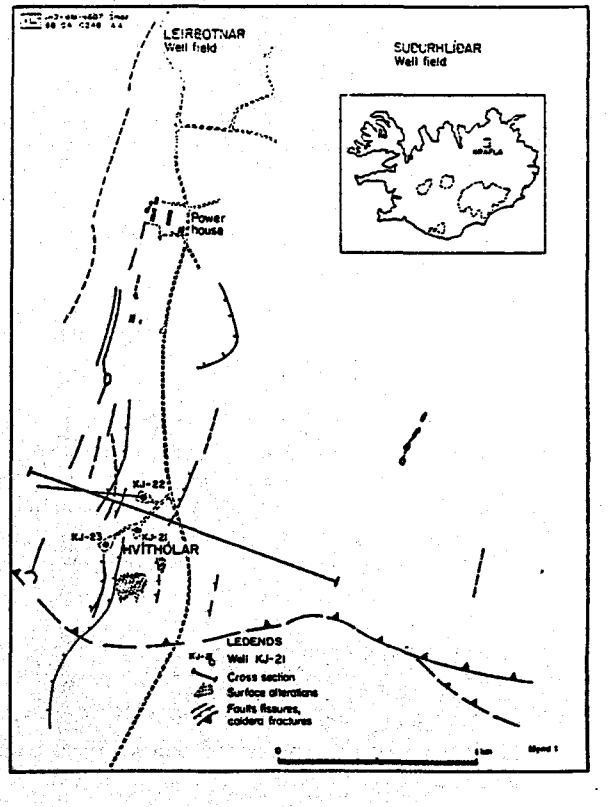

Figure 1. The Krafla-Hvíthólar well field.

Geological data indicate horizontal layering of basalts, hyaloclastites, and vertical or inclined intrusions (Ármannsson et al., 1987; Árnason, et al., 1984). There are no strong indications of reservoir connections between the Hvíthólar field and other parts of the Krafla area. Before production, the temperature in the field increased with depth down to 700 – 800 m, where it reached a maximum. Below 800 m there was a temperature reversal. The temperature at the bottom of well KJ-23 (1968 m) was 235°C. A fault separates KJ-23 from the upper part of KJ-22, and from all of KJ-21, and acts as a barrier between the wells. Since

KJ-22 is directionally drilled, it crosses this barrier at around 900 m depth (figure 2). A pressure drop of 6.5 bar across the fault was recorded.

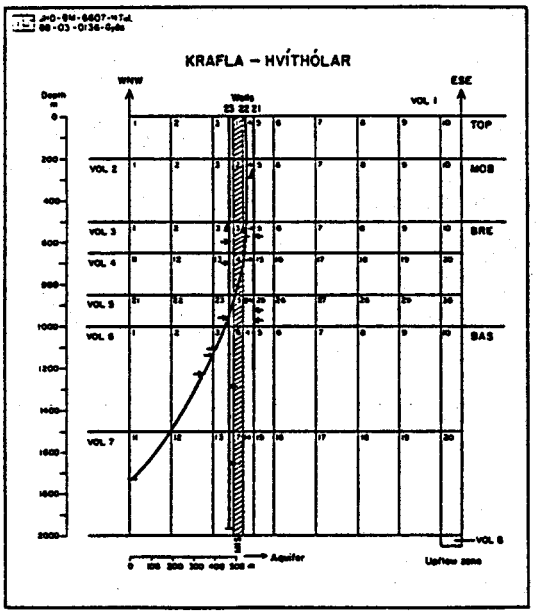

Figure 2. The two-dimensional distriubuted parameter model.

The computer program SHAFT79 (Pruess and Schroeder, 1980) was used for the simulation. In this program, flow through a porous medium is assumed. Several simulation studies have been performed on Icelandic high-enthalpy geothermal fields using this assumption, with good results (Böðvarsson, 1987; Böðvarsson et al., 1984 and 1986), even though the flow in Krafla and other high-enthalpy areas in Iceland is primarily through fractures and the storage is mostly in the rock matrix. The program furthermore assumes the reservoir fluid to be pure water, and the effects of gases and dissolved minerals are neglected. This should be a reasonable approximation because the gas and mineral content of the Hvíthólar reservoir fluid is low.

A two-dimensional model for the natural state of the Hvíthólar system is presented below. Field data from all three wells was used to develop the model.

CONCEPTUAL MODEL

All the available information on the field was used to construct the conceptual model. The undisturbed formation temperature is shown in figure 3. The temperature is similar at all the wells, though slightly higher at well KJ-21 in the depth range 600 – 1200 m. The highest temperature is about 250°C at wells KJ-22 and KJ-23, and 270°C at well KJ-21. The temperature at wells KJ-22 and KJ-23 falls to 190°C at 1400 m, where it increases again.

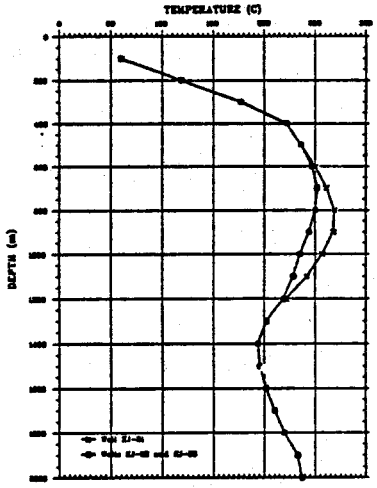

Figure 3. The estimated undisturbed formation temperature at wells KJ-21, KJ-22 and KJ-23.

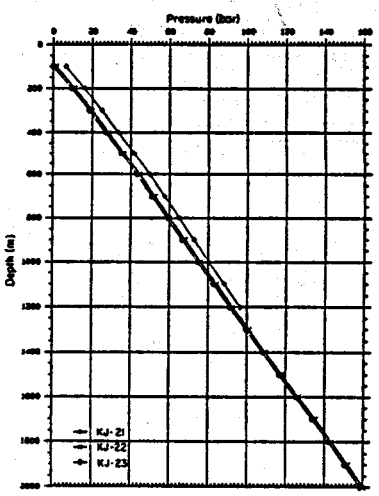

Figure 4. The estimated initial pressure at wells KJ-21, KJ-22, and KJ-23.

The estimated undisturbed inital pressure is shown in figure 4. The initial pressure is estimated to be 6.5 bar higher at well KJ-21 than at well KJ-23. This pressure difference is probably due to a barrier (fault/dyke) between these wells.

The temperature inversion and pressure distribution suggest that hot water is flowing towards the west on top of colder water. Well KJ-21 and the upper aquifers in well KJ-22 tap fluid from a reservoir east of well KJ-21. The lower aquifers in well KJ-22 (below 1000 m) and the aquifers in well KJ-23 are fed by a colder reservoir, which is probably connected to a north-south fissure swarm. This fissure swarm could be connected to the Krafla-Leirbotnar geothermal reservoir (Böðvarsson et al., 1984).

Drill cuttings from the three wells suggest a horizontal

layering of basalts, hyaloclastites, and vertical or inclined intrusions. At the top there is about a 200 m thick layer, consisting primarily of fresh basaltic lavas, which are highly permeable and porous. Below it, extending to about 500 m depth, comes altered hyaloclastite with low porosity and permeability. This layer acts as a cap on the geothermal system. The next 500 m are primarily composed of more porous and permeable basalt breccias. Most of the aquifers are located in this layer. Below about 1000 m depth intrusions become more numerous and the permeability of the basalt decreases. Few aquifers are found below 1000 m depth.

THE COMPUTER MODEL

The wells are clustered together and therefore provide limited information on the lateral distribution of pressure and other parameters. The vertical structure in the geology and temperature is known but over a short lateral distance. Because of the limited lateral spread of the data, a two-dimensional model, i.e. a vertical cross section, was chosen. The cross section cuts the well field from WNW to ESE (figure 1). This way the model is close to being perpendicular to one of the main strike directions but parallel to the flow from the east. If the direction of the cross section had been at a right angle to the one chosen, very limited lateral and vertical changes would have been observed in the pressure and temperature data, and the model would therefore have been less appropriate for correlating the inflow to the system and other parameters.

In figure 2 the wells are projected onto the cross section. The cross section extends 600 m west of well KJ-21 and 1000 m to the east of it. Because of the geological structure of the geothermal system, the cross section was divided into five different geological units, each with different reservoir parameters. These units were further divided into smaller elements with different parameters (porosity, permeability). Table 1 lists the main parameters for the different units.

The geological unit MIS represents the fault between the wells and acts as a barrier. Its thickness is 50 m. The boundary nodes VOL 1 - VOL 8 control the inflow to, and the outflow from, the system and represent the surface. The node VOL 1 represents the atmosphere with an annual mean temperature around 5°C, and a pressure of one bar.

The boundary nodes are large enough to maintain constant temperature and pressure (table 2), even under the addition or withdrawal of large quantities of fluid. A constant temperature gradient and hydrostatic pressure are assumed in the nodes, which are not connected to each other. Because of their capacitive properties, these nodes can partly account for flow from the north along the north-south fissure swarm. Boundary node VOL 8 represents the upflow zone. To simulate the natural heat conduction from the earth a heat flux of 2 W/m^2 to the bottom unit was assumed. This value is the same as that used for Krafla-Leirbotnar (Böðvarsson, et al., 1984), but is an order of magnitude too high for Hvíthólar. This has little effect on the results of the simulation, except that it could accelerate the creation of two-phase condition.

Table 1. Element properties: Values of the parameters.

Name	Permeability* (10^{-15} m^2)	Porosity (%)	Density (kg/m^3)	Thermal conductivity (W/m°C)
TOP 1-10	10	15	2650	1.5
MOB 1-10	$2x10^{-3}$	5	2650	1.1
BRE 1-9	10	5	2650	1.7
BRE 11-19	10	5	2650	1.7
BRE 21-29	10	5	2650	1.7
BRE 10,20,30	10/20	5	2650	1.7
BAS 1-9	1.2	5	2650	1.7
BAS 11-19	1.2	5	2650	1.7
BAS 10,20	1.2/20	5	2650	1.7
MIS 1	0.45	5	2650	1.7
MIS 2	0.45	5	2650	1.7
MIS 3	0.45	5	2650	1.7
MIS 4	0.45	5	2650	1.7
MIS 5	0.45	5	2650	1.7
MIS 6	0.45/0.2	5	2650	1.7
MIS 7	0.45/0.2	5	2650	1.7

* Horizontal permeability/vertical permeability

Table 2. Boundary nodes.

Name	Temperature (°C)	Pressure (bar-a)
VOL 1	5.2	1.0
VOL 2	85.0	23.60
VOL 3	105.0	41.50
VOL 4	121.2	55.90
VOL 5	137.9	70.70
VOL 6	168.8	97.30
VOL 7	216.3	139.8
VOL 8	300	167.00

The values for the different parameters for each unit are essentially the same (table 1) as for the Leirbotnar and Suðurhlíðar fields (Böðvarsson et al., 1984). The values selected for porosity and thermal conductivity are the same as for the other fields. The porosity is 5% in all units except in the unit TOP, where it is 15%, and the heat capacity is 1000 J/kg°C in all units. The relative permeability of the water-steam mixture is assumed to be a linear function of steam saturation. Steam becomes immobile at 5% steam saturation as does water at 30% water saturation. This assumption has given good results for the Krafla fields (Böðvarsson et al., 1984).

NATURAL CONDITIONS

The objective of the study was to simulate the natural conditions in the Hvíthólar geothermal system prior to production, i.e. the prevailing temperature and pressure distributions at that time. Undisturbed temperature and hydrostatic pressure gradients (figures 3 and 4)

were assumed in the system at the beginning of the simulation. An upflow zone, recharged by the boundary node VOL 8, is assumed east of well KJ-21.

The porosity and permeability in the different units were then changed along with the recharge rate in the upflow zone until a match with the initial temperature and pressure was reached. In the "best" model, near steady-state conditions were reached in about 900 years. At this point the changes in temperature and pressure everywhere in the system were less than 0.5°C and 0.5 bar, respectively, over 30 years.

Figures 5 and 6 show the natural state temperature and pressure distributions in the cross section, and figures 7 and 8 the calculated temperature and pressure profiles, for wells KJ-21 and KJ-23.

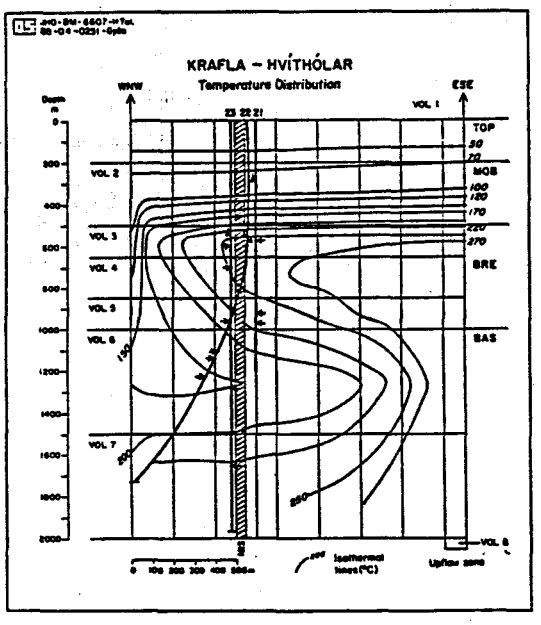

Figure 5. Calculated temperature distribution in the Krafla-Hvíthólar system.

By adjusting the permeability in the barrier (MIS), a pressure difference of 6.5 bar across the barrier could be obtained, in agreement with well measurements. In order to match the lower temperatures below 800 m, the upflow was directed along the east edge of the cross section by assigning a higher vertical than horizontal permeability to these elements. This is reasonable in view of the fracture/fault nature of the system.

In the "best" model the fluid turned out to be two-phase in the top layer of BRE from the barrier (MIS) to the east edge. In the upflow zone, two-phase conditions occurred in the BRE elements but not in the BAS elements. In the actual system it is not known whether the fluid was two-phase at 600 m depth in well KJ-21 prior to production, but is considered unlikely. The fluid at that depth was, however, expected to be at the boiling temperature. It should be noted that the presence of two-phase conditions in the model will influence the production predictions.

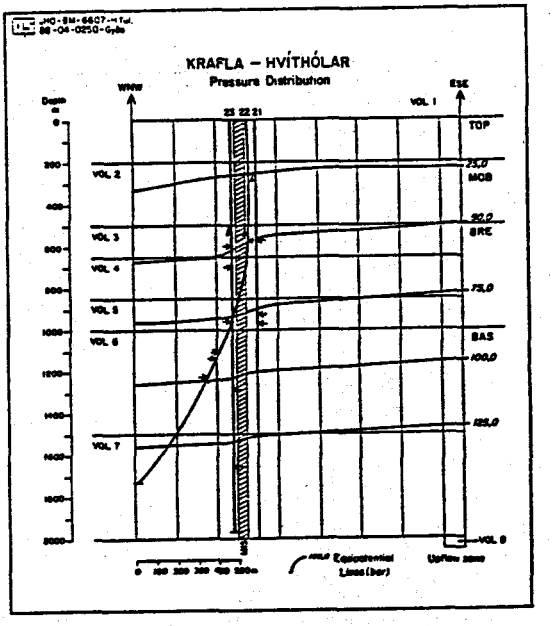

Figure 6. Calculated pressure distribution in the Krafla-Hvíthólar system.

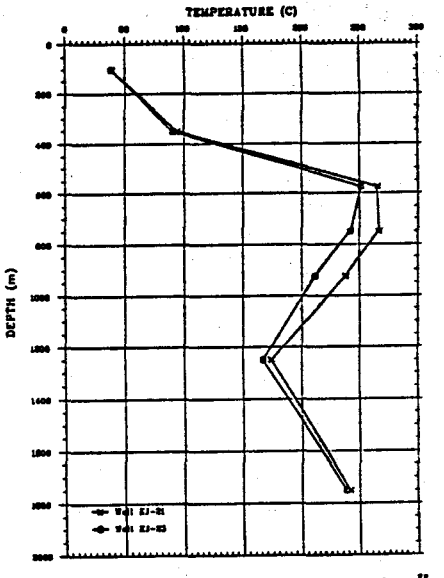

Figure 7. Calculated formation temperature at wells KJ-21 and KJ-22, prior to production.

PRODUCTION

The production histories for wells KJ-21 and KJ-22, from October 19, 1982, when KJ-21 was put into production, and until the end of 1987, are shown in figures 9 and 10, respectively. Well KJ-22 was not put into production until August 19, 1983, but the same time scale is used for both wells. The "best" model was calibrated against the production data. The end product of the natural state model was used as the initial condition for this calibration.

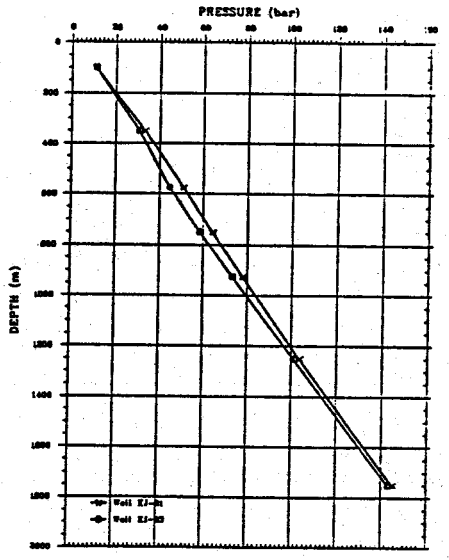

Figure 8. Calculated initial pressure at wells KJ-21 and KJ-22, prior to production.

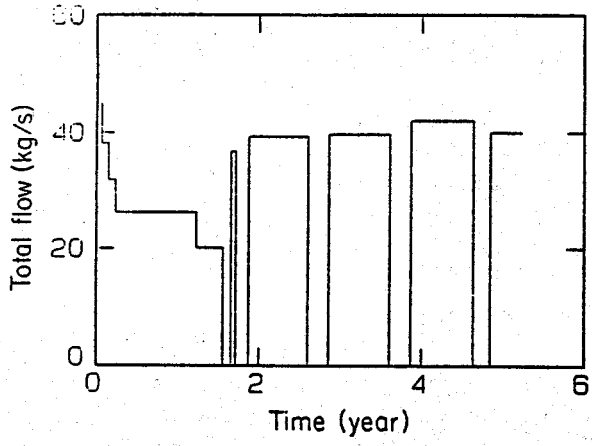

Figure 9. Well KJ-21, production history.

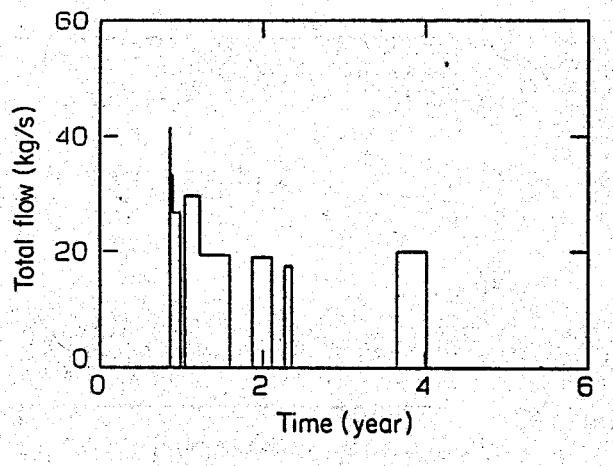

Figure 10. Well KJ-22, production history.

To simulate the production, several sinks were added to the model, approximately where the aquifers are located in the wells. In this way the pressure drawdown in the reservoir was simulated. Figure 11 shows the calculated pressure at 750 m depth in well KJ-21, and the corresponding measured pressures at 700 m and 800 m. In the simulation the production from each sink was varied until the "best" match was found. The results indicate that just over 60% of the total output comes from the upper aquifer at 600 m depth in well KJ-21, and the rest from the lower one at 975 m depth. The elements BRE 5 and BRE 25 indicate these two aquifers. In well KJ-22 about 40% of the total output comes from the upper, hotter aquifers (BRE 4) and 60% from the lowest (BAS 2).

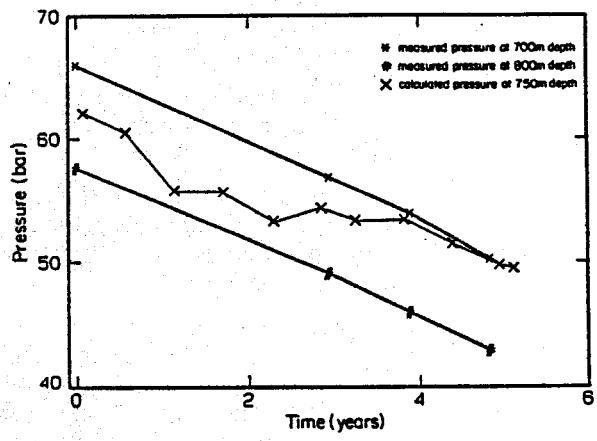

Figure 11. Calculated and measured pressure in well KJ-21.

The calibration against the production data indicated that the required lateral thickness for this two-dimensional model to sustain the production was of the order of 500 m. Furthermore, the natural recharge to the hot reservoir was estimated to be about 10 kg/s of fluid at 300°C.

As can be seen from figure 11, the calculated pressure response matches the observed one rather well. The applicability of the two-dimensional natural state model to exploitation studies of this system is, however, limited for the following reasons. The model is just two-dimensional, and the grid blocks are large. The third dimension, north-south, is kept constant, which means that mass production affects the whole thickness (N-S). One of the major strike directions in the area is N-S, which means the permeability could be greater in that direction close to the main fissures. Pressure drawdown in the production area could therefore cause an inflow from the north or the south. This is only partially accounted for by the present model, in the boundary nodes.

PREDICTION

After obtaining the "best" model and calibrating it against the production history, it was employed to predict pressure and temperature changes in the future. It should be kept in mind that this model is rather rudimentary, and therefore gives only a general idea about the system's response to further production. Three cases were examined.

1. Same production scheme as is currently employed at Hvíthólar. Well KJ-21 produces 40 kg/s (60% from 600 m and 40% from 975 m) nine months a year. The well is shut in during the months of June, July and August. Well KJ-22 produces 20 kg/s (40% from 600 m and 60% from 1100 m), and is shut in two weeks for every one it is in production. Well KJ-22 is also shut in during the months of June, July and August.
2. Same as case 1 except the wells are not shut in during the summer months, i.e. constant production during the whole year.
3. The lower aquifer in well KJ-22 is closed off, and it is assumed that the upper aquifer produces 8 kg/s for the whole year. Production from well KJ-21 is the same as in case 1.

Figures 12 – 14 show these three cases. For cases 2 and 3 the pressure drops so rapidly in the upper aquifer in well KJ-21 that production from the well stops after about a year, 275 days in case 2, and 473 days in case 3. Production from the system can be maintained much longer, however, under the present scheme (rest for three months a year). It appears that some kind of equilibrium is reached after about seven years, in late 1994. The pressure at the upper aquifer is then rather low or about 20 bar. In these calculations, the total flow is kept constant, and the increasing steam fraction of the fluid mixture is ignored. This could mean that less total flow is required for the same energy output from the well. Under real-life conditions the energy production can be constant, while the total fluid production declines. This would mean that the pressure drop at the wells is less than that calculated here, over the same period of time.

Temperature changes are small in all cases, at the most around 16°C at the upper aquifer in well KJ-21 for case 1. Temperature equilibrium is reached when the wells have dried up and only steam is produced.

CONCLUSIONS

A simple two-dimensional model of the Krafla-Hvíthólar geothermal system was developed, one which can simulate the pressure and temperature distribution in its natural state. This model was calibrated against the production history of the system, and employed to make rough predictions for future production.

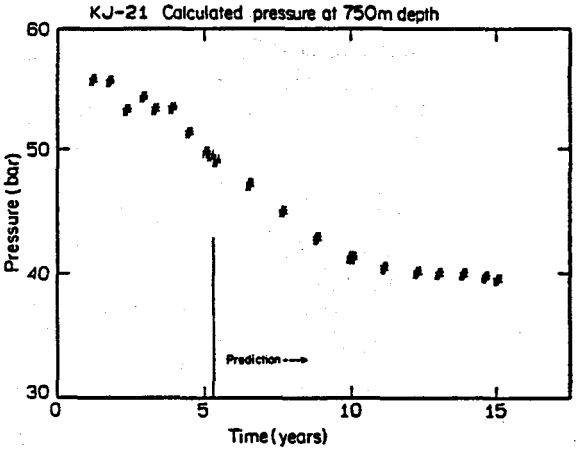

Figure 12. Prediction case 1, pressure at 750 m depth.

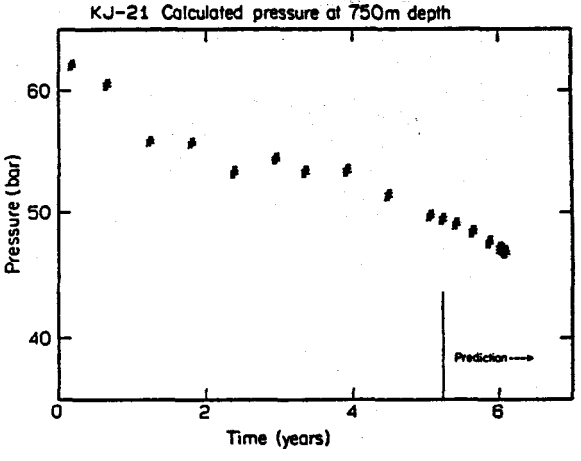

Figure 13. Prediction case 2, pressure at 750 m depth.

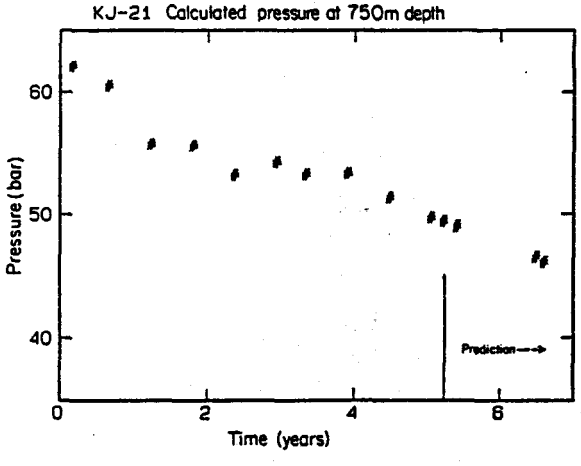

Figure 14. Prediction case 3, pressure at 750 m depth.

In the model, 60% of the fluid produced from well KJ-21 is from the upper aquifer (600 m) and about 40% from the lower (975 m). About 40% are produced from the upper aquifers in well KJ-22 and 60% from the lowest.

Natural recharge into the hot reservoir is estimated to be about 10 kg/s of 300°C fluids.

The system is rather small, probably somewhere between 0.3 and 0.5 km^3, which could correspond to 500 m in a north-south direction, a thickness of 500 – 1000 m (at a depth of 500 – 1500 m), and 1000 m in an east-west direction.

Under the current production scheme the system is predicted to last ten additional years, at the most.

FUTURE WORK

It has been recommended to the power plant operators (Landsvirkjun) that the model should be modified and the third dimension included. The recommendations are:

1. Modify the current two-dimensional model to obtain a better fit to the field data.
2. Add the third dimension, and thereby allow for directionally dependent inflow to the producing wells, as well as changes in their enthalpy and flow.
3. Include well-by-well simulation or refine the grid to match better the characteristics of individual wells.
4. Make new predictions for the Krafla-Hvíthólar system.

ACKNOWLEDGEMENT

We would like to thank Landsvirkjun (The National Power Company) for allowing us to publish this data.

REFERENCES

Ármannsson, H. and Steingrímsson, B., 1984: Krafla. Hola KJ-22. Upphitun, upphleyping og blástur. OS-84008/JHD-02 B (in Icelandic).

Ármannsson, H., Guðmundsson, Á., and Steingrímsson, B. S., 1987: Exploration and development of the Krafla geothermal area. Jökull no. 37, pp 13-30.

Árnason, K., Eyjólfsson, B., Gunnarsson, K., Sæmundsson K. and Björnsson, A., 1984: Krafla - Hvíthólar, Jarðfræði- og jarðeðlisfræðileg könnun 1983. OS-84033/JHD-04. Unnið fyrir Rafmagnsveitur ríkisins – Kröfluvirkjun (in Icelandic).

Böðvarsson, G. S., Pruess, K., Stefánsson V. and Elíasson, E. T., 1984: The Krafla Geothermal Field, Iceland: 2. The Natural State of the System. Water Resources Research, Vol 20, No 11, pp. 1531-1544.

Böðvarsson, G.S, Pruess K., Stefánsson V., Steingrímsson B., Björnsson S., Gunnarsson Á., and Gunnlaugsson E., 1986: Natural State Model of the Nesjavellir Geothermal Field, Iceland. Proceedings, Eleventh Workshop on Geothermal Reservoir Engineering Stanford University, Stanford, California. pp. 109-115.

Böðvarsson, G. S., 1987: Líkanreikningar fyrir jarðhitakerfi Nesjavalla. I. The Nesjavellir Geothermal Field, Iceland. Prepared for The Reykjavík Municipal Heating service, Reykjavík, Iceland.

Guðmundsson, Á., Steingrímsson, B., Friðleifsson, G. Ó., Tryggvason, H. and Sigurðsson, Ó., 1982: Krafla, hola KJ-21. Borun vinnsluhluta holunnar, frá 293 m til 1200 m. OS-82119/JHD-35 B, (in Icelandic).

Guðmundsson, Á., Steingrímsson, B. S., Sigursteinsson, D., Guðmundsson, G., Friðleifsson, G. Ó., Tryggvason H. and Sigurðsson, Ó., 1983: Krafla, hola KJ-22. Borun vinnsluhluta holunnar, frá 567 m til 1877 m. OS-83071/JHD-22 B (in Icelandic).

Pruess, K., Schroeder, R. C., 1980. SHAFT79 User's Manual. LBL-10861 Lawrence Berkeley Laboratory, Berkeley, California, U.S.A.

Steingrímsson, B. S., Ármannsson H. and Benjamínsson, J., 1983: Krafla. Hola KJ-21. Upphitun, upphleyping og blástur. OS-83013/JHD-03 B, (in Icelandic).

Steingrímsson, B. S., Guðmundsson, Á., Guðmundsson, G., Friðleifsson, G. Ó., Tulinius H. and Sigurðsson, Ó., 1984: Krafla, hola KJ-23. Borun og rannsóknir. Lokaskýrsla. OS-84032/JHD-03, unnið fyrir Rafmagnsveitur ríkisins – Kröfluvirkjun (in Icelandic).

PROCEEDINGS, Fourteenth Workshop on Geothermal Reservoir Engineering
Stanford University, Stanford, California, January 24-26, 1989
SGP-TR-122

EVALUATION OF RESERVOIR MODEL PREDICTIONS FOR THE OLKARIA EAST GEOTHERMAL FIELD, KENYA

G. S. Bodvarsson,* K. Pruess,* C. Haukwa‡ and S. B. Ojiambo‡

*Earth Sciences Division
Lawrence Berkeley Laboratory
1 Cyclotron Road
Berkeley, California 94720

‡Kenya Power Company Ltd.
Electricity House
Harambee Avenue
Nairobi, KENYA

ABSTRACT

In 1984 a detailed three-dimensional well-by-well model was developed for the Olkaria geothermal field in Kenya. The model was calibrated against the production history of the field over the period 1977 through 1983, using porosities and permeabilities as adjustable parameters. During this period two 15-MW_e Units were put on-line at Olkaria; the third 15 MW_e Unit commenced operation in March 1985. The numerical model was used to predict the performance of the Olkaria wells and these predictions have been compared with the observed well behavior for the period 1984 to 1987. In general, the model predictions show satisfactory agreement with the observed well behavior, especially for those wells that had production histories exceeding two years. The predicted steam rates for most of the wells were accurate to within 1 kg/s for the period considered and the steam rate decline was well predicted by the model. Some differences between the observed and predicted total flow rates and enthalpies of individual wells were seen, especially in those wells with large enthalpy variation or unorthodox increases in total flow rate. The model also predicted that 3 make-up wells would be needed by the end of 1987, which is consistent with the observed decline in total steam rates. New performance predictions have been made using an updated model, including the effects of wastewater reinjection.

INTRODUCTION

The Olkaria East geothermal field has been producing electrical power since 1981 when the first of three 15 MW_e Units started operation. The other two 15 MW_e Units came on-line in 1982 and 1985, respectively, bringing the plant capacity to the current level of 45 MW_e.

Concurrent with the development of the Olkaria East wellfield, exploration drilling was carried out in other parts of the Olkaria field (Fig. 1). This exploration activity has been successful and has delineated two new areas for development. These are the Olkaria Northeast area, around the 700 series wells (north of the Olkaria East field) and the Olkaria West area around the 300 series wells (west of the Olkaria Hill). A decision has been made to continue development in Olkaria Northeast with a 60 MW_e power plant, planned to be commenced in 1992. In order to aid in the development of the geothermal development at Olkaria, a series of numerical simulation studies have been carried out.

The first study was conducted in 1980 with the objective of evaluating if fluid production should be limited to the rather thin vapor zone (about 100 m thick), or if the long term reservoir performance would improve with combined production from the vapor zone and the underlying two-phase zone (Bodvarsson et al., 1982). The second simulation study addressed the effects of adding a second 15 MW_e Unit on the long-term reservoir performance. Finally in 1984, a detailed three-dimensional model of the Olkaria East field was developed, which represented all wells individually. This model was calibrated against the existing flow rate and enthalpy histories of all wells for the period 1977-1983. The model results indicated that power generation of 45 MW_e at Olkaria East was possible.

With the commencement of the third 15 MW_e Unit significant flow rate declines were observed in many wells, as well as considerable enthalpy changes. This was of sufficient concern to lead to updating of the three-dimensional model with production data for the period 1984-1987; the work was completed in 1988. The updating of the model allowed for an evaluation of the accuracy of the model predictions during this period in terms of flow rates and enthalpies of all wells. This paper briefly describes the three-dimensional model of Olkaria East and evaluates its predictive performance. It also describes the model modifications that were necessary to match the additional data and the new performance predictions.

THE THREE-DIMENSIONAL MODEL

The three-dimensional model consists of three layers, with the top 100 m thick layer representing the initial vapor zone and the bottom two layers (250 and 500 m thick) representing the underlying two-phase liquid-dominated zone. These vertical dimensions and number of layers were considered sufficient to adequately represent the initial thermodynamic conditions of the reservoir and the major feed zones of the wells. The areal discretization of the model allows for individual grid block representation of all wells (Fig. 2) and extends

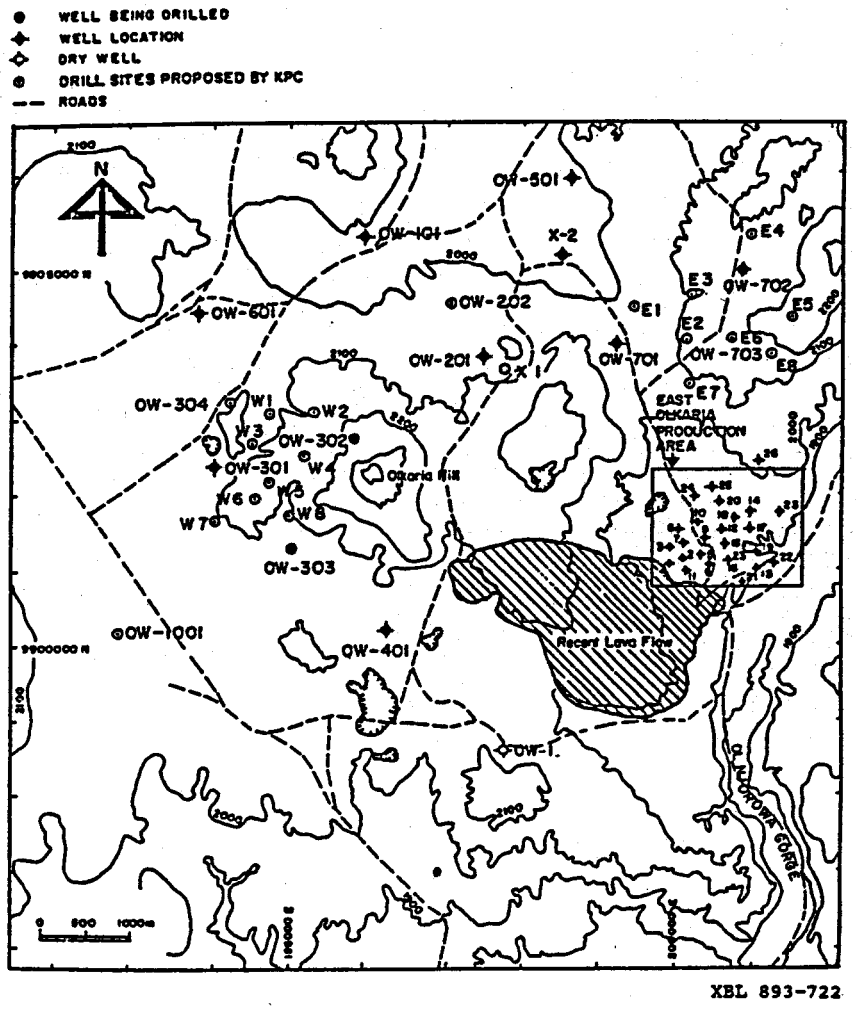

Figure 1. Locations of exploration wells and Olkaria East production wells.

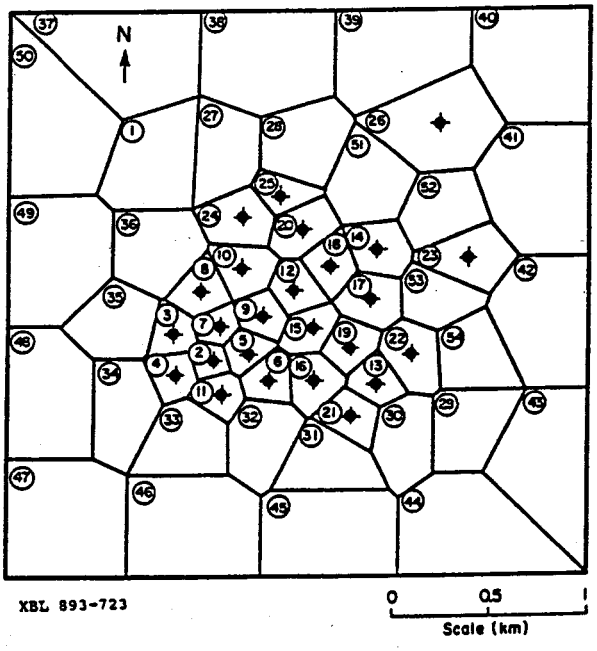

Figure 2. Areal view of grid used in the numerical model.

over an area of some 9 km^2. Because of the two-phase conditions in the reservoir, this assumed areal extent of the reservoir is sufficiently large for the system to act as if it is infinite.

The three-dimensional model was calibrated against the flow rate and enthalpy histories of all wells, using reservoir porosities and permeabilities and productivity indices of the wells were used as adjustable parameters. As an example, Figure 3 shows the history match for well 11. The history match yielded average permeabilities of 7.5 md and 4.0 md in the steam zone and the underlying liquid-dominated zone, respectively. This corresponds to an average well transmissivity of about 3.5 Dm (Darcy-meters) which is similar to the average transmissivity determined from short-term well tests.

Following the history match, performance predictions were made, that indicated that power generation in excess of 45 MW$_e$ would be possible for 30 years at Olkaria East. It was recommended that the well spacing of future wells should exceed 300 m (11 wells per km^2) due to large interference of the present wells (average

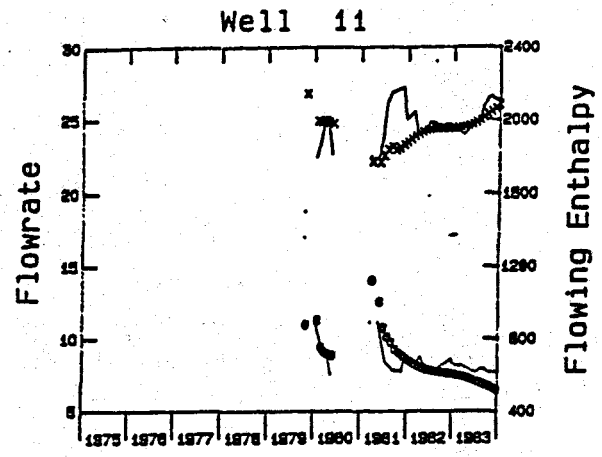

Figure 3. History match with flowrates and enthalpies for well 11 during the period 1977 through 1983.

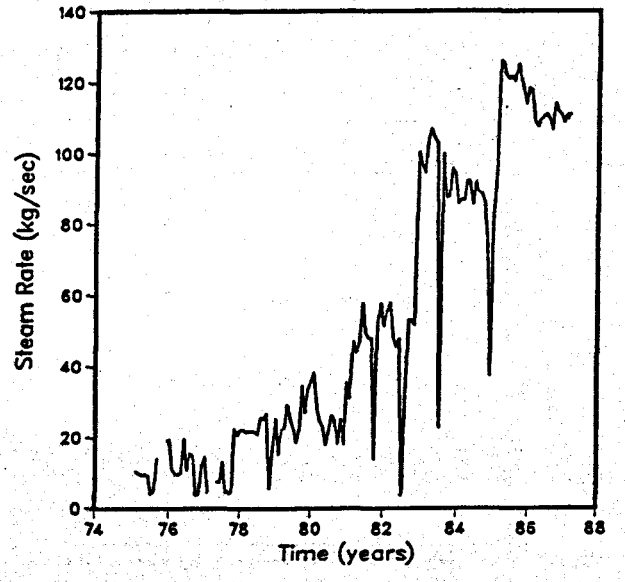

Figure 4. Total steam production versus time for Olkaria East wells.

well spacing of 225 m). For all of the different exploitation and reinjection scenarios flow rate and enthalpy predictions were made for each well and the necessary replacement wells, so that the predictions could be directly compared to future well data. More details of the model are given by Bodvarsson et al (1987a, b), and Svanbjornsson et al. (1983) describe the reservoir conditions at Olkaria.

FIELD PERFORMANCE 1984–1987

During the exploitation of the Olkaria East reservoir 1981 to 1987, significant changes have occurred in well outputs. The total steam rate of all wells is given in Figure 4 and reflects the early testing of wells (period 1975 to 1981) and the startup of the three Units (the first 15 MW_e Unit in 1981, the second one in 1982 and the third one in 1985). The average steam rate of the wells (Fig. 5) also shows large variations during the early flow testing, as wells with different production capacities were tested. A significant increase in the average steam rate for the wells is seen in 1982, reflecting the fact that the wells feeding Unit 2 are in general better producers than those feeding Unit 1. The considerable decline in the average steam rate since 1985 is due to production from wells feeding Unit 3, with the associated reservoir pressure decline and well output decline. Table 1 gives a summary of the effects of the Unit 3 start-up on producing wells for Units 1 and 2. Many of these wells show considerable flow rate decline (1.5 to 4.0 kg/s) and an accompanied enthalpy rise (100-200 kJ/kg). It is rather interesting that the effects for most wells are felt very quickly after the start-up of Unit 3 (generally less than 1 month) in spite of the two-phase conditions of the reservoir. It is probable that this is due to single-phase vapor conditions in the expanding vapor zone, which allows rapid areal propagation of pressure changes.

The average enthalpy of the produced fluids (Fig. 6) shows that most of the wells produce high enthalpy fluids averaging about 1800 kJ/kg during the flow testing period (1975-1981). After Unit 1 came on-line in 1981, the average enthalpy increased rapidly to about 2200 kJ/kg due to the expanding vapor zone and well interference. This trend continued when Units 2 and 3 commenced so that in 1987 the average enthalpy was near 2500 kJ/kg, or close to that of saturated steam (≈ 2800 kJ/kg).

It is of interest to evaluate how well the three-dimensional model predicted the performance of the wells during the period 1984 through 1987. This was achieved by incorporating the flow histories of the wells

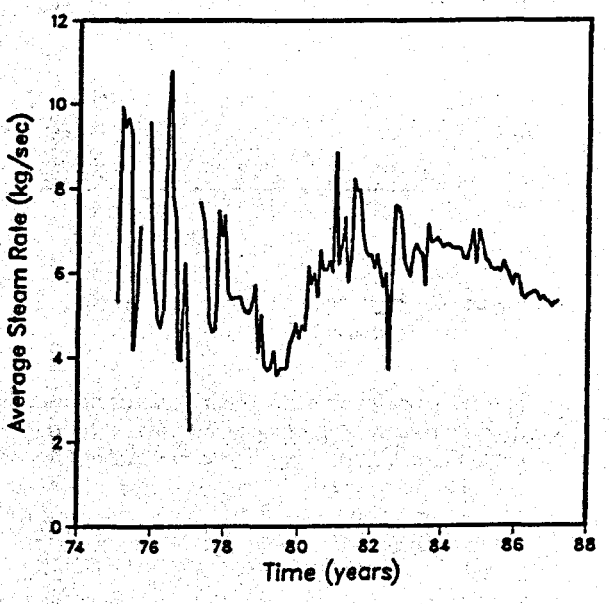

Figure 5. Average steam rate per well versus time for Olkaria East wells.

Table 1. Effects of Unit 3 wells coming on-line on the performance of other Olkaria East wells.

Well	Flow rate change (kg/s)	Enthalpy change (kJ/kg)	Steam rate change (kg/s)	Comments
2	0	0	0	
5	0	0	0	
6	0	0	0	
7	?	?	?	masked by well 8
10	1.5	200	0	small lag time (layer 3 well)
11	2.0	0	1.0	small lag time (layer 3 well)
12	3.5	200	2.5	small lag time (layer 2-3 well)
13	(0.5)	(200)	0	6-month lag time (layer 2 well)
14	0	0	0	
15	0	0	0	layer 3 well
16	4.0	100	3.0	small lag time (layer 3 well)
17	1.5	150	1.0	small lag time
18	2.0	150	0.5	small lag time (layer 3 well)
19	0	0	0	layer 3 well

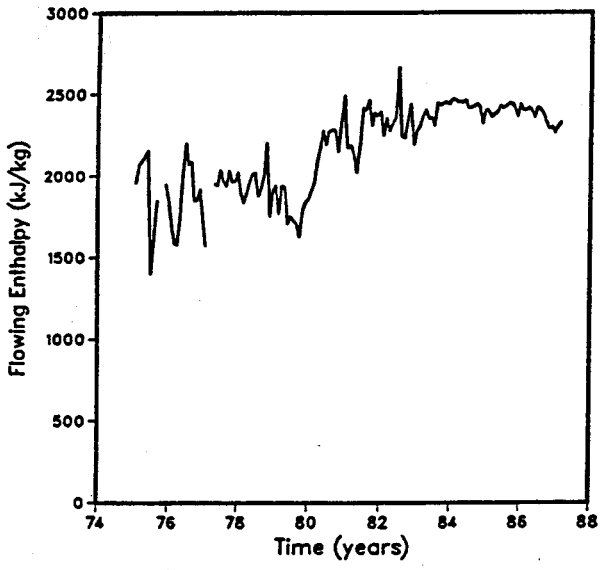

XBL 893-727

Figure 6. Average enthalpy of the produced fluids versus time.

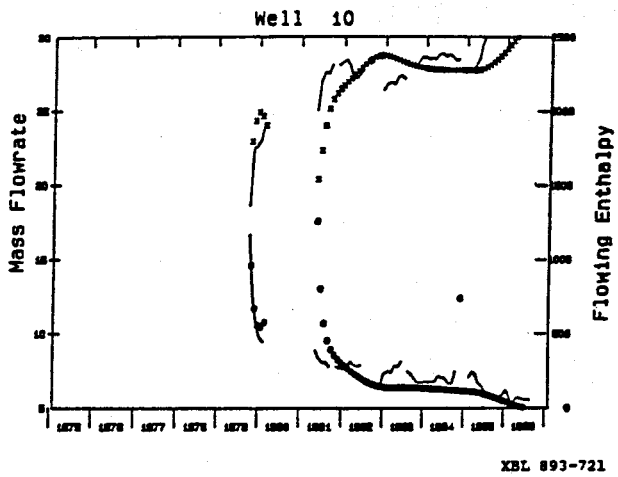

XBL 893-721

Figure 7. Comparison between predicted and observed flowrates and enthalpies (1984-1987) for well 10.

into the model, computing their performances during the four years and comparing the results with the observed data. Figures 7 and 8 give these comparisons for wells 10 and 11, respectively. The predicted flow rate and enthalpy behavior of well 10 agrees very well with that observed even to the extent that the late time rapid rise in enthalpy and decline in total flow rate is predicted. In the case of well 11 the predictions of the flow rate and enthalpy trends are rather poor, as the model overpredicts enthalpies by up to 500 kJ/kg and underpredicts the total flow rate by some 2 kg/s. However, it is most important that the steam rate at the separators is adequately predicted, as this controls how soon replacement wells are needed. Figure 9 shows that in spite of the rather poor enthalpy and flow rate predictions for well 11, the steam rate predictions are reasonably good.

In general, the model predicted adequately the steam rates and their decline for about 75% of the wells. For wells which had very short production history the model calibration was not sufficient to allow for reliable well performance predictions. Also, some of the wells showed

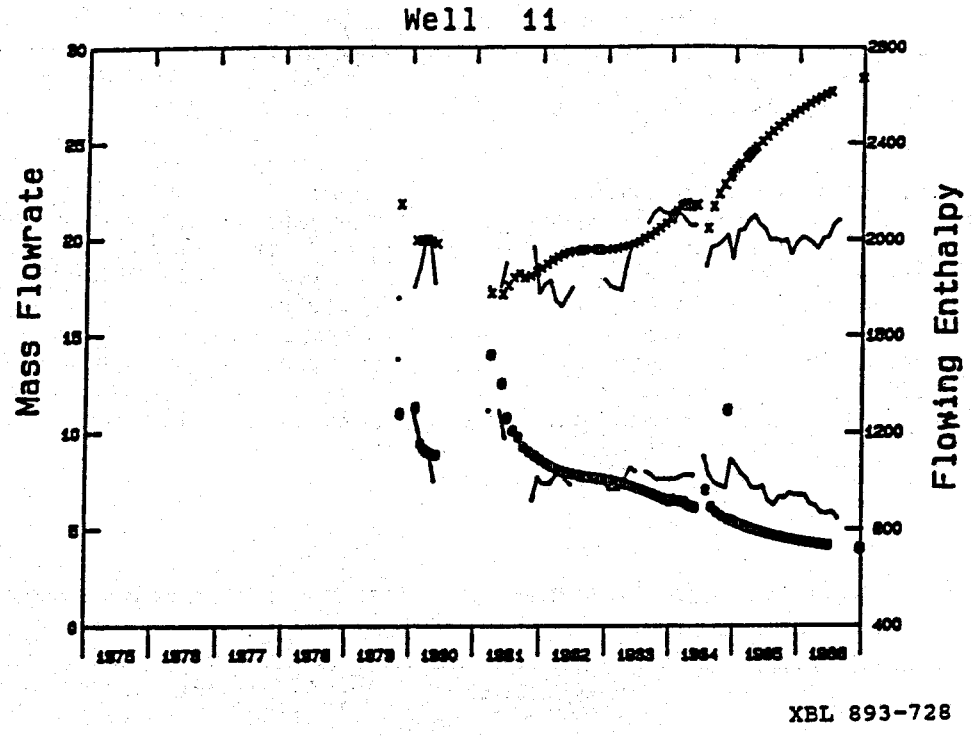

Figure 8. Comparison between predicted and observed flowrates and enthalpies (1984-1987) for well 11.

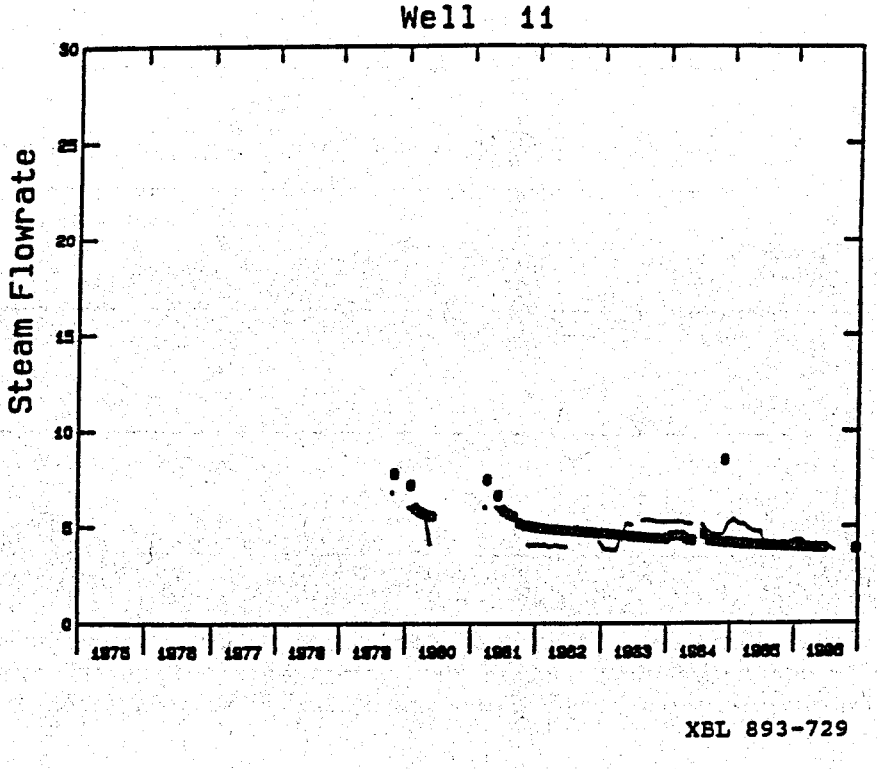

Figure 9. Comparison between predicted and observed steam rates (1984-1987) for well 11.

very unorthodox behavior during the period 1984-1987, including large flow rate increases with little enthalpy changes. This type of behavior can only be explained by temporal permeability changes, which are not included in the model.

The best evaluation of the model performance is to compare the overall predicted steam rate decline of all wells with that observed. This is a direct measure of how accurately the model predicted the number of replacement wells needed during the period 1984-1987, which is very important from the standpoint of the plant operation and the economics of the project. It turned out that the predicted decline in the total steam rate agreed very well with that observed, so that the model prediction of 3 make-up wells needed by the end of 1987 was correct.

Another test of the model concerned the relative contributions of the feed zones of the wells. Before the model was developed in 1984, the Kenya Power Company (1984) estimated the relative contributions of the various well feed zones using geochemical data (Table 2). These estimated relative contributions were used as initial "guesses" in the model development during the iterative history matching. However, these estimates had to be modified during the history matching, primarily because of the observed enthalpy transients. For many of the wells the enthalpies rose from 1500-1800 kJ/kg to over 2300 kJ/kg over a period of a year to a few years. This behavior is clearly inconsistent with majority of flow coming from steam zone feeds, but results from localized boiling around the feed zones in the liquid-dominated zone.

Table 2. **Relative contributions of different feeds for Olkaria East wells, based on estimates from the flowing pressure surveys, the numerical model, and geochemical data.**

Well	Zone	Pressure Surveys		Numerical Model		KPC (1984)
		Flow (%)	Enthalpy (kJ/kg)	Flow (%)	Enthalpy (kJ/kg)	Flow (%)
4	Steam	30	2800	18	2800	90
	Upper liquid	70	1500	82	1500	10
	Lower liquid					
9	Steam					50
	Upper liquid					
	Lower liquid	100	2435	100	2400	50
11	Steam	?		28	2840	60
	Upper liquid					
	Lower liquid	?		72	1930	40
13	Steam	26	2800	32	2830	90
	Upper liquid	74	1640	68	2390	10
	Lower liquid					
14	Steam	65	2800	66	2830	30
	Upper liquid	35	2485	34	2150	70
	Lower liquid					
15	Steam	35	2800	26	2840	20
	Upper liquid					
	Lower liquid	65	2150	74	2800	80
16	Steam	16	2800	5	2840	20
	Upper liquid					
	Lower liquid	84	2520	95	2330	80
17	Steam	6	2800	31	2840	33
	Upper liquid	0		12	2800	33
	Lower liquid	94	2000	57	2730	33

Table 2. Continued.

Well	Zone	Pressure Surveys		Numerical Model		KPC (1984)
		Flow (%)	Enthalpy (kJ/kg)	Flow (%)	Enthalpy (kJ/kg)	Flow (%)
	Steam	29	2800	11	2840	10
18	Upper liquid	0		10	2800	10
	Lower liquid	61	2600	79	2540	80
	Steam					
19	Upper liquid					
	Lower liquid	1000	2300	100	2470	100
	Steam	45	2800			
20	Upper liquid	0		8	2590	25
	Lower liquid	55	2480	92	2160	75
	Steam	29	2800	29	2850	80
21	Upper liquid	71	2550	71	1800	20
	Lower liquid					
	Steam	19	2800	20	2850	90
22	Upper liquid	81	2450			
	Lower liquid	0		80	2000	10
	Steam	54	2800	38	2800	90
23	Upper liquid	46	2220			
	Lower liquid	0		62	2220	10
	Steam					20
24	Upper liquid	0		25	2000	10
	Lower liquid	100	2200	75	2180	70

The model estimates of relative feed zone contributions have been compared to those obtained from the analysis of flowing pressure surveys using a multiple feed zone wellbore model (Bjornsson and Bodvarsson, 1987). As an example, Figure 10 shows the analysis for well 16, which yields the majority of the fluid inflow from the liquid-dominated zone (84%), in good agreement with the model results. Note also the high enthalpy of the feed zone at 1150 m depth, indicating a large degree of boiling around the well. As shown in Table 2 the results of the flowing surveys analysis yielded relative contributions of the feed zones that generally agree well with the model results. However, this is by no means a reliable check on the model as the results of the analysis of flowing pressure surveys are often very non-unique.

UPDATING OF THE MODEL

Although the three-dimensional model predicted the performance of many wells adequately, parameter modifications were necessary to match other wells. This new round of history matching involved all of the available data from 1977 through 1987. In general, little changes in productivity indices of the wells and permeabilities of the different layers were required. For a few wells the productivity indices of the steam zone feed zones had to be increased to maintain stable flow. The permeability distribution in the wellfield required rather localized changes around individual wells, but the average permeabilities of the steam zone (≈ 7.5 md) and the underlying liquid-dominated zone (≈ 4 md) remained unchanged. The permeability adjustments were primarily needed to properly represent the effects of Unit 3 coming on-line.

The main parameter adjustment needed for the model was an increase in the average porosity of the liquid-dominated zone from 2% to 4%. We believe that this parameter change reflects an artifact of the porous medium model used for this fractured reservoir. The need for a higher average porosity in the liquid zones in the present simulations is probably due to increasing

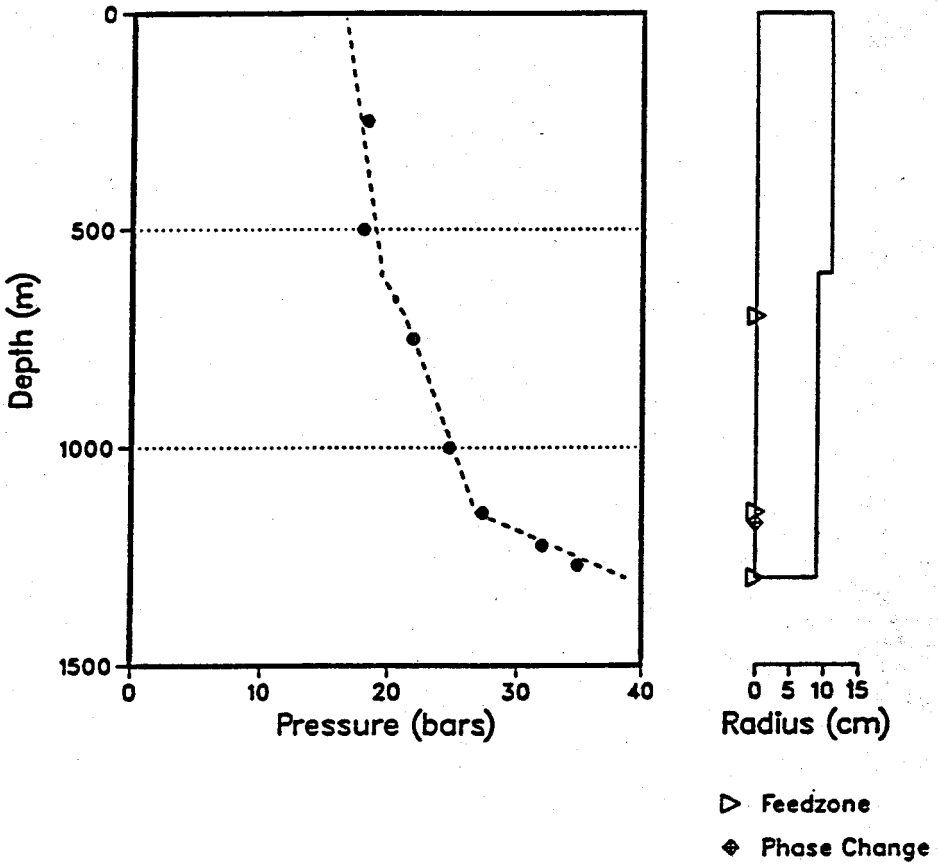

OLKARIA WELL OW-16
Pressure log during discharge. Measured 30-april-1981
Downhole pressures calculated for the following conditions.

Wellhead pressure (bar abs.)	:	16.50
Wellhead temperature (C)	:	202.00
Wellhead dryness	:	0.017
Wellhead enthalpy (kJ/kg)	:	2440.00
Wellhead total flow (kg/s)	:	13.00

Feedzone no:	Depth (m)	Flow (kg/s)	Enthalpy (kJ/kg)
1	766.0	2.0000	2800.1
2	1150.0	10.0000	2520.0
3	1300.0	1.0000	1054.3

XBL 893-730

Figure 10. Analysis of a flowing pressure survey for well 16.

recharge from the high-porosity matrix blocks to the fractures. At early time fracture effects dominate as localized fluid depletion is occurring near the wells. The rapid rise in enthalpy of many of the Olkaria wells at early production times is controlled by the low fracture porosity (the volume fraction occupied by the fractures) and the complex fracture/matrix interactions. This early rise in fluid enthalpy can only be represented in our porous medium model by small porosities near the wells, which most likely will lead to conservative performance predictions.

After significant fluid production has taken place the enthalpy of the produced fluids is controlled by the enthalpy of fluids recharging the wellfield. At this time the effects of fractures are not as important, except of course in locations where colder fluids are migrating from outer regions to the reservoir. In the present simulation, data are available for a 10-year period and we believe that currently the enthalpies of most wells are controlled by fluids recharging the wellfield. It was found during the history match iterations that porosities of 2% in the liquid zones outside the wellfield caused fluids with high enthalpy to recharge the wellfield, and consequently the enthalpies of the producing wells were too high. The 4% porosity seemed to provide the proper enthalpy of fluids recharging the wellfield. In the earlier

history match simulations (Bodvarsson et al., 1987a) the production period was too short to allow reliable estimates of the porosity of the recharge zones to be made.

Figure 11 shows, as an example, the porosity and permeability distribution in the lower liquid zone. The figure shows that a rather wide range of porosities (1-10%) and permeabilities (1->15 md) are needed to match the data. In general, high permeabilities are needed close to the best producers (e.g. wells 12, 15 and 16) and low porosities close to those wells that showed large enthalpy increases during the early production period. It is acknowledged that the porosity and permeability distribution shown in Figure 11 is by no means unique, as other (probably similar) distributions would also yield reasonable history matches for all wells.

PERFORMANCE PREDICTIONS

The updated numerical model shows that the effects of Unit 3 on the well flow rates and enthalpies have subsided, and new quasi-steady conditions have been reached in the system. It is estimated that four replacement wells need to be drilled to bring the plant up to maximum capacity (48 MW_e; the rated capacity is 45 MW_e). Figure 12 shows the predicted plant outputs until the end of 1991, assuming that these replacement wells will be drilled and connected. The first replacement well is assumed to be on-line by the end of 1989 and the last one by the end of 1990. The model predicts that the plant output will gradually decline to 38 MW_e before the first replacement well comes on-line. The model was used to investigate various alternatives for future development of Olkaria East including effects of reinjecting the waste water.

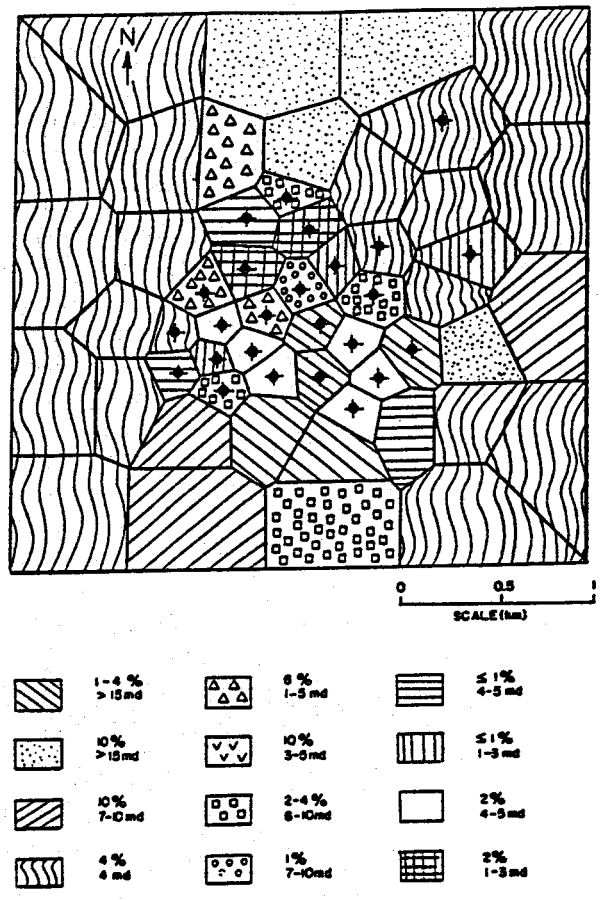

Figure 11. Estimated permeability and porosity distributions for the lower liquid zone.

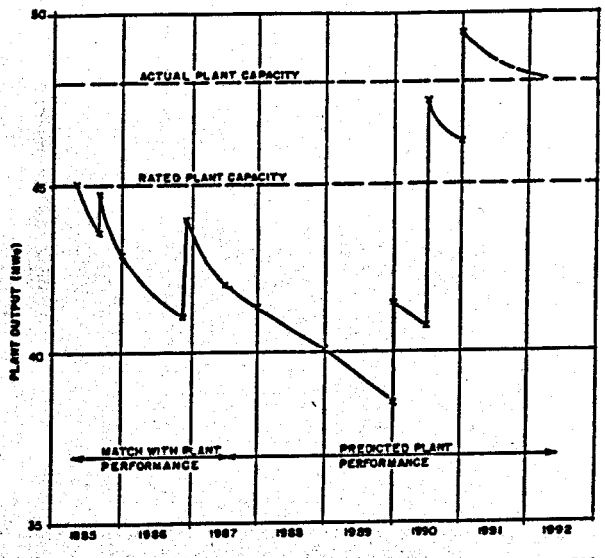

Figure 12. Predicted power plant output for the period 1987 through 1991.

ACKNOWLEDGEMENTS

The authors thank B. Steingrimsson and C. Doughty for technical review of this paper. Analysis of flowing pressure surveys by B. Steingrimsson is most appreciated. This work was supported by the Kenya Power Company Ltd. and in part by the Assistant Secretary of Conservation and Renewable Energy, Office of Renewable Energy Technologies, Geothermal Technology Division, of the U.S. Department of Energy under contract No. DE-AC03-76SF00098.

REFERENCES

Bjornsson, G. and Bodvarsson, G. S., 1987. "A multi-feedzone wellbore simulator," Geothermal Resources Council Trans., **11**, 503-507.

Bodvarsson, G. S., Pruess, K., Lippmann, M. J. and Bjornsson, S., 1982. "Improved energy recovery from geothermal reservoirs," *J. Pet. Tech.*, 34, 9 1920-1928.

Bodvarsson, G. S., Pruess, K., Stefansson, V., Bjornsson, S. and Ojiambo, S. B., 1987a. "East Olkaria geothermal field, Kenya, 1. History match with production and pressure decline data," *J. Geophys. Res.*, **92**, B1, 521-539.

Bodvarsson, G. S., Pruess, K., Stefansson, V., Bjornsson, S. and Ojiambo, S. B., 1987b. "East Olkaria geothermal field, Kenya, 2. Performance predictions, *J. Geophys. Res.*, **92**, B1, 541-554.

Kenya Power Company, Ltd., 1984. Status report on steam production, report prepared by Merz and McLellan and Virkir Ltd., Nairobi, Kenya, 95 p.

Svanbjornsson, A., Mathiasson, M., Frimannsson, H., Arnorsson, S., Bjornsson, S., Stefansson, V. and Saemundsson, K., 1983. "Overview of geothermal development at Olkaria in Kenya," Proc. Ninth Workshop on Geothermal Reservoir Engineering, Stanford University, Stanford, CA, 65-72.

PROCEEDINGS, Fourteenth Workshop on Geothermal Reservoir Engineering
Stanford University, Stanford, California, January 24-26, 1989
SGP-TR-122

RESULTS OF WELL LOGGING OPERATIONS AT THE AHUACHAPAN GEOTHERMAL FIELD, EL SALVADOR

Bert Dennis, Ray Jermance, Robert Lawton, Los Alamos National Laboratory
Alejandro Quintinilla and Juan Berganza, a Comision Ejecutiva Hidroelectrica del Rio Lempa

ABSTRACT

Well logging operations were performed in eight of the geothermal wells at Ahuachapán. A series of high temperature instruments, including temperature/rabbit, caliper, fluid velocity/temperature/pressure (STP) and fluid sampler were deployed in each well. The caliper tool was used primarily to determine the possible chemical deposit buildup in the casing or liner, and in one well to investigate a suspected break in the casing.

STP logs were obtained form six of the eight wells at various flow rates ranging from 30 to 70 kg/s. A static STP log was also run with the wells shut in to provide data to be used in the thermodynamic analysis of several production wells.

INTRODUCTION

The Ahuachapán geothermal field is located in the northwest section of El Salvador about 120 km from San Salvador (see Fig. 1). The first geothermal electric power power generating plant in Central America came on-line in 1975 in Ahuachapán. The generating capacity grew from an initial 30 megawatts (MW) to 95 MW in a six year period. Over 40 wells have been drilled in the Ahuachapán field. The high quality geothermal resource at one time produced 42% of the electrical power used in El Salvador. In recent years, however, productivity of generated power has dropped primarily due to declining well production.

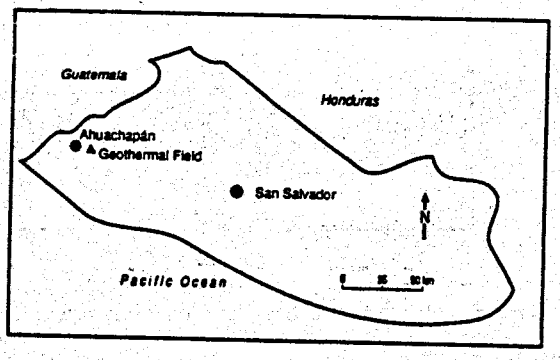

Fig. 1. Map of El Salvador, showing location of Ahuachapán..

La Comision Ejecutiva Hidroelectrica del Rio Lempa (CEL) is the agency of the Salvadoran government responsible for the Ahuachapán geothermal operations.

The Los Alamos well logging team, in collaboration with CEL focused on the problem of declining well production. The objectives in making downhole measurements with the high-temperature logging tools developed at Los Alamos were to determine whether the production declines could be attributed to individual well damage, reduction in the central reservoir pressure or a combination of these and other factors. The well logging data could improve existing reservoir models of the Ahuachapán field. Studies of the data will provide input for an integrated reservoir engineering investigation that will culminate in the design and implementation of an effective spent brine reinjection program.

WELL LOGGING OPERATIONS

The Ahuachapán field operations included downhole measurements in three production wells: AH-1 , AH-32, and AH-20. AH-1 was a good production well located near the center of the geothermal field (Fig 2). AH-32 was drilled in the

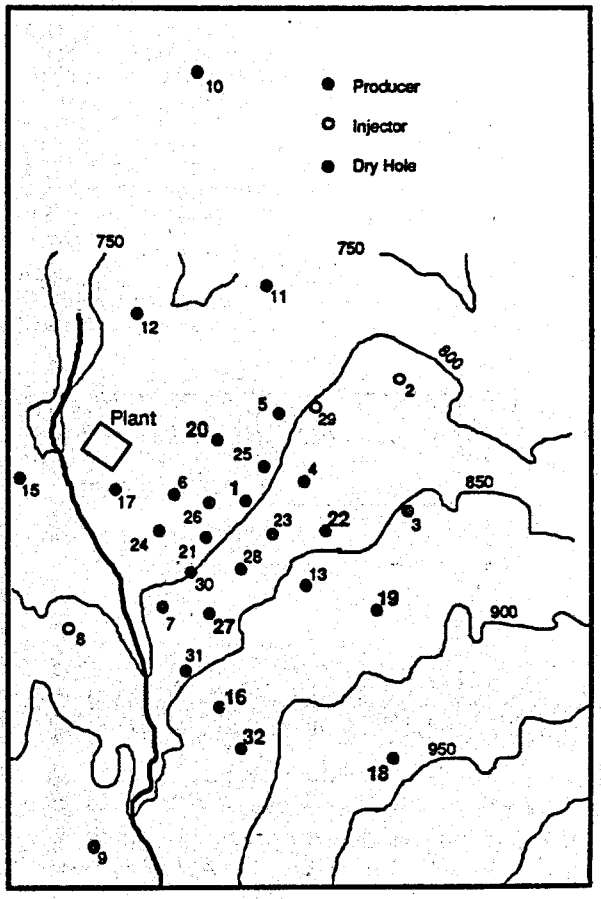

Fig. 2. Schematic map of the Ahuachapán Geothermal Field, showing well locations.

southern most section of the exploration area and AH-20, a damaged well, was located just east of the power plant. The well completion schedule for the three wells is given in Table 1.

Table 1
Well Completion Schedule

Well Number	AH-1	AH-32	AH-20
Casing size ,mm	244.5	244.5	340.
Liner size, mm	none	193.7	244.5
Openhole diameter ,mm	222.3	215.9	n/a
Bottom of casing	457	490	449
Top of liner ,m -	-	470	423
Bottom of liner, m	-	1500	850
Bottom of hole, m	1195	1504	853

193.7 mm (7-5/8 in.), 216 mm (8-3/4 in.) 244.5 mm (9-5/8 in.), 340 mm (13-3/8 in.

Production well AH-1

The first well, AH-1, was located near the base compound at well AH-6. A relatively large cleared area surrounded this well made it the best place to rig up the logging equipment for the first time at Ahuachapán. It was necessary to go through this procedure, taking the time to explain and demonstrate each step in order to train the CEL operators on safe field procedures. Information regarding the production of AH-1 included the reported water level at 525 m, the main production zone at 554 m and a maximum temperature of 225°C. The maximum flow rate was 54 kg/s with a flowing wellhead pressure of 5.9 kg/cm^2 (0.4 psi). The shut in pressure could build up to 3543 kg/cm^2 (248 psi).

A temperature survey was run in AH-1 from the surface to 100 m. The temperature tool had the ring gage or "rabbit" attached to provide clearance information regarding this wellbore prior to deploying the more expensive downhole instruments. The temperature log, run with the well shut in (static), shows the water level or liquid to vapor interface at 590 m Fig. 3. The casing in AH-1 was cemented in to a depth of 457 m from the surface. The wellbore was open hole from there to 1195 m. Maximum temperature measured was 231°C.

The combination fluid velocity (spinner)/temperature/pressure instrument can provide the data necessary to investigate the thermodynamic behavior of the geothermal well. Mass flow rates can be calculated knowing the fluid density, flow area and fluid velocity. Fluid densities can be determined if the temperatures, pressures and vapor qualities are known. Vapor quality can be calculated assuming no total heat loss (enthalpy) throughout the borehole using the value of enthalpy at the liquid interface.

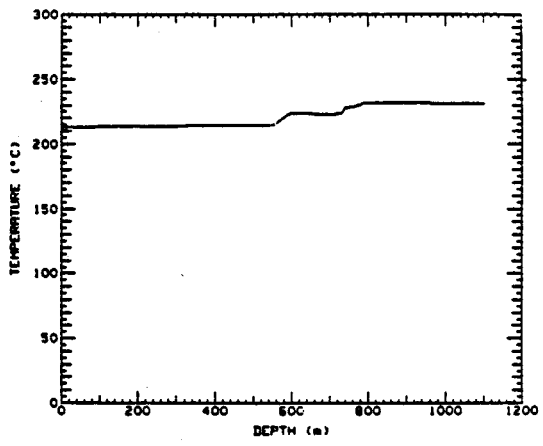

Fig. 3. Static temperature/rabbit survey, well AH-1.

The STP tool was run in AH-1 starting at a depth of 100 m and logging the well to 1100 m. The first survey was run with the well shut-in (static) to provide for "in-situ" calibration information for the pressure and spinner transducers. A second log was run with the well flowing at approximately 30kg/s. The temperature data from this survey shows that the vapor to liquid interface is at 600 m (Fig. 4) which agrees with pressure (based on temperature) intersection plotted in Fig.5.

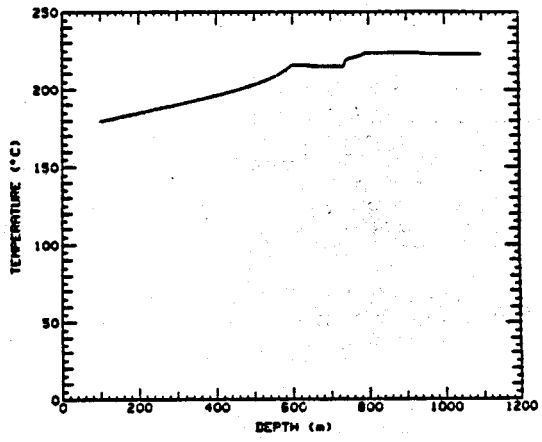

Fig. 4. STP temperature survey, well AH-1, 30 kg/s flow.

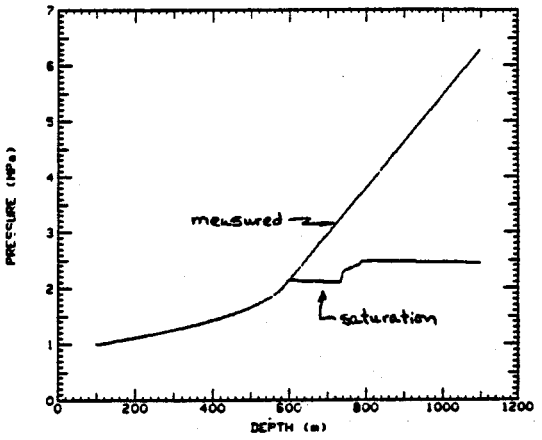

Fig. 5. Pressure data and saturation pressure, well AH-1, 30 kg/s flow.

The spinner output in Hertz vs depth is plotted in Fig. 6. A problem with the trigger level in the electronic counter that measures spinner frequency inhibited the data acquisition between the depths from 280 m to 410 m in the vapor region of the wall. This plot does indicate major production zone around 500 m and 580 m.

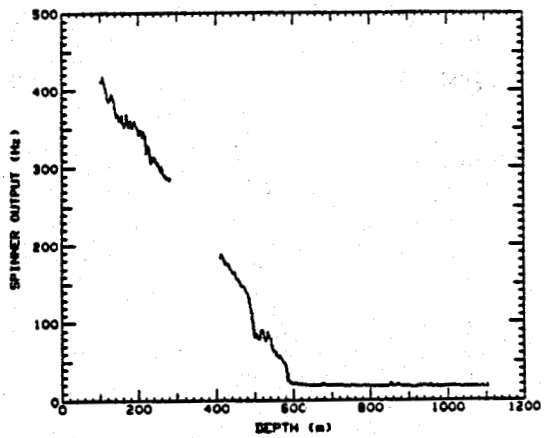

Fig. 6. STP spinner survey, well AH-1, 30 kg/s flow.

The fluid velocity is obtained by subtracting the tool velocity or logging rate from the indicated spinner values. The spinner or velocity transducer is normally calibrated for each log. This *in-situ* calibration is determined from the spinner data and the tool velocity (time vs depth data) in the liquid region of the well during the static survey. The proportionality constant used for the spinner for this series of logs was 0.0318 m/s/Hz. The mass flow rates were calculated as a function of depth and the results are shown in Fig.7. The average mass flow in the

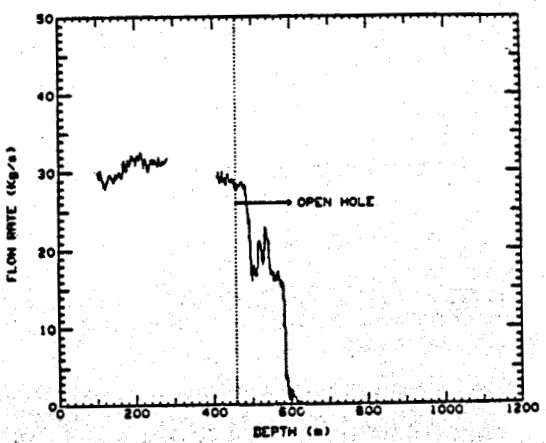

Fig. 7. Calculated flow rate, well AH-1, 30 kg/s flow.

casing is about 30 kg/s.. Vapor quality was also calculated using the value of enthalpy at the liquid interface and is plotted in figure 8.

A third STP survey was conducted with the well open to full flow. The mass flow rate (Fig. 9) indicates an additional production zone between 640 m and 660 m. Mass flow rate in the casing averages 58 kg/s., which is in agreement with the reported flow rate. Vapor quality calculated for the higher flow rate is plotted in Fig. 10.

Damaged Well AH-20

Well AH-20 was of considerable interest because steam was emerging at the surface around the outside of the wellhead. There was speculation that the well damage might have been parted casing near the depth that the liner was hung or that the cement around the casing shoe had deteriorated. The well was "killed" by pumping cold water down the casing into

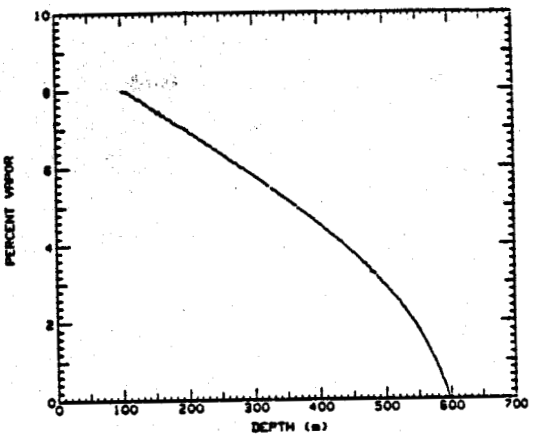

Fig. 8. Vapor quality, well AH-1, 30 kg/s flow.

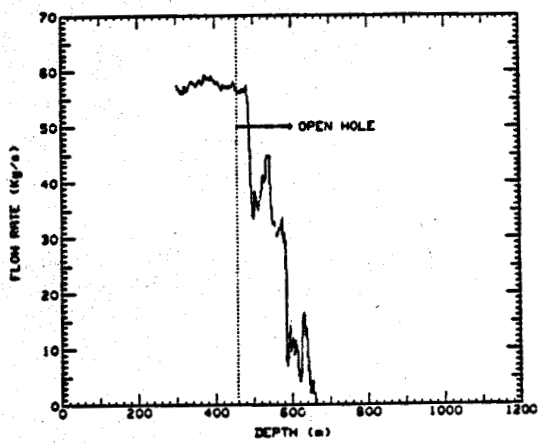

Fig. 9. Calculated flow rate, well AH-1, 58 kg/s flow.

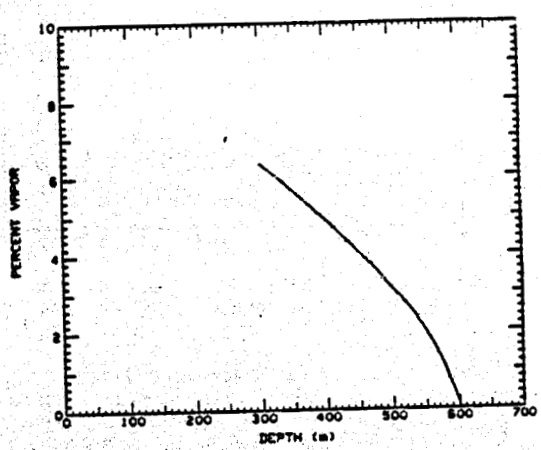

Fig. 10. Vapor Quality, well AH-1, 58 kg/s flow.

the borehole. Other information received form CEL concerning AH-20 indicated a main production zone at 455 m with a secondary zone at 700 m. The liquid/vapor interface was reported to be at 525 m and the maximum temperature was 219°C. Prior to killing the well, the static wellhead pressure was 3043 kg/cm^2 (213 psi) and flowing pressure was 8.9 kg/cm^2 (0.6 psi).

Since AH-20 was in the killed status and cold water was still being pumped down the well, no pressure lock was required during the logging operations. The temperature/rabbit tool was deployed to a depth of 827 m where it set down 23 m above the bottom of the liner. The temperature log (Fig. 11) clearly shows the cold water interface and the area where fluid is leaving the wellbore. This data also indicates that this interface can move up and down the wellbore when the pumps are turned on or off for short periods.

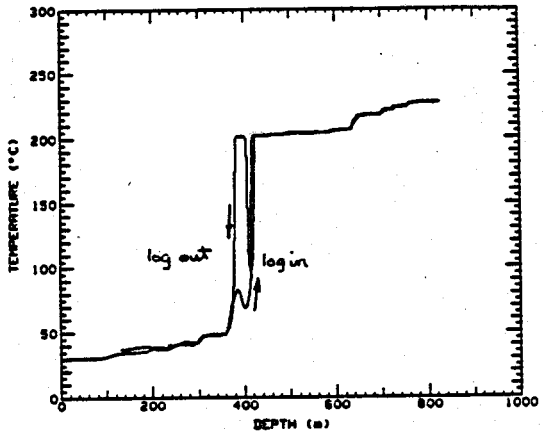

Fig. 11. Temperature/rabbit survey, well AH-20.

The STP log confirms the evidence of the fluid leaving the wellbore at 420 m as shown by the STP temperature data Fig. 12 and the spinner output data Fig. 13.

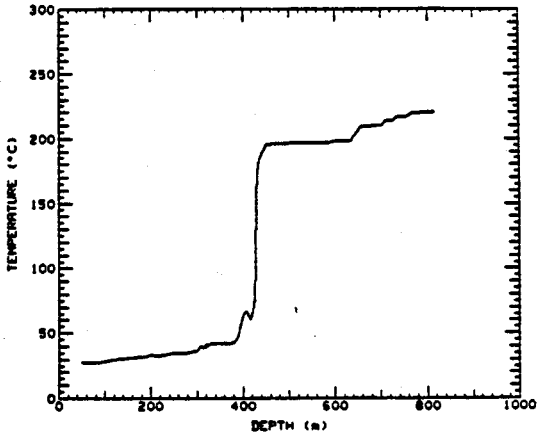

Fig. 12. STP temperature survey, well AH-20.

The 3-arm caliper tool was deployed to 800 m and the the well logged up to the surface. There is evidence of chemical build up in liner below 700 m (which may account for the set down of the temperature/rabbit at 826 m) and some around the lower part of the casing. There are no indications of a break in either the casing string or the slotted liner (Fig. 14). It appears that the fluid is leaving near the casing shoe which could indicate a bad cement zone.

Production Well AH-32

AH-32 was a good production well with a reported mass flow rate of 70 kg/s.. Maximum temperature was 241°C and the well head pressure shut-in was 2285.6 kg/cm2 (160 psi). There were several production zones with locations estimated

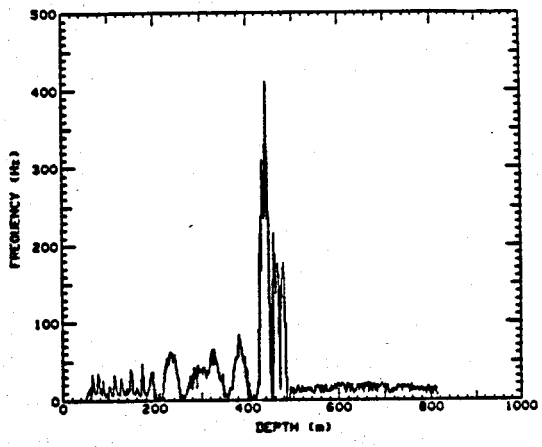

Fig. 13. STP spinner survey, well AH-20.

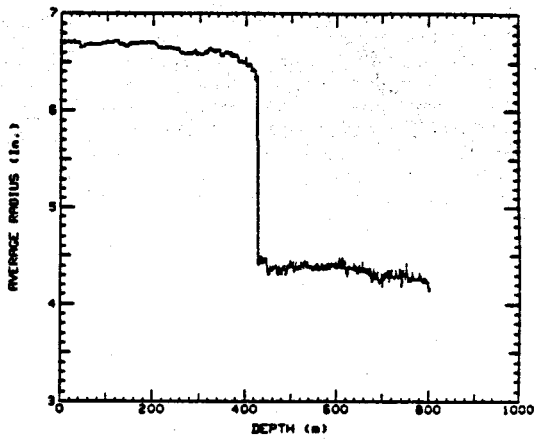

Fig. 14. Three arm caliper survey, well AH-20.

at 775 m (two phase flow). 800 m, 1000, and 1400 m. The major production zones were reported to be at the 1000 m and 1400 m depth.

The first temperature log was started in the well under flowing conditions. The temperature/rabbit tool was lowered in the casing to 50 m and stopped at this depth while the flow line was opened to allow a flow rate of 45 kg/s.. The tool was then run in the well until a set down at 470 m stopped the tool. The tool would not enter the slotted liner under the flow conditions and the well had to be shut in. The temperature log was run to a depth of 1450 m under static conditions and back up the hole to the surface. There were no obstructions encountered in AH-32 other than the top of the liner. Maximum temperature measured was 241°C. The 3-arm caliper tool was run in AH-32 under shut in (static) flow conditions. The arms were deployed at 1400 m and the caliper survey logged to the surface. The top of the liner was tagged at 465 m. No evidence of chemical build-up in the well was observed in the data (Fig. 15).

Difficulties were encountered when running the STP tool in AH-32. The higher pressure at the wellhead at an initial flow rate of 45 kg/s and the light weight of the tool (36.3 kg , or 80 lbs) prevented the tool from entering the well. The tool, therefore, was deployed to a depth of 200 m with the well shut in. The well was again opened to a flow rate of 45 kg/s and the tool desended to 470 m were it would not enter the slotted liner. The flow rate was then decreased to 20 kg/s and the STP log run from 480 to 1450 m at this lower flow rate.

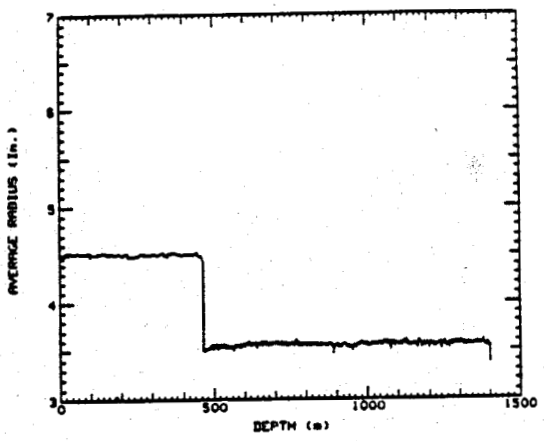

Fig. 15. Three arm caliper survey, well AH-32.

The liquid to vapor interface was measured at 840 m as shown by both the STP temperature data (Fig. 16) and the measured and saturation pressures calculated at temperature (Fig. 17). The measured pressures above the liquid surface are lower than the saturation pressures which means the vapor was in the superheated region. Using the pressure and temperature data and assuming no heat loss in the two phase region the calculated vapor quality for the 20 kg/s flow rate is shown in Fig. 18.

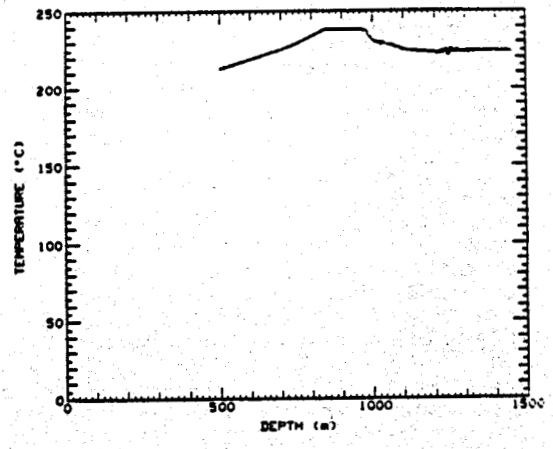

Fig. 16. STP temperature survey, well AH-32, 20 kg/s flow.

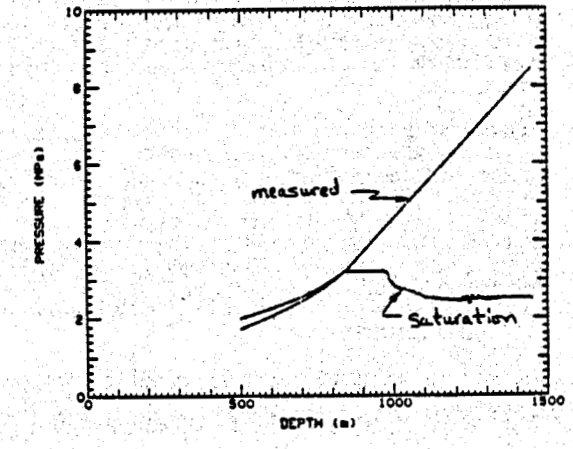

Fig. 17. Measured and saturation pressures, well AH-32, 20 kg/s flow.

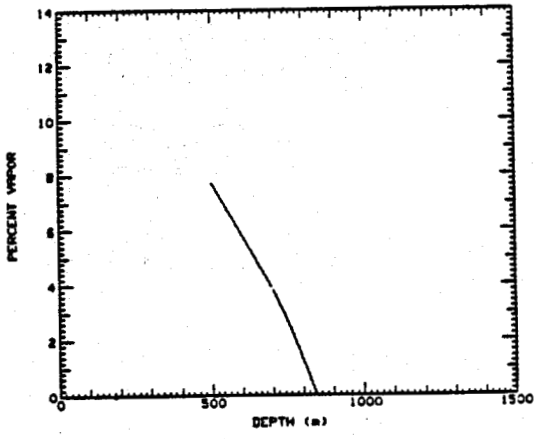

Fig. 18. Vapor quality, well AH-32, 20 kg/s flow.

The output of the fluid velocity transducer (spinner) is plotted in Fig. 19. A proportionality constant for the spinner can be determined from the data obtained in the liquid region of the well. The spinner output in Hertz for both the log in and the log out is proportional to the fluid velocity plus the tool velocity. Tool velocities are calculated from the time and depth data recorded during the logging operation. The proportionality constant for the spinner in AH-32 was calculated to be 0.0739 m/s/Hz. Notice the negative frequency counted during the log out in the liquid region which means the impellars were rotating in a reverse direction coming out of the hole. There was very little fluid flow if any up the well below 980 m.

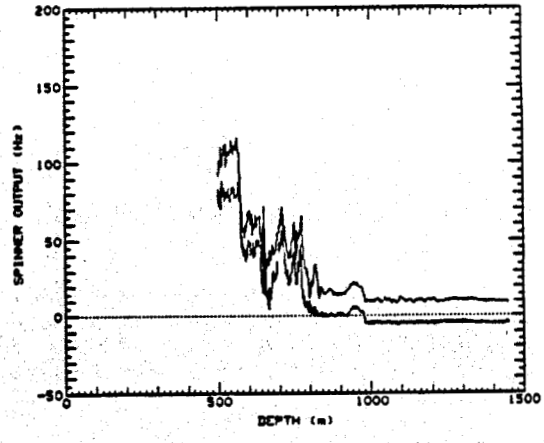

Fig. 19. STP spinner survey, well AH-32, 20 kg/s flow.

Knowing the velocities and thermodynamic properties of the flowing fluid ,mass flow rates can be calculated. In the case of AH-32 all of the data for the flowing log was taken in the slotted liner below the casing. In this case the diameter of the open hole would be applicable to calculate the mass flow rate but since this diameter throughout the open hole is not well defined the calculated mass flow rates are quite erratic. Using a constant 215.9 mm (8.5 in.) diameter for the open hole is not a good assumption. A second STP log was run from 500 m to 1200 m at a flow rate of 45 kg/s. The data from the temperature data (Fig. 20) and the measured pressure and calculated saturation pressure (Fig. 21) show the liquid to vapor interface at 860 m. The vapor above the 860 m depth is in the superheat region. Vapor quality for this second flowing

log is plotted in Fig. 22. The spinner data again shows a major production zone starting at 980 m but there is little evidence of production zones below this depth (Fig. 23).

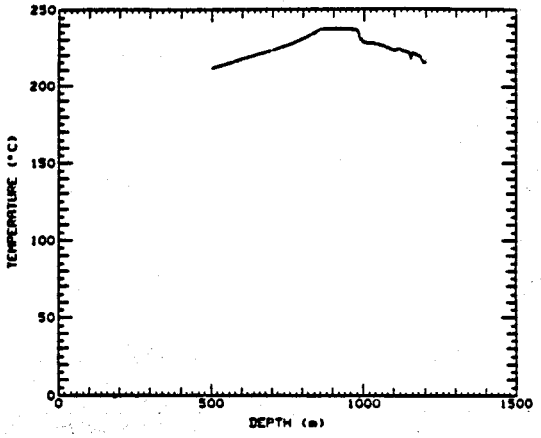

Fig. 20. STP temperature survey, well AH-32, 45 kg/s flow.

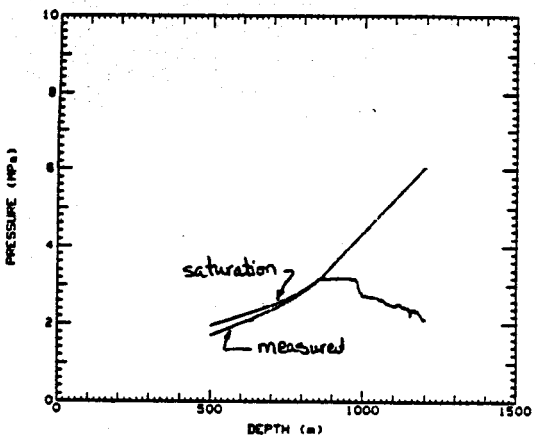

Fig. 21. Measured and saturation pressures, well AH-32, 45 kg/s flow.

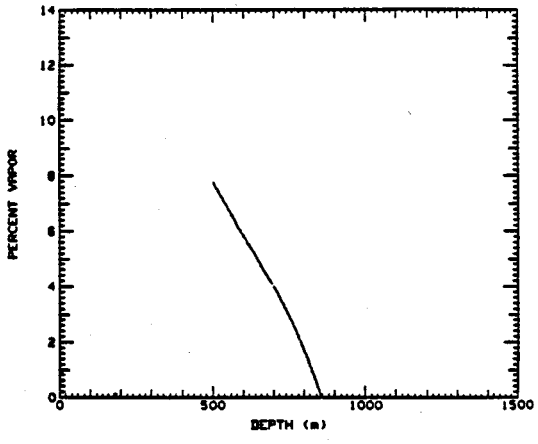

Fig. 22. Vapor quality, well AH-32, 45 kg/s flow.

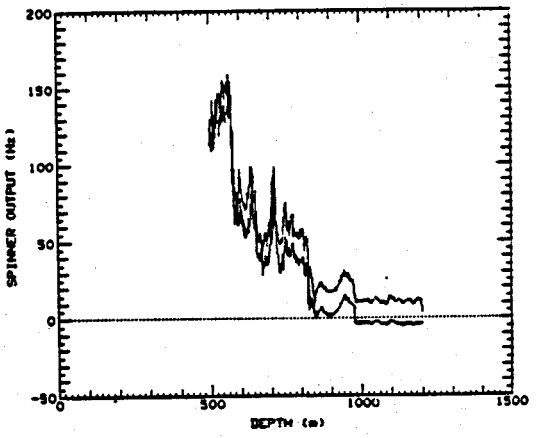

Fig. 23 STP spinner survey, well AH-32, 45 kg/s flow.

A third flowing log was started at 500 m with the well open to 60 kg/s. The spinner was working fine but 2 broken centralizers on the tool prevented it from going down the well and the log was terminated.

CONCLUSIONS

The maximum temperature in the geothermal wells in the Ahuachapán field approached 250°C. Wellhead pressures were reported to be as high as 4285 kg/cm^2 (300 psi) and flow rates reached 70 kg/s. The downhole instruments and associated equipment were capable of continuous and repeated performance in this severe geothermal environment. The wellhead pressures in some wells were, however, higher than initially anticipated and caused problems when first starting the logging tools downhole. This was especially true for the lighter STP tool. Although a new impeller design was implemented during the later phases of the Ahuachapán operations, it was evident that more mass must be added to the STP sonde. A sub had been designed that will easily be assembled in the field between the cable head and the uphole end of the tool. This subassembly will add about 54 kg (120 lbs) of mass. These improvements will now allow the STP to provide required measurements in the entire wellbore under maximum flow conditions.

The high temperature STP and 3-arm caliper tools can provide all of the data necessary to determine the thermodynamic fluid properties of the production wells when wellbore conditions are applicable. For the thermodynamic analysis to be meaningful, it is necessary that the diameters of the completed well sections of casing, liners and open hole be known. There must also be a liquid to vapor interface that is well defined with the liquid region of sufficient depth to provide the "in-situ" calibration of the respective downhole transducers.

Non-producing wells can result from wellbore damage during the drilling and well completion operations or from long term effects. Non-producing wells may also be the result of the well location in the field. The nature of such wells are not well known especially when they occur in the vicinity of good producers. The logging systems used in the Ahuachapán operations often provide information that can result in appropriate analysis and interpretation.

ACKNOWLEDGEMENT

This work was part of a United States Agency for International Development (USAID) program, and was overseen by the Regional Office for Central American Programs in Guatemala City.

PROCEEDINGS, Fourteenth Workshop on Geothermal Reservoir Engineering
Stanford University, Stanford, California, January 24-26, 1989
SGP-TR-122

DC Resistivity at the Ahuachapán Geothermal Field, El Salvador

James B. Fink, Geophynque International, U.S.A.
Mauricio de la Fuente D., Geociencias Aplicadas, S. A., Mexico
Carlos Rodriquez, CEL, El Salvador
Dan J. Cash & Michael Gerety, Los Alamos National Laboratory, U.S.A.

ABSTRACT

Deep dc resistivity surveying has been performed at the Ahuachapán Geothermal Field in western El Salvador. The field lies on the north base of the volcanic range that runs the length of the country and is the site of a significant active geothermal powerplant. The technical purpose of the surveying was to assess the geophysical properties of the geothermal regime around the existing field. The survey was carried out as a colinear dipole-dipole survey using dipole spacings of 500m and 1000m, and dipole separations of up to fourteen dipole lengths. Results included (1) the observation that the geothermal reservoir was not readily detectable due to surface lithologic changes and extensive cultural effects, (2) the hydrothermally altered areas are readily recognized by their low resistivities, (3) local lithologies appear to be mappable based on their *in situ* resistivities, (4) the greater field logistical convenience of the shorter 500m dipole spacings is negated by the increase in topographic effects, and (5) if appropriate dipole separations are used, there is no need to run surveys of both 500 and 1000 meter dipole spacings to gather shallow and deep information.

INTRODUCTION

A deep resistivity geophysical survey was performed at the Ahuachapán geothermal field (AGF), the site of a 90 megawatt powerplant, in western El Salvador between November 1987 and May 1988. The survey was part of a project of geothermal resource evaluation and technology transfer program sponsored by Los Alamos National Laboratory (LANL) and funded by the United States Agency for International Development (USAID). The results of two survey lines are presented in this paper; however, two additional lines have recently been completed and will be presented in a future report.

OBJECTIVES

The technical objectives of the resistivity program were designed to study particular aspects of the geothermal resources of the Ahuachapán region by defining the electrical characteristics of the known geothermal reservoir such that adjacent areas may be investigated and compared. Specifically,

1. identifying and mapping the relevant physical properties related to shallow geothermal production so that the Chipilapa area to the east may be better evaluated, and
2. determining the deep electrical characteristics beneath the volcanic mountains to the south of Ahuachapán to evaluate the geothermal and recharge potential in that area.

LOCATION

The AGF, as shown in Fig. 1, is located at the western end of El Salvador immediately north of a chain of volcanic mountains that run the length of El Salvador. Site elevation is approximately 800 meters. The mountains to the south rise to approximately 1800 meters. None of the volcanoes is active but some are young enough to have well defined craters. The geothermal field is named after the nearby town of Ahuachapán in the state of Ahuachapán.

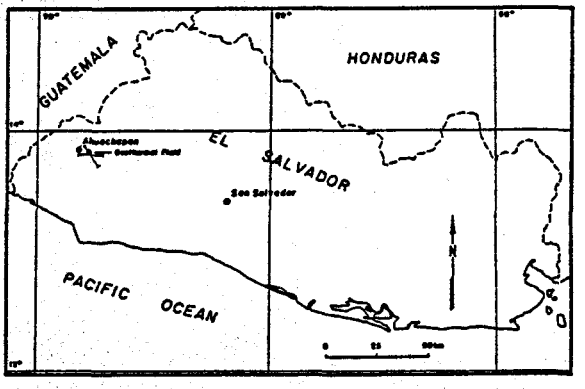

Fig. 1. Location map of the Ahuachapán Geothermal Field, El Salvador.

METHOD

Resistivity Surveying

The method of electrical resistivity surveying employed a dipole-dipole array with dipole spacings of 500 and 1000 meters. Lines 1 and 2 shown in Fig. 2 consisted of 24 line kilometers.

In order to assure adequate shallow resistivity information, dipole separations of 0.1, 0.5, 1.0, 1.5, 2.0, 3.0, 4.0, 5.0, and 6.0 were used to collect the 1000 meter dipole data, and the 500 meter dipole data were gathered using separations of 0.2 and integer intervals of 1 through 14. The reduced data are presented in logarithmic pseudosection format. The objectives of using two dipole spacings were to enhance the lateral and near-surface resolution with the shorter dipole spacing (500m) and to allow deeper penetration with the larger spacing (1000m). Both of these objectives were achieved successfully. Indeed, the combination of field logistics and resultant data suggest that future work may be satisfactorily performed with only the 500m spacing, *if adequate current is injected into the ground.* In situations where adequate current is not achievable, larger dipole spacings must be used.

Previous resistivity work performed by CEL included Schlumberger array vertical electrical soundings (VES's) in a grid covering the Ahuachapán area and extending to the northeast towards Turin. This grid is outlined in Fig. 2. Qualitative and quantitative data comparisons between the dipole-dipole array work and the VES's are quite good. The dipole-dipole data, because of instrumental design, allowed deeper penetration with minimal interference from electromagnetic (EM) response, whereas the VES data, because of instrumental design limitations, appeared to suffer from EM response at the larger spacings. The data for the larger current-electrode spacings for the VES's were qualitatively corrected for the EM response but the quantitative interpretation for those spacings was still questionable.

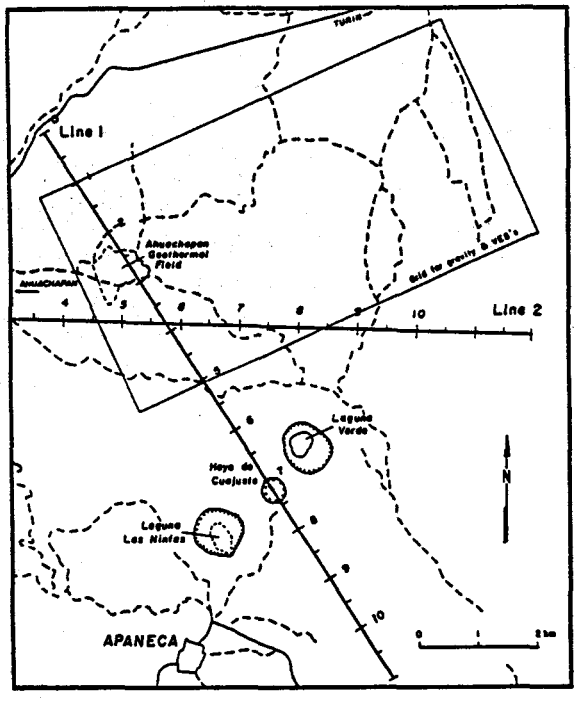

Fig. 2. Location map of Lines 1 and 2 for the dipole-dipole dc resistivity program of 1987-1988.

Survey Program

The survey consisted of four lines, three of which were oriented due east-west, approximately parallel to each other, and eight kilometers long. These lines were one-half kilometer apart and located so that they would connect the known area of the AGF to the Chipilapa area by crossing the southwestern corner of the grid of existing VES data. This would then extend the resistivity information to the south of the grid. The fourth line (Line 1) was oriented approximately N25°W so that it would cross the western end of the VES grid, cross the established limits of the AGF, and extend to the south over the mountains.

Data Presentation

Dipole-dipole data are generally presented in pseudosection format. This method of data presentation displays the collected data in a manner such that the horizontal scale is linear distance and is scaled in units of dipole length and the vertical scale is in units of dipole separation and may be either linear or logarithmic. The vertical axis is positive downward. Although the appearance is that of a geologic section, we must emphasize that the location of the plotted points is not necessarily representative of depth.

Topographic Modeling

The effects of topography on a resistivity survey are well known. These effects are due mostly to two causes: lack of collinearity of the four electrodes represented by any given data point, and compression or expansion of the equipotentials observed on the earth's surface related to the transmitting dipole.

For the work herein, the method of Schwarz-Cristoffel conformal transformation was used to approximate the topographic effects. This method allows the topography along the survey line to be modeled as if it were a two-dimensional structure. In the case of Line 1, where it crosses the Hoyo de Cuajuste crater, there are severe topographic effects and they are not two-dimensional. However, the 2-D model results give a qualitative idea of the trends and magnitudes of effects anticipated from the modeled structures.

Topographic effects are determined by the severity of the topography relative to the dipole size. At Ahuachapán, topographic effects were maximum where the line crossed the highest elevation and the Cuajuste crater. Ridges produce an increase of the observed apparent resistivities, in this case with 1000m dipoles, up to fifty percent greater than a flat surface. Valleys, or flanks of ridges, reduce the observed apparent resistivities, approximately twenty-five percent less using 1000m dipoles. In spite of the large topographic effects present, the general patterns present in the uncorrected 1000 meter apparent resistivity pseudosection were still present after removing the topographic effects suggesting that lithologic changes occurred sympathetically with the topography. Prior to geologic modeling, the modeled 2-D topographic effects were subtracted from the observed field data.

Geologic modeling

Modeling of apparent resistivity due to complex earth structures is more computationally intensive than the topographic modeling. For this work, 2-D geologic models using a finite element algorithm were used to approximate the observed data. The finite-element routine used is a commercially available program.

Drilling has shown that the AGF reservoir is limited in lateral extent and therefore three-dimensional. Nevertheless, 2-D approximations are the most readily available and should suffice to guide the interpretation of the observed data. Physical property values for the model were based on reported laboratory-measured physical properties performed by CEL and estimated physical properties from short-dipole-spacing field data. The laboratory resistivity measurements were made for a frequency range of 5 to 10,000 Hz and three pressures of 100, 500, and 1000 psi. The laboratory results show reservoir rocks (andesite and breccia) to have true resistivities in the range of 5 to 50 ohm-meters, whereas overlying tuffs and lavas range from 10 to 1000 ohm-meters. The reported trends of increasing resistivity with decreasing frequency are acknowledged, but extrapolation to dc is not prudent as induced polarization effects are also inferred to be present in the laboratory data. The inverse relationship of resistivity with pressure at the lower frequencies is also acknowledged. This would only tend to decrease the observed apparent

resistivities in the field data. Although there appears to be a tendency for the tuffs and lavas to be of moderate to high true resistivity, hydrothermal alteration of any of the lithologies present will produce low resistivities.

INTERPRETATION

LINE 1 (a = 1000m)

Observed values ranged from 2.3 to 250 ohm-meters. In general, the apparent resistivities fall into two groups, low (2 to 20 ohm-meters) and moderate (20 to 200 ohm-meters). The low values correlate with the surface expression of hydrothermally-altered lithologies and with deeper stratified lithologies, most likely those of the andesites and saturated agglomerates in the lower Quaternary San Salvador Formation. There is no evidence in the resistivity data that older lithologies such as the Pliocene Balsamo Formation were detected. The moderate apparent resistivities correlate with the shallower tuffs and lavas where they appear to form cap-rock and in the high-topographic-relief area where the survey line crosses the mountains.

Line 1 (a=1000m) data are shown in logarithmic pseudosection in Fig. 3. Increased data density was desired in the immediate vicinity of the AGF, so the received data were collected with half-dipole moves for the transmitter resulting in double density coverage. The portion of the AGF crossed by the line is between stations 2 and 3. Blank spaces occurring beneath dipoles 4-5 and 6-7 indicate unreliable or unreadable data.

A qualitative investigation of the data in Fig. 3 indicates considerable variation in the near-surface apparent resistivities. The lowest values (3.8 ohm-meters) for the shallowest data occur at station 5 which was located among fumaroles. Low values also occur at the AGF (5.5 ohm-meters) and next to Cerro Blanco (another hydrothermally altered area) at station 6 (4.0 ohm-meters). In the high-density portion of the pseudosection these low apparent resistivities are flanked by slightly higher values ranging from 5 to 17 ohm-meters.

Moderate-valued near-surface apparent resistivities occur to the extreme northern and southern ends of the line and midway between stations 3 and 4. The northern end of the line is in a cultivated area. Generally, shallow data are artificially low due to the increased soil moisture content typical of cultivated areas. Consequently, the slightly-higher-valued shallow data seen in this area demonstrate that the lower-valued shallow data seen elsewhere are not due solely to surface moisture. The moderate-valued apparent resistivities occurring in the southern end of the line are in the area of outcrop and high topographic relief. Therefore, they would be expected to be higher-valued than data in lower, cultivated areas. The significance of the very low values mentioned previously is that they occur where extensive hydrothermal alteration is quite evident at surface. With increasing depth (pressure), saturation, and temperature, the true resistivities should decrease considerably. Therefore it is expected that lower apparent resistivities should appear for larger dipole separations, especially in the vicinity of the geothermal field where extensive hydrothermal alteration has taken place.

Of particular interest is the moderately-valued shallow data between stations 3 and 4. These data are flanked by lower values. Therefore, this local, moderately-resistive area probably represents a near-surface, relatively unaltered lithologic block that may be representative of caprock material. The block is likely 100 to 200 meters thick and perhaps up to a kilometer wide in the direction of the survey line and is restricted to the area between stations 3 and 4.

The lowest values occur immediately beneath this localized, near-surface, moderately-resistive block. Model data show that the low closure for the 3 ohm-meter contour is a constructive interference phenomenon and that more representative true resistivities would be around 5 to 10 ohm-meters. The interference phenomenon results from the lower near-surface resistivities which modeling suggests to be around 5 ohm-meters or less.

With increasing dipole separation the apparent resistivities appear to increase (for example, between stations 4 and 5) perhaps suggesting a deep, resistive medium. The presence of a deep resistive body or layer is unresolvable due to the fact that surface resistivities also increase to the south which, as already indicated, will produce constructive interference for the larger spacings.

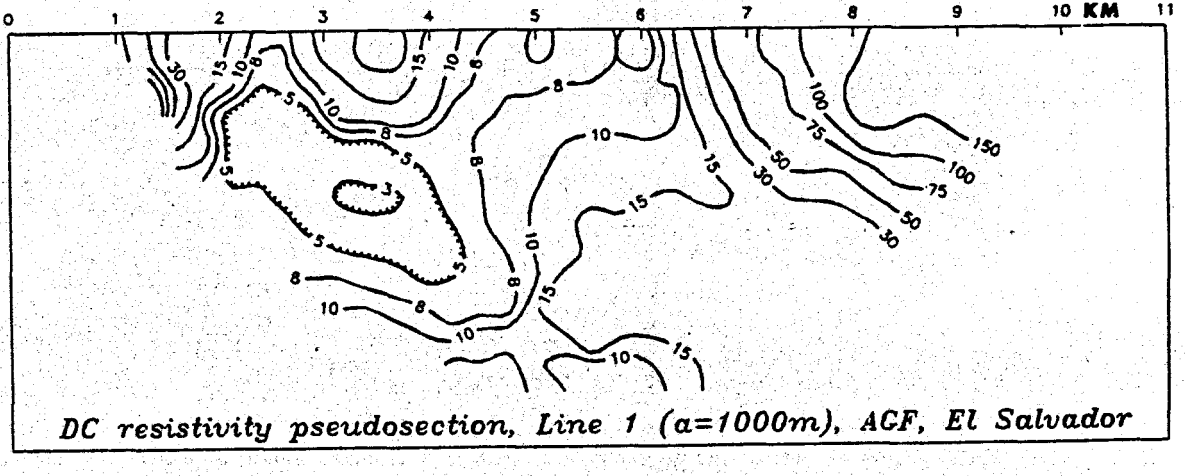

Fig. 3. Pseudosection of Line 1 showing the apparent resistivities logarithmically contoured in ohm-meters for 1000 meter dipole spacing.

The gradient indicated in the contoured data between stations 6 and 7 suggests a lithologic change occurring on the north slope of the mountains. This gradient location coincides with the contact between the Laguna Verde volcanics and the central graben pyroclastics. The moderately resistive material likely represents the unaltered Laguna Verde mountain-building volcanics. This is supported by the constancy of the shallower apparent resistivities to the south of the gradient that suggest the lithology remains the same within the vicinity of the survey line.

Geologic model

A geologic model for Line 1 is presented in Fig. 4. This model is based on the 1000 meter dipole data. Four media of different true resistivities were used to generate the model: medium 1 (100 ohm-meters); medium 2 (10 ohm-meters); medium 3 (500 ohm-meters); and medium 4 (5 ohm-meters). In the immediate vicinity of the AGF only media 1, 2, and 4 are relevant for the purpose of defining reservoir characteristics.

Model medium 1 (100 Ω-m)

Medium 1 is intended to represent the unaltered (or only partially altered) surface pyroclastics and lavas of younger San Salvador age. The moderate resistivity of 100 ohm-meters suggests limited hydraulic permeability and good potential for caprock formation. Medium 1 is vertically limited to the upper 600 meters. Laterally, medium 1 is modeled at the north end of the line, between stations 5 and 9, and in the previously-discussed isolated block between stations 3 and 4. In general, the base of medium 1 corresponds to the contact between reservoir lithologies and overlying lithologies. The depth to this contact in well AH-12 is reported at 550 meters, whereas in wells AH-1 and AH-20 the depth is 450 to 500 meters. In an area of variable lithology this is considered good agreement.

Model medium 2 (10 Ω-m)

Medium 2 represents lower resistivity material occurring from 300 meters to depth (greater than 1000 meters) and forming a vertical "plume" between stations 3 to 5. This plume-like vertical extension of lower resistivities corresponds very well with the shallow depths to high temperatures between stations 3 and 4. The northern extent or contact of the plume-like low resistivities occurs at station 3 and is coincident with a vertical fault. To the south, the plume-like feature contacts lower resistivity material (medium 4) at station 5 beneath the soccer-field fumaroles. Two lesser blocks of medium 2 are modeled at surface near station 7 to the south and between stations 1 and 2 to the north. These lesser blocks are regarded as being transitional material, probably less altered, between media 4 and 1. The thickness of these blocks is 100 meters, which corresponds well with the known alluvial thickness.

Model medium 3 (500 Ω-m)

Medium 3 represents a high resistivity medium occurring to the south of station 7 and corresponding to the aforementioned Laguna Verde volcanics of the high plateau in the vicinity of Apaneca. Enough resistivity data are available in that area to suggest that the Laguna Verde volcanics overlie more conductive lithologies represented by medium 2. Although medium 2 shows continuity from the AGF to approximately station 9, there is nothing else in the electrical data to support continuity for the thermal characteristics. Nevertheless, this area should not be disregarded for future geothermal potential.

Model medium 4 (5 Ω-m)

Medium 4 is intended to represent extensive hydrothermal alteration regardless of lithology. The close association of the low apparent resistivities with the fumarolic activity and surface alteration suggest that these low resistivities are likely a result of high porosity and high clay content. Hydraulic permeability is probably higher than the less altered lithologies in spite of the increase in clay content.

Although no medium 4 is presented in the model below 600 meters, a simple trade-off exists from the modeling standpoint. Consider the large, irregular block of medium 4 beneath stations 2 to 3. By removing some of that block of medium 4 and placing it below 600 meters in the same general area would produce similar model results. This exemplifies the inherent non-uniqueness of any modeling procedure. The choice of not modeling medium 4 beneath 600 meters was made to determine the resolvability of a conductive deep body with this particular data set. *In this instance*, a deep body of only moderate resistivity contrast with the overlying material is very difficult to detect, *because of the complexity of the overlying geology*. On the other hand, in an area of less surface complexity such as extensive caprock and minimal surface

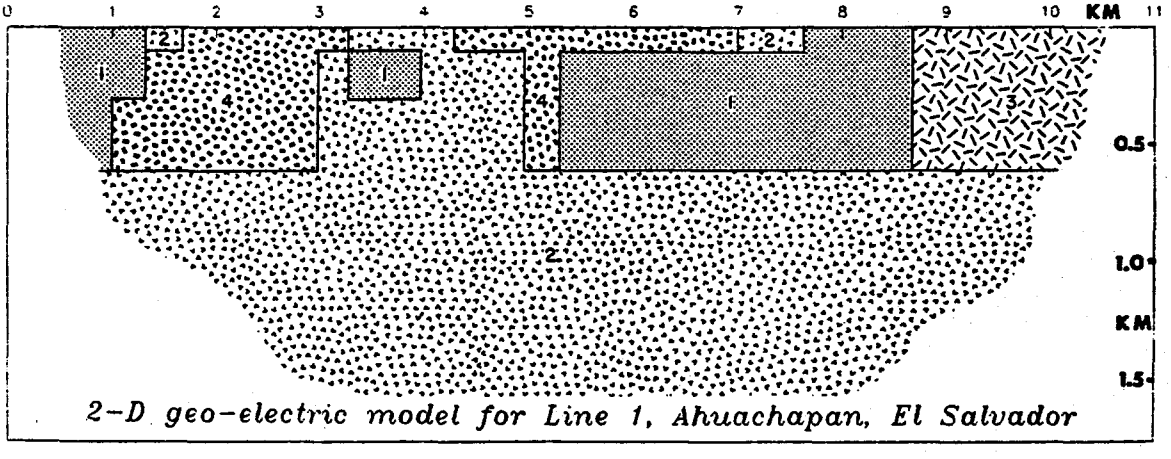

Fig. 4. Two-dimensional geo-electric model for Line 1 based on topographic corrected apparent resistivity data using a finite element program.

alteration, a deep conductive body should be readily mappable.

LINE 1 (a = 500m)

Figure 5 shows the data for Line 1 (a = 500m). As might be expected from the 1000 meter dipole data, the observed resistivities range from 1.8 to 250 ohm-meters. To be as compatible as possible, data were collected for dipole separations ranging from 0.2 to 14. Within the accuracy of the method, the 1000 meter and 500 meter pseudosections are very similar. The same pattern exists for the two sections and consequently the same interpretation would apply. The differences that are observed are not significant enough to warrant modeling changes.

This similarity of results illustrates two important points. First, there is probably no need to collect data at both 1000 and 500 meter dipole spacings as long as; 1. shallow data are collected for the larger dipole spacings, or 2. deeper data are collected for the shorter dipole spacings. The original work plan was oriented towards using the 1000 meter dipole data for deep investigation and the 500 meter dipole data for shallower control. The field work performed at AGF shows that both situations may be satisfied with a single dipole spacing, if appropriate dipole separations are used.

Topographic effects for the shorter dipole spacing are considerably larger and more complex. Figure 6 shows the modeled topographic effects in the vicinity of the Cuajuste crater. In this case the ridge effects may increase the apparent resistivities by up to 100% whereas the valley effects decrease apparent resistivities by approximately 50%. These extremes in topographic corrections suggest that the logistical advantage of shorter dipole sizes may be offset by more complex topographic effects in the resultant data.

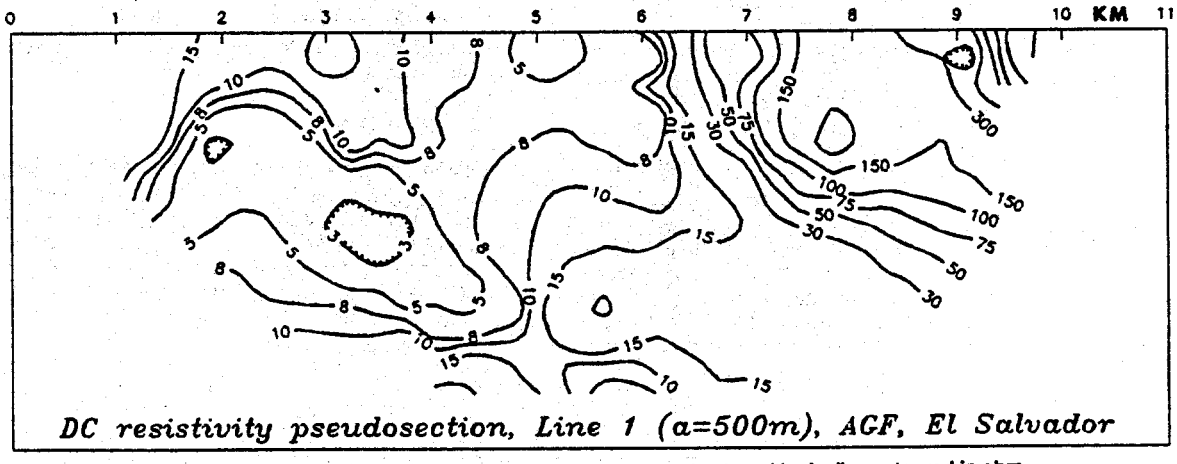

Fig. 5. Pseudosection of Line 1 showing the apparent resistivities logarithmically contoured in ohm-meters for 500 meter dipole spacing.

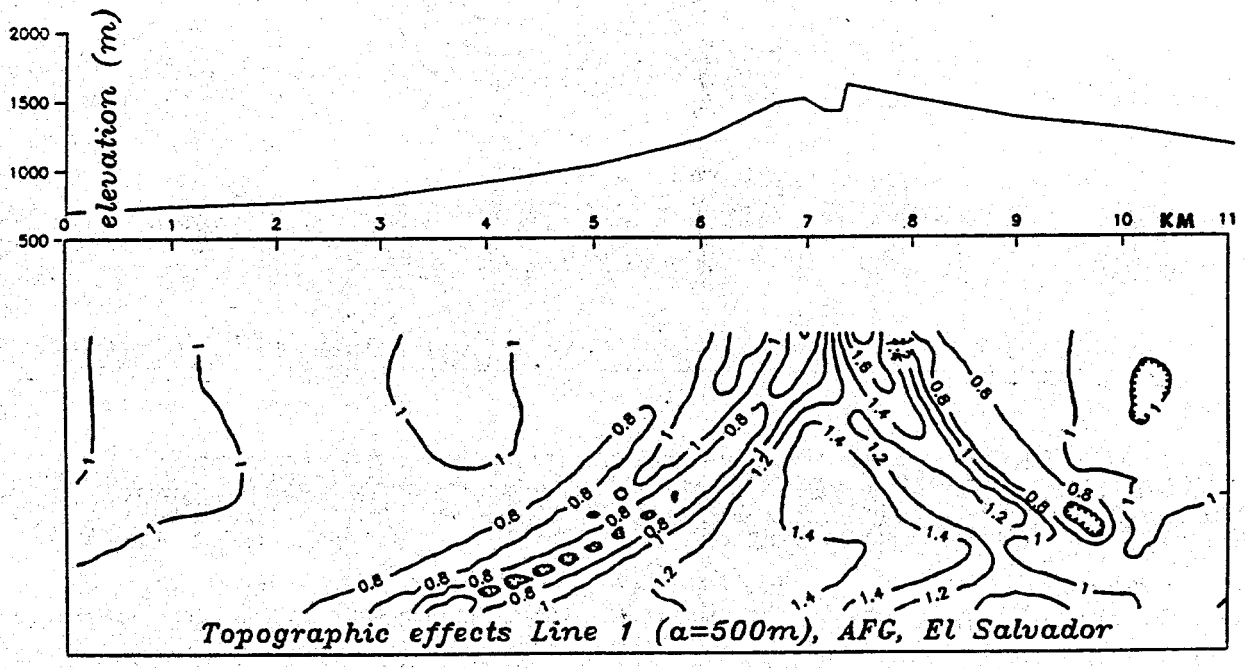

Fig. 6. Logarithmic pseudosection of topographic effects on Line 1 due to the mountains south of the site for 500 meter dipole spacings.

LINE 2 (a = 1000m)

Line 2 is oriented approximately east-west and crosses Line 1 roughly 250 meters north of station 4. The point of intersection on Line 2 is approximately 250 meters west of station 6 (see Fig. 2). Apparent resistivities ranged from 3.4 to 105 ohm-meters. With only a few exceptions, the entire pseudosection shows resistivities less than 20 ohm-meters, however, the general pattern of low-to-high apparent resistivities is surprisingly similar to that of Line 1. The similarity of pattern would be desirable for two-dimensional modeling if the features appeared parallel. They do not appear parallel and do demonstrate the three-dimensionality of the area.

The apparent resistivity data are presented in Fig. 7. The lowest near-surface resistivities occur at station 4 near the Agua Shuca fumaroles. The low apparent resistivities appear to extend to station 5, located just east of the Rio Los Ausoles. Higher resistivities are encountered at station 7 and are suggestive of the localized moderate resistivity block occurring on Line 1 between stations 3 and 4. There does not appear to be a direct connection between these two localized resistive blocks. At surface, another low resistivity area occurs to the east around station 10 which is reasonably close to the Cuyanausul fumaroles. These near-surface, apparent resistivity lows further support the previous observation that they are associated with extremely altered lithologies.

Topographic corrections were not determined for Line 2. The eastern end of the line encountered moderate topographic relief but the lack of severe relief and the non-orthogonal two-dimensionality of the topography encountered minimized the necessity and usefulness of topographic corrections, in this instance.

The most salient feature of Line 2 is the presence of an apparent resistivity low beneath stations 4 to 6. It is most likely that this feature is related to the aforementioned hydrothermally-altered lithologies. This feature is quite similar to the apparent resistivity low occurring on Line 1 beneath stations 2 to 4 in the immediate vicinity of the AGF. Interestingly, both wells AH-8 and AH-9 (which bracket Line 2 between stations 4 and 5) are non-productive. The geologic logs indicate that the more permeable agglomerates are missing in these two holes but the temperature logs indicate that relatively high temperatures are still present.

The consistent values of 10 to 15 ohm-meters is suggestive of an elevated thermal environment between stations 7 and 11. The lack of shallow, more resistive material that could serve as caprock is somewhat of a drawback but not so much that the area should be disregarded. This area lies between the Chipilapa and Cuyanausul surface expressions.

The deeper appearing localized highs and lows in the apparent resistivities are likely the result of interference effects from surface features.

LINE 2 (a = 500m)

As with Line 1, the shorter dipole data display a pattern quite similar to that of the larger dipoles. Apparent resistivities ranged from 3.3 to 127 ohm-meters. Differences in the observed values do not justify any change in interpretation of the larger dipole pseudo-section. The similarity of the 500 and 1000 meter dipole data on both lines indicates that sufficient information is available with only one dipole spacing if the appropriate dipole separations are used.

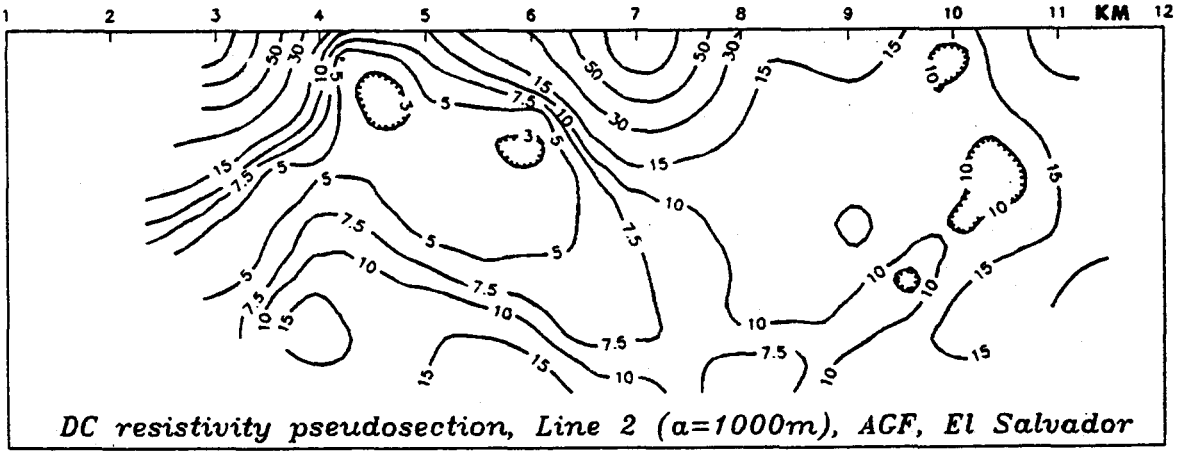

Fig. 7. Pseudosection of Line 2 showing the apparent resistivities logarithmically contoured in ohm-meters for 1000 meter dipole spacing.

SUMMARY

The apparent resistivity data collected for Lines 1 and 2 at the AGF display a three-dimensional complex geologic picture. Two-dimensional modeling demonstrates that known lithologies may be identified (where unaltered) by a limited range of resistivities. Reservoir rocks have interpreted true resistivities of less than 10 ohm-meters. Younger overlying rocks range from 20 to 200+ ohm-meters. Both of these lithologies may be hydrothermally altered to have resistivities below 5 ohm-meters.

The known reservoir at the AGF does not appear to have a sufficiently diagnostic electrical signature to stand out relative to the interference effects of the near-surface altered lithologies and possible cultural effects. It is not unusual for a fracture-flow hydraulic regime to show little or no electrical resistivity contrast with the country rock. One of the results of a magnetotelluric survey performed previously indicated that the reservoir was a high-resistivity body relative to the country rock. These relatively-high resistivity characteristics are not seen in either the VES's or dipole-dipole dc data.

The severe topography encountered on Line 1 does not pose an interpretational problem with 1000 meter dipole data as long as it is taken into account. The 500 meter dipole data suffer more from the topography but should not be left out of consideration for future work because the shorter dipoles have other logistical advantages.

ACKNOWLEDGMENTS

This resistivity survey was part of a USAID technology transfer program administered by LANL. The data were collected by CEL Salvadoran geophysicists using equipment designed and built by Los Alamos National Laboratory LANL.

Personnel from CEL directly involved in the on-site field operations were: Mr. Carlos Rodriguez, Mr. Manuel Ernesto Monterrosa, and various geophysical staff members. Personnel from CEL involved in supporting the field operations were: Dr. Gustavo Cuéllar, Mr. David Vega, Mr. Mauricio Retana, Mr. Alejandro Quintanilla, and Mr. Jose Alonzo Martinez.

Personnel involved on site from LANL were: Dr. Dan J. Cash, geophysicist; Mr. Michael T. Gerety, geophysicist, and Mr. Richard A. Fenster, electronics engineer.

Personnel involved from Geophynque International were: Mr. James B. Fink, geophysicist.

Personnel involved from Geociencias Aplicadas were: Dr. Mauricio F. de la Fuente Duch, geophysicist; Mr. Alfonso Ochoa, geophysicist; Mr. Antonio Cano, geophysicist; and Mr. David Brito, geophysicist.

Electric Log Modeling: A Tool for Determining Hydraulic Properties of Reservoirs

Presented by
Pascal Bidaux (CSNR)

No final copy was received by press time

Calculations of Reservoir Parameters from Physical and Chemical Well Test Data

Presented by
David Nieva (IIE)

No final copy was received by press time

PROCEEDINGS, Fourteenth Workshop on Geothermal Reservoir Engineering
Stanford University, Stanford, California, January 24-26, 1989
SGP-TR-122

LBL-26509

ON RELATIVE PERMEABILITY OF ROUGH-WALLED FRACTURES

K. Pruess and Y. W. Tsang

Earth Sciences Division
Lawrence Berkeley Laboratory
1 Cyclotron Road
Berkeley, California 94720

and

Department of Materials Science and Mineral Engineering
University of California, Berkeley

ABSTRACT

This paper presents a conceptual and numerical model of multiphase flow in fractures. The void space of real rough-walled rock fractures is conceptualized as a two-dimensional heterogeneous porous medium, characterized by aperture as a function of position in the fracture plane. Portions of a fracture are occupied by wetting and non-wetting phase, respectively, according to local capillary pressure and accessibility criteria. Phase occupancy and permeability are derived by assuming a parallel-plate approximation for suitably small subregions in the fracture plane. Wetting and non-wetting phase relative permeabilities are calculated by numerically simulating single phase flows separately in the wetted and non-wetted pore spaces. Illustrative examples indicate that relative permeabilities depend sensitively on the nature and range of spatial correlation between apertures.

INTRODUCTION

Most high-temperature geothermal reservoirs are situated in formations with predominant fracture permeability. In many of these systems two-phase flow of liquid water and vapor occurs in the fractures naturally, or will be induced from boiling in response to fluid production. Geothermal wells will usually produce at commercially viable rates only if they intercept sufficiently permeable fracture zones. Multiphase flow in fractures also occurs in oil and gas production, and in the vicinity of geologic repositories for heat-generating nuclear wastes.

When analyzing multiphase flows it is important to carefully distinguish between fluid phases and components. Liquid water and water vapor constitute a single-component two-phase system, while mixtures of water and oil, or water and natural gas, are two phase systems consisting of at least two components. (Oil and natural gas themselves may contain many different components or chemical species). Single-component two-phase systems may behave rather differently than their two-component counterparts. For example, a gas (vapor) phase can evolve inside a body of liquid water by phase transformation (boiling) in response to suitable changes in temperature or pressure. The vapor phase need not be geometrically connected to a contiguous body of vapor. This is in contrast to two-component two-phase systems, where the phase composition in a region can only change if an invading phase can access the region through a continuous flow path. In addition to issues of phase occupancy, phase mobilities are also different in single-component two-phase systems. Through a thermodynamic analysis, Verma (1986) showed that vapor bubbles cannot get trapped at pore throats in concurrent vapor-liquid flow, while under suitable capillary pressure conditions the non-wetting phase in a two-component system may get trapped.

Given the wide occurrence and practical importance of multiphase flows in fractures, it is surprising that very little quantitative information on such flows is available. Experimental work has demonstrated multiphase flow effects in fractures (Barton, 1972; Bawden and Roegiers, 1985), but we are not aware of any measurements of fracture relative permeabilities in the literature. The lack of laboratory data is probably due to difficulties in controlling and measuring phase saturations in fractures. Standard laboratory techniques such as gamma ray or microwave attenuation devices are sensitive to the volumetric composition of a multiphase system. The void volumes present in fractures, however, are invariably small compared to sample volumes and interstitial voids in unfractured material, so that the application of volumetric methods meets with great difficulties and inaccuracies.

From a theoretical viewpoint the subject of multiphase flow in fractures has also received very little attention. The chief obstacle here seems to be that until recently there was a lack of credible models for pore space geometry in natural rock fractures. Evans and coworkers have used capillary theory to study the multiphase flow behavior of systems of idealized parallel-plate fractures (Evans, 1983; Evans and Huang, 1983; Rasmussen et al., 1985), and of wedge-shaped fractures with continuously varying apertures (Rasmussen, 1987). Newly developed

imaging techniques (Gentier, 1986; Pyrak-Nolte et al., 1987; Hakami, 1988) have led to the conceptualization of fractures as two-dimensional heterogeneous porous media, with flow taking place in intersecting channels of varying aperture (Tsang and Tsang, 1987; Wang et al., 1988; Montazer et al., 1988). These emerging concepts open the way for new theoretical approaches to multiphase flow in fractures.

TWO-DIMENSIONAL POROUS MEDIA

In the hydrologic literature fractures have often been idealized as the void space enclosed between two parallel plates. "Real" rock fractures, however, have rough surfaces with numerous contact points. Recent observations indicate that the topography of fracture walls may have fractal structure (Brown and Scholz, 1985; Wang et al., 1988). In this paper we focus on "small" fractures in hard rock, with apertures typically in the submillimeter range, as opposed to fracture zones which consist of a layer of highly permeable material sandwiched between rock of low permeability. Fracture zones may have widths of order 0.1 to 1 m and have a three-dimensional pore structure. In contrast, the small fractures considered here consist of the void space enclosed between two impermeable surfaces, which in a topological sense constitutes a two-dimensional porous medium. Quantitatively this can be described by specifying the two boundary surfaces, $z_i = z_i(x,y)$ for $i = 1, 2$. Alternatively, one can specify the midplane $z = (z_1 + z_2)/2$ and the local aperture $b(x,y) = z_2 - z_1$. For simplicity we assume fractures to be planar in the following (z = const.); however, this assumption is made only for convenience and is not necessary for our model. The important property of the fracture model developed here is the two-dimensional nature of the pore space.

Several different techniques have been used to experimentally characterize apertures of rough-walled fractures, including linear profilometer scans (e.g. Gentier, 1986), two-dimensional imaging from replicas of the pore space made by injection of Woods' metal or epoxy resins (Pyrak-Nolte et al., 1987; Gale, 1987; Gentier et al., 1989), and application of fluid drops of known volume (Hakami, 1988). Different scales of spatial correlation among apertures have been noted experimentally (Gentier, 1986). In various instances fracture apertures have been found to follow a skewed distribution well approximated by a log-normal distribution (Gentier, 1986; Gale, 1987; Hakami, 1988). Figures 1 and 2 show examples of fracture pore spaces simulated by computer (see below).

Adopting a finite spatial resolution $\Delta x \times \Delta y$ results in a discretized representation of fracture apertures, with average aperture being b_{ij} in the element $(x_i - \Delta x/2, x_i + \Delta x/2; y_j - \Delta y/2, y_j + \Delta y/2)$ of the fracture plane. In the calculations reported below we use a 20×20 grid to discretize a 40mm × 40mm portion of a fracture plane, so that $\Delta x = \Delta y = 2$mm (Figures 3 and 4). For convenience, we will use a shorthand notation (i,j) for an element of the fracture plane. Discretized representations of fracture apertures can be generated from continuous distributions through stochastic techniques, or they can be directly obtained from laboratory specimen by digitizing pore space images into a finite number of "pixels".

In the present study, we use geostatistical methods to generate discretized aperture distributions in the fracture plane. In most cases we use a lognormal distribution of apertures with an exponential spatial covariance. The aperture generation code COVAR (William and El-Kadi, 1986) was modified to allow for anisotropic covariance. The input parameters to the aperture generation code are $\log b_0$, σ, λ_x, and λ_y, which denote, respectively, the mean and standard deviation of the lognormal distribution, and the spatial correlation lengths in x and y directions.

Figures 1 and 2 show stochastic realizations of lognormal aperture distributions in a fracture plane with different length and anisotropy of spatial correlation. The parameters for these distributions are given in Table 1, and the discretized counterparts are shown in Figures 3 and 4.

RELATIVE PERMEABILITY MODEL

It is well established that for single-phase flow the permeability of a parallel-plate fracture of aperture b is given by

$$k = \frac{b^2}{12} \tag{1}$$

This permeability is present over a flow sheet of width b so that, when normalized to a unit thickness perpendicular to the fracture, the average permeability is

$$\bar{k} = \frac{b^3}{12} \tag{2}$$

whence the term "cubic law" for this relationship. In two-phase conditions, the capillary pressure between wetting and non-wetting phases is given by

$$P_c = \frac{2\gamma \cdot \cos\alpha}{b} \tag{3}$$

where γ is the surface tension between wetting and non-wetting phases, and α is the contact angle between the wetting phase meniscus and the fracture wall. We adopt the convention of taking $P_c > 0$, and we assume that the contact angle for water-vapor (or wetting-nonwetting phase) is 0.

The crucial concept developed in this paper can now be stated as follows: As far as multiphase flow properties are concerned, a rough-walled fracture with position-

dependent aperture is assumed to behave locally like a parallel-plate fracture with the same average aperture (Brown, 1987). Thus, a fracture element with aperture b_{ij} has a single-phase permeability $b_{ij}^2/12$, and its phase occupancy is governed by the local capillary pressure $P_{ij} = 2\gamma/b_{ij}$. In "quasistatic" conditions of low pressure gradients (low capillary number), when both wetting and non-wetting phase have access to the fracture element (i,j), it will contain wetting phase if $P_c < P_{ij}$, non-wetting phase if $P_c > P_{ij}$. Note that this assumption ignores possible effects from wetting phase which may be held by small-scale roughness or by adsorptive forces in the walls of fracture elements the bulk of which would be drained (Pruess et al., 1988). Mineral coatings may also play a role in complicating phase occupancy and mobility (N.G.W. Cook, private communication).

Our procedure for calculating capillary pressures and relative permeabilities can now be described as follows.

(1) Obtain a discretized representation b_{ij} of fracture apertures for a finite rectangular domain, either by generating a stochastic realization of a suitable aperture distribution, or by directly digitizing an image of the pore space (see Figures 3 and 4).

(2) Define a cutoff-aperture b_c, corresponding to a capillary pressure $P_c = 2\gamma/b_c$, and occupy all apertures smaller than b_c with wetting phase, all larger apertures with non-wetting phase. (This occupancy rule ignores global accessibility criteria which may be very important in two-component flow; it is appropriate for single-component vapor-liquid systems.) Calculate the saturation S_{cw} (and $S_{cnw} = 1 - S_{cw}$) corresponding to the cutoff capillary pressure P_c by directly summing the wetted pore volume.

(3) Apply suitable constant-pressure conditions at the boundaries of the fracture, and simulate fluid flow in the network of occupied fracture elements. (In our simulations, flow is taking place in the x-direction, with no-flow boundaries at y = 0 and y = 1; see Figures 3 and 4.) The steady-state flow rate obtained when only apertures less than b_c are occupied will yield the effective wetting phase permeability; a similar simulation with only apertures larger than b_c occupied will yield the effective non-wetting phase permeability. It should be noted that it is only under conditions of small capillary number that the two-phase flow problem in the fracture plane separates into two single-phase flow problems. When sizeable pressure gradients are present the flowing phases will be able to invade otherwise "forbidden" pores.

(4) Division of the effective phase permeability by the single-phase permeability (all apertures occupied) yields the relative permeability at saturation S_{cw}. Repeat the procedure for a range of b_c (and S_{cw}) to obtain the entire relative permeability and capillary pressure curves.

NUMERICAL SIMULATIONS

In order to implement the procedure outlined above it is necessary to derive the transmissivity between fracture elements of different aperture. Consider a "connection" (flow contact) between two fracture elements with apertures b_n and b_m, respectively (Figure 5). Neglecting non-linear flow effects at the juncture, the total pressure drop between n and m can be expressed as

$$\begin{aligned} P_n - P_m &= (P_n - P_i) + (P_i - P_m) \\ &= F_{mn} \frac{\mu}{\rho} \left\{ \frac{D_n}{k_n A_n} + \frac{D_m}{k_m A_m} \right\} \end{aligned} \tag{4}$$

Here P_i denotes the pressure at the interface, F_{mn} is the mass flow rate, μ is fluid viscosity, ρ is density, and D_n, k_n, A_n are nodal distance, permeability, and cross-sectional area for flow in fracture element n, respectively (likewise for element m). Introducing an effective permeability k_{mn} and connection area A_{mn}, the pressure drop can also be written as

$$P_n - P_m = F_{mn} \frac{\mu}{\rho} \frac{D_n + D_m}{k_{mn} A_{mn}} \tag{5}$$

Equating the expressions (4) and (5), and inserting for flow area $A_n = b_n \times \Delta y$, similarly for A_m, and using Eq. (1) for permeability, we obtain

$$k_{mn} A_{mn} = \frac{(D_n + D_m)\Delta y}{12 \left\{ \frac{D_n}{b_n^3} + \frac{D_m}{b_m^3} \right\}} \tag{6}$$

indicating that only the product of effective interface permeability k_{mn} and interface area A_{mn} is defined. For the numerical implementation we find it convenient to take $k_{mn} = k = \text{const.}$ for all flow connections. With this convention we obtain

$$A_{mn} = \frac{(D_n + D_m)\Delta y}{12k \left\{ \frac{D_n}{b_n^3} + \frac{D_m}{b_m^3} \right\}} \tag{7}$$

for "active" (occupied) connections; $A_{mn} = 0$ for inactive connections.

We have incorporated these equations into our general-purpose simulator "MULKOM" (Pruess, 1983, 1988). Additional minor code changes were made to improve the calculational efficiency for small fracture domains, in which individual fracture elements, represented as separate grid blocks, have small linear dimensions of order 1 mm. The modifications include specification of a fictitious very large fluid viscosity (of order 10^6 Pa·s) to scale up pressure differences between neighboring grid blocks and thereby diminish numerical cancellation errors, and automatic adjustment of time step and convergence criteria to expedite and recognize attainment of a steady state. From the numerical simulation we obtain

the total steady-state flow rate F across the fracture between boundaries separated by a distance L and held at a pressure difference of ΔP. A straightforward application of Darcy's law gives the following expression for effective permeability

$$k = \frac{F}{A} \frac{\mu}{\rho} \frac{L}{\Delta P} \qquad (8)$$

The permeability in Eq. (8) is normalized to a cross-sectional area A, which we take to be $1\,m^2$; i.e., it is assumed that the modeled fracture segment is embedded in a cross-sectional area of $1 \times 1\,m^2$.

RESULTS AND DISCUSSION

The accuracy of the numerical simulation procedure was verified by comparison with computations using an electric resistor analog. Simulations were then performed for a number of discretized realizations of lognormal and normal aperture distributions with different mean values and spatial correlation lengths. Figures 6 and 7 show results for wetting and nonwetting phase relative permeabilities, respectively, for the two aperture distributions of Figures 3 and 4 (parameters as given in Table 1). The different data points in Figures 6 and 7 correspond to different cutoff apertures b_c.

Before discussing the simulation results presented in Figures 6 and 7 it should be emphasized that these are to be considered a first rough illustration of the trends; due to various approximations and idealizations involved they are not expected to provide a quantitatively valid evaluation of fracture relative permeabilities. The test calculations performed so far indicate that relative permeability predictions depend sensitively on the details of spatial correlation between apertures; a realistic description of these correlations is required before quantitatively useful results can be obtained. Other limitations arise from the stochastic nature of the aperture distributions; calculations for a reasonably large number of realizations would be needed before firm conclusions can be drawn. The rather coarse discretization (20×20) of the fracture plane and the five-point finite difference scheme used here result in grid orientation errors (Forsythe and Wasow, 1960; Yanosik and McCracken, 1979). By restricting flow connections to the four nearest neighbors with a shared interface, the five-point scheme will produce an overestimate of flow interference between phases.

The most remarkable feature of the relative permeability curves shown in Figure 6 is the apparent strong interference between the phases: Immobile nonwetting phase saturation is extremely large, about 84%, and a saturation "window" in which both phases would be mobile is virtually non-existent. This contrasts with the behavior shown in Figure 7, where immobile nonwetting saturation is a more modest (although still large) 51.5%, and there is a considerable range of saturations over which both phases can flow simultaneously. In our calculations so far we have generally found that a significant window of two-phase mobility exists only for anisotropic aperture distributions, with considerably larger spatial correlation length in the direction of flow than perpendicular to it.

Our wetting phase relative permeabilities appear to be generally similar to experimental results for (three-dimensional) porous media (Osoba et al., 1951; Johnson et al., 1959; Brooks and Corey, 1964), while non-wetting phase relative permeabilities are predicted to drop off rather rapidly with increasing wetting phase saturation.

This can be understood from the characteristics of the lognormal distribution, in which there are many relatively small apertures and a small number of large apertures. In the absence of long-range spatial correlations between apertures (see Figure 1), a contiguous flow path for nonwetting phase can only be maintained when in addition to all the large apertures also some of the smaller apertures contain nonwetting phase. In other words, a relatively large nonwetting phase saturation is required before nonwetting phase can flow.

Phase interference is generally stronger in two-dimensional than in three-dimensional porous media, because there are fewer alternative routes for bypassing inaccessible pores. (In percolation theory parlance, two-dimensional media have a smaller coordination number). Anisotropic spatial correlation, with larger correlation length in the direction of flow, tends to segregate the small aperture and the large aperture pathways (see Figure 2). This diminishes phase interference and broadens the saturation window for two-phase mobility (Figure 7). The sudden jump in non-wetting phase relative permeability at $S_W = 48.5\%$ occurs because of a single pore throat located near $x = 0.5$, $y = 0.3$ (see Figures 2 and 4).

At the present time there are no reliable observational data with which our predictions for fracture relative permeabilities can be compared. However, there is some evidence from fractured geothermal reservoirs which suggests that the sum of liquid and vapor relative permeabilities is close to 1 over the entire range of saturations (Grant, 1977; Pruess et al., 1983, 1984; Bodvarsson et al., 1987). Such behavior is not necessarily in disagreement with our findings; in fact, it is straightforward to identify geometric characteristics of fracture aperture distributions that would lessen or completely eliminate interference between phases, and thereby give rise to larger wetting and nonwetting phase relative permeabilities at intermediate saturations.

For example, it is quite conceivable that fractures commonly have certain long-range spatial correlations between apertures. These could be provided by channels or rivulets formed by mechanical erosion or mineral dissolution processes. Another possibility is that field-determined relative permeabilities could pertain to an aggregate response of several fractures of different magnitude, with wetting phase flowing in the smaller frac-

tures, nonwetting phase in the larger ones. Under such conditions of segregated flow the sum of wetting and nonwetting phase relative permeabilities would be near 1 at all levels of saturation.

In addition to geometric characteristics of the fracture pore space, there is a purely thermodynamic effect that could enhance nonwetting phase permeability in single-component two-phase flow. As was shown by Verma (1986), phase transformation effects will prevent vapor bubbles from getting trapped at pore throats in concurrent vapor-liquid flow. Verma's analysis indicates that phase change processes will in effect enable vapor flow to take place even if there is no contiguous flow path for the vapor phase. This effect would generally enhance nonwetting phase relative permeability in single-component two-phase systems (a volatile fluid and its vapor) in comparison to two-component systems.

CONCLUDING REMARKS

We have developed a new conceptual approach for wetting and nonwetting phase relative permeabilities in real rough-walled rock fractures. Our method utilizes a quantitative description of the fracture pore space in terms of an aperture distribution, which can be obtained either through direct laboratory measurements on fracture specimens, or by means of stochastic computer-generated realizations of mathematical distribution functions. The crucial concept used in our method is that the capillary and permeability properties of a fracture can be approximated by a parallel-plate model locally. This is a hypothesis which requires further experimental and theoretical study.

First applications of the method involved computer simulation of flow in fractures with synthetic (lognormal) aperture distributions. It was found that interference between phases is generally strong. The sum of wetting and nonwetting phase relative permeabilities is much less than 1 at intermediate saturations, unless there are long-range spatial correlations among apertures in the direction of flow. Such correlations are likely to occur commonly in fractures in the form of channels or rivulets. Even so, first results seem to indicate that immobile nonwetting phase saturations in fractures may be large, of order 50%. However, this result may only be applicable to two-component two-phase systems, such as water and gas (or air), or water and oil. In geothermal reservoirs we are dealing with essentially single-component (water) two-phase systems. In these systems phase change provides an additional degree of freedom in two-phase flow, which will diminish or eliminate blocking of one phase by the other, and thereby enhance nonwetting phase relative permeability. Contributions from matrix flow, neglected in this paper, will also tend to lessen phase interference.

There is some evidence from fractured geothermal reservoirs that the sum of liquid and vapor relative permeabilities is close to 1 at all saturations. We suggest that this feature may be due to the indicated phase transformation effects rather than due to fracture flow, as has often been assumed in the geothermal literature. All else being equal, the sum of wetting and nonwetting phase relative permeabilities at intermediate saturations should be smaller in fractures than in three-dimensional porous media, because of the reduced possibility for bypassing inaccessible pores.

The relative permeability functions shown in Figures 6 and 7 were obtained for highly idealized aperture distributions, with no explicit allowance for phase change effects in vapor-liquid flow. They are not expected to give a realistic outlook on relative permeabilities in fractured geothermal reservoirs. Work is continuing to apply the method developed in this paper to conditions and parameters of practical interest.

ACKNOWLEDGEMENT

For a careful review of the manuscript and the suggestion of improvements, the authors are indebted to M. Lippmann and J. Wang. This work was supported by the Geothermal Technology Division, U.S. Department of Energy, under Contract No. DE-AC03-76SF00098.

REFERENCES

Barton, N. R. (1972). "A Model Study of Air Transport from Underground Openings Situated Below Groundwater Level," Proceedings, Symposium International Society for Rock Mechanics, Stuttgart, pp. T3-A1-T3-A20.

Bawden, W. F. and J. C. Roegiers (1985). "Gas Escape from Underground Mined Storage Facilities - A Multiphase Flow Phenomenon", Proceedings, International Symposium on Fundamentals of Rock Joints, Björkliden, 15-20 September, pp. 503-514.

Bodvarsson, G. S., K. Pruess, V. Stefansson, S. Björnsson, and S. B. Ojiambo (1987). "East Olkaria Geothermal Field, Kenya. 1. History Match with Production and Pressure Decline Data", *Journal of Geophys. Res., 92,* (B1) 521-539.

Brooks, R. H. and A. T. Corey (1964). "Hydraulic Properties of Porous Media", Hydrol. Paper 3, Civ. Eng. Dept., Colorado State University, Fort Collins, CO., 27 pp.

Brown, S. R. (1987). "Fluid Flow Through Rock Joints: The Effect of Surface Roughness", *Journal of Geophys. Res., 92,* (B2) 1337-1347.

Brown, S. R. and C. H. Scholz (1985). "Broad Bandwidth Study of the Topography of Natural Rock Surfaces", *Journal of Geophys. Res., 90,* 12,575-12,582.

Evans, D. D. (1983). "Unsaturated Flow and Transport through Fractured Rock - Related to High-Level Waste Repositories", Final Report - Phase I, Department of Hydrology and Water Resources, University of Arizona, prepared for U. S. Nuclear Regulatory Commission, Report NUREG/CR-3206, March.

Evans, D. D. and C. H. Huang (1983). "Role of Desaturation on Transport through Fractured Rock", in *Role of the Unsaturated Zone in Radioactive and Hazardous Waste Disposal*, J. W. Mercer, P. S. C. Rao, and I. W. Marine (editors), Ann Arbor Science, pp. 165-178.

Forsythe, G. E. and W. R. Wasow (1960). *Finite-Difference Methods for Partial Differential Equations*, John Wiley and Sons, Inc., New York, London.

Gale, J. E. (1987). "Comparison of Coupled Fracture Deformation and Fluid Flow Models with Direct Measurements of Fracture Pore Structure and Stress-Flow Properties", Proceedings, 28th U. S. Symposium on Rock Mechanics, Tucson, AZ, June 29-July 1, pp. 1213-1222.

Gentier, S. (1986). Morphologie et Comportement Hydromécanique d'une Fracture Naturelle dans un Granite Sous Contrainte Normale, Doctoral Thesis, Université d'Orléans, Orléans, France.

Gentier, S., D. Billaux and L. van Vliet (1989). "Laboratory Testing of the Voids of a Fracture", to appear in *Int. Jour. Rock Mech. and Rock. Eng.*

Grant, M. A. (1977). "Permeability Reduction Factors at Wairakei", paper 77-HT-52, presented at AICHE-ASME Heat Transfer Conference, Salt Lake City, Utah, August.

Hakami, E. (1988). Water Flow in Single Rock Joints, Licentiate Thesis, Lulea University of Technology, Lulea, Sweden, November.

Johnson, E. F., D. P. Bossler and V. O. Narmann (1959). "Calculation of Relative Permeability from Displacement Experiments", *Trans., AIME, 216*, 370-376.

Montazer, P., F. Thamir and P. Harrold (1988). "Anisotropic Relative Permeability in a Plane Fracture", paper presented at International Conference on Fluid Flow in Fractured Rocks, Atlanta, GA, May 15-18.

Osoba, J. S., J. G. Richardson, J. K. Kerner, J. A. Hafford and P. M. Blair (1951). "Laboratory Measurements of Relative Permeability", *Pet. Trans., AIME*, 47-55.

Pruess, K. (1988). "SHAFT, MULKOM, TOUGH: A Set of Numerical Simulators for Multiphase Fluid and Heat Flow", *Geotermia, Rev. Mex. Geoenergia, 4*, (1) 185-202 (also: Lawrence Berkeley Laboratory Report LBL-24430).

Pruess, K. (1983). "Development of the General Purpose Simulator MULKOM", Annual Report 1982, Earth Sciences Division, Lawrence Berkeley Laboratory Report LBL-15500.

Pruess, K., G. S. Bodvarsson and V. Stefansson (1983). "Analysis of Production Data from the Krafla Geothermal Field, Iceland", paper presented at Ninth Workshop on Geothermal Reservoir Engineering, Stanford University, Stanford, CA, December.

Pruess, K., G. S. Bodvarsson, V. Stefansson and E. T. Eliasson (1984). "The Krafla Geothermal Field, Iceland, 4. History Match and Prediction of Individual Well Performance", *Water Resources Research, 20*, (11) 1561-1584.

Pruess, K., J. S. Y. Wang and Y. W. Tsang (1988). On Thermohydrological Conditions near High-Level Nuclear Wastes Emplaced in Partially Saturated Fractured Tuff. Part 2. Effective Continuum Approximation, Lawrence Berkeley Laboratory Report LBL-24564, January. (To appear in *Water Resources Research.)*

Pyrak-Nolte, L. J., L. R. Myer, N. G. W. Cook and P. A. Witherspoon (1987). "Hydraulic and Mechanical Properties of Natural Fractures in Low Permeability Rock", paper presented at Sixth International Congress on Rock Mechanics, Montreal, Canada, August.

Rasmussen, T. C. (1987). "Computer Simulation Model of Steady Fluid Flow and Solute Transport through Three-Dimensional Networks of Variably Saturated, Discrete Fractures", in D. D. Evans and T. J. Nicholson (eds.), Flow and Transport through Unsaturated Fractured Rock, Geophysical Monograph 42, American Geophysical Union, pp. 107-114.

Rasmussen, T. C., C. H. Huang and D. D. Evans (1985). "Numerical Experiments on Artificially-Generated, Three-Dimensational Fracture Networks: An Examination of Scale and Aggregation Effects", in International Association of Hydrogeologists (ed.), Memoirs, Vol. XVII, pp. 676-682.

Tsang, Y. W. and C. F. Tsang (1987). "Channel Model of Flow through Fractured Media", *Water Resources Res., 23*, (3) 467-479, March.

Verma, A. K. (1986). Effects of Phase Transformation on Steam-Water Relative Permeabilities, Doctoral Dissertation, University of California, Berkeley, CA, March (also: Lawrence Berkeley Laboratory Report LBL-20594).

Wang, J. S. Y., T. N. Narasimhan and C. H. Scholz (1988). "Aperture Correlation of a Fractal Fracture", *Journal Geophys. Res., 93*, (B3) 2216-2224.

Williams, S. A. and A. I. El-Kadi (1986). COVAR - A Computer Program for Generating Two-Dimensional Fields of Autocorrelated Parameters by Matrix Decomposition, Report, International Groundwater Modeling Center, Holcomb Research Institute, Butler University, Indianapolis, Indiana.

Yanosik, J. L., and T. A. McCracken (1979). "A Nine-Point, Finite Difference Reservoir Simulator for Realistic Prediction of Adverse Mobility Ratio Displacements", *Soc. Pet. Eng. J.*, 253-262, August.

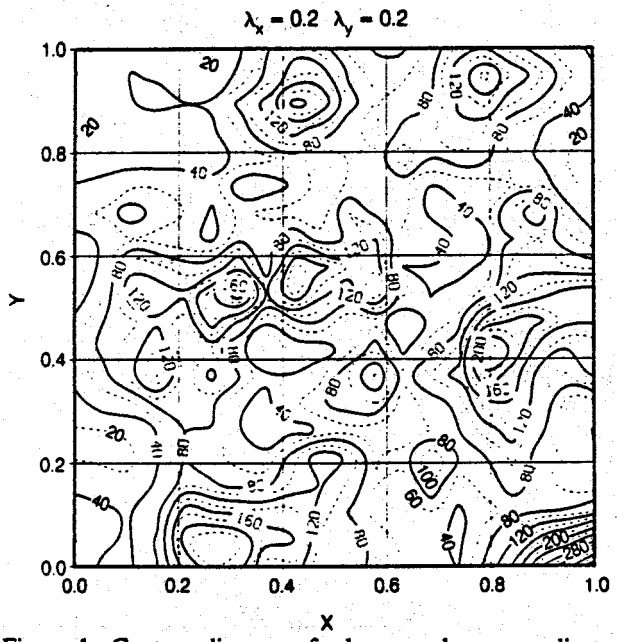

Figure 1. Contour diagram of a lognormal aperture distribution in a fracture plane with isotropic spatial correlation (Case 1, Table 1).

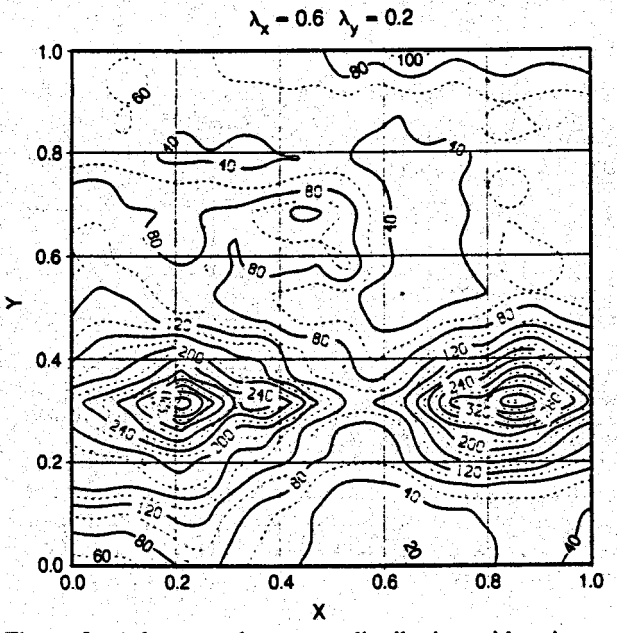

Figure 2. A lognormal aperture distribution with anisotropic spatial correlation (Case 2, Table 1).

Table 1. Parameters for lognormal aperture distributions

	Case 1	Case 2
mean aperture (μm)	81.8	81.8
standard deviation	0.43	0.43
x-spatial correlation	0.20	0.60
y-spatial correlation	0.20	0.20

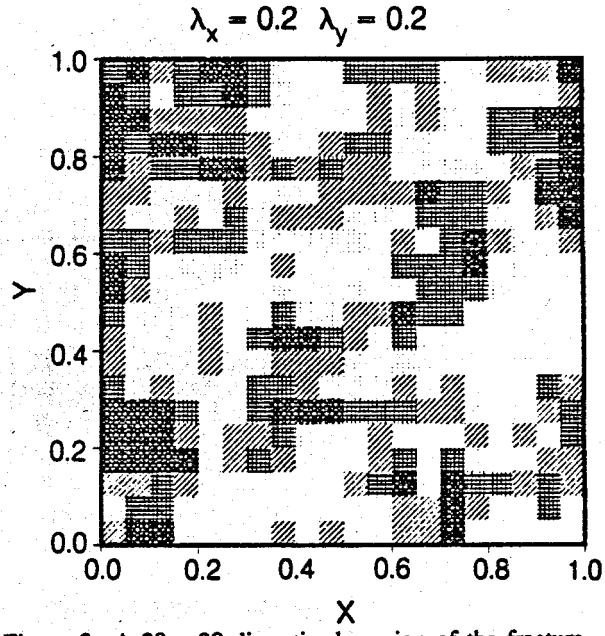

Figure 3. A 20 x 20 discretized version of the fracture apertures shown in Figure 1. Lighter shading corresponds to larger apertures.

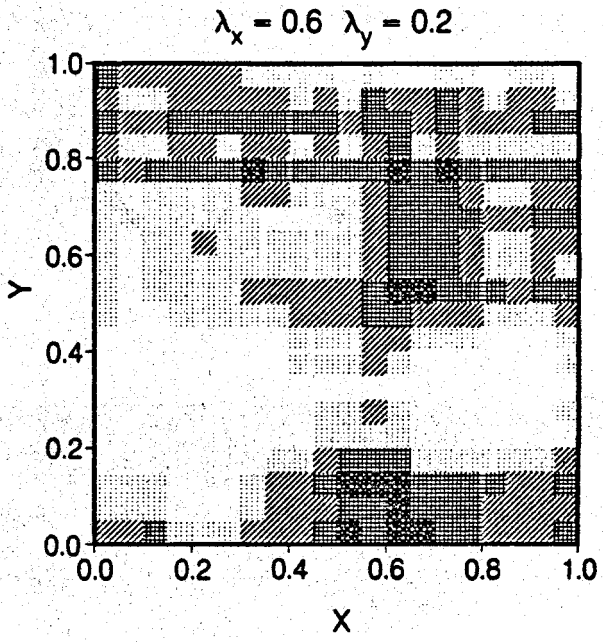

Figure 4. A 20 x 20 discretized version of the fracture apertures shown in Figure 2.

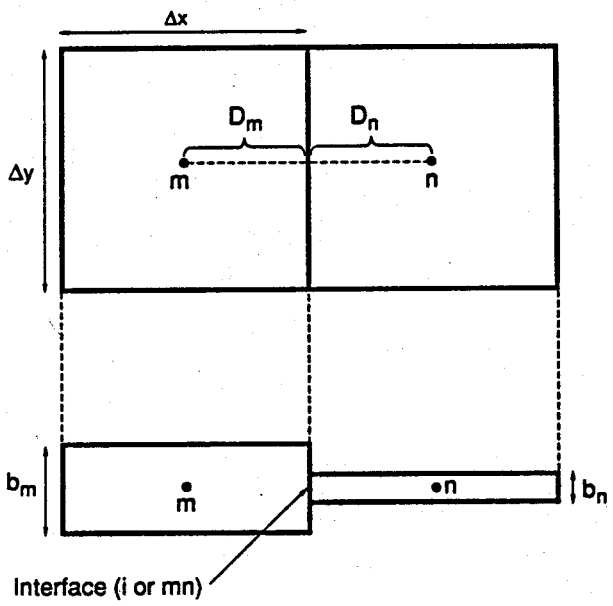

Figure 5. Schematic of a connection between two fracture elements, looking down onto the fracture plane (top), and giving an elevation view (bottom).

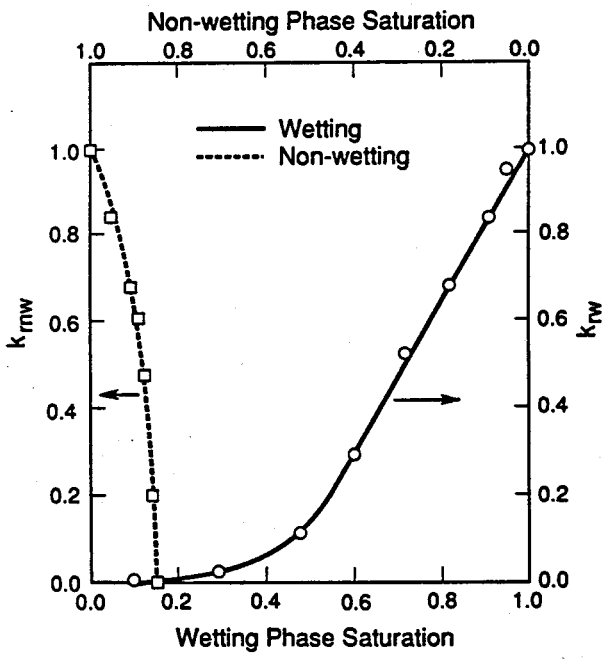

Figure 6. Simulated wetting and nonwetting phase relative permeabilities for the lognormal aperture distribution og Figures 1 and 3.

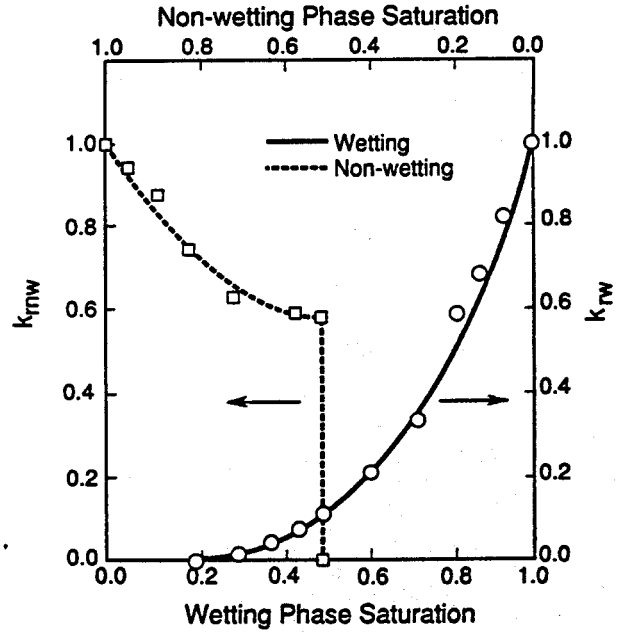

Figure 7. Simulated wetting and nonwetting phase relative permeabilities for the lognormal aperture distribution of Figures 2 and 4 with long-range anisotropic spatial correlation.

PROCEEDINGS, Fourteenth Workshop on Geothermal Reservoir Engineering
Stanford University, Stanford, California, January 24-26, 1989
SGP-TR-122

The Rise and Fall of Chloride in Larderello Steam

A.H. Truesdell[1], F. D'Amore[2], and J.R. Haizlip[3]

[1] U.S. Geological Survey, Menlo Park, Calif.
[2] Int. Inst. for Geothermal Research, Pisa, Italy
[3] GEO Operator Corp., San Mateo, Calif.

ABSTRACT

Significant amounts of Cl appeared in steam from upflow zones of Larderello in the early 1960s. The general pattern of Cl concentration includes: a rapid rise, a more or less constant plateau (coincident with a low, stabilized flow rate), and rapid decrease generally after 1980. The rise correlates with a general decrease in pressure throughout the field presumably due to the disappearance of liquid in the two-phase, vapor-dominated reservoir. The plateau may be related to the distance from centers of upflow and inhomogeneities in the temperature and chemistry of deep brine. The decrease is correlated with the start of liquid introduction from reinjection and drilling losses and particularly with the time of breakthrough of steam formed from injected water. This history suggests that when liquid was exhausted in some areas and pressure dropped, other areas suffered accelerated boiling and dried out as well, allowing high-Cl steam formed from boiling of deep brine to move upward to reach the wells. The introduction of liquid after 1980 reversed the process. A similar situation may be occurring now at The Geysers, California.

INTRODUCTION

Chloride in steam from Larderello was mentioned by Allegrini and Benvenuti (1970) as an important factor in corrosion of pipelines. At that time (1960s), Cl in steam in "considerable quantities" was "rather rare," with only 22 of 188 wells listed carrying >5 ppm and only 10 wells with >10 ppm. The Cl was considered to be carried as NH_4Cl (which is neutral in solution) despite evidence that some condensate drains carried high concentrations of Fe^{++} as well as Cl^-, indicating H^+ corrosion. They contributed the critical observation that Cl in superheated steam was noncorrosive but became corrosive when it contacted liquid water. D'Amore et al. (1977) showed that steam with more than 1 ppm Cl was limited to zones of intense exploitation (Fig. 1), where superheating of steam is most common. HCl was identified as the probable form of Cl in steam, but the formation of HCl was considered to be limited to reaction of $CaCl_2$ with silica. D'Amore and Truesdell (1979) considered Cl in steam to indicate boiling of a deep, high-Cl brine and pointed out that Cl in steam from three Larderello wells had appeared in low concentrations (0-5 ppm) when first analyzed in 1963 and increased until at least 1977, reaching 22 ppm in steam from one well.

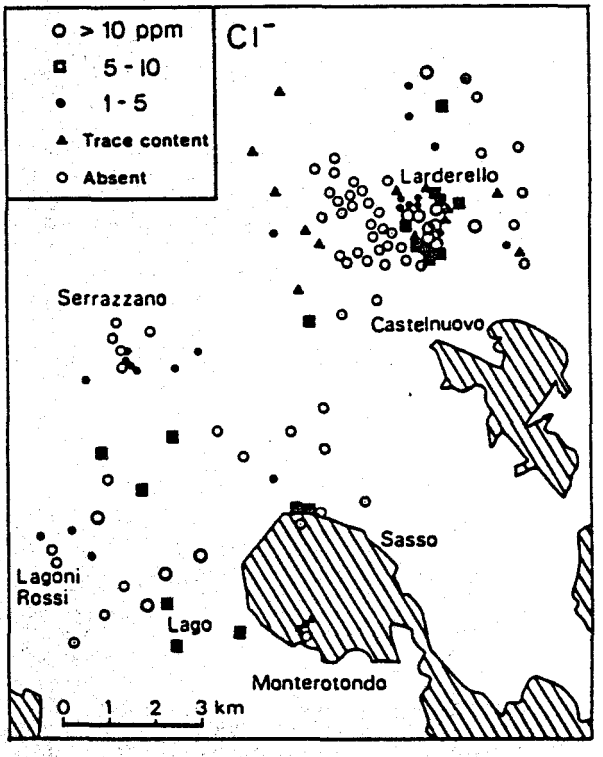

Figure 1. Chloride concentrations in Larderello steam from D'Amore et al. (1977).

D'Amore and Pruess (1986) extended the observations of D'Amore and Truesdell (1979) on temporal changes in steam composition and correlated Cl in steam with the increase of the apparent reservoir vapor saturation ("y" values). Recently, Haizlip and Truesdell (1988) and Truesdell et al. (1988) reconsidered the origin of Cl in geothermal steam and concluded that it is carried as HCl volatilized from Cl brine under conditions of low pH, high Cl, and/or high temperature. Condensate at normal reservoir temperatures would completely scrub HCl from steam, so transport is limited to superheated steam with a dry pathway from the boiling brine. The occurrence of Cl in Larderello steam was briefly describ-

ed by Truesdell et al. (1988) but will be discussed here at greater length, and the reasons for its rapid rise and (after 1980) fall will be considered in relation to reservoir processes.

OBSERVED CL IN LARDERELLO STEAM

Chloride in steam was not routinely analyzed at Larderello before 1963. Earlier, only steam from wells showing high corrosion was analyzed for Cl, as well as Na^+, SiO_2, and other nonvolatile salts, which indicate entry of liquid from the reservoir. The low values for Cl found in the first fieldwide analyses suggest that Cl was below detection (<1 ppm) in most wells before 1960. Of 45 wells for which we have detailed chemistry, Cl when first measured (in 1963 for most wells, up to 1982 for newer wells) was below detection in 14 wells, 1-2 ppm in 15 wells, 2-5 ppm in 7 wells, 5-15 ppm in 6 wells, and >15 ppm in 3 wells.

Thirteen wells located in different zones of Larderello were chosen for detailed study (Fig. 2). These wells have a range of Cl contents and temperature (Table 1) typical of wells considered to be in upflow zones on the basis of relatively high Cl and B and relatively low CO_2 and NH_3 in produced steam (D'Amore and Truesdell, 1979). Changes in Cl concentration with time for these wells are shown in Figures 3-5. The patterns shown are similar. Cl concentrations start low (below 5 ppm for 5 wells, below about 15 ppm for all but 2 wells) and increase rapidly, reaching a more or less broad plateau from 7-10 years after the first measurement until 1980 to 1983. After 1980 most wells showed a sharp decrease in Cl, which was temporary for some wells, and continued for others at least through 1985-1986, which is the limit of our data. Other data for these wells are shown in Table 2, including typical gas analyses and reservoir temperatures calculated from wellhead physical data and from gas geothermometers.

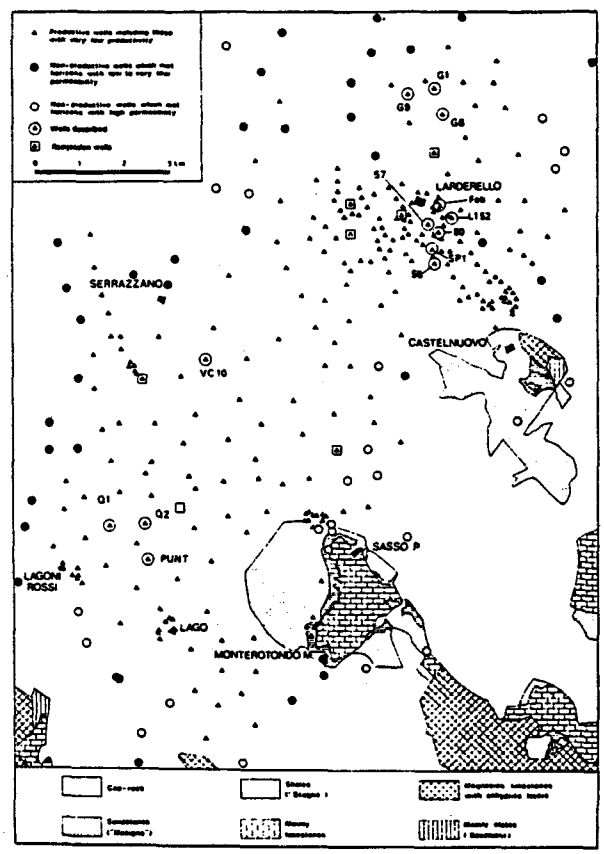

Figure 2. Locations of wells studied and reinjection wells.

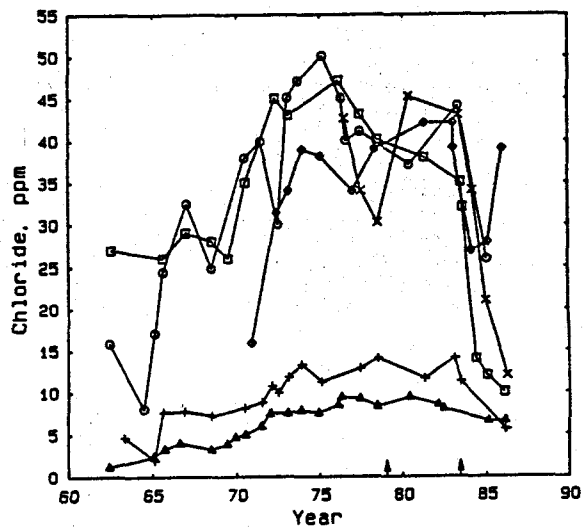

Figure 3. Chloride concentrations in steam from central Larderello wells (L56, pluses; L57, squares; L80, circles; L152, crosses; Fab, triangles; SP1, diamonds). The earlier arrow indicates the start of injection. The later arrow indicates the breakthrough of steam vaporized from this water.

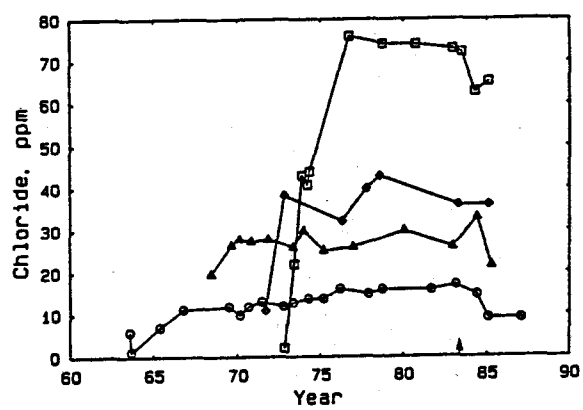

Figure 4. Chloride concentrations in steam from western Larderello wells (VC10, circles; Q1, triangles; Q2, squares, Punt, diamonds). The arrow indicates the start of injection.

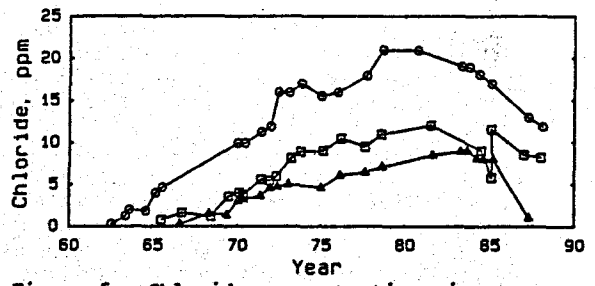

Figure 5. Chloride concentrations in steam from northern Larderello wells (G1, circles; G6, squares; G9, triangles).

Data in D'Amore and Truesdell (1979) and D'Amore and Pruess (1986) suggest that, for wells in the central zone of Larderello drilled before 1950, the appearance of Cl in steam (extrapolated to zero ppm) correlates with the stabilization of steam flow at 10-20% of initial values. For these earlier wells the time of chloride appearance seems to be about 1957.

INDICATIONS OF RESERVOIR DRYING AT LARDERELLO

The accepted model for vapor-dominated geothermal systems (after White et al., 1971) consists of a liquid-saturated condensate zone, a vapor-dominated two-fluid-phase zone, and a deep boiling brine. In the natural state, steam produced from the boiling brine flows upward in the vapor-dominated zone along large fractures and conduits, and condensate flows downward on surfaces and discontinuous small fractures to replenish the deep brine. Although deep temperatures (>350°C) have been measured at Larderello (Cappetti et al., 1985), the deep brine has never been satisfactorily sampled; however it must exist to provide upflowing steam to maintain system temperatures and heat flow.

In the natural state the vapor-dominated reservoir at Larderello was drier than that at The Geysers (1 wt % of total fluid at Larderello compared with 5% at The Geysers, Nathenson and Muffler, 1975 using methods from Nathenson, 1975) and extensive production has dried it further. The production of super-heated steam from wells in all parts of Larderello indicates complete drying of the upper parts of the reservoir near well bottoms but does not prove that the entire vapor-dominated reservoir above the brine was dry.

The drying of the reservoir and the production of superheated steam are clearly related to the decline of reservoir pressure. Measurements in newly exploited zones as well as thermodynamic arguments (James, 1968; Truesdell and White, 1973) indicate that natural state Larderello pressures and temperatures at the top of the vapor-dominated reservoir were near 32-35 ata and 235-240°C. These conditions are consistent with coexistence of vapor and liquid. Pressures in intensely exploited zones of Larderello dropped rapidly (Ferrara et al., 1970; Celati et al., 1976). Early shallow wells in central Larderello showed lower pressures (30 ata) probably resulting from natural discharge. By 1943 pressures in the top of the reservoir in the central Larderello and Castelnuovo zones had declined to 10 ata, and by 1952 the entire Larderello and Castelnuovo zones showed similar low pressures. In 1975 pressures in the reservoir top were near 5 ata.

Although pressures dropped rapidly in response to production, temperatures in the vapor-dominated zone changed very little. The wells studied by D'Amore and Truesdell (1979, 1980) showed nearly constant wellhead and reservoir temperatures after the end of production from vaporized near-well liquid. Declining pressures with near-constant temperature result in drying of the reservoir and superheating of steam. Indications of drying from pressure decline and steam superheating are, however, limited to the upper part of the vapor-dominated zone where most wells have their main steam entries. Processes occurring deeper in the vapor-dominated zone, particularly near the deep brine, would not be revealed by these observations.

Calculations by Haizlip and Truesdell (1988) show that the production and transport of HCl in geothermal systems require the boiling of high-Cl (or low-pH) brine at temperatures above 300°C and the existence of dry pathways through zones of lower temperature. The only part of the system where Cl-containing steam could be generated is the deep brine because sufficiently high temperatures and Cl contents of liquids are found only there. The rapid increase of Cl in Larderello steam is unlikely to have resulted from changes in the deep brine such as a sudden increase in brine salinity, acidity, or temperature. The drying of the vapor-dominated zone is the most likely factor. Cl-bearing steam must have come from the >300°C boiling brine and must have traveled by an entirely dry path to the well because any lower-temperature, lower-Cl liquid would have scrubbed almost all Cl from the steam.

IMPLICATIONS FOR RESERVOIR BEHAVIOR

The nearly simultaneous appearance of high-Cl steam from wells within intensely exploited zones (e.g., central Larderello, Fig. 3) or in nearby wells (e.g., Gabbro, Fig. 4) indicates drying of these parts of the reservoir within a short time period. This probably resulted from pressure equalization and lateral transfer of steam. With continued production, pressure in the reservoir will be maintained as long as both liquid and vapor coexist. As soon as drying is complete, the pressure drops and steam from still-wet zones, where pressures are higher, flows to the dry zone. The lateral flow accelerates the drying of wetter parts and they eventually dry. As soon as steam conduits to the boiling brine are dry, pressures drop and steam in these conduits becomes

superheated. The pressure drop increases boiling of deep brine and the now dry conduits no longer scrub Cl from steam boiled off the brine. Cl contained in deep steam is now able to reach the wells and does so at about the same time throughout the connected volume.

The appearance of Cl in widely separated areas at the same time might result instead from similar exploitation histories with drying of these areas occuring coincidentally. However, exploitation histories at Larderello are not the same. Intense modern exploitation of central Larderello began about 1950 with many wells drilled earlier. In 1951 total flow reached 2500 t/h (Sestini, 1970). This was two times the flow from earlier producing wells. Some of our study wells from the central Larderello area started production early (Fab, 1941; L57, 1949; L56, 1950; and L80, 1951) and some later (SP1, 1963 and L152, 1976). Other zones were developed later. Gabbro was produced after 1960 (G1, 1962; G6, 1964; and G9, 1966). The western area was producing less than 600 t/h before 1957 and only reached 1000 t/h in 1962. Our examples also started production relatively late (VC10, 1963; Q1, 1967; Q2, 1972; and Punt, 1971).

Given this uneven history of exploitation it seems unlikely that coincidence produced the similarity of chloride appearance and increase between, for example, the Gabbro wells developed in the mid-1960s and Fab, L56 and L80 developed from 1940-1950. The distance from central Larderello to Gabbro is 3-4 km, so lateral flow is acceptable. Lateral flow to Larderello was in fact indicated in the study by Brigham and Neri (1979) of the Gabbro zone. The distance from central Larderello to Q1 and Q2 is 9-10 km and lateral flow is less likely. The similarity of the chloride curves of these wells to those for Larderello wells is less marked. However, these wells do not show evidence of a long period of production of low-Cl steam, indicating that somehow there was less available liquid in the vapor-dominated reservoir, perhaps through vaporization and lateral flow to other zones.

Gradual increase of Cl over a period of 7-10 years suggests that low-Cl steam generated from boiling of condensate mixes with an increasing fraction of deep, high-Cl steam. The mixing occurs after low-Cl steam has become superheated by passage through dry zones. Conduits from the brine to the zone of mixing and from there to the surface are dry but liquid water still is present further from the wells (and possibly in nearby matrix blocks) to provide low-Cl steam. Apparently the proportion of deep steam increases until almost all steam was from deep boiling brine and the Cl contents of produced steam stabilizes.

The plateau in Cl contents, which differs in concentration in different wells and different zones, may reflect the equilibrium concentrations of HCl boiled from brines of different temperature, pH, or Cl content. The calculations of Haizlip and Truesdell (1988) show that 100 ppm HCl could originate from boiling at 350°C of brine with 20,000 ppm Cl (like seawater) and pH near 5 or with 100,000 ppm Cl and pH near 6. pH is most likely buffered by feldspar-mica reactions to values near 6 so the more concentrated brines are indicated. At 300°C only 10 ppm Cl would be generated from these brines, suggesting higher temperatures in agreement with deep drill-hole results.

Variations of Cl concentrations with time (e.g., Figs. 3-5) suggest that drying of much of central Larderello and parts of western Larderello occurred in 1955-1960 and that drying of parts of the northern zone occurred in 1960-1965. Wells starting production after 1970 (SP1 in Fig. 3) show moderately high initial Cl and rapid increase suggesting a small amount of initial low-Cl steam from near wellbore liquid that was quickly exhausted. Within these zones there is apparently rapid lateral steam flow and high lateral permeability. More detailed examination of steam Cl could indicate details of connectivity between wells within zones and in interzone areas.

THE EFFECT OF WATER INJECTION AND DRILLING WATER LOSS

Drying of large parts of the Larderello reservoir has resulted in low steam flow and electricity production with large amounts of heat left in the reservoir. This additional heat may be exploited through injection of additional water to increase pressure and steam flow (Cappetti et al., 1982).

Water was introduced into the Larderello reservoir both as injected condensate from cooling towers and also from lost circulation during drilling of new wells. Relating changes in Cl to these events is complicated because reinjection and new drilling were part of a program for the rejuvenation of the Larderello field and both started at about the same time (Cappetti et al., 1982; Bertrami et al., 1985). The wells chosen for study are away from areas of natural recharge and water introduced by this means is not a consideration. We have shown on Figures 3 and 4 approximate times of the start of injection of cooling tower condensate and, for the central area, the time when breakthrough of steam generated from injected condensate was detected isotopically (D'Amore et al., 1987).

Although exact timing of liquid introduction is not available, the general correspondence of sudden decrease in steam Cl contents with liquid injection and, for the central zone, with breakthrough of steam from injected liquid are in reasonable agreement. The data suggest that introduction of liquid produced the Cl decrease through the action of newly generated low-Cl steam and liquid itself.

Mixing of new low-Cl steam may explain the data for some wells in which the decrease was small or temporary, perhaps resulting from a short period of water introduction (as from nearby drilling).

Wells with large, permanent (at least to 1986) decreases in Cl are apparently affected not only by the introduction of low-Cl steam but also of liquid that scrubbed Cl from deep steam. The mechanism of liquid introduction is suggested by the simulations of Calore et al. (1986), which indicated that injected liquid moves mostly vertically downward unless it encounters lower permeability that causes lateral spreading. At Larderello this lateral spreading of liquid would be expected to occur at the bottom of the two-phase vapor-dominated reservoir where increased permeability from mineral solution by downward-flowing condensate gives way to decreased permeability from mineral precipitation by boiling brine. (Pruess et al. (1987) also suggest decreased permeability at this location.) If the contrast in permeability is sufficiently great, liquid could be carried to some distance from its source. Direct introduction of liquid would scrub Cl from deep steam and eliminate superheating at least locally. After the steam left the liquid it might again become superheated, but it would no longer have a supply of HCl. The behavior of Cl in produced steam thus depends on the quantity and location of introduced liquid and also on details of lateral and vertical permeability within the reservoir. Quantitative study of the Cl data along with details of injection and drilling and of other reservoir observations (interference for example) could provide information about reservoir structure at the bottom of the vapor-dominated zone and the top of the brine zone.

A CONCEPTUAL MODEL

The reservoir processes suggested by the changes in Cl of Larderello steam are illustrated by Figure 6. This cartoon is telescoped in time and space showing on the left side the evolution of an expanding dried and decompressed zone of the reservoir just after it has contacted the deep brine. Steam from the not yet dried two-phase (vapor and liquid) zone is flowing from the left into the dry zone. The source of this saturated, low-Cl steam is vaporization of condensate induced by exploitation pressure decline. The lack of Cl in this steam results from its source in boiling of low-Cl liquid at normal reservoir temperature and from passage through the still wet reservoir, which would scrub any Cl in the steam. This saturated, low-Cl steam becomes superheated by isothermal decompression as it flows through the dried zone.

A flow of high-Cl steam is shown entering the dry zone from below where it originates from boilng of saline, high-Cl brine. Temperatures are not shown but must include a relatively steep gradient between the part of the brine that is initially above 350°C and the 250°C vapor-dominated reservoir. The high-Cl steam mixes in the dried zone with low-Cl steam (from lateral flow) and flows to the well. The path from the boiling brine to the well bottom is entirely dry and low-Cl steam that was once saturated has become superheated before mixing. Thus, no scrubbing of chloride occurs and the well produces more or less diluted high-Cl steam. Before the dried zone encountered the deep brine, Cl in steam from the brine would have been scrubbed by condensate in the reservoir and would have contributed steam but not Cl to the production.

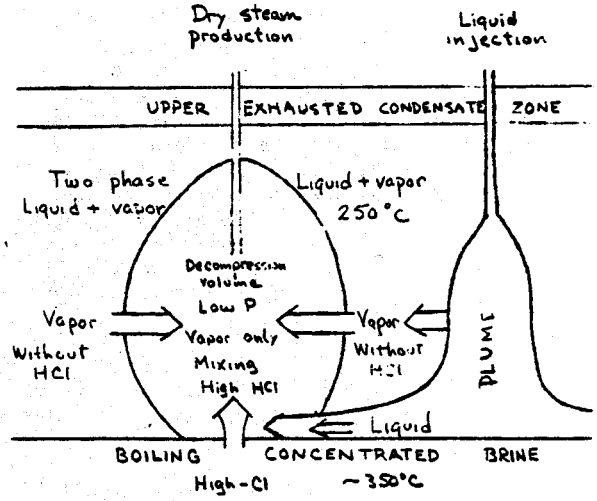

Figure 6. Cartoon of reservoir processes influencing chloride concentrations in steam.

On the right side of the cartoon is shown a plume of liquid (and saturated steam) from an injection well or circulation lost during drilling. Saturated steam from vaporization of liquid contributes to the mixture of high- and low-Cl steam in the dried zone feeding the production well. More importantly, liquid water from the plume is spreading laterally along the high permeability at the base of the vapor-dominated reservoir above the low-permeability original brine interface (at the center of the cartoon). This liquid water has just encountered the dried zone and is about to overtake the high-Cl steam rising from the boiling brine. When this happens steam from the high-Cl brine will become saturated and Cl will be scrubbed into the liquid. As the steam continues to flow upward through the dried zone it will become super-heated again but will not increase in Cl contents. If the flow of liquid diminishes, these processes will reverse themselves. All of these processes occur below the bottoms of most wells at depths sufficiently great that none of the physical characteristics of the produced steam would indicate their occurrence.

FURTHER IMPLICATIONS OF THE MODEL

The general drying of the Larderello reservoir indicated by the appearance of Cl in produced steam has further implications for the exploitation of the field and explains some observations that were poorly understood. A negative implication is that for much of the field (where high stabilized Cl concentrations occurred) the supply of stored liquid in the condensate and vapor-dominated zones of the reservoir has been exhausted. The evaporation of this stored liquid provided the early high flows of low-temperature steam described by D'Amore and Truesdell (1979). A more positive implication is that the stabilized flow of wells with high Cl comes from the boiling of a deep brine. Boiling of deep brine might be expected to be a more stable source than evaporation of liquid in either the relatively thin condensate zone or the originally rather dry vapor-dominated zone. Using this model the long-term increase in average steam temperature at Larderello is simply the result of progressive drying of low-temperature sources of steam and possibly by their replacement by higher temperature steam from boiling of deep hot brine. This last requires the heating of conduits from the brine.

Finally, the model has implications for the future of The Geysers. Exploitation at The Geysers started in the 1960s compared with 1930s at Larderello. Cl in steam at Larderello appeared in 1960, signalling general drying of the upper parts of the reservoir. Cl in steam at The Geysers has appeared in the mid-1980s (Haizlip and Truesdell, 1988) and most probably also signals widespread drying of the vapor-dominated reservoir at The Geysers. This has the same implications for steam production as at Larderello except that The Geysers vapor-dominated zone is thicker and deep steam would have further to travel to the wells, possibly resulting in lower pressures.

ACKNOWLEDGMENTS

We were greatly helped in our interpretation by Romano Celati and Claudio Calore of the IIGS. The paper was helped by reviews from Cathy Janik and Manny Nathenson of the USGS. Finally, we wish to thank the Ente Nazionale per l'Energia Elettrica who provided the data.

REFERENCES

Allegrini, G. and Benvenuti, G., 1970, Corrosion characteristics and geothermal power plant protection: Geothermics, v. 2, pt. 1, p. 865-881.

Bertrami, Rino, Calore, Claudio, Cappetti, Guido, Celati, Romano and D'Amore, Franco, 1985, A three-year recharge test by reinjection in the central area of Larderello field: analysis of production data: Geothermal Resources Council Transactions, v. 9, p. 293-298.

Brigham, W.E. and Neri, G., 1979, Preliminary results on a depletion model for the Gabbro zone: Proc. 5th Workshop Geotherm. Res. Eng., Stanford Report SGP-TR-40, p. 212-221.

Calore, C., Pruess, K. and Celati, R., 1986, Modeling studies of cold-water injection into fluid-depleted, vapor-dominated geothermal reservoirs: Proc. 11th Workshop Geotherm. Res. Eng., Stanford, p. 161-168.

Cappetti, G., Giovannoni, A., Ruffilli, C., Calore, C. and Celati, R., 1982, Reinjection in the Larderello geothermal field: Proc. Int. Conf. on Geothermal Energy, Florence, Italy, May 1982, p. 395-407.

Cappetti, G., Celati, R., Cigni, V., Squarci, P., Stefani, G. and Taffi, L., 1985, Development of deep exploration in the geothermal areas of Tuscany, Italy: Geotherm. Resourc. Counc. 1985 Int. Symp. Geothermal Energy, Int. Volume, p. 303-309.

Celati, R., Squarci, P., Taffi, L. and Stefani, G.C., 1976, Study of water levels in Larderello region geothermal wells for reconstruction of reservoir pressure trend: Proc. Int. Symp. about Geothermal Energy in Latin America, Guatemala City, Oct. 18-23, 1976, p. 501-526.

D'Amore, F., Celati, R., Ferrara, G.C. and Panichi, C., 1977, Secondary changes in the chemical and isotopic composition of the geothermal fluids in Larderello field: Geothermics, v. 5, p. 153-163.

D'Amore, F., Fancelli, R. and Panichi, C., 1987, Stable isotope study of reinjection processes in the Larderello geothermal field: Geochimica et Cosmochimica Acta, v. 51, p. 847-856.

D'Amore, F. and Pruess, K., 1986, Correlations between steam saturation, fluid composition and well decline in vapor-dominated reservoirs: Geothermics, v. 15, p. 167-183.

D'Amore, F. and Truesdell, A.H., 1979, Models for steam chemistry at Larderello and The Geysers: Proc. 5th Workshop Geotherm. Res. Eng., Stanford, p. 283-297.

D'Amore, F. and Truesdell, A.H., 1980, Gas thermometry for drill-hole fluids from vapor-dominated and hot-water geothermal fields: Proc. 6th Workshop Geotherm. Res. Eng., Stanford, Calif., p. 351-360.

Ferrara, G.C., Panichi, C. and Stefani, G., 1970, Remarks on the geothermal phenomenon in an intensively exploited field: results of an experimental well: Geothermics Special Issue 2, v. 2, pt. 1, p. 578-586.

Haizlip, J.R. and Truesdell, A.H., 1988, Hydrogen chloride in superheated steam at The Geysers geothermal field, California: Proc. 13th Workshop Geotherm. Res. Eng., Stanford, Calif. (in press).

James, Russell, 1968, Wairakei and Larderello; geothermal power systems compared: New Zealand Journal of Science, v. 11, no. 4, p. 706-719.

Nathenson, Manuel, 1975, Physical factors determining the fraction of stored energy recoverable from hydrothermal convection

systems and conduction dominated areas: U.S. Geological Survey Open-File Report 75-525, 38 p.
Nathenson, M. and Muffler, L.J.P., 1975, Geothermal resources in hydrothermal convection systems and conduction-dominated areas, in Assessment of geothermal resources of the United States: U.S. Geological Survey Circular 726, p. 104-121.
Pruess, K., Celati, R., Calore, C. and Cappetti, G., 1987, On fluid and heat transfer in deep zones of vapor-dominated geothermal reservoirs: Proc. 12th Workshop Geotherm. Res. Eng., Stanford, p. 89-96.
Sestini, G., 1970, Superheating of geothermal steam: Geothermics Special Issue 2, v. 2, pt. 1, p. 622-648.
Truesdell, A.H. and White, D.E., 1973, Production of superheated steam from vapor-dominated geothermal reservoirs: Geothermics, v. 2, no. 3-4, p. 154-173.
Truesdell, A.H., Haizlip, J.R., Armannsson, H. and D'Amore, F., 1988, Origin and transport of chloride in superheated geothermal steam: Geothermics (in press).
White, D.E., Muffler, L.J.P., and Truesdell, A.H., 1971, Vapor-dominated hydrothermal systems compared with hot-water systems: Economic Geology, v. 66, p. 75-97.

Table 1. Physical and Chemical Data for Typical Wells in Upflow Areas of Larderello

Well	Max. Steam Temp., (°C)	Depth (m)	Period	Average Steam (ppm) Cl	H_3BO_3	NH_3
VC10	260	>1600	1976-84	15±2	335±29	130±10
Q1	250	>1000	1970-84	30±4	430±30	116±18
Q2	255	>1000	1977-84	72±5	487±44	90±8
PUNT	250	>1000	1973-85	37±4	352±36	103±16
LA80	240	~600	1970-83	39±8	344±26	125±7
LA57	248	~500	1970-83	37±7	330±32	118±17
SP1	250	>1000	1973-86	36±5	340±10	109±11
LA56	237	~600	1973-83	12±1	257±25	141±17
FAB	240	~600	1976-83	8±1	199±20	240±10
G1	242	>1000	1977-84	19±1	276±37	168±12
G6	250	~800	1973-84	10±1	206±16	209±27
G9	237	~980	1978-85	9±1	211±32	190±7
LA152	245	>1000	1976-84	40±6	362±37	100±10

Table 2. Typical Steam Chemistry for Wells from Table 1

Well	Date	Gas/Steam (molal ratio)	CO_2	H_2S	H_2	CH_4	N_2 (volume, percent)	$t_{(Res)}$ °C	$t_{(H2S)}$ °C	$t_{(H2)}$ °C
VC10	1981	12.4	91.29	3.15	3.43	1.52	0.65	260	254	262
Q1	1981	12.1	90.07	3.49	3.52	1.95	0.97	265	259	265
Q2	1981	15.3	90.11	3.68	3.69	1.81	0.71	275	266	271
PUNT	1978	12.0	90.91	3.19	3.70	1.66	0.54	265	254	266
LA80	1981	32.1	93.70	2.04	1.65	1.55	1.06	260	255	254
LA57	1981	32.9	93.72	1.87	1.67	1.63	1.10	265	254	254
SP1	1975	29.7	93.24	2.08	1.83	1.85	1.01	265	255	256
LA56	1978	29.8	94.31	1.73	1.58	1.37	1.01	255	250	250
FAB	1981	22.5	93.57	1.91	1.89	1.29	1.40	250	248	253
G1	1981	38.6	95.44	1.64	1.56	0.72	0.64	260	252	254
G6	1981	44.2	95.76	1.22	1.25	0.98	0.78	250	243	250
G9	1981	48.2	96.17	1.06	1.23	1.25	0.93	245	240	250
LA152	1981	26.5	93.40	1.80	2.00	1.60	1.10	260	249	257

$T_{(Res)}$ is measured from ENEL data (±10°C); $t_{(H2S)}$ and $T_{(S)}$ are values computed from semiempirical equations 12 and 11 of D'Amore and Truesdell (1980, 6th Stanford Res. Eng. Workshop).

PROCEEDINGS, Fourteenth Workshop on Geothermal Reservoir Engineering
Stanford University, Stanford, California, January 24-26, 1989
SGP-TR-122

A FLUID FLOW MODEL OF THE COSO GEOTHERMAL SYSTEM: DATA FROM PRODUCTION FLUIDS AND FLUID INCLUSIONS

by

J. N. Moore[1], M. C. Adams, B. P. Bishop[2], and P. Hirtz[3]
1. University of Utah Research Institute
2. California Energy Company, Inc.
3. Thermochem, Inc.

ABSTRACT

Coso is one of several high-temperature geothermal systems associated with recent volcanic activity in the Basin and Range province. Within this fracture-dominated system, temperatures as high as 340°C have been measured at depths of less than 2.5 km. Chemical analyses of the production fluids show that steep gradients in the salinities, gas concentrations, and temperatures occur within the reservoir. Salinities and CO_2 contents range from 1.05 wt.% TDS and 0.95 wt.% CO_2 in the southern part of the field to 0.37 wt.% TDS and 0.06 wt.% CO_2 in the north and east.

Fluid inclusion data have been used to characterize the compositions and temperatures of the reservoir outside the production zones. Homogenization temperatures of the fluid inclusions ranged from 328° to less than 100°C. Ice- and clathrate-melting temperatures indicate that the fluids have salinities up to 1.4 equivalent wt.% NaCl and variable but significant CO_2 contents.

The chemical and fluid inclusion data define a plume of thermal fluid that rises from depth in the south, and travels outward toward the north and east.

INTRODUCTION

Detailed hydrogeochemical models of geothermal reservoirs are needed to locate production and injection wells and to numerically predict the effects of long-term production. In order for these models to be useful, they must describe the temperature, salinity, and gas distributions within the reservoir, the interactions between reservoir fluids, the extent of boiling and mixing, and the velocity and direction of fluid movement through the geothermal system. Because of the drilling and completion techniques currently in use, fluid samples collected from production wells can only provide a partial view of the reservoir. In this paper, we illustrate how production and fluid inclusion data can be combined to develop a detailed hydrogeochemical model of the fracture-dominated geothermal system at Coso. This investigation is part of an ongoing study being performed through an agreement between California Energy Company and the Earth Science Laboratory Division/University of Utah Research Institute.

The Coso geothermal field is located at the western edge of the Basin and Range province on the China Lake Naval Weapons Center in Inyo County, CA (Fig. 1). The thermal area is associated with a series of Pliocene to Pleistocene rhyolite domes which trend north-south through the Coso Range. The geothermal system is localized along discrete zones of fracture permeability in the underlying crystalline metamorphic basement. Surface manifestations of the system include fumaroles and acid-sulfate springs in the northern and eastern portions of the field at Devil's Kitchen and Coso Hot Springs.

To date, California Energy Company, as operator for the Coso Geothermal Project, has completed 66 wells ranging in depth from 400 to 2500 m and 10 core holes ranging from 600 to 1300 m in depth. Measured temperatures in the production wells range from 230°C in the shallow portion of the system in the north to 340°C at depths of 2500 m in the south. The first 30 MW power plant at Coso began operation in July of 1987. By early 1989, four additional units will be in operation, increasing the generating capacity to 123 MW..

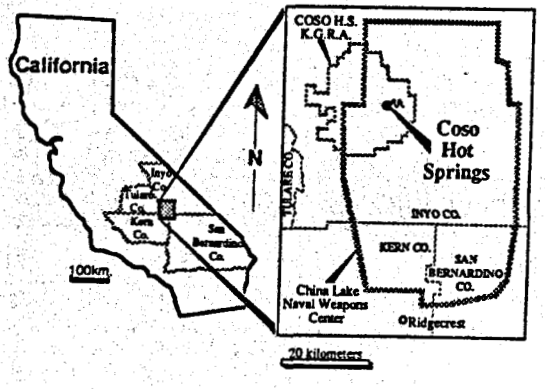

Figure 1. Location map of the Coso geothermal system.

CHEMISTRY OF THE PRODUCTION FLUIDS

Collection of gas and liquid samples from the production wells has been an important component of the development program at Coso. The data base discussed in this paper includes chemical analyses from 27 wells drilled throughout the field. Samples from these wells were collected using a mini-cyclone separator.

Many of the production wells display a greater measured enthalpy than that predicted by the chemical geothermometers. These differences in enthalpy appear to be caused by a

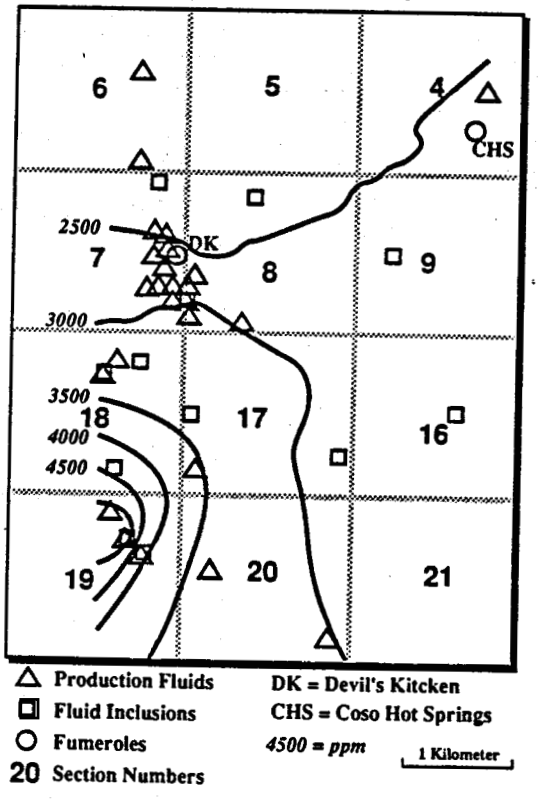

Figure 2. Plan map of the Coso geothermal field showing well locations and calculated Cl concentrations of reservoir fluids.

combination of boiling around the wellbore (excess enthalpy) and the addition of steam from the reservoir (excess steam). However, because the discharge enthalpies were not measured for every well at the time of sampling, quartz adiabatic- boiling geothermometer temperatures have been used for consistency to estimate the composition of the reservoir from the fluid samples. More detailed reconstructions of the reservoir chemistries are in progress. Table 1 presents representative compositions of the reservoir fluids calculated by this method.

The fluid compositions define steep gradients in salinities, gas concentrations, and temperatures across the reservoir. Figure 2 is a plan map of the field contoured with respect to the calculated Cl contents of the reservoir fluids. Wells that define the high-chlorinity region in the southern part of the field all produce from depths greater than 1525 m. In contrast, wells drilled outside the 3500 ppm contour produce from shallower depths. The corresponding salinities range from 1.05 wt.% TDS in the south to 0.37 wt.% TDS in the north.

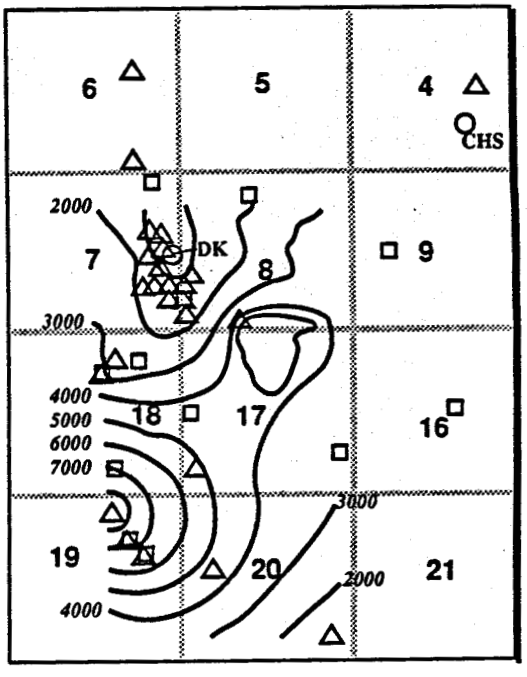

Figure 3. CO_2 concentrations in production fluids. See Fig. 2 for explanation.

Variations in CO_2, shown in Figure 3, mimic the Cl variations with the exception of the CO_2 depression in the north. Gas depletion in the north may be caused by boiling, as indicated by the occurrence of fumaroles in this area.

The relationship between the Na/K geothermometer temperatures (Truesdell, 1976) and the Cl contents of the recalculated fluids is shown in Figure 4. Because the Na/K geothermometer is a logarithmic function of the concentrations of these elements, mixtures of different temperature endmembers that have not chemically reequilibrated will define a curve that is concave downward

Table 1. Representitive analyses of production fluids from the Coso geothermal system. Concentrations are are in ppm and are restored to pre-flash conditions based on the silica geothermometer temperatures. Quartz = quartz geothermometer temperatures (Fournier and Potter, 1982) in deg C , Na/K = Na/K geothermometer temperatures (Truesdell, 1975).

Well	52-7	77-7	24-20	33-19	72-19	73-19
Date	2/88	1/87	1/88	6/88	9/86	5/87
Na	1480	1731	1949	2801	2850	1934
K	206	324	390	700	927	552
Ca	11.4	25.3	9.0	36.8	75.0	36.6
Mg	< 0.18	< 0.16	0.21	< 0.10	< 0.35	< 0.15
SiO_2	423	463	549	700	711	661
B	63	67	64	113	119	61
Li	10.9	15.1	18.4	36.3	45.3	29.9
Sr	2.43	2.58	1.42	0.77	2.79	2.08
Cl	2329	3041	3301	5121	5729	3763
F	3.20	N.A.	N.A.	2.25	1.91	1.49
HCO_3	95.5	40.4	98.6	30.2	23.3	31.4
SO_4	49.9	37.2	41.4	11.6	5.0	5.5
TDS	4615	5709	6355	9573	10468	7048
Quartz	240	249	268	307	310	296
NA/K	226	267	277	313	363	337
Total Gas	2477	1428	4678	9842	7967	9389
CO2	2449	1412	4644	9545	7786	9224
H2S	14.3	15.0	20.9	188.8	159.8	141.7
NH3	0.472	0.473	0.530	0.694	3.776	0.547
Ar	0.181	0.012	0.038	1.569	0.059	0.103
N2	9.65	1.14	9.02	94.02	9.19	18.85
CH4	0.444	0.093	0.737	4.004	1.118	1.989
H2	0.038	0.043	0.040	1.859	1.077	0.568

on a Cl-enthalpy plot. The degree of curvature increases as the salinity of the diluting fluid decreases. Equilibration to the mixture temperature results in a straight-line relationship between the geothermometer values and the Cl concentrations. The linear trend shown in Figure 4 indicates that the fluids at Coso are related by mixing, and that they have reequilibrated after mixing. The high-temperature end-members are produced from wells in section 19, and have Na/K geothermometer temperatures of 362°C and Cl contents of approximately 6000 ppm. Although it is not possible to determine uniquely the temperature of the diluting fluid from the Cl- enthalpy relationships, the data suggest that it is not much lower than about 140°C.

Comparison of chemical analyses from individual wells sampled at different times indicates that part of the scatter in Figure 4 results from local mixing of the reservoir fluids. The repeat analyses indicate that SO_4 contents of the fluids can vary as much as 100% and that increasing SO_4 correlates with decreasing geothermometer temperatures and increasing calcite scaling and total S content. In contrast, the Cl content shows no systematic correlation with SO_4 concentration. Thus, the observed compositional variations may be the result of mixing between reservoir fluids of different temperature but similar Cl concentrations, with the cooler fluids enriched in Ca, HCO_3, and SO_4 due to equilibration with calcite and anhydrite.

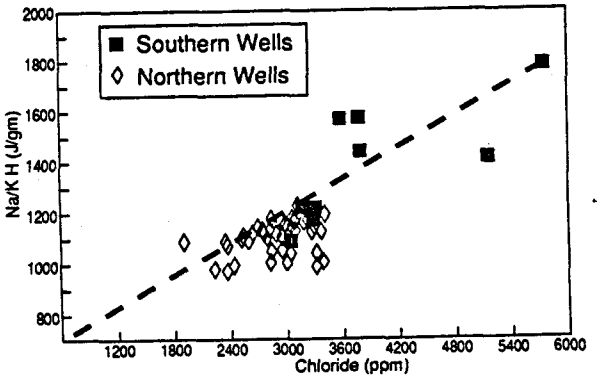

Figure 4. Enthalpy-Cl relationships of the production fluids.

FLUID INCLUSIONS

Fluid inclusions from 12 thermal gradient and production wells were studied to better characterize the composition of the reservoir fluids. Microthermometric measurements were made on approximately 1200 two-phase, liquid-rich inclusions in quartz, calcite, and anhydrite. The majority of the inclusions studied were secondary or pseudosecondary in origin and 3 to 10 microns in size. Although the temperature and salinity relationships discussed below indicate that most of these inclusions are related to the present geothermal system, a few inclusions found in quartz and anhydrite recorded salinities in excess of 6 equivalent wt.% NaCl. Such high salinity fluids are unlikely to be related to the present thermal system, and therefore these data were not included in Figures 5a-c.

Vapor-rich inclusions are found throughout the field but are most common in the upper several hundred meters of the northern and eastern wells. The presence of vapor-rich inclusions is significant because they provide evidence of boiling within the reservoir. Unfortunately, it was not possible to make reliable microthermometric measurements on them because of their small size (less than 10 microns).

Homogenization temperatures (Th) of the fluid inclusions ranged from 328° to less than 100°C. The data are grouped in Figures 5a-c according to the locations of the wells. Wells drilled in the southern part of the field are located in sections 17 through 20. The northern wells are in sections 7 and 8, while eastern wells are located in sections 9 and 16. Figure 5a shows that fluid inclusions in the upper 1200 m of the southern wells define conductive gradients but plot close to the boiling point curve at greater depths. In contrast, the thermal profiles in the shallow portions of the northern and eastern wells follow boiling point curves (Figs. 5b and c).

Ice-melting temperatures (Tm-ice) of the inclusions range from 0.0° to -2.8°C. These data are summarized in Figure 6. The plot shows that, in general, the apparent salinity of the inclusion fluids increases with increasing Th. Many individual samples, however, display large variations in Tm-ice but relatively little variation in Th. For example, Tm-ice of secondary fluid inclusions in quartz from 372 m in well 41-8 ranged from -2.2° to -0.4°C whereas the corresponding homogenization temperatures varied by only 7°C (236° to 243°C). Hedenquist and Henley (1985) described similar relationships from the Broadlands geothermal system and suggested that variations in Tm-ice of individual samples could be due to differences in the gas contents of the inclusions.

If the assumption is made that the gas is primarily composed of CO_2, as is the case at Coso, then the gas contents of the inclusions can be esti-

mated from the range in their freezing-point depressions. For the example given above, the CO_2 content would be 4.5 wt.%. This value is obviously too high, because clathrate begins to form at 3.7 wt.%, and the freezing temperature would be positive. Thus, the artificially high concentration calculated by this method is at least in part due to natural variations in the salinities of the fluids (see Fig. 2).

A few of the inclusions from the eastern and northern wells have positive melting temperatures, which ranged from +0.3° to +1.9°C. Even though it was not possible to identify optically the last solid phase to melt in these inclusions because its refractive index is similar to that of the liquid, the observations described above suggest that the positive temperatures represent the melting of CO_2 clathrate. A minimum estimate of the CO_2 contents of these inclusions can be obtained by combining the decomposition curve of clathrate in pure water (Bozzo et al., 1975) with Henry's Law relationships and the Th values of the inclusions. These calculations yield CO_2 contents up to 4.5 wt.%.

For comparison with the fluid inclusion data, the freezing point depressions of the production fluids were calculated using a procedure similar to that of Hedenquist and Henley (1985). The data are shown in Figure 6 along with the fluid inclusion measurements. It can be seen from this figure that the salinities and temperatures of the production fluids are a subset of the fluid inclusion values. The geographic trends found in the production data are also evident from the fluid inclusion data. Fluids from the southern wells are the most saline, while those in the east and north have the lowest salinities. The vertical spike defined by the northern wells in Figure 6 reflects the high gas contents of the fluids trapped at shallow depths. These wells lie along the same zone as the gas-depleted production fluids, implying that the higher gas contents of the inclusion fluids reflects condensation of steam and gas released from the deeper fluids during boiling.

The least diluted fluid is contained in fluid inclusions sampled at a depth of 1859 m in Well 72-19, which is located in the southern part of the field. Fluid inclusions from this depth have an average Th of 322°C. The Tm-ice of these inclusions ranged from -0.6° to -1.6°C with the majority being -0.8°C. We infer from these data that the inclusion fluid has an apparent salinity of 1.4 equivalent wt.% NaCl, and a maximum CO_2 content of 2.4 wt.%. These values are slightly higher than the production fluids from this well, which have a salinity of 1.05 wt.% TDS and a CO_2 content of 0.95 wt.%. Although the higher apparent salinities of the fluid inclusions from well 72-19 may represent a more saline parent fluid than is found in the production zones, the higher gas contents of the inclusions are probably the result of gas transfer and enrichment due to boiling. Gas enrichment is likely since the majority of the highest-temperature inclusions have the lowest gas contents.

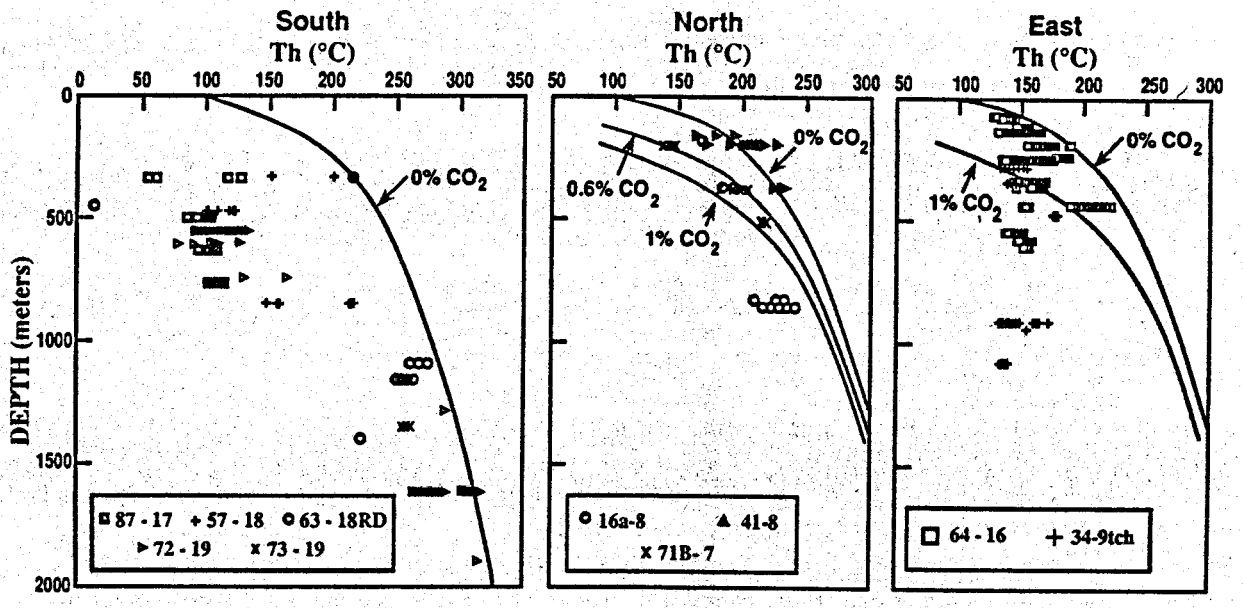

Figure 5a-c. Th-depth relationships for each of the three areas studied. Boiling point curves for a 0.3 wt% NaCl fluid with variable CO_2 contents are shown for reference.

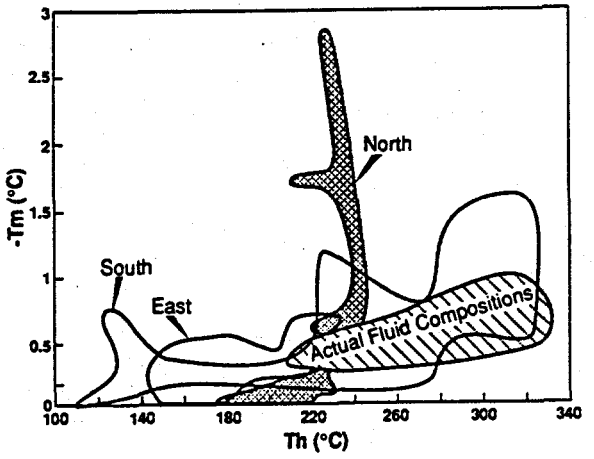

Figure 6. Th-Tm diagram summarizing the fluid inclusion and production fluid data.

CONCLUSIONS

Exploration and production drilling within the Coso geothermal system has provided an unusually complete suite of fluid and rock samples for chemical and petrologic studies. In this paper, we have combined chemical analyses of the production fluids with the results of fluid inclusion measurements to develop a detailed hydrogeochemical model of this dynamic geothermal system. This model defines a plume of hot water that originates deep in the southern part of the field and then migrates to the north and east through the fractured crystalline basement rocks.

As the deep reservoir fluid moves laterally and vertically away from the center of upwelling, it is progressively diluted by low-salinity water. Both the fluid inclusion and enthalpy-Cl data indicate that the diluting fluid has a temperature between 120° and 140°C. Estimates of the high-temperature endmember range from 322° to 360°C.

The pattern of fluid movement appears to be controlled by decreasing depth to permeable rocks north and east of section 19. Variations in permeability with depth are reflected in the abundance of veins and the widespread evidence of boiling at shallow depths in the north compared to the south.

Evidence for boiling includes CO_2 depletions of the fluids, vapor-rich inclusions, and fumarolic activity. In addition, CO_2 enrichments in fluid inclusions indicate that steam and gas have been added to some of the geothermal fluids.

The close correspondence of production fluid chemistry and fluid inclusion data demonstrates that these methods, used in conjunction, can provide detailed models of geothermal systems. In contrast, neither the chemical nor the fluid inclusion studies independently yields a hydrogeochemical model that adequately describes this reservoir.

ACKNOWLEDGEMENTS

We would like to thank J. Moore of the California Energy Company and C. Austin of the Naval Weapons Center for making this study possible. Samples and data made available by California Energy Company for this work are greatly appreciated. Funding for this work was provided by the Department of Energy, under contract no. DE-AC07-85ID-12489.

REFERENCES

Bozzo, A. T., Chen, H-S., Kass, J. R., and Barduhn, A. J., 1975, The properties of the hydrates of chlorine and carbon dioxide: Desalination, v. 16, p. 303-320.

Fournier, R. O., and Potter, R. W., II, 1982, A revised and expanded silica (quartz) geothermometer: Geothermal Resources Council Bulletin, Vol. 11, No. 10, 1982, p. 3-12.

Hedenquist, J. W., and Henley, R. W., 1985, The importance of CO_2 on the freezing point depression of fluid inclusions: evidence from active geothermal systems and implications for epithermal ore deposition: Economic Geology, v. 80, p. 1379-1406.

Truesdell, A. H., 1976, Summary of section III-geochemical techniques in exploration: Second United Nations Symposium on the Development and Use of Geothermal Resources, San Francisco, May 1975, v. 1, p. liii-lxiii.

PROCEEDINGS, Fourteenth Workshop on Geothermal Reservoir Engineering
Stanford University, Stanford, California, January 24-26, 1989
SGP-TR-122

SELF-POTENTIAL ANOMALY CHANGES AT THE EAST MESA AND CERRO PRIETO GEOTHERMAL FIELDS

N. E. Goldstein, S. Halfman*, R. F. Corwin† and J. Alvarez R.‡*

*Earth Sciences Division, Lawrence Berkeley Laboratory,
University of California, Berkeley, California 94720

†Consultant, El Cerrito, California 94530

‡ Coordinadora Ejecutiva de Cerro Prieto,
Comisión Federal de Electricidad, Mexicali, B.C., Mexico

ABSTRACT

Repetitive self-potential (SP) surveys recently completed over two producing geothermal fields, Cerro Prieto and East Mesa, ten years after the original surveys gave us an unprecedented opportunity to see whether SP changes over the fields are related to pressure gradients associated with massive fluid movements; i.e., production, injection and natural recharge. A strong correlation between SP and production was observed at Cerro Prieto where the anomaly position has shifted eastward, and where we were able to model the new anomaly on the basis of actual production rates and the hydrogeology. On the other hand, we were unable to explain the East Mesa anomalies on the basis of what we presently know about production rates and the hydrogeology of that system. The SP voltages over the East Mesa area are smaller, and non-geothermal sources effects are more apparent. We suspect, as well, that electrochemical (diffusional) potentials are caused by fault-guided leakage of thermal fluids in the shallow clay caprock.

INTRODUCTION

Most geothermal fields are reported to have an associated self-potential (SP) anomaly of tens to over several hundred millivolts (Corwin and Hoover, 1979). Although the interpretation of these voltages has proved difficult in the past due to the multiplicity of causes (e.g., electrokinetic, thermoelectric, and chemical diffusion effects), lack of laboratory and field data, and the lack of interpretative techniques, recent advances indicate that the main mechanism is related to the electrokinetic effect. That is, these so-called streaming potentials are generated by subsurface flows of water, both natural and induced by geothermal fluid extraction and injection activities (Ishido et al., 1983; Ishido et al., 1987). SP measurements made near individual geothermal production and injection wells being tested show that changes of 5 to 10 mV occur as the wells are subjected to short-term flow and injection tests (Ishido et al., 1983; Sill, 1983a). Although these voltages are close to the typical SP noise level of ± 5 mV, the voltage anomalies over a large multi-well geothermal field would be many times larger.

An unprecedented opportunity to study production-related SP effects occurred recently when we obtained SP data sets over two producing geothermal fields; East Mesa and Cerro Prieto. SP surveys had been run over both fields ten years earlier (Corwin et al., 1978; Corwin et al., 1981), and thus it was also hoped that the repeat surveys would show changes correlative to changes in production activities. East Mesa and Cerro Prieto are a fortunate choice of fields for comparative studies because they share a few common geological features, yet have had markedly different production histories. Both reservoirs occur in nearly horizontal deltaic sediments of the Salton Trough and both systems have been under increasing development and exploitation between the survey years. On the other hand, there exist many significant differences in the physical parameters of the systems, chemistry of their brines, and their production rates and histories.

DATA ACQUISITION PROCEDURES

Attempts were made to resurvey the two fields in the same fashion as the original surveys, but this was impossible to do for reasons discussed in this section. For the most part surveys could be rerun along the same lines and with the same type of equipment; copper-copper sulfate electrodes and a 10 Mohm impedance digital multimeter. Because of geothermal activities some survey line had to be relocated, other lines were extended to expand the surveys into newer production areas. Telluric noise monitoring was carried out during surveys to check for periods of anomalously strong noise.

With minor exceptions both East Mesa surveys were carried out using the fixed reference technique in

which one electrode remains fixed at a base and is connected to the multimeter via a very long wire. In this mode of operation, multiple base stations were required (14 for the 1987 survey), and loop errors were distributed to help minimize cumulative errors. In 1987, a 100-m station separation was used. These data are higher in resolution and better in quality than the 1978 data for which a 200-m station separation was used.

Data acquisition techniques used at Cerro Prieto consisted of both the fixed reference and the less desirable "leapfrog" technique in which both electrodes move in an alternating fashion along the survey line. The 1978 Cerro Prieto survey was conducted almost entirely using the reference electrode technique and station separations of 100 to 350 m. Due to the increased cultural activity and loss of easy access to some areas, the 1988 survey was done entirely using the leapfrog method with a 100-m measuring dipole (Rodríguez, 1988). The leapfrog mode is highly susceptible to cumulative random errors along a line. Errors at line crossing points were distributed around loops to help minimize this problem.

The corrected voltages were all then smoothed by means of a 5-point moving average to help remove small voltage perturbations due to various noise sources, that is telluric noise, man-made electrical noise, and background geologic noise due to point-to-point variations in soil moisture and chemistry. This is a low-pass filtering operation which preserves the long spatial wavelengths in the data, but which changes individual readings up to 20-30 mV. The smoothed data sets were then hand contoured. Both new SP contour maps display more detail than the original maps. This is due to the closer station spacing used in the two recent surveys, and additional (fill-in) survey lines. Such differences make direct comparisons of the results difficult. Another consideration when comparing repeat surveys, particularly those at Cerro Prieto, is the difference in background voltage levels. This difference may be due simply to the choice of reference station.

CERRO PRIETO RESULTS

The initial SP survey was conducted in late 1977 and early 1978 when production was limited to the shallow α reservoir. At that time approximately 12 wells were producing 750 tonnes/hr (≈250 L/s) from a reservoir region 1.0 to 1.4 km below the surface. Steam separated at the wellheads was delivered to the original 75 MWe plant (Units I and II of the CPI plant). The SP contours (Fig. 1) showed a dipolar anomaly, peak-to-peak voltage of 160 mV, whose axis trended N-S and was centered over the original production area (Corwin et al., 1978; Fitterman and Corwin, 1982). The dipolar anomaly may be explained in terms of fluid recharge by waters ascending through the sandy gap of the otherwise impermeable O Shale unit (Halfman et al., 1986a).

The second SP survey was carried out by Jorge Rodríguez Bahena of CFE in March 1988. At that time the installed electric generating capacity had increased to 620 MWe with the expansion of the CPI plant and the addition of two new 220 MWe plants (CPII and CPIII), that went on line in 1986-1987. Most steam for the three plants was provided by brine from deeper reservoir regions (primarily the β reservoir) located east of the original production area (Halfman et al., 1986a; 1986b). Brine reinjection has been insignificant. Not unexpectedly, the 1988 survey (Fig. 2) reveals that the SP anomaly has changed. Among the more significant changes are the following:

(1) the dipolar anomaly is less clear,

(2) the steepest SP gradients have shifted eastward a distance of over 2 km to a position that appears to correlate with the surface projection of the Fault H zone (Halfman et al., 1986b),

(3) the voltage amplitude variations have increased up to 20% along some lines.

INTERPRETATION OF THE CERRO PRIETO DATA

To determine whether the 1988 SP data are, in fact, production related, we attempted to numerically model the SP using known production data for the month of the surveys, the hydrogeologic-lithofacies model for the system, and the subsurface geophysical parameters, either measured directly (electrical resistivity and temperature) or inferred from reservoir models (permeability). Thus far, we have focussed our attention on a single northwest-southeast trending profile, Line E–E′, for which there is a lithofacies cross-section and a recently updated model of geothermal fluid flow (Halfman et al., 1986b). In addition, the profile is roughly normal to the steepest SP gradients, and it crosses an area of significant geothermal production. Figure 3 shows the simplified lithofacies section, with the interpreted geothermal fluid flow patterns, and the geothermal production intervals. Northwest of Fault H production is from 2.2 km, the upthrown side of the β reservoir in Sand unit Z. Southeast of the Fault H production comes mainly from a depth of 2.6 to 2.8 km in the downthrown Sand Z unit. Temperatures in the β reservoir are 320-350°C. Less is known about the deeper γ reservoir (unit K) and so it has been excluded from this study.

To calculate the surface SP along profile E–E′ we used a program SPXCPL written by Sill and Killpack (1982) and modified for easier use at LBL. A complete discussion of the basis for these calculations is beyond the scope of this paper (see for example Nourbehecht, 1963; Sill, 1983b), so it shall suffice to say

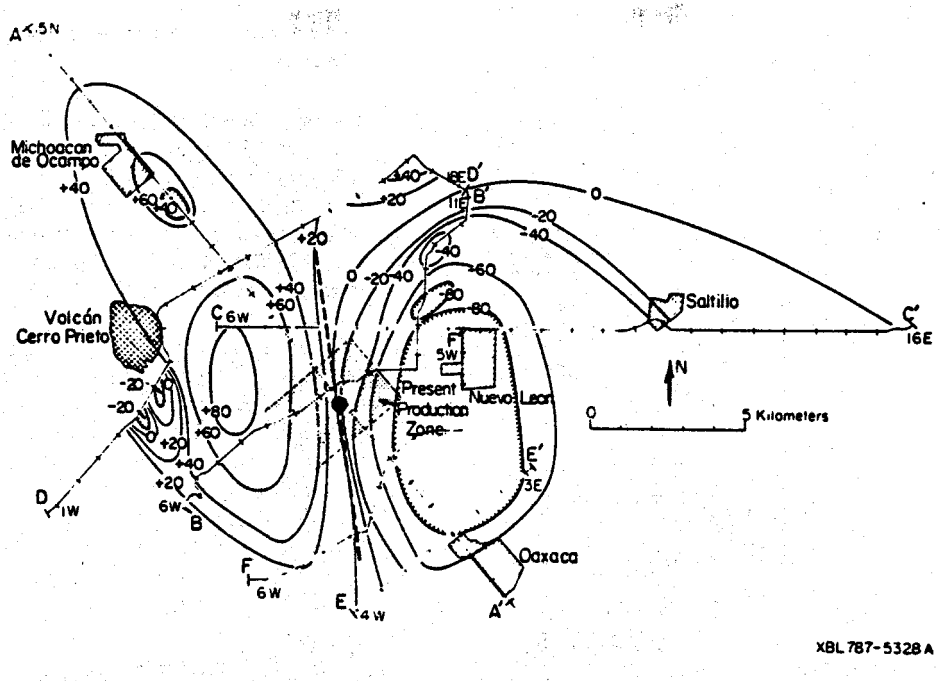

Fig. 1. The 1977-78 Cerro Prieto SP contour map.

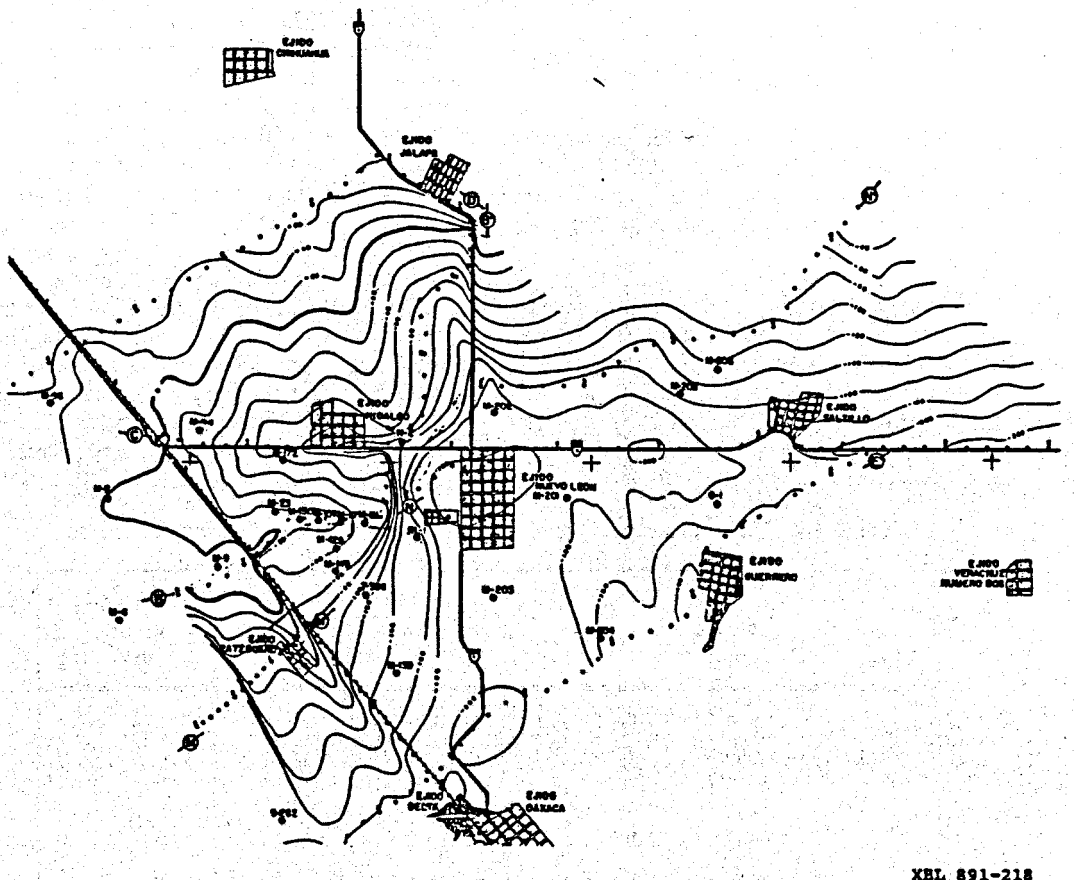

Fig. 2. The 1988 Cerro Prieto SP contour map.

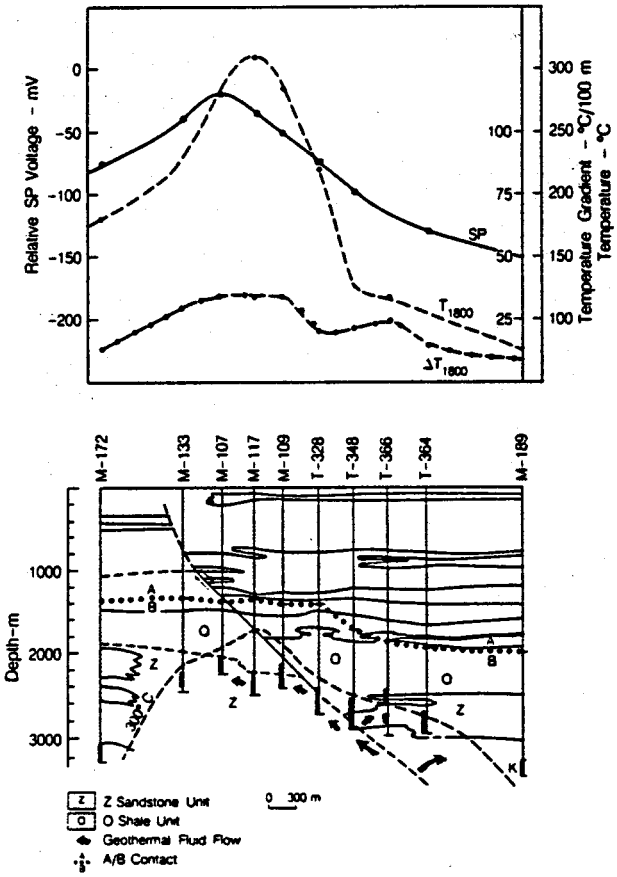

Fig. 3. Simplified lithofacies section for the north-south Line E–E′ (after Halfman et al., 1986b). Also shown is the SP voltage profile plotted against the subsurface temperature and temperature gradient at 1800 m depth.

that SPXCPL solves separately for the electric potentials in the earth subject to a distribution of pressure (flow or electrokinetic) sources and thermal (thermoelectric) sources. SPXCPL solves the 2-D coupled flow problem by explicitly modeling both the primary flow (fluid flux, heat flux) and the induced secondary electric potentials that arise from the primary flows (Onsager, 1931).

Figure 4 shows the flow model constructed and used, and Table 1A lists the parameters for the model. The two large negative flow sources (II and IV) account for actual well production from the upthrown and downthrown sides of the β reservoir, respectively, during March 1988. The positive flow sources simulate recharge effects.

We were able to obtain a reasonable fit to the observed SP anomaly after relatively few iterations (Fig. 5). Electrical resistivity values are reasonably well constrained by surface and wellbore surveys and so these were not varied. Unit permeabilities had to be reduced by about half the values used by Halfman et al. (1986a), and the values for the electrokinetic coupling coefficient, a critical parameter in the modeling exercise, were taken from tables of representative values for sands and shales.

We found that the location and magnitude of recharge sources is essential for fitting the SP anomaly. The SP low in the southeast part of the survey area requires both shallow lateral fluid flow in Unit 2 and deeper lateral recharge in the Z Sand unit from the southeast. The fit improved after we eliminated recharge source I, simulating deep Z Sand recharge from the northwest. The fit improved more after we eliminated source V which simulates deep vertical recharge to the β reservoir. This came as a bit of a surprise because it contradicts the hydrogeologic model showing a deep source of fluid ascending the H fault (Halfman et al., 1986b) and feeding both the β and γ reservoirs. It must be pointed out that the SP is not conclusive evidence for the presence or absence of recharge. First, the SP calculations are highly model specific and nonunique. Second, the final model is also highly dependent on the choice of profile to be fitted and data accuracy along that profile. However, these numerical tests clearly point out the sensitivity of SP surface voltages to recharge sources.

Table 1A. Unit Parameters for Cerro Prieto SP Model: Pressure Sources

Unit	Geologic Designation	Electrical Resistivity (ohm-m)	Permeability (md)	Electrokinetic Coupling Coeff. (mV/atm)
1		2	10	5
2		20	50	20
3		6	10	5
4		0.5	50	50
5	Shale O	6	0.5	5
6	Sand Z	3	50	100
7		10	5	5

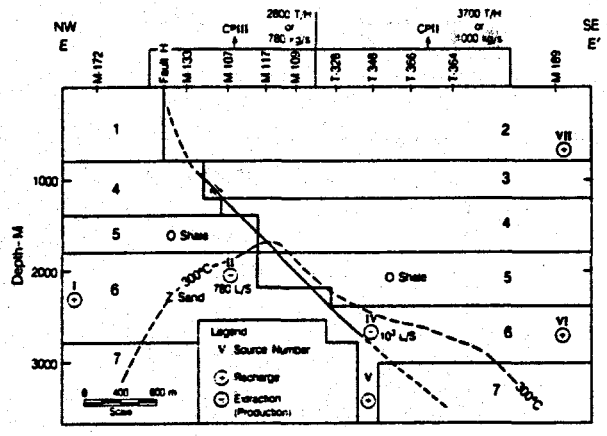

Fig. 4. Two-dimensional hydrologic flow model used to model SP effects at Cerro Prieto.

To see how much the SP data was affected by thermoelectric currents, we next calculated the voltages due to a distribution of thermal sources. A reasonable fit to the subsurface temperature distribution was obtained by using 70 sources, each 0.25 x 10^6 Watts, in the region outlined in Figure 6, and the rock thermal parameters shown in Table 1B. Although a closer fit to subsurface temperatures could have been achieved, modeling was terminated when it became apparent that the peak thermoelectric voltage at the surface is less than 4 mV, and less than the noise level of the field data.

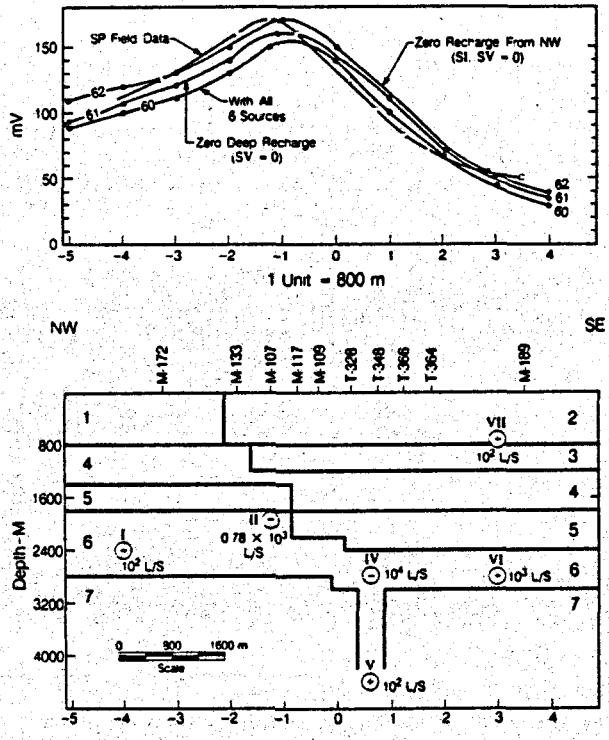

Fig. 5. Numerical model results for different cases of recharge (60, 61 and 62 refer to the data file numbers). Horizontal distance resolution is 200 m.

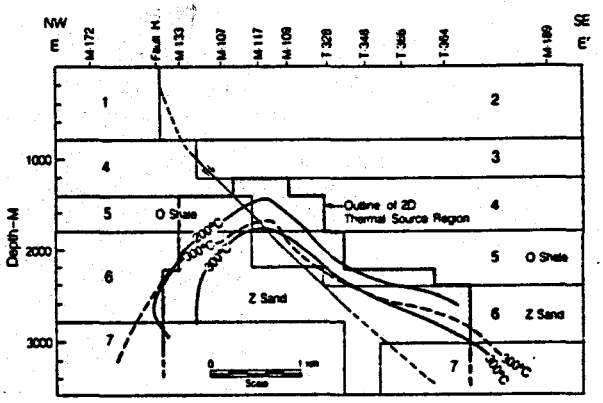

Fig. 6. Two-dimensional thermal model for Cerro Prieto used to calculate thermoelectric SP voltages. Seventy point sources, 0.25 x 10^6W each were used, but produce only a broad negative anomaly of < 4 mV (peak). The solid isotherm lines are calculated, the dashed line is measured.

EAST MESA RESULTS

The 1978 East Mesa SP survey (Fig. 7) was conducted after several wells had been drilled and tested by Republic Geothermal, U.S. Bureau of Reclamation (Burec), and Magma Power Company, but prior to large-scale, continuous geothermal production. A broad dipolar anomaly (90 mV peak-to-peak) was modeled by using charge separations along three steeply dipping pairs of planes; two that run northwesterly through Section 6 (T. 16 S., R. 17 E.), roughly between the Burec and Republic wells (Corwin et al., 1981). Because these planes were found to correlate with the traces of known or suspected faults, Corwin et al. (1981) concluded that conditions along faults were causing the SP voltages. However, known subsurface temperature and pressure gradient and estimated electrokinetic and thermoelectric coupling coefficients for the rocks all seemed far too low to account for the anomaly amplitude. They suggested that another mechanism might be generating the source currents.

Aside from enhanced resolution, the 1987 data appear relatively unaltered and unaffected by production activities (Fig. 8). Because of the higher data density, the 1987 data set has a much richer and more complex pattern of 10 to 30 mV (after smoothing) highs and lows, but the relations between discrete SP variations and production activities are subtle. During the first two weeks of December 1987 when the second survey was made, two binary power plants were in operation and a third was being prepared for start-up. Production wells in Section 7 were delivering approximately 200 L/s to the 10 MWe (gross) Magma plant. To the north, another 11 production wells, most in the southern part of Section 30, were producing approximately 500 L/s for the Ormesa I (30 MW

Table 1B. Unit Parameters for Cerro Prieto SP Model: Thermal Sources

Unit	Geologic Designation	Electrical Resistivity (ohm·m)	Thermal Conductivity (W/m·°C)	Thermoelectric Coupling Coeff. (mV/°C)
1		2	2	0.05
2		20	2	0.10
3		6	2	0.30
4		0.5	2	0.10
5	Shale O	6	1.8	0.30
6	Sand Z	3	2	0.10
7		10	2.5	1.00

gross) plant. Another seven production wells in Sections 5 and 6 were in the last stages of testing prior to the start-up of the Ormesa II (20 MW gross) plant. Geothermal fluids are produced from depths of 1.2 to 2.1 km and are injected into offset wells at depths of 0.9 to 1.5 km.

In view of the amount of fluid produced and injected (the pressure sources), the SP amplitude variations are small. A few of the discrete anomalies seem to be non-geothermal in origin. For example, a new 50 mV low around well 18-28 is probably due to oxidizing well casing, and the persistent 20 mV low at the west end of Line D may be due to a pump motor along the East Highline Canal. Small highs adjacent to the East Highline Canal may be due to fluid leakage. Other small discrete anomalies do seem to correlate with geothermal activities. In particular, notice that a the original 60 mV high in the southwest corner of the survey area has become a complex pattern of 30 mV highs to 20 mV lows. The E-W trending low running through Sections 7 and 8 correlates with injection wells 46-7, 46-7B, and 84-7, while the adjacent high on the south correlates with production wells 48-7, 48-7A, 48-7B and 88-7. This correlation is illustrated in Figure 9 which shows the smoothed SP data for Line A, a south-to-north profile, passing through several wells, including production well 88-7 and injection well 84-7, 700 m apart.

The observed SP anomaly could be fitted in only a very rough way to this production-injection doublet. A pair of 300 L/s sources at 800 m depth yielded the

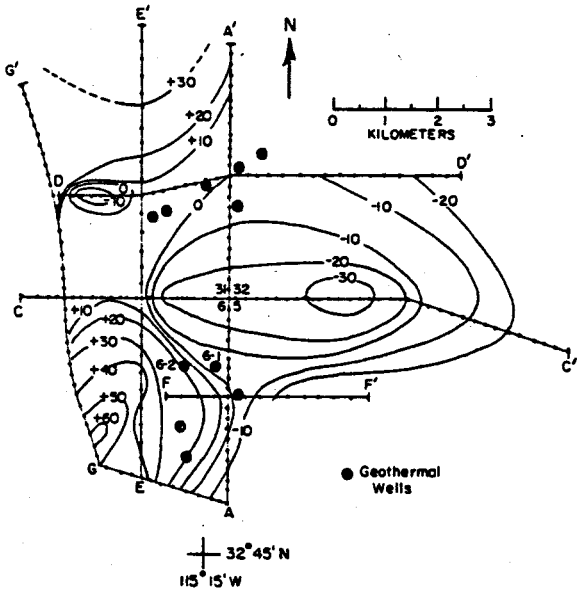

Fig. 7. The 1978 East Mesa SP contour map.

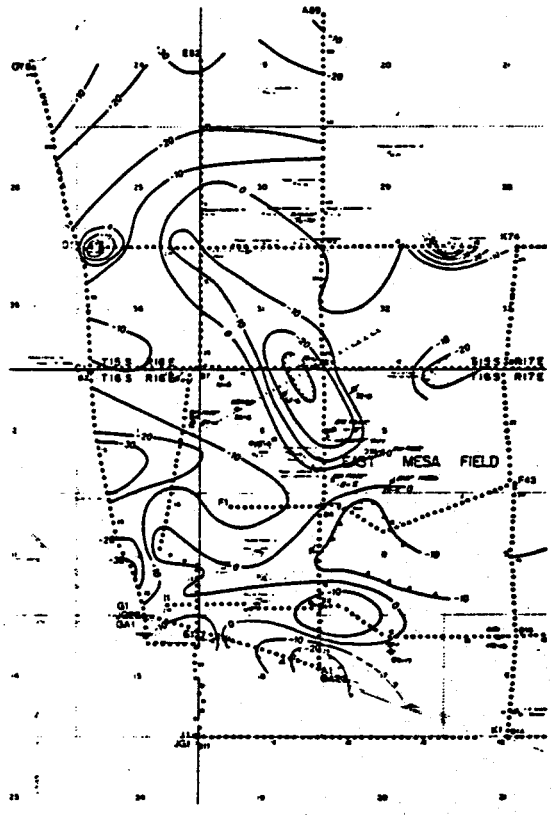

Fig. 8. The 1987 East Mesa SP contour map.

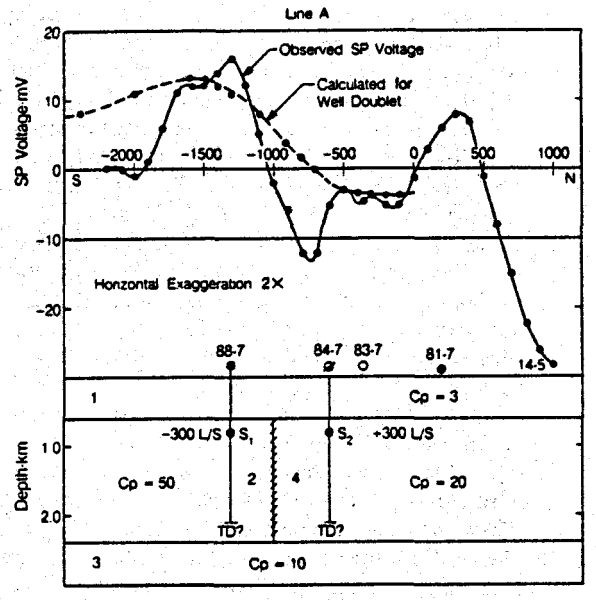

Fig. 9. SP model for the south end of East Mesa Line A (north-south).

observed voltages. Model parameters are listed in Table 2A and 2B. To get the asymmetry in the SP curve one can alter source strengths and source depths. Alternatively, as shown in Figure 9, we can also introduce a boundary between the two wells across which zone the electrokinetic cross-coupling changes. A fault boundary in this area has been indicated by offsets in the clay caprock thickness and from interference tests. The amplitude of the calculated dipolar anomaly seems to match the field data for the assumed pressure source strengths, but the steep gradients in the observed SP curve shape indicate shallower source currents. We cannot match the steep gradients unless we bring both pressure sources closer to the surface and, at the same time, reduce the thickness of the clay caprock layer, layer 1. As there is no justification for this model, we are led to conclude that the data cannot be explained by a well doublet alone. Moreover, as we learned later, actual source depths are deeper and source I is only about 30 L/s (T. Hinrichs and J. Tennison, personal communications, 1989). Thus, the true doublet anomaly should have a very small peak amplitude and a broader dipolar voltage form.

Comparing the general appearances of both data sets again, we also see that the broad dipole negative of the 1978 data has been replaced by a narrow northwest-trending 30 mV low. This interesting feature also correlates with one of the normal faults (down-to-the-west) inferred from drill hole data and the heat flow anomaly (T. Hinrichs, personal commun., 1986). A cross-section normal to anomaly strike and through several ORMAT wells is shown in Figure 10. The gradients of the observed SP anomaly indicate a source at a depth of around 600 m, the approximate depth of the contact between the low permeability clay cap and the underlying reservoir rocks (Riney et al., 1979; Goyal and Kassoy, 1981). However, calculations reveal that neither a thermal nor a pressure source at this depth can explain the anomaly. A thermal source at or below the contact, and which produces the appropriate subsurface temperatures yields only a small (≈1 mV) positive SP. A pressure

Table 2A. Unit Parameters for East Mesa SP Models: Pressure Sources

Unit	Geologic Designation	Electrical Resistivity* (ohm-m)	Permeability** (md)	Electrokinetic Coupling Coeff. (mV/atm)
1	Clay Cap	4.5	1	3
2	Reservoir Rocks	2.0	100	50
3	Deeper Sediments	5.0	5	10
4	Reservoir Rocks	2.0	100	20

Table 2B. Unit Parameters for East Mesa SP Models: Thermal Sources

Unit	Geologic Designation	Electrical Resistivity (ohm·m)	Thermal** Conductivity (W/m·°C)	Thermoelectric Coupling Coeff. (mV/°C)
1	Clay Cap	4.5	1.44	0.3
2	Reservoir Rocks	2.0	2.06	0.1

*Meidav and Furgerson, 1971
**Goyal and Kassoy, 1981; Riney et al., 1979

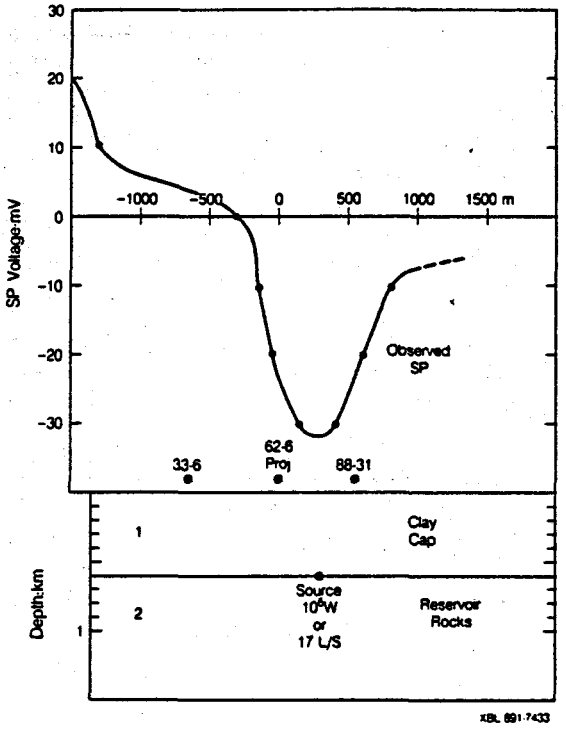

Fig. 10. SP model for a section though the -30 mV anomaly at East Mesa.

source with of magnitude 17 L/s, as calculated by Goyal and Kassoy (1981) to get the right energy balance for the hydrothermal system, gives the proper (negative) voltage, but generates only a weak SP effect of about 1 mV at the surface. Either our model and model parameters are in error, or as Corwin et al. (1981) concluded, a more significant SP mechanism exists. It has been suggested that fluid leakage into the clay cap may be creating an electrochemical potential.

CONCLUSIONS

SP resurveys over the East Mesa and Cerro Prieto geothermal fields show a number of differences from surveys made 10 years earlier. Part of the differences can be attributable to better data quality and higher data density of the recent surveys. However, it seems particularly evident that the shift in the Cerro Prieto anomaly can be explained by production-recharge differences. At the time of the initial survey in 1978 production for the CPI plant came from the shallow α reservoir with thermal fluid recharge ascending a "sandy gap" in the otherwise impermeable Shale O unit. At the time of the resurvey in 1988, production has been greatly expanded to the east with most fluids produced from the deeper β reservoir and thermal recharge guided, in part, by the Fault H. A numerical model for electrokinetic SP currents fits the 1988 production data and the current hydrogeologic model reasonably well. One of the important findings from the modeling exercise is the sensitivity of the SP to deep recharge.

By way of contrast, we had no success in fitting the East Mesa SP to production-related effects. East Mesa data reveal a complex assortment of small (20 to 30 mV) positives and negatives. A few of these correlate to man-made sources (e.g., redox reaction of a well casing and pumps) or to non-geothermal fluid flow (e.g., leakage from the East Highline Canal). Attempts to model individual SP anomalies using production-injection well doublets, natural convective flow and thermal sources gave anomalies with the wrong sign, that were too small in amplitude and/or too broad. Our models may be inaccurate, but there also could be another source of SP voltage. As evidenced by the apparent shallow nature of SP sources at East Mesa, it is possible that the anomalies are electrochemical and result from thermal fluid leakage guided by faults that penetrate the clay caprock. It also seems that for reasons of temperature, fluid chemistry (i.e., speciation) and rock chemistry, the East Mesa system is not as effective at causing streaming potentials as Cerro Prieto.

In spite of our difficulties in modeling the East Mesa data, we have shown that where an accurate hydrogeologic model, well production data, and subsurface rock parameters are available, carefully made repetitive SP surveys may be able to help understand and estimate fluid recharge in the system.

ACKNOWLEDGMENTS

We would like to acknowledge our colleagues in industry with whom we had numerous helpful discussions. These include Chan Swanberg, Zohn Ziagos and James Tennison of GEO, Tom Hinrichs of Magma Power, and Doug Miller of ORMAT, all of whom reviewed and discussed East Mesa data with us. We had extremely useful discussions with Marcelo Lippmann (LBL) on the Cerro Prieto system. Mike Wilt installed his modified version of program SPXCPL on the LBL computer and advised us on the use of this code. We would also like to thank our colleagues of the Coordinadora Ejecutiva de Cerro Prieto, Comisión Federal de Electricidad, for carrying out the SP survey and making the results available. These include Francisco Bermejo, Benjamín Terrazas and Jorge Rodríguez Bahena.

The East Mesa SP survey and the modeling study was supported by the Assistant Secretary for Conservation and Renewable Resources, Office of Renewable Technologies, Geothermal Technology Division of the U.S. Department of Energy, under Contract No. DE-AC03-76SF00098.

REFERENCES

Corwin, R. F. and Hoover, D. B., (1979), "The Self Potential Method in Geothermal Exploration," *Geophysics*, V. 44, p. 226-245.

Corwin, R. F., Morrison, H. F., Díaz, C. S. and Rodríguez B., J., (1978), "Self-Potential Studies at the Cerro Prieto Geothermal Field," Proc. First Symp. on the Cerro Prieto Geothermal Field, Baja California, Mexico, Lawrence Berkeley Laboratory, LBL-7098, p. 204-210.

Corwin, R. F., DeMoully, G. T., Harding R. S., Jr. and Morrison, H. F., (1981), "Interpretation of Self-Potential Survey Results from the East Mesa Geothermal Field, California," *J. Geophys. Res.*, V. 86, p. 1841-1848.

Fitterman, D. V. and Corwin, R. F., (1982), "Inversion of Self-Potential Data from the Cerro Prieto Geothermal Field, Mexico," *Geophysics*, V. 47, p. 938-945.

Goyal, K. P. and Kassoy, D. R., (1981), "A Plausible Two-Dimensional Vertical Model of the East Mesa Geothermal Field, California," *J. Geophys. Res.*, V. 86, p. 10719-10733.

Halfman, S. E., Lippmann, M. J. and Bodvarsson, G. S., (1986a), "Quantitative Model of the Cerro Prieto Field," Proc. 11th Workshop Geothermal Reservoir Engin., Stanford Univ., SGP-TR-84, p. 127-134.

Halfman, S. E., Manõn, A. and Lippmann, M. J., (1986b), "Update of the Hydrogeologic Model of the Cerro Prieto Field Based on Recent Well Data," Trans. Geothermal Resources Council, V. 10, p. 369-376.

Ishido, T., Mizutani, H. and Baba, K., (1983), "Streaming Potential Observations, using Geothermal Wells and In-Situ Electrokinetic Coupling Coefficients under High Temperatures," *Tectonophysics*, V. 91, p. 89-104.

Ishido, T., Kikuchi, T. and Sugihara, M., (1987), "The Electrokinetic Mechanism of Hydrothermal-Circulation-Related and Production-Induced Self Potentials," Proc. 12th Workshop Geothermal Reservoir Engin., Stanford Univ., SGP-TR-109, p. 285-290.

Meidav, T. and Furgerson, R., (1971), "Electrical Resistivity for Geothermal Exploration in the Imperial Valley," in Rex, R. W. et al., Cooperative Geological-Geophysical-Geochemical Investigations of Geothermal Resources in the Imperial Valley Area of California: Univ. Calif. Riverside, UCR/IGPP-71-2, p. 43-89.

Nourbehecht, B., (1963), "Irreversible Thermodynamic Effects in Inhomogeneous Media and their Applications to Certain Geoelectric Problems," Unpub. Ph.D. thesis, MIT, Cambridge, MA.

Onsager, L., (1931), "Reciprocal Relations in Irreversible Processes I," *Phys. Rev.*, V. 37, p. 405-426.

Riney, T. D., Pritchett, J. W., Rice, L. F. and Garg, S. K., (1979), "A Preliminary Model of the East Mesa Hydrothermal Systems," Proc. 5th Workshop Geoth. Reser. Eng., Stanford Univ., SGP-TR-40, p. 211-214.

Rodríguez B., J., (1988), "Informe Sobre el Estudio de Potencial Espontáneo en el Campo Geotérmico de Cerro Prieto," Comisión Federal de Electricidad, Coordinadora Ejecutiva de Cerro Prieto, Superintendencia General de Estudios, internal report.

Sill, W. R., (1983a), "Final Report, Interpretation of Self-Potential Measurements during Injection Tests at Raft River, Idaho," Earth Sciences Laboratory, Univ. Utah Res. Inst., DOE/ID/12709-103, ESL-120, 20 p.

Sill, W. R., (1983b), "Self-Potential Modeling from Primary Flows," *Geophysics*, V. 47, p. 76-86.

Sill, W. R. and Killpack, T. J., (1982), "SPXCPL: Two-Dimensional Modeling Program of Self-Potential Effects from Cross-Coupled Fluid and Heat Flow," Univ. of Utah Res. Inst., DOE/ID/12079-60, ESL-74, 26 p.

PROCEEDINGS, Fourteenth Workshop on Geothermal Reservoir Engineering
Stanford University, Stanford, California, January 24-26, 1989
SGP-TR-122

CALCULATION OF STEAM FRACTIONS IN VAPOUR-DOMINATED GEOTHERMAL SYSTEMS USING AN EMPIRICAL METHOD

R A McCartney and G W Lanyon

GeoScience Limited, Falmouth Business Park, Bickland Water Road,
Falmouth Cornwall, TR11 4SZ, UK

ABSTRACT

Steam fractions can be calculated via an empirical method using the steam fraction model conditions developed by earlier researchers (eg Giggenbach, 1980; D'Amore et al, 1982). The only exception is that prior knowledge of the reactions controlling the gas composition of the reservoir fluid is not required. Two techniques, one graphical and the other numerical, of calculating steam fractions by this new method are presented and their respective performances are assessed. The advantages and limitations of the new method compared with previous steam fraction calculation methods are discussed.

INTRODUCTION

In recent years numerous investigations have been directed towards the use of gas geochemistry as a reservoir evaluation tool for vapour-dominated geothermal fields. Most interest has centred upon the calculation of steam fractions (y) from wellhead steam gas compositions due to their possible use in the estimation of reservoir fluid reserves. The steam fraction is defined as the proportion of produced steam which is original reservoir vapour as opposed to vaporised reservoir liquid. Since the initial studies of Giggenbach (1980), 12 types of steam fraction calculation have been proposed in the literature for use on vapour-dominated systems (D'Amore et al, 1982; D'Amore and Celati, 1983; D'Amore et al, 1983; D'Amore and Truesdell, 1985; D'Amore et al, 1987), all of which are based on the same mixing/boiling model.

One of the principal uncertainties with current steam fraction calculation methods lies in the need for prior knowledge of the reactions controlling the gas composition of the reservoir fluid, and the thermodynamic equilibrium constants of these reactions. If either are incorrect, the calculated steam fractions will be erroneous. Previous researchers have relied on gas equilibrium calculations from liquid-dominated systems, or mineralogical evidence, to determine the most likely reactions at equilibrium in vapour-dominated systems (see Table 1). It is difficult, however, to determine which, if any, of these reactions are valid for any given selection of produced steam samples. For example, Arnorsson (1985) has found that the Fischer-Tropsch reaction (Reaction 7, Table 1) is not in equilibrium in all geothermal waters over 200°C and yet this reaction has been widely incorporated in previous steam fraction calculations (Table 1). Likewise, where multiple generations of secondary minerals are present, it is not always evident which are controlling the fluid gas composition.

D'Amore and Pruess (1986) have recently found that the current calculation methods do not produce correct steam fractions unless all fluids derived from production sites feeding a well have the same chemical composition (ie they are derived from the same fluid type; McCartney and Haizlip, this volume). In this paper we introduce an empirical steam fraction calculation technique which has an advantage over previous methods in that it does not require knowledge of the reactions controlling the gas composition of fluids in vapour-dominated reservoirs. Instead, it utilises the new condition imposed by D'Amore and Pruess (op cited). The new method also differs from those used previously in that it is applied to sets of steam analyses as opposed to individual samples. We discuss the potential use and limitations of the new technique.

STEAM FRACTION MODEL CONDITIONS AND MOLE RATIO DATA

All current steam fraction calculation methods are based on a vapour-liquid boiling model which incorporates the following conditions:

1 Liquid and vapour are in phase and chemical equilibrium in the reservoir.

2 The reactions and thermodynamic equilibrium constants controlling the gas composition of both phases in the reservoir are known.

3 The temperature of the reservoir fluid is known.

TABLE 1 EQUILIBRIUM REACTIONS USED IN PREVIOUS STEAM FRACTION CALCULATIONS

YNN		$NH_3 = \frac{1}{2}N_2 + \frac{3}{2}H_2$	Ref 1
YCN1		$3C + 4NH_3 = 3CH_4 + 2N_2$	Ref 1
YCN2		$C + NH_3 + \frac{1}{2}H_2 = \frac{1}{2}N_2 + CH_4$	Ref 1
YCN3		$C + \frac{1}{2}N_2 + \frac{3}{2}H_2 = NH_3 + CH_4$	Ref 1
YH	(a)	$H_2O = H_2 + \frac{1}{2}O_2$	Ref 1
	(b)	$CH_4 + 2H_2O = CO_2 + 4H_2$	
YS	(a)	$H_2S = H_2 + \frac{1}{2}S_2$	Ref 1
	(b)	$CH_4 + 2H_2O = CO_2 + 4H_2$	
YHC (≡ YFT)		$CH_4 + 2H_2O = CO_2 + 4H_2$	Ref 3
YSC		$10H_2O + CH_4 + 6FeS_2 = 2Fe_3O_4 + 12H_2S + CO_2$	Ref 3
YFT		$CH_4 + 2H_2O = CO_2 + 4H_2$	Ref 4
Y_C		$CO_2 + H_2 = CO + H_2O$	Refs 5,6
Y_{C_2}		$CH_4 + 3CO_2 = 4CO + 2H_2O$	Ref 5
YHSH (YSHC in Ref 6)		$Fe_3O_4 + 6H_2S = 2H_2 + 3FeS_2 + 4H_2O$	Refs 6,7
YHSC		$Fe_3O_4 + 6H_2S + CO_2 + 2H_2 = 3FeS_2 + 6H_2O + CH_4$	Ref 7

Ref 1 D'Amore et al (1983)
Ref 2 D'Amore and Gianelli (1984)
Ref 3 D'Amore et al (1982)
Ref 4 D'Amore and Celati (1983)
Ref 5 Bertrami et al (1985)
Ref 6 D'Amore et al (1987)
Ref 7 D'Amore and Truesdell (1985)

4 Whilst the liquid may boil and be transferred as steam along with the original vapour, there is no mass gain or loss during transport from the reservoir to the wellhead.

5 The gases do not re-equilibrate either chemically or between phases at any stage between the production site and the wellhead.

6 All fluids derived from production sites feeding a well have the same chemical composition.

A further condition of current methods is that the simple mixing model of Equation 1 is obeyed.

$$C_s = C_v.y + C_l.(1-y) \quad (1)$$

Our new model conditions only differ from those above in that condition 2 is ignored.

The distribution of gases between the reservoir liquid and vapour phases can be described by the partition coefficient:

$$B = C_v/C_l \quad (2)$$

Partition coefficients are temperature dependent and can generally be described by equations such as (see D'Amore and Truesdell, 1986 for a review):

$$\text{Log } B = a + bT \quad (3)$$

For gases normally analysed in steam from vapour-dominated geothermal systems, the order of affinity for the vapour phase (ie the order of decreasing distribution coefficient) is:

$$N_2 > H_2 > CH_4 > CO_2 > H_2S > NH_3$$

The partition coefficients of each of these gases are in excess of unity below the critical temperature, but decline as temperature increases. From Equations 1 and 2 it is evident that these gases favour the vapour phase and that as the steam fraction increases, so will the gas concentrations in produced steam samples given our model conditions.

Produced steam gas data sets which satisfy our model conditions display a distinctive distribution on graphs depicting mole ratio (A/B) against A, B or C concentration (see Figure 1, where A, B and C are gaseous species). Curves such as those in Figure 1 are generated through the use of Equations 1 and 2 for all gases, and by knowing the reservoiar temperature and vapour (or liquid) composition. The shape of the data curves is determined by the partition coefficients of the gases (and therefore the reservoir temperature) involved on the graph. The species which are more soluble in the liquid phase and have a lower partition coefficient are enriched in produced steam which has a lower steam fraction and, therefore, a lower gas concentration. Mole ratios tend to be more constant at higher steam fractions because most of the gas resides in the vapour phase; high dilution with vaporised liquid is usually required before the mole ratios in the

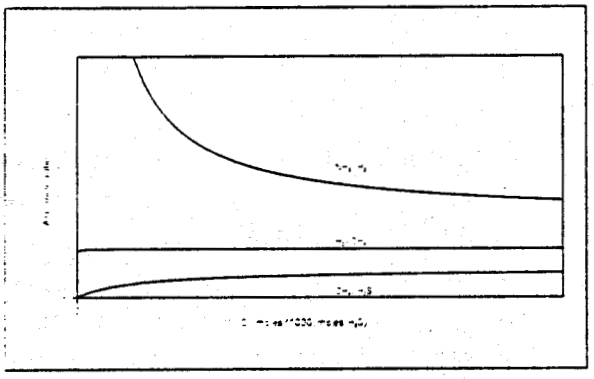

FIGURE 1 EXAMPLE MODEL DATA TRENDS. CURVES WERE GENERATED USING EQUATIONS 1 AND 2, GIVEN C_v AND B_i WITH y AS A VARIABLE

steam change significantly. Thus, the position of data along the curves is determined by the steam fraction of the produced steam sample. Data satisfying the model are also sensitive to the vapour (and liquid) phase gas concentrations and mole ratios which determine the position of the curves relative to the x and y axes, respectively.

CALCULATION OF STEAM FRACTIONS USING A MANUAL FITTING TECHNIQUE

Steam gas mole ratio data, which are evidently sensitive to the steam fraction of a produced steam sample and the vapour (or liquid) phase composition of the reservoir fluid, can be useful in two ways when displayed on graphs such as that in Figure 1. Firstly, they may be used to identify data which potentially satisfy the model conditions described above. For example, examination of data on such graphs will indicate which samples, and which gas analyses of those samples, follow the trends predicted by the model conditions.

Secondly, if the data appears to satisfy the model conditions, and an estimate of reservoir temperature is available, the observed data on the graphs can be 'fitted' by a mixing line such as those shown in Figure 1 after initial selection of the appropriate vapour (or liquid) phase composition. This allows estimation of the steam fraction of each of the samples used in the 'fit'. For example, fitting can be achieved by initially estimating the vapour mole ratios from the mole ratios in the highest gas samples (which will have the highest steam fraction). The vapour gas concentrations can then be selected and using Equations 1 and 2 for all gases involved, mixing lines can be generated and compared with the field data. Better visual fits of the mixing lines to the data can be achieved by judicious variation of the vapour composition. Equations 1 and 2 can then be used with the best-fit vapour composition to calculate one steam fraction for each gas analysed in each sample. These steam fractions can be used to determine the average steam fraction for the sample and errors on each. Evidently, the method also provides an estimate of the reservoir vapour (and liquid) composition.

This method is tedious and prone to bias so we have developed an automated minimisation technique for the calculation of steam fractions based on similar principles to those of the manual fitting method.

CALCULATION OF STEAM FRACTIONS USING A MINIMISATION TECHNIQUE

The minimisation technique also produces estimates of the steam fraction for each sample and the reservoir vapour composition, but does so through the solution of a set of simultaneous equations (one for each gas of every sample):

$$C_{sij} = C_{vi} \cdot y_j + C_{vi}\,(1-y_j)/B_i(T_j) + \varepsilon_{ij} \qquad (4)$$

All the samples need to be analysed for the same gases and the minimum necessary for the calculation is two gases.

It is also assumed that the temperatures of all samples (T_j) are the same and this constant temperature must be provided as an input to the algorithm.

If B values are large or y is close to 1, the equations reduce to:

$$C_{sij} = C_{vi} \cdot y_j + \varepsilon_{ij} \qquad (5)$$

In such cases it will be impossible to estimate the values of C_{vi} or y_j since any solution (y_j, C_{vi}) will be indistinguishable from the solution (y_j/R, $C_{vi}.R$) where R is any constant. This scaling effect is the major source of error in fitting Equation 4. Our model pays special attention to this scaling error.

Let

$$s = \sum_{j=1}^{Ns} \sum_{i=1}^{Ng} \frac{(C_{sij} - C_{vi} \cdot y_j - C_{vi}(1-y_j)/B_i)^2}{\sigma_{ij}^2} \qquad (6)$$

σ_{ij} are estimates of sampling/analytical error and would typically be found from the analysis of duplicate samples. Partial differentiation with respect to C_{vi} and y_j leads to:

$$\frac{ds}{dy_j} = -2 \sum_{i=1}^{Ng} \frac{(C_{sij} - C_{vi} \cdot y_j - C_{vi}(1-y_j)/B_i)}{\sigma_{ij}^2} (C_{vi} - C_{vi}/B_i) \qquad (7)$$

and

$$\frac{ds}{dC_{vi}} = -2 \sum_{j=1}^{Ns} \frac{(C_{sij} - C_{vi} \cdot y_j - C_{vi}(1-y_j)/B_i)}{\sigma_{ij}^2} \left(y_j + \frac{1-y_j}{B_i}\right) \quad (8)$$

For any set of y_j, C_{vi} that minimise S, we must have $dS/dy_j = 0$ for all j and $dS/dC_{vi} = 0$ for all i. Given estimates of the steam fractions y_j^{K-1}, we can use Equation 7 to derive new estimates of the vapour concentrations C_{vi}^K. Similarly we can use the C_{vi}^K in Equation 8 to derive new steam fraction estimates y_j^K. We have expanded Equations 7 and 8 into explicit equations for y_j and C_{vi}, these are Equations 9 and 10.

$$y_j^K = \frac{\sum_i (C_{sij} - C_{vi}^K/B_i)/\sigma_{ij}^2}{\sum_i (C_{vi}^K - C_{vi}^K/B_i)^2/\sigma_{ij}^2} \quad (9)$$

$$C_{vi}^K = \frac{\sum_j C_{sij} \left(y_j^{K-1} + \frac{1-y_j^{K-1}}{B_i}\right)/\sigma_{ij}^2}{\sum_j \left(y_j^{K-1} + \frac{1-y_j^{K-1}}{B_i}\right)^2/\sigma_{ij}^2} \quad (10)$$

The calculation follows the following procedure:

a Set all initial estimates $y_j 0$ to 0.5 for all j. Set the iteration count k to 0.

b Increment k.

c Calculate C_{vi}^K from Equation 9.

d Calculate y_j^K from Equation 10.

e If the relative change in any parameter C_{vi} or y_j is greater than a given tolerance (eg 1%) go back to step b.

At this point we have derived estimates y_j^K and C_{vi}^K, however because of the ill conditioned nature of the equations (4), we now rescale the y_j^K by a common factor R such that $S(y_j/R, C_{vi}^K * R)$ is a minimum. If the computed factor R is not close to 1 (ie within 0.005), we now go back to step b. Otherwise the algorithm has converged, typically this rescaling occurs between two and five times before convergence.

A number of numerical test cases were examined to evaluate the performance of the method (Table 2). Dummy sample analyses were generated using Equation 11. The sampling/analytical errors were set to 10% RSD for each gas. The y_j were randomly selected from a uniform distribution. The vapour concentration was as shown in Table 3. Different sets of samples were generated for each test case.

$$C_{sij} = \left(C_{vi} + e_{ij}\right) \left(y_j + \frac{(1-y_j)}{B_i}\right) \quad (11)$$

TABLE 2 TEST CASES USED IN MODELLING

	No of Samples	Y range	Temperature (°C)	Gases Used	Mean Error	SD	Mean % Error	SD of % Error
1	50	0-1	240	All	0.02	0.07	5	14
2	50	0-1	240	NH_3, H_2	-0.02	0.07	-5	17
3	50	0-1	240	H_2, CH_4	-0.06	0.33	-12	57
4	50	0-1	220	All	-0.10	0.08	-20	10
5	50	0-1	260	All	+0.12	0.11	26	15
6	10	0-1	240	All	0.02	0.16	10	34
7	10	0-1	240	NH_3, H_2	0.06	0.17	18	43
8	10	0-1	240	H_2, CH_4	No convergence			
9	25	0-0.2	240	All	0.01	0.02	14	23
10	25	0-0.2	240	NH_3, H_2	0.03	0.04	44	53
11	25	0-0.2	240	H_2, CH_4	No convergence			
12	25	0.8-1.0	240	All	0.65	0.41	-11	55
13	25	0.8-1.0	240	NH_3, H_2	No convergence			
14	25	0.8-1.0	240	H_2, CH_4	No convergence			
15	10	0-0.2	240	All	0.00	0.02	7	24
16	10	0-0.2	240	NH_3, H_2	0.05	0.20		
17	10	0-0.2	240	H_2, CH_4	No convergence			

TABLE 3 RESERVOIR VAPOUR COMPOSITION*

Moles/1000 moles H_2O	
CO_2	3.6469
H_2S	0.3234
NH_3	0.1756
N_2	0.1019
CH_4	0.9303
H_2	1.0363

* Calculated from Truesdell et al (1987) (Central and West Geysers medium sample, Table 1) assuming y=0.5

Six gases were used in the calculations (CO_2, H_2S, NH_3, CH_4, H_2) and partition coefficients were determined from the equations of D'Amore and Truesdell (1986). The temperature was generally set to 240°C except in cases 4 and 5. For each test case the percentage error between the original and estimated steam fractions have been calculated (Table 2)*.

RESULTS

The test cases produced the following results.

1 The principal errors are related to the scaling of the y values.

2 As indicated earlier, the method fails where either steam fractions or partition coefficients are high (Figure 3).

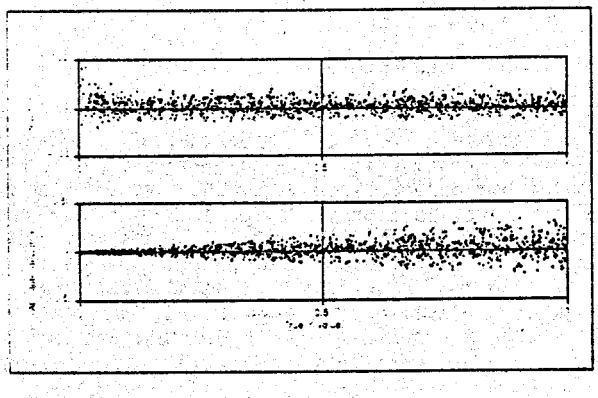

FIGURE 2 TEST CASE 1 : COMPARISON OF THE PERCENTAGE AND ABSOLUTE ERRORS BETWEEN THE TRUE AND CALCULATED STEAM FRACTIONS

* We have only quoted percentage errors for samples with steam fractions greater than 0.01, and absolute errors for all samples. This is because the percentage errors of lower steam fraction samples distort what are relatively constant values in higher steam fraction samples (Figure 2).

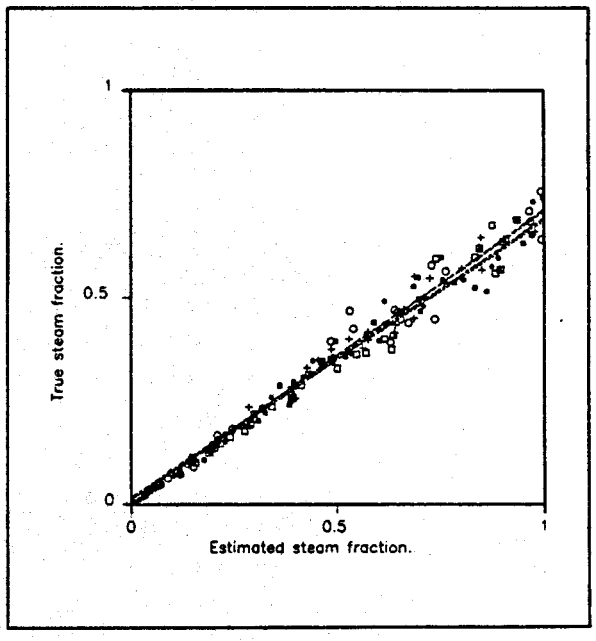

FIGURE 3 TEST CASE 3 : RELATION BETWEEN THE TRUE AND CALCULATED STEAM FRACTIONS. DIFFERENT SYMBOLS REPRESENT DIFFERENT DATA SETS. DASHED LINES ARE 'BEST-FIT' LINES

3 Reasonable results are achieved when a) at least one gas used in the calculation has a low partition coefficient (eg NH_3); b) the spread in sample gas concentrations (and steam fractions) is large and c) low steam fraction samples are present (eg Figure 4). In test case 1 85% of the calculated steam fractions are within 20% of the input values (eg Figure 2).

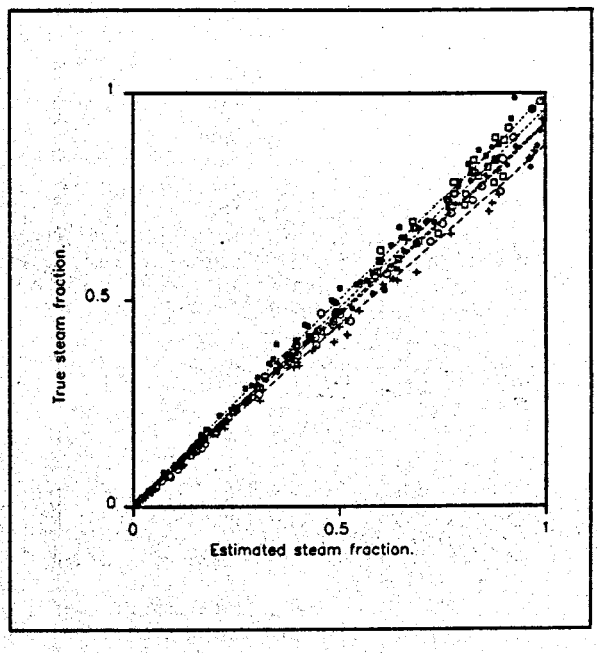

FIGURE 4 TEST CASE 1 : RELATION BETWEEN THE TRUE AND CALCULATED STEAM FRACTIONS. DIFFERENT SYMBOLS REPRESENT DIFFERENT DATA SETS. DASHED LINES ARE 'BEST-FIT' LINES

4 The accuracy and precision of the method increases with the number of samples.

5 Where the input temperature is over-estimated so are the steam fractions. Steam fractions are correspondingly under-estimated when the input temperature is lower than that of the reservoir.

We examined the test case mole ratio data and the corresponding vapour liquid mixing lines generated via the calculated vapour composition and Equations 1 and 2. In each case the fit of the mixing line to the mole ratio data was as good as that expected from hand-fitting (Figure 5). Indeed the limitations of the minimisation method and the ideal conditions for its use are those anticipated when using the manual fitting method. Mole ratio data evidently provides an independent check on the reliability of the steam fractions calculated by the minimisation technique.

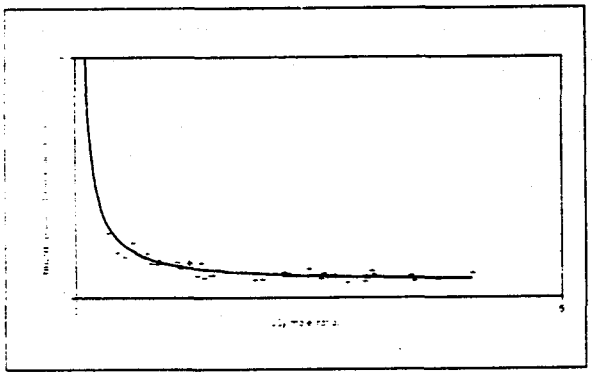

FIGURE 5 EXAMPLE OF THE RELATION BETWEEN THE MINIMISATION DERIVED VAPOUR-LIQUID MIXING LINE AND A TEST DATA SET

DISCUSSION

The principal advantages of the above empirical methods compared with existing steam fraction calculation techniques are a) no information concerning the reservoir reactions are required, and b) the data upon which the new methods are most likely to be successful can be readily identified. It should be noted however, that a good correlation between the mixing line and sample data only indicates that the data could be produced under the conditions defined by the model. We are currently investigating the processes and conditions which may mimic the mole ratio trends produced by the steam fraction model, but actually produce erroneous steam fraction values.

At this stage, the disadvantages of the technique might be perceived as being the relatively stringent data requirements, the accuracy and precision of the calculated steam fractions and the need to know the reservoir temperature. Although few localities produce the type of data required by the calculation method, it may be appplied to the Unit 15 area at The Geysers (McCartney and Haizlip, this volume; McCartney and Haizlip, 1989).

The precisions quoted earlier include the sampling/analytical error associated with the data, and as such may be acceptable for certain applications. On the other hand, the calculated empirical steam fractions could be compared with those calculated by existing methods to help determine which reactions are indeed controlling gas compositions in the reservoir fluid. More precise steam fractions could then be calculated using existing methods incorporating these reactions. It is hoped that the accuracy and precision may also be improved by refinement of our current numerical technique.

More accurate steam fractions depend on knowing the reservoir temperature at which the reservoir vapour and liquid equilibrated. Whilst endeavours should be made to use other information to correctly estimate the reservoir temperature, it is evident that even errors in the calculated steam fractions of +/- 20°C do not significantly affect the estimates of the steam fractions when the overall accuracy and precision of the method are considered.

CONCLUSIONS

We have presented two empirical methods for calculating steam fractions of steam samples from vapour dominated systems. The methods rely on the assumption that the steam is being produced from a single fluid type, however assumptions concerning reaction equilibria are not required. Steam gas mole ratio data may be used to identify samples to which the methods may be applied, and to check the accuracy of the calculated steam fractions.

ACKNOWLEDGEMENTS

We thank GeoScience Limited, a wholly owned subsidiary of Geothermal Resources International, Inc, for permission to publish this paper. We are indebted to J Haizlip for her discussion and support of our work and to Drs A S Batchelor and R H Curtis who provided helpful reviews of our paper. We are grateful for the help in producing the paper provided by P Davies and J Pearson. It was the work of Drs F D'Amore and A H Truesdell who initiated our interest in steam fraction calculations.

NOMENCLATURE

a,b	Constants in Equation 3
B	Gas partition coefficient
C_l	Concentration of gas in reservoir liquid (moles/1000 moles H_2O)
C_s	Concentration of gas in produced steam (moles/1000 moles H_2O)

C_v	Concentration of gas in reservoir vapour (moles/1000 moles H_2O)
E_{ij}	Sampling/analytical error in sample j for gas i
i	Gas identifier
j	Sample identifier
K	Iteration count in numerical scheme
N_g	Number of gases analysed
N_s	Number of samples
T	Reservoir temperature estimate (°C)
y	Steam fraction
σ_{ij}	Estimate of sampling/analytical error
e_{ij}	Gaussian random variable

REFERENCES

Arnorsson S (1985). Gas pressures in geothermal systems. Chem Geol, vol 49, pp 319-328.

Bertrami R, Cioni R, Corazza E, D'Amore F and Marini L (1985). Carbon monoxide in geothermal gases - Reservoir temperature calculations at Larderello (Italy). Geotherm Res Counc Trans, vol 9, pt 1, pp 299-303.

D'Amore F and Celati R (1983). Methodology for calculating steam quality in geothermal reservoirs. Geothermics, vol 12, pp 129-140.

D'Amore F, Celati R and Calore C (1982). Fluid geochemistry applications in reservoir engineering (vapour-dominated systems). Proc 9th Workshop on Geothermal Reservoir Engineering, Stanford University, California. pp 295-307.

D'Amore F, Celati R, and Calore C (1983). Hypothesis of possible equilibria between N_2 and other gases at Larderello and Cerro Prieto. Proc 9th Workshop on Geothermal Reservoir Engineering, Stanford University, California, pp 247-252.

D'Amore F, Fancelli R, Saracco L and Truesdell A H (1987). Gas geothermometry based on CO content : Application in Italian geothermal fields. Proc 12th Workshop on Geothermal Reservoir Engineering, Stanford University, California, pp 221-229.

D'Amore F and Gianelli G (1984) Mineral assemblages and oxygen and sulphur fugacities in natural water-rock interaction processes. Geochim Cosmochim Acta, vol 48, pp 847-857.

D'Amore F and Pruess K (1986). Correlations between steam saturation fluid composition and well decline in vapour-dominated reservoirs. Geothermics, vol 15, pp 167-183.

D'Amore F and Truesdell A H (1985). Calculation of geotehrmal reservoir temperatures and steam fractions from gas compositions. Geotherm Res Counc Trans, vol 9, pp 305-310.

D'Amore F and Truesdell A H (1986). A review of solubilities and equilibrium constants for gaseous species of geothermal interest. CNR report, 33 pp.

Giggenbach W F (1980). Geothermal gas equilibria. Geochim Cosmochim Acta, vol 44, pp 2021-2032.

McCartney R A and Haizlip J R (1989). Anomalous behaviour of hydrogen in steam from vapour-dominated geothermal systems. This volume.

McCartney R A and Haizlip J R (1989). Gas pressures at The Geysers geothermal field, California : Comparison with liquid-dominated systems and implications for boiling processes. Proc 6th Symposium in Water-Rock Interactions, Malvern, England.

Truesdell A H, Haizlip J R, Box W T and D'Amore F (1987). Fieldwide chemical and isotopic gradients in steam from The Geysers. Proc 12th Workshop on Geothermal Reservoir Engineering, Stanford University, California, pp 241-246.

PROCEEDINGS, Fourteenth Workshop on Geothermal Reservoir Engineering
Stanford University, Stanford, California, January 24-26, 1989
SGP-TR-122

THE HYDROGEOLOGIC-GEOCHEMICAL MODEL OF CERRO PRIETO REVISITED

M. J. Lippmann, A. H. Truesdell,† A. Mañón M.,‡ and S. E. Halfman,**

*Lawrence Berkeley Laboratory
Berkeley, CA 94720

†U.S. Geological Survey
Menlo Park, CA 94025

‡Comisión Federal de Electricidad,
Mexicali, BC, Mexico

ABSTRACT

As the exploitation of the Cerro Prieto, Mexico, geothermal field continues, there is increasing evidence that the hydrogeologic model developed by Halfman et al. (1984, 1986) presents the basic features controlling the movement of geothermal fluids in the system. At the present time the total installed capacity at Cerro Prieto is 620 MWe requiring the production of more than 10,500 tonnes/hr of a brine-steam mixture. This significant rate of fluid production has resulted in changes in reservoir thermodynamic conditions and in the chemistry of the produced fluids.

After reviewing the hydrogeologic-geochemical model of Cerro Prieto, some of the changes observed in the field due to its exploitation are discussed and interpreted on the basis of the model.

INTRODUCTION

The Cerro Prieto field has been extensively studied by the Comisión Federal de Electricidad (CFE) of Mexico and by various U.S. groups participating in cooperative agreements between CFE and the U.S. Department of Energy (DOE).

The exploration and development of the Cerro Prieto field and the early changes resulting from its exploitation have been discussed in numerous papers and reports; a recent summary is given by Lippmann and Mañón (1987). The purpose of this paper is to review generally accepted hydrogeologic and geochemical models developed for the Cerro Prieto geothermal system and illustrate how these models can explain the changes being observed as the exploitation of the field continues.

NATURAL STATE HYDROGEOLOGICAL MODEL

The hydrogeological model of Cerro Prieto that best describes the movement of geothermal fluids in the system under natural state conditions is that of Halfman et al. (1984, 1986). The model developed on the basis of electric, lithologic and temperature well logs, as well as on information on well completion, demonstrates the importance of lithology and faults in controlling fluid circulation.

The Halfman et al. natural state model shows that in the Cerro Prieto system there is circulation of geothermal fluids generally from east to west. Hot (about 350°C) fluids enter the system from the east-southeast, and are discharged in the area of surface manifestations located west of the wellfield (Figs. 1 and 2). The geothermal fluids seem to ascend from depth through the SE-dipping, normal fault H. (The results of recent isotope and self-potential surveys have given further evidences of fluid movement through this fault; Stallard, et al., 1987; Goldstein et al., this volume).

As the hot fluids flow up fault H, they tend to move laterally into the more permeable layers (Figs. 2 and 3). An unknown amount recharges the deepest reservoir identified so far (gamma reservoir); it corresponds to layer K found below 3300 m depth (Fig. 3). The bulk of the hot fluids flow westward into layer Z (beta reservoir) following the general east-west gradient prevalent in the system; only a smaller fraction seem to penetrate layer Z east of the fault (Fig. 3).

The westward movement of the geothermal fluids has an upward component since it follows the bottom of the less permeable shale layer O, which is dipping toward the northeast. In the region of well M-10A (Fig. 2) a significant part of the fluids manages to ascend because of the absence of a shale caprock; this region has been called the "sandy gap". The rest of the fluids move into the western continuation of the beta reservoir (below 1600 m depth in the western area of the field).

The movement of fluids through the sandy gap was reflected by the self-potential anomaly observed in 1977 over the Cerro Prieto field (Goldstein et al., this volume). As the hot fluids ascend through the gap, boiling occurs. The vertical flow of the geothermal fluids is eventually stopped at about 1000 m depth by the presence of low permeability sandy materials sealed by mineral precipitation (Lippmann and Bodvarsson, 1983). At this point, the fluids continue to flow westward through a shallower permeable layer (alpha reservoir), between about 1000 and 1500 m depth. The alpha reservoir is restricted to the western region of the field, i.e., west of the railroad tracks (Fig. 1). It generally corresponds to the hatched region shown in the west-central part of Figure 2. Under natural state conditions the westward movement of hot fluids in

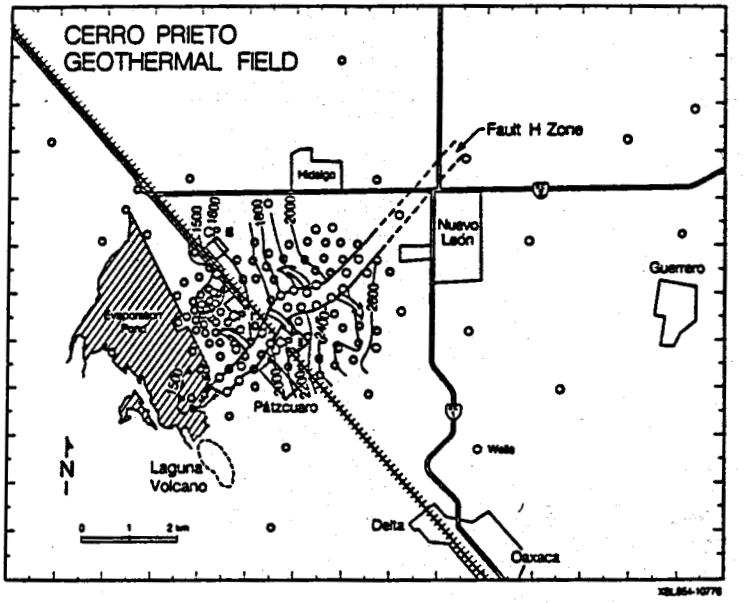

Figure 1. Cerro Prieto. Depth (in meters) to the top of the Sand Unit Z (see Fig. 2). The arrows indicate the direction of geothermal fluid flow away from fault H. The fault zone is shown at the beta reservoir level (from Halfman et al., 1986)

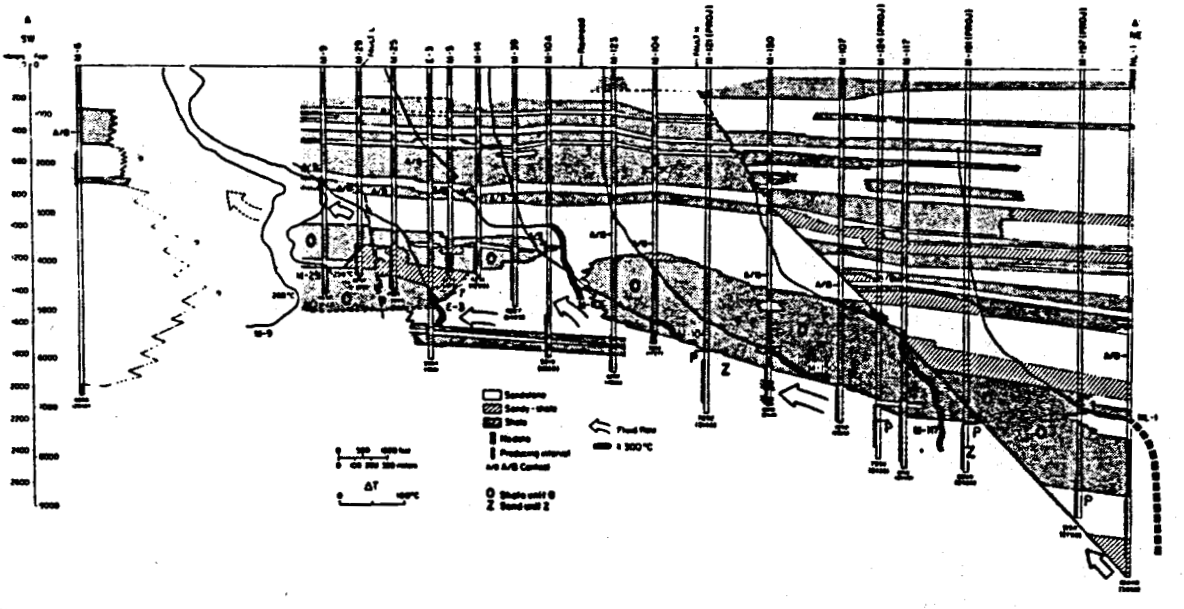

Figure 2. Southwest-northeast geologic cross section of the Cerro Prieto field showing schematically the lithology and the flow of geothermal fluids (from Halfman et al., 1984)

the alpha reservoir continues somewhat west of the normal fault L. However, most of the fluids flow up this fault (Fig. 2), reaching a shallower aquifer where mixing occurs with colder ground waters. Some of the hotter fluids leak to the surface west of the wellfield.

The important control of fault H on the recharge of geothermal fluids to the Cerro Prieto system is made evident by the high production rates being observed in wells with open intervals within, or near the fault zone. As an example, Figure 4 illustrates the excellent production characteristics of well M-147; the initial enthalpies of the

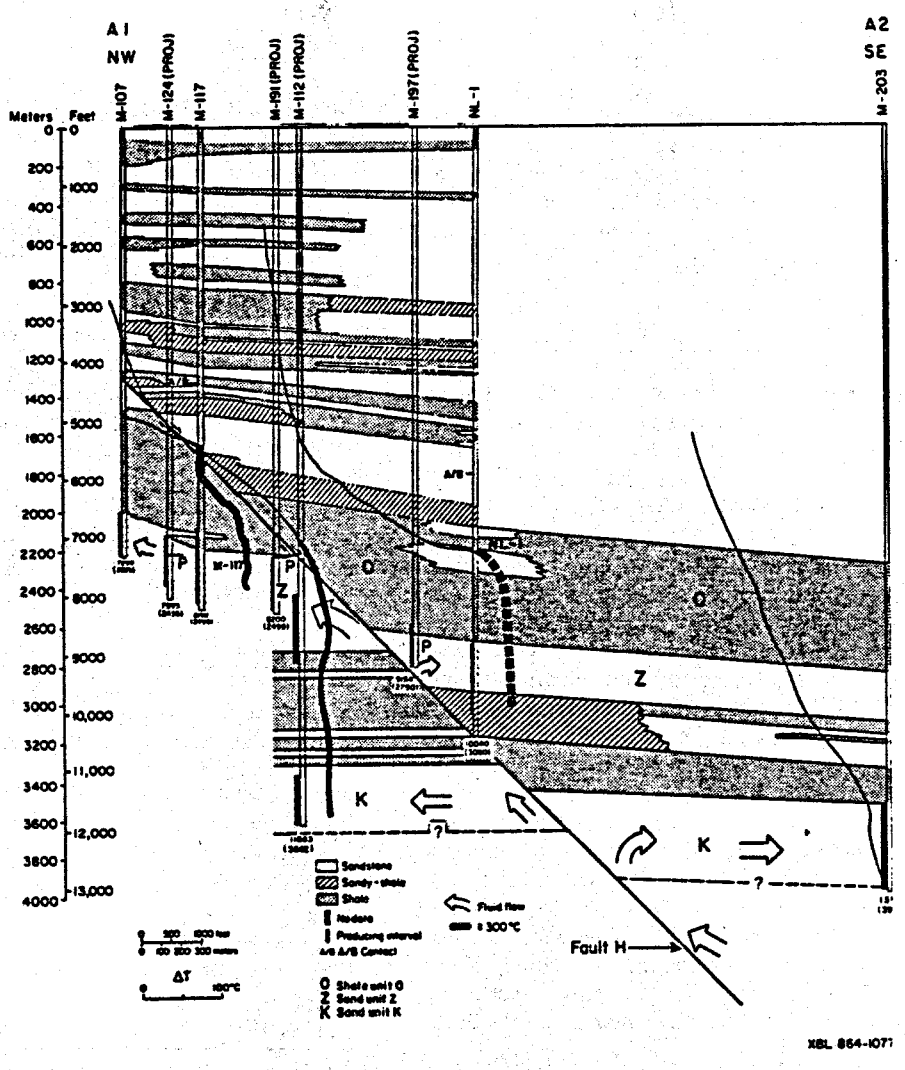

Figure 3. Northwest-southeast cross section of the eastern Cerro Prieto wellfield showing geothermal fluid flow pattern (after Halfman et al., 1986)

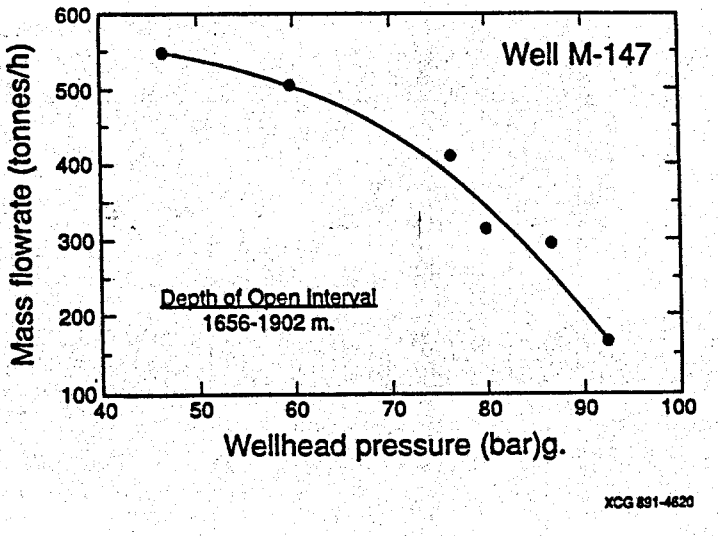

Figure 4. Characteristic curve for well M-147 (after Mercado and Bermejo, 1987).

produced fluids exceeded 2000 kJ/kg. The high production rates, enthalpies and wellhead pressures recorded in M-147 have led Mercado and Bermejo (1987) to postulate that it is fed by a fracture connected to a steam chamber located below the producing reservoir. We do not necessarily agree with their hypothesis of a deep steam chamber; we consider that the behavior of M-147 is related to its proximity to fault H through which hot compressed liquid recharges the system.

NATURAL STATE GEOCHEMICAL MODEL

The original temperatures and sources of the Cerro Prieto field reservoir fluids, as well as the processes active in the system mainly after the start of fluid production, have been discussed in several papers and summarized by Truesdell et al. (1984b) and Truesdell (1988).

Initial hydrogeologic models of the Cerro Prieto field were mainly developed on the basis of geochemical information (e.g., Mercado, 1976). Later models, like the one discussed above, had to show the "subsurface plumbing" inferred from the interpretation of the chemistry of the initially produced fluids. Thus, there is general agreement between the natural state circulation models developed for Cerro Prieto by geologists, reservoir engineers and geochemists.

Geochemical studies established the origin of the geothermal brines as mixtures of Colorado River water and marine hypersaline brine contained in the deltaic sediments of the Mexicali Valley (Fig. 5). These studies also showed that N_2 and Ar originate from the atmosphere, CO_2, H_2S, HC, ^4He and NH_3 from thermal metamorphism of sediments, and a minor amount of ^3He from magmatic sources.

EXPLOITATION HISTORY OF CERRO PRIETO

Before the initial 37.5 MWe unit began operating in April 1973, long-term production tests of wells completed in the alpha reservoir had been carried out. Very little data are available for this early period. However, starting in 1973 careful records have been kept on the rate of production and on the chemistry of the produced fluids.

The present installed electrical generating capacity at Cerro Prieto is 620 MWe. Initially the total capacity at the field grew slowly, but in 1986-87 it expanded substantially, as indicated in Table 1. Accordingly, the rate of fluid production has significantly increased (Fig. 6). To date only small-scale reinjection tests have been carried out; all the separated brine is being disposed into a evaporation pond located west of the wellfield (Fig. 1). Recently, the pond has been expanded to cover an area of about 16 km^2 (Mercado and Bermejo, 1988).

Table 1

Installed electrical generating capacity at Cerro Prieto

Date	Total installed capacity (MWe)
April 1973	37.5
October 1973	75
January 1979	112.5
March 1979	150
November 1981	180
January 1986	400
September 1986	510
June 1987	620

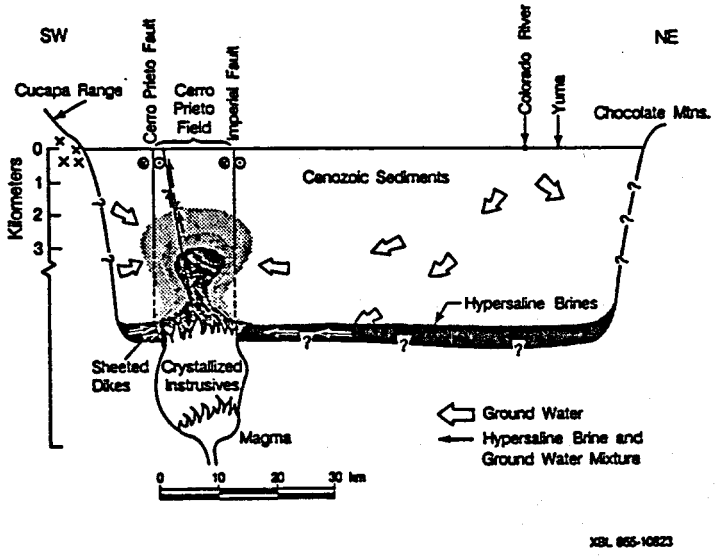

Figure 5. Schematic diagram of the geology and fluid flow across the Mexicali Valley (from Halfman et al., 1986).

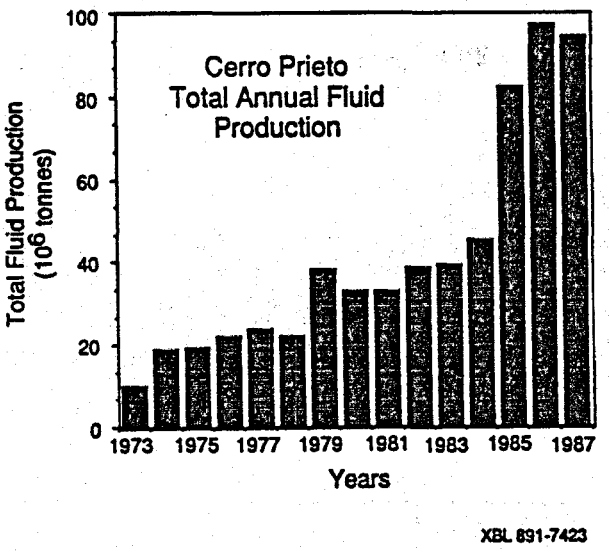

Figure 6. Total annual fluid production at Cerro Prieto.

Due to the large fluid extraction rate, significant changes have been observed in the reservoirs and production wells. The bulk of available information on reservoir changes is on the alpha reservoir, the first one to be exploited. Even though fluid production from the beta reservoir began in the late 1970s, only a few studies have dealt with the changes occurring in this reservoir. There are no data on the evolution, if any, of the gamma reservoir; only a few wells (e.g., M-112) are producing from it.

For administrative purposes the present wellfield has been divided into three areas: CPI (Cerro Prieto I), west of the railroad tracks; CPII, the southeastern area; and CPIII, the northeastern area.

Response of the alpha reservoir to production

As indicated earlier, the alpha reservoir is restricted to the region west of the railroad tracks (CPI). Between 1973 and 1980 most of the fluids produced at Cerro Prieto came from this, the shallowest (1000-1500m depth), hot water aquifer. Exploitation of the alpha reservoir continues but on a smaller scale as a reduced production enthalpy (i.e., steam/water ratio) make some of the wells uneconomical. These are being replaced by new wells completed in the deeper beta reservoir ("E-wells").

As a consequence of production, the pressure in the alpha reservoir has dropped, resulting in localized boiling around some of the wells and an increased influx of colder, less saline water (Grant et al., 1984; Truesdell et al.; 1984a). Large excesses in enthalpy temperatures and deficiencies in silica temperatures compared to Na-K-Ca temperatures indicate initial boiling around some wells (Janik et al., 1982; Nehring and D'Amore, 1984; Truesdell et al., 1984a; 1989). With time, these boiling zones tend to expand and stabilize; the history of well M-31 illustrates such behavior (Fig. 7). This type of well response can be simulated by a radially symmetric system showing a constant pressure boundary at a given distance from the well (Fig. 8). Boiling has deposited large amounts of quartz and calcite in the near-well region resulting in flow declines, sometimes leading to the loss of wells (Truesdell et al., 1984a)

As the alpha reservoir is bounded below by low permeability rocks, and above and to the west by an interface of colder waters (Fig. 9), pressure drawdown results in cold recharge from the west and/or through fault L (Fig. 2) that breaches the overlying shale layer. Once in the reservoir, the cooler waters tend to sweep the hot waters as they move toward the producing wells (Grant et al., 1984; Truesdell and Lippmann, 1986). Because of their location near the natural recharge areas or in less exploited parts of the field, some of the alpha wells never developed a boiling zone (e.g., M-42; Grant et al., 1984).

Fault L, which under natural state conditions allowed the upward leakage of geothermal fluids, now acts as conduit to the downward flow of colder groundwater into the reservoir. The evolution of the chemistry of the fluids produced by wells completed in the alpha reservoir clearly indicates the importance of this fault in the cold-water recharge of this aquifer (Truesdell and Lippmann, 1986; Stallard et al, 1987).

Response of the beta reservoir to production

The beta reservoir is officially considered to have been discovered in 1974 in the eastern part of the field with the drilling of well M-53. It was not until later studies by Halfman et al. (1984) that it became evident that some earlier wells in the southern region of CPI had partially penetrated this reservoir (e.g., M-51 completed in 1972). The beta reservoir extends over most of the Cerro Prieto field. It is found below about 1600 m depth, deepening towards the east (layer Z in Figs. 1 and 2).

Even though fluid production from this reservoir began in the late 1970s in the southwestern (i.e., southern CPI) and southeastern (i.e., CPII) regions of the field, it increased markedly with the completion of the deeper E-wells in CPI (started in 1980) and more recently with the start up of the new CPII and CPIII power plants (Table 1).

Only a small number of studies have been made on the response of the beta reservoir to production. However, a general picture of its behavior can be obtained from the available wellhead data. Because of its significant depth, and with its top and bottom sealed boundaries (Figs. 2 and 3), the beta reservoir has restricted natural fluid recharge. This is especially true in the eastern areas which presently are being heavily exploited. In the CPI region lateral influx from the west seems to be readily available; a similar situation could exist along the southeastern edge of the field.

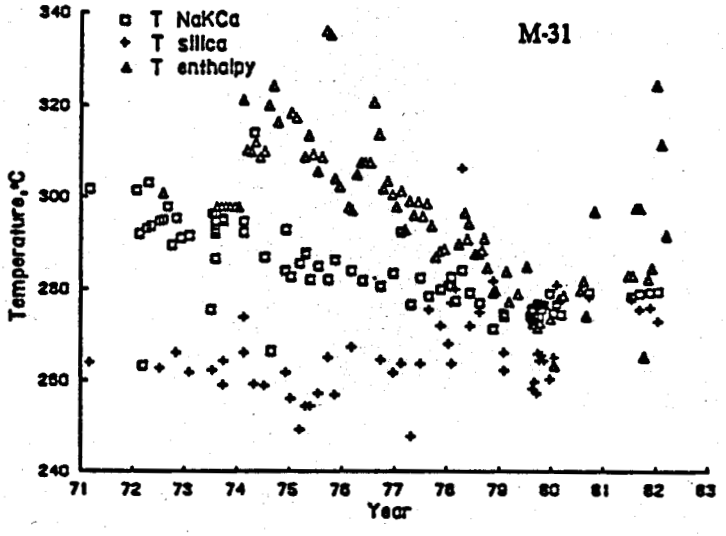

Figure 7. Chemical and enthalpy temperature history of well M-31. (from Truesdell et al, 1984a)

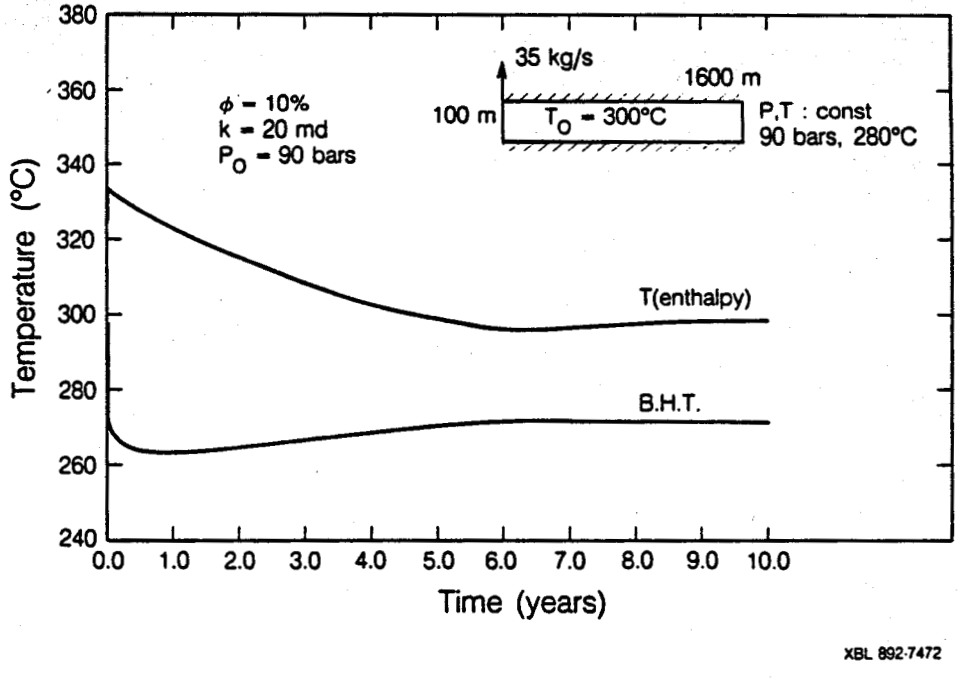

Figure 8. Numerically simulated enthalpy and bottomhole temperatures (B.H.T.) for a radially symmetric system with a constant pressure and temperature boundary.

Most beta wells show high production rates and temperatures initially. The enthalpy of the produced fluids tends to increase immediately due to reservoir boiling (indicated by excess steam). Evidences of boiling in the beta reservoir have been reported by Semprini and Kruger (1984), Stallard et al. (1987), de León Vivar (1988), and Truesdell et al. (1989).

In many wells of the eastern region (e.g., M-147 discussed above) a decrease in flowrate has been observed, that has been generally attributed to casing problems, but may be also due to mineral deposition in and around the well because of reservoir boiling, especially in CPIII (a more careful analysis of downhole data is needed). On the other hand, the precipitation of silica in the wellbores and/or wellhead separators is a significant problem in the southeastern region of the field (CPII). This indicates that in this region reservoir boiling is not yet extensive.

In some E-wells of CPI a decrease of fluid chloride content has been observed that could be explained by the advance of cold water entering the beta reservoir from

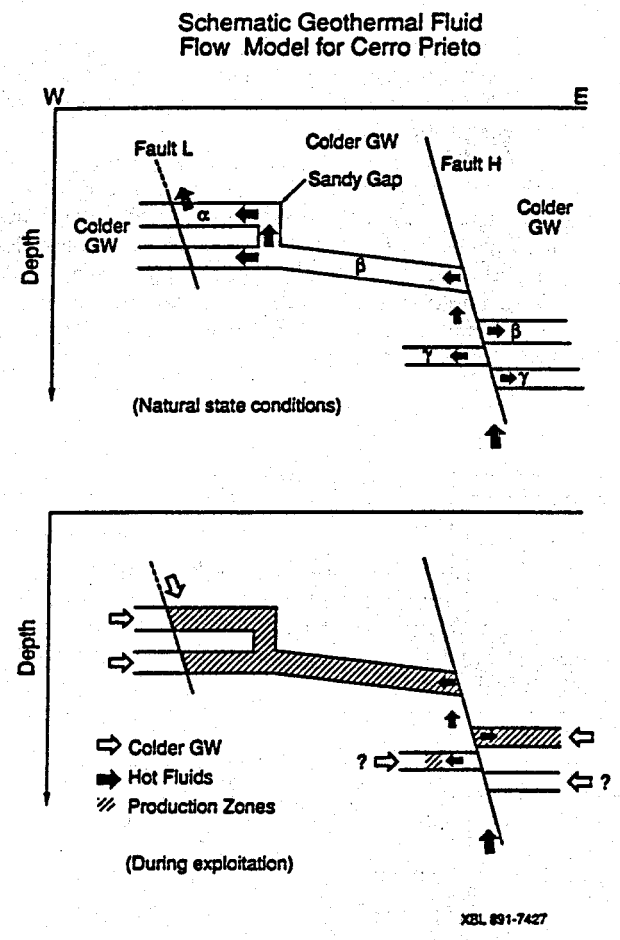

Figure 9. Schematic fluid flow model for Cerro Prieto.

the western edge of the field (A cold water sweep similar to the one occurring in the alpha reservoir; Truesdell et al., 1989).

There is a remarkable spatial correlation between the boiling zone in the beta reservoir and the location of fault H. Semprini and Kruger (1984) and Stallard et al.(1987) have shown boiling zones that generally agree with the position of this fault. More striking is the correspondence between de León Vivar's (1988) distribution of wells showing reservoir boiling and Halfman et al.'s (1986) trace of the fault H at reservoir level (Fig. 10). There is clear evidence that the boiling beta wells are located near the fault zone or in the upthrown block of fault H. A simplified model of the beta reservoir simulating its natural recharge and response to production (Fig. 11), shows that because of relative elevation, location of producing areas, and restricted recharge, the boiling in this reservoir tends to start in the upthrown block of the fault.

Figure 11a shows a schematic two-dimensional (x - z plane), one-meter thick (y axis) numerical simulation model of the Cerro Prieto beta reservoir system. Zone 1 correspond approximately to CPI and CPII, and Zone 2 to CPIII. Figure 11b describes the assumed conditions that were used to compute the pre-exploitation mass flow and temperature distributions. No heat and mass transfer was allowed between the reservoirs and surrounding formations. LBL's MULKOM code (Pruess, 1988) was used in the calculations.

For these particular conditions, 87.5 % of the recharged water flows into the upthrown Zone 1; only 12.5% into Zone 2. The computed temperatures are quite uniform

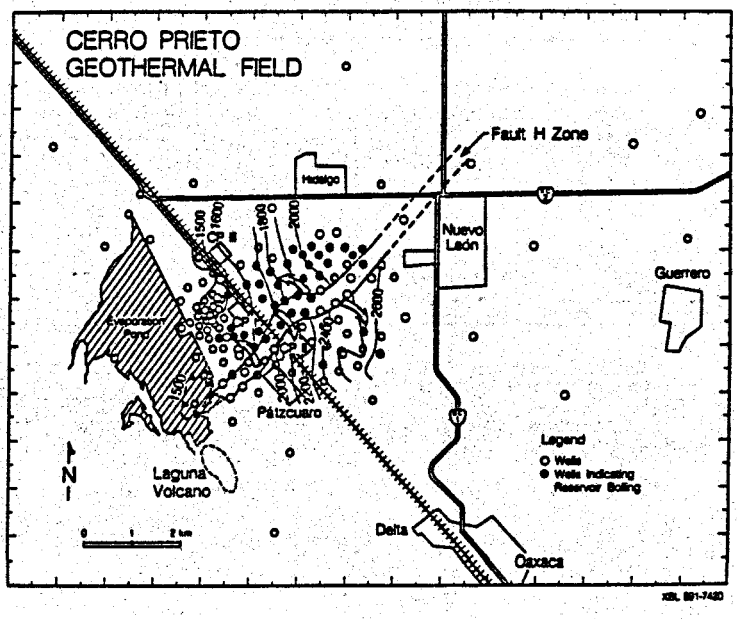

Figure 10. Location of wells indicating reservoir boiling (de León Vivar, 1988) and of the fault H zone (see Fig. 1).

under these "natural state" conditions, varying between 342 and 350 °C; no boiling is observed.

Figure 11c describes the exploitation conditions that were assumed for the model. The system is produced at a total rate 40 times the natural recharge, while the hot (350 °C) recharge is assumed to be 10 times the natural value because of pressure drawdown. Figure 11d shows the temperature distribution and location of the boiling zone in the system after three years of production. The effects of lateral cold-water recharge are reflected by the isotherms; thermal fronts are advancing toward the producing areas, but have not yet reached them. The boiling is restricted to the upthrown block near the fault since this particular region is isolated from the recharge areas.

The model shows that the boiling zone collapses with time because of increasing system recharge and cooling. Note that at 3 years (Fig. 11d) the total recharge slightly exceeds total production.

Even though models like the one described in Figures 9 and 11 are very schematic, they can reproduce some of the behavior of the beta reservoir. These simple models may be used to outline a production/injection program at Cerro Prieto that could reduce the boiling and induced cold water recharge, and the related reservoir plugging and cooling.

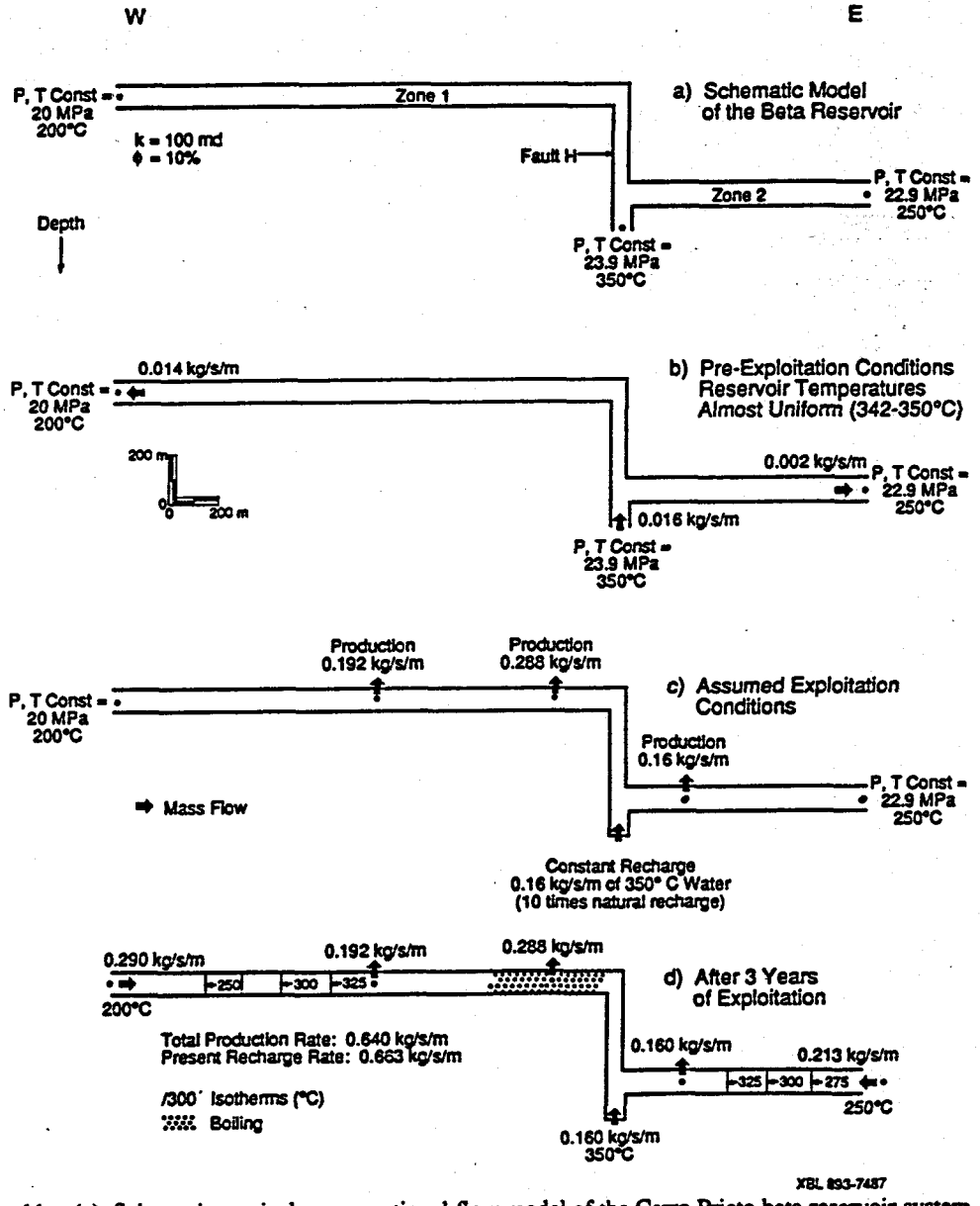

Figure 11. (a) Schematic vertical cross-sectional flow model of the Cerro Prieto beta reservoir system.
(b) Pre-exploitation (initial) flow and temperature conditions.
(c) Assumed exploitation regime.
(d) Temperature distribution, fluid flows and location of boiling zone after 3 years of production.

CONCLUSIONS

We find a surprisingly clear control of fluid circulation in the Cerro Prieto field by faults and lithology. The simple geothermal fluid flow model given in Figure 9, describes in very general terms the natural state circulation of hot fluids in the system, as well as the recharge that results from pressure drawdown due to exploitation.

It was shown that simple models can explain the behavior of individual wells and large regions of the Cerro Prieto geothermal system. Development of a reservoir management plan for this highly-productive field requires more detailed numerical simulations. This effort is being carried out in parallel by CFE and LBL scientists who are studying the system using three-dimensional numerical models that are quite sophisticated. The basic understanding of geothermal field processes obtained here from analyzing simplified models is providing valuable guidance in the development of more detailed numerical simulation models of Cerro Prieto.

ACKNOWLEDGEMENTS

We wish to thank Norman Goldstein and Karsten Pruess of LBL for discussing and reviewing the paper. Special thanks are due to our colleagues of the Superintendencia General de Estudios of the Coordinadora Ejecutiva de Cerro Prieto of CFE for providing the field data used in this study. Finally, we want to acknowledge the assistance of Diana Parks in producing the paper. This work was supported by the Assistant Secretary for Conservation and Renewable Energy, Office of Renewable Technologies, Division of Geothermal Energy of the U.S. Department of Energy under contract DE-AC03-76SF00098.

REFERENCES

de León Vivar, J., 1988. "Presencia de dos fases en el yacimiento del campo geotérmico de Cerro Prieto," *Geotermia, Rev. Mex. de Geoenergía, 4*, 1, 203-211.

Goldstein, N.E., Halfman, S.E., Corwin, N.E., and J. Martínez R., 1989. "Self-potential anomaly changes at the East Mesa and Cerro Prieto geothermal fields," (this volume).

Grant, M.A., Truesdell, A.H., and Mañón M., A., 1984. "Production induced boiling and cold water entry in the Cerro Prieto geothermal reservoir indicated by chemical and physical measurements," *Geothermics, 13*, 1/2, 117-140.

Halfman, S.E., Lippmann, M.J., Zelwer, R., and Howard, J.H., 1984. "Geologic interpretation of geothermal fluid movement in Cerro Prieto Field, Baja California, Mexico", *Amer. Assoc. Petroleum Geologists Bull., 68*, 1, 18-30.

Halfman, S.E., Lippmann, M.J., and Gilreath, J.A., 1985. "Cerro Prieto case history: Use of wireline logs to characterize a geothermal reservoir," *Soc. Pet. Eng. Jour., 25*, 6, 793-803 (LBL-12379).

Halfman, S.E., Mañón, A., and Lippmann, M.J., 1986. "Update of the hydrogeologic model of the Cerro Prieto field based on recent well log data," *Geothermal Resources Council Trans., 10*, 369-375.

Janik, C.J. et al., 1982. "Carbon-13 variations in fluids from the Cerro Prieto geothermal system," Proc. Fourth Symposium on the Cerro Prieto Geothermal Field, 535-541, Comisión Federal de Electricidad, Mexico.

Lippmann, M.J. and Bodvarsson, G.S., 1983. "Numerical studies of the heat and mass transport in the Cerro Prieto geothermal field, Mexico," *Water Resources Research, 19*, 3, 753-767.

Lippmann, M.J. and Mañón, A., 1987. "The Cerro Prieto geothermal field," *Geothermal Science and Technology, 1*, 1, 1-38.

Mercado, S., 1976. "Movement of geothermal fluids and temperature distribution in the Cerro Prieto geothermal field, Baja California, Mexico," Proc. 2nd UN Symp. Development and Use of Geothermal Resources, 487-492.

Mercado, S. and Bermejo, F.J., 1987. "Mecanismo de producción del pozo M147 de la central geotermoeléctrica de Cerro Prieto II," Proc. Internat. Symp. on Develop. and Exploit. of Geothermal Resources, Oct. 5-9, 1987, Cuernavaca, Mexico, 214-220.

Mercado S. and Bermejo, F.J., 1988. "Ecological aspects on Cerro Prieto geothermal field," *Trans., Geothermal Resources Council, 12*, 95-99.

Nehring, N.L. and D'Amore, F., 1984. "Gas chemistry and thermometry of the Cerro Prieto, Mexico, geothermal field," *Geothermics, 13*, 1/2, 75-89.

Pruess, K., 1988. "SHAFT, MULKOM AND TOUGH: A set of numerical simulators for multiphase fluid and heat flow," *Geotermia, Rev. Mex. de Geoenergía, 4*, 1, 185-202.

Semprini, L. and Kruger, P., 1984. "Relationship of radon concentration to spatial and temporal variations of reservoir thermodynamic conditions in the Cerro Prieto geothermal field," *Geothermics, 13*, 1/2, 103-115.

Stallard, M.L. et al., 1987. "Patterns of change in water isotopes from the Cerro Prieto geothermal field, Baja California, Mexico," *Geothermal Resources Council Trans., 11*, 203-210.

Truesdell, A.H., 1988. "Geochemical models for reservoir processes at Cerro Prieto, Mexico," Proc. Intern. Symp. on Geothermal Energy, Nov. 10-14, 1988, Kumamoto and Beppu, Japan, 59-62.

Truesdell, A.H., D'Amore, F., and Nieva, D., 1984a. "The effects of localized boiling on fluid production at Cerro Prieto," *Geothermal Resources Council Trans., 8,* 223-229.

Truesdell, A.H. and Lippmann, M.J., 1986. "The lack of immediate effects from the 1979-1980 Imperial and Victoria earthquakes on the exploited Cerro Prieto geothermal reservoir," *Geothermal Resources Council Trans., 10,* 405-411.

Truesdell, A.H., Nehring, N.L., Thompson, J.M., Janik, C.J. and Coplen, T.B., 1984b. "A review of progress in understanding the fluid geochemistry of the Cerro Prieto geothermal system," *Geothermics, 13,* 1/2, 65-74.

Truesdell, A. H., Terrazas, B., Hernández, L., Janik, C., Quijano, L. and Tovar, R., 1989. "The response of the Cerro Prieto reservoir to exploitation as indicated by fluid geochemistry," paper to be presented at the April 4-5, 1989, Symposium on Cooperative Geothermal Research of the United States and Mexico, San Diego, CA.

PROCEEDINGS, Fourteenth Workshop on Geothermal Reservoir Engineering
Stanford University, Stanford, California, January 24-26, 1989
SGP-TR-122

ANOMALOUS BEHAVIOUR OF HYDROGEN IN STEAM FROM VAPOUR-DOMINATED GEOTHERMAL SYSTEMS

R A McCartney[1], J R Haizlip[2]

[1] GeoScience Limited, Falmouth Business Park, Bickland Water Road, Falmouth, Cornwall, TR11 4SZ, UK.

[2] GEO Operator Corporation, 1825 South Grant Street, Suite 900, San Mateo, California 94402, USA.

ABSTRACT

The ratios of gases in dry steam produced from the vapour-dominated reservoir of the Unit 15 steam field at The Geysers in Northern California, USA, can be explained by a model incorporating mixing between original reservoir vapour and vaporised reservoir liquid. However, hydrogen analyses are anomalous in that they are apparently enriched in the produced steam compared with levels predicted by this model. This enrichment appears to be caused primarily by fluid-rock interactions during boiling in the reservoir, although well casing corrosion reactions during production are also contributary. Hydrogen enrichment also appears to be present in the northwestern area of The Geysers and at the vapour-dominated geothermal systems of Larderello, Italy, suggesting its occurrence may be widespread. The calculation and interpretation of steam fractions and water-rock interaction models could be significantly affected by this hydrogen enrichment phenomenon.

INTRODUCTION

The Geysers (northern California, USA) and Larderello (Tuscany, Italy) are the largest and most heavily exploited vapour-dominated geothermal systems in the world. They have been extensively studied from both reservoir engineering and geological viewpoints which have provided pre- and post-production conceptual models (eg White et al, 1971; Pruess, 1985; Walters et al, 1988). In recent years the importance of geochemical and isotopic studies has been recognised through the evaluation of the effects of recharge and reinjection, and the interest in reservoir liquid-vapour ratios (eg Panichi et al, 1974; D'Amore and Truesdell, 1979; D'Amore et al, 1982, 1983, 1987; Truesdell et al, 1987; Haizlip and Truesdell, 1988).

Due to the larger volume of published data, most geochemical research has concentrated on the Larderello field. No previous studies of The Geysers have involved a detailed examination of steam gas compositions although a general model for the field has been proposed (Truesdell et al, 1987). In contrast, this present study presents some results from a major investigation of steam gas data collected by GEO Operator Corporation (GEOOC) from Unit 15 at The Geysers (Figure 1). The data were evaluated by GeoScience Limited and GEOOC, both wholly owned subsidaries of Geothermal Resources International Inc. This investigation has produced a conceptual model of the area involving the production of steam from a mixture of both vaporised liquid and vapour* sources (McCartney and Haizlip, 1989). Some anomalies to the model exist although the most evident involves hydrogen which appears to be enriched in steam produced from low gas steam

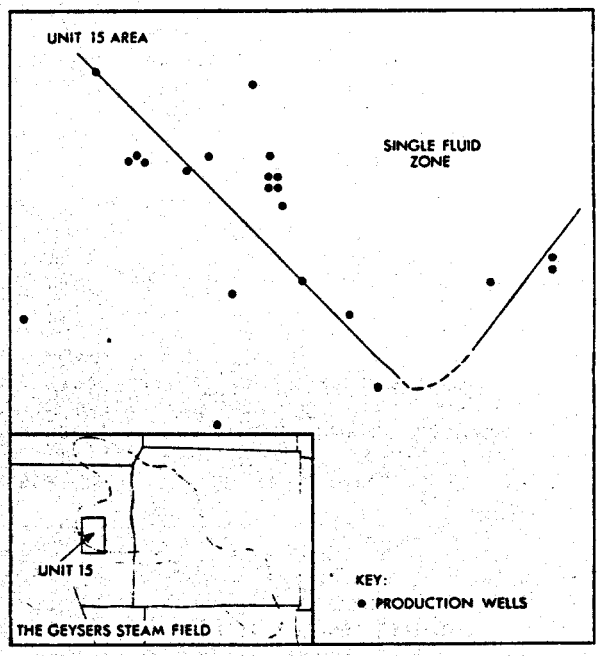

FIGURE 1 LOCATION OF THE UNIT 15 AREA AT THE GEYSERS AND THE SUGGESTED ZONE OF PRODUCTION FROM THE SINGLE FLUID SOURCE.

* 'Vapour' in this text refers to vapour which has equilibrated with reservoir liquid and rock at the reservoir temperature. The term 'steam' is used generically to refer to a vapour phase (eg it can be used where the fluid is a mixture of vaporised liquid and 'vapour').

wells. Unpublished data from the northwestern area of The Geysers, and of published data from Larderello (D'Amore et al, 1983, 1987), indicate that this might be a widespread phenomenon.

The purpose of this paper is to present the evidence for hydrogen enrichment in steam produced from low gas wells at The Geysers and Larderello, examine the possible causes of this anomalous behaviour, and offer an explanation for the observations. As hydrogen is commonly used in the calculation of reservoir temperatures and steam fractions, the implications of hydrogen enrichment to such calculations are also discussed.

EVIDENCE FOR THE ANOMALOUS BEHAVIOUR OF HYDROGEN AT UNIT 15

Truesdell et al (1987) noted that the total gas concentrations in steam from The Geysers range from approximately 150 to 65 000 ppmw. The general order of dominancy in the gas phase is:

$$CO_2 > H_2 > CH_4 > NH_3, H_2S > N_2$$

CO_2 is typically 50-70 mole percent of the dry gas whilst the proportion of hydrogen usually ranges from 10 to 20 mole percent. At Unit 15, a similar order of gas dominancy is present with steam total gas concentrations ranging from approximately 1000 to 15 000 ppmw. All gas concentrations increase with increases in CO_2 concentration. The average proportions of CO_2 and H_2 are approximately 60 and 16 mole percent in the dry gas, respectively.

McCartney and Haizlip (1989) selected 290 steam samples, which had been collected from Unit 15 wells between 1979 and 1988, for examination. These were collected under conditions of full, stable production flow and are believed to be free of significant air contamination as all samples contained less than 5 mole percent N_2 in the dry gas. Their interpretation suggests that a number of wells from a geographically defined area at Unit 15 (Figure 1) derive their steam from a single, two-phase, fluid type* under similar reservoir conditions.

The distribution of a gaseous constituent between a liquid and a vapour phase can be described through the use of a laboratory derived distribution coefficient (Bi, where i is a gaseous constituent) which is the ratio of the gas molality in the vapour phase to the gas molality in the liquid phase. In terms of the constituents normally analysed in produced steam, the order of affinity for the vapour phase based on distribution coefficients at temperatures observed at The Geysers and Larderello (~240-260°C) is (see D'Amore and Truesdell, 1986, for a summary; Haizlip and Truesdell, 1988):

$$N_2 > H_2 > CH_4 > CO_2 > H_2S > HCl > NH_3 >> H_3BO_3$$

where, N_2 is the least 'soluble' gas and only H_3BO_3 has a distribution coefficient less than unity (ie partitions preferentially into the liquid phase).

Given that (a) the single fluid type is produced from the reservoir as steam, (b) no mass loss occurs through condensation between the production source and the wellhead, (c) no gas-gas or water-rock interaction occurs during or after boiling of the liquid phase, and (d) the gases obey their distribution coefficients, the change in gas composition with change in fraction of produced steam derived from vaporised liquid is qualitatively, if not quantitatively, predictable. As the proportion of vaporised liquid increases, gas concentrations decrease, and the fraction of the more liquid soluble gases increases in the produced steam phase. As an example, because BCH_4 is greater than BH_2S, the H_2S/CH_4 mole ratio of steam is higher at lower gas concentrations where the fraction of vaporised liquid in the produced steam is dominant over the fraction of original vapour. Single fluid type wells at Unit 15 show such a trend (Figure 2) which can be explained by assuming mixing between vaporised liquid and original vapour (Equation 1; after D'Amore et al, 1982) given the above conditions.

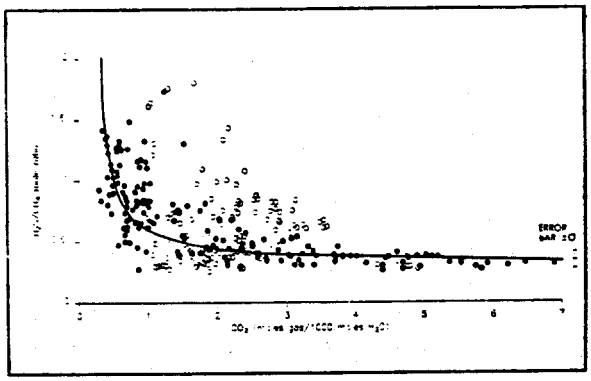

FIGURE 2 VARIATION OF H_2S/CH_4 MOLE RATIO WITH CO_2 CONCENTRATION FOR UNIT 15 STEAM SAMPLES. SOLID LINE REPRESENTS A BOILING/MIXING MODEL FIT THROUGH SINGLE FLUID SOURCE SAMPLES (SOLID CIRCLES). OPEN CIRCLES REPRESENT SAMPLES FROM ANOMALOUS WELLS.

$$C_s = C_v.y + C_l.(1-y) \quad (1)$$

where, C_s = Concentration of gas in produced steam (moles/1000 moles H_2O)

* A fluid type may be single- or two-phase and is defined as one which has a distinct and identifiable chemical composition. Where both liquid and vapour fractions are present, both are assumed to be in chemical and phase equilibrium in the reservoir.

C_v = Concentration of gas in reservoir vapour (moles/1000 moles H_2O)

C_l = Concentration of gas in reservoir liquid (moles/1000 moles H_2O)

y = Fraction of produced steam which is reservoir vapour

CH_4, H_2S, CO_2 and NH_3 data appear to support the proposed Unit 15 model but H_2 data do not. This can be illustrated by the variation in H_2/CH_4 mole ratios and CO_2 concentrations for single fluid type samples at Unit 15 (Figure 3). Whilst the distribution coefficients predict an almost constant H_2/CH_4 ratio during boiling/mixing, the field data indicates that H_2 is relatively enriched in the low gas wells and possibly also in the higher gas wells (the H_2 enrichment may not be large enough to take the H_2/CH_4 ratio out of the range of the error bars in the higher gas wells). All other gas ratios involving H_2 show the same anomaly. Although we realise that the anomaly could be caused by relative depletions in all the other gases we think that their strong correlation with the liquid-vapour mixing model makes it more likely that only hydrogen is enriched. In the following section we examine the possible causes of this effect on the single fluid type wells.

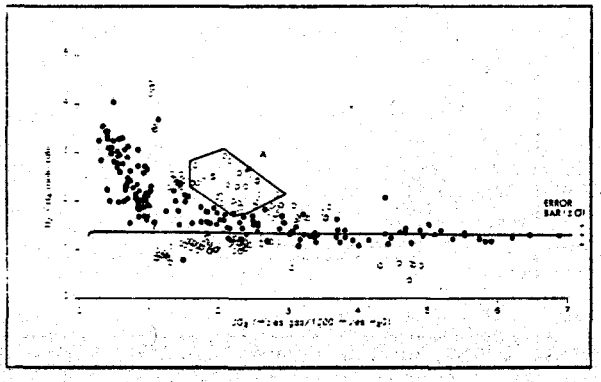

FIGURE 3 VARIATION OF H_2/CH_4 MOLE RATIO WITH CO_2 CONCENTRATION FOR UNIT 15 STEAM SAMPLES. SOLID LINE REPRESENTS BOILING/MIXING MODEL FIT THROUGH SINGLE FLUID SOURCE SAMPLES (240°C, SOLID CIRCLES). OPEN CIRCLES REPRESENT SAMPLES FROM ANOMALOUS WELLS (SEE TEXT). SAMPLES IN AREA A ARE BELIEVED TO BE AFFECTED BY CONDENSATION.

INTERPRETATION

Distribution coefficients

The trend in H_2 data (Figure 3) may be explained by the incorrect determination of laboratory H_2 distribution coefficients. That is, H_2 has a greater affinity for the reservoir liquid phase than indicated by published data (see D'Amore and Truesdell, 1986). If the 'true' distribution coefficient is in the region 30-60 (ie similar to that of H_2S) as opposed to 597 at 240°C, the single fluid data are closely fitted by the above model. Although variations in calculated partition coefficients exist between experimental results, they are not large enough to produce H_2 distribution coefficients as low as 30-60 at 240°C. Likewise, temperature variations which may occur in the reservoir as a result of boiling cannot explain the H_2 enrichment if all gases are in phase equilibrium. This is because the order of distribution coefficients noted above is maintained across the range of interest (ie 170-240°C).

Condensation

The low gas wells generally produce steam at low flow rates which may make them prone to wellbore condensation. If condensation occurs between the reservoir steam production site and the wellhead sampling point, all gases will become concentrated in the steam phase and the proportion of less liquid soluble gases in the produced steam will increase as long as all the gases obey their distribution coefficients. Thus, it is possible that the H_2 enrichment over CH_4 could result from condensation of steam which originally had a gas content much lower than that observed. However, simulations of Raleigh-type condensation (after D'Amore and Truesdell, 1979) indicate that this process is unlikely to explain the H_2 data. Even starting with gas concentrations less than 1 ppmw total gas, and condensing more than 99.9% steam causes an insignificant increase in the H_2/CH_4 mole ratio.

Boiling/mixing conditions

As long as the model criteria discussed above are obeyed, and only a single fluid type is present, variations in the boiling or mixing conditions in the reservoir do not affect the overall ratios of gases observed at different CO_2 concentrations. For example, consider the case where (a) steam (vapour or a vapour/vaporised liquid mixture) is continuously produced from a site, (b) liquid continuously boils in reponse to pressure decline, and (c) the gases in the remaining liquid and steam phases always satisfy the distribution coefficients (McCartney and Haizlip, 1989). Even in this case, as the proportion of vaporised liquid increases relative to the proportion of vapour in the produced steam, the more liquid soluble gases will always appear enriched relative to the less liquid-soluble gases, and vice-versa.

Gas transfer kinetics

Glover (1970) found that H_2S and CO_2 do not necessarily obey their gas distribution coefficients during flashing which is probably a result of relatively (for the process) slow gas transfer kinetics between liquid and steam phases. Likewise he found that each gas was affected to a different extent suggesting that

the rates of transfer vary between gases. This effect might extend to other processes and provides a possible mechanism of H_2 enrichment in the steam phase. For example, given the condensation model discussed above, if H_2 entered the condensate at a slower rate than CH_4 then the H_2/CH_4 ratio in the remaining steam phase would increase to a greater extent than suggested by our previous calculations. However, further calculations indicated that even if H_2 does not enter the condensate at all, the H_2/CH_4 mole ratio in the steam phase increases only slightly, primarily because of the poor solubility of CH_4 in the liquid phase. Thus, slow H_2 uptake by the liquid phase during condensation could not have induced the observed H_2 trend.

H_2 might leave the liquid phase at a slower rate than other gases during boiling such that the remaining liquid, when completely vapoarised, produces low gas steam anomalously enriched in H_2. Although this process might occur we do not favour it as a cause of H_2-enrichment. Conceptually, any liquid which starts boiling will continue to do so until it is all vaporised. The presence of superheating in wells from this area shows that this has happened. Likewise, steam from a number of sites in different states of boiling will probably supply a well. Linking this conceptual model with the gas kinetics hypothesis would suggest that hydrogen-enriched and -depleted steam will enter each well at the same time. This is inconsistent with the fact that low gas wells have produced only H_2-enriched steam for at least nine years.

Fluid inhomgeneities

Inhomogeneities might exist in the H_2 composition of the reservoir fluid whilst the CO_2, H_2S and CH_4 compositions remain homogenous. For example, this could be caused through mineralogical variations or through mixing with unequilibrated reinjected fluids; there is no evidence for natural recharge at Unit 15 (GEOOC, unpublished data).

Wells affected by reinjection would tend to produce low gas steam due to the higher liquid content of the source fluid and because the reinjected liquids may react with the reservoir rocks prior to vaporisation and production they may potentially become enriched in H_2 over all other gases. Increases in deuterium, oxygen-18 and tritium in produced steam, since reinjection started at Unit 15, indicate that up to 60% of production from some wells comes from reinjected fluid, and the proportions are highest in some of the low gas wells. However, samples collected from the low gas wells before reinjection began show the same H_2 enrichment as observed in later samples suggesting that reinjection is not the cause of this effect. Although reinjection might perhaps add to the general scatter of the data about the boiling/mixing model trend in Figure 3, the fact that more recent data follows the gas mole ratio distributions of earlier samples may indicate that re-injected fluids equilibrate to a large extent in the reservoir prior to production.

Steam produced from a single fluid type will have almost constant H_2/CH_4 mole ratios over a range of CO_2 concentrations if the distribution coefficients and the model conditions discussed above are obeyed. If a range of reservoir fluid types exist in the reservoir where only the H_2 composition varies and CO_2, H_2S and CH_4 are constant, then the vapour, liquid and produced steam phases may have a range of H_2/CH_4 mole ratios. Thus, the low gas samples might represent samples of high vapoarised liquid content, produced from such a range of reservoir fluid types (Figure 4). There are, however, two factors which suggest that this is not the case. Firstly, although Unit 15 wells have been monitored under varying production conditions for over nine years there is little evidence of a range of vapour-liquid mixing lines which would support the presence of a range of H_2 fluid types (see Figures 3 and 4). Many of the data which might represent examples of these fluids are in fact low gas samples affected by wellbore condensation (samples marked A in Figure 3, McCartney and Haizlip, 1989). Secondly, we have no evidence of mineralogical variations across the reservoir which might explain why H_2 concentrations should vary in the single fluid type, whilst leaving H_2S, CH_4 and CO_2 concentrations constant.

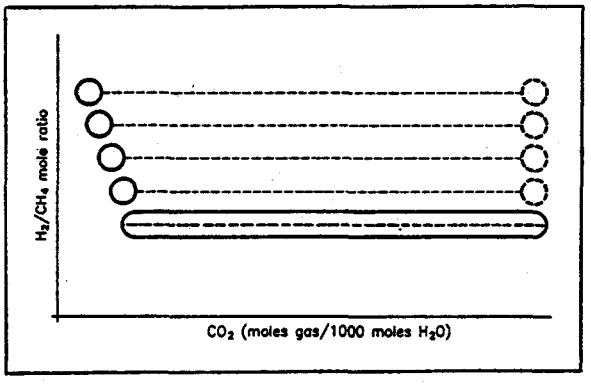

FIGURE 4 EXAMPLE OF THE DISTRIBUTION OF DATA EXPECTED FROM A FLUID SOURCE WITH INHOMOGENEOUS H_2 CONCENTRATIONS BUT HOMOGENEOUS CO_2, H_2S AND CH_4 CONCENTRATIONS. DASHED CIRCLES REPRESENT HYPOTHETICAL VAPOUR COMPOSITIONS, SHADED AREAS REPRESENT UNIT 15 DATA, AND DASHED LINES REPRESENT BOILING/MIXING LINES CONNECTING VAPOUR AND VAPOURISED LIQUID SAMPLES. NOTE THAT BECAUSE THE DISTRIBUTION COEFFICIENTS OF H_2 AND CH_4 ARE SIMILAR, THE MIXING LINES ARE ALMOST HORIZONTAL.

Fluid-solid interactions

Pruess et al (1985) presented evidence for the active production of CO_2 after the onset of boiling in the Larderello reservoir. Boiling produces a decline in gas partial pressures and results in disequilibrium between the residual liquid and the host rock. Whilst liquid remains, there is a thermodynamic driving force for gas production. If H_2 is produced at Unit 15 in this way, or H_2 is

produced at a faster rate than other gases, then such a process would result in the H_2 enrichment we observe. Given the remarkable consistency of the CH_4, H_2S and CO_2 data over time to the single fluid model, we believe that H_2 is the only gas which might be significantly produced 'in excess', if the process is occurring at all. The reaction of prehnite/pyrrhotite to epidote/pyrite (Equation 2) is an example of the type which might be generating the excess H_2. This reaction has been proposed to buffer H_2 in liquid-dominated systems by Arnorsson and Gunnlaugsson (1985) and is also compatable with the mineralogy observed at The Geysers (Sternfeld, 1981).

$$4FeS + 2Ca_2Al_2Si_3O_{10}(OH)_2 + 2H_2O =$$

$$2FeS_2 + 2Ca_2FeAl_2Si_3O_{12}(OH) + 3H_2 \quad (2)$$

Produced steam may be enriched in H_2 generated during corrosion of well casing and the steam gathering system. Minor, and in some cases more significant, condensation is common at Unit 15 and corrosion is localised where steam condenses and the condensate contacts carbon steel (eg Giggenbach, 1979). Analyses of corroded pipe indicate the presence of high levels of H_2 whilst the most common corrosion product is magnetite. This suggests that a reaction such as that in Equation 3 is important and the poor solubility of H_2 in the condensate will favour partitioning of excess H_2 into the produced steam phase.

$$3Fe + 4H_2O = Fe_3O_4 + 4H_2 \quad (3)$$

Pyrite and pyrrhotite are also corrosion products at Unit 15 and their formation could generate H_2 (Equations 4 and 5). However, their occurrence is much less frequent than that of magnetite, and the lack of evidence for H_2S depletion in the lower gas wells suggests that Reaction 3 is the dominant mechanism of H_2 production during well casing and pipe corrosion.

$$Fe + 2H_2S = FeS_2 + 2H_2 \quad (4)$$

$$Fe + H_2S = FeS + H_2 \quad (5)$$

Despite the presence of corrosion products, we have performed mass balance calculations based on Reaction 3, observed corrosion rates of well casings, and cumulative steam production, which indicate that only 5-15% of the excess H_2 is likely to have been derived from well casing corrosion reactions.

EVIDENCE FROM OTHER AREAS

We have also examined steam gas mole ratio data from GEOOC's lease in the northwestern area of The Geysers and some from Larderello (D'Amore et al, 1983, 1987) where gas levels are much higher than at Unit 15. Total gas concentrations in the former area are in the higher ranges for The Geysers (quoted earlier) whilst at Larderello they typically range from approximately 17 000 to 20 0000 ppmw. As at The Geysers, CO_2 is by far the dominant gas over H_2 at Larderello (typically > 90, and 1-2, mole percent in the dry gas respectively).

We have not, as yet, performed detailed studies on either area and therefore do not suggest that the conditions present in these localities are similar to those at Unit 15. However, mole ratio data from both areas display a distribution with respect to CO_2 concentration which is similar to that seen at Unit 15 (eg H_2 appears to be enriched in lower gas wells; see Figures 5 and 6). One exception is that both H_2 and CH_4 appear to be enriched over CO_2 in lower gas steam from Larderello (Figure 6). It is unlikely that these apparent enrichments are the result of CO_2 depletion in these samples because Pruess et al (1985) have presented strong evidence to suggest that 'excess' CO_2 is present in steam from Larderello due to fluid-rock interaction during boiling.

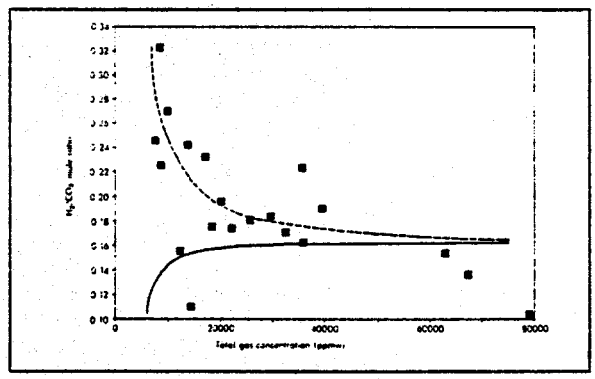

FIGURE 5 VARIATION OF H_2/CO_2 MOLE RATIO WITH CO_2 CONCENTRATION FOR STEAM SAMPLES FROM THE NORTHWESTERN AREA OF THE GEYSERS. EACH SOLID SQUARE REPRESENTS THE AVERAGE VALUE FOR A WELL. SOLID LINE REPRESENTS THE TREND EXPECTED FOR DATA DERIVED FROM A SINGLE FLUID TYPE. DASHED LINE SHOWS THE OBSERVED TREND.

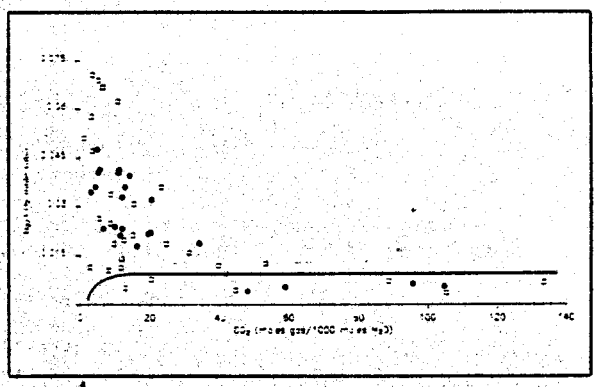

FIGURE 6 VARIATION OF H_2/CO_2 MOLE RATIO WITH CO_2 CONCENTRATION FOR LARDERELLO STEAM SAMPLES. FILLED CIRCLES (D'AMORE ET AL, 1983) AND OPEN SQUARES (D'AMORE ET AL, 1987). SOLID LINE REPRESENTS THE TREND EXPECTED FOR DATA DERIVED FROM A SINGLE FLUID TYPE.

Any of the processes discussed above for Unit 15 might be responsible for H_2 generation in the northwestern area of The Geysers and

Larderello. However, at this stage there is only evidence supporting H_2 generation through corrosion of well casings and production pipelines in the northwest Geysers. At this site magnetite, pyrite and pyrrhotite have been identified as corrosion products suggesting that the the reactions shown in Equations 3 to 5 are occurring during production. We have no information on corrosion products at Larderello but given the fact that 'excess' CO_2 appears to be generated by fluid-rock interactions in the reservoir (Pruess et al, 1985), it is possible that H_2 is also generated by such reactions. The same process would explain the behaviour of CH_4 in the lower gas wells.

CONCLUSIONS

H_2 enrichment of steam gas has been identified at Unit 15, The Geysers, and may also be occurring in other areas of both The Geysers and Larderello. At Unit 15 we have evidence that this effect may be caused, in part, by steam-well casing interactions during production although the major source of 'excess' H_2 appears to be fluid-rock interactions which take place during boiling in the reservoir.

Given the potential widespread presence of H_2 enrichment, it is evident that field data should be carefully evaluated prior to using them in H_2 influenced steam fraction, geothermometry or fluid-rock interaction calculations. In the case of Unit 15 data, we estimate that approximately 14 ppmw H_2 has been added to the steam through one of the processes considered above and this should be subtracted from low gas wells, and possibly also higher gas wells prior to use in such calculations. Errors will be largest if use is made of low gas mole ratio data incorporating H_2. If in doubt about the validity of H_2 data, we suggest non-H_2 influenced calculations are performed.

ACKNOWLEDGEMENTS

We thank Geothermal Resources International, Inc, and its wholly owned subsidiaries GeoScience Limited and GEO Operator Corporation for permission to use previously unpublished data. Thoughtful reviews by Drs A S Batchelor and J Combs are greatly appreciated. We also thank P Davies and J Pearson for help in producing the paper. We acknowledge the work of Drs A H Truesdell and F D'Amore for stimulating our interest in the behaviour of gases in vapour-dominated geothermal systems.

REFERENCES

Arnorsson S, Gunnlaugsson E (1985). New gas geothermometers for geothermal exploration : Calibration and application. Geochim Cosmochim Acta, Vol 49, pp 1307-1325.

D'Amore F, Celati R, Calore C (1982). Fluid geochemistry applications in reservoir engineering (vapour-dominated systems). Proc 9th Workshop on Geothermal Reservoir Engineering, Stanford University, California, pp 295-307.

D'Amore F, Celati R, Calore C. (1983). Hypothesis of possible equilibria between N_2 and other gases at Larderello and Cerro Prieto. Proc 9th Workshop on Geothermal Reservoir Engineering, Stanford University, California, pp 247-252.

D'Amore F, Fancelli R, Saracco L, Truesdell A H (1987). Gas geothermometry based on CO content : Application in Italian geothermal fields. Proc 12th Workshop on Geothermal Reservoir Engineering, Stanford University, California, pp 221-229.

D'Amore F, Truesdell A H (1979). Models for steam chemistry at Larderello and The Geysers. Proc 5th Workshop on Geothermal Reservoir Engineering, Stanford University, California, pp 283-297.

D'Amore F, Truesdell A H (1986). A review of solubilities and equilibrium constants for gaseous species of geothermal interest. CNR report, 33 pp.

Giggenbach W F (1979). The application of mineral phase diagrams to geothermal corrosion. Proc NZ Geothermal Workshop, Part 1, pp 217-226.

Glover R B (1970). Interpretation of gas compositions from the Wairakei field over ten years. Geothermics, Vol 2, Part 2, pp 1355-1366.

Haizlip J R, Truesdell A H (1988). Hydrogen Chloride in superheated steam and chloride in deep brine at The Geysers geothermal field, California. Proc 13th Workshop on Geothermal Reservoir Engineering, Stanford University, California.

McCartney R A, Haizlip J R (1989). Gas pressures at The Geysers geothermal field, California : Comparison with liquid-dominated systems and implications for boiling processes. Proc 6th Symposium on Water-Rock Interactions, Malvern, England.

Panichi C, Celati R, Noto P, Squarci P, Taffi L, Tongiorgi E (1974). Oxygen and hydrogen isotope studies of the Larderello (Italy) geothermal system. In: Isotope techniques in groundwater hydrology, International Atomic Energy Agency, Vienna, Vol 2, pp 3-28.

Pruess K (1985). A quantitative model of vapour-dominated geothermal reservoirs as heat pipes in fractured porous rock. Geotherm Res Counc Trans, Vol 9, pp 353-361.

Pruess K, Celati R, Calore C, D'Amore F (1985). CO_2 trends in the depletion of the Larderello vapour-dominated reservoir. Proc 10th Workshop on Geothermal Reservoir Engineering, Stanford University, California, pp 273-278.

Sternfeld J N (1981). The hydrothermal petrology and stable isotope geochemistry of two wells in The Geysers geothermal field, Sonoma County, California. MSc thesis, Univ of California, Riverside, Report No UCR/IGPP 81/7, 202 pp.

Truesdell A H, Haizlip J R, Box W T, D'Amore F (1987). Fieldwide chemical and isotopic gradients in steam from The Geysers. Proc 12th Workshop on Geothermal Reservoir Engineering, Stanford University, California, pp 241-246.

Walters M A, Sternfeld J F, Haizlip J R, Drenick A F, Combs J B (1987). A vapour-dominated reservoir exceeding 600°F at The Geysers, California. Proc 13th Workshop on Geothermal Reservoir Engineering, Stanford University, California.

White D E, Muffler L P J, Truesdell A H (1971). Vapour-dominated hydrothermal systems compared with hot-water systems. Econ Geol, Vol 66, pp 75-97.

PROCEEDINGS, Fourteenth Workshop on Geothermal Reservoir Engineering
Stanford University, Stanford, California, January 24-26, 1989
SGP-TR-122

THE OCCURRENCE OF ACID-LEACHED GRAYWACKE AT THE GEYSERS, SONOMA COUNTY, CALIFORNIA

Jeffrey Sternfeld and Mark Walters

GEO Operator Corporation
1330 North Dutton Avenue, Suite A
Santa Rosa, CA 95401

ABSTRACT

Acid-leached[1] graywacke has been identified in 15 of 19 GEO wells in the Northwest Geysers. The altered graywacke is characterized by a bleached appearance and a high degree of secondary dissolution porosity/permeability. Minerals deposited in vugs and veins include large (up to 30mm) doubly terminated quartz crystals, bladed calcite, pyrite, pseudohexagonal pyrrhotite, albite, potassium feldspar and kaolinite. Alunite, trace amounts of iron oxides, opaline silica and possibly sulfur are also observed. The dissolution features and the morphologies of the replacement minerals suggest that these rocks were subject to a complex history of boiling and low pH dissolution. The dissolution features include the leaching and replacement of detrital albite and selected matrix phyllosilicates. The acid-leached zones are generally encountered above the steam-bearing reservoir rocks and may represent the shallowest levels of the geothermal system. Examination of older GEO mudlogs and publically available data indicate that similar zones are present throughout The Geysers field.

INTRODUCTION

An abundant number of doubly terminated quartz crystals, approximately 2 mm. long, were encountered in mud drilled samples over several 3-9 m. intervals in GEO Operator's Prati 1 well in 1981. Because these crystals were unattached to any rock matrix, their origin was unknown at that time. In subsequently drilled GEO wells, various combinations of: large clear euhedral quartz crystals (up to 30 mm. in length); pseudohexagonal pyrrhotite and euhedral calcite and quartz; bleached graywacke and quartz; and clear calcite and euhedral quartz, were observed in drill samples from many of GEO's steam wells in the Northwest Geysers. Because the samples of these materials were small fragments and constituted only a relatively small percentage of rotary drill cuttings, a hypothesis for a common origin was not made. Then in 1988, GEO blew a partially bridged well to the atmosphere to clean it out. Among the ejecta from the well were about 8 kgs. of white, bleached graywacke fragments up to 5 cm. across, composed primarily of euhedral quartz, white clay, bladed calcite, sulfides including pyrite and pyrrhotite and bleached graywacke with dissolution cavities. Because the location of the bridge was known

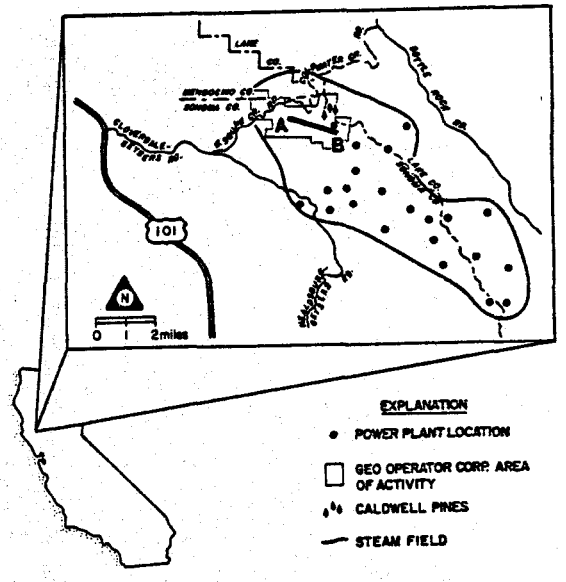

Figure 1: Map of The Geysers with location of cross section (A-B) of Figure 2.

[1] Used here to describe observed dissolution textures. Term is not analogous to acid-sulfate alteration.

approximately, the position of the bleached graywacke in the wellbore was determined to be at a depth of approximately 1,260 m. and correlated with an increase in drilling penetration rate. We have identified similarly altered rocks in other wells using the following criteria:

- abundant euhedral quartz, sometimes doubly terminated
- a bleached appearance to the graywacke
- clear, euhedral calcite
- lost circulation zones
- increased drilling penetration rates
- occurrence near or above the top of the steam reservoir.

It was determined that 15 of GEO's 19 wells encountered acid-leached graywacke. Laboratory studies were subsequently made to determine the characteristics of this rock. This paper reports the preliminary results of that work.

As Figure 2 shows, the acid-leached graywacke is discontinuously encountered above steam-bearing rocks in geothermal wells in the Northwest Geysers. Although the geothermal system vents at the surface in the central and southeast portions of The Geysers steam field, there are few surficial hydrothermal manifestations in the Northwest Geysers (Walters et al, 1988). It is worthwhile to note that the shallowest occurrences of acid-leached graywacke shown in Figure 2 also are in close proximity to the few weak surficial manifestations in the Northwest Geysers.

Mineralogy

The acid-leached graywacke ejected from the well has a light gray to bleached white appearance with a highly porous sponge-like texture. Relict sedimentary textures and structures are poorly preserved or absent. Veinlets and veins up to 4 mm. across and irregular cavities up

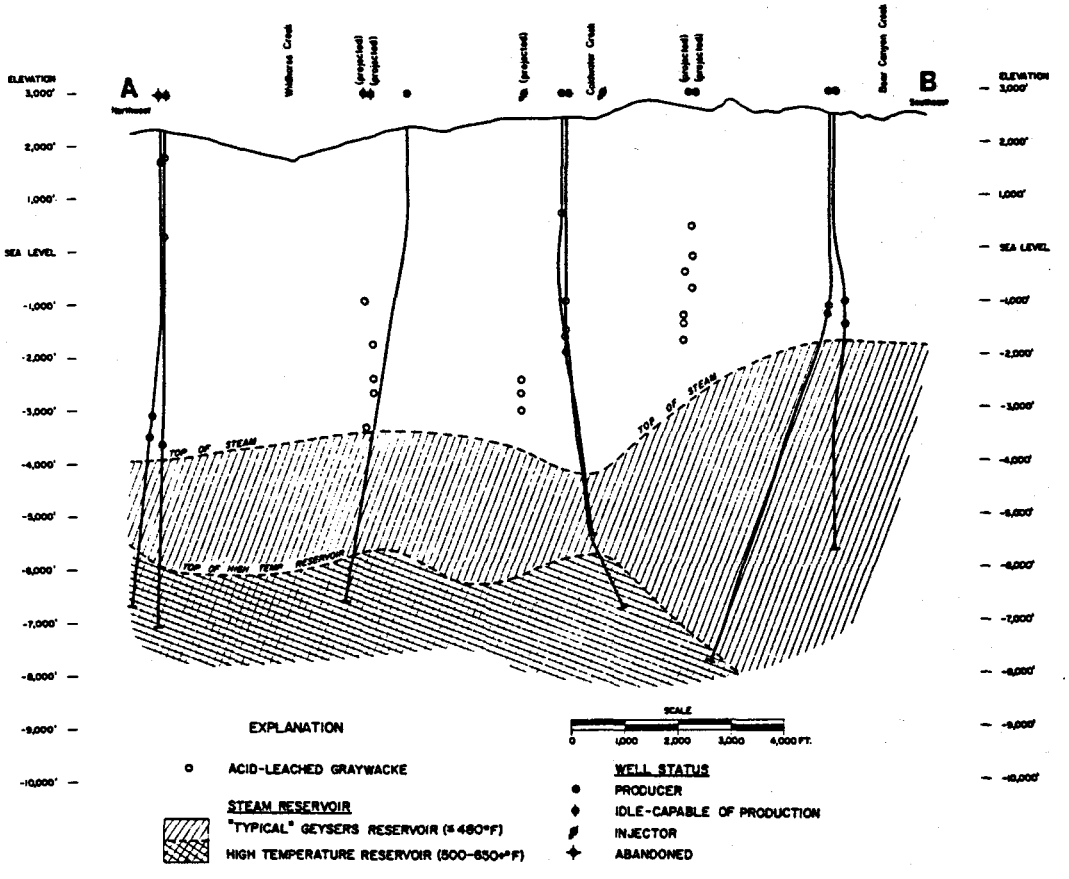

Figure 2: Cross section through the Northwest Geysers area of Figure 1 showing occurrence of acid-leached rocks relative to the steam reservoir.

to 5 mm. are common. The cavities and open fractures are ubiquitously lined with very fine to millimeter-sized quartz crystals and often infilled with other minerals including calcite, pyrite and pyrrhotite. There is also evidence for brecciation and cementation of rotated graywacke fragments.

The characteristic fracture-fill mineral assemblages consist of colorless euhedral and traces of doubly terminated quartz crystals ranging in size from <.1 mm. to 25 mm. in length; subordinant amounts of massive white quartz; bladed to rhombohedral white to colorless calcite crystals (up to 1.5 mm.) and crystal aggregates; disseminated pyrite cubes (<.05 mm.) and pyrite aggregates up to 3 mm. in length; and pseudohexagonal crystals of pyrrhotite up to 1.0 mm. in size. There are also minor amounts of soft, powdery, white to bluish white, very finely granular mineral(s). This material lacks crystalline geometries under the binocular stereoscope and locally forms botryoidal masses. XRD analyses of the powdery material indicate the presence of albite, potassium feldspar and kaolinite. Trace amounts of reddish brown iron oxides and a yellowish granular material, possibly sulfur or jarosite, are also observed.

In order to study the alteration characteristics of acid-leached graywacke, several pieces of the well ejecta, as well as graywacke cuttings ("GW" of Table I) originating approximately 75 m. above the estimated depth of the ejected material, were studied using whole rock geochemical analysis, X-ray diffraction analysis and petrographic analysis.

The samples of altered graywacke referenced in Table I are: A-1, altered material with no visible veining or dissolution features but with recognizable sedimentary textures; A-2, altered graywacke with abundant quartz crystals; A-3, altered graywacke with abundant calcite and quartz crystals; and A-4, altered graywacke with significant amounts of the white granular material.

Sample "GW" is typical of the graywackes from the Northwest Geysers. It is a medium dark greenish gray, weakly metamorphosed, textural type 1.0 graywacke. It is composed (see Table 1) of quartz, plagioclase, chlorite, illite (with a broad 100% peak indicative of some mixed montmorillonite layers) and traces of montmorillonite. In thin section, framework grains of quartz, twinned albite and lithic fragments (argillite, chert, greenstone) with trace amounts of detrital epidote, muscovite, biotite and sphene are observed in a heterogeneous matrix of phyllosilicate cements, chlorite, phengite and incompetent deformed grains of claystone. Grain boundaries in the graywacke are sharp and well defined. The Franciscan metamorphic minerals consist of minor pumpellyite after plagioclase and incipient lawsonite in the matrix.

Petrographic observations of the altered graywacke reveal a pervasive silicic replacement and recrystallization of the original graywacke. The altered material is composed of microcrystalline to subhedral prismatic quartz grains surrounded by a relatively homogeneous fine-grained matrix of sericite and chlorite, with sporadic disseminated cubic pyrite. Relict quartz grains, when present, display embayed or corroded, pitted boundaries and lithic grains are typically rounded and partially replaced. Plagioclase grains are totally absent.

The bulk of the altered graywacke has a web texture of small (<0.1 mm. to 0.5 mm.) irregular quartz blebs in a matrix of fibrous to scaly, fine-grained sericite and chlorite. Near large mineralized veins, open fractures and cavities, the material develops a coarser (0.1 to 1.0 mm.) decussate texture of subidioblastic prismatic quartz crystals with minor amounts of interstitial fibrous sericite and trace amounts of chlorite. Less commonly, irregular patches of calcite are also observed intergrown with, or replacing, the sericitic matrix.

XRD-derived mineralogies (see Table 1) support the thin section observations. The altered material is composed chiefly of quartz and sericite (micaceous illite with an extremely strong 8.8° 2θ peak) with trace to minor amounts of chlorite and pyrite. Plagioclase and smectite are absent and the relative percentage of chlorite is lower compared to the unaltered graywacke. It should be noted that in sample A-4, the observed white granular material proved to be authigenic albite and alkali feldspar. However, in samples A-2 and A-3 kaolinite and alunite were identified.

TABLE I

XRD MINERALOGY

Semi-quantitative Analyses in Weight Percent

	GW	A-1	A-2	A-3	A-4
Quartz	55.0	77.0	85.9	87.4	73.7
Plagioclase[1]	29.0				3.4
Chlorite	6.2	7.1	4.0	1.7	4.0
Illite	4.3				
Sericite[2]		12.8	7.5	2.3	6.9
Calcite	4.3			5.3	1.3
Pyrite		1.3	1.7	2.7	3.7
Alkali Feldspar		1.9			2.0
Kaolinite			1.0	0.8	
Alunite (?)			Tr.		
Pyrrhotite				Tr.	

[1] Albite
[2] Micaceous illite

GW Typical Graywacke
A-1 Altered Graywacke
A-2 Altered Graywacke with drusy quartz
A-3 Altered Graywacke with drusy calcite
A-4 Altered Graywacke with white material

Albite, alkali-feldspar and kaolinite could not be petrographically identified. There were localized concentrations of a fine-grained, mosaic silicate mineral but it was not possible to identify it as feldspar or quartz. Trace amounts of a colorless to pale green, fibrous to scaly, very fine-grained phyllosilicate mineral were observed coating some quartz crystals and infilling the interstitial spaces between quartz and calcite crystals, but it was not possible to optically identify this material as kaolinite, sericite or chlorite.

Geochemistry

Comparisons between the whole rock geochemical values for unaltered and altered graywackes are presented in Figure 3. The plots clearly illustrate the selective leaching of plagioclase, smectite clays and clorite, and the introduction of silica and sulfur. Sodium (Na) found primarily in plagioclase is virtually absent in the altered material. Calcium (Ca) and strontium (Sr) are also severely depleted, probably as a result of the dissolution of pre-existing calcite veins and secondarily due to the destruction of pre-existing smectite clays. Additional evidence for the dissolution of the matrix chlorites and clays is exhibited by the depletion of iron (Fe), magnesium (Mg), manganese (Mn) and titanium (Ti).

The differences in the degree of alteration and recrystallization between samples A-1 and A-2 are reflected in their chemical characteristics. Sample A-1, which is only moderately altered and contains less secondary quartz and more secondary sericite than A-2, exhibits increased values of potassium (K), aluminum (Al) and titanium (Ti), and small decreases in Fe, Mg and Mn. Silica (Si) remains unchanged. Sample A-2, which is predominated by drusy quartz and contains smaller volumes of sericite and chlorite than A-1, exhibits a strong increase in Si, unchanged K, and strong depletions of Al, Fe, Mg, Mn and Ti.

Fluid Inclusions Geothermometry

Quartz and calcite crystals from the altered ejecta graywacke as well as

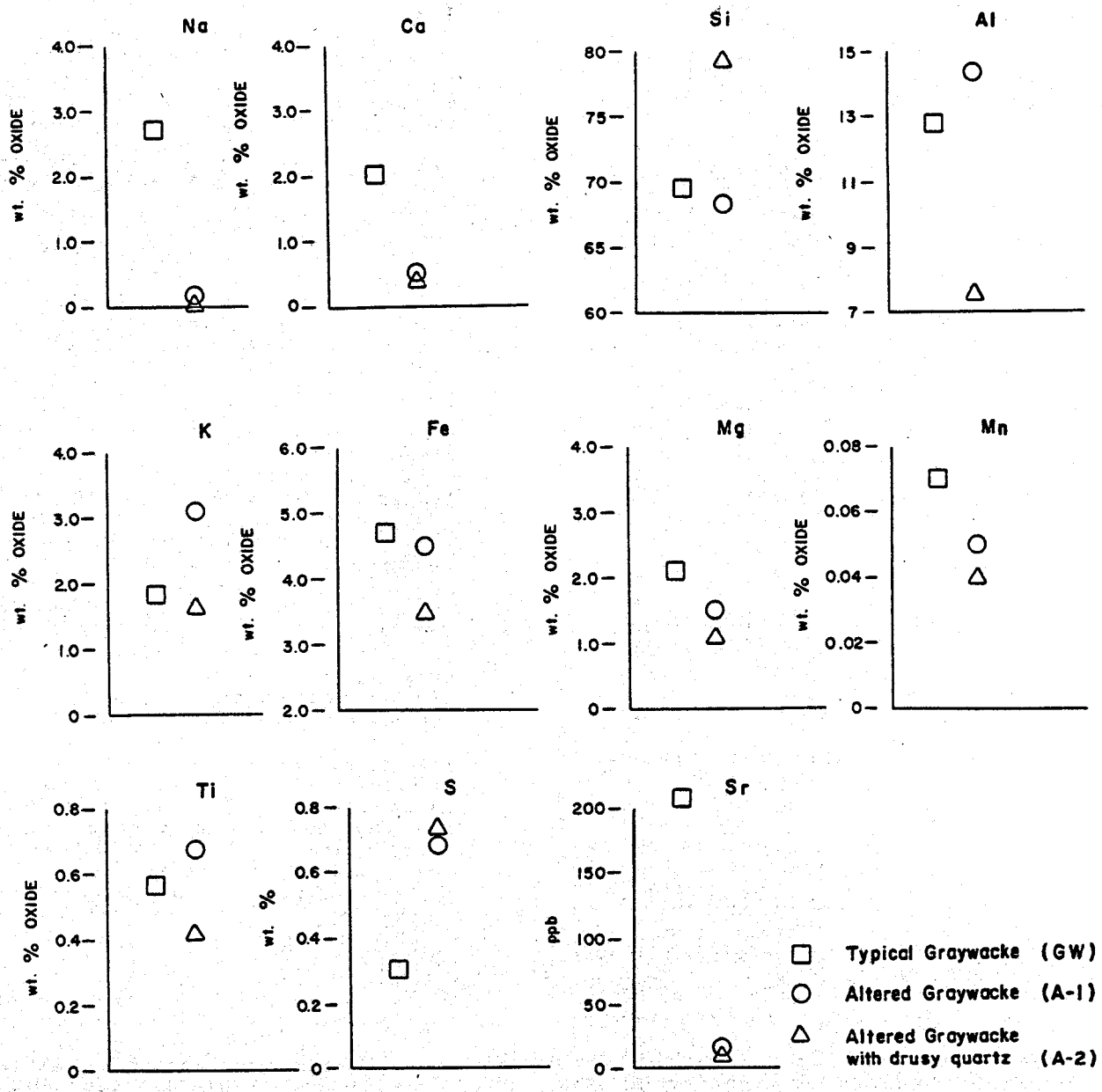

Figure 3: Whole rock geochemical compositions of altered graywacke and unaltered graywacke.

crystals from acid-leached graywacke zones in two other wells were analyzed. However, only preliminary results are available at this time. Vapor-filled inclusions associated with both primary and secondary liquid-rich inclusions were identified in some of the euhedral quartz crystals. Although no data on vapor-rich inclusions were obtained, petrographic relationships suggest that the vapor and liquid-rich inclusions were deposited as a result of boiling.

The homogenization and ice melting temperatures of liquid-rich inclusions vary widely but tend to plot into two distinctive groupings. One group, composed of primary and secondary inclusions from quartz and calcite, has homogenization temperatures that range between 280° to 320°C but have highly variable ice melting temperatures. These ice melting temperatures range from -2.4°C to -0.2°C which correspond to apparent salinities of 2.7 to 0.4 wt.% NaCl equivalent. The second group, composed of secondary

inclusions from quartz, are tightly clustered with homogenization temperatures of 230 to 240°C and ice melting temperatures of -0.1 to -0.4°C.

The fluid inclusions may represent different generations of fluids in the reservoir. Another possibility is that these inclusions are related to subsurface boiling. The 280-320°C temperatures approach the boiling point curve for low saline waters at the depths that these crystals originated (Haas, 1971) and the 230-240°C correspond to the predicted temperatures at depth in a 2-phase vapor-dominated reservoir (White et al., 1971). The variation in the apparent salinities of the high temperature group could be a function of fluctuating CO_2 levels in a boiling environment (Moore, J., verbal communication).

Conclusions

The acid-leached graywacke encountered in the GEO Northwest Geysers steamfield is a product of complex alteration processes. The graywacke displays a unique bleached appearance, and a cellular texture with abundant dissolution features. It is composed of a unique silica+sericite-+chlorite matrix which has replaced pre-existing plagioclase grains and matrix illites and chlorites. Infilling the open spaces in the bleached graywacke is an assemblage of quartz+sericite+calcite+pyrite+pyrrhotite with trace amounts of authigenic albite, alkali feldspar, kaolinite and alunite.

The assemblage of pore-filling minerals is similar to the adularia-sericite-type of epithermal ore deposits which are formed by the interaction of hot neutral pH chloride waters with meteoric waters (Heald et al., 1987). However, the observed bleached appearance, the dissolution textures, the leaching of plagioclase and the presence of alunite and kaolinite must have been caused by acidic conditions. The open cavities and pore spaces existed before the precipitation of the sericite-adularia-type minerals which are indicative of neutral pH waters. The logical source of the acidic fluids is the condensation of volatiles, primarily H_2S and CO_2, released through boiling at depth. Evidence for subsurface boiling can be found in the fluid inclusion homogenization temperatures and their variable ice melting temperatures.

Thus, we have the situation where low pH fluids, generated from boiling fluids at depth, altered the graywacke. Subsequently, the pore spaces were filled by boiling neutral pH fluids. Finally, the traces of kaolinite and alunite indicate that low pH conditions returned to the fracture network after the neutral waters had boiled away.

The altered graywackes with dissolution features and evidence for boiling represent the highest elevations reached by geothermal fluids. The fluids subsequently began to boil down toward present day reservoir levels. The distribution of altered graywacke lies above, or within the upper levels of the typical Geysers steam reservoir (see Figure 2). To date, no occurrences of bleached graywacke have been identified within the lower portions of the typical steam reservoir nor within the high temperature (650°F) reservoir (Walters et al., 1988). However, trace amounts of calcite with pyrrhotite inclusions have been observed in the typical reservoir especially where clusters of entries are separated by barren intervals hundreds of feet thick.

There is evidence in the public domain that indicates to us that rocks affected by dissolution and/or boiling may occur throughout The Geysers steamfield. Although we have not inspected the rocks, some or all of our criteria for acid-leached rocks appear to be met in the following Geysers wells outside of GEO Operator leases:

1. The drilling of the Ottoboni State 2, 6, and 13 wells in the Northwest Geysers produced notable occurrences of euhedral quartz crystals according to mudlogs on file with the California Division of Oil and Gas (D.O.G.). The quartz crystals for Ottoboni State 13 were described as being doubly terminated.

2. Moore (1980) describes a core from Thermal 10 in The Geysers Resort area which closely fits the mineralogical and chemical criteria for acid-leached rocks we have studied in the Northwest Geysers. Moore attributes "Boiling and subsequent loss of CO_2...in the deposition of calcite, quartz and adularia..."

3. A core report on open file with the D.O.G. for the Lakoma Fame - 6 well in the Central Geysers describes a very permeable and vugular greenstone with calcite veins and quartz crystals up to 25 mm. in length.

4. W.T. Box (Verbal Communication) reports that veins in graywacke with dissolution features are also present in wells in the Southeast Geysers.

Acknowledgements

We thank Geothermal Resources International, Inc. for financial support of this work and permission to publish. We also thank Dr. Jim Combs, Dr. Chandler Swanberg and two anonymous reviewers for their review of this paper and Steve Mason, Linda Johnson and Michelle Michaelis for manuscript preparation.

XRD patterns were made by Utah Research Institute (UURI). Fluid inclusion microthermometry was conducted by Dr. Joe Moore and Michele Lemieux of UURI.

References

Haas, J.L., 1971, The Effect of Salinity on Maximum Thermal Gradient of a Hydrothermal System at Hydrostatic Pressure. Econ. Geol., v.66, pp.940-946.

Heald, P., Foley, N.K., and Hayba, D.O., 1987, Comparative Anatomy of Volcanic-Hosted Epithermal Deposits: Acid-Sulfate and Adularia-Sericite Types. Econ. Geol., v.82, pp. 1-26.

Moore, D., 1980, Hydrothermal Minerals in The Geysers Steam Field, California and their Potential Use in Exploration. Proceedings of the Sixth Workshop on Geothermal Reservoir Engineering, Stanford University, Stanford, CA, pp.361-366.

Walters, M.A., Sternfeld, J.N., Haizlip, J.R., Drenick, A.F., Combs, J., 1988, A Vapor-Dominated Reservoir Exceeding 600°F. at The Geysers, Sonoma County, CA. Proceedings of the Thirteenth Workshop on Geothermal Reservoir Engineering, Stanford University, Stanford, CA., in press.

White, D.E., Muffler, L.J.P., Truesdell, A.H., 1971, Vapor-Dominated Hydrothermal Systems Compared to Hot-Water Systems. Econ. Geol., v.66, pp. 75-97.

PROCEEDINGS, Fourteenth Workshop on Geothermal Reservoir Engineering
Stanford University, Stanford, California, January 24-26, 1989
SGP-TR-122

COLD-WATER INJECTION INTO SINGLE- AND TWO-PHASE GEOTHERMAL RESERVOIRS

S. K. Garg and J. W. Pritchett

S-CUBED
P. O. Box 1620
La Jolla, California 92038-1620

ABSTRACT

Approximate analytical solutions are derived for cold water injection into single- and two-phase "porous medium" geothermal reservoirs. A numerical geothermal reservoir simulator is used to verify the applicability of the analytical solutions for pressure transient analysis. In accordance with these numerical results, the analytical solutions indicate that the pressure buildup behavior during injection into either a single-phase-liquid or two-phase reservoir is governed by the kinematic viscosity of the cold injected fluid. The fall-off pressures after cold water injection into a single-phase liquid reservoir (except for very early shutin times) are primarily controlled by the kinematic viscosity of the *in situ* (hot) reservoir fluid. For two-phase reservoirs, however, the fall-off behavior is considerably more complex and cannot be fully described by the analytical solution developed in this paper.

INTRODUCTION

Traditionally, cold-water injection testing of geothermal wells takes place shortly after the well is completed. Cold water is injected into the well at a known rate for a period of time, and then injection ceases. Pressures are recorded within the well both during the "buildup" part of the test (during injection) and the "fall-off" part (after injection). The interpretation of these pressure histories to yield formation properties requires consideration of nonisothermal (and possibly two-phase) fluid flow in porous and fractured rocks.

For an isothermal constant rate injection test, the line-source (Theis) solution implies that a plot of pressure increase versus logarithm of time (semi-log plot) asymptotically approaches a straight line after a short initial period. The slope of this line yields the mobility-thickness product. The intercept of the straight line may be used to compute either the skin factor or the total formation compressibility. Pressure fall-off data are often plotted as a function of log $(t + \Delta t)/\Delta t$, where t denotes the production time and Δt is the shutin time; these data also asymptotically approach a straight line with a slope identical with that of the buildup straight line.

Numerical simulation techniques have been employed by several authors (see e.g. Benson and Bodvarsson, 1982; Garg and Pritchett, 1984) to investigate cold-water injection into single-phase (liquid) and two-phase (liquid water/steam) "porous medium" reservoirs. Injection of cold water into a geothermal reservoir results in the outward propagation of a cold front of which the radius increases in proportion to the square root of time; during the subsequental fall-off phase, the cold front is more or less stationary. In two-phase reservoirs, a condensation front moves ahead of the cold front; the radius of the condensation front also increases with the square root of time, but, unlike the cold front, the condensation front does not remain stationary during the fall-off phase.

Numerical results (Garg and Pritchett, 1984) indicate that pressure buildup data from both single- and two-phase reservoirs can be interpreted by the semi-log method provided that the fluid properties (viscosity, density) of the cold injected fluid are used. Fluid properties for the *in situ* hot water are required to interpret pressure fall-off data after injection into single-phase reservoirs. Fall-off data for two-phase reservoirs, however, exhibit rather complex behavior and do not appear to be useful for deducing formation properties.

Cold water injection testing often takes place just after drilling and logging operations have been completed. In these cases, a relatively small region containing cold water (cold spot) is usually present immediately surrounding the well. The effect of such a cold spot on pressure buildup behavior was numerically investigated by Benson and Bodvarsson (1982). The pressure buildup data initially follow a straight line on the semi-log plot with a slope reflecting the fluid properties of the inner cold zone. Later, the pressure disturbance propagates into the outer hot region, and a straight line with a slope corresponding to the fluid properties of the hot region is obtained. With a preexisting cold spot, the cold front radius is finite initially and does not change significantly at early times. For long injection periods, however, the cold front moves away from the well and its radius once again becomes proportional to the square root of time. Under these conditions, a straight line with the slope determined by the properties of the cold

injected fluid is observed. The pressure fall-off data are affected only slightly by the presence of the cold spot.

Geothermal reservoirs are often found in fractured volcanic foundations. The effects of fractures on pressure buildup and pressure fall-off behavior have been numerically examined by, among others, Bodvarsson, *et al.* (1984) and O'Sullivan (1987). Simulation results show that for practical injection times and realistic formation properties, the pressure buildup data yield a straight line on semi-log paper whose slope depends upon fluid properties (viscosity and density) evaluated at the average temperature (i.e. average of the injected cold water and the *in situ* hot water). Note that in this case, the cold front expands differently; the radius increases with the fourth-root of time instead of the square root. If the injection period is sufficiently long (usually not feasible in practical situations), the thermal front will once again revert to expansion in proportion to the square root of time (Bodvarsson and Tsang, 1982), and the final slope of the pressure buildup straight line will depend only upon the properties of the cold injected fluid. According to Bodvarsson, *et al.* (1984), pressure fall-off data are often hard to interpret due to rapid heating of fluid in the fractures.

In this paper, we derive analytical solutions for cold water injection into single- and two-phase "porous medium" geothermal reservoirs. It should be recognized at the outset that the physical problem treated herein (porous medium at a uniform initial temperature) is somewhat idealized in that complications arising from the presence of a cold spot and/or fractures are ignored. These analytical solutions should nevertheless be useful for illustrating essential features of pressure buildup and fall-off response in geothermal reservoirs.

MATHEMATICAL FORMULATION

Consider a fully penetrating injection well located in an infinite porous medium reservoir of thickness h. We neglect any variations in either formation or fluid properties in the vertical direction. The latter assumption implies that we are restricting our attentions to either single-phase (liquid water) systems or to two-phase (liquid water + steam) systems with steam saturation less than the residual gas saturation. (Any mobile steam in the pores will tend to migrate towards the top of the formation and thus invalidate the assumption of uniformity of fluid properties in the vertical direction.) At time t = 0, we start injecting cold fluid at a temperature T_c into the well at a constant mass rate of injection $\dot{M}$. The cold-water injection ceases after a time t_{inj}. The injection of cold-water is accompanied by the propagation of a thermal front into the reservoir. Assuming that (1) the reservoir rock and the pore fluid are in thermal equilibrium, and (2) global heat conduction is negligible, the radial location (r_{thm}) of the thermal front at time t ($< t_{inj}$) is given by:

$$r_{thm} = (\eta t)^{0.5}, \tag{1}$$

where

$$\eta = \frac{\dot{M}}{\pi\, h\, \rho_c} \frac{(\rho c)_\ell}{(1-\phi)\,(\rho c)_r + \phi\,(\rho c)_\ell}$$

ϕ = porosity,

ρ_c = density of injected water,

$(\rho c)_r$ = specific heat of formation per unit formation volume,

$(\rho c)_\ell$ = specific heat of water per unit liquid volume.

Although $(\rho c)_\ell$ varies somewhat with temperature, for the present purpose it suffices to regard $(\rho c)_\ell$ as a constant.

Since the pressure disturbance propagates faster then the thermal front, in two-phase reservoirs a condensation front will form which moves outward ahead of the thermal front. The spatial location of the condensation front (r_{cond}) at time t ($< t_{inj}$) is given by

$$r_{cond} = (\lambda\, t)^{0.5} \tag{2}$$

where λ is an undetermined constant. Since under two-phase conditions fluid pressure (p) is a unique function of temperature (T), both the pressure p^* and temperature T^* at the condensation front must be higher than the initial reservoir pressure p_i and temperature T_i. To estimate p^*, we note that initially (i.e. prior to injection), a unit volume of the reservoir contains fluid mass M_i:

$$M_i = \phi\,(\rho_{wi}\, S_{wi} + \rho_{gi}\, S_{gi}) \tag{3}$$

where

S_{wi} = initial liquid saturation (= 1 - S_{gi}),

S_{gi} = initial gas saturation ($\leq S_{gr}$),

S_{gr} = residual gas saturation,

ρ_{wi} = liquid water density at temperature T_i,

ρ_{gi} = steam density at temperature T_i.

The total energy H_i contained in this volume prior to injection is:

$$H_i = (1-\phi)\,\rho_r\, c_r\, T_i + \phi\,(\rho_{wi}\, S_{wi}\, h_{wi} + \rho_{gi}\, S_{gi}\, h_{gi}) \tag{4}$$

where h_{wi} (h_{gi}) denotes the enthalpy of saturated liquid water (steam) at temperature T_i. After condensation, the unit volume contains only liquid water at temperature T^*; the mass of liquid is:

$$M = \phi\, \rho_w \tag{5}$$

where ρ_w denotes the density of liquid water at temperature T^*.

A comparison of Equations (3) and (5), shows that a mass increment Δm must be added to the unit volume to compensate for the condensed steam:

$$\Delta m = M - M_i = \phi(\rho_w - \rho_{wi} S_{wi} - \rho_{gi} S_{gi}). \quad (6)$$

Since only the liquid phase is mobile, the specific enthalpy of the added mass (Δm) is equal to h_{wi}. An energy balance can, therefore, be written as follows:

$$H_i = (1-\phi) \rho_r c_r T^* + \phi \rho_w h_w - \Delta m h_{wi} \quad (7)$$

where h_w is the enthalpy of liquid water at temperature T^*. Substituting for Δm from Equation (6) into Equation (7), and noting that:

$$p^* = p_i + \Delta p = p_i + \left(\frac{dp}{dT}\right)_{T=T_i} (T^* - T_i)$$

$$c_w = \left(\frac{dh_w}{dT}\right)_{T=T_i}$$

we obtain:

$$p^* = p_i + \frac{\phi \rho_{gi} S_{gi} (h_{gi} - h_{wi})}{(1-\phi) \rho_r c_r + \phi \rho_{wi} c_w} \left(\frac{dp}{dT}\right)_{T=T_i}. \quad (8)$$

Equation (8) shows that the condensation pressure increases in proportion to the initial reservoir steam saturation. For reasonable values of the parameters, it is easy to verify from Equation (8) that $(p^* - p_i)$ is at most of the order of 10^4 Pa (0.1 bar).

In the case of cold water injection into a single-phase hot water reservoir, the reservoir contains cold water with temperature T_{inj} (i.e. temperature of the injected water) for $r \leq r_{thm}$, and hot water with temperature T_i (i.e. initial reservoir temperature for $r \geq r_{thm}$). The pressure behavior in these two flow regimes is governed by:

$$\frac{\partial p_j}{\partial t} - D_j \frac{1}{r} \frac{\partial}{\partial r} \left[r \frac{\partial p_j}{\partial r} \right] = 0 \quad (9)$$

where j = 1 and 2 denote the cold water and hot water regions respectively. The diffusivity D_j (j = 1,2) is given by:

$$D_j = \frac{k}{\phi \rho_j \nu_j C_j}, \quad j = 1,2 \quad (10)$$

where ρ_j and ν_j denote the density and kinematic viscosity of the liquid in the jth region. The total formation compressibility C_j is related to uniaxial formation compressibility C_m and liquid compressibility C_{wj} as follows:

$$C_j = C_m/\phi + C_{wj} \qquad j = 1,2 . \quad (11)$$

We assume that the reservoir is initially at a uniform pressure p_i, and that the fluid is injected at a constant mass rate $\dot{M}$ into a well of radius r_w. The boundary conditions at r_w and at infinity are:

$$r \left.\frac{\partial p_1}{\partial r}\right|_{r=r_w} = - \frac{\dot{M} \nu_1}{2\pi h k} \quad (11a)$$

$$\lim_{r \to \infty} p_2 (r, t) = p_i \quad (11b)$$

For the sake of mathematical convenience, the boundary condition at $r = r_w$ is usually replaced by the "line source" approximation:

$$\lim_{r \to 0} r \frac{\partial p_1}{\partial r} = - \frac{\dot{M} \nu_1}{2\pi h k} . \quad (11a')$$

In addition to the boundary conditions (11), we have the following continuity conditions on mass flow and pressure at the thermal front ($r = r_{thm}$):

$$\left(\frac{k}{\nu_1}\right) \frac{\partial p_1}{\partial r} = \left(\frac{k}{\nu_2}\right) \frac{\partial p_2}{\partial r} \quad (12a)$$

$$p_1 = p_2 \quad (12b)$$

Equations (1) and (9) through (12) completely specify the problem of cold water injection into a hot water reservoir.

Next, consider cold water injection into an initially two-phase reservoir. In this instance, the reservoir contains three flow regimes: (1) a cold water zone, $0 \leq r \leq r_{thm}$, (2) a hot water zone, $r_{thm} \leq r \leq r_{cond}$, and (3) a two-phase zone, $r \geq r_{cond}$. The pressure behavior is once again governed by Equation (9) with j = 1,2,3. The diffusivities for the cold and hot water regions are given by Equations (10) and (11) with j = 1,2. The effective diffusivity for the two-phase region D_3 can be expressed as:

$$D_3 = \frac{k}{\phi \rho_3 \nu_3 C_3} \quad (13)$$

where ρ_3 and C_3 denote the density of the flowing mixture and the total compressibility of the two-phase region, respectively. Since the steam phase is immobile, we have:

$$\rho_3 = \rho_2$$

$$\nu_3 = \nu_2 / k_{r\ell} \quad (14)$$

where $k_{r\ell}$ denotes the liquid phase relative permeability. The total two-phase compressibility C_2 is given sufficiently accurately by the following approximate expression (Grant and Sorey, 1979):

$$\phi\, C_3 = \langle \rho c \rangle \left[\frac{(\rho_w - \rho_g)^2}{\rho_w \rho_g (h_w - h_g)}\right] (T + 273.15) \quad (15)$$

where

$$\langle \rho c \rangle = (1-\phi)\, \rho_r\, c_r + \phi\, \rho_w\, c_w\, S_w .$$

For present purposes, the two-phase compressibility C_3 may be evaluated at the initial reservoir conditions. Boundary conditions (11a′), (12a) and (12b) apply in this case as well; the condition at infinity (11b) is, for this case,

$$\lim_{r \to \infty} p_3\,(r,t) = p_i \,. \quad (11b')$$

Continuity of mass flow and pressure across the condensation front yields three additional boundary conditions at $r = r_{cond}$:

$$\left[\frac{k}{\nu_2}\right] \frac{\partial p_2}{\partial r} = \left[\frac{k}{\nu_3}\right] \frac{\partial p_3}{\partial r} \quad (16a)$$

$$p_2 = p^* \quad (16b)$$

$$p_3 = p^* . \quad (16c)$$

PRESSURE BUILDUP RESPONSE

To develop a solution for pressure buildup response during cold-water injection, we note that a general solution for Equation (9) can be written as:

$$p_j = a_j\, E_1\,(r^2/4\, D_j\, t) + b_j \quad (17)$$

where a_j and b_j are constants of integration, and E_1 is the exponential integral function

$$E_1\,(x) = \int_x^\infty \frac{e^{-u}}{u}\, du \,. \quad (18)$$

For cold-water injection into a liquid reservoir, we have four boundary conditions (11a′, 11b, 12a, 12b) to determine four unknowns (a_j, b_j, $j = 1,2$). The reservoir pressure response can, therefore, be written as:

$$0 \le r \le r_{thm} : p_1 = p_i + \frac{\dot{M}\nu_1}{2\pi\, h\, k} \left\{E_1\left[r^2/4\, D_1 t\right] - E_1\,(\eta/4\, D_1) + \gamma_{12}\, E_1\,(\eta/4\, D_2)\right\} \quad (19a)$$

$$r_{thm} \le r : p_2 = p_i + \frac{\dot{M}\nu_1\, \gamma_{12}}{4\pi\, h\, k} E_1\left[r^2/4\, D_2 t\right], \quad (19b)$$

where

$$\gamma_{12} = (\nu_2/\nu_1)\, \exp\left\{-\frac{\eta}{4\, D_1}\,(1 - D_1/D_2)\right\}. \quad (19c)$$

It is straightforward to verify that the exponential term in Equation (19c) is, for all practical purposes, equal to unity. This implies that the pressure buildup response of the hot water region is independent of the pressure response of the cold water region.

In case of injection into a two-phase reservoir, there are seven equations (11a′, 11b′, 12a, 12b, 16a, 16b, 16c) for seven unknowns (a_j, b_j, $j = 1,2,3$; λ). The pressure buildup response for this case is given by:

$$0 \le r \le r_{thm} : p_1 = p^* + \frac{\dot{M}\nu_1}{2\pi\, hk} \left\{E_1\left[r^2/4\, D_1 t\right] - E_1\,(\eta/4\, D_1) + \gamma_{12}\left[E_1\,(\eta/4\, D_2) - E_1\,(\lambda/4\, D_2)\right]\right\} \quad (20a)$$

$$r_{thm} \le r \le r_{cond} : p_2 = p^* + \frac{\dot{M}\nu_1\, \gamma_{12}}{4\pi\, h\, k} \left\{E_1\left[r^2/4\, D_2 t\right] - E_1\,(\lambda/4\, D_2)\right\} \quad (20b)$$

$$r_{cond} \le r : p_3 = p_i + \frac{\dot{M}\nu_1}{2\pi\, hk}\, \gamma_{12}\, \gamma_{23}\, E_1\left[r^2/4\, D_3 t\right] , \quad (20c)$$

where

$$\gamma_{23} = (\nu_3/\nu_2)\, \exp\left\{-\frac{\lambda}{4\, D_2}\,(1 - D_2/D_3)\right\}. \quad (20d)$$

and λ is the root of

$$p^* = p_i + \frac{\dot{M}\nu_1}{4\pi\, hk}\, \gamma_{12}\, \gamma_{23}\, E_1(\lambda/4\, D_3) . \quad (20e)$$

Since $\gamma_{12} \simeq \nu_2/\nu_1$, Equation (20b) implies that the pressure response of the hot water region can be decoupled from the pressure response of the cold-water region. The two-phase diffusivity D_3 is much smaller than the single-phase diffusivity D_2; thus, the exponential term in Equation (20d) will always exceed unity. It, therefore, follows that the pressure response of the two-phase region is given by the line source solution with $\dot{M}$ replaced by $\dot{M}^*$

$$\dot{M}^* = \dot{M} \exp\left\{-\frac{\lambda}{4 D_2}\left(1 - D_2/D_3\right)\right\} \geq \dot{M}. \qquad (21)$$

As noted earlier, the condensation pressure p^* will only slightly exceed the initial pressure (by an amount of the order of 10^4 Pa). It is now apparent from Equation (20c) that in the two-phase region, the pressure changes induced by injection are likely to be quite small.

PRESSURE FALL-OFF RESPONSE

The self-similar solutions developed in the preceding section for pressure buildup response do not, strictly speaking, apply for pressure falloff. After cold water injection ceases, the radii of the thermal and condensation fronts no longer grow in proportion to the square root of time. The thermal front is stationary for $t > t_{inj}$. The condensation front, however, displays a more complex behavior (Garg and Pritchett, 1984). In this section, we will present approximate solutions for the shutin phase of the cold water injection test.

For cold-water injection into a single-phase (liquid) reservoir, the pressure buildup response of the hot water region is independent of the cold water zone. Since most injection tests last only a few days at most, the cold water front is likely to advance a small distance (say < 10 meters) into the reservoir. On cessation of cold-water injection, the cold zone will govern the pressure fall-off behavior for only a very short time (a few seconds). For practical purposes, the cold-water region will act like a skin zone. The pressure fall-off response can, therefore, be approximated as:

$$p_w\left(t_{inj}+\Delta t\right) = p_i + \frac{\dot{M}\,\nu_1\,\gamma_{12}}{4\pi\, h\, k}$$

$$\left\{E_1\left[\frac{r_w^2}{4 D_2\,(t+\Delta t)}\right] - E_1\left[\frac{r_w^2}{4 D_2\,\Delta t}\right]\right\} \qquad (22)$$

where $p_w\,(t_{inj} + \Delta t)$ denotes the pressure in the well at a shutin time Δt. Employing the usual logarithmic approximation for the exponential integral function, it is straightforward to show from Equation (22) that a plot of p_w versus log $[(t + \Delta t)/\Delta t]$ will yield a straight line with slope m equal to

$$m = \frac{1.15\,\nu_2\,\dot{M}}{2\pi\, k\, h}. \qquad (23)$$

The corresponding results for pressure buildup response in both single- and two-phase reservoirs (Equations 19a and 20a) imply that ν_2 in Equation (23) should be replaced by ν_1.

The fall-off response for injection into an initially two-phase reservoir is rather complex. According to Garg and Pritchett (1984), the fall-off data can be subdivided into the following three parts:

1. For large values of $(t + \Delta t)/\Delta t$ (i.e. small shutin times), the pressure response is essentially governed by the condensed fluid region. Because of the large contrast in single- and two-phase diffusivities, the two-phase region remains practically unaffected during this time period, and the condensed fluid region behaves like a reservoir with a constant pressure $(= p^*)$ boundary.

2. For moderate values of $(t + \Delta t)/\Delta t$, the well pressure is essentially constant $(= p^*)$. During this period, the condensation front starts moving towards the wellbore. At the end of this period, the condensation front becomes coincident with the edge of the thermal front.

3. For large values of buildup time Δt, the pressure response is governed by the two-phase region.

Since p^* is unlikely to differ appreciably from p_i in most practical situations, only the fall-off response for early shutin times (see Item 1 above) is likely to be useful for deducing formation properties. (In many cases, these early fall off data may be dominated by wellbore storage effects, and it may well be impossible to obtain any useful information regarding formation transmissivity.) Accordingly the pressure fall-off response can be approximately represented by the following relations:

$$p_w(t_{inj}+\Delta t) = p_2\,(t_{inj}+\Delta t) \qquad \text{for } p_2 \geq p^*$$
$$= p_3\,(t_{inj}+\Delta t) \qquad \text{for } p_2 < p^*, \qquad (24)$$

where

$$p_2\left(t_{inj}+\Delta t\right) = p^* + \frac{\dot{M}\,\nu_1\,\gamma_{12}}{4\pi\, k\, h}$$

$$\left[E_1\left(r_w^2/4\,D_2\,(t_{inj}+\Delta t)\right)\right.$$

$$\left. - E_1\left(r_w^2/4\,D_2\,\Delta t\right) - E_1\left(\lambda/4\,D_2\right)\right]$$

$$p_3\,(t_{inj}+\Delta t) = \min\left\{p^*,\ p_i + \frac{\dot{M}\,\nu_1}{4\pi\,h\,k}\,\gamma_{12}\gamma_{23}\right.$$

$$\left.\left[E_1\left(r_w^2/4\,D_3(t_{inj}+\Delta t)\right)\right.\right.$$

$$\left.\left. - E_1\left(r_w^2/4\,D_3\,\Delta t\right)\right]\right\}$$

Equation (24) implies that for small values of shutin time Δt, the pressure fall-off response is controlled by the properties of hot liquid region, and that the formation kinematic mobility (kh/ν_2) is given by Equation (23).

NUMERICAL RESULTS

To investigate the limits of applicability of the preceding theory, the THOR reservoir simulator (Pritchett, 1982) was used in one-dimensional radial geometry to generate pressure buildup-falloff histories associated with cold water injection into single- and two-phase reservoirs. The radially infinite reservoir is simulated using a 100-zone ($\Delta r_1 = \Delta r_2 = \ldots = \Delta r_{10} = 0.1$ m, $\Delta r_{11} = f\,\Delta r_{10}$, $\Delta r_{12} = f\,\Delta r_{11}$, ..., $\Delta r_{100} = f\,\Delta r_{99}$) radial grid. The growth factor f is chosen such that no signal reaches the outer radius of the grid during the time scale of interest. We consider a fully penetrating injection well located in a reservoir of thickness h = 100 m. The well is represented as an integral part of the grid by assigning to the well block (Zone 1) sufficiently high permeability and porosity; fluid injection is specified as a mass source in the well block. The reservoir rock properties selected are listed in Table 1. Case 1 was designed to represent a single phase reservoir; the initial temperature and pressure are 300°C and 8.5917 MPa respectively. Note that these pressure and temperature conditions lie along the saturation line for pure water. The initial fluid state in Case 2 was assumed to be two-phase with pressure and steam saturation being 8.5917 MPa and 0.05 respectively; the initial steam saturation is taken to be equal to the residual gas saturation (Table 1). In both the cases, cold water (temperature = 100°C) is injected at a constant mass rate of 10 kg/s for $t_{inj} = 10^6$ s; the well is then shut in for $\Delta t = 2 \times 10^6$ s.

To evaluate the analytical solutions, we require several properties for water. For liquid water at 100°C, the following values for liquid density, viscosity and specific heat were assumed:

Liquid water density	=	962.3 kg/m^3,
Liquid dynamic viscosity	=	2.80×10^{-4} Pa-s
Liquid specific heat	=	4197 J/kg°C
Liquid compressibility	=	5.92×10^{-10} Pa^{-1}.

TABLE 1

	Wellblock (i = 1)	Rock Matrix 2 ≤ i ≤ 100
Porosity, ϕ	0.9999	0.1000
Permeability k, m^2	5×10^{-11}	5×10^{-14}
Uniaxial Formation Compressibility C_m, MPa^{-1}	0	0
Rock Grain Density ρ_r, kg/m^3	1	2650
Rock Grain Thermal Conductivity K_r, W/m°C	0.00	5.25
Heat Capacity c_r, kJ/kg°C	0.001	1.00
Relative Permeabilities $k_{r\ell}$, k_{rg}	Straight-line*	Straight-line*
Residual Liquid Saturation $S_{\ell r}$	0.00	0.30
Residual Gas Saturation S_{gr}	0.00	0.05

* $k_{r\ell} = (S_\ell - S_{\ell r})/(1 - S_{\ell r})$ for $S_\ell \geq S_{\ell r}$

$k_{rg} = (S_g - S_{gr})/(1 - S_{gr})$ for $S_g \geq S_{gr}$.

The reservoir initially contains liquid water and/or steam at a temperature of 300°C; this *in situ* fluid is assumed to have the following properties:

Liquid water density	=	712.5 kg/m^3
Steam density	=	46.2 kg/m^3
Liquid water enthalpy	=	1345 kJ/kg
Steam enthalpy	=	2749 kJ/kg
Liquid dynamic viscosity	=	8.87×10^{-5} Pa-s
Steam dynamic viscosity	=	$1.98\ 10^{-5}$ Pa-s
Liquid compressibility	=	$1.99\ 10^{-9}$ Pa^{-1}
Liquid specific heat	=	5700 J/kg°C.

Figures 1 and 2 compare the simulated pressure buildup and fall-off histories for injection into a single-phase reservoir with the analytical solutions (Equations 19a and 22). The numerical results are generally in good agreement with the analytical solutions. The slopes of straight lines agree within four percent (Figures 1 and 2). Despite the good agreement, there are small differences (10 to 20 kPa for pressure buildup and < 10 kPa for pressure fall off) between the numerical and analytical results (Figures 1 and 2). The analytical solutions, were derived by

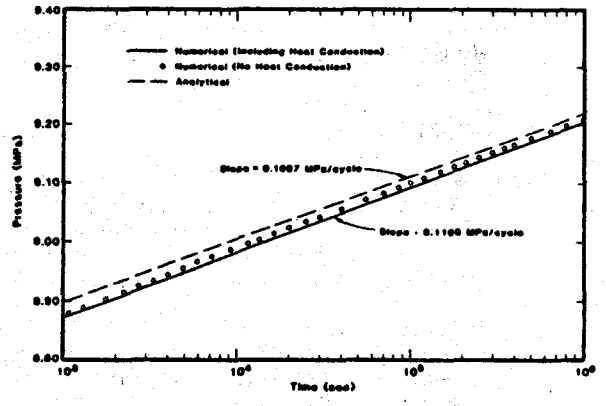

Figure 1. Simulated pressure buildup history for cold water injection into a single-phase hot water reservoir (Case 1).

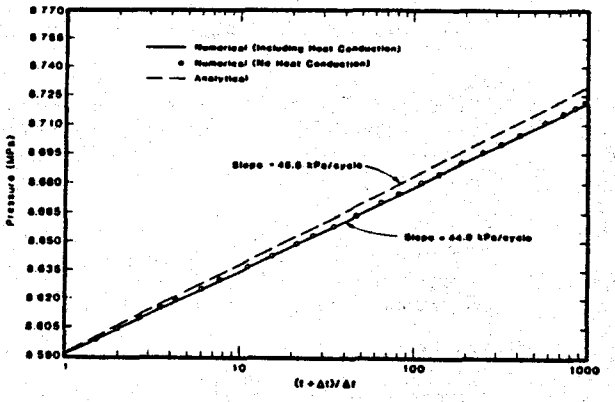

Figure 2. Simulated pressure falloff history subsequent to cold water injection into a single-phase hot water reservoir (Case 1).

assuming that the global heat conduction is negligible; the numerical reservoir simulator, however, incorporates the effects of such heat conduction. To investigate the effects of global heat conduction, we repeated the numerical calculations by eliminating the heat conduction terms in the reservoir simulator. As can be seen from Figure 1, some of the discrepancy between the numerical and analytical solutions is clearly due to heat conduction. It should also be noted that the numerical simulations employ a finite wellbore size as opposed to a well of zero radius assumed in obtaining the analytical solutions. The effect of finite wellbore size should vanish for large injection times; Figure 1 shows that the numerical solution does indeed tend to approach the analytical solution at late times. Finally, we note that discretization errors (time step, spatial resolution, etc.) may also contribute to the observed differences between analytical and numerical results.

The simulated pressure buildup history for cold-water injection into a two-phase reservoir (Case 2) is shown in Figure 3; the numerical results are in good agreement with the analytical solution. Again, the slope of the pressure-buildup curve is governed by the kinematic

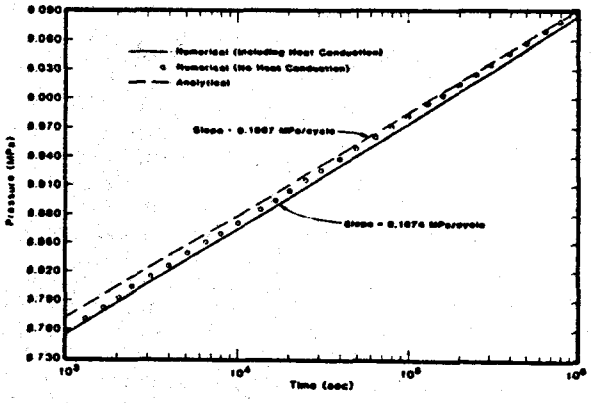

Figure 3. Simulated pressure buildup history for cold water injection into a two-phase (liquid-water/steam) reservoir (Case 2).

viscosity of the cold injected fluid. Figure 4 compares the early to intermediate shutin time simulated fall-off response with the approximate analytical solution, Equation (24). The fall-off response prior to $\Delta t \sim 10^3$ s is principally governed by the condensed (cold and hot water zones) fluid region. It is seen from Figure 4 that the analytical solution, Equation (24), may be used to represent these early to intermediate time fall-off data approximately. In practical situations, complications such as wellbore storage and skin may, however, render the early fall-off data useless for inferring formation properties.

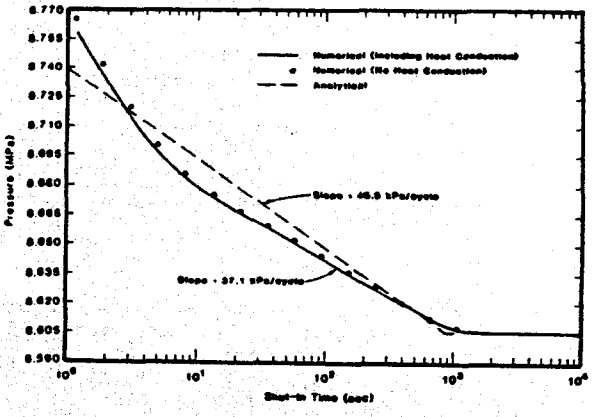

Figure 4. Early to intermediate time pressure fall-off response for cold-water injection into a two-phase reservoir (Case 2).

CONCLUDING REMARKS

The principal goal of this paper was to develop analytical solutions for cold water injection into single- and two-phase porous medium geothermal reservoirs. The analytical solutions obtained herein closely approximate pressure buildup behavior of both single- and two-phase reservoirs; these solutions indicate that the pressure response beyond the thermal front is essentially governed by the properties of the *in situ* fluid. The analytical solutions for pressure buildup (i.e. during the injection phase) can in principle be

used to analyze pressure interference effects in nearby wells as well as the pressure response in the injection well itself. Approximate solutions are also given for pressure fall off response after cold water injection ceases. For injection into a single-phase reservoir, the fall off response, except for very early shutin times, is controlled by the kinematic viscosity of the hot reservoir fluid. Two-phase reservoirs exhibit rather complicated fall-off behavior. The early and intermediate shutin time fall-off response is principally governed by the condensed fluid region; the analytical solution can be used to approximate this early/intermediate time response. Practical problems (e.g. wellbore storage, skin) are, however, likely to render the early fall-off data useless for analysis purposes. The late time fall-off pressure history in two-phase reservoirs is in principle controlled by the two-phase zone. Since cold-water injection produces only small pressure increases in the two-phase zone, the signal to noise ratio is likely to render this part of the fall-off response difficult to interpret.

In order to derive the analytical solutions, it was necessary to make certain simplifying assumptions. More specifically, it was assumed that cold water (at a uniform temperature) is injected at a constant mass rate into a "porous medium" reservoir with uniform properties. As noted elsewhere in this paper, cold water injection is usually performed shortly after well completion; injection tests in these cases amount to injecting water with a time-varying temperature into a reservoir at a nonuniform temperature. Furthermore, geothermal reservoirs are often found in fractured volcanic rocks, and in some cases cannot be adequately represented as porous media. Thus, depending upon the actual field conditions, the analytical solutions obtained in this paper may or may not be applicable in specific situations. The analytical solutions should nevertheless be useful for deriving a first estimate of reservoir properties; numerical simulation techniques may then be utilized to refine these estimates.

REFERENCES

Benson, S. M. and G. S. Bodvarsson (1982), "Non-Isothermal Effects During Injection and Falloff Tests," Paper presented at the 57th Annual Meeting of the Society of Petroleum Engineers, New Orleans, Louisiana.

Bodvarsson, G. S. and C. F. Tsang (1982), "Injection and Thermal Breakthrough in Fractured Geothermal Reservoirs," *Journal of Geophysical Research, Vol. 87,* pp. 1031-1048.

Bodvarsson, G. S., S. M. Benson, O. Sigurdsson, V. Stefansson, and E. T. Eliasson (1984), "The Krafla Geothermal Field, Iceland: 1. Analysis of Well Test Data," *Water Resources Research, Vol. 20,* pp. 1515-1530.

Garg, S. K. and J. W. Pritchett (1984), "Pressure Transient Analysis for Two-Phase Geothermal Wells: Some Numerical Results," *Water Resources Research, Vol. 20,* pp. 963-970.

Grant, M. A. and M. L. Sorey (1979), "The Compressibility and Hydraulic Diffusivity of a Water-Steam Flow," *Water Resources Research, Vol. 15,* pp. 684-686.

Pritchett, J. W. (1982), "User's Guide to the THOR Thermal Reservoir Simulator," Report SSS-R-83-5795, S-CUBED, La Jolla, California (September).

Sullivan, M. J. (1987), "Aspects of Geothermal Well Test Analysis in Fractured Reservoirs," *Transport in Porous Media, Vol. 2,* pp. 497-517.

PROCEEDINGS, Fourteenth Workshop on Geothermal Reservoir Engineering
Stanford University, Stanford, California, January 24-26, 1989
SGP-TR-122

Tracer Testing at Los Azufres

Roland N. Horne *, *Hector Puente* **

* *Stanford University*
** *Comision Federal de Electricidad*

1. Summary

Up until February 1987, nearly 8 million tonnes of water had been reinjected at Los Azufres, mainly at wells Az-40, Az-15, and Az-7. Six tracer tests had been performed up to the most recent one in July 1987. No tracer was recovered in any of the tests. We reviewed the format used in the tracer tests, and the implications of the null responses. Based on the results, it appears as if reinjection into wells Az-7 and Az-8 is unlikely to affect reservoir performance detrimentally. Since tracer return times seem to be long at Los Azufres, further tracer testing is probably not warranted--as an alternative, long time monitoring of liquid and gas chemistry (such as chloride and nitrogen) may identify the longer term transport of injected fluid through the reservoir.

2. Reinjection History at Los Azufres

Reinjection has taken place at Los Azufres since 1982, and there has been no difficulty accepting the entire waste water flow from the five wellhead units. Table 1 summarizes the total quantities of water injection up to February 1987. Altogether about 8 million tonnes of water had been injected by that time. The principal injection sites have been wells Az-40 and Az-15 in the Northern Sector, and wells Az-7 and Az-8 in the Southern Sector. Recently, well Az-31 has been added as an injector in the Southern Sector. Well Az-1 has been proposed as a potential reinjection site, based on its proximity to the central power station site. At the present time, well Az-40 accepts most of the fluid from the Northern Sector, and well Az-7 accepts most of the fluid from the Southern Sector.

Table 1: Summary of injection in to Los Azufres (up to Feb, 1987)

Well	Volume Injected (m^3)	Until
Az-1	49,342	Oct. 1984
Az-3	39,021	Dec. 1984
Az-7	1,506,013	Feb 1987
Az-8	73,569	Aug. 1986
Az-15	2,181,618	Aug. 1986
Az-40	3,899,338	Feb. 1987

The total fluid injection requirement for the field will be about 700 tonnes/hour. Well Az-7 can, by itself, accept at least 425 tonnes/hour without raising the water level in the casing by more than 10 meters (from a static level about 450 meters below the casing head). It has not been demonstrated that well Az-7 can accept more than this (as only 425 tonnes/hour is available for testing), but it seems highly probable that well Az-7 could accept even the entire 700 tonnes/hour required. Well Az-8 has been demonstrated to be able to accept at least 225 tonnes/hour, so between these two wells, there is already sufficient proven reinjection capacity for the 50 Mw development.

There does not seem to have been any problems with deposition in the reinjection wells, but well Az-40 has shown evidence of casing corrosion due to the dissolution of acidic alteration products into the water from Laguna Verde.

3. Tracer Tests at Los Azufres

A total of six tracer tests have been performed at Los Azufres (see Table 2). The first of these used 1000 kg of potassium iodide, the other five all used radioactive Ir^{192}. All of the tests were of the well-to-well type. In two of the tests, the wells were flowed only briefly after the injection; thus, the probability of a return of the tracer being detected was low--and in fact none was seen. Even in the other four tests, in which injection was continuous, no tracer was ever detected, even after 2 or 3 months of monitoring.

Table 2: Tracer tests performed at Los Azufres

Date	Injection	Method	Tracer	Monitored	Response
8/8/83	Az-8	contin.	1000kg KI	Az-2,26	none
3/14/84	Az-43	11 days inj	4.1GBqIr^{192}	Az-5,13, 32	none
8/31/84	Az-26	contin.	7.4GBqIr^{192}	Az-18,31	none
9/20/84	Az-7	contin.	14.8GBqIr^{192}	Az-2,16	none
			16D	none	
3/28/85	Az-33	No inj.	14.8GB Ir^{192}	Az-6,46, 17,36,	none
				38,24	none
7/30/87	Az-8	contin.	12.0GBqIr^{192}	Az-26	none

The following paragraphs describe each of the six tracer tests in detail.

The first test was conducted in 1983 by the personell of the Instituto de Investigaciones Electricas (IIE) in collaboration with Stanford University. In this study, 1000 kg of Potassium Iodide (KI) was injected into well Az-8, which was receiving the total water production from well Az-2. Wells Az-2 and Az-16 were monitored for the return of the Iodide, as well as for changes in sodium, potassium and lithium. The monitoring continued for three months. No tracer was detected in either Az-2 or Az-16.

Following the lack of success with KI, it was decided to use radioactive materials as tracers in subsequent studies. Iridium-192 (Ir^{192}), with a half-life of 74 days, was selected since it was possible to acquire it within Mexico, and since it was easy to handle and detect. In the second tracer test, 4 GBq of Ir^{192} were injected into well Az-43 on March 14, 1984, using separated water from well Az-13. Monitoring for the return of the tracer was continued for five months at wells Az-5, Az-13, Az-19 and Az-32, as well as at the springs at Laguna Verde and Laguna Maritaro.

The third tracer test was conducted in the South-East zone, where 7.4 GBq of Ir^{192} were injected into well Az-26 with the separated water from well Az-18. This injection was completed on August 31, 1984, and water samples from wells Az-18 and Az-31 as well as from the Los Azufres springs were monitored for a period of four months.

In the same year, 1984, one more study in the Southern zone was performed. The well selected was Az-7, into which was injected 14.8 GBq of Ir^{192}. The observation wells were Az-2, Az-16 and Az-16D. Injection started on September 20, and monitoring continued for four months.

Next, in 1985 it was decided that more tests would be done in the central part of the Southern zone, known as Tejamaniles. Well Az-33 was selected to receive 14.8 GBq of Ir^{192}. Injection took place on March 28, 1985, and wells Az-6, Az-17, Az-24, Az-36, Az-38 and Az-46 were monitored. It is important to note that, except for Az-46, all the monitored wells produced dry steam. Monitoring was continued for seven months after the injection.

Finally, the sixth and last study was again done in the South-Eastern zone. In this case 12 GBq of Ir^{192} were injected into well Az-31, on July 30, 1987, using the separated water from wells Az-18 and Az-26, and from the Laguna de Los Azufres. This last test lasted four months.

4. Discussion of the Tracer Tests

As can be appreciated from the preceding descriptions, there was intensive study of the fluid movement in the Southern zone through the use of tracers. In spite of all these studies, there still remains an uncertainty about the chemical stability of the tracers once the reservoir pressure and temperature was reached. Nor is the tracer/rock interaction fully understood, and adsorption of the tracer may have been a factor that reduced the effectiveness of the investigations.

In hindsight, it is possible to pinpoint some errors and omissions in the tests so that they will serve as a precedent for the reformulation of this type of study. In particular, the first test made use of natural chemicals present in the fluids (such as Cl^- and Na^+) in addition to the artificial tracers.

In the second test, in the Northern zone, the radioactive tracer injected into well Az-43 was displaced by 40 t/hr of separated water from well Az-13. The injection continued at constant rate for 11 days. An important detail here is that once the injection was concluded, well Az-43 was shut for two months before being reopened again for another test. The water produced at that time was analyzed in attempt to detect any indications of the tracer initially introduced. None was found, suggesting that the tracer was either retained or migrated so far into the reservoir that it could no longer be detected.

The next three tests in the Southern zone were all similar, in that each of them monitored the chemistry of the springs in the area, which was found to behave similarly to that of the observation wells.

The final test at Los Azufres, which used Az-31 as the injection well, can be considered in general as the least reliable of the group. This is due to the fact that there was no adequate control of the samples nor of the measurements made on them. There were also periods of time in which no measurements were taken due to problems with the detectors. Thus the information from this test is practically impossible to interpret.

Based on this synthesis of the work done on tracer testing at Los Azufres, there are four major points that can be summarized:

(a) It would be important to perform a laboratory study to determine the effects of adsorption of the tracer onto the rock. Otherwise there would be continuing uncertainty over this phenomenon.

(b) It is necessary to describe a dispersion model for the tracer in order to define the frequency of sampling needed in each case. For example, in the first study the sampling rate was proportional to the square root of the elapsed time since injection.

(c) It is necessary to understand the effect of change of phase of the fluid containing the tracer. This is important in places like Los Azufres, where wells in the Southern zone produce mainly dry steam. Perhaps the tracer that is contained will eventually be condensed at the side of this zone.

(d) It is necessary to revise the methodology for the detection of the radioactivity present in the fluid produced from the wells. The importance of this can be appreciated by examining the measured response when the detector is placed in the water vessel without much attention to its position. This can be quite different to the response of the same detector when it is centralized in the vessel. Much smaller dispersion of the values can be seen once the detector is centralized.

5. Interpretation

Some of the tests are of particular importance; namely, those in which tracer was injected into well Az-7, well Az-8, and well Az-31. These wells are to be used for reinjection during plant operation; therefore, it is important to know where the reinjected water went. As discussed in the previous section, the test at well Az-31 encountered some problems, and the observation well Az-26 could not be produced (for mechanical reasons) until some time after the injection commenced. Thus, the (null) result of this test is rather inconclusive. On the other hand, tracer injection into wells Az-7 and Az-8 was effectively achieved, yet no return was detected at the two closest production wells (Az-2 and Az-16). We must conclude either (a) the tracer was retained within the field by some mechanism or (b) the return occurred after the monitoring was terminated, or was at such a low concentration as to escape detection.

To examine these possibilities we looked for changes in chemical composition at well Az-16. Since well Az-7 has been injecting for some time, it is to be expected that chloride concentrations in the reservoir may increase (since chloride is concentrated in the reinjection water due to the separation of the steam). In fact, an increase in chloride concentration at well Az-16 has been observed. Other explanations for this increase are possible--for example, the well could be drawing fluid of higher chloride concentration from greater depth. On the other hand, a much more definite piece of evidence was discovered in the nitrogen content of the production from well Az-16. Nitrogen concentration at well Az-16 is higher than the nitrogen solubility of the geothermal fluid--indicating that nitrogen (which is injected into the reservoir through the open wellhead at well Az-7) is mobile through the reservoir in both dissolved and gaseous forms. Well Az-6 also shows an increasing nitrogen content.

There is an obvious source for this abnormally high Nitrogen. It is observed that well Az-7 sucks large quantities of air into its wellhead, which is open to the atmosphere. The exact quantity entrained is not known, however the suction at the well head is sufficiently vigorous to warrant caution for the personell working in its vicinity. It is reasonable to assume therefore that the intake of air is substantial. More than that, the intake is known to have been occuring periodically (time period of order of minutes) throughout the time that reinjection has taken place there.

Thus, it appears evident from this "natural tracer" that water reinjected into well Az-7 does return to well Az-16, and perhaps to well Az-6 as well. In order to estimate the rate of movement of the reinjected water, we examined historical data of chloride and nitrogen production at well Az-16, as well as nitrogen production at well Az-6, and we recommended that an attempt be made to estimate the rate of nitrogen intake into well Az-7. Figures 1 and 2 show the nitrogen production as a function of time in wells Az-6 and Az-16. Other contributing evidence was obtained by plotting the argon and argon/nitrogen ratios in wells Az-6 and Az-16 (Figures 1 and 2) which demonstrate that the gases are atmospheric in origin.

It is evident from these plots that the transit time from well Az-7 towards wells Az-6 and Az-16 is of the order of months, which suggests why the radioactive tracers were never detected. This is an encouraging conclusion from the point of view of reinjection, as it suggests that thermal breakthrough of the reinjected water will be slow between these particular wells.

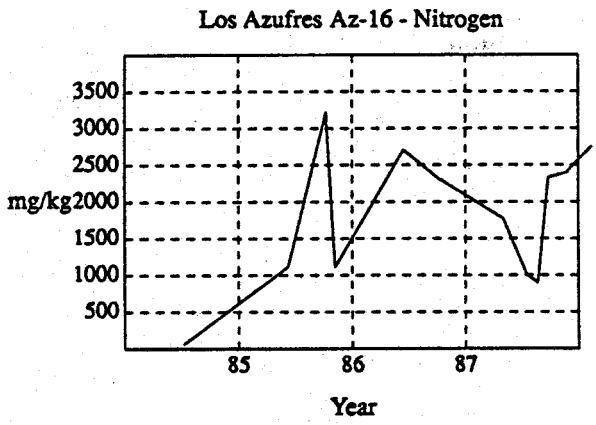

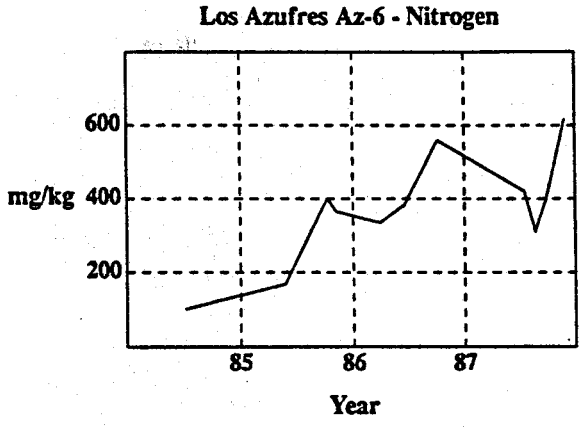

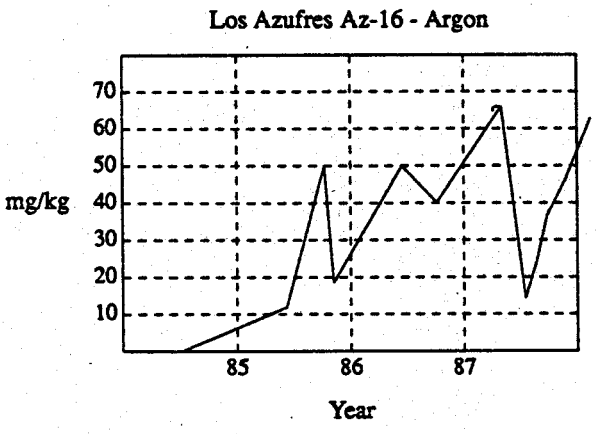

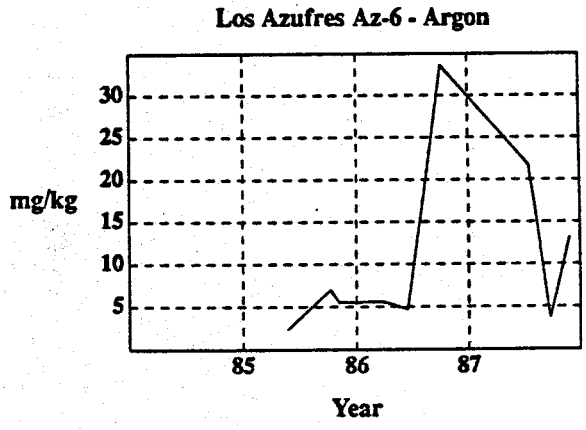

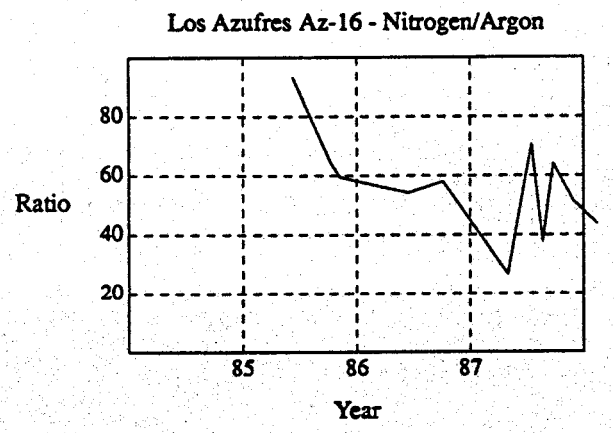

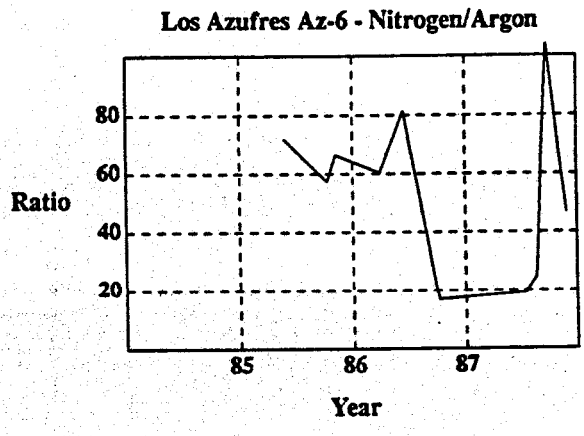

Figure 1: Gas production values for Az-16

Figure 2: Gas production values for Az-6

References

Iglesias, E.R.: "Reporte de avance del primer intento de utilizacion de trazadores en el Campo Geotermico de Los Azufres", Memorias de la Primera Reunion Interdisciplinaria CFE-IIE, Los Azufres, Mich., Mexico, Nov. 22-24, 1983, pp 161-170.

Aragon, A.A.: "Uso de trazadores radioactivos en la Zona Norte del Campo Geotermico de Los Azufres", Informe Interno 1385-004, Dep. Yaciemientos, CFE, (1985).

Oficina de Reinyeccion CFE: "Reporte de trazadores radioactivos en la Zona Sur del Campo Geotermico de Los Azufres, Mich.", Reporte Interno, 1386-005, Dep. Yaciemientos, CFE, (1986)

PROCEEDINGS, Fourteenth Workshop on Geothermal Reservoir Engineering
Stanford University, Stanford, California, January 24-26, 1989
SGP-TR-122

LONGEVITY CALCULATIONS FOR HDR GEOTHERMAL RESERVOIRS

Derek Elsworth

Waterloo Centre for Groundwater Research
University of Waterloo, Waterloo
Ontario, Canada N2L 3G1

ABSTRACT

A conceptual model is presented to describe thermal recovery from a semi-infinite hot dry rock (HDR) geothermal reservoir containing an equidimensional permeable zone. Transient behaviour may be represented uniquely by five dimensionless parameters. Variation in production temperature (T_D) with time (t_D) is influenced by reservoir throughput (Q_D), thermal porosity (Φ_D) and depth ratio (a/z). Of these, only throughput (Q_D) exercises significant control on transient performance, the parameter being directly proportional to reservoir circulation rate and inversely proportional to the effective radius of the stimulated zone. Steady production temperature (T_D) is indexed to throughput (Q_D) and depth ratio (a/z), only. Steady production temperatures are always highest for a host medium bounded by a proximal constant temperature surface and lowest for an insulated boundary. Boundary effects are insignificant for reservoir burial depths up to an order of magnitude greater than the reservoir radius. A threshold behaviour in time (t_DQ_D) is evident for very large reservoir throughput (Q_D). This bounding behaviour describes, in dimensionless time (t_DQ_D), the maximum rate at which thermal depletion may occur. This state is evident for large dimensionless throughput magnitudes (Q_D) corresponding directly with high circulation rates within the reservoir. Predictions compare favourably with results from a 300-day circulation test at the Fenton Hill Geothermal Energy Site, New Mexico.

INTRODUCTION

The original concept for HDR geothermal energy production involved propagation of a massive hydraulic fracture to facilitate full hydraulic connection with a secondarily introduced borehole. This concept spawned a number of conceptual models to allow evaluation of thermal drawdown within the hydraulically closed system for single (Gringarten and Sauty, 1975) and multiple fractures (Gringarten and Witherspoon, 1973. Gringarten et al., 1975). Recent attempts to stimulate HDR reservoirs have resulted in inflation of a voluminous and roughly equidimensional region through which complex flow paths penetrate (Baria et al., 1987; Fehler, 1987). The equiaxed form of this zone of permeability enhancement may be discerned from both the passive seismic record and the results of tracer testing (Robinson and Tester, 1984).

The following suggests a conceptual model to represent the thermal drawdown behaviour of a spherical stimulated zone embedded within impermeable host rock.

CONCEPTUAL MODEL

A schematic of the reservoir model is illustrated for free surface and insulated caprock conditions in Figures 1 and 2, respectively. Thermal energy is withdrawn from the system through circulation of fluid within a spherical and hydraulically closed zone of radius, a. The secondary porosity of this zone is assumed constant and of magnitude, ϕ, with the external medium returning zero secondary porosity. Fluid is circulated at constant volumetric flow rate, q_F, with a prescribed injection temperature T_{F_i} and unknown outlet temperature $T_{F_o}(t)$. The following assumptions are germane to the model:

1. All spatial, temporal, and material parameters are assumed constant with time excepting the outlet fluid temperature, $T_{F_o}(t)$.

2. Fluid temperature within the stimulated zone is prescribed as uniform and of magnitude T_{F_o}, neglecting any spatial dependence. This condition requires that the blocks comprising the stimulated zone remain in thermal equilibrium with the circulating fluid; a condition that is justified as block size, and therefore thermal diffusion length, is reduced.

3. Thermal transport within the spherical stimulated zone is by forced convection and in the surrounding medium by pure conduction.

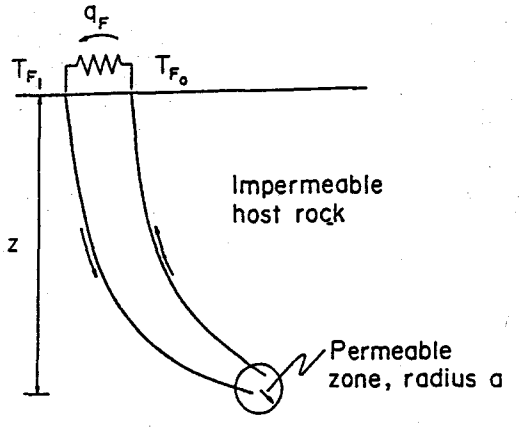

Figure 1. Circulation geometry for constant surface temperature HDR model

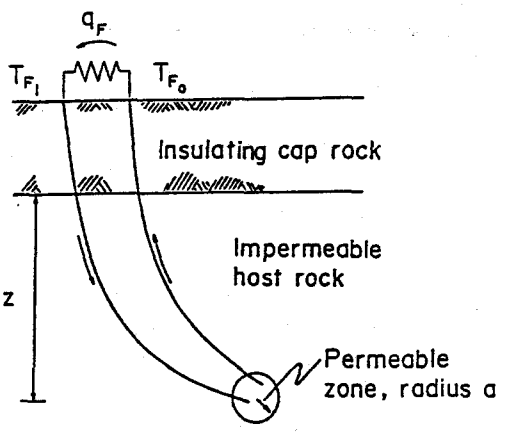

Figure 2. Circulation geometry for insulated caprock HDR geothermal reservoir model

ENERGY BALANCE

An energy balance relationship may be defined for the production zone. Thermal energy is withdrawn from the system by uniform drawdown within the spherical reservoir. This drawdown in turn stimulates a conductive heat flux, $q_T(a,t)$, from the surrounding rock where equivalence is maintained on the periphery of the spherical zone between the temperatures of the circulating fluid (T_{F_o}) and the external rock medium. In this manner, the energy balance equation may be stated as

$$q_T(a,t) = q_F\rho_F c_F(T_{F_o}(t) - T_{F_i}) + \frac{4}{3}\pi a^3 \rho_S c_S \frac{\partial T_{F_o}(t)}{\partial t} \qquad (1)$$

where, the three component terms, from left to right, represent: (i) the conductive heat flux supplied from the external host rock; (ii) the thermal flux removed from the system through forced convection; and (iii) the thermal inertia of the system. The heat capacity of the fluid is incorporated as $\rho_F c_F$ and the aggregated heat capacity of the fluid saturated reservoir zone is given as $\rho_S c_S=(1-\phi)\rho_R c_R+\phi\rho_F c_F$ where $\rho_R c_R$ is the heat capacity of the rock.

Initial conditions are applied to equation (1) where the system is initially at rest and the temperature distribution is prescribed by the geothermal gradient, T_R. At the initiation of thermal drawdown, heat flux to the reservoir volume is stimulated through $q_T(a,t)$. The magnitude of this flux is determined directly from solution of the spherically symmetric intial value problem for conductive heat flow to a spherical source (eg. Carslaw and Jaeger, 1959). With this final component, equation (1) may be solved to represent thermal recovery from a spherical reservoir within an infinite medium. Image theory is used to approximately represent the behaviour of a semi-infinite host medium for the constant surface temperature and zero flux conditions represented by Figures 1 and 2, respectively. Linear superposition in time, through Duhamel's theorem, is used to formally evaluate equation (1) for the inifinite and semi-infinite cases. The interested reader is referred to Elsworth, (1989), for further information regarding transient solution.

COMPUTATIONAL RESULTS

The transient thermal production behaviour is uniquely represented by five dimensionless parameters, namely:

$$T_D=\frac{(T_{F_i}-T_{F_o})}{(T_{F_i}-T_R)} \qquad (2a)$$

$$Q_D=\frac{q_F\rho_F c_F}{K_R a} \qquad (2b)$$

$$\Phi_D=\frac{\rho_S c_S}{\rho_R c_R} \qquad (2c)$$

$$t_D=\frac{K_R t}{\rho_R c_R a^2} \qquad (2d)$$

and

$$a/z \qquad (2e)$$

where K_R is the thermal conductivity of the intact rock surrounding the reservoir and z is the depth of the reservoir below the surface or insulating caprock as illustrated in Figures 1 and 2. The controlling parameters are therefore dimensionless output temperature (T_D), dimensionless circulation rate (Q_D), dimensionless thermal porosity (Φ_D). dimensionless time (t_D), and dimensionless depth ratio (a/z).

As a specialization of the general transient result, the steady long term behaviour is given by

$$T_D=\left[1+\frac{1}{4\pi}Q_D\left(1\pm\frac{a}{2z}\right)\right]^{-1} \qquad (2)$$

where the positive and negative signatures applied against the dimensionless depth ratio refer to cases of zero flux and constant (with time) temperature constraints on the surface of the half-space, respectively. This suggests that thermal supply from the exterior, by conduction, is most significant for small circulation rates, Q_D. This intuitive result is reinforced by the significant magnitude of the dimensionless temperatures that may be recovered. As $Q_D\rightarrow 0$, no thermal drawdown is experienced, and hence thermal recovery remains finite even as $t_D\rightarrow\infty$. This result is important for geothermal energy production schemes operating under low circulation rates since thermal recovery magnitudes are guaranteed. For production at larger circulation rates, knowledge of the transient thermal drawdown is important in predicting useful lifetimes.

TRANSIENT BEHAVIOUR

Of prime interest in determining the projected longevity of energy production is knowledge of the reduction in reservoir production temperature, T_D, as a function of dimensionless time, t_D, for different production rates, Q_D. The results are represented most compactly if thermal drawdown (T_D) is represented as a function of the product t_DQ_D. This method of compressing the time dimension is used throughout the following.

Thermal histories are most markedely sensitive to variations in the circulation rate, Q_D and less sensitive to the thermal porosity, Φ_D, which is sensibly restricted to a relatively narrow band of variation. For igneous rocks, the thermal porosity term Φ_D will always be greater than unity. Physical constants representative of granite as the host and water as the percolating fluid impart $\Phi_D\cong 1.1$ for an unrealistically high secondary porosity of 10%. As secondary porosity is reduced ($\phi\rightarrow 0$), the dimensionless reservoir porosity term approaches

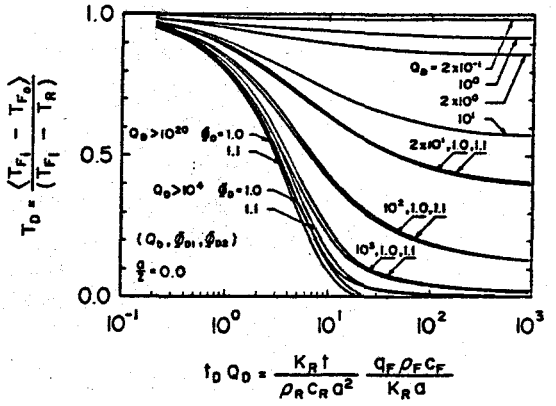

Figure 3. Thermal drawdown histories for a reservoir within an infinite host medium. Thermal porosities (Φ_D) of 1.0 and 1.1.

unity. A suitable range for the reservoir porosity parameter would therefore appear to be $1.0\leq Q_D\leq 1.1$.

Results for temperature histories in an infinite medium (a/z=0) are reported in Figure 3. As a natural consequence, the solution exhibits uniform rock temperature at the periphery of the permeable zone. It is apparent that thermal history is sensitive to Φ_D only for large dimensionless throughputs Q_D. For $Q_D<10^1$ the results are indistinguishable for the two thermal porositites Φ_D of 1.0 and 1.1. Even for large Q_D values the discrepancy appears insignificant. The sense of the modification to the thermal histories suggests that increased porosities slightly forestall thermal depletion. As evidenced in equation (3) and also in Figure 3, long-term (steady) withdrawal temperatures remain finite and, more importantly, significant for throughput values, Q_D less than 10^3.Depending on the threshold temperatures required to ensure efficient energy conversion, the productive life of the geothermal reservoir may remain unbounded.

For very large magnitudes of Q_D, a threshold behaviour is apparent. Figure 3 illustrates the predicted temperature as $Q_D\rightarrow\infty$. This behaviour corresponds to high circulation rates where the thermal supply from the surrounding rock becomes negligible. In this instance, solution of equation (1) with $q_T(a,t)=0$ becomes $T_D=\exp\left[-3t_DQ_D/4\pi\right]$ resulting in the limiting curvature of Figure 3 for $Q_D=10^{20}$. Physically, the limiting behaviour corresponds to thermal drawdown in a sphere of radius a, embedded within an insulating medium. The total thermal energy extracted at full depletion is given by the product of sphere volume, specific heat capacity of that volume and

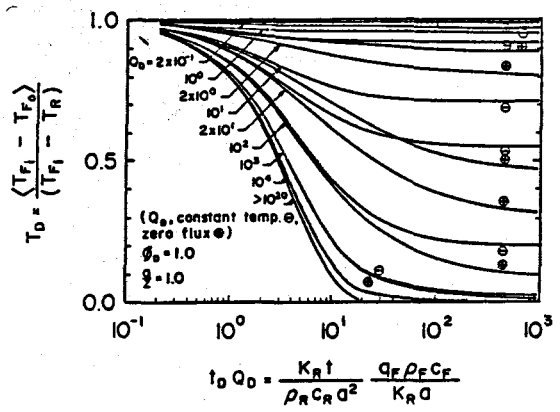

Figure 4. Thermal drawdown histories for a reservoir within a semi-infinite host medium. Depth ratio a/z=1.0. Positive and negative demarcations represent insulating caprock and constant surface temperature constraints, respectively.

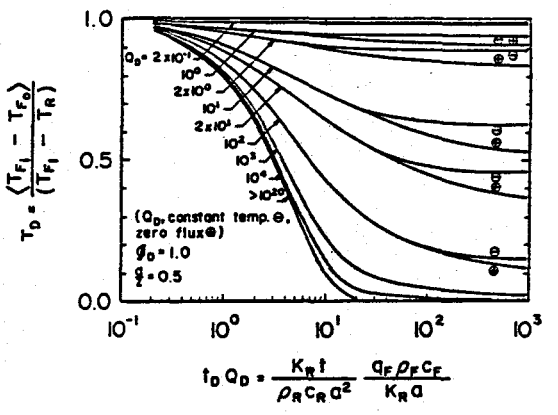

Figure 5. Thermal drawdown histories for a reservoir within a semi-infinite host medium. Depth ratio (a/z)=0.5. Positive and negative demarcations represent insulating caprock and constant surface temperature constraints, respectively

temperature change. For fixed thermal diffusivities of the host medium, together with a constant reservoir dimension, a, the thermal histories are moved laterally (earlier) in real time by one order of magnitude for every increase in real circulation rate (q_F) of one order of magnitude. Thus, as anticipated, the energy production rate is directly conditioned by the circulation rate through the system. Intuitively, minimal thermal depletion is evident in Figure 3 for small flow rates q_F or large reservoir diameters as evidenced by small values of dimensionless throughput Q_D.

The thermal response of semi-infinite systems are bounded, in the most extreme case, by a depth ratio, a/z, of unity. Although results are physically meaningless for the instance of a constant temperature surface, comparisons are useful since thermal histories bound candidate responses for all depth ratios between unity and zero. Semi-infinite responses are illustrated in Figure 4 for a depth ratio of unity. The influence of an insulated surface is to reduce the ultimate steady outlet temperature T_D over that of the infinite case. This result appears reasonable since a reduced volume, and hence thermal reservoir, is available for depletion in the semi-infinite case. Conversely, the presence of a surface retained at constant (ambient) temperature elicits a more favourable (hotter) thermal response to that of the inifnite case. The influence of boundaries is only significant for intermediate values of dimensionless throughput Q_D and even in these instances is only apparent at large dimensionless times $t_D Q_D$ The range $10^{-1}<Q_D<10^{3}$ brackets this boundary sensitive region. The branching of thermal histories occurs earlier in dimensionless time with decreasing throughput Q_D.

Thermal responses for depth ratios of one half are illustrated in Figure 5. Similar to the results for a/z=1, the influence of boundaries are only significant in the range $10^{-1}<Q_D<10^{3}$. As the reservoir depth a/z decreases to 10^{-1}, the results for bounded reservoirs are indistinguishable from the infinite case and may be correctly interpolated from Figure 3.

From knowledge of thermal response, depletion times may be directly determined to aid in defining useful lifetimes of individual reservoir configurations. Ultimate withdrawal temperatures may be determined from equation (3). The time required for the outlet temperature to reach fifty per cent and ninety-five per cent of the steady temperature values are defined as $t_D{}^{50}Q_D$ and $t_D{}^{95}Q_D$, respectively. These results are illustrated in Figure 6 for the limiting cases of bounded and infinite reservoir geometries for all significant values of Q_D. Reservoirs bounded by a constant temperature surface deplete more rapidly than either insulated or infinite geometries. This behaviour is most marked in the very long-term performance as evidenced by the $t_D{}^{95}Q_D$ parameter.

FENTON HILL HDR RESERVOIR

Comparison is possible between predictions elicited from the thermal recovery model and results from a 300-day circulation test conducted at the Fenton Hill experimental reservoir in New Mexico. Results are reported from Run Segment 5 of Experiment 217 in Zyvoloski et al. (1981), where long-term circulation was induced between the injection level at 2903 m and withdrawal level at 2708 m below surface. The known separation of the

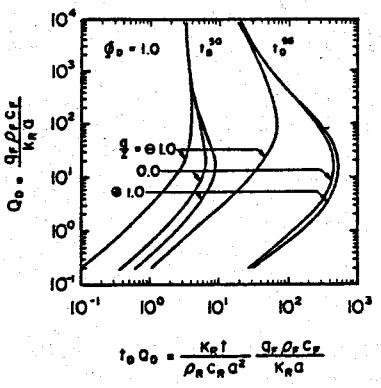

Figure 6. Variation is 50 percent and 95 percent depletion times with dimensionless throughput Q_D for thermal porosity Φ_D=1.0. Results for insulating caprock (+) and constant surface temperature (−) conditions.

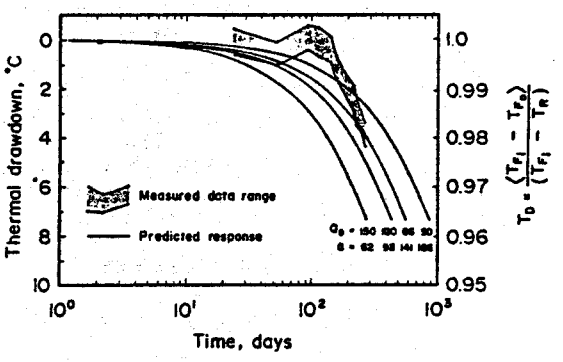

Figure 7. Measured and predicted responses of the Fenton Hill Geothermal Reservoir during a 300-day circulation test.

injection and withdrawal points together with available seismic data suggest a permeable zone or reservoir diameter of the order of 200 m. The single undefined input parameter is the dimension of the permeable zone. An estimated radius of a=100 m yields a dimensionless throughput of Q=93 for known flow rates and reasonable reservoir parameters. Predicted thermal drawdowns are reported in Figure 7 in real time for dimensionless throughputs spanning 50 to 150. These magnitudes correspond to reservoir radii of 186 m to 62 m and show some correspondence with the data recovered from the 300-day circulation test. This correspondence is encouraging given the reasonableness of the physical parameters utilized in the comparison, however, the test duration is too brief to yield a conclusive comparison. Furthermore, the initial response is most strongly conditioned by thermal depletion of the immediate permeable zone. Only later in the drawdown history will the influence of external heat supply from around the spherical zone become apparent.

If, from the data of Figure 7, a dimensionless throughput (Q_D) of 100 is assumed reasonable for this physical system, the full thermal drawdown history may be determined directly from Figure 3. The dimensionless time axis ($t_D Q_D$) may be converted to real time by requiring that a=100 m. The time axis then spans from 10^2 days (0.27 years) on the left hand side to 10^6 days (2,740 years) on the right hand side allowing the full thermal depletion history, and consquently the productive lifetime and output during this lifetime, to be projected. As noted previously, the thermal productivity of the reservoir remains unbounded in time as a result of the external heat supply.

CONCLUSIONS

A simple conceptual model is proposed to represent the thermal performance of HDR geothermal energy systems where thermal energy is supplied from the surrounding medium. Behaviour is shown to be insensitive to the proximity of thermal barriers (as evidenced through a/z) and the magnitude of the secondary porosity (as evidenced through Φ_D). Although the magnitude of thermal porosity exerts little influence on thermal recovery, it would be expected to strongly influence pumping costs required to maintain any given circulation rate, q_F. Small increases in Φ_D may disproportionately increase circulation rates and, thereby, increase the appropriate magnitude of dimensionless throughput, Q_D.

Significant steady heat production rates are estabilshed for all dimensionless throughputs (Q_D) greater than 10^3. The long-term dimensionless temperature (T_D) is indexed through the dimensionless variables of throughput Q_D and depth ratio, a/z, only. Higher steady production temperatures are recovered for low circulation rates q_F or large reservoir radii, a.

The condition corresponding to zero external heat supply from the surrounding rock medium is represented by the response as $Q_D \rightarrow \infty$. Physically, this condition corresponds to extremely high circulation rates, q_F, or small reservoir radii, a. This bounding behaviour describes, in terms of dimensionless time ($t_D Q_D$), the maximum rate at which thermal depletion may occur. This threshold state is

indexed directly to dimensionless throughput Q_D and is apparent for $Q_D > 10^3$.

Large radii or low circulation rate systems exhibit the most desirable thermal behaviour in the long-term. This response is further conditioned, however, by the flow impedence characteristics of the stimulated zone and cannot, therefore, be viewed in isolation.

ACKNOWLEDGEMENTS

The foregoing represents partial results of work supported by the National Science Foundation under Grant No. MSM-8708976. The assistance of Steven Birdsell, Michael Fehler, and Bruce Robinson, of Los Alamos National Laboratory, in providing data from the Fenton Hill reservoir is gratefully acknowledged.

REFERENCES

Baria, R., A.S.P. Green, and R.H. Jones, (1987) "Anomalous Seismic Events Observed at the CSM HDR Project", Proceedings International Workshop on Forced Fluid Flow through Strong Fractured Rock Masses, Commission of European Communities, EUR 11164/1, April, pp. 321-336.

Carslaw, H.S. and J.C. Jaeger, (1959) "Conduction of Heat in Solids," 2nd edition. Clarendon, Oxford.

Elsworth, D. (1989) "Theory of Thermal Recovery from a Spherically Stimulated HDR Reservoir," J. Geophys. Res., in press.

Gringarten, A.C. and P.A. Witherspoon (1973 "Extraction of Heat from Multiple Fractured Hot Dry Rock," Geothermics, 2(3/4), pp. 119-122.

Gringarten, A.C., P.A. Witherspoon, and Y Ohnishi (1975) "Theory of Heat Extraction from Hot Dry Rock," J. Geophys. Res, 80(8), pp. 1120-1124.

Gringarten, A.C. and J.P. Sauty (1975) "A Theoretical Study of Heat Extraction from Aquifers with Uniform Regional Flow," J. Geophys. Res., 80(35), pp. 6956-6962.

Robinson, B.A. and J.W. Tester (1984) "Dispersed Fluid Flow in Fractured Reservoirs: An Analysis of Tracer-Determined Residence Time Distributions," J. Geophys. Res., 89(B12), 10, pp. 374-384.

Zyvoloski, G.A. et al. (1981) "Evaluation of the Second Hot Dry Rock Geothermal Reservoir: Results of Phase I, Run Segment 3," Los Alamos Scientific Laboratory, LA-8940-HDR, 94 pages.

PROCEEDINGS, Fourteenth Workshop on Geothermal Reservoir Engineering
Stanford University, Stanford, California, January 24-26, 1989
SGP-TR-122

A Combined Heat Transfer and Quartz Dissolution/Deposition Model For a Hot Dry Rock Geothermal Reservoir

Bruce A. Robinson and John Pendergrass

Earth and Space Sciences Division
Los Alamos National Laboratory
Los Alamos, NM 87545

ABSTRACT

A kinetic model of silica transport has been coupled to a heat transfer model for a Hot Dry Rock (HDR) geothermal reservoir to examine the effect of silica rock-water interactions on fracture aperture and permeability. The model accounts for both the dissolution and deposition of silica. Zones of local dissolution and deposition were predicted, but their effect on aperture and permeability were fairly small for all cases studied. Initial rock temperature, reservoir size, and the ratio of rock surface area to fluid volume have the largest effect on the magnitude of silica mass transfered between the liquid and solid phases.

INTRODUCTION

Dissolution and deposition processes can have a large impact on plant operations and reservoir performance in both Hot Dry Rock (HDR) geothermal reservoirs and conventional geothermal systems undergoing fluid reinjection. For example, the deposition of dissolved silica in surface equipment and the injection wellbore is a well-known phenomenon which adversely affects plant operations (Cuellar, 1975, Bohlman et al., 1981, Rothbaum and Anderton, 1975, and Gudmundsson and Bott, 1979). Also, dissolution and deposition in the reservoir can affect the permeability by decreasing or increasing the flow path size (Rimstidt and Barnes, 1980, Horne, 1982, Robinson, 1982). For example, Horne (1982) reported that the problem of decreasing permeability near reinjection wells at the Hatchobaru and Otake geothermal fields in Japan may be caused by silica deposition.

Rock-water interactions in geothermal reservoirs are complex processes in which the mineralogy of the solid phase, chemical content of the fluid, and temperature all affect the behavior of the system. Nonetheless, simplified mathematical expressions have been proposed for certain minerals such as quartz. The behavior of quartz is among the most important in geothermal reservoirs because of the potential for large quantities of material to be dissolved or precipitated.

It is essential to combine a rock-water interaction model with a heat transfer model because of the strong dependence of temperature on quartz dissolution and deposition. Heat extraction from a HDR reservoir creates a thermal cooling front which is initially located near the injection wellbore and progresses with time toward the production wellbore. The produced fluids are reinjected without removal of dissolved silica. Thus, a driving force exists for deposition of silica on the cool rock near the injection wellbore, while a driving force exists for dissolution of the hot rock at distances beyond where the thermal effects of reinjection are felt. Since the temperature field within the reservoir is constantly changing due to heat extraction, the location in the reservoir where dissolution and deposition occur will change with time. The effect of these phenomena on permeability can be estimated by assuming that for flow through a fractured medium, dissolution or deposition of quartz results in a widening or narrowing of the fracture aperture. The magnitude of the aperture change is in turn related to the change in permeability through a relationship such as the cubic law.

In the present study, we present a model which couples a rate law for quartz dissolution and deposition to a HDR reservoir heat transfer model. The model is used to predict the rate of quartz dissolution and deposition in the reservoir and the effect of these rock-water interactions on the flow geometry and permeability within the reservoir.

MODEL DEVELOPMENT

Rock-Water Interaction Model. In a HDR geothermal reservoir, the produced fluid is reinjected after extracting the heat in a heat exchanger. The mass balance for dissolved silica in a closed-loop recirculating system is shown in Figure 1. Since some water loss to the host rock is always experienced, make-up fluid is added to the injection fluid to achieve a constant production flow rate. Therefore, the injection concentration C_{in} is

$$C_{in} = f_m C_m + (1-f_m)C_p \qquad (1)$$

where f_m is the make-up fluid flow fraction (typically 0.1-0.2), C_m is the make-up fluid

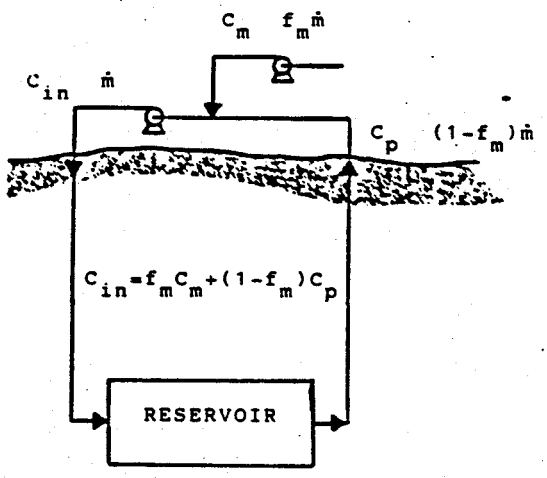

Figure 1. Mass balance on dissolved silica in a closed-loop HDR reservoir.

concentration, and C_p is the production fluid concentration. In practice, $C_m < C_p$, so that the production fluid is diluted with make-up fluid before reinjection.

The outlet concentration C_p is controlled by dissolution and deposition processes occurring in the reservoir. A commonly used rate law for quartz dissolution or deposition in a batch reactor is

$$\frac{dC}{dt} = ka^*(C^\infty - C) \qquad (2)$$

where t is time, a^* is the surface area to fluid volume ratio, k is the rate constant for quartz dissolution/deposition, and C^∞ is the saturation or equilibrium concentration of quartz in water. The temperature dependence of the equilibrium concentration was obtained by Rimstidt and Barnes (1980):

$$C^\infty = 6\times10^4 \times 10^{(1.881-2.028\times10^{-3}T-1560/T)} \qquad (3)$$

where T is the temperature in K and C^∞ has units of parts per million (ppm) as SiO_2.

The temperature dependence of dissolution rate constant k was determined by Robinson (1982) to be

$$k = 10^{(0.433-4090/T)} \qquad (4)$$

where the units of k are m/s. Finally, since fluid flow in HDR reservoirs occurs within fractures, a relationship for a^* is obtained by assuming the fracture can approximated by the parallel flat plate model:

$$a^* = \frac{2f_q}{w} \qquad (5)$$

In Eqn. (5), w is the mean fracture aperture and f_q is the fraction of quartz in the rock.

For modeling purposes, we assume that the fluid travels in plug flow between the wellbores, although in reality a distribution of solute residence times is always observed. For this parametric study, which is designed to evaluate the importance of dissolution and deposition processes, this assumption will not affect the results. For plug flow, dt = dx/u, and Eqn. (2) becomes

$$\frac{dC}{dx} = \frac{ka^*}{u}(C^\infty - C) \qquad (6)$$

To place this equation in terms of variables which can be measured directly, we make the substitution $u = \dot{m}L/V_f\rho_l$, where $\dot{m}$ is the fluid mass flow rate, L is the reservoir length, V_f is the reservoir fluid volume, and ρ_l is the density of water. Then, Eqn. (6) becomes

$$\frac{\partial C}{\partial x} = \frac{V_f\rho_l ka^*(C^\infty - C)}{\dot{m}L} \qquad (7)$$

This equation, coupled to the heat transfer model described below, is solved using finite difference techniques to obtain the steady state concentration as a function of position. Each time the temperature pattern is recalculated, a new steady state concentration profile is determined.

In addition to computing the concentration profile within the reservoir at various times, it is informative to examine the cumulative mass of silica dissolved from or deposited on the rock surfaces at each position in the reservoir. For a given time interval Δt, the mass of silica dissolved or deposited per unit length of reservoir m_q is given by

$$m_q = \frac{10^{-6}\rho_l \Delta t V_f ka^*(C^\infty - C)}{L} \qquad (8)$$

The quantity of silica dissolved or deposited can be related to the fractional change in the average fracture aperture by assuming a fracture flow geometry. Figure 2 shows the assumed geometry for both the rock-water interactions and the heat transfer model. Fluid flows along a series of parallel fractures of equal aperture w and fracture spacing S, with each fracture accepting the same flow rate. For the timestep Δt, the fractional aperture change Δw, which is equal to the volume change of quartz divided by the fluid volume, is

$$\Delta w = \frac{-Lm_q}{\rho_q V_f} = \frac{-LSm_q}{\rho_q w V_r} \qquad (9)$$

where ρ_q is the density of quartz and V_r is the total reservoir rock volume.

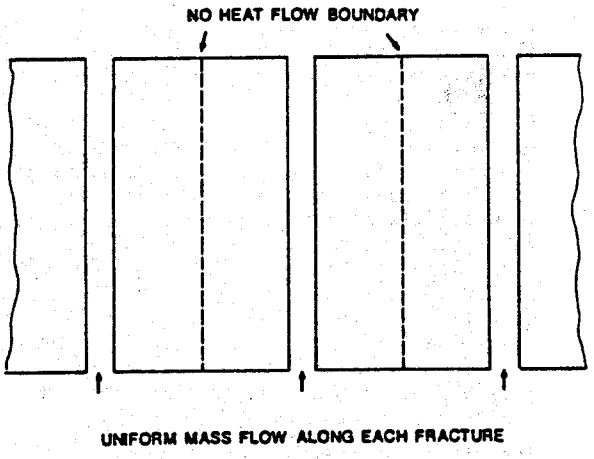

Figure 2. Fracture geometry for the heat transfer model.

Heat Transfer Model. The heat transfer model, based on the schematic diagram of Figure 2, was first treated analytically by Gringarten et al. (1975) for constant flow rate and inlet temperature. In the rock, the one-dimensional transient heat flow equation

$$\frac{\partial T}{\partial t} = \alpha \frac{\partial^2 T}{\partial x^2} \qquad (10)$$

is coupled to an energy balance equating convection in the fluid to conduction in the rock at the interface, which in terms of the variables used above, is:

$$\frac{\partial T}{\partial x} = \frac{LS\dot{m}c_f}{2k_r V_r} \frac{\partial T}{\partial y} \qquad (11)$$

In these equations, α is the rock thermal diffusivity, c_f is the fluid heat capacity, and k_r is the rock thermal conductivity. Due to symmetry, the boundary condition in the rock is a no-heat flow condition at the center of the rock block. To simulate time-varying flow rate and inlet temperature conditions, the model was solved by finite difference techniques. The model was verified by comparison to the solution of Gringarten et al. (1975) for constant flow rate and inlet temperature.

Figure 3 shows the internal temperature profiles at different times during heat extraction for different values of the fracture spacing S. For small S, the thermal wave passes through the reservoir as a sharp front. This extreme is sometimes referred to as volumetric heat extraction, since almost all of the heat within the rock volume is extracted. For large S, the front is more diffuse and significant temperature gradients remain within the rock blocks.

MODEL RESULTS

Figures 4a, b, and c demonstrate the behavior of the model for a typical set of reservoir

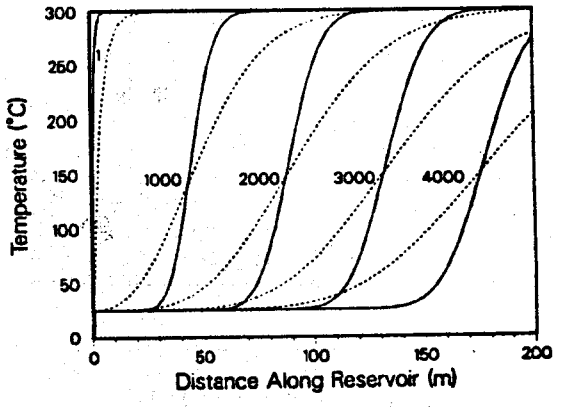

Figure 3. Temperature profiles at different times (in days) during long-term operation. Solid curves: S=2m, Dashed curves: S=10m.

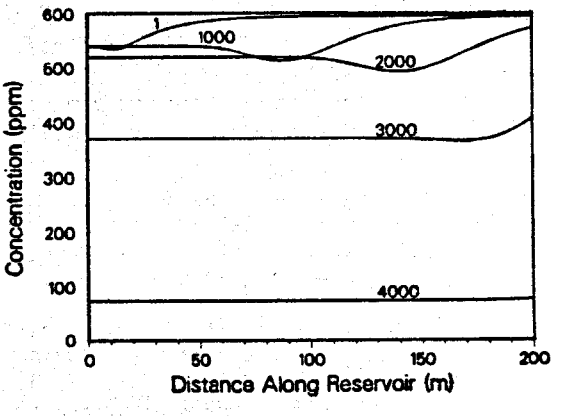

Figure 4a. Concentration profiles (time in days).

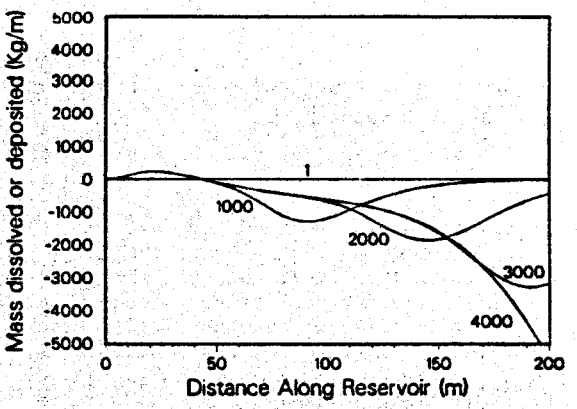

Figure 4b. Mass transfer profiles (time in days).

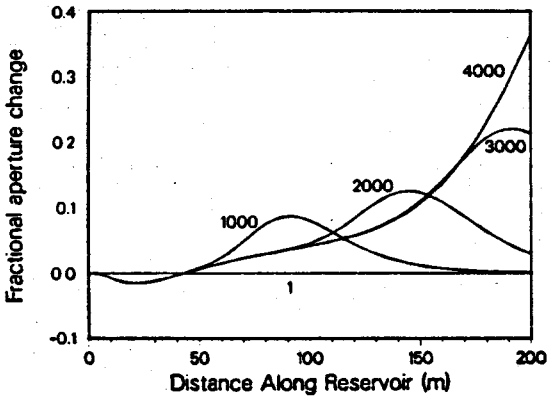

Figure 4c. Fractional aperture change profiles (time in days).

Figure 4. Internal profiles during long-term operation (time in days). T_r=300°C, S=10m, V_f=1.3x10^{8}m^3, $\dot{m}$=15kg/s, f_m=0.1, L=200m.

conditions (T_r=300°C, S=10m, V_f=1300m^3, $\dot{m}$=15kg/s, V_r=1.3x10^{8}m^3, f_m=0.1, and L=200m). Figure 4a shows the computed silica concentration profiles at different times during heat extraction. The fluid enters the reservoir supersaturated ($C>C^\infty$) due to cooling near the injection well, creating a driving force for deposition. The position of the thermal front dictates the location of the deposition. Although the largest driving force for deposition exists in the coolest region of the reservoir (near the inlet), the rate constant k is too small for significant deposition to occur. Deposition occurs in the transition region of rising temperature with distance, and the thermal wave is accompanied by a deposition front. When the fluid reaches the hotter portions of reservoir, deposition ceases and dissolution begins, resulting in an increase of dissolved silica, in this case to a maximum value of C^∞.

Dissolution and deposition result in residual silica depletion or buildup along the flowpath over time. Figure 4b shows the mass of silica dissolved or deposited per unit length of reservoir, and Figure 4c is the corresponding fractional aperture change. The amount of dissolution or deposition is controlled by the fraction of fresh make-up fluid in the injection fluid. For example, if f_m=1, the quantity of dissolved silica would be much greater, while if f_m=0 the net amount of silica removed from the reservoir would be zero. Deposition leaves a small zone of decreased aperture near the injection wellbore, but the magnitude of the change is small. Dissolution creates a larger zone of increased aperture and permeability which travels with the thermal wave. However, this zone is localized, rather than present across the entire reservoir. Therefore, the overall flow impedance, or pressure drop per unit flow rate, is unlikely to be much improved.

Figure 5 shows the effect of the mean fracture spacing S on the fractional aperture change after 2,000 days of operation. Small fracture spacings result in a sharp thermal front and more localized zone of dissolution and deposition. Thus, dissolution in a reservoir with larger fracture spacings results in a different residual pattern of the aperture profile. However, in all cases the effect on the permeability will be somewhat mitigated by the fact that significant portions of the reservoir remain at the initial aperture, unaffected by dissolution or deposition.

The effect of initial rock temperature on the dissolution and deposition processes is examined in Figure 6. Higher temperatures increase both the reaction rate and the magnitude of the changes possible from equilibrium considerations. Thus the changes in aperture are more pronounced at higher temperatures.

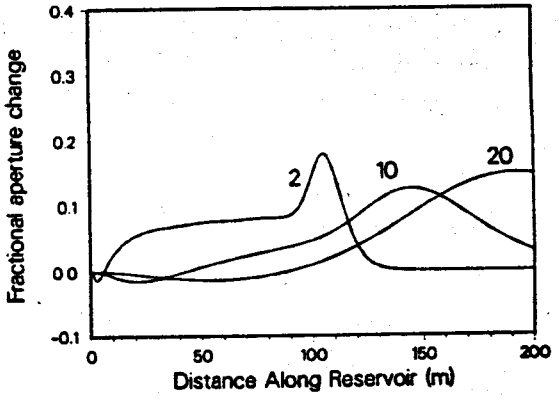

Figure 5. Fractional aperture change profiles for different fracture spacings S (after 2000 days).

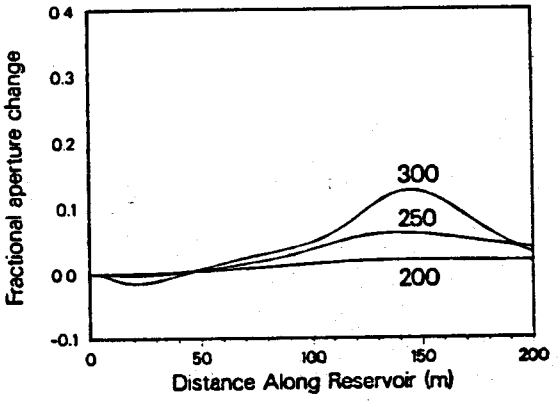

Figure 6. Fractional aperture change profiles for different initial rock temperatures T_r (after 2000 days).

DISCUSSION

Whenever a solution is undersaturated or supersaturated, the potential exists for dissolution or deposition. However, the amount of material exchanged between the solid and liquid phases depends on the kinetics of the reactions. In all cases examined, the deposition kinetics were such that a zone of decreased aperture was left near the injection wellbore. However, the effect on the crack width and permeability was found to be small. The zone of increased aperture and permeability due to dissolution was usually localized within a fraction of the reservoir length. Thus the effect on the overall flow impedance is also likely to be small.

In the silica mass balance model assumed (Eqn. (1)), it is assumed that heat is extracted without flashing the brine. In energy conversion schemes in which the brine is flashed, the reinjected liquid has a much higher concentration of all dissolved species, including silica. Thus, the potential exists for more severe deposition near the injection wellbore. One advantage of the binary cycle energy conversion schemes usually proposed for HDR reservoirs is that deposition problems are minimized by keeping the brine liquid.

When assessing the effect of rock-water interactions on permeability, we must recognize that other effects will occur simultaneously to either enhance or negate the effects of dissolution and deposition. First, thermal stress cracking of the rock is thought to occur near the injection well (Tester et al., 1986), increasing the permeability and competing with the effect of deposition. Also, pressures are highest near the injection wellbore, which, according to current theories of flow through fractured rocks, cause the fractures to dilate and the permeability to increase (Brown and Fehler, 1989). Finally, the effect of dissolution on the aperture and permeability will depend on the location of the quartz grains relative to the asperities upon which the fracture faces rest. In fact, if the asperities are largely quartz, dissolution would cause the fracture faces to collapse on each other, lowering the aperture and permeability. Clearly, when estimating the effect of rock-water interactions on the permeability of a HDR reservoir, these phenomena must be considered. However, they are beyond the scope of this study.

Another area in which further study is warranted is in the form of the rate law used to describe quartz dissolution and deposition. In the present study, a single rate equation with a common rate constant was assumed to model both dissolution and deposition. Although Rimstidt and Barnes (1980) claim that the reaction is reversible and Eqn. (2) is valid, some studies have stated that in the temperatures of interest for HDR reservoirs, the deposition of silica is controlled by amorphous silica rather than quartz (e.g. White et al., 1956). Others have noted the possibility of both homogeneous and heterogeneous nucleation mechanisms for silica precipitation (Gudmundsson and Bott, 1979). Finally, Makrides et al. (1978), and Marsh et al. (1975) examined the effect of pH on the reaction kinetics. However, other than the model of Rimstidt and Barnes (1980), no comprehensive model of quartz dissolution and silica deposition has been proposed which includes the temperature dependence of the reactions. Therefore, Eqn. (2) was used in the present study. Future work should incorporate more complex laws for quartz dissolution and deposition when they become available.

CONCLUSIONS

A quartz dissolution/deposition kinetic model has been coupled to a heat transfer model to examine the silica rock-water interactions occurring in a HDR geothermal reservoir. The temperature dependence of the reaction rates makes modeling of the temperature pattern within the reservoir essential. Near the injection well, where temperatures are lovest, the fluid is supersaturated with respect to dissolved silica, and a driving force exists for deposition. However, under all conditions studied, the computed deposition rate was insufficient to cause significant decreases in the fracture aperture near the injection well. Dissolution occurs in the hotter portions of the reservoir, but its effects are usually localized: only a fraction of the total flow system experiences an increase in fracture aperture. Thus, permeability enhancement due to dissolution will probably be small.

In future studies, these model results should be compared to the results of calculations of thermal stress cracking and pressure dependent dilation of joints to assess the relative importance of rock-water interactions. Furthermore, when available, rate laws incorporating the effect of pH and different silica phases such as amorphous silica should be coupled to the heat transfer model to refine the results presented here.

NOMENCLATURE

a^*	surface area to fluid volume ratio (m^{-1})
C	concentration (ppm)
c_f	heat capacity of the fluid (J/kg-K)
C_{in}	inlet silica concentration (ppm)
C_m	make-up fluid silica concentration (ppm)
C_p	production fluid silica concentration (ppm)
C^∞	equilibrium silica concentration (ppm)
f_m	make-up fluid flow fraction
f_q	fraction of quartz in the rock
k	reaction rate constant (m/s)
k_r	thermal conductivity of the rock (W/m-K)
L	reservoir length (m)
$\dot{m}$	fluid mass flow rate (kg/s)
m_q	mass of quartz dissolved or deposited per unit length of reservoir (Kg/m)
S	mean fracture spacing (m)

T	temperature (K)
T_r	initial rock temperature (K)
u	fluid velocity (m/s)
V_f	reservoir fluid volume (m^3)
V_r	reservoir rock volume (m^3)
w	mean fracture aperture (m)
x	flow path direction (m)
α	rock thermal diffusivity (m^2/s)
ρ_l	fluid density (kg/m^3)
ρ_q	quartz density (kg/m^3)

ACKNOWLEDGEMENTS

This work was performed under the auspices of the U.S. Department of Energy, Geothermal Technology Division. We thank S. Birdsell for reviewing this paper.

REFERENCES

Bohlman, E. G., Shor, A. J., Berlinski, P., and Mesmer, R. E., "Silica Scaling in Simulated Geothermal Brines," Oak Ridge National Laboratory Report No. TM-7681 (1981).

Brown, D. W., and Fehler, M. F., "The Pressure/Water-Loss Behavior of a Hydraulically Stimulated Region of Deep Naturally Jointed Crystalline Rock," presented at the 14th Workshop on Geothermal Reservoir Engineering, Stanford University, Stanford, CA (1989).

Cuellar, G., "Behavior of Silica in Geothermal Waste Waters," Second U.N. Symposium on the Development and Use of Geothermal Resources, San Francisco, CA (1975).

Gringarten, A. C., Witherspoon, P. A., and Ohnishi, Y., "Theory of Heat Extraction from Hot Dry Rock," J. Geophys. Res., 80, 1120-1124 (1975).

Gudmundsson, J. S., and Bott, T. R., "Deposition of Silica from Geothermal Waters on Heat Transfer Surfaces," Desalination, 28 (1979).

Horne, R. N., "Geothermal Reinjection Experience in Japan," Soc. Petrol. Eng. J., 495-503 (1982).

Makrides, A. C., et al., "Study of Silica Scaling From Geothermal Brines," U. S. Dept. of Energy Report Number COO-2607-5 (1978).

Marsh, A. R., Klein, G., and Vermeulen, T., "Polymerization Kinetics and Equilibria of Silicic Acid in Aqueous Systems," Laverence Berkeley Laboratory Report Number LBL-4415 (1975).

Rimstidt, J. D., and Barnes, H. L., "The Kinetics of Silica-Water Reactions," Geochim. et Cosmochim. Acta, 44, 1683-1699 (1980).

Robinson, B. A., "Quartz Dissolution and Silica Deposition in Hot Dry Rock Geothermal Systems," S. M. Thesis, MIT, Cambridge, MA (1982).

Rothbaum, H. P., and Anderton, B. H., "Removal of Silica and Arsenic from Geothermal Discharge Waters by Precipitation of Useful Calcium Silicates," Second U.N. Symposium on the Development and Use of Geothermal Resources, San Francisco, CA (1975).

Tester, J. W., Murphy, H. D., Grigsby, C. O., Potter, R. M., and Robinson, B. A., "Fractured Geothermal Energy Growth Induced By Heat Extraction," paper presented at the 56th SPE California Regional Meeting, Oakland, CA, SPE 15124, (1986).

White, D. E., Brannock, W. W., and Murata, K. J., "Silica in Hot-Spring Waters," Geochim. et Cosmochim. Acta, 10 (1956).

PROCEEDINGS, Fourteenth Workshop on Geothermal Reservoir Engineering
Stanford University, Stanford, California, January 24-26, 1989
SGP-TR-122

A DOWNHOLE PUMP TEST ON A 2 KM DEEP HOT DRY ROCK GEOTHERMAL SYSTEM

Nazroo M F and Bennett T S

Camborne School of Mines Geothermal Energy Project
Rosemanowes, Quarry, Herniss, Penryn, Cornwall, UK.

SUMMARY

During the continuing long-term circulation programme of the 2 km deep Hot Dry Rock (HDR) geothermal system at Camborne, a downhole pump was installed in the production well and used to investigate the effects of sub-hydrostatic pressure on reservoir performance. This condition is expected to occur naturally in a 6 km deep HDR reservoir.

Tracer test results showed a change in the flow distribution but no overall change in the effective circulating volume of the reservoir and this was confirmed by the unchanged thermal behaviour of the reservoir. Although the production flow rate did increase during the test the impedance was also increased and indicated that the increased effective stress acting on the joints close to the production well was causing them to close up.

INTRODUCTION

For the past eight years the Camborne School of Mines has been developing and investigating a Hot Dry Rock (HDR) geothermal system at a depth of 2 km in Cornish granite. The current system consists of three wells drilled to depths of between 2100 and 2600 m (Figure 1). The main circulating reservoir lies between Wells RH12, the injection well, and RH15, the production well. The third well, RH11, produces at a rate of only 2 to 3 l/s and is thought not to be well connected to the main reservoir.

Since 1985 the reservoir has been circulated continuously and a variety of tests have been carried out to evaluate its performance. At the end of 1986, in addition to continuing the characterisation studies of the existing reservoir, work was started on a detailed engineering assessment for the creation of a prototype commercial HDR system at a depth of 6 km in the Cornish granite.

One area of importance that was investigated was the behaviour of the system when the production well was operated under sub-hydrostatic conditions using a downhole pump (DHP). This allowed the effective stress conditions which would exist in a 6 km deep system being operated under normal circulation, to be simulated, and the performance of a reservoir with a well producing under sub-hydrostatic conditions to be investigated.

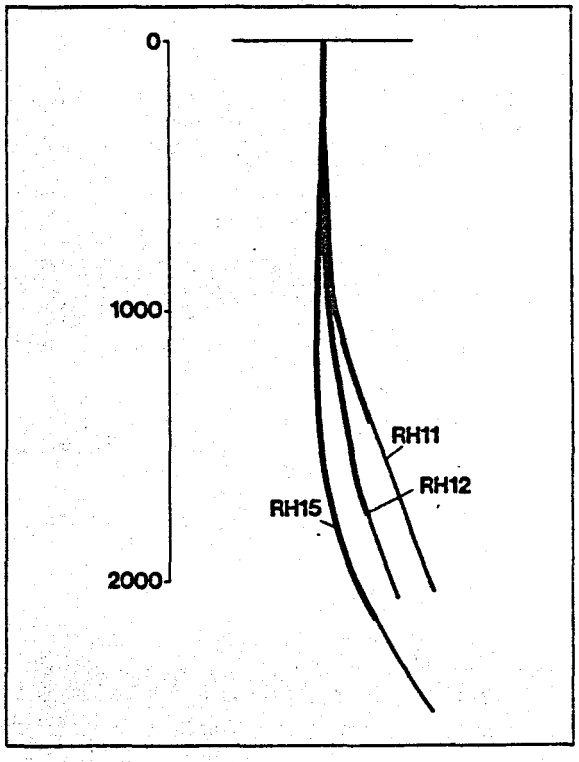

Figure 1 Well layout at the Camborne School of Mines HDR Project, Cornwall.

DESIGN

The major objective of the DHP test was to simulate partially the effective stress conditions which would be encountered when operating a deep system and to assess the effect these conditions would have on flow in the reservoir.

The effective normal stress across a vertical joint whose strike is aligned in the direction of the maximum principal stress is given by:

$$\sigma n' = \sigma h - Po$$

where: $\sigma n'$ = effective normal stress

σh = minimum principal horizontal stress

Po = hydrostatic pressure

The minimum earth stress at a depth of 6 km is predicted to be in the range 70-86 MPa. There are many uncertainties associated with this prediction as it is obtained by an extrapolation of data obtained at depths of up to 2.5 km. However, it is thought that the lower end of the stress range is the most likely (Pine and Kwakwa, 1988). If the production water is at a temperature of 220°C, the hydrostatic pressure at the bottom of the production well will be approximately 54 MPa, which is 6 MPa sub-hydrostatic, because of the lower density of the hot production water. This would be reduced to 4 MPa sub-hydrostatic if the well is pressurised to prevent the water flashing to steam in the wellbore. Therefore, the effective stress across joints orientated in the direction of the maximum principal stress at 6 km will be approximately 14 MPa. This compares with an effective stress under normal conditions of 10 MPa at a depth of 2 km.

By operating the DHP to give a drawdown head of approximately 4 MPa at a depth of 2km in the existing reservoir, it was possible to partially simulate the effective stress conditions in a 6 km deep system being operated without a DHP.

TEST PROCEDURE

The original intention was to deploy the DHP whilst the injection flow rate was 35 l/s, but this was changed when the flow rate had to be reduced to 22 l/s a few weeks before the start of the test, because the high flow rates had caused a large amount of microseismicity. As a result the test was run against a background of decreasing reservoir pressure and production flow rate.

Initially RH15 was drawn down by 4.5 MPa until a near steady state was achieved at which point two surface to surface, fluorescein tracer tests were run. The injection flow rate was then increased to 25 l/s and conditions were allowed to stabilise, so that a tracer test could be run with an unchanged drawdown on RH15. Following this the pump was put on its maximum production rate which resulted in a drawdown of 4.8 MPa and another tracer test was run. Finally, the pump was throttled back to produce a drawdown of 2.2 MPa and the last tracer test was carried out just before the pump was removed. The overall length of the experiment was 78 days.

RESULTS

HYDRAULIC DATA

Steady state data are presented in Table 1, and are those which describe the conditions under which the tracer tests were run. The changes in operating conditions during the DHP test are shown in Figure 2 along with the flow rates. The temperature data are shown in Figure 3.

DATE	08 AUG	14 SEP	06 OCT	13 OCT	23 OCT	11 NOV	13 DEC
RH12							
Wellhead pressure (MPa)	9.5	9.0	9.8	9.8	9.8	9.9	9.4
Flow rate (l/s)	21.7	21.7	25.2	25.3	25.4	25.4	22.8
RH15							
Wellhead pressure (MPa)	0.2	-4.5	-4.4	-4.6	-2.2	0.2	0.2
Flow rate (l/s)	15.2	16.4	17.9	18.3	16.8	15.5	14.9
Temperature (°C)	57.4	59.0	58.5	58.7	58.4	55.6	53.7
RH11							
Wellhead pressure (MPa)	0.2	0.2	0.2	0.2	0.2	0.2	0.2
Flow rate (l/s)	2.4*	2.1	2.3	2.3	2.4	2.5	2.3
Temperature (°C)	52.8	50.6	51.8	51.8	52.2	52.9	51.8
*Impedance (MPa/l/s)	0.61	0.82	0.79	0.79	0.72	0.63	0.61
Overall recovery (%)	81.1	85.3	80.2	81.4	75.6	70.9	78.2
RH15/RH12 recovery	70.0	75.6	71.8	72.3	66.4	61.8	67.7

* not steady-state
* Impedance = pressure drop between RH12 and RH15/RH15 production flow

Table 1 Steady state conditions

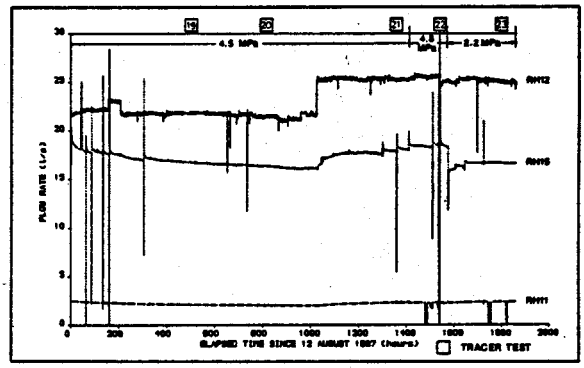

Figure 2 Flow rates, drawdown and tracer test during the downhole pump experiment.

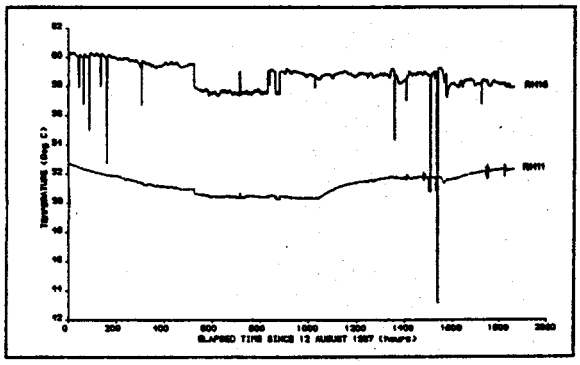

Figure 3 Wellhead temperatures during the downhole pump test.

The recovery (calculated as RH15 production flow divided by RH12 injection flow) at 21 l/s injection with a 4.5 MPa (460 m) drawdown, was 75% and was better than the recovery at the same flow rate in normal circulation, which was 69.5%.

During the period when the injection flow rate was 25 l/s, the drawdown in RH15 was initially kept at about 4.4 MPa (460 m) and then increased for a week to 4.6 MPa (480 m) before being decreased to 2.2 MPa (230 m). When the drawdown was 4.6 MPa the production flow rate was 18.3 l/s and the recovery 72%. With the drawdown reduced to 2.2 MPa, the production flow rate declined to 16.8 l/s and the recovery decreased to about 66%.

Analysis of the RH12 production logs indicated that the flow distribution before and after the pump test remained unchanged. No logging could be conducted on the production well during the test, but production logs were carried out before and after the test. These showed only small changes in percentage flow contributions from the various producing zones. The general trend of a 1°C per month thermal drawdown, which had been occurring throughout the previous year, continued during the DHP test, as confirmed in Figure 3. Note that in Figure 3 there is a sharp drop in temperature of 2°C, at 520 hours and a sharp rise of 2°C, at 840 hours. This is a result of a fault in the data acquisition system and is not a real change in temperature.

TRACER DATA

Tracer tests provided an important means of comparing the behaviour of the reservoir under normal circulating conditions with that under sub-hydrostatic conditions. A number of tracer tests, using the inert tracer sodium fluorescein, had been run throughout the circulating period prior to the test. These had been carried out during steady state conditions, and provided adequate data against which the DHP test tracer tests could be compared (CSM, 1986). The tracer tests are interpreted on the basis of plug flow in the wellbores and fractures, so that the highly dispersed nature of the tracer determined residence time distributions is attributed to variations in flow path lengths and flow rates within the reservoir.

Five tracer tests, each using 2 kg of sodium fluorescein, were conducted during the DHP test and a further two tracer tests were run after the pump had been removed. The results of the DHP tracer tests are summarised in Table 2 and an RTD curve for test no 20 is shown, along with those from the tests immediately preceding and following the DHP test, in Figure 4.

TEST NUMBER	19	20	21	22	23
Test start date	1 Sep	14 Sep	6 Oct	13 Oct	23 Oct
Test start time	09:00	09:00	09:00	09:00	09:00
Test duration (hours)	72	72	72	84	90
Tracer type	NaFl NH_4Br	NaFl	NaFl EtAc	NaFl	NaFl EtAc
Injection flow rate (l/s)	21.7	21.7	25.2	25.3	25.4
Production flow rate (l/s)	16.8	16.5	17.9	18.3	16.8
Injection pressure (MPa)	9.1	9.1	9.8	9.8	9.8
RH15 water level (m)	460	460	460	480	230
RH15/RH12 recovery (%) •	7.4	76.0	71.0	72.3	66.1
Breakthrough time (hours)	3.6	3.4	3.2	3.4	3.6
Breakthrough volume (m^3) *	81	65	69	86	81
Time to peak conc (hours)	6.2	6.4	6.0	5.6	6.2
Volume to peak conc (m^3)	375	380	387	369	375
Modal volume (m^3) *	238	243	250	232	238
Median volume (m^3) *	1917	1722	1707	1574	1488
Tracer recovery (%)	56.7	59.4	57.6	59.7	58.6

• Recovery = 15V/12I
* Wellbore volume = 137 m^3 (RH12 vol = 69 m^3; RH15 vol = 68 m^3)

Table 2 Results of tracer tests during the downhole pump test

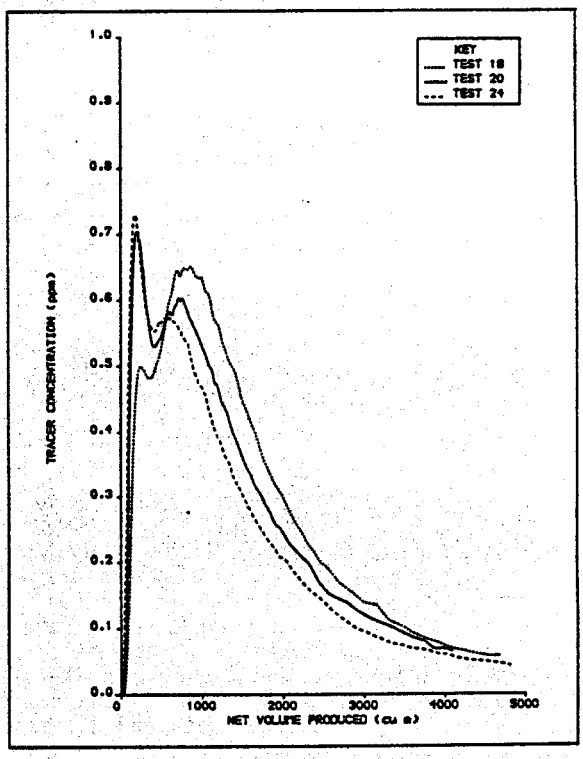

Figure 4 Inert tracer results for tests 18, 20 and 24.

DISCUSSION

HYDRAULIC AND THERMAL BEHAVIOUR

During the period when the injection flow

rate was 21 l/s, the recovery declined continuously until just before the increase in injection flow to 25 l/s. It is likely that the high production flow rate in the early part of the test was in part due to the production of water that was in storage. It is most probable that the continued decline in the production flow rate was due to the area affected by joint closure, caused by the increased effective stress acting across the joints, increasing as the region influenced by the DHP gradually increased.

A very small drop in pressure (0.5 MPa) was observed at RH12 which occurred soon after the start of the test. This small pressure drop at RH12, together with the sub-hydrostatic pressure imposed by the DHP at RH15, resulted in the impedance being increased, as shown in Figure 5.

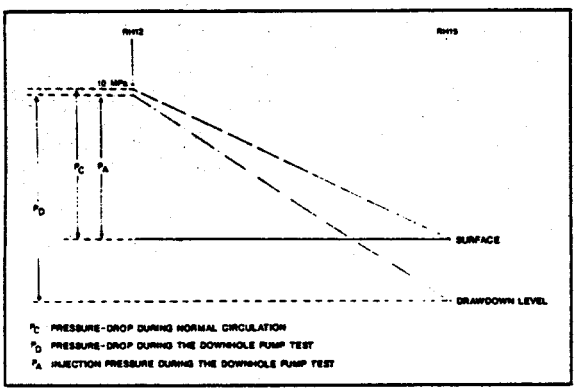

Figure 5 Comparison of pressure distribution with and without downhole pump.

In the DHP test an imposed sub-hydrostatic pressure of up to 4.6 MPa only produced a reduction in injection overpressure of 0.5 MPa (PA-PC). As the reduction in injection pressure is small compared with the drawdown, the impedance was greater using the DHP even though the production flow was generally higher than under normal circulating conditions.

Although the production flow in each stage of the test declined continuously, there was no stage during which the recovery fell below that which would be expected at the same injection flow rate in normal circulation. The improved recovery also resulted in a re-distribution of the flow in the reservoir as shown by the tracer data and discussed in the following section.

The slight increase in production temperature above that recorded immediately before the test is due to the heat given off by the pump motors. The rate of decline of the production water temperature, which had been observed for several months before the test, was unaffected by the introduction of the DHP.

Immediately following the test, the recovery fell to about 61%, which was lower than the expected value of about 68% under normal circulation conditions at an injection flow rate of 25.4 l/s. This was probably due to water going into storage and a re-adjustment of the joint apertures after the return to hydrostatic effective stress conditions. Two months after the end of the downhole pump test the recovery had returned to about 68%.

TRACERS

The effect of operating the production well under sub-hydrostatic conditions and increasing the pressure drop across the reservoir appeared to cause a major change in the flow paths as shown in the RTD curves (Figure 4). However, a change in the shape of this curve was starting to occur before the start of the DHP test with the first peak gradually becoming more prominent as the injection flow rate (and thus injection pressure) was increased during earlier experiments. It is likely that the DHP test helped to enhance this effect.

The initial peak is considered to be associated with the breakthrough flow path and the second peak with a number of other paths. Data from previous tests showed that the breakthrough feature was not dependent on pressure changes within the reservoir (CSM, 1986) and this was confirmed by the DHP test. The change in shape of the RTD curves at the start of the DHP test occurred because some of the flow paths associated with the second peak are probably pressure dependent and the reduction in hydrostatic head on the production well was sufficient to cause the near-well flow paths to close up and therefore reduce their contribution. However, the overall water recovery from the production well was higher than during normal circulation, so more fluid may have been forced through the breakthrough feature as a result of the increased pressure drop across it.

The tracer tests which had been run before the pump test were showing a general decrease in the peak concentration and an increasingly diffusive tail. This occurred as the injection flow rate was increased and had indicated that the reservoir was growing and becoming more diffuse. The shapes of the tails of the tracer tests run during the DHP experiment were similar to those of the two tests which were run immediately before and after it. The median volume, which represents the volume of the major flow paths in the reservoir, decreased during the DHP test to a level which was equivalent to that observed during earlier tests at similar production flow rates. It is suspected that this was due to the rapid decrease in injection flow rate prior to the start of the test rather than an effect of the DHP. Therefore, it is thought that there can have

been no large volumetric changes as a result of operating the production well under sub-hydrostatic conditions.

The marginal change in impedance, along with the small volumetric changes seen in the tracer data, suggests that the region affected by sub-hydrostatic conditions was close to the production well.

CONCLUSIONS

The DHP test was used to simulate conditions anticipated in a 6 km deep system and, although it was not possible to run for a sufficient length of time to allow totally steady state conditions to be established, some important conclusions can be drawn.

1 The overall recovery improved during the DHP test compared with that achieved during normal circulation.

2 The continued decline in production flow rate indicates that joints were closing up as a result of the increased effective stress and, therefore, that joint apertures will be reduced when operating a system under sub-hydrostatic conditions.

3 Following as from 2 above, it is probable that the greater part of the buoyant drive caused by sub-hydrostatic conditions at the production well will be required to overcome increased resistance to flow through the paths in the region affected by the sub-hydrostatic conditions, unless these flow paths are held open using proppants placed close to the production well.

4 The tracer data indicated that there was no major change in the effective volume of the reservoir during the DHP test, although there was a change in the flow distribution of the system.

ACKNOWLEDGEMENTS

The design and operation of the DHP test was under the direction of Mr K A Kwakwa, of GeoScience Ltd, Falmouth, UK - and the authors wish to thank him for his guidance and help.

The work reported in this paper was carried out under UKAEA Contract No E/5A/CON/151/2034, sponsored by the UK Department of Energy, to whom the authors are grateful for permission to publish their work.

REFERENCES

Camborne School Of Mines Geothermal Energy Project. (1986). Phase 2B Tracer Results. Internal report 2B-40, 1986. (ETSU G137-P10).

Pine R J and Kwakwa K A. (1988). Experience with hydrofracture stress measurements to depths of 2.6 km and implications for measurements to 6 km in the Carnmenellis granite. Second Int Workshop on Hydraulic Fracturing Stress Measurements. Minneapolis, Minnesota, USA, 1988.

PROCEEDINGS, Fourteenth Workshop on Geothermal Reservoir Engineering
Stanford University, Stanford, California, January 24-26, 1989
SGP-TR-122

THE CONTROLLING INFLUENCE OF NATURAL JOINT CONTINUITY ON THE CREATION OF HDR SYSTEMS-EXPERIENCE AND MODELLING

P Ledingham and G W Lanyon

GeoScience Limited, Falmouth Business Park, Bickland Water Road
Falmouth, Cornwall, TR11 4SZ, UK

ABSTRACT

A brief outline of the development of conceptual designs in Hot Dry Rock geothermal reservoirs, based on heat extraction requirements, leads to todays favoured volumetric models, which depend on the stimulation of natural jointing. Evidence from field experiments is used to demonstrate that no new flow paths have been created by stimulation, and that the nature, particularly continuity, of the natural jointing has a controlling influence on reservoir development.

The paper goes on to show how fracture network models can play a significant role in understanding the development process, and presents a small study undertaken to illustrate the joint continuity problem. The study shows how only a very small number of the larger joints may be required to form a connection between two wells, and how under these circumstances a low area flow path may be created.

It is concluded that connections are likely with only a small percentage of the fractures considered, and that there is a significant likelihood of creating a 'short circuit' connection in the types of network tested. The probability of such a connection increases with the size of the fractures. It is accepted that the size of natural joints is one of the hardest parameters to measure.

PERFORMANCE REQUIREMENTS FOR HOT DRY ROCK RESERVOIRS

Exploitation of geothermal energy by Hot Dry Rock (HDR) technology is essentially a heat mining process (eg Ledingham, 1986). The objective is to move heat from the rock to the surface by the medium of circulating water and, therefore, the design of HDR reservoirs is dictated by heat extraction requirements. These define minimum rates and temperatures which are commercially acceptable.

Maximum rates and temperatures are defined by the physical limitations imposed primarily by depth, pumping power requirements, and potential temperature drawdown.

Armstead and Tester (1987) concluded that these requirements dictate the following four attributes that any potential reservoir design must have:

1 A very large contact area between the working fluid and the hot rock.

2 Adequate conductive communication between the working fluid and a sufficient volume of hot rock to ensure a long lifetime.

3 Sufficient void volume in the reservoir to ensure that the working fluid exits at as high a temperature as possible, even when circulated at rates well in excess of the economic minimum.

4 A configuration of voids and flow paths that offer minimum impedance to the passage of the working fluid, so minimising pumping power, while also containing it within the reservoir to avoid loss to non-productive regions.

The essential paradox of the creation of HDR reservoirs is immediately evident; the need to create a large heat transfer area and yet allow water to flow easily through it. The most efficient hydraulic system would consist of a single, wide fracture between injection and production points, but this would be inadequate in heat extraction terms. In contrast, a large diffusive system, with narrow, tortuous flow paths and many dead ends may have a very large heat transfer area, but be inadequate in terms of efficiency of fluid transport.

In the design of HDR reservoirs, heat extraction requirements were used to derive heat transfer areas, hence rock volumes, and hence inter well spacing, which is one of the fundamental reservoir design parameters.

This design evolution required assumptions about the available heat transfer area available in a given rock volume, and the effectivenes with which the available area is swept by the circulating fluid.

For example, the targets set out for the design of the Camborne School of Mines (CSM) Phase II reservoir were based on heat transfer

calculations, which dictated that an effective heat transfer area of two million square metres was required. This was translated into an active rock volume of 200 million cubic metres, assuming that one square metre of heat transfer area would be available from every 100 cubic metres of rock.

The one in a hundred factor incorporated both the area-volume ratio and the swept-available area ratio. The rock volume could be translated into an approximate reservoir geometry to specify the well spacing. For example, 450 m by 150 m, with a well spacing of 300 m. An assumed flow path width of 1 mm gives rise to a circulating volume of 2000 cubic metres.

THE EVOLUTION OF HDR CONCEPTS

In recognition of the paradoxical nature of the requirements for a successful HDR system, researchers have strived to develop the best possible compromise reservoir.

Los Alamos National Laboratory (LANL) developed the first conceptual model, comprising a single artificial penny shaped fracture with an injection point at the bottom and a production point at the top. The realisation that to satisfy the heat extraction requirements this fracture would need to be impossibly big led to the development of the multiple artificial fracture models.

At CSM, learning from the LANL experience, emphasis was placed on the role of natural jointing in the reservoir creation process. Researchers at CSM assumed that the stimulation of natural jointing would dominate over the creation of artificial fractures, and a volumetric reservoir would be created.

The evolution of these concepts is shown schematically in Figure 1 a), b) and c), respectively.

Volumetric models are probably the favoured variety today, although they exist in various forms with various assumed configurations. The reservoirs at LANL and CSM both appear to be generally volumetric, although there seem to be a small number of major, probably vertical, structures which tend to dominate the flowing characteristics (Figure 1c).

It is interesting to note that earlier concepts have not been completely abandoned (eg Kappelmeyer and Rummel, 1987; Tosaya et al, 1988).

STIMULATION

Similar approaches to stimulating large volumes of naturally jointed hard rock masses have been adopted at LANL and CSM. The role of stimulation is to enhance the passage of flow through the potential reservoir region, either by improving existing flow paths or by creating new ones.

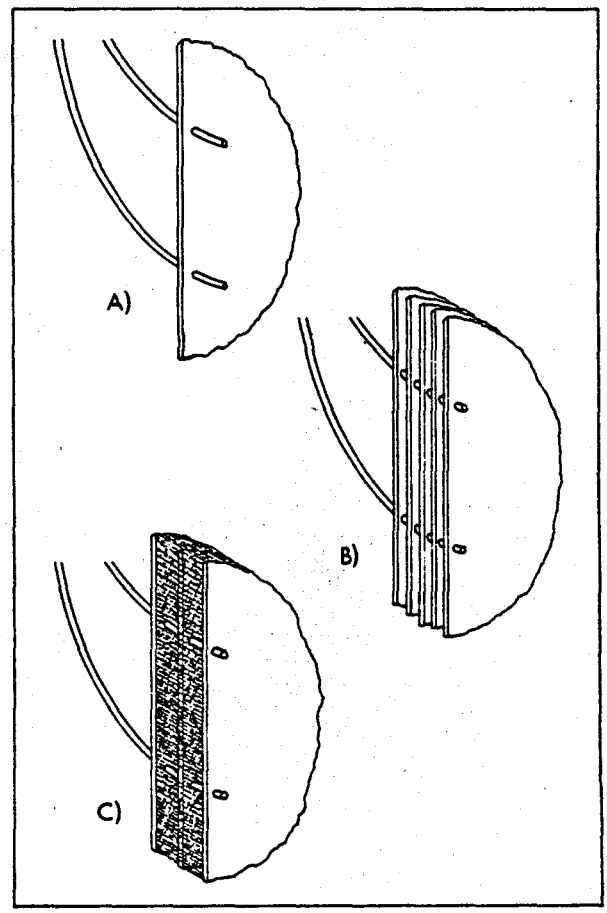

FIGURE 1 a) SINGLE PENNY SHAPED FRACTURE
b) MULTIPLE PENNY SHAPED FRACTURES
c) VOLUMETRIC SYSTEM WITH DOMINATING VERTICAL FEATURES

Three kinds of improvement of a flow path seem to be potentially possible; increasing the aperture, lengthening, and widening of the flow channel in the joint. Widening here refers to increasing the breadth of the flow channel, or increasing the effective swept area.

There is no doubt that apertures can, and have been improved significantly at the wellbores in all the major field trials of stimulation techniques. This increase can be supported for some distance into the rock mass, but spreading flow and dissipating pressure reduces the stimulating potential of the fluid, and the aperture enhancement reduces.

The length of 'wide aperture' flow paths can therefore be increased to some extent, but at some distance away from the injection point, the stimulation will effectively stop and continued flow will only be possible if the joint has sufficient 'undisturbed' flow capacity. Physical extension of joints by fracturing away from the wellbore is highly unlikley.

The various tracer studies carried out at LANL and CSM (Armstead and Tester, 1987) have shown that the modal volumes of circulating systems are significantly less than the potentially available volume in the joints between the wells. It follows that the effective heat transfer area, or swept area, is less than the joint area available, and it is reasonable to conclude that flow exists in channels in joints.

It is unclear from field experiments whether stimulation increases the breadth of these flow channels, or what proportion of the potential heat transfer area is in fact swept by the fluid. This has significant bearing on the relationship between required area and active rock volume described earlier. However, no increase in channel width will be useful if the flow capacity of the joint is inadequate.

In conceptual terms, therefore, it appears that stimulation can succeed in improving the passage of fluid through the rock mass, possibly for some distance away from the wellbore, but that there is some point beyond which flow can only progress further if there is a pre existing flow path. If this point is nearer to the injection well than the stimulated region around the production well, the wells will not be hydraulically connected unless they were so in the undisturbed state.

There is significant evidence from the Camborne work to support this hypothesis. When the first two deep wells were drilled, geophysical logging showed hundreds of natural joints intersecting each well, but even the earliest hydraulic testing, at low flow rates, showed that only a very few accepted or produced significant quantities of fluid (CSM, 1983).

By the end of the development and circulation stages of the system, some 20 million gallons of water had been circulated, and several vigorous injections had been carried out into both wells, often at pressures in excess of the minimum earth stress. Despite this activity, and although the distributions altered, the flowing joints in the developed system were the same ones that flowed at the outset.

Whilst there was an obvious improvement in the circulation performance of the system (CSM, 1984) the stimulation process did not create any new flow paths identifiable at the wells.

Even more striking was the behaviour of the third deep well, drilled into part of the 'reservoir' developed below the first two wells. Geophysical, and production logging during a gas lift production test identified the joints and flowing zones in the well. All the flowing zones correlated with joints but, as before, only a small number of the joints flowed.

The well was stimulated by a 1.2 million gallon injection of medium viscosity gel at very high pressures and rates (Pine, 1987). Geophysical logging showed that extensive axial fracturing of the wellbore had taken place, but production logging during and after the stimulation demonstrated that the artificial fracture did not accept fluid at any time (CSM, 1988). The only zones in the well which accepted fluid, and which have subsequently produced fluid during circulation experiments, were the joints which flowed just after the well was drilled.

It is therefore clear that the distribution, nature, and particularly the continuity of undisturbed natural joints in the potential resevoir region have a controlling influence on the development of that system.

Conventional fracture models used in HDR development are based on regular, mostly grid-like, joint patterns which have artificially high joint continuities, and which consequently overestimate the degree of stimulation and communication between wells. To properly understand the HDR environment and its potential for exploitation, fracture network models which more accurately reflect the natural situation are required.

FRACTURE NETWORK MODELS

It is the focus on natural joints and the 3D geometry of the reservoir that make fracture network models attractive. Because they treat fractures explicitly, they are well suited to answering questions about the geometry of flow paths, and flow to area relationships. The incorporation of stochastic network generation means that they can provide answers to questions about the engineering risk of short circuits or high water loss.

Fracture network modelling originated from work on the long term safety of underground repositories for nuclear waste. Much of the original work is related to the joint Swedish - American project at Stripa (eg Rouleau, 1985; Witherspoon, 1979)

A major feature of the models is their reliance on probabilistic methods for generating the fracture network. It is impossible to delineate every fracture in a given reservoir region, and it is therefore necessary to extrapolate inter-well fracture occurrence using statistical methods. This means that models must be run many times to understand the possible variation in results due to the random element. Similarly, any results from the model must incorporate the observed variation. In practice, results are given in terms of mean behaviour and confidence limits.

Three dimensional network models are now in use for modelling groundwater flow around hypothetical underground repositories. It is important to understand the assumptions behind these models, and the problems with using them

at great depth.

Network models are based on the following simplifying assumptions, they are drawn from Robinson (1986):

° The rock mass is impermeable.

° Joint properties can be described by stochastic distributions.

° There is no head loss across intersections.

Individual models make further assumptions such as planar flow within the fracture or channelled flow between intersections. Some models even allow some matrix permeability, but most models follow the above assumptions.

It is possible that some of the above assumptions while valid for shallow disposal sites, are not appropriate for models of deep reservoirs at high rock stresses.

There is one further important assumption, that flow can be modelled by using a finite number of fractures. This number must inevitably be smaller than the total number of discontinuities (faults, joints, microcracks...) in the rock. At some point it is necessary to set limits on what minimum size of fracture will be included in the model. A simple cut-off can be derived from the system used to measure the presence of fractures, such a cut-off is valid as long as it can be shown that no appreciable flow occurs away from those fractures that have been detected. Lanyon (1988) used fracture statistics from borehole televiewer logs on the basis that all major flows could be associated with fractures shown on these logs.

FRACTURE NETWORK INPUT DATA

A major problem in fracture network modelling is the acquisition of input data. If the model is to be used as a predictive engineering tool, rigorous conditions must be met by the input data. This may be prohibitively expensive or impossible for some fracture parameters.

Orientation data has, in general, been relatively simple to collect and analyse for sample bias. Aperture data can be collected from packer tests, but assumptions must be made about the underlying distribution of fracture aperture. These assumptions may cause problems because of the dominating effect of a few large aperture fractures on flow. Figure 2 shows aperture data from a test borehole at Carwynnen in Cornwall (Heath and Durrance, 1984). Note the dominating effect of the permeability of the three largest fractures.

Size and shape data are very difficult to extract from exposure data and impossible to extract from borehole data. Fracture density can be found from fracture spacing data if

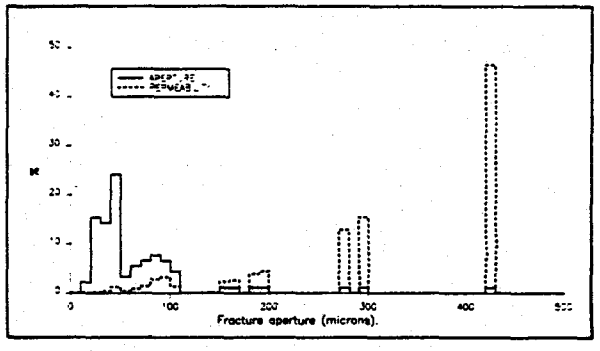

FIGURE 2 FRACTURE APERTURE AND PERMEABILITY DATA FROM HEATH AND DURRANCE (1984)

assumptions are made about the fracture extent.

It is also important to determine any correlations between parameters. Long et al (1987) outlined methods for creating hypothetical fracture networks from borehole data which will have comparable hydraulic properties to those of the measured system. In general, the networks produced will be statistical analogues of the real system.

A SIMPLE GEOMETRIC MODEL

The rest of this paper outlines how a network model can be used to study the particular problem of prediciting joint cointinuity between two wells in an HDR doublet, and how the inter-well connectivity is affected by fracture size.

The model is based on a percolation theory approach. Fractures from two sets are generated according to a random process to form a complete fracture network around and between the wells (Figure 3). The fractures

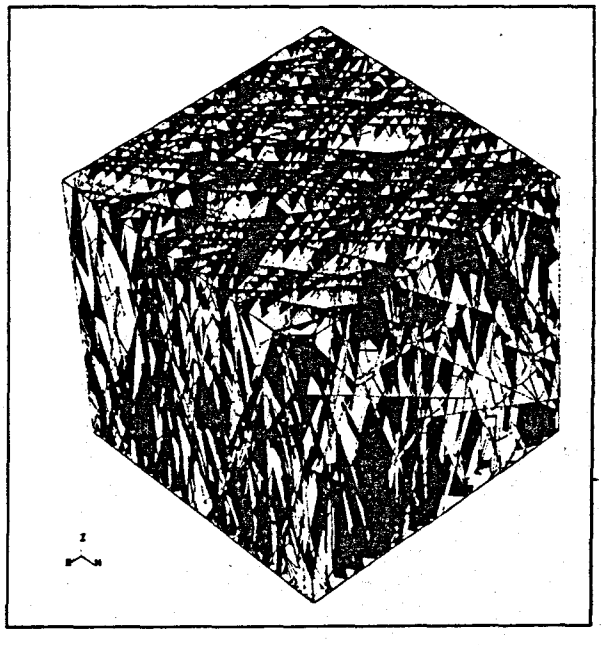

FIGURE 3 SIMULATION OF 50 M CUBE SHOWING ALL FRACTURES

are then considered in order of descending aperture until a link between the two wells is created.

Since the biggest, and therefore the most transmissive, fractures are considered first, the first connection generated will be the one with the highest minimum aperture (ie all other connections include lower aperture fractures). Where the distribution of fracture aperture is highly skewed such a connection will dominate the hydraulic performance of the reservoir.

A 'typical' HDR doublet configuration was used; two wells deviated at 30 degrees from the vertical, separated by 300 m vertically, with open hole lengths of 300 m. A stimulated zone of 20 m radius was assumed around both wells.

Fractures were modelled as constant radius discs whose centres were uniformly distributed by a Poisson process. Numerical experiments, comprising a minimum of 50 realisations were run with fracture radii of 20, 30, 50, and 75 m. The fractures existed in two orthogonal sets offset at 20 degrees to the well direction.

The fracture density was related to the radius used, and was set in each case so that there was a constant mean value of one square metre single sided fracture area per cubic metre of rock. This area to volume ratio was based on the fracture data acquired at CSM and reflects the high frequency of jointing that was measured, typically a joint in the boreholes every two to three metres.

In each realisation, three parameters were derived for the first connection:

1 The percentage of total fracture area needed to form the connection.

2 The number of fractures in the connection.

3 An estimate of flowing surface area of the connection.

The flowing surface area was calculated as the bounding convex polygon formed from all fracture and well intersections on a fracture (see Figure 4).

The model is purely geometric and does not include a flow solving system. Although dead ends are removed from the fracture network, any loops in the connection may be counted as contributing to the surface area. This means that this area estimate is probably optimistic.

MODELLING RESULTS AND DISCUSSION

Figure 5 shows a plot of the flowing surface area of the interwell connection against the percentage of total fracture area needed for connection to occur. It is clear that, in all

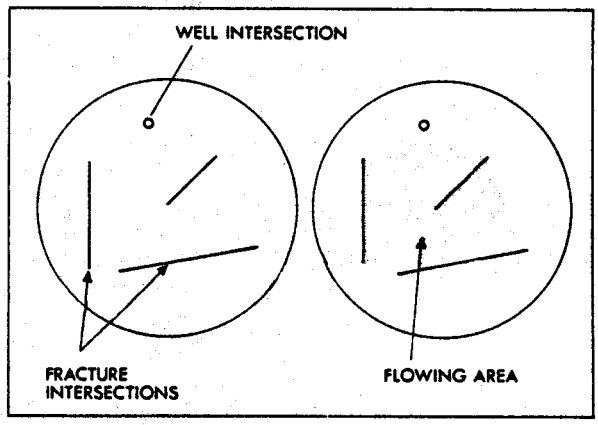

FIGURE 4 ILLUSTRATION OF 'FLOWING AREA' DEFINITION IN THE GEOMETRIC MODEL

cases run, only a small percentage of the total fractures in the model were required to form a connection, and that in the case of the largest joints, only one or two percent were necessary.

This is consistent with the observation at both large scale field experiments that only a very small percentage of natural joints flow.

Where only a few joints were required, the resulting surface area of the connection was rather small, representing the undesirable 'short circuit' connection. In order to achieve a heat transfer area of one million square metres (500 000 single sided area), at least three percent of fractures must be involved, this percentage increasing as fracture size decreases.

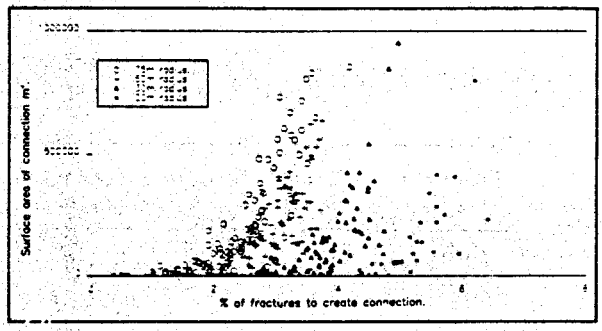

FIGURE 5 COMPARISON OF FRACTURE PERCENTAGE WITH CONNECTION AREA, FOR DIFFERENT FRACTURE RADII

Note that this only represents the first connection. Other connections will increase the area available, but are likely to be subordinate in terms of hydraulic performance to the first one, particularly where the fracture aperture distribution is skewed.

Figure 6 demonstrates that there is a significant risk of developing a 'short circuit' connection. It shows the distribution of generated flowing surface area for each fracture radius considered. In each case the distribution is skewed towards low area. No trends dependent on fracture radius

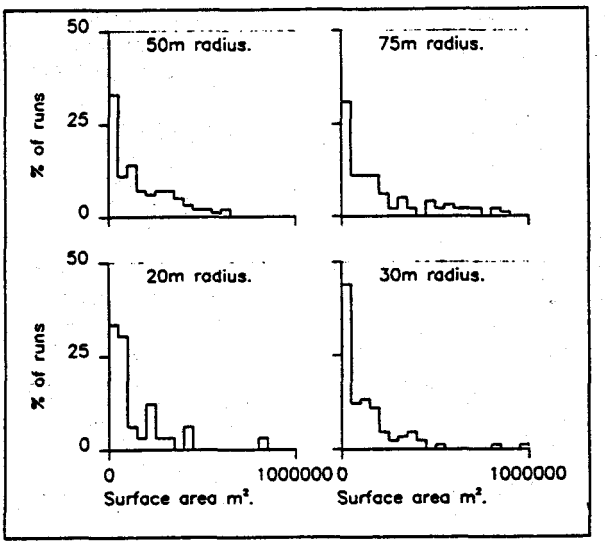

FIGURE 6 COMPARISON OF INTERCONNECTION 'FLOW AREA' FOR VARYING FRACTURE RADII

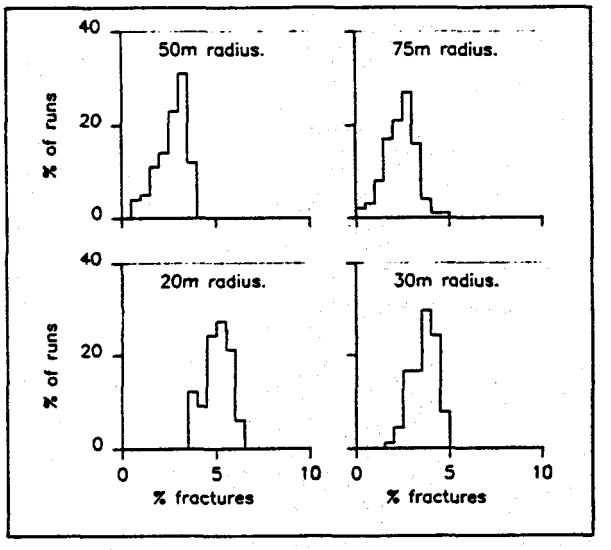

FIGURE 7 COMPARISON OF PERCENTAGE OF FRACTURES NEEDED FOR INTERCONNECTION

are apparent, but only a relatively few (50 to 100) realisations were carried out.

Figure 7 shows the distribution of the percentage of fractures required to form a connection at each fracture radius. In general, the unsurprising trend emerges that fewer large radius joints are required than small radius ones.

The same trend is apparent in Table 1, which shows the percentage of runs where very low surface area connections existed, formed solely of fractures in the top one and two percent. This circumstance becomes increasingly more likely with increasing fracture radius.

TABLE 1 FREQUENCY OF LOW SURFACE AREA CONNECTIONS

Fracture radius	% Connected by top 1%	% Connected by top 2%
20 m	0	0
30 m	0	1%
50 m	4%	20%
75 m	5%	30%

CONCLUSIONS

1 Experimental results from two major field trials of HDR technology have demonstrated the controlling influence of the character and continuity of natural joints on the creation of successful circulating systems.

2 The importance of realistic fracture network models has been established, and a small study relating to the joint continuity problem has been carried out.

3 The study demonstrated how the presence of a few large joints forming a connection between the wells could dominate the behaviour of the system, and that there was a significant probability, in the fracture networks tested, that a low area connection could be formed.

The probability depended largely on the assumed radius of the fractures in the model.

4 The study produced numerical experimental results consistent with field experiments, and suggested that original estimates of joint properties used in conceptual designs were reasonable.

5 Fracture network models offer a valuable tool for the design and understanding of the processes involved in creating HDR systems. Probably the greatest problem facing the modelling effort is the acquisition of reliable input data.

REFERENCES

Armstead H C H, Tester J W (1987). Heat Mining; A new source of energy. Published by E and F N Spon Ltd, New York, pp 68-69, 255-305.

Camborne Geothermal Energy Project (1988). Circulation results (1983-1986). ETSU Report G137-P5.

Camborne School of Mines Geothermal Energy Project (1983). Low flow rate hydraulic tests (RT2019-RT2041). Internal report Group 1, Pt 4, Vol 1, 110 pp.

Camborne Geothermal Project (1988). Viscous stimulation of hot dry rock reservoirs. ETSU Report G137-P13.

Heath M J, Durrance E M (1984). Radionuclide migration in fractured rock: hydrological investigations at an experimental site in the Carnmenellis granite, Cornwall. Report AERE-R-11402.

Kappelmeyer O, Rummel F (1987), Hanover. Geolog Jb, E 39, pp 252.

Lanyon G W (1988). Interconnection and flow in 3D joint networks. GeoScience Report to ETSU.

Ledingham P (1986). Heat Mining, Geothermal Energy Research in Cornwall. Mining Magazine, March Vol.

Long J C S, Karasaki K, Billaux D (1987). The creation of hypothetical fracture networks from borehole data. LBL-22090 Earth Sciences Division Annual Report 1986.

Pine R J (1987). The design and observed effects of medium viscosity, large volume fluid injection for HDR development in jointed rock. Proc Workshop on forced flow through strong fractured rock masses, Garchy, France, April 12-15.

Robinson P C (1986). Flow modelling in three dimensional fracture networks. Report AERE R 11965.

Rouleau A, Gale J E (1985). Statistical characterisation of the fracture system in the Stripa granite, Sweden. Int J Rock Mech Min Sci, Vol 22, pp 353-367.

Tosaya C, Findikakis A, Cochrane F (1988). Preliminary reservoir design and screening for a commercial Hot Dry Rock geothermal prospect. Trans 1988 Geothermal Resources Council annual meeting, pp 485-490.

Witherspoon P A, Wang J S Y, Iwai, Gale J E (1979). Validity of cubic law for fluid flow in a deformable fracture. Report LBL-9557, SAC-23 for the Swedish American co-operative programme.

PROCEEDINGS, Fourteenth Workshop on Geothermal Reservoir Engineering
Stanford University, Stanford, California, January 24-26, 1989
SGP-TR-122

RESERVOIR PHYSICS AND HOT DRY ROCK IN CURRENT NATIONAL R/D PROJECTS

Seiichi Hirakawa*, Yoshinori Miyazaki** and Yoshiteru Satoh***

* University of Tokyo, Emeritus Professor
** Geological Survey of Japan, Tsukuba, Japan 305
*** National Research Institute for Pollution & Resources
Tsukuba, Japan 305

ABSTRACT

National geothermal energy development program in Japan began in the early 1970's as one of the Sunshine Project (R/D on new energy technology). The program has been funded by the Sunshine Project Promotion Headquarters, Agency of Industrial Science and Technology, Ministry of International Trade and Industry. The main targets of geothermal energy project are to develop (1)technology for exploration and extraction of hot hydrothermal energy, (2) technology for power generation using geothermal hot water (10MW class binarycycle test plant), (3)technology for hot dry rock power generation systems, (4)technology for multi-phase utilization of geothermal energy and preservation of environment. The FY1988 total budget for all national geothermal R/D programs is about 5386 million Yen (43 million US dollars,1$=125 Yen). NEDO (New Energy and Industrial Technology Development Organization) established in 1980 by the government and private sector plays the main role in promoting national energy development with participation by several national institutes such as GSJ(Geological Survey of Japan), NRIPR(National Research Institute for Pollution & Resources), Tohoku Industrial Research Institute and so on. This paper presents the introduction of main national R/D projects which are going on, and will focus on the reservoir physics and hot dry rock project.

INTRODUCTION

One of the NEDO projects, confirmation study of the effectiveness of prospecting techniques for deep geothermal resources, began in 1980 with the objective of developing geothermal exploration techniques and confirming the results of various geophysical and geological surveys by drilling a deep geothermal wells. Two different geothermal model areas, Sengan and Kurikoma, were chosen for this purpose. FY1988 is a final year for this project and evaluation work is being done for the results of various surface exploration technologies with comparison of deep drilling data. New R&D program will be started following this project, and its emphasis is directed at producing two- and three-dimensional models of geothermal reservoirs, and surveying to locate and to map fractures of hydrothermal systems from the surface and within wells. Sengan and Kurikoma projects are first summarized, and then new future program for the fractured reservoir is discussed.

The hot dry rock project at Hijiori site in Yamagata prefecture has been operated by the New Energy and Industrial Technology Development Organization (NEDO) since 1985. Many experiments of the hot dry rock system are planned from 1989, and NRIPR (National Research Institute for Pollution and Resources) of MITI is in charge of analysis of logging data and circulating data. NEDO and NRIPR will be responsible for the future program of the hot dry rock in Hijiori. Discussion is concentrated on the current HDR research in National Project.

RESERVOIR PHYSICS IN SENGAN PROJECT

The Sengan area is in Akita and Iwate prefectures in northern Japan, and three geothermal power plants in operation, Onuma, Matsukawa and Kakkonda, are located within this area. Sengan area is a high potential area for a large geothermal energy, and it will be of importance to establish the geothermal exploratory techniques for identifying and mapping unknown hydrothermal system at depth in this area. Heat sources are probably the feeding magma of young volcano group as Mt.Yakeyama and Mt.Hachimantai, and its geothermal reservoir layer is assumed to be located in the Neogene Tertiary System underlying each of the volcanic materials.

Many geophysical and geological surveys in addition to gravity, geochemical and

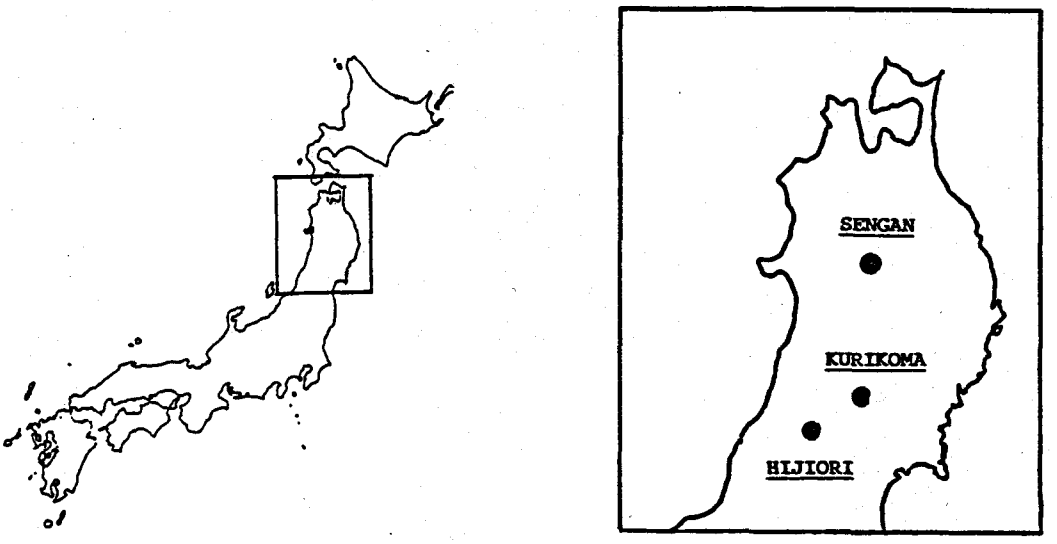

Figure 1: Location Map

aeromagnetic surveys, were applied in Sengan to make a geothermal subsurface model, such as refraction method, magnetotelluric exploration, Schlumberger electrical surveys, heat flow surveys by 200-800m wells, core dating by ESR (Electron Spin Resonance), Tubel method and so on. Geological Survey of Japan joins this Sengan project in the analysis of geologic structure, geochronological study, borehole geochemistry, thermophysical modeling, DC resistivity and magnetotelluric method. Geological study of the basement rocks around the central part of the Sengan geothermal area revealed that Mesozoic and Paleozoic siltstone, shale and chert are distributed in the Yuze and Ryugamori districts, and sedimentary rocks underwent the contact metamorphism by intrusive rocks. But no evidence for Pre-Tertiary igneous rocks was found out in the studied area. The isotopic compositions of surface water in Sengan area correlate inversely to the altitude of the sampling sites (-0.25‰/100m for $\delta^{18}O$). In some wells, it shows abnormally low $\delta^{18}O$ values with respect to the altitude of the well. Temperature logging data of deep wells and physical properties of core samples were extensively collected for the thermophysical modeling of the Sengan field. A forward modeling of the temperature structure has been continued to find out the subsurface temperature distribution at depth consistent with well logging data of surface temperature. Geothermal model of Sumikawa area, north part of Sengan area, is considered as follows.

Heat sources are assumed to be the deep of Mt.Yakeyama and Mt.Hachimantai. The individual heat source situates in the center of a up-flow zone and several hydrothermal convection systems are formed. Steam cap has been formed at the top of the reservoir, and lake deposite and Quaternary andesitic volcanics are considered to be this cap rocks. Fracture System of Sumikawa area was formed in relation closely to the volcanic activities, and geothermal fluids predominantly flows through these fractures.

In Nov. 1987, a deep confirmative well (N61-SN-7D) was drilled to depth of 2486m (8287 ft). The drilling location of this well was based upon the subsurface prediction of probable existence of geothermal reservoir at depth. Mud-logging was started from a depth of 1111m (3703ft), and aerated drilling operations were started from a depth of 1924m (6413ft). Drill cuttings were collected at every 5 meter and core was also collected at 1505m, 1921m, 2292m and 2484m. Several geophysical well loggings were conducted for the N61-SN-7D such as temperature logging, electrical logging, dual latero logging, neutron logging, density logging and spectro gamma logging. After a 7 inch slotted and uncemmented liner was installed, injection test and warm-up test were conducted. The permeability-thickness product (kh) of the N61-SN-7D is 3.11-9.38 darcy-m by multi-flow injection-test and kh calcuated by fall-off curve is 7.73 darcy-m. From the results of the hydrostatic-pressure balance and geophysical well logs, the major lost circulation zone is inferred to be at 2325m (7750ft) depth. The highest calculated static temperature is 304°c at 1800m (6000ft). This temperature, however, is not considered to correspond with the static formation temperature because of large circulation losses during a drilling operation. In 1988,

a production test for this well N61-SN-7D was conducted, and its data are as follows.

Steam	161 t/hr
Hot water	318 t/hr
Reservoir temperature	272 °c
Well head pressure	12.5 kg/cm²
Liquid chemistry	neutral Nacl type

It was found that the geothermal energy of this N61-SN-7D well corresponds to 16 MW power generation, and this is the biggest productivity for a single geothermal well in Japan. This success encourages the continuing effort to develop geothermal resources deeper than conventional 1000-1500m depth.

RESERVOIR PHYSICS IN KURIKOMA PROJECT

The Kurikoma area is centered on the Onikobe caldera in Miyagi prefecture, and a geothermal reservoir layer is thought to exist in fissures extending from the upper portion of the Pre-Tertiary granitic basement to lake deposits at the base of the caldera. Kurikoma project began in 1980, and airborne infrared thermal image surveys were conducted in this year over an area about 200 km² including the Onikobe caldera. Magentotelluric (MT) exploration and the electrical (Schlumberger) method were also conducted for the subsurface resistivity structure of Kurikoma field. GSJ revealed that the basement beneath the caldera was 1-2 km depth from the surface with two-dimensional inverse modeling technique of the MT data. It was also found that there exists a horst structure in Katayama area which is the most active geothermal manifestation area. This horst may be playing the important role for the conduit of hydrothermal up-flow system by providing the vertical faults. Other geophysical data such as gravity and aeromagnetic data were already surveyed and collected in this area. A total of six 1500 m class well were drilled for geological surveys, subsurface temperature distribution and core analyses.

The result of two-dimensional multi-layer analysis shows that gravity anomalies are consistent with the features of the granitic basement or the upper green-tuff layers, and short wavelength Bouguer anomalies seems to correspond to the distribution of lake deposits and/or andesitic lava. The three dimensional structure in the Kurikoma area was also obtained on the assumption of three homogeneous layer model under the control information of basement outcrop. 3D hydrothermal numerical modeling in the Onikobe area is being conducted with IFDM codes of geothermal simulation program.

HDR IN HIJIORI PROJECT

After the field studies of hydraulic fracturing at Yakedake which is the first test site for hot dry program in Japan, Hijiori in Yamagata prefecture was selected as another substantial test field to extract geothermal energy from a hot dry rock. Two wells, SKG-1 and SKG-2, had been drilled for geothermal survey at Hijiori. The depth of SKG-2 is 1802m, and the temperature at its bottom is about 250°c. The basement rock (granodiorite) lies below a depth of 1460m and the artificial reservoir was intended to be made in this basement rock by drilling and hydraulic fracturing.

In 1984, logging and pumping tests were conducted to get information for hydraulic fracturing. The natural inflow was 1.0 m³/h, and a well head pumping pressure at flow rate of 0.4 m³/min was 6 MPa. Lost circulations were detected at depth of 1530m to 1540m, 1570m to 1580m, and 1620m to 1640m. As a result of these tests, a full hole pressurization was selected as a hydraulic fracturing method. In 1985, 7" casing was installed from the surface to a depth of 1788m in SKG-2. Permeabilities of the basement rock at depth of 1788m to 1802m were estimated from 1 to 10 microdarcy.

In October 1986, a hydraulic fracturing was conducted by injecting about 1000 m³ of water at depth of 1788m to 1802m in SKG-2 well. Flow rates were 2 to 6 m³/min and well head pressures were 11 to 16 MPa. 380 m³ of hot water were vented from SKG-2 well after this injection. Microseismics were observed by 8 seismic sensors at 100m depth and a downhole triaxial geophone in SKG-1. Hypocentral locations of about 30 high-quality events indicated that microseismics occurred at 200m to 400m south of SKG-2 and at depth of 1500m to 1800m. The number of microseismic events, however, was insufficient for finding out the location of the hydraulically fractured zone.

In 1987, a new well, HDR-1, was drilled in the south of SKG-2 to confirm the artificial fractured reservoir created by 1986 hydraulic fracturing operation. The bottom of HDR-1 & SKG-2 well was 30m apart at depth. 9 5/8" casing was installed in HDR-1 from the surface to a depth of 1500m, and 8 1/2" borehole was left open below 1500m. In Nov. 1987, 380 m³ of water were injected into SKG-2 in order to confirm that HDR-1 was bored through the hydraulically fractured zone. Flow rates were 0.7 to 1.5 m³/min and well head pressures were 8 to 11 MPa. The maximum production flow rate was 0.01 m³/min which was only 1 % of the injection flow rate. Weak temperature anomalies were found at depth of 1743m and 1786m in HDR-1 well.

In July 1988, an additional stimulation was conducted to improve the hydraulic

communication between SKG-2 and HDR-1. An injection of water into SKG-2 was for 11 hours, and a total 2000m³ of water was injected. Flow rates were 2 to 6 m³/min and well head pressures were 4 to 15 MPa. After the injection, the well head of SKG-2 was opened, and an estimated amount of vented hot water was approximately 400 m³.

The well head of HDR-1 was opened before the start of the injection, and water flow from HDR-1 started at about six hours after the start of the injection. The production flow rate from HDR-1 was about 0.1 m³/min at the beginning, but the temperature of produced water increased gradually. When the water temperature reached 100 °c, hot water and steam were spouted and the flow rate of this hot water, as high as 154 °c, was estimated over 2 m³/min. The flow rate decreased rapidly after half hour later and it was less than 0.2 m³/min. Another spout of hot water & steam started after about two days later, and it continued for about 30 minutes. The maximum flow rate of this second spout was estimated at about 2 m³/min and its temperature was 158 °c. The production flow continued until the well head of HDR-1 was closed. A total amount of the produced water was about 350 m³ but that of the produced steam was not measured.

The hydraulic communication was improved by this stimulation, but the intermittent spout of hot water and steam had not been expected at all. About a hundred microseismic events were observed during this injection, and most events occurred in the south to SKG-2 at depth of 1400m to 1800m.

In August 1988, a short circulating operation was conducted in order to evaluate characteristics of the fractured reservoir. The injection flow rate was 1 m³/min and it was changed to 0.5 m³/min. This flow rate was changed again to 1 m³/min and maintained at this value until the end of the injection. A total 14000 m³ of water were injected in SKG-2. A venting of SKG-2 was started immediately after the end of the injection, and about 170 m³ of hot water was vented.

Water flow from HDR-1 was started immediately after the injection. Hot water was produced from HDR-1 intermittently, and the production flow rate was not constant. The maximum flow rate was about 0.5 m³/min and the maximum temperature at the well head of HDR-1 was 124 °c. A total 4500 m³ of hot water was produced until the well head of HDR-1 was closed. The total volume produced from HDR-1 was 32 % of that of the injected water into SKG-2. The amount of the produced steam is not included in this recovery. PTS logging in HDR-1 revealed that hot water flowed into HDR-1 through several fractures across this well. It was also found that flushing of hot water occurred in HDR-1 and the depth of flushing point moved up and down. Although tracer test was operated two times using tracer KI, concentration of tracer was not identified partially because the production flow rate from HDR-1 changed so frequently. Microseismic observation was conducted but few events were observed.

In addition to the hot dry rock program, a development of instruments has been carried out. A PTS log and a borehole televiewer were made, and they were now in operation. An triaxial geophone will be made which can be operated at temperature up to 250 °c and at a hydraulic pressure down to a depth of 1800m for eight hours. An improved borehole television is also being developed for a high temperature condition.

A TREND IN FUTURE

Geothermal reservoir descriptions including HDR project about a geological structural model and reservoir parameters have been based primarily on the geophysical interpretation. Spatial information about reservoir parameter variations can be inferred from the data of well drilling and reservoir geophysics.

A majority of geothermal reservoir belongs to the fractured media type. The present exploration techniques and assessment for this fractured reservoir is still incomplete and its maturity will be future tasks. In the stage of reservoir survey and evaluation, it is important to understand individual fractures and to estimate the quantity of resources. The final goal of our program for fractured reservoir is to locate and predict subsurface characteristics of fractured reservoir. This means the determination of the location, orientation, extent, porous or sealed, aperture etc of fractures in reservoirs at depth. The following new geophysical methods are planned to be applied for the geothermal reservoir in new program.

Electromagnetic Array Profiling (EMAP)
Cross-hole seismic tomography
Vertical Seismic Profiling (VSP)
High precision seismic reflection

Electromatromagnetic Array Profiling is already being tested in Sumikawa area, and its results will be checked with conventional MT method and with a deep well data.

Two shallow experimental wells S-1 & S-2 (500m) and two deep wells (2000m) are planned to be completed for testing the technical feasibility of these new geophysical methods and to develop the special tools for these methods. In 1988, Tanna area in Shizuoka prefecture was chosen for the shallow experimental field for VSP and seismic

tomography, and a first shallow S-1 well will be drilled in this winter. Another shallow S-2 well is planned to be completed in 1989 near S-1 site. The drilling location of deep wells (2000m class) is not decided yet.

The Hijiori HDR reservoir will be evaluated experimentally and theoretically. Before these evaluations, another deeper HDR reservoir will be tested by the hydraulic fracturing and drilling of a new well, HDR-2. The final hot dry rock system at Hijiori site will consist of dual extraction systems by 1989. One is a hydraulic fractured zone at a depth of 1800m between SKG-2 and HDR-1, while another will be a fractured zone at a depth of 2200m between HDR-1 and HDR-2.

CONCLUDING REMARKS

The Sunshine Geothermal Program in Japan is now 14 years long, and many fruitful results were completed. This paper introduced one of the geothermal exploration program in Sengan and Kurikoma area, and hot dry rock project in Hijiori site. It also refered to the new geothermal project specially oriented for the fractured reservoir system. The development and testing of improved geophysical methods for determining fracture characteristics of geothermal reservoir rocks are very important, and will help to improve the characterization and assessment of actual geothermal reservoirs.

ACKNOWLEDGEMENT

The authors express our appreciation to the Sunshine Project Promotion Headquaters, AIST, MITI, especially to Mr. Masanori Yoshikai, senior officer for development program (Geothermal Energy) for publishing this paper in the 14th Workshop Proceedings on Geothermal Reservoir Engineering, Stanford Geothermal Program.

year	million Yen	(Million $)
1980	5,603	(44.8)
1981	7,218	(57.7)
1982	7,040	(56.3)
1983	6,275	(50.2)
1984	6,116	(48.9)
1985	6,217	(49.7)
1986	5,977	(47.8)
1987	5,092	(40.7)
1988	5,386	(43.1)

Table 1: A Trend of Geothermal Program Budget

Geothermal Energy Projects Budget -- FY 1988

	million Yen	(million $)
Geothermal Exploration	1,456	(11.6)
Geothermal Survey	1,380	(11.0)
Drilling Technology	294	(2.4)
Binary Cycle Generation	1,441	(11.5)
Hot Dry Rock Research	758	(6.1)
Others	57	(0.5)
Total	5,386	(43.1)

Table 2: Geothermal Energy Projects Budget -- FY 1988

PROCEEDINGS, Fourteenth Workshop on Geothermal Reservoir Engineering
Stanford University, Stanford, California, January 24-26, 1989
SGP-TR-122

THE COMMERCIAL REQUIREMENTS FOR AN HDR RESERVOIR SUPPLYING A DOUBLE FLASH POWER PLANT

A S Batchelor, R H Curtis and P W Moore

GeoScience Limited, Falmouth Business Park, Bickland Water Road,
Falmouth, Cornwall, TR11 4SZ, UK

ABSTRACT

Hot Dry Rock (HDR) geothermal systems have been under investigation by research groups in several countries for the past 18 years. This work has cost in excess of $240 million and has probably utilised more than 1000 man years of effort. However, the central problem of developing an adequate heat extraction region with the correct hydraulic properties has still not been solved.

The results from the large field experiments suggest that the heat transfer areas are formed by the pre-existing natural fractures in the reservoir region and that HDR systems will be dependant upon the natural interconnections in the fractures forming flow paths to extract the heat. This means that the reservoir geometry will be predetermined by the interaction of the selected injection and production positions with the joint network, despite the fact that some form of stimulation may be necessary to reduce the resistance to flow. Work is already in hand to understand the nature of suitable joint distributions and, secondly, to determine if the results from an exploration well can be used to support continuing a project into a development phase.

In addition, measurements must be made in the reservoir that give an early indication of heat transfer area, hence, allowing longevity assessments to be made to ensure that an individual project can be funded properly.

This paper presents some results from a continuing sensitivity analysis of the performance of a HDR system based on a double flash plant for a commercial project based in the UK. It shows that it is possible that geological constraints on HDR reservoirs may restrict the commercial application of the process in the near future. However, the indications are that HDR does have a viable future under the right circumstances but the research effort on reservoir behaviour is in need of adequate direction and requires operational experience of longterm flow in fractured systems.

INTRODUCTION

The idea of using subterranean heat from formations that do not contain large and exploitable volumes of water or steam has been discussed for more than a century (Starkie-Gardner, 1885). However, modern interest in Hot Dry Rock (HDR) systems really began in the late 1960's with the pioneering work at the Los Alamos National Laboratory, New Mexico (Smith, 1973) and several countries have now supported major research programmes. Much of this work has been presented comprehensively by Armstead and Tester, 1987, in their book 'Heat Mining'.

All of the current concepts for HDR systems under field investigation have three common factors:

- Injection wells with pumps
- A heat transfer region, the HDR reservoir
- Production wells

The HDR reservoir has been the main focus of attention and considerable disagreement still exists on the nature and form of the reservoir amongst the various groups working on HDR.

The major research expenditures to date are estimated to be:

	US$ million
USA, primarily Fenton Hill (Murphy, priv comm)	132
UK, primarily Rosemanowes (£27 million)	47
Japan, NEDO, Tohoku, CRIEPI and NRIPR (Kobayashi, (priv comm) (Yen 3484 million)	27
France	8
Germany, Falkenberg, Urach, Fenton Hill	33
	$ 247 m

This includes EEC contributions to national programmes but excludes items like the OECD Mages project ($2 million ?) and expenditure in the USSR.

Internationally, the current annual spend is approximately $15 million.

The majority of this money has been spent by national government research programmes with research organisations and, generally, they have studied various aspects of generating the necessary heat transfer area within the body of hot rock.

However, despite the very considerable effort (say 1000 man years) and obvious international financial support, the original goal of finding an engineering solution for the reservoir creation phase has not been reached. At the current level of comprehension of the behaviour of fractured rocks at depth, it seems clear that a less ambitious approach may be more successful.

The one common factor that has emerged in most of the larger scale field programmes with wellbore interlinking has been that the flow paths were formed by the naturally occurring joints and fractures despite local artificial fracturing near the wellbore. The research programme in the UK was specifically planned to exploit the natural fractures, while the programmes at Los Alamos, USA, Mayet de Montagne, France and Falkenberg, West Germany were originally planned to create 'penny-shaped' artificial fractures in solid rock.

The main implication of the observation that the natural joints dominate the system behaviour is that the maximum accessible heat transfer area is predetermined by the chosen position of the injection and production well locations in the existing joint network. All the far field links in the joints will already be in place, even though the initial apertures may be too small for adequate flow behaviour.

The in situ stress field, the in situ fluid pressure and the distribution and extent of the jointing are the key factors that must be known or modelled for any given site before the reservoir geometry can be considered. This topic is discussed further in the paper by Ledingham and Lanyon (this volume) at this meeting but, in principle, HDR systems in jointed rocks are as site dependant as any other form of geothermal or mineral exploitation. The problem is to quantify the nature and extent of geologically suitable sites before considering the modification of the natural characteristics of joints themselves. This geological constraint is a possible restriction on the original concept of HDR systems that could be placed anywhere and simply drilled to a depth necessary to reach the desired temperature. At the moment there is insufficient information to know if this is an onerous restriction.

We decided to constrain the specification of the reservoir by matching a potential power sales contract to the ideal system behaviour before attempting further hypothetical modelling of reservoir behaviour. The key issue was to tie a specific plant behaviour to HDR systems with various features and determine the required performance characteristics of the system to achieve financial viability.

POWER SALES CONTRACT

The UK electricity utilities are currently state owned but, in 1990/91, the government have planned stock floations to make them private companies. Retail sales of electricity will be handled by local distribution companies who will purchase the power from any of the generator companies provided that 20% of that power is from 'non fossil sources'; in reality, this is protection for the nuclear power plants rather than any attempt to support large scale HDR developments! The distribution companies will also be able to generate power and participate in generation projects.

Looking at the market potential for HDR in the UK's privatised system, there are two major points which have to be noted:

i The privatised generating companies will contain the old base load fossil-fuelled and nuclear generating capacity. These will still be the rolling giants which work on very long payback periods, although changes are being made in order to attract investment.

ii The emphasis for new generating capacity in the UK is aimed at the load between base and peak demand. It follows that tariff negotiations for power purchases are going to be far more lucrative in this sector and small payback periods may well be achievable, effectively creating the real competition in the supply industry.

This means that the provision of small base load generating capacity by HDR, or in fact any other source, will not be supported nationally. Arguments based on specific local demands will still hold for Cornish HDR in such a system, but any consideration of widespread development in the UK must be highly unlikely unless the large generating utilities take responsibility for the development at some stage.

We have considered an HDR system based in Cornwall which is more than 200 miles from the nearest major power plant and has the best prospects for a deep HDR system in the UK (Batchelor, 1987).

The purchase tariffs in the UK for the energy and capacity payments have a premium scale based on time and duration related to both national and local demand profiles. Typically the variation can be from 1.7 p (3 c) to 17.1 p (31 c) per kWh. However, in levelised terms including capacity, for a station running at constant output, the price is likely to be 2.7 p/kWh (4.8 c). This may not

be the best method for operating an HDR plant.

The desirable contract has the following elements:

- Basic capacity payment for proven performance.
- Bonus capacity payment for proven extra performance at set times.

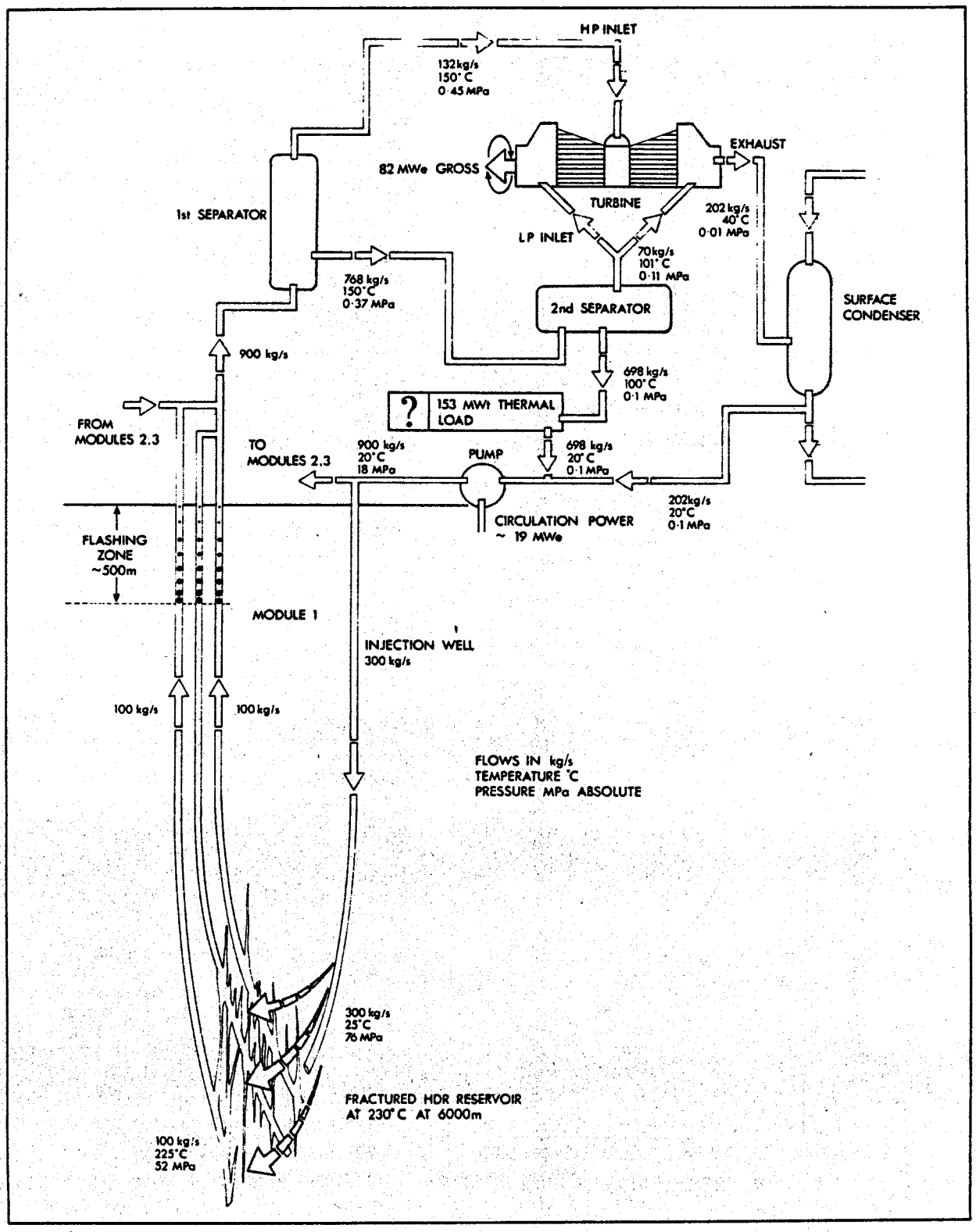

FIGURE 1 A CONCEPTUAL 63 MWe NET DOUBLE FLASH PLANT WITH AN HDR SYSTEM IN CORNWALL

- Energy payments based on set demand patterns.
- Bonus payments for energy delivered at peak times on notice from the utility.

The typical diurnal variations in energy payment are between approximately 1.7 p (3 c) and 7.9 p (14 c) between night and day during the high demand periods of November to February.

The tariffs are designed to attract generation systems that can follow demand without major capital investment in excess capacity. To maximise revenue from such a tariff, an HDR system needs the capability to vary its output significantly.

THE DOUBLE FLASH HDR SYSTEM

Figure 1 shows a conceptual double flash system for UK conditions coupled to an HDR system using twelve wells in three modules of four wells. The gross power from the plant in this example is 82 MWe with a parasitic power of 19 MWe for the circulation pumps.

Sensitivity to temperature, hence depth

Part of the sensitivity analysis was based on varying the production temperatures from 150 to 250°C to identify the influence of the depth and temperature on performance. Figure 2 shows the specific brine requirements for power generation under local conditions and it can been seen that moving to 4500 m at 150°C would reduce the gross power by a factor of three because the specific brine consumption increases from 11 kg/sMW to 33 kg/sMW. However, the parasitic power remains similar so the net power varies from 63 MWe to 8 MWe or nearly an eight fold reduction in saleable power.

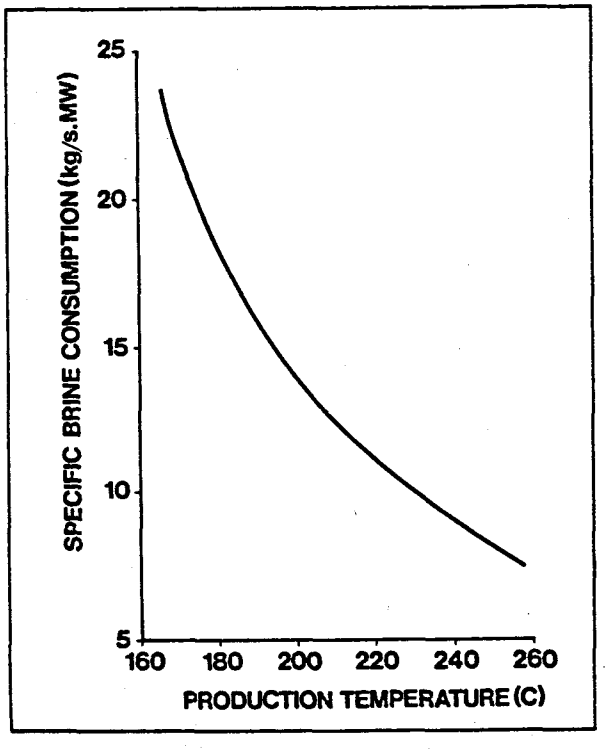

FIGURE 2 SPECIFIC BRINE CONSUMPTION AS A FUNCTION OF RESERVOIR TEMPERATURE FOR A DOUBLE FLASH PLANT IN CORNWALL

Drilling costs as function of depth

We chose to cost each well on an AFE basis rather than use a drilling cost algorithm of uncertain accuracy. This exercise required great patience from the suppliers once the engineering studies had established the limitations to the well designs. The majority of this work was undertaken by Southern International and was based on actual experience gained during the drilling of the Gravberg #1 well at Siljan in Sweden.

An example of the variations on the basic drilling costs is given in Table 1. The values include all casing and completion hardware and assume that the rig was purchased and amortised over four wells.

TABLE 1 AN EXAMPLE OF VARIATIONS IN WELL COST WITH DEPTH (based on 8.5 in completion)

Depth (m)	Injection wells	Production wells
5000	M$4.467	M$4.533
5500	M$5.12	M$4.88
6000	M$5.8	M$5.6

The absolute values in Table 1 may be in error by 20% but the relative values are much more reliable. Overall, the variation in drilling related costs from 5000 m to 6000 m of 25% is not outweighed by the doubling of the saleable power output if the risks of HDR at 5000 m are similar to those at 6000 m.

This study also concluded that drilling and completing wells below 6000 m at the necessary diameters was beyond current technology.

A commercial HDR plant in the UK

The overall study to maximise return and minimise risk, but assuming success at each stage, gave the following general specification for an HDR plant in the UK.

- Individual turbines 15-30 MWe
- Two to three turbines per plant
- 12-15 wells per plant
- 20-40 Ha sites
- 125-175 kg/s evaporative cooling losses
- 25-75 kg/s circulation losses

- 20-25% parasitic power for pumps
- Six years to build a system
- System costs £2200 ($4000) to £3000 ($5400) plus per kW
- 95-98% availability

OVERALL MODEL

Figure 3 shows an overall model of the system where the gross power from the plant is a linear function of mass flow rate at a given temperature but the parasitic power is a power function of the mass flow rate. Typically, the value of the index is between 1.5 and 2.5 for the systems studied.

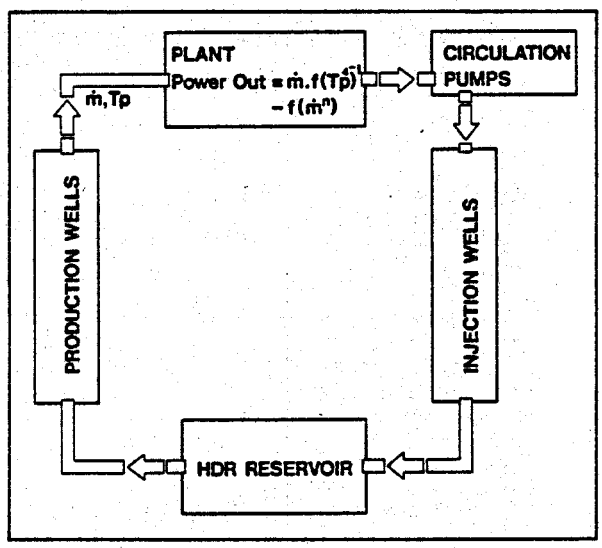

FIGURE 3 MODEL ELEMENTS OF AN HDR SYSTEM

Injection well behaviour

The field work shows that injection pressures can be raised to the point where the losses increase rapidly or the onset of sustained microseismicity indicates joint motions in the reservoir region. Typically, this limit has been set in Cornwall by the prevailing least principal stress and the in situ fluid pressure. The relationship between pressure and flow rate has been found to be linear over the range of pressures and flow rates that are useful for HDR systems, hence the hydraulic power requirements are related to the square of the flow rate in simple terms. Therefore it seems likely that the injection side would run at a maximum flow rate limited by the operational pressure limit. This value can be estimated from experimental data available from Los Alamos and Rosemanowes.

Figure 4 shows a curve of 'losses' vs injection pressure from the Rosemanowes experiments; it can be seen that there is a sharp departure from the linear trend at approximately 10 MPa in this case.

For the conceptual design at 6000 m, the anticipated least stress is 70 MPa with an in situ fluid pressure of 56 MPa. This means that the maximum overpressure during operation at the inlet point to the reservoir is 14 MPa. The head losses in the injection well are anticipated to be 4 MPa, hence 5.4 MW of hydraulic power are needed per module and 19 MWe of prime mover power are needed for the three modules.

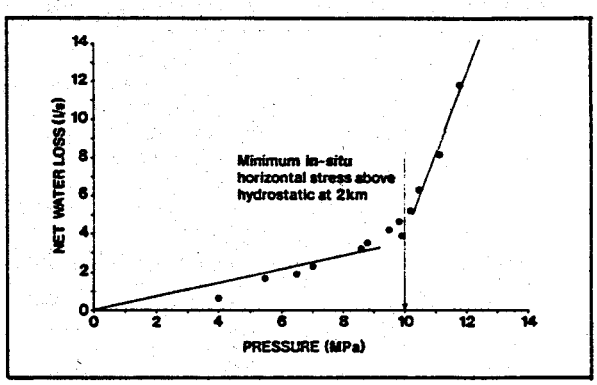

FIGURE 4 WATER LOSS RATE AS A FUNCTION OF INJECTION PRESSURE AT ROSEMANOWES

Production well performance

A flashing wellbore simulator was used to predict well behaviour setting flow rates to 100 kg/s and surface, flashed conditions to 0.5 MPa, 75 psi. The simulator is based on that from Parlaktuna, 1985.

The flowing downhole pressures can be seen in the example here to be 52 MPa or 4 MPa below the in situ formation pressure. In this way it is possible to have a degree of control over the losses that may be anticipated from the circulation loop. The validity of the simulator behaviour has been tested against published data and well tests run by GEO in wells up to 3000 m deep. Its validity in modelling the flow in a 6000 m well is unproven.

The depth of this model system helps the flow behaviour by providing a substantial bouyant pressure drive that is enhanced by the wellbore flashing. The actual pressure difference across the reservoir will be between 16 and 20 MPa with flow path resistances of 0.18 to 0.2 MPa/kg/s, values that have not yet been attained in practice.

Cyclic behaviour

The plant cannot operate over a wide range of mass flows; indeed if the production flow rate is decreased substantially then the heat losses in the wellbore will reduce the output temperatures.

The obvious way to enhance the performance is to cut the parasitic power by reduced pumping. At the moment when the pumps are cut the peak output will reach some major fraction of the gross power and this will then diminish as the

production rate falls. Figure 5 shows the flow reduction following a pump rate change at Rosemanowes. It can be seen that a 60% reduction in injection resulted in only a 15% loss of production after 24 hours.

This production is coming from stored fluid that is not necessarily in the main flow channels and could be extracting heat from regions not cooled by steady circulation. The flowing 'huff-puff' mode could be enhanced by diverting more power to the circulation pumps at night during the low tariffs to maximise revenues during the day. In times of severe demand for one to two hour peaks when the maximum possible value is attached to the power (ten times the basic rate), the full power output from the plant could possibly be achieved by stopping the pumps for a short period.

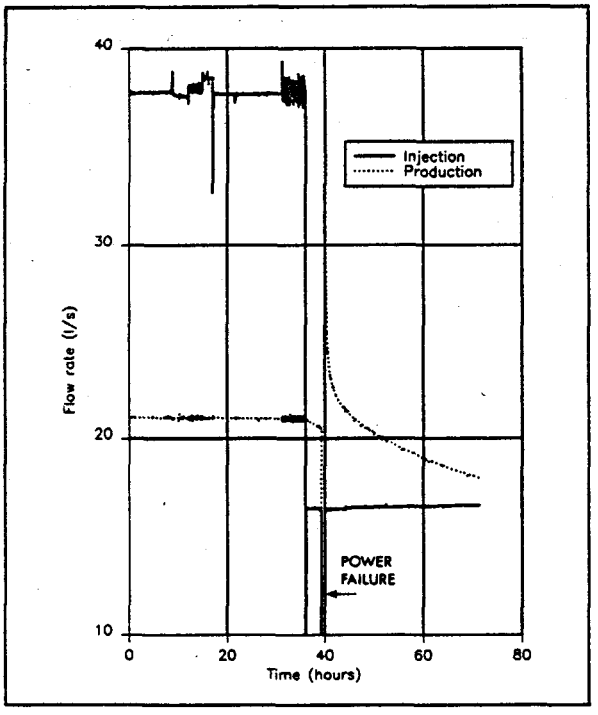

FIGURE 5 INJECTION AND PRODUCTION FLOWS BEFORE AND AFTER INJECTION RATE STEP

Various models show that the annual revenue from load following could be enhanced by 25 to 50% on the correct tariff structure to suit an HDR operation. Even so, the capital cost of the conceptual project is estimated at £145 million ($253 million or $4027/kw) and the best predicted annual gross revenues are only £18 million ($31 million). While this might represent a reasonable project in a mature industry with well understood risks, it is not a viable operation today without government development support.

SIZE OF THE RESERVOIR

The extraction of 900 kg/s at 225°C is a thermal power production of 727 MWt or 242 MWt per module. Over 25 years, cooling to 200°C, 1.43 x 10 MJ will be extracted from each module. To support such an extraction the rock volumes associated with the flowing pathways in the joint network need to be between 1500 million and 6000 million cubic metres of rock. This is much larger than some of the original calculations based on simple models. This wide variation depends on the assumptions in the various thermal modelling methods. The volume can be represented by cubes of 1100 m to 1800 m in length or slabs 300 m wide and 2200 m to 4400 m square. This implies interwellbore distances of the order of 600 m to 1000 m to avoid using too small a volume of rock.

The Ledingham and Lanyon paper (this volume) highlights the probability of forming a 'short-circuit' with interwell distances of the order of 300 m because of the low number of fractures involved. At the distances mentioned above, some 8 to 10% of the fractures could be involved and the short circuit risk is reduced.

REALITY

The various stimulations used to date have not achieved low resistance wellbore linking with adequate surface areas, even at distances of 300 m despite the fact that they were some of the largest massive stimulations ever attempted. The reality is that the sheer scale of the dilated reservoir volume , 2000 to 6000 cubic metres, plus the losses, means that the pumping requirements and job durations become unrealistically large if attempted in one operation. It is possible that cumulative, smaller stimulations, as proposed originally by LANL, may be used to reach the desired volume but it is difficult to envisage reliable completion systems.

However, if the far field natural fracture system already contains an adequate distribution of fractures and stimulation is only necessary to form a local effective access to the joints, the problem appears more tractable. Further work, as outlined by Ledingham and Lanyon, is already underway to determine the joint and fracture patterns that will support HDR operations without the need for massive stimulation operations and their associated geophysical monitoring. This will enable the basic reservoir requirements to be assessed in comparision to those available from nature.

To support this work, an exploration well to 6000 m into a region of the granite in Cornwall that is known to be heavily fractured near surface has been planned. This well is likely to be drilled as part of another R&D project but the data may be used to determine if conditions would warrant further work in the UK.

CONCLUSIONS

We believe that the grand dream of HDR is approachable in the long term if simple and less glamourous steps are taken first.

The understanding of how natural fracture systems link to form flowing reservoirs is a major goal of most geothermal operations, yet an understanding of those fracture patterns that are likely to be successful for HDR has not been achieved.

The failure of the various attempts to create commercial sized reservoirs by massive stimulation means it is worth reconsidering the idea of HDR systems that do not need such stimulations, eg the GEO-HEAT idea, Bodvarsson, 1974 and 1975. Once the conditions for possible success have been identified, it will be feasible to review the restrictions that may be placed on this class of HDR system.

HDR must be seen to deliver a success in the near term after the huge expenditures to date. It seems realistic to seek hot and fractured conditions that require no or limited stimulation for an operational project while the basic understanding of flow in fractured systems is developed. The existing base of dry geothermal wells provides an ideal opportunity to move the technology ahead at least cost and risk.

The system studies show that the power can be sold profitably if a reservoir can be generated whose performance meets or exceeds the values used in this paper.

The next steps to move HDR ahead towards such a goal are suggested to be:

Generic - Operate an HDR loop in a hot fractured formation with minimum stimulation.

Site specific - Drill a single hole to full depth to understand the in situ fracturing and fluid conditions. The decision for the work beyond those stages can then be based on reliable information.

ACKNOWLEDGEMENTS

The views and opinions expressed in this paper are the personal opinions of the authors alone. The authors are grateful for permission to publish this paper by GeoScience Limited. Terry Brittenham of Southern International and Bob Tucker of Geothermal Resources were major contributors to the feasibility study of HDR systems at varying depths and temperatures and their help is acknowledged along with the support of Dr J B Combs, GEO and the staff of GeoScience in the UK.

This version of the paper should be considered a draft and it may be amended in the final version.

REFERENCES

Armstead C H, Tester J W (1987). Heat mining; a new source of energy. Published by E&FN Spon, New York, 478 pp.

Batchelor A S (1987). Development of hot-dry-rock geothermal systems in the UK. IEE Proc, vol 134, pt A, no 5, pp 371-380.

Bodvarsson G S (1974). Geothermal resource energetics. Geothermics, vol 3, no 3, pp 83.

Bodvarsson G S, Reistad G M (1975). Econometric analysis of forced geo-heat recovery for low temperature use in the Pacific North-West. Proc UN Geothermal Symp, San Francisco, Ca, USA, vol 3, pp 1559-1654.

Gardner J S (1885). Can underground heat be utilised?. Geological Mag, Decade III, vol 2, pp 371-380.

Ledingham P L, Lanyon G W (1989). The controlling influence of natural joint continuity on the creation of HDR systems-experience and modelling. Workshop on Geothermal Reservoir Engineering, Stanford, Ca, USA.

Parlaktuna M (1985). Two phase wellbore simulator and analysis of reinjection data from Svartsergi, Iceland. UNU Geothermal Training Programme, Iceland, report no 1985-7.

Smith M C (1973). Geothermal energy. Los Alamos Scientific Laboratory, New Mexico, USA, LASL report 5289.

PROCEEDINGS, Fourteenth Workshop on Geothermal Reservoir Engineering
Stanford University, Stanford, California, January 24-26, 1989
SGP-TR-122

STABILITY OF TWO PHASE ZONES BELOW FISSURED CAPROCK

Y. Yano and T. Ishido

Geological Survey of Japan
Higashi 1-1-3
Tsukuba 305, Japan

INTRODUCTION

Many geothermal reservoirs contain two-phase (water/steam) flow regions under natural-state conditions. Vapor-dominated reservoirs are characterized by the predominance of such regions (and occasionally dry steam zones), but even liquid-dominated reservoirs frequently contain two-phase regions which overlie part or all of the liquid filled volume below. Production-induced reservoir pressure decline will cause the two-phase flow region to grow. Owing to compressibility effects, the response characteristics of two-phase regions and of liquid zones are very different. Consequently, it is important to properly understand the development and flow characteristics of reservoirs containing two-phase zones.

The purpose of this paper is to study the conditions required for the development of a two-phase zone in a particular Japanese geothermal reservoir. The complicated behavior of two-phase systems may now be treated using numerical simulation techniques. Ingebritsen (1987) examined three different kinds of vapor dominated reservoirs which can evolve in the natural state. He suggested that there are several basic types of two-phase zones which have different sizes and characteristic pressure profiles. The differences arise from differences in formation properties.

EVOLUTION OF A TWO-PHASE ZONE

As Ingebritsen (1987) demonstrated, even though small-scale two-phase regions may develop naturally in the absence of overlying confining beds, a caprock layer to prevent cold-water downflow is an essential prerequisite for the formation of large-scale two-phase regions. Hence, it is important to incorporate confining caprock layers in theoretical studies of the development of two-phase geothermal reservoirs.

In Japan, crustal motions and volcanic activity have created numerous faults and fracture zones in geothermal areas. If a vertical fracture penetrates the caprock overlying a two-phase region, steam may flow upward through the crack and create a fumarole at the surface. The liquid water within the two-phase region may flow either upward or downward, depending on the natural deep recharge rate which supplies the reservoir.

The Ginyu reservoir, located within the Kirishima thermal area in southern Japan, is characterized by a natural two-phase region below a caprock layer which is locally penetrated by a fractured zone through which steam flows upward to supply surface fumaroles (Kodama and Nakajima, 1988). The effective vertical permeability of the fractured area which penetrates the caprock must be at least ten millidarcies based upon measured fumarole heat output and observed underground pressures. Despite the relatively small volume of the two-phase region, its presence has a profound influence upon the response of the reservoir to a four-year history of well discharge (Kitamura, *et al.*, 1988). The role of the fissured zone as it influences the two-phase region and the underground pressure distribution proved to a critical issue in a recent numerical modeling study of the natural state of the Ginyu.reservoir (Maki, *et al.*, 1988).

MODEL DESCRIPTION

In the interests of simplicity, for the present study we chose to represent the Ginyu reservoir as a two-dimensional vertical section as indicated in Figure 1; this rather simplified model incorporates many of the major structural features of the reservoir. Quantitative details concerning this representation are summarized in Table 1. The so-called "convective-radiative" boundary condition was imposed upon heat flow along the upper surface; a volumetric energy sink was imposed in each uppermost grid block of strength:

$$e(\text{watts/m}^3) = 1 - T_b/10 \qquad (1),$$

where T_b is the instantaneous block temperature in degrees Celsius. This is intended to represent an upward heat flux of:

$$H(\text{watts/m}^2) = K_{bl}(T_b - T_{air}) \,/\, L \qquad (2),$$

where L is the thermal boundary layer thickness, K_{bl} is the boundary layer thermal conductivity (taken as 5 watts/m°C), and T_{air} is air temperature. For most of the upper blocks, we adopted the particular values L = 1 meter,

T_{air} = 10°C. In the uppermost block containing the fissure itself, we used L = 10 m and T_{air} = 100°C to maintain two-phase conditions.

Numerical calculations were all performed using the THOR reservoir simulator (Pritchett, 1988), which is designed to solve multidimensional unsteady multi-phase problems in geothermal reservoir flow. Calculations were carried out using the CRAY computer system located at the RIPS computer center at Tsukuba.

NUMERICAL RESULTS

Figures 2 and 3 illustrate the computed results for a case in which the deep inflow rate was prescribed as 100 kg/s. The internal energy of the inflowing fluid is 1130 kJ/kg, corresponding to liquid water at 260°C. These illustrations show the situation at t = 4986 years, by which time a nearly steady state is reached. A small two-phase zone with high steam saturations has formed within the fissure and extends into the upper part of the reservoir. A less pronounced two-phase zone is also present near the surface below the lower-topography area to the left.

Presumably, if the deep inflow is insufficient, surface waters will flow downward through the fissure and escape from the system through the horizontal conduit. This critical flow rate may be estimated as:

$$M_{esc} \approx k_{horiz} A_{horiz} (P_a - P_b) / (\nu L_{horiz}) \quad (3),$$

where k_{horiz}, A_{horiz} and L_{horiz} are the permeability, cross-section area and length of the horizontal conduit. The kinematic viscosity of water is represented by ν. P_b is the boundary pressure (P_1) applied at the conduit outlet (see Figure 1) and P_a is the initial hydrostatic pressure below the fissure at the elevation of the conduit (8.5 MPa). For kinematic viscosity, a value appropriate for water at 200°C (1.5×10^{-7} m^2/s) was assumed. It may reasonably be assumed that, if the deep inflow rate (M_o) exceeds the above "escape" rate (M_{esc}), then fluid will flow upwards into the fissure; otherwise, downflow will occur. Using the above numerical values, a critical flow rate of 47 kg/s may be obtained; in the present calculation, M_o = 100 kg/s, resulting in upflow in the fissure.

The stable steam zone should increase in size if the inlet flow (M_o) is reduced. To investigate this possibility, we carried the above numerical calculation further in time, but reduced this parameter to 80 kg/s for the interval 5000 - 10,000 years and then imposed an additional reduction (to 60 kg/s) for the interval 10,000 - 15,000 years. The distribution of the two-phase region at about this point (14,960 years) is shown in Figure 4. As expected, two-phase flow has become more extensive. Further reductions in flow rate were imposed thereafter; M_o was reduced by 6 kg/s every 1000 years, reaching a final value of 30 kg/s at 19,000 years. Prior to 17,000 years, the input rate exceeds the above critical rate (47 kg/s) required to maintain upflow, and the two-phase region continues to grow. After this time, however, cold water begins to flow downward through the fissure collapsing most of the two-phase zone. Figure 5 shows the shrunken two-phase zone at 17,590 years (at which time M_o = 42 kg/s).

In the preceding calculations, the internal energy of the fluid entering the system at depth (1130 kJ/kg) was relatively low, corresponding to liquid conditions at about 260°C. Under these circumstances, as discussed above, the inflow rate must exceed a critical value (47 kg/s) to avoid downflow of cold groundwater into the reservoir through the vertical fissure. If, however, the deep recharge fluid is sufficiently energetic, it may be possible to sustain a stable two-phase region even at lower recharge rates.

To investigate this possibility, a calculation was performed with relatively low inflow rate (30 kg/s) but with a much higher inflow fluid internal energy (1810 kJ/kg). This value corresponds to saturated liquid water at near-critical conditions (20.3 MPa, 367°C). Since the pressure at the bottom of the computing volume is substantially lower, this condition amounts to the introduction of a two-phase mixture directly into the bottom surface of the computational volume. As Figure 6 shows, by 4954 years a stable situation was reached with a huge two-phase region filling much of the upper portion of the volume and extending downward to the hot fluid source.

Thus, if the input power is sufficient, a stable two-phase zone can occur even if the inflow rate is less than the critical value given by Equation (3). The reason is simply that, in the high-energy case, steam saturations become so high in the upper part of the two-phase region that the liquid phase becomes nearly immobile and the pressure distribution approaches vapor-static (instead of hydrostatic, as in the low-energy case). The effect is to reduce P_a in Equation (3) substantially, reducing the minimum flow rate required to sustain fissure discharge.

CONCLUSIONS

A two-phase zone may form in the upper part of a geothermal reservoir even if the caprock is penetrated by a vertical fissure, so long as either (1) sufficient deep fluid mass recharge is present, or (2) the deep input power is great enough. Two-phase zones sustained by high mass flow rates are qualitatively different from those created by high heat flow. In the high-mass-flow case, the two-phase zone is relatively small in size, and decreases in size as recharge rate increases above a certain critical value. So long as the inflowing fluid enthalpy is relatively modest (consistent with single-phase flow at depth), flow rates below the critical value will fail to create a two-phase region and cold water will flow downward through the fissure into the reservoir. The critical mass flow rate may be estimated

using a simple algebraic model. On the other hand, if the inflowing fluid is sufficiently energetic (such that steam is injected directly into the reservoir from below), an extensive two-phase region may result even if the inflow rate is significantly less than the critical value; in this case, the two-phase region will be characterized by relatively low pressures, approaching vapor-static conditions.

REFERENCES

Ingebritsen, S. E. (1987), "Vapor-Dominated Zones within Hydrothermal Convection Systems," *Twelfth Workshop on Geothermal reservoir Engineering*, Stanford University, Stanford, California, SGP-TR-109, pp. 291-296.

Kitamura, H., T. Ishido, S. Miyazuki, I. Abe and R. Nobumoto (1988), "NEDO's Project on Geothermal Reservoir Engineering - A Reservoir Engineering Study of the Kirishima Field, Japan," *Proc. 13th workshop on Geothermal Reservoir Engineering*, Stanford University.

Kodama, M. and T. Nakajima (1988), "Exploration and Exploitation of the Kirishima Geothermal Field," *Jour. of Japan Geothermal Energy Assoc., Vol. 25, No. 3*, pp. 201 - 230 (in Japanese with English abstract).

Maki, H., T. Ishido, I. Abe, R. Nobumoto and Y. Oikawa (1988), "A Modeling Study of the Natural State of the Kirishima Field," *Proc. International Symposium on Geothermal Energy, 1988, Exploration and Development of Geothermal Resources,"* Kumamoto and Beppu, Japan, pp. 144-147.

Pritchett, J. W. (1988), "THOR User's Manual," SSS-IR-88-9408, S-CUBED, La Jolla, California, 109 p.

GEOMETRY

entire system:	width=2850m, height=1900m(right edge), thickness=500m
reservoir(A):	width=1050m, height=800m (along edge)
vertical conduit:	width=100m, center location=950m from right end
horizontal conduit:	height=100m, center depth=450m from surface
fissure:	width=50m

ROCK PROPERTIES (Symbols A-D are shown in Figure 1.)

Absolute permeability(m^2)(A:10^{-13}, B:4.0×10^{-14}, C:10^{-15}, D:2.0×10^{-17}).
Relative permeability: linear functions with residual liquid saturation=0.3, residual steam saturation=0.05.
Rock grain heat capacity(Joules/kg°C) = 1000(all).
Rock grain thermal conductivity(watts/m°C) = 2.5(all).
Rock grain density(kg/m^3) = 2700(all).
Porosity A=B:0.1, C=D:0.01

BOUNDARY CONDITIONS AND SOURCE/SINK

Sides:	insulated for both heat and mass except for horizontal conduit. P_1 in Figure 1 is 4.6×10^6 pascals.
Surface:	convective-radiative condition (see text). pressure = 1.013×10^5 pascals.
Bottom:	heat flux (2HFU for left 1100m, 5HFU for right 1750m except for vertical conduit). Hot water supply into vertical conduit: fluid internal energy=1.13×10^6 (Joules/kg) for models in Figures 2-5, see text for mass (M_0).

INITIAL CONDITIONS

Pressure:	hydrostatic pressure.
Temperature:	conductive profile according to heat flux from bottom.

Table 1: Parameters used for the numerical simulation.

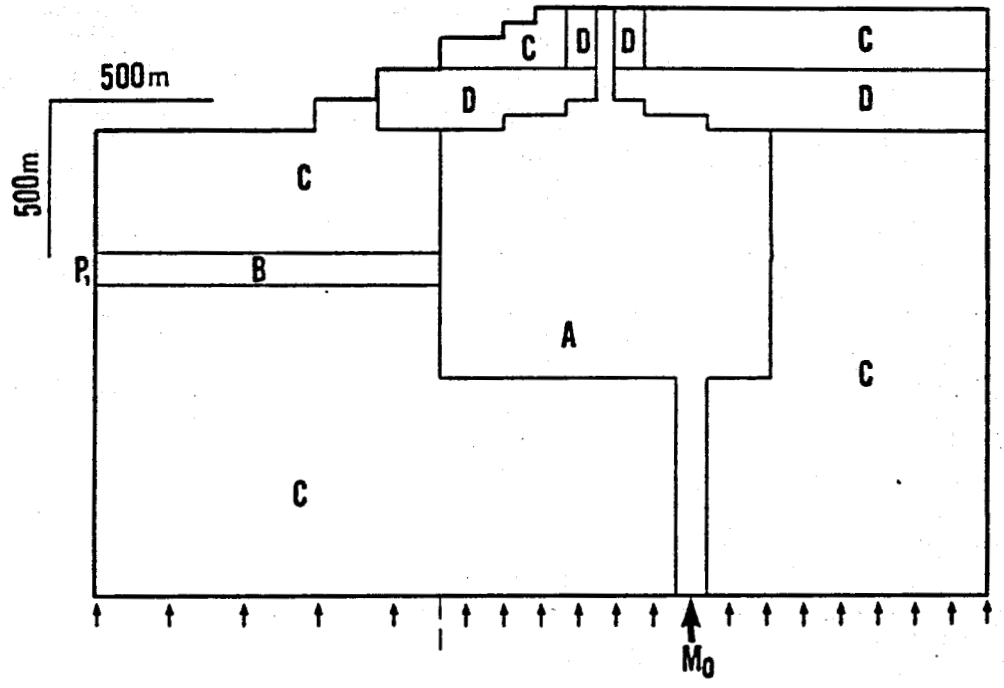

Figure 1. Two-dimensional model used for numerical simulation. Letters A,B,C and D indicate the rock type. See Table 1 for formation parameters.

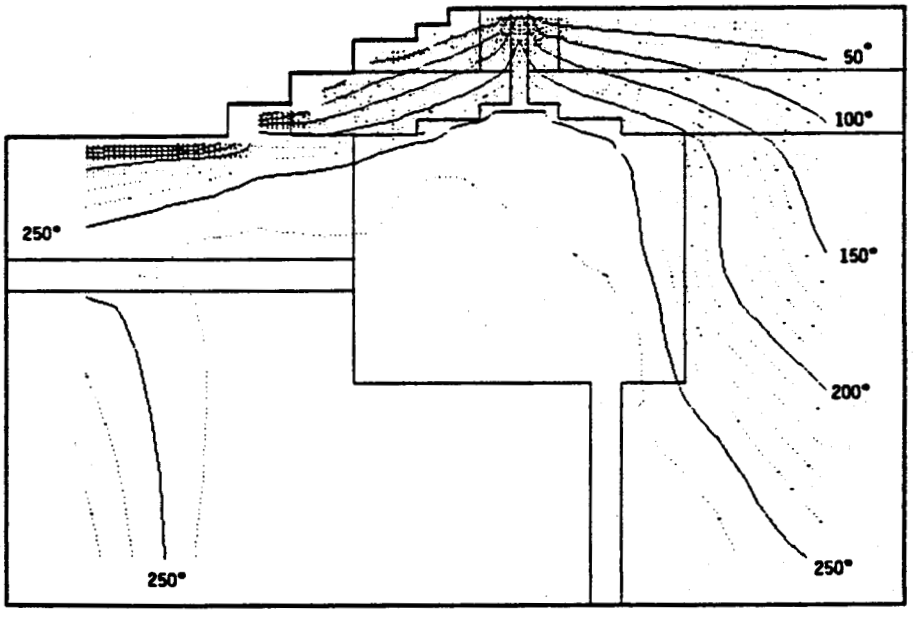

Figure 2. Computed temperatures at 4986 years for M_o = 100 kg/sec.

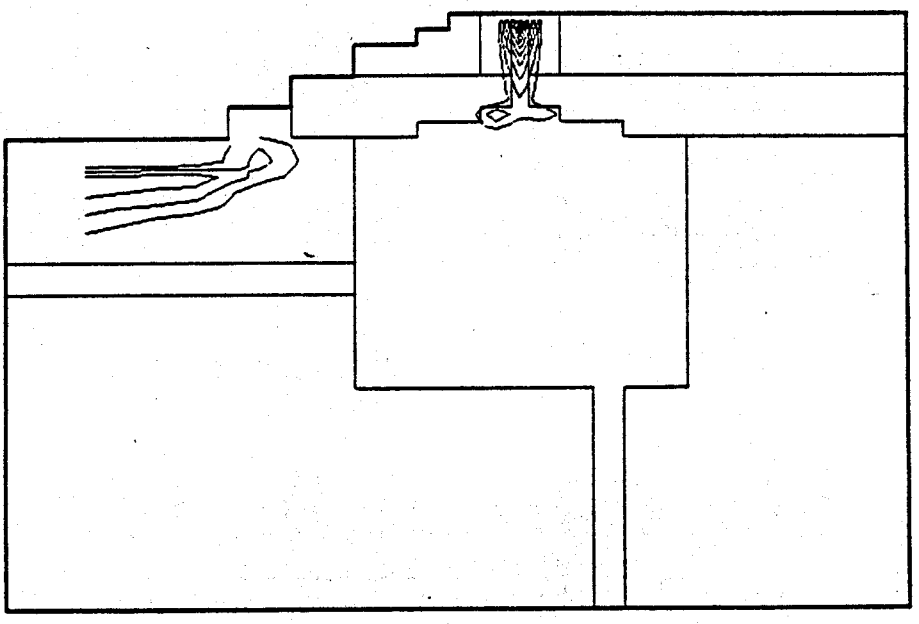

Figure 3. Computed steam saturation at 4986 years for M_o = 100 kg/sec. Contour interval is 0.05.

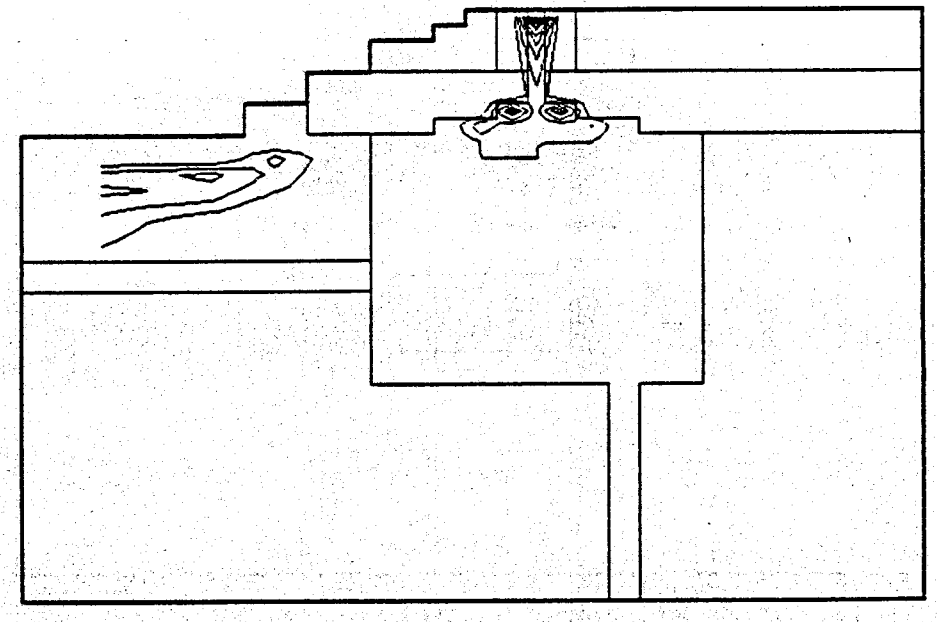

Figure 4. Computed steam saturation at 14,960 years with reduced mass input (M_o = 60 kg/sec).

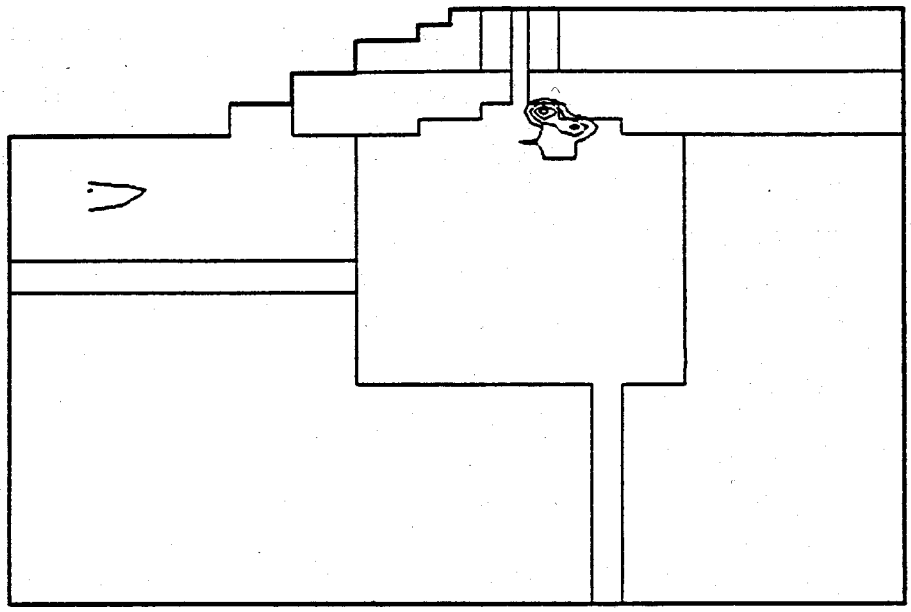

Figure 5. Steam saturation at 17,590 years.

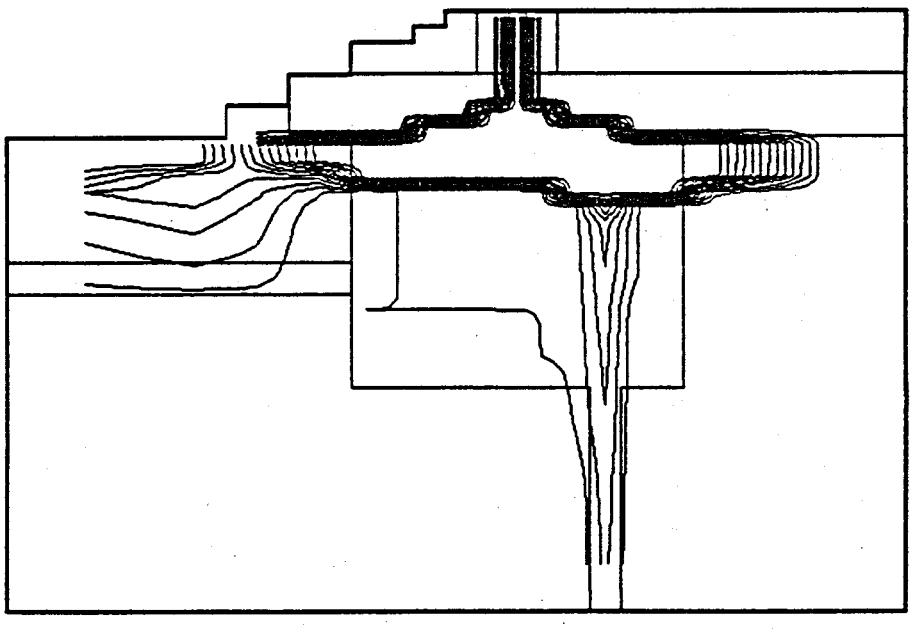

Figure 6. Computed steam saturation at 4954 years with small mass input (M_o = 30 kg/sec) of high internal energy (1810 kJ/kg) fluid.

Preliminary Modelling Studies

by
Cesar Suarez (CFE), Karsten Pruess (LBL), and Marcello Lippman (LBL)

No final copy was received by press time

PROCEEDINGS, Fourteenth Workshop on Geothermal Reservoir Engineering
Stanford University, Stanford, California, January 24-26, 1989
SGP-TR-122

DOUBLET HEAT SWEEP MODEL WITH BOUNDED INITIAL TEMPERATURE DISTRIBUTION

S. T. Lam and P. Kruger
Stanford Geothermal Program
Stanford University
Stanford, CA 94305

ABSTRACT

The SGP 1-D Heat Sweep Model has been improved to simulate production fluid cooldown under partial reinjection recharge through a fractured hydrothermal reservoir with a given temperature distribution. The model was developed as a 1-D doublet flow model with the assumption of equal and linear flow through a series of N crescents each carrying 1/N of the reinjection recharge flowrate. For a uniform initial reservoir temperature infinite in geometry for doublet flow, the heat content available above a useful abandonment temperature increases rapidly with increasing crescent number. The result is a very long cooldown time to the abandonment temperature. The improved model limits the volume of the reservoir at mean initial temperature to a defined geometry. In the absence of field data on temperature distribution around an isolated injection-production well pair, several possibilities are explored; for example, uniform temperature in a cylinder of radius equal to one half of the distance between the well pair, with temperature distribution decreasing as 1/N thereafter. Other distributions examined are a step function, a normal distribution, and an exponential decline from the line normal to the well pair. The simulated cooldowns resulting from these temperature distributions are compared to the prior results reported for uniform temperature distribution at two Mexican geothermal fields. The first is the La Primavera well pair scheduled for the first power unit. The simulations were based on preliminary data on the actual temperature distribution at the flow horizon. The second is the isolated well pair in the El Chino zone of the Los Azufres geothermal field, where little temperature data are available. The results show considerable decline in cooldown time to the abandonment temperature. When measured temperature distributions are made, the model can be changed to reflect doublet flow more accurately. This will require a more complicated heat sweep model.

INTRODUCTION

The Stanford Geothermal Program 1-D Heat Sweep Model was developed as a means of estimating energy extraction by reinjection recharge in fractured-rock geothermal resources in a simple way when reservoir and production data are sparse. The model is especially useful in new and undeveloped fields where only limited geologic, thermodynamic, and production data are available and where recharge experience in non-productive wells does not exist. The model calculates production fluid temperature based on estimated condition of reservoir structure, return flow geometry, and mean thermal properties of the reservoir formation for given steady production conditions. A description of the original 1-D linear heat sweep model was given by Hunsbedt, Lam, and Kruger (1984) and several applications are listed in Kruger (1988).

The linear model was improved by Lam (1986) to provide ability to examine more complex flow geometries and mixing of reinjected recharge fluid with resource fluid while maintaining the simple 1-D nature of the simulations. The linear heat sweep model now allows for radial return flow of reinjected fluid and for fluid mixing at the production zone of sweep fluid at its heat-extracted temperature with resource fluid cooling at a constant rate. More recently, doublet flow was added as another flow geometry in which the intrinsic 2-D nature of doublet flow is approximated as 1-D flow by linear flows in a series of flow crescents extending normal to the line through the doublet pair of injection-production wells. The hydrologic flow between wells in a uniform flow field was described by Grove, Beetem, and Sower (1970). The 1-D doublet heat sweep model calculates the heat extraction as linear heat sweeps in the series of flow crescents. A description of the model is given in Lam and Kruger (1987).

One of the simplifications made in the heat sweep model is an assumption of a uniform-temperature formation of hot, fractured rock blocks encompassing the reinjection return flow geometry between

the injection and production wells. The extractable heat content of this mass of rock above the recharge temperature is given by

$$H = [\phi\rho wVwCw+(1-\phi)\rho rVrCr]*(To-Tr) \quad (1)$$

where ϕ = formation porosity
ρ = mean phase density
V = swept formation volume
C = phase specific heat
To = mean initial formation temperature
Tr = recharge fluid temperature
and w,r refer to water and rock phases, respectively.

The assumption of a uniformly-distributed thermal energy reservoir is adequate for the linear and radial return flow geometries in that the uncertainty in the flow boundaries is probably not much greater than the unknown non-uniformity in the reservoir structural and thermal characteristics. On the other hand, this assumption for the intrinsic 2-D doublet flow model with its series of expanding crescent flow volumes is not adequate for two reasons: (1) the use of a uniform high initial temperature for the outer crescents involves a reservoir volume much greater than the resource volume resulting in an unrealistic extractable heat content; and (2) the streamline flow away from the direct path to the production well makes a negligible contribution to the cooldown to abandonment temperature but provides a long period of production fluid at the mean initial reservoir temperature. The result of these two phenomena results in an overestimation of the cooldown time to the abandonment temperature.

To evaluate the effect of temperature distribution on the extraction of heat from large rock blocks and still maintain the 1-D nature of the doublet flow model, an exercise was carried out to observe the effect of varying the initial temperature distribution in the flow geometry on the cooldown behavior of the produced fluid. The distributions were arbitrarily set normal to the axis of the injection-production well pair with a uniform temperature in each crescent. Figure 1 shows the series of assumed initial temperature distributions: (1) a circular reservoir of radius one-half the well separation distance containing half of the injection return flowrate with temperature further away declining with crescent number, N, as 1/N; (2) a step function, with crescent number distance taken from the temperature-depth profiles estimated by Maciel (1988) for the well pair PR2-PR1 at the La Primavera geothermal field; (3) a normal distribution to the same external temperature distance as the step function; and (4) an exponential temperature decline from the well pair

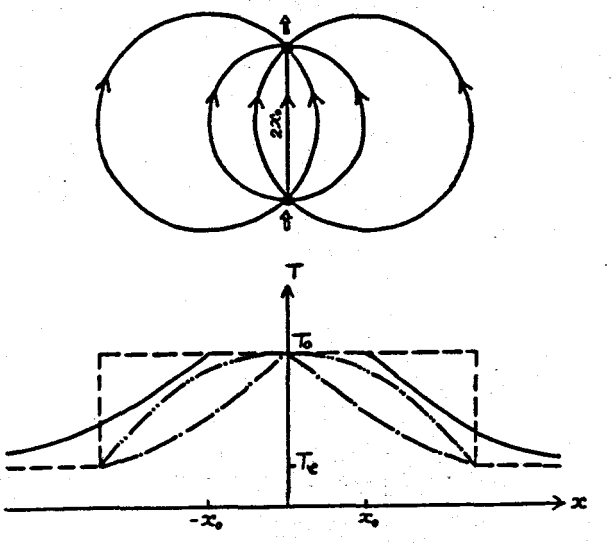

Figure 1. Temperature distributions for doublet flow simulations: (a) doublet flow as a series of crescents bounded by streamlines; (b) circular, step, normal, and exponential temperature distributions.

axis to the same external temperature distance. The same fractional distances were used for the El Chino well pair Az3-Az9 in the Los Azufres geothermal field.

1-D DOUBLET HEAT SWEEP MODEL WITH TEMPERATURE DISTRIBUTION

The 1-D Heat Sweep Model describes thermal energy extraction from a distribution of fractured rock blocks in a linear reservoir of uniform width and depth (Hunsbedt, et al, 1984). Energy extraction is based on the heat transfer from an irregular-shaped rock block investigated by Kuo et al (1977) and extended by Iregui, et al (1978) to an ensemble of rock blocks by size distribution. The ensemble is modeled as lumped equivalent-volume spheres with thermal time constant, τ , given by Hunsbedt, et al (1978) as

$$\tau = R^2/3\alpha\ (0.2 + 1/Bi) \quad (2)$$

where R = equivalent radius of the rock blocks
α = rock thermal diffusivity
Bi = rock Biot number (= hR/k)
h = reservoir heat transfer coefficient
k = rock thermal conductivity

The rate of heat extraction is determined by both the thermal time constant for the rock block distribution and the mean residence time of the recharge fluid from the reinjection well to the production well. The 1-D model is formulated in heat transfer equations for both the fluid and rock phases, in terms of the rock thermal time constant and fluid residence time. The equations are transformed into Laplace space and solved analytically. The resulting rock and fluid temperatures are converted into real space temperatures with the numerical algorithm reported by Stehfest (1970).

The linear and radial flow models have been useful in simulations involving numbers of injection or production wells or where structural features can act as boundaries to reinjection return flow. For single injection-production well pairs having no apparent reservoir boundaries, doublet return flow represents the maximum flow time for heat extraction from the reservoir formation as the series of crescent flows result in a spectrum of arrival times. The doublet flow field, sketched in Figure 1a is a series of streamlines emanating from the injection well, extending as circular arcs centered on the normal to the middle of the well pair axis, and converging at the production well. For a uniformly thick reservoir, doublet flow is two-dimensional.

Development of the 1-D doublet heat sweep model was described by Lam and Kruger (1987). The 2-D recharge return flow and associated heat transfer is approximated adequately with the 1-D linear heat sweep model by dividing the total flow field into a large number of flow crescents bounded by streamlines, such that the equivalent mean flow velocity through each narrow crescent characterizes the actual velocity in that crescent. The average flow velocity is uniform and constant in each crescent. The result is an overprediction of heat transfer from the rock blocks to the fluid in the early phase of the transient near the injection well, and underprediction of heat transfer near the midsection. The errors are mainly cancelled over the total sweep flow in each crescent. By integrating the sweep flow and heat transfer of the series of crescents arriving at the production well, the produced fluid temperature is simulated for the given production flowrate.

Generally, the production flowrate exceeds the reinjection flowrate, especially where the separated steam is discharged from the generating-unit turbine. The difference in flow is replaced by mixing the recharge sweep flow with resource fluid near the production well. The resource fluid is considered to originate at a remote location and cool with time at an exponential rate due to entry of colder groundwater or percolation from above. Cooling rates of -0.005/yr have been observed at several geothermal fields.

To estimate the importance of temperature distribution in the doublet flow model as it effects heat transfer in the series of flow crescents, the four different initial temperature distributions away from the well pair axis (shown in Figure 1b) were considered to represent a large spread of heat content available for recharge extraction. The first assumes a circular reservoir boundary with diameter equal to the well pair axis. Within the boundary, the initial temperature is To, decreasing to a given external temperature, Te, outside the boundary as 1/(N-NC/2), where N is the crescent number outside the boundary and NC is the total number of crescents. This temperature distribution should result in the largest extractable heat content above the abandonment temperature, Ta, specified for a given type of generator turbine. It is noted that for doublet flow, half of the crescents, NC/2, are contained within the circular boundary.

The second temperature profile is a step distribution, with a uniform reservoir initial temperature, To, to a given crescent number, and beyond that, a uniform external temperature, Te. The third temperature profile assumes each crescent has a uniform initial temperature which decreases exponentially as a function of distance from the well-pair axis. This distribution should result in the smallest extractable heat content above the abandonment temperature. The initial temperature Ti for crescent i at distance y from the axis is given by

$$Ti = To * \exp[-y/ya * \ln(To/Te)] \quad (3)$$

where ya = maximum distance from well-pair axis at Ta
To = initial temperature at the well-pair axis.

The fourth temperature profile assumes each crescent has a uniform initial temperature which decreases along a normal (bell-shaped) distribution from the well axis. This distribution most-closely follows observed temperature profiles and should account for the most-likely extractable heat content above the abandonment temperature. For this distribution, the initial temperature for crescent i at distance y from the well axis is given by

$$Ti=To*\exp[-((y/ya)*\mathrm{sqrt}(\ln(To/Te)))^2] \quad (4)$$

THE TWO CASE STUDIES

(A) La Primavera Doublet PR2-PR1

The La Primavera geothermal field is located in the State of Jalisco near the city of Guadalajara. The field currently has 8 completed wells, of which 7 are considered for commercial production. Three of these wells, PR1, PR8, and PR9, have been designated for use with the two 5-MW generating units expected in 1989. The non-productive well, PR2, is being considered as a reinjection well for these two units. A study to evaluate the potential for premature thermal breakthrough by the reinjected fluid in this well to the three production wells was reported by Kruger, et al (1988) based on preproduction data compiled by the field operating staff.

For reinjection recharge into well PR2 consisting of brine flow from the separators and condensate from the turbines, the return flow geometry was examined as small-angle radial flow to each well individually, as large-angle radial flow to the three wells collectively, and as doublet flow to the central well. The simulated cooldown curves for the sweep and mixed fluids for this case, based on an infinite initial temperature distribution, are shown in Figure 2a. The key compiled input data for the estimate were initial temperature of 277 C, recharge temperature of 70 C, injection flowrate of 69.8 kg/s, (65% of the production flowrate), with reservoir fluid makeup declining in temperature at a rate of -0.005 /y, and a mean formation porosity of 10 %. The reservoir thickness for return flow was estimated as 410 m over the well separation distance of 1180 m.

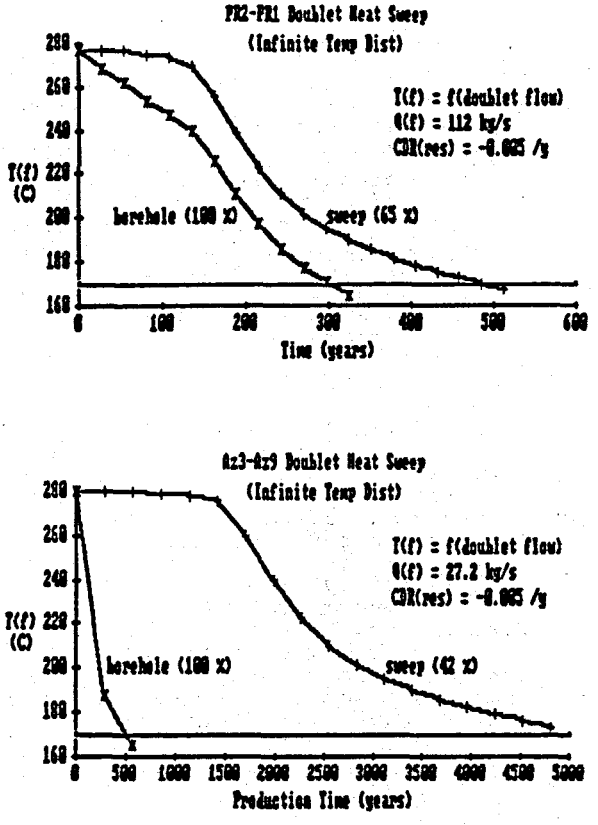

Figure 2. Production fluid cooldown results for the sweep fluid arriving at the production well and the mixed borehole fluid estimated by doublet flow with infinitely uniform initial reservoir temperature for (top) the La Primavera PR2-PR1 well pair and (bottom) the El Chino (Los Azufres) Az3-Az9 well pair.

(B) El Chino (Los Azufres) Doublet Az3-Az9

The Los Azufres geothermal field is located in the State of Michoacan, about midway between Guadalajara and Mexico City. The field consists of a number of production zones, named after the predominant local faults. The three zones currently with portable 5-MW wellhead generating units are the Tejamaniles zone in the south, the Maritaro zone in the north, and the El Chino zone in the center. The El Chino zone at present has a single production and reinjection well pair, Az9 and Az3, respectively. The zone is located between the El Chino, Laguna, and San Alejo faults which may act as reservoir boundaries for the El Chino reservoir.

A preliminary doublet-flow cooldown analysis for this well pair was reported by Lam and Kruger (1987) for the infinite initial temperature distribution. The simulated cooldown curves for this case are shown in Figure 2b. The heat-sweep time of 5000 years to abandonment temperature was very long compared to the mixed-fluid cooldown time of 500 years (and the no-reinjection cooldown time of 150 years), both based on a constant resource fluid cooldown rate of -0.005 /yr. The key compiled input data for El Chino well pair were initial temperature of 280 C, recharge temperature of 70 C, injection flowrate of 11.3 kg/s (42% of the production flowrate), with the same resource fluid cooldown rate of -0.005 /yr, and a mean porosity of 10 %. The reservoir thickness for return flow was estimated as 240 m over the measured separation distance of 2007 m.

RESULTS

The 1-D Doublet Heat Sweep Model was adjusted for this study to output the temperature distribution as a function of distance in terms of crescent number. The results, common to the two case studies, are shown in Figure 3. The circular reservoir model (Fig 3a) shows the constant initial temperature to crescent number 25, half of the 50 crescents used for the symmetric half field. This crescent number corresponds to a distance of one well-pair radius, whereas the 50th crescent is at a distance of more than 23 well-pair radii. The other distribution reach the assumed external temperature of 145 C at crescent number 31, corresponding to the abandonment temperature distance on the temperature profiles compiled by the La Primavera staff.

The studies for two well-pair doublet flows under markedly different flow conditions show significant thermal cooldown behavior with reinjection recharge. The La Primavera doublet is relatively closer together (1180 m) than the El Chino doublet (2007 m) with a correspondingly greater reinjection flowrate (68% of 102 kg/s compared to 42% of 27.2 kg/s)at essentially the same initial production temperature.

The results of the simulations for the two well-pair cases are shown as sweep fluid and mixed fluid cooldown curves to the abandonment temperature of 170 C, corresponding to the minimum saturated steam pressure of 8 bar required to operate the 5-MW unit turbines. Figure 4 shows these curves for the La Primavera well pair and Figure 5 for the El Chino well pair. The rapid drop in temperature from the observed initial bottomhole temperature results from the unrealistic colder water production from the crescents outside the thermal reservoir (50 % for the circular reservoir and about 30 % for the other three temperature distributions normal to the actual temperature profiles). The resulting production fluid cooldown times to abandonment temperature for these case studies are listed in Table 1 with the results obtained in the previous studies for the infinitely uniform initial temperature distribution. The calculated heat content of the recharge reservoir above the abandonment temperature and the amount of thermal energy extracted by the sweep fluid for each of the four temperature distributions is given in Table 2.

For the La Primavera doublet, the data show that the cooldown time to abandonment temperature for the circular uniform distribution, comprising half of the number of crescents, is less than half of the time for the infinitely uniform temperature distribution. The cooldown time falls between those for the step and normal distributions. The time for the normal distribution, considered the most realistic one in view of the temperature contours estimated by the La Primavera staff, falls between the step distribution and

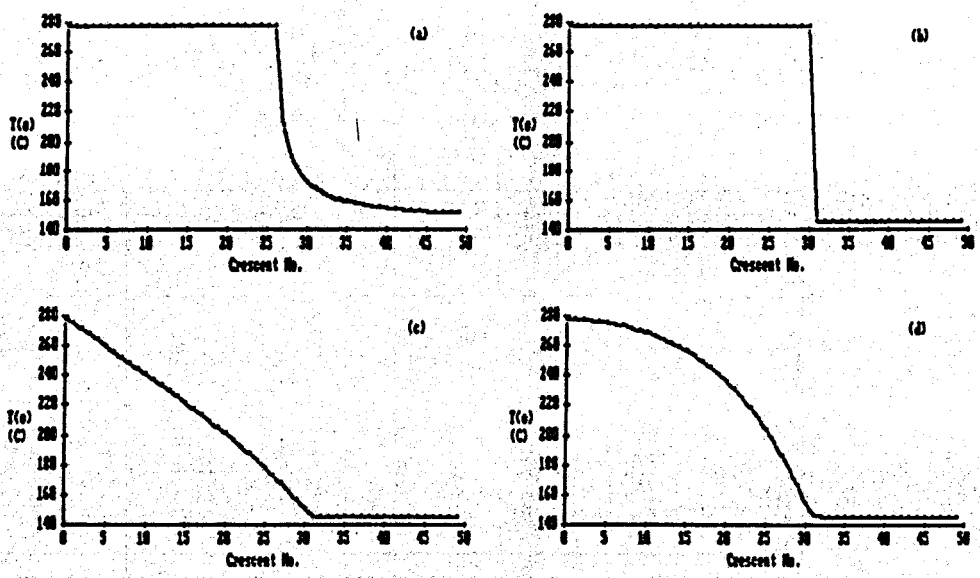

Figure 3. Temperature distribution output from the simulations: (a) circular reservoir with external decreasing temperature to abandonment temperature; (b) step function to given crescent number; (c) exponential decline; (d) normal distribution. For scale, crescent no. 25 is at 1 well-axis radius, crescent 50 is at 23 well-axis radii.

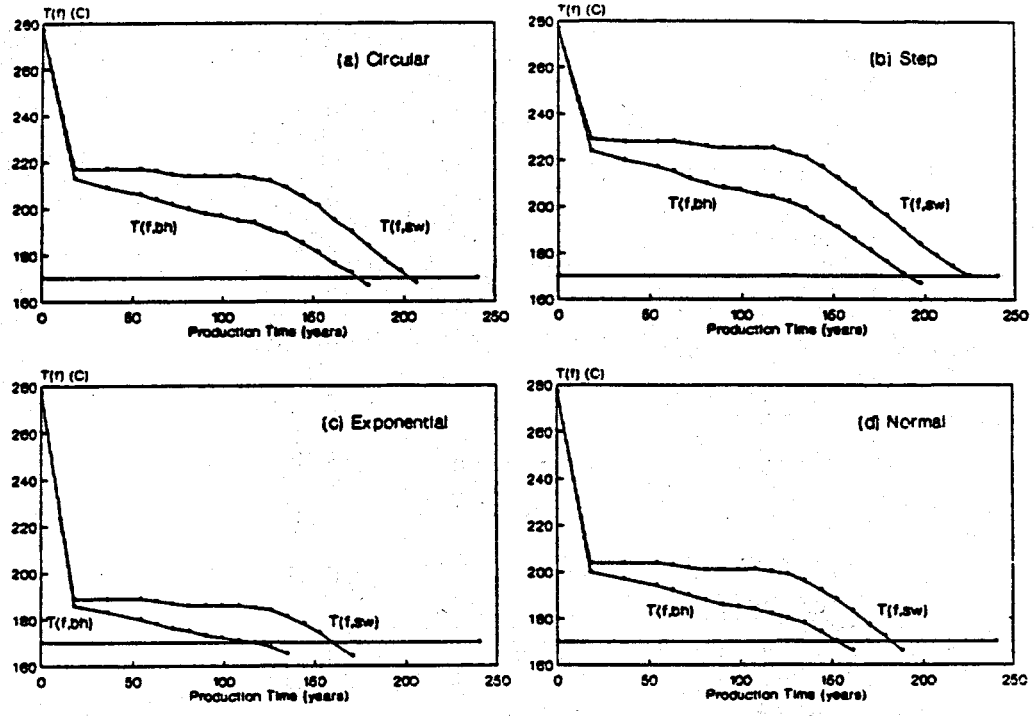

Figure 4. Cooldown results for the La Primavera PR2-PR1 well pair doublet for the given temperature distributions.

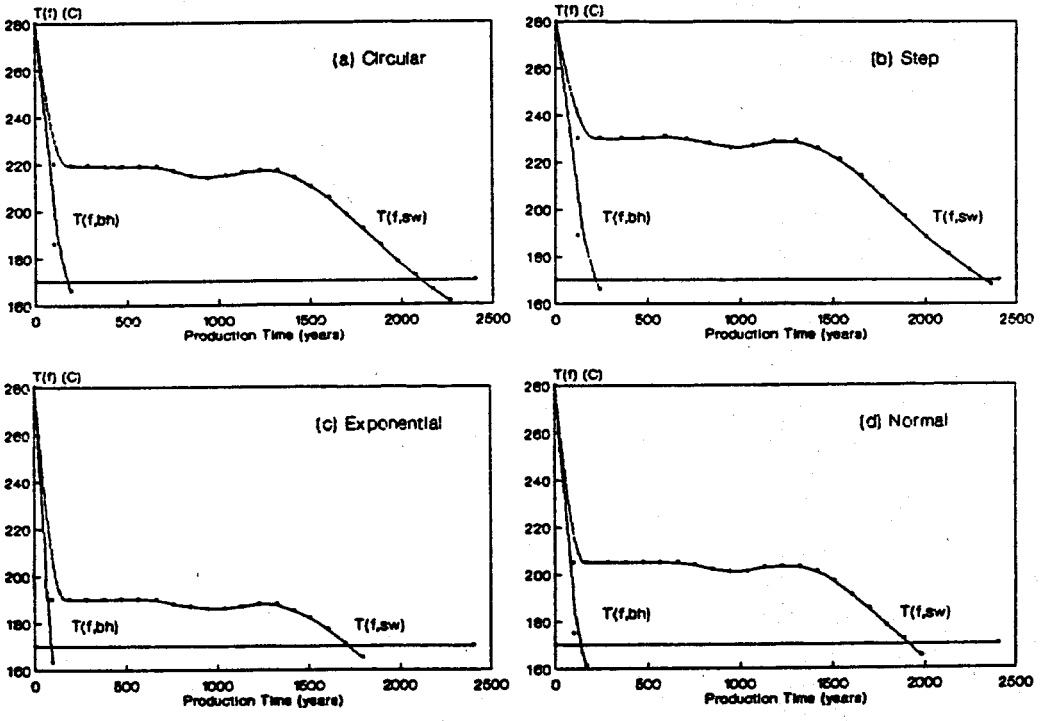

Figure 5. Cooldown results for the El Chino Az3-Az9 well pair doublet for the given temperature distributions.

Table 1
Comparison of Cooldown Times by Temperature Distribution

Assumed Temperature Distribution	Time to Ta = 170 C La Primavera PR2-PR1 Sweep Fluid (y)	La Primavera PR2-PR1 Mixed Fluid (y)	El Chino Az3-Az9 Sweep Fluid (y)	El Chino Az3-Az9 Mixed Fluid (y)
Infinite	484	297	5180	503
Circular	202	173	2110	165
Step	224	191	2320	206
Exponential	159	114	1720	67
Normal	182	153	1910	118

Table 2
Heat Extraction by Reinjection Recharge

Assumed Temperature Distribution	La Primavera PR2-PR1 Heat Content (10^{18} J)	La Primavera PR2-PR1 Heat Extr'd (10^{18} J)	La Primavera PR2-PR1 Fractn Extr'd (%)	El Chino Az3-Az9 Heat Content (10^{18} J)	El Chino Az3-Az9 Heat Extr'd (10^{18} J)	El Chino Az3-Az9 Fractn Extr'd (%)
Circular	30.9	0.296	0.96	52.2	0.511	0.98
Step	28.9	0.347	1.20	48.6	0.595	1.22
Exponential	28.7	0.197	0.69	48.3	0.349	0.72
Normal	28.7	0.248	0.86	48.4	0.429	0.89

the more rapidly declining exponential distribution. The heat content for the circular reservoir with rapid temperature falloff after 25 crescents is somewhat greater than the others with 31 crescents to abandonment temperature. The heat extraction varies as the distribution type, ranging from about 0.7 to 1.2 percent.

The data for the El Chino case reflects the difference in sweep reservoir volume and reinjection rate with much longer cooldown times. The range for all of the initial temperature distributions is less than half of the 5000 years observed for the infinite uniform temperature distribution. The relative times for the four initial temperature distributions are about the same as for the La Primavera doublet. The circular reservoir again shows a cooldown time between those for the step and normal distributions and the normal distribution between those for the step and exponential distributions. The heat content calculated for this larger flow doublet is correspondently larger. The heat extracted by recharge return flow sweep is also larger with about the same fractional extraction of thermal energy. The relative similarity in the heat sweep for these two doublets may be due to the similar reservoir properties for fracture spacing, porosity, and initial temperatures.

CONCLUSIONS

In a geothermal reservoir with a large separation distance between injection and production wells relative to the reservoir mean fracture spacing, and with no apparent flow boundaries, the doublet return flow serves as a reasonable flow geometry for the well pair system. In unexploited geothermal resources, the initial temperature distribution for the whole reservoir is generally not known. In such cases the assumption of an initial temperature distribution becomes necessary. This study showsthat the assumption of a fractured-rock reservoir with temperature normally distributed away from the production well zone results in estimated cooldown times with enhanced energy recovery smaller than those estimated for an extended uniform temperature distribution. The estimated cooldown times also fall between those for the larger heat content of the step distribution and the exponential temperature decline. The corresponding results in terms of heat extraction from theformation can be estimated from the given reservoir thermophysical properties. The two case studies with available preproduction data show the relative cooldown times for these initial temperature distributions compared to the results with the assumption of an infinitely uniform temperature distribution. In contrast to the almost complete extraction of the heat content above the abandonment

temperature for the small and well-defined linear and radial flow geometries, the doublet flow geometry with its essentially infinite expanse and very large heat content, shows a very small heat extraction fraction (of the order of one percent in the cases studied) as reinjection recharge fluid at the injection temperature breaks through in the shortest crescents.

REFERENCES

Grove, D.B., Beetem, W.A., and Sower, F.B., Fluid Travel Time between a Recharging and Discharging Well Pair having a Uniform Flow Field, Water Res. Res. 6, 1404-1410 (1970).

Hunsbedt, A., P. Kruger, and A.L. London, Energy Extraction from a Laboratory Model Fractured Geothermal Reservoir, J.Petrol.Tech., 30, No.5, 712-718 (1978)

Hunsbedt, A., Lam, S.T., and Kruger, P., User's Manual for the 1-D Linear Heat Sweep Model, Report SGP-TR-75, Stanford Geothermal Program, Stanford University, 1984.

Iregui, R., A. Hunsbedt, P. Kruger, and A.L. London, Analysis of Heat Transfer and Energy Recovery in Fractured Geothermal Reservoirs, Report SGP-TR-31, Stanford Geothermal Program, Stanford University, 1978.

Kruger, P., The Role of Heat Sweep in Reinjection of Cooled Geothermal Fluids, Geotermia, 4, 247-253 (1988).

Kuo, M.C.T., P. Kruger, and W.E. Brigham, Shape-Factor Correlations for Transient Heat Conduction from Irregular-Shaped Rock Fragments to Surrounding Fluid, Paper 77-HT-54, AIChE-ASME Heat Transfer Conference, ASME, August, 1977.

Lam, S.T., Chapter 6 (1986) in PhD Thesis (in preparation).

Lam, S.T. and Kruger, P., 1-D Doublet Heat Sweep Model, Proceedings, 9th NZ Geothermal Workshop, (University of Auckland, NZ, November, 1987)

Maciel, R., La Primavera Geothermal Field, CFE, Guadalajara, Mexico, private communication, 1988.

Stehfest, H., Numerical Inversion of the Laplace Transform, Algorithm No. 368, Comm.ACM, 13, No.1 47-49, 1970.

PROCEEDINGS, Fourteenth Workshop on Geothermal Reservoir Engineering
Stanford University, Stanford, California, January 24-26, 1989
SGP-TR-122

SIMULATION OF PRESSURE RESPONSE DATA FROM GEOTHERMAL RESERVOIRS BY LUMPED PARAMETER MODELS

Gudni Axelsson

National Energy Authority, Grensásvegur 9, 108 Reykjavík, ICELAND

ABSTRACT

Detailed numerical modeling of geothermal reservoirs is time consuming, costly and requires large amounts of field data. Lumped parameter modeling is in some cases a cost effective alternative. A method has been developed that tackles simulation of pressure response data by lumped models as an inverse problem and therefore requires very little time. This method of lumped modeling has been used successfully to simulate data from several low-temperature geothermal reservoirs in Iceland. The lumped simulators have been used to predict future pressure changes and they provide information on the global hydrological characteristics of the geothermal reservoirs.

INTRODUCTION

Modeling of geothermal systems, as a tool for resource assessment, has grown significantly during the last decade. Rapid advances have been made in the development of numerical simulators for detailed and complex modeling of such systems (Bodvarsson et al., 1986). Yet detailed numerical modeling of complex fluid/rock systems, such as geothermal reservoirs, is both time consuming and costly. In addition distributed parameter modeling of geothermal reservoirs requires large amounts of geological, geophysical, geochemical and hydrological data.

Other methods for modeling geothermal systems are available. The most appropriate approach, for a particular modeling study, is determined by the available field data as well as the objectives of the study. In situations where available funds, field data and time are limited, detailed modeling may not be feasible. Lumped parameter modeling is in such cases a viable alternative. Lumped parameter models have been developed for many geothermal reservoirs (Grant et al., 1982; Bodvarsson et al., 1986). Wairakei in New Zealand (Fradkin et al., 1981) and Svartsengi in Iceland (Kjaran et al., 1979; Gudmundsson and Olsen, 1987) can be mentioned as examples. Bodvarsson (1966) discusses the usefulness of lumped methods of interpreting geophysical exploration data.

Energy from several low-temperature ($\lesssim$150 °C) geothermal reservoirs in Iceland is used for space heating by various district heating services. A limited number of wells have been drilled into many of these reservoirs. But data on the production from the fields as well as data on the pressure in one or two observation wells are often available. Funds for detailed modeling may not be available to the smaller district heating services.

In this paper an effective method of lumped parameter modeling, which has been used successfully for pressure response data from several Icelandic geothermal reservoirs, is discussed. This method tackles the simulation problem as an inverse problem. It automatically fits analytical response functions of lumped models to the observed data by using a non-linear iterative least-squares technique for estimating the model parameters. The theoretical background of this method will briefly be presented, but the details are given by Bodvarsson and Axelsson (1986) and Axelsson (1985).

THEORY AND SOLUTION METHOD

Consider a general lumped network of the type sketched in Figure 1 consisting of a total of N capacitors or boxes with capacitances (storage coefficients) κ. A capacitor has the mass capacitance κ when it responds to a load of liquid mass m with a pressure $p = m/\kappa$. The capacitors are pairwise connected by up to N(N-1)/2 conductors (resistors) of conductances σ_{ik} ($\sigma_{ii} = 0$). The mass conductance of a conductor is σ when it transfers $q = \sigma\Delta p$ units of liquid mass per unit time at the impressed pressure differential Δp. The particular element σ_{ik} connects the i'th and k'th capacitors and because of linearity $\sigma_{ik} = \sigma_{ki}$. The network is open in the sense that the i'th capacitor is connected by a conductor of conductance σ_i to an external capacitor that maintains equilibrium pressure of magnitude zero. The network is closed when $\sigma_i = 0$ for i = 1,2 . . . N.

Let $p_i(t)$ be the pressure in the i'th capacitor and $q_{ik}(t)$ be the mass flow from the k'th to the i'th element. Then the basic equations are the mass flow equation

$$q_{ik} = \sigma_{ik}(p_k - p_i) \qquad (1)$$

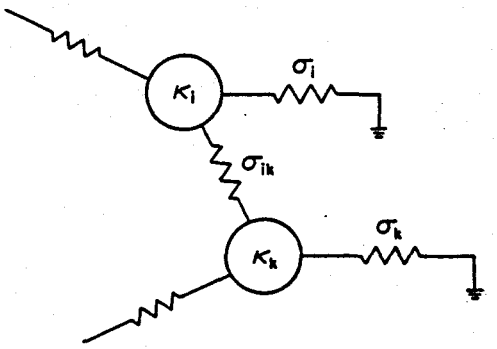

Figure 1. *General lumped capacitor/conductor network.*

and the equation for conservation of mass

$$(2) \qquad \kappa_i \, dp_i/dt = \sum_{k=1}^{N} q_{ik} - \sigma_i p_i + f_i$$

where f_i represents an external source mass flow into the i'th capacitor. Inserting (1) into (2) one obtains the basic system equations in matrix form

$$(3) \qquad \mathbf{K}\, d\vec{p}/dt + \mathbf{A}\vec{p} = \vec{f}$$

where the vectors and matrices are defined as follows

$$\mathbf{K} = [\kappa_i \delta_{ik}]$$

$$(4) \qquad \mathbf{A} = [(\sum_j \sigma_{ij} + \sigma_i)\delta_{ik} - \sigma_{ik}]$$

$$\vec{p} = (p_i), \quad \vec{f} = (f_i).$$

To obtain general solutions of the system of equations (3), one first derives the response of the network to an impulsive drive of the the k'th capacitor, at time t = 0^+, given by

$$(5) \qquad f_i = 0 \text{ for } i \neq k, \quad f_k = \delta_+(t)$$

Here $\delta_+(t)$ is the delta function in time, centered at t = 0^+. The response to this particular drive is $\vec{h}_k(t)$, the k'th impulse response vector of the network that is the solution of (3) with $\vec{f}$ given by (5). If the network is driven by a general causal drive $\vec{f}(t)$, and can be taken to be in equilibrium at t = 0, the response is obtained by the convolution

$$(6) \qquad \vec{p}(t) = \sum_{k=1}^{N} [\int_0^t \vec{h}_k(t-\tau) f_k(\tau)\, d\tau], \quad t>0$$

Equation (3) can be solved by considering the associated eigenvector problem

$$(7) \qquad \mathbf{A} = \lambda \mathbf{K}\vec{\tau}$$

where $\vec{\tau}$ and λ are the eigenvectors and eigenvalues respectively. Equation (7) has up to N non-negative eigenvalues. The matrix **A** can be diagonalized as follows

$$(8) \qquad \mathbf{T}'\mathbf{A}\mathbf{T} = \Lambda \quad or \quad \mathbf{A} = \mathbf{K}\mathbf{T}\Lambda\mathbf{T}'\mathbf{K}$$

where Λ is a diagonal eigenvalue matrix, **T** the eigenvector matrix formed out of the column vectors $\vec{\tau}_j$ and **T**′ the transpose of the matrix T. The solution of (3) with a drive given by (5) is then given by

$$(9) \qquad \vec{h}_k(t) = \mathbf{T}e^{-t\Lambda}\mathbf{T}'\vec{\Delta}_k, \quad t>0$$

where $\vec{\Delta}_k$ is a vector having only one non-vanishing component equal to unity at the k'th entry.

The response of the i'th capacitor to an impulsive drive of the k'th capacitor is given by

$$(10) \qquad h_{ik}(t) = \sum_{j=1}^{N} \tau_{ij}\tau_{kj}\, e^{-\lambda_j t}, \quad t>0.$$

In practical situations a step response is often more convenient than the impulse response. The response of the i'th capacitor to a mass flow input q_k, for t>0, into the k'th capacitor is obtained by applying equation (6)

$$(11) \qquad p_{ik}(t) = q_k \sum_{j=1}^{N} \frac{\tau_{ij}\tau_{kj}}{\lambda_j} [\,1 - e^{-\lambda_j t}], \quad t>0.$$

It should be mentioned that closed networks have a singular matrix A such that $\lambda_1 = 0$. The corresponding eigenvector has the components $\tau_{i1} = V^{-1/2}$ where $V = \Sigma\kappa_i$. The solution (10) remains valid, but in the case of the step response (11) the first term of the sum becomes t/V.

To simulate pressure response data from a liquid-dominated geothermal reservoir an appropriate lumped model is chosen. Water is produced from one of the capacitors at a variable rate $q(t)$, the rate of production from the geothermal reservoir. The resulting pressure $p(t)$ is then observed in any given capacitor of the lumped model. One can write

$$(12) \qquad p(t) = \int_0^t h(t-\tau)\, q(\tau)\, d\tau$$

where h is the impulse response of the lumped model for the specific production and observation capacitors. The impulse response is given by equation (10) which can be rewritten

$$(13) \qquad h(t) = \sum_{j=1}^{N} m_j\, e^{-m_{j+N}t}$$

where N is the number of capacitors in the lumped model chosen. An iterative non-linear least-squares technique (Menke, 1984) is used to fit equations (12) and (13) to the observed data $p(t)$ and estimate the parameters m_i, which in turn depend on the properties of the model (Bodvarsson and Axelsson, 1986).

The observed pressure data is written as

$$(14) \qquad p_i = p(t_i); \quad t_i = i\Delta t, \quad i = 1,2 \ldots M,$$

where Δt is a fixed time interval, and the flow rate data is approximated by

$$(15) \qquad q(t) = q_i \text{ for } (i-1)\Delta t \leq t < i\Delta t$$

Equation (12) can be written as

$$\vec{g}(\vec{m}) = \vec{p} \tag{16}$$

where $\vec{g}$ is a vector-valued function and

$$\begin{aligned} &\vec{m} = (m_i), \quad i = 1,2 \ldots 2N \\ &\vec{p} = (p_i), \quad i = 1,2 \ldots M \\ &\vec{g} = (g_i); \quad g_i(\vec{m}) = p(t_i) \end{aligned} \tag{17}$$

Expanding equation (16) into a Taylor series the following iterative scheme can be set up to estimate the best fitting parameters $\vec{m}$ of a given model

$$\begin{aligned} &\mathbf{G}_n \, \Delta\vec{m}_{n+1} = \vec{p} - \vec{g}(\vec{m}_n^{est}) \\ &\vec{m}_{n+1}^{est} = \vec{m}_n^{est} + \Delta\vec{m}_{n+1} \end{aligned} \tag{18}$$

where $\vec{m}_0^{est}$ is an initial guess for the parameters and the matrix G is defined as

$$(\mathbf{G}_n)_{ij} = \left. \frac{\partial g_i}{\partial m_j} \right]_{\vec{m} = \vec{m}_n^{est}}, \quad j = 1,2 \ldots 2N \tag{19}$$

The least squares solution of (18) is given by (Menke, 1984)

$$\Delta\vec{m}_{n+1} = (\mathbf{G}_n^T \mathbf{G}_n)^{-1} \mathbf{G}_n^T \left[\vec{p} - \vec{g}(\vec{m}_n^{est})\right] \tag{20}$$

$$n = 0,1,2, \ldots$$

where $\mathbf{G}_n^T$ is the transpose of $\mathbf{G}_n$.

SIMULATION RESULTS FROM ICELAND

Field examples

The procedure outlined above has been used successfully to simulate pressure response data from several low-temperature (<150 °C) geothermal reservoirs in Iceland. Most of these reservoirs provide hot water for local district heating services. The locations of four geothermal fields, that will be presented as examples here, are shown in Figure 2. In each of these four cases long records of pressure response data are available. The pressure changes resulting from variable production from the fields have been monitored as water level changes in one or two observation wells. The water level data and data on the production are presented in Figures 4 through 7. Data on the subsurface geology of three of these reservoirs are, however, limited.

The Hamar-field in N-Iceland is a small geothermal field utilized by a district heating service that serves Dalvík, a small town of 1400 inhabitants. Production from the field started in 1969. Two production wells, with feed zones between depths of 500 and 800 m, are currently in use and the water temperature is 64 °C. Several wells have been drilled into the reservoir, but all within an area of 50x50 m. In view of limited research funds available to this small community and

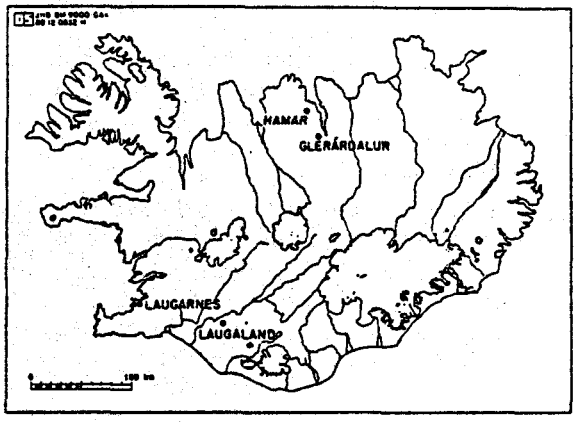

Figure 2. *Location of the low-temperature geothermal fields.*

the limited field data, lumped parameter modeling was used to estimate the production capacity of the Hamar-reservoir (Axelsson, 1988).

The Glerárdalur-field in N-Iceland is one of four small geothermal fields utilized by a district heating service that serves Akureyri, a town of about 13,000 inhabitants. Production from the field started in 1982 and currently one well is used for production. The main feed zone is at 450 m depth and the water temperature is 61 °C. Most of the wells drilled into the reservoir are shallow (100-300m) exploration wells. Due to the limited field data, lumped parameter modeling was determined to be appropriate for the Glerárdalur-reservoir (Axelsson et al., 1988).

The Laugarnes-field in SW-Iceland is considerably larger than the two fields mentioned above. It is one of three fields currently utilized by the Reykjavík Municipal Heating Service that serves about 130,000 inhabitants. Production from the field started in 1930 but increased greatly after 1962. About 44 deep (>500m) wells have been drilled into the field and the deepest well is over 3000 m deep. The major feed zones are between depths of 700 and 1300 m and the water temperature is between 115 and 135 °C. Considerable amounts of data are available on the geological characteristics of the Laugarnes-reservoir. A continuous water level record was, however, only available from one well. In this case lumped modeling and detailed numerical modeling were carried out simultaneously, in order to simulate the pressure response of the field and to estimate its production capacity (Reykjavík Municipal Heating Service, 1986).

The Laugaland-field in S-Iceland is a small geothermal field used by a district heating service that serves two small towns, Hella and Hvolsvöllur, with a total of 1200 inhabitants. Production from the field started in 1982. Three deep wells have been drilled into the field. Two of these wells are productive with the main feed zones

between depths of 400 and 900 m. The water temperature is between 85 and 100 °C. Due to limited research funds as well as limited field data, lumped parameter modeling was used to model the Laugaland-reservoir (Georgsson et al., 1987).

Simulations

A closed three capacitor lumped model, as shown in Figure 3, was used to simulate the pressure response data from each of the four reservoirs. These were four different models in the sense that the parameters of the models were different. Water is produced from the first capacitor (κ_1) and the pressure is monitored in the same capacitor. The first capacitor can be considered as representing the innermost part of each geothermal reservoir, the second one as outer and deeper parts of the reservoir and the third one possibly as the surrounding recharge part of each reservoir. These recharge parts may be colder than other parts of the geothermal systems.

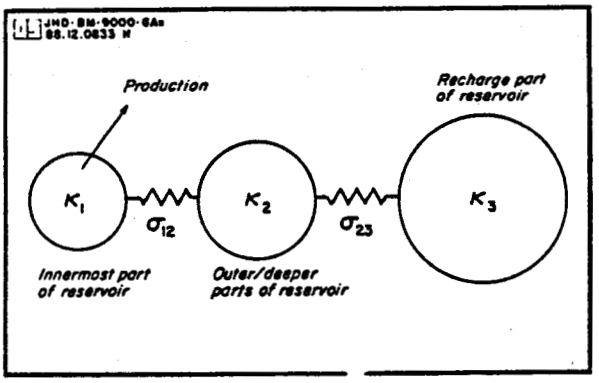

Figure 3. *General three capacitor lumped parameter model used in simulations.*

The simulations were carried out automatically by a computer. A first guess of the lumped model parameters was made and then the parameters were changed by the iterative process described above until a satisfactory fit was obtained. No assumptions were made *a priori* on the properties of the reservoirs. The results of the simulations, that is comparisons between observed and calculated water levels, are presented in Figures 4 through 7 and the parameters of the best fitting lumped models are given in Table 1 below.

Table 1 *Parameters of the best fitting lumped models*

	Hamar	Glerár-dalur	Laugar-nes	Lauga-land
$\kappa_1(ms^2)$	70.0	59.0	773	46.3
$\kappa_2(ms^2)$	6220	666	20900	3400
$\kappa_3(ms^2)$	124000	6080	364000	7100
$\sigma_{12}(10^{-5}ms)$	51.3	3.37	36.8	1.73
$\sigma_{23}(10^{-5}ms)$	18.5	1.89	61.8	9.96

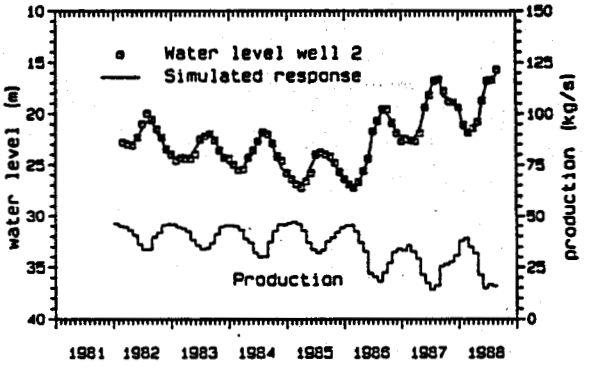

Figure 4. *Comparison of observed and calculated water level changes in the Hamar-reservoir in N-Iceland.*

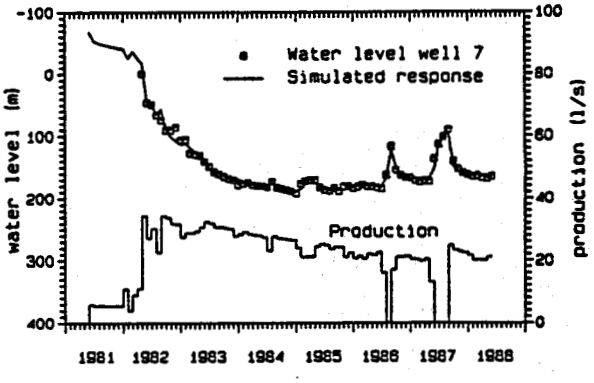

Figure 5. *Comparison of observed and calculated water level changes in the Glerárdalur-reservoir in N-Iceland.*

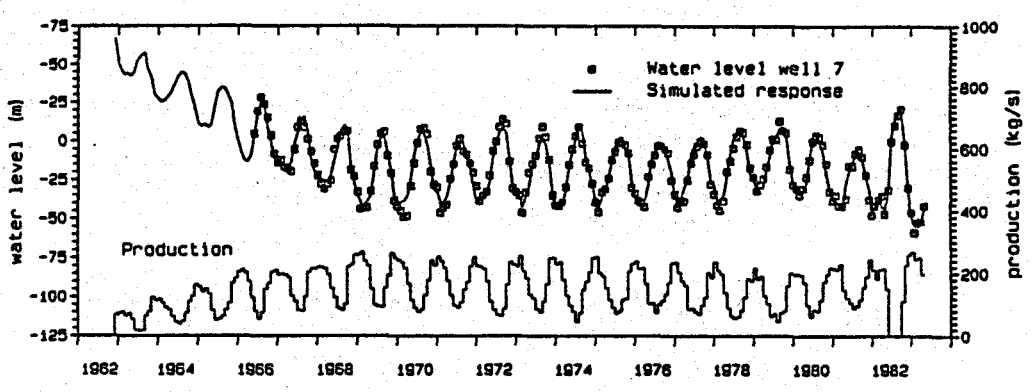

Figure 6. *Comparison of observed and calculated water level changes in the Laugarnes-reservoir in SW-Iceland.*

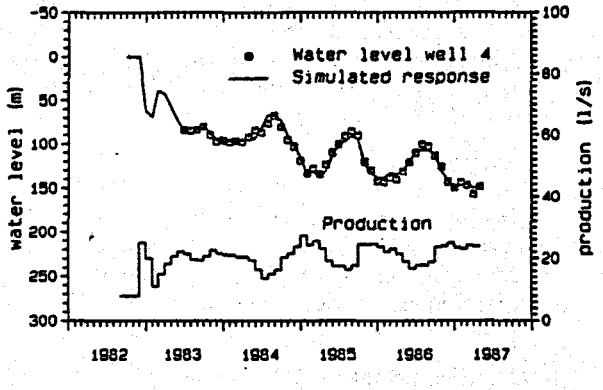

Figure 7. *Comparison of observed and calculated water level changes in the Laugaland-reservoir in S-Iceland.*

Discussion

Considering the results in Figures 4 through 7 one sees that the match between observed and calculated water level changes is quite satisfactory. This is so in spite of the simplicity of the models. The reason for this is the diffusive nature of the pressure response of geothermal systems. In using a closed three capacitor model there are five adjustable parameters which produce a very satisfactory match.

The parameters in Table 1 reflect clearly the highly variable productivity of the four fields. The models for the more productive fields have a higher total capacitance as well as higher conductivity values. The Laugarnes-field, which is the most productive, has the highest capacitance. The Hamar-field is somewhat less productive, which is reflected in a lower capacitance. The conductivity values for the Laugarnes and Hamar fields are, however, similar. The productivities of the Glerárdalur and Laugaland fields are quite poor. The total capacitance, as well as the conductivity values, are an order of magnitude greater for the Hamar and Laugarnes fields than for the Glerárdalur and Laugaland fields.

Capacitance, or storage, in a liquid-dominated geothermal system can result from two types of capacitive effects (storage mechanisms). The capacitance may on one hand be controlled by liquid/formation compressibilty. In that case the capacitance of a capacitor in a lumped model is given by

$$\kappa = V \rho c_t \qquad (21)$$

where V is the volume of that part of the reservoir in question the capacitor simulates, ρ the liquid density and c_t the compressibility of the liquid saturated formation. The compressibility is given by

$$c_t = \phi c_w + (1-\phi) c_r \qquad (22)$$

where c_w is the compressibility of the water and c_r the compressibility of the rock matrix. The capacitance may on the other hand be controlled by the mobility of a free surface. Then

$$\kappa = A \phi / g \qquad (23)$$

where A is the surface area of that part of the reservoir in question a capacitor simulates, ϕ its porosity and g the acceleration of gravity.

If the total capacitances of the Hamar and Laugarnes fields were solely due to compressibilty, based on equation (21) and porosities between 5 and 10 %, they would have to cover areas of the order of 1000 - 5000 km^2. Such large areas are unacceptable. Their capacitance must partially be due to free surface mobility. In that case the Hamar and Laugarnes systems would only cover areas of 10 - 70 km^2 (equation (23)). Therefore the third capacitor in the models for the Hamar and Laugarnes reservoirs appears to represent some unconfined part of the

hydrological systems, perhaps the groundwater system in each area. It is also likely that some parts of the Glerárdalur and Laugaland systems are unconfined as well.

The interpretation of the conductivity values is not straight forward. The conductivity values reflect the permeability in the systems, but they also depend on their internal geometry. Because of the limited knowledge on the subsurface geological characteristics of the systems the conductivity values will not be interpreted further.

The main objective of modeling a geothermal system is to assess its production potential. In the cases discussed here the lumped models were used to predict the pressure changes in the reservoirs in question for different cases of future production. The maximum allowable drawdown in the fields determines the maximum potential of the systems. Two examples of such predictions are presented in Figures 8 and 9 below.

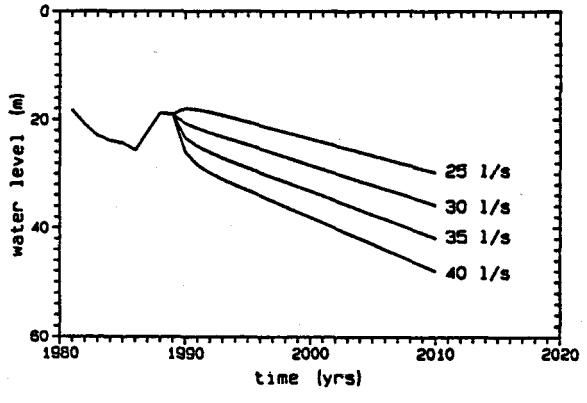

Figure 8. *Predicted water level changes in the Hamar-reservoir in N-Iceland.*

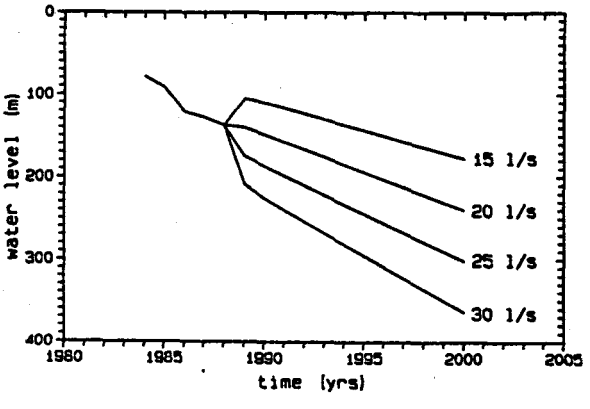

Figure 9. *Predicted water level changes in the Laugaland-reservoir in S-Iceland.*

CONCLUDING REMARKS

A method of simulating pressure response data from liquid-dominated geothermal reservoirs by simple lumped parameter models has been developed. The method uses an automatic non-linear least-squares iterative technique which requires very little time compared to more detailed/complex numerical modeling techniques. The use of this method is appropriate in cases where data on subsurface conditions are scarce but where the pressure response of a reservoir has been monitored carefully for some time. In such cases highly detailed/complex modeling, being much more costly, can hardly be justified. This method can also be used as a first stage in a modeling study of a reservoir as well as to provide independent checks on results of more complex modeling techniques.

Lumped parameter models can simply be considered as distributed parameter models with a very coarse spatial discretization (Bodvarsson et al., 1986). But the method presented here tackles the modeling as an inverse problem which requires far less time than direct, or forward, modeling. This makes lumped parameter simulations highly cost effective.

Examples of simulations of pressure response data from four low-temperature geothermal reservoirs in Iceland show that quite a satisfactory match between observed and calculated data can be obtained. Because of the satisfactory degree of approximation achived by the lumped models they have a strong power of predicting the future evolution from the observed past.

Detailed numerical modeling has also been performed for the Glerárdalur and Laugarnes fields (Axelsson and Tulinius, 1988; Reykjavík Municipal Heating Service, 1986). A comparison of the pressure data match by the two methods shows that in both cases the lumped models were able to match the pressure data with the same accuracy as the detailed numerical models. The time required for the lumped modeling, however, was only a fraction of the time required for the more detailed modeling.

At this point, it is appropriate to emphasize that a clear distinction has to be made between liquid reservoirs and reservoirs of thermal energy. In the individual areas, the extent of each type of reservoir depends on local geological and physical conditions. This paper deals with modeling of the liquid reservoirs only. Variations in temperature within the systems are not taken into account. This is justified by the fact that significant changes in the temperature of the water produced have not been observed in any of the cases presented here. It appears evident, however, that some parts of the liquid reservoirs of the Hamar and Laugarnes systems are unconfined. These two geothermal reservoirs are possibly connected to local groundwater systems and the recharge into the systems

may be cold groundwater. Thus the temperature of the water produced from the two fields may eventually decrease. In cases where changes in temperature and/or chemical content have been observed, lumped models can also be developed to simulate such data and to predict the future evolution.

ACKNOWLEDGEMENTS

I would like to thank the Dalvík District Heating Service, the Akureyri District Heating Service, the Reykjavík Municipal Heating Service and the Hella/Hvolsvöllur District Heating Service for allowing puplication of the data from the Hamar, Glerárdadalur, Laugarnes and Laugaland geothermal fields.

REFERENCES

Axelsson, G., 1988, The Hamar geothermal field in Svarfaðardalur. The production capacity of production wells of the Dalvík District Heating Service (in Icelandic), report OS-88053/JHD-11, National Energy Authority, Reykjavík, 68 pp.

Axelsson, G., 1985, Hydrology and thermomechanics of liquid-dominated hydrothermal systems in Iceland, Ph.D. Thesis, Oregon State University, Corvallis, Oregon, 291 pp.

Axelsson, G. and H. Tulinius, 1988, The Glerárdalur geothermal field. Simulation calculations and future predictions (in Icelandic), report GAx/HTul-88/01, National Energy Authority, Reykjavík, 26 pp.

Axelsson, G., H. Tulinius, Ó.G. Flóvenz and Þ. Thorsteinsson, 1988, Geothermal resources of the Akureyri District Heating Service (in Icelandic), report OS-88052/JHD-10, National Energy Authority, Reykjavík, 35 pp.

Bodvarsson, G., 1966, Direct interpretation methods in applied geophysics, **Geoexploration, 4**, 113-138.

Bodvarsson, G. and G. Axelsson, 1986, The analytical framework of the simulation of liquid reservoir response functions by lumped element models, **J. Eng. Ass. Iceland, 71** (in press).

Bodvarsson, G.S., K. Pruess and M.J. Lippmann, 1986, Modeling of geothermal systems, **J. Pet. Tech.** (Sept. 1986), 1007-1021.

Fradkin, L.J., M.L. Sorey and A. McNabb, 1981, On identification and validation of some geothermal models, **Water Resour. Res., 17**, 929-936.

Georgsson, L.S., A. Ingimarsdóttir, G. Axelsson, M. Kjartansdóttir and Þ. Thorsteinsson, 1987, Laugaland in Holt county. Well GN-1 and production 1982-1987 (in Icelandic), report OS-87022/JHD-04, National Energy Authority, Reykjavík, 65 pp.

Grant, M.A., I.G. Donaldson and P.F. Bixley, 1982, **Geothermal Reservoir Engineering**, Academic Press, New York, 369 pp.

Gudmundsson, J.S. and G. Olsen, 1987, Water-influx modeling of the Svartsengi Geothermal field, Iceland, **SPE Reservoir Engineering** (Feb. 1987), 77-84.

Kjaran, S.P., G.K. Halldorsson, S. Thorhallson and J. Eliasson, 1979, Reservoir engineering aspects of Svartsengi geothermal area, **Geoth. Resources Council Trans., 3**, 337-339.

Menke, W., 1984, **Geophysical Data Analysis: Discrete Inverse Theory**, Academic Press, Orlando, 260 pp.

Reykjavík Municipal Heating Service, Orkustofnun and Vatnaskil Consulting Engineers, 1986, The Laugarnes geothermal field. Production history and future outlook (in Icelandic), Reykjavík District Heating Service report (August 1986), 129 pp.

PROCEEDINGS, Fourteenth Workshop on Geothermal Reservoir Engineering
Stanford University, Stanford, California, January 24-26, 1989
SGP-TR-122

HYDROGEOLOGIC MODEL OF THE AHUACHAPAN GEOTHERMAL FIELD, EL SALVADOR

C. Laky, M. J. Lippmann,* G. S. Bodvarsson,* M. Retana† and G. Cuellar†*

*Earth Sciences Division
Lawrence Berkeley Laboratory
University of California
Berkeley, California 94720

† Comision Ejecutiva Hidroelectrica del Rio Lempa
P. O. Box 01-478
San Salvador, El Salvador

ABSTRACT

A hydrogeological model of the Ahuachapan geothermal field has been developed. It considers the lithology and structural features of the area and discerns their impact on the movement of cold and hot fluids in the system. Three aquifers were identified, their zones of mixing and flow patterns were obtained on the basis of temperature and geochemical data from wells and surface manifestations.

INTRODUCTION

As a part of a reservoir evaluation effort the Earth Sciences Division of the Lawrence Berkeley Laboratory (LBL) in cooperation with the Comision Ejecutiva Hidroelectrica del Rio Lempa (CEL) and the Los Alamos National Laboratory, has developed a hydrogeological model of the Ahuachapan geothermal field in El Salvador, Central America. The model is based upon data on the geologic/stratigraphic structure and initial thermodynamic conditions of the field.

This paper describes the hydrogeological model in terms of geological cross sections, the inferred faults and their effects on fluid flow, the various aquifers present and their temperature distributions.

GEOLOGIC SETTING OF AHUACHAPAN

El Salvador is almost entirely underlain by Tertiary to Holocene volcanic rocks and debris. From the Pacific Ocean toward the north, the country can morphologically be divided into five regions: the Coastal Plains, the Coastal Ranges, the Pacific Volcanic Chain, the Great Interior Valley (or Central Graben), and the Northern Mountain Ranges.

Of interest here is the Pacific Volcanic Chain, which is a line of young volcanoes that extends across El Salvador parallel to the Pacific Coast. It is closely associated with the high enthalpy geothermal fields in the country. Although Ahuachapán is the only area currently being exploited, exploration is being carried out at the Berlin, Chinameca, Chipilapa, San Vicente, Coatepeque and other areas.

The geologic structure of the Ahuachapan area is strongly influenced by the regional tectonics of Central America, where several lithospheric plates interact with one another (Weyl, 1980). El Salvador is located on the Caribbean Plate which is underthrust by the Cocos Plate. This subduction is responsible for the chain of active volcanos extending between Guatemala and Costa Rica and for the fracture tectonics of the area.

El Salvador is one of the world's most intense seismic areas, giving rise to different interpretations of the country's complex geologic structure. Wiesemann (1975) identified seven fault trends listed as: WNW-ESE, NW-SE, NE-SW, NNE-SSW, N-S, E-W, and NNW-SSE. Most faults are considered normal but those with horizontal displacements are said to be right-lateral on the W-E and WNW-ESE fault zones. The NNE- to NE-trending fault system is considered an important zone of left-lateral strike-slip faulting.

The Ahuachapán field is located in the northwestern sector of the Laguna Verde volcanic complex, on the southern flank of the Central Salvadorean Graben. It is about 5 km northwest of Laguna Verde, an extinct, andesitic, stratovolcano, approximately 1800 masl.

METHODOLOGY

This study has been undertaken to better define the stratigraphy and the fault/fracture characteristics in the geothermal system. This information is needed for the evaluation of fluid movement within the system. Careful analysis of the lithology encountered in the 32 deep wells drilled in the field (Fig. 1) revealed the presence of four major lithologic units (Table 1). The lithologic data were supplemented by temperature and pressure logs, data on loss of circulation zones, assumed aquifer locations, and core data. Mineralogical and geochemical data were contoured and the results compared to the inferred fault map (Aunzo et al., 1989). Cross-sections with their corresponding isotherms were drawn through the area. Previous structural maps of the area were analyzed as well as numerous papers and unpublished reports.

Table 1.
Lithologic units and aquifers identified at Ahuachapán

Formation	Rock Type	Unit	Aquifer
San Salvador (Quaternary)	colluvium, altered pyroclastics and lavas (Holocene)	Surficial Materials	Shallow Aquifer
	pyroclastics, andesites (Pleistocene)	Young Agglomerates	Regional Saturated Aquifer
	andesites, tuffs (Plio-Pleistocene)	Ahuachapán Andesites	Saline Aquifer (reservoir)
Balsamo (Pliocene)	breccias, agglomerates andesites	Older Agglomerates	Saline Aquifer

GEOLOGIC MODEL

Lithology

The known lithologic column at Ahuachapán consists mostly of the San Salvador Formation (Table 1) with only the basement rock from the Balsamo. The column has previously been divided into the following units: upper brown tuff, gray ignimbrite, pink ignimbrite, lower brown tuff, gray agglomerate, blue ignimbrite, old andesitic lavas, and ancient agglomerate (Jonsson, 1970). For this study, four major units have been defined, which are similar to those of Aumento et al. (1982). These are: Surficial Materials (SM), Young Agglomerates (YG), Ahuachapán Andesites (AA), and Older Agglomerates (OG).

The Surficial Materials occur in the top 100-150m and contain the "Shallow Aquifer". Beneath this unit there is a sequence of young pyroclastics and andesites, 300 to 800 m thick. These are the Young Agglomerates where losses in circulation are attributed to the "Regional Saturated Aquifer". Below these rocks one finds the Ahuachapán Andesites, a highly fractured 200 to 600 m thick unit that hosts the "Saline Aquifer," which is the main geothermal reservoir. The permeability of this unit is enhanced by columnar jointing and contact surfaces. The lower part of the Younger Agglomerates is highly hydrothermally altered, forming an impermeable barrier between the Saturated and Saline Aquifers. The Older Agglomerates (basement rocks) consist of dense breccias, agglomerates and andesites with little matrix permeability, but some fracturing.

Faults

The structure of the Ahuachapán field appears to be dominated by seven major and five minor faults (Fig. 2). These faults have been identified on the basis of lithologic logs, aerial photographs and existing structural maps.

The Surficial Materials are rarely displaced by the faults.

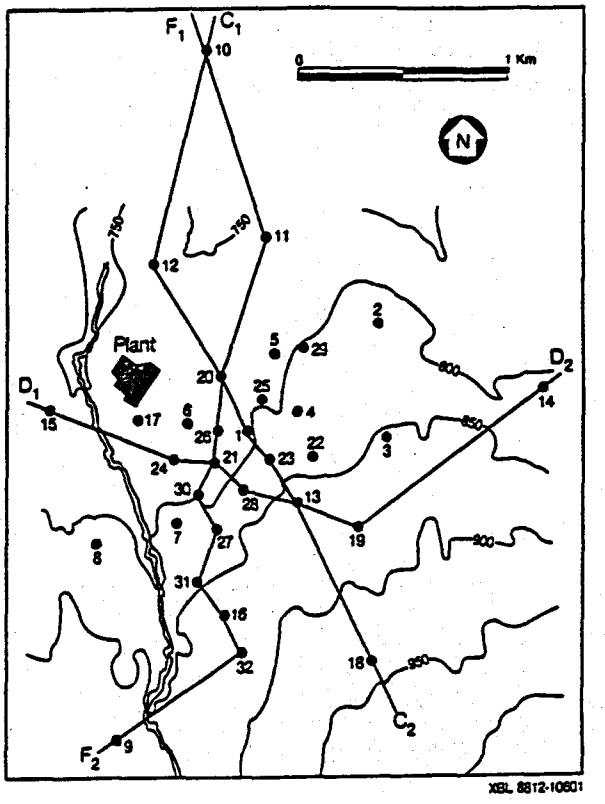

Figure 1. Location of the geothermal wells and cross-sections in the Ahuachapan geothermal field.

Young Agglomerates are of fairly uniform thickness except in wells AH-18 and AH-32, which is believed to be due to a high-angle reverse fault (Fault 10), and in AH-14 on the outskirts of the field. Within the wellfield, the Ahuachapan Andesites are fairly uniform in thickness with small displacements due to recent faulting. However, near the boundaries of the field these andesites have not been found (e.g., in wells AH-8, AH-9, and AH-10). In wells AH-2, AH-11, AH-12, AH-14, AH-18, AH-19, and AH-32 the Ahuachapan Andesites are found at a lower elevation than in the center of the wellfield. The Older Agglomerates are not penetrated by most of the wells so their extent is largely inferred. However, in AH-8, AH-9, and AH-10 these agglomerates are found at the elevation usually occupied by the Ahuachapan Andesites. This suggests an unconformity and a possible erosional surface.

HYDROGEOLOGIC MODEL

Aquifers

Three aquifers have been identified at Ahuachapán: the Shallow Aquifer, the Regional Saturated Aquifer, and the Saline Aquifer. This classification is based on the chemistry of the fluids and the pressure response of the aquifers to seasonal variations in precipitation. The three aquifers appear to coincide with the lithologic units discussed above (Table 1).

The Shallow Aquifer is unconfined and shows very rapid response to precipitation. The waters are generally of calcium carbonate type, locally sulfatic with residues below 0.5 gm/l (Romagnoli et al., 1976). In the wellfield the temperatures in this aquifer range from 40° to 100 °C, with decreasing temperatures toward the north.

The Regional Saturated Aquifer is recharged by direct infiltration but its response to variations in rainfall is much slower than that of the Shallow Aquifer. The water is of calcium-sodium carbonate type, with residues generally below 0.4 g/l (Romagnoli et al., 1976). In the wellfield the temperatures in the Regional Saturated Aquifer range from 110° to 130 °C (Aunzo et al., 1989), decreasing toward the north where a temperature of 46 °C was recorded in M-1, an exploratory drill hole.

The Saline Aquifer (geothermal reservoir) is thought to be recharged from the volcanic belt of Laguna de las Ninfas-Laguna Verde and Cerro de las Ranas, southeast and east of the wellfield. In this belt, deep water infiltration is facilitated by the presence of highly permeable volcanic chimneys. The waters of the Saline Aquifer are of sodium chloride type and high salinity (residues up to about 22 g/l; Romagnoli et al., 1976). The temperatures range from 214° to 240 °C in the reservoir with inferred minimum recharge temperatures of 245° to 250 °C (Aunzo et al., this volume).

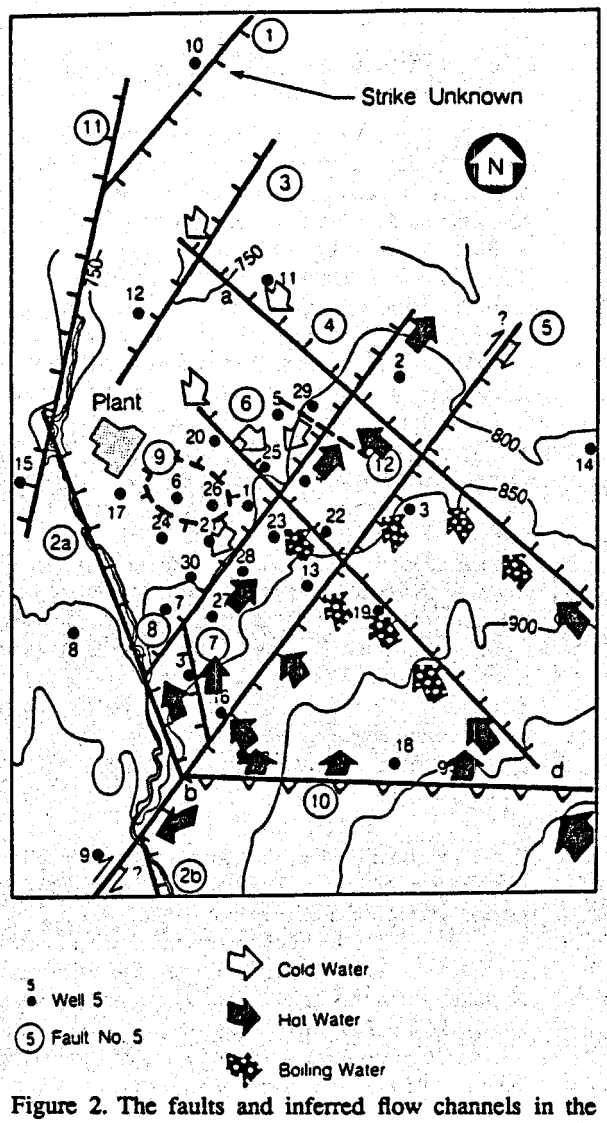

Figure 2. The faults and inferred flow channels in the Ahuachapan field.

Initial Thermodynamic Conditions

The initial pressure in the different aquifers reflect limited hydraulic communication between them as their hydraulic potentials are different (Fig. 3). The hydraulic potential is lowest in the Saline Aquifer and therefore there is a potential for cold water recharge into the reservoir from the overlying Saturated Aquifer. Within the geothermal reservoir (Saline Aquifer) there is no significant variation in hydraulic potential; and at the reference level of 200 masl the pressure is about 36 bar-g. Some of the cold peripheral wells (e.g. wells AH-10, AH-12, AH-15), which are not in hydraulic communication with the geothermal reservoir, have pressures exceeding 40 bar-g at the 200 masl level.

Figures 4 and 5 show the initial temperature distributions at Ahuachapan for 200 masl and sea level elevations, respectively. Both of these distributions basically reflect temperatures in the Ahuachapan Andesites. At 200 masl

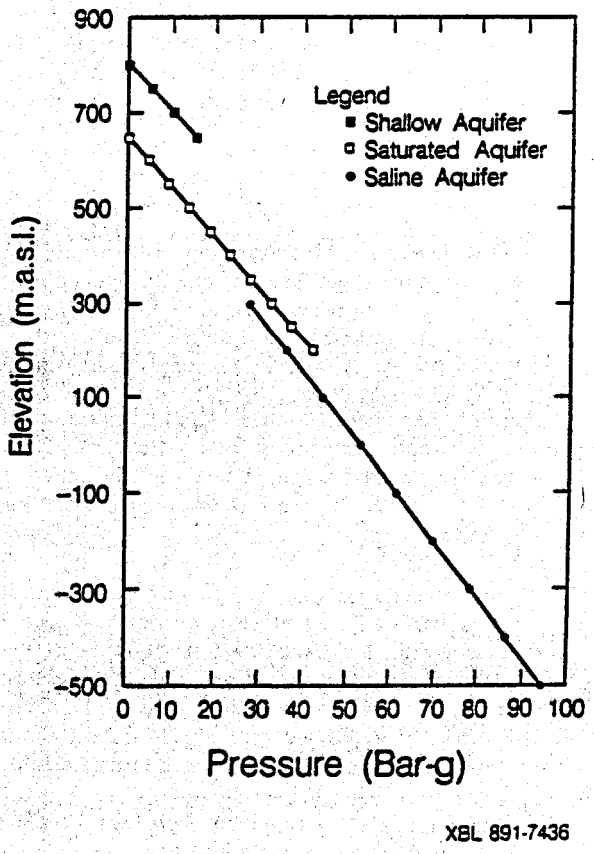

Figure 3. Plots of fluid pressure vs. elevation for the different aquifers.

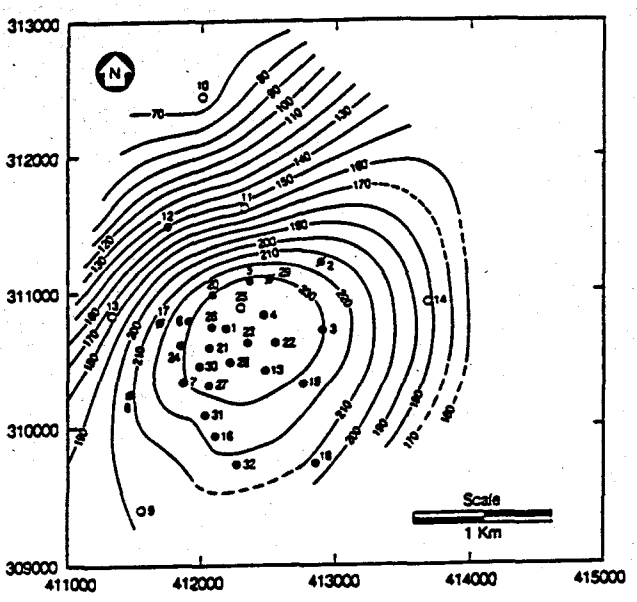

XBL 891-7437

Figure 4. Initial temperatures distribution (in °C) at 200 masl.

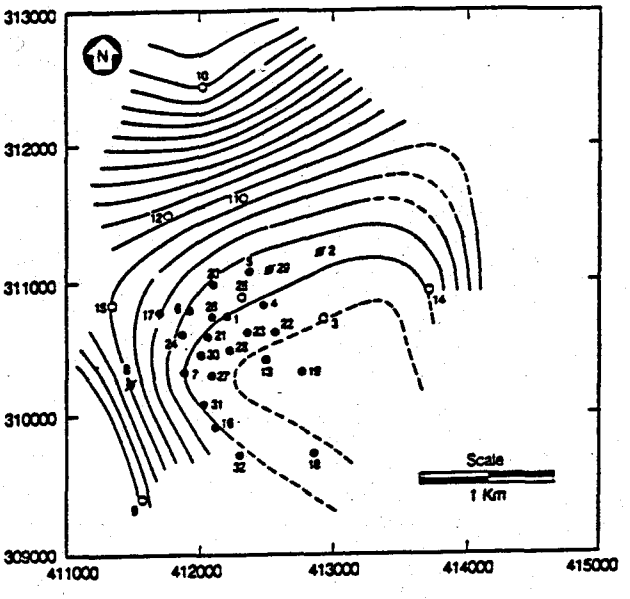

XBL 891-7432

Figure 5. Initial temperature distribution (in °C) at mean sea level elevation.

the highest temperatures are found in the center of the wellfield (230-235°C), whereas at sea level elevation the highest temperatures (240-245°C) are found in the southeast part of the wellfield. This clearly suggests that the upflow zone is southeast of the present wellfield, probably beneath the Laguna Verde volcanic complex. Exploitation has greatly affected the thermodynamic conditions of the system as discussed by Steingrimsson et al. (this volume).

Fluid Movement

In the field, the groundwater flow in the Shallow Aquifer is not significantly affected by the faults since few movements have been recent enough to displace the Elluvials. A study of well circulation losses suggests a rather uniform permeability in these less consolidated materials.

In the Regional Saturated Aquifer groundwater flow tends to be influenced by the fault pattern. The role of Faults 4, 5, and 6 seems to be especially important (Fig. 2), as indicated by the lost circulation zones observed during drilling.

The flow in the geothermal reservoir is also controlled by the faults. Most notably to the north and west, where Faults 3 and 11 act as barriers and limit the extent of the reservoir. Fault 4 is seen to cause similar effects to the northeast. This is strongly supported by the temperature distributions in the reservoir (Figs. 4 and 5). Other faults act primarily as conduits to flow rather than flow barriers.

Several geologic cross sections have been developed and illustrate the lithology, faulting and temperature distribution in the field (Figs. 6, 7 and 8). The locations of these cross sections are shown in Figure 1. Cross section $C_1 - C_2$ (Fig. 6) traverses the field from north to south. The sharp decline in temperature north of Fault 3 indicates that it acts as a barrier to flow, although the Ahuachapan Andesites are found north of this fault; north of Fault 1 the AA unit is not found. The isotherms clearly show that the Young Agglomerates act as a caprock to the system and the increasing depth to the reservoir (the AA unit) toward the south. The faults offset the AA from 50 to 200 meters. The cross section shows that in the natural state a small two-phase zone was present in the reservoir.

Cross section $D_1 - D_2$ (Fig. 7) represents an west-east traverse of the field. The isotherms indicate that Fault 2a acts as a barrier to the hot water flow, resulting in low temperatures in well AH-15. Only a thin AA unit is found in this well. The section also shows continuity of the reservoir to the east, although the depth to the AA is somewhat greater. In the center of the wellfield, the isotherms suggest reversals in many of the wells, although the extent of the reversals is poorly known due to the limited well depths. The cross section shows a good correlation between temperature contours and lithology.

Cross section $F_1 - F_2$ (Fig. 8) spans the field from the north to the southwest. Due to the circuitous route of this section several of the faults are crossed twice. This does not include Fault 9 which bounds the dome-like structure around wells AH-6 (not shown) and AH-26. Faults 1 and 2b displace the AA unit, which is not found in wells AH-9 and AH-10. This cross section again shows the inferred two-phase zone, evidence of temperature inversions and the good correlation between temperatures and lithology.

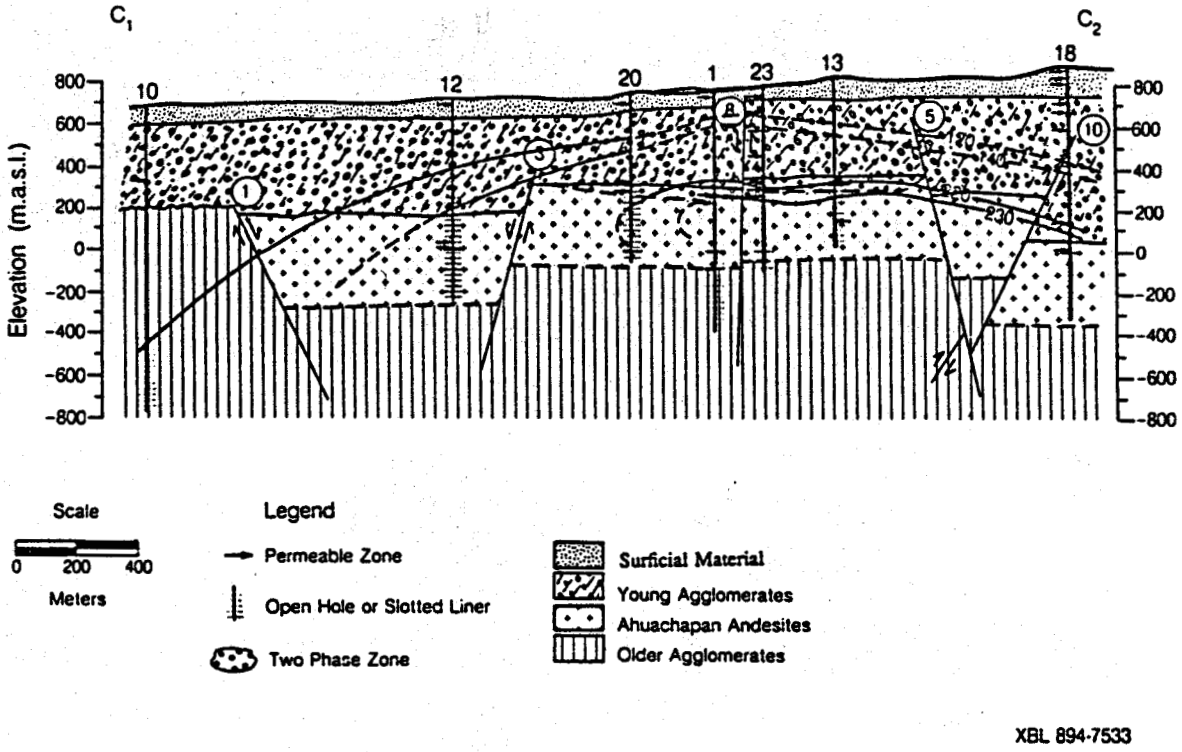

Figure 6. Section $C_1 - C_2$: cross-section through wells AH-10 to AH-18 showing lithology, faults, and isotherms.

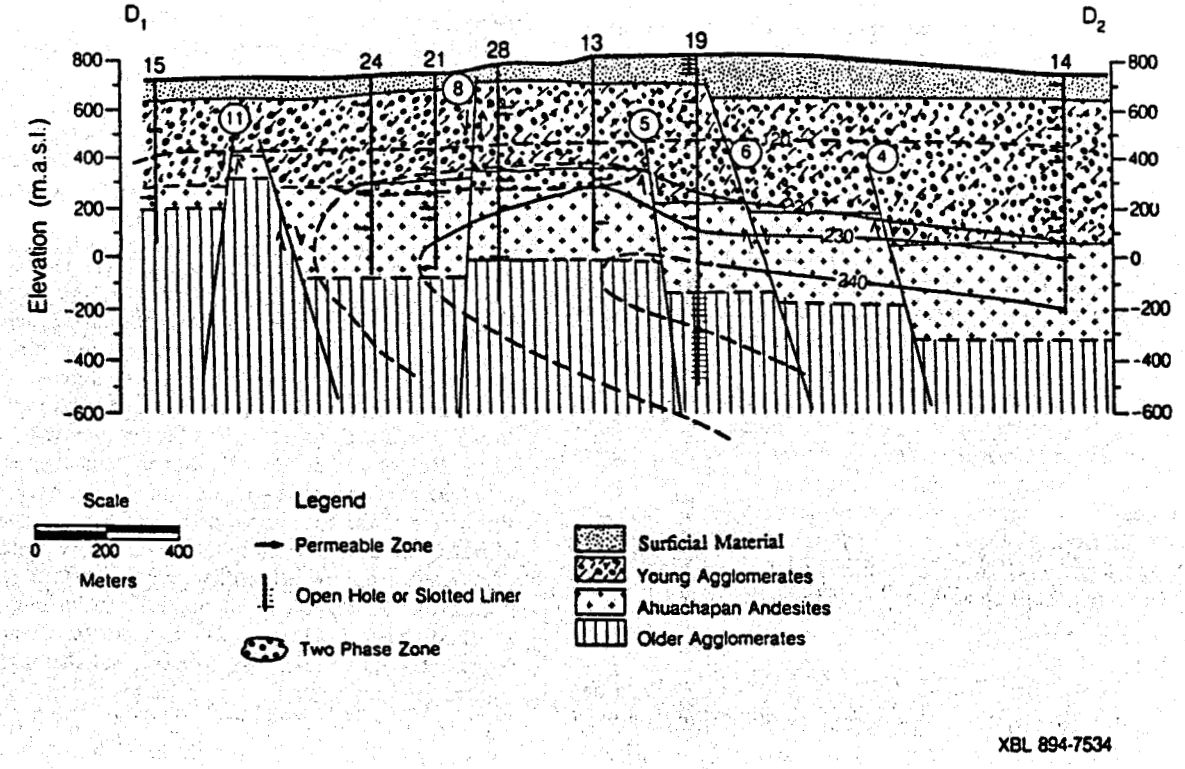

Figure 7. Section $D_1 - D_2$: cross-section through wells AH-15 to AH-14 showing lithology, faults, and isotherms.

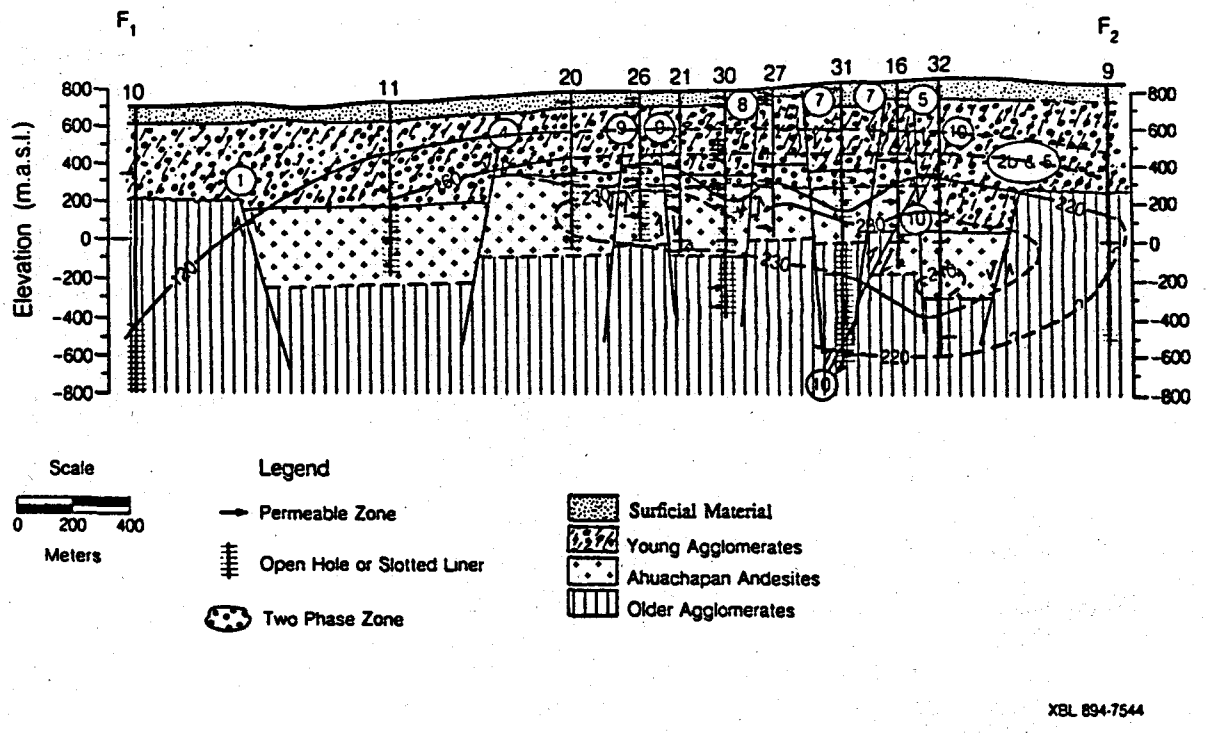

Figure 8. Section $F_1 - F_2$: cross-section through wells AH-10 to AH-9 showing lithology, faults, and isotherms.

THE AHUACHAPAN–CHIPILAPA GEOTHERMAL SYSTEM

In the vicinity of Ahuachapan, geothermal surface manifestations are spread over more than 100 km^2 (Fig. 9). These manifestations can be divided into high temperature fumaroles and steaming grounds on the northern slopes of the volcanoes located in the southern part of the area, and hot (40-100 °C) springs on the plain north of Ahuachapan.

The major fumaroles are: Cuyanausul on the northern slopes of Cerro Cuyanausul, east of Laguna Verde (outside the area shown in Fig. 9); El Sauce on the northern slopes of Laguna Verde; Agua Shuca and Playon de Ahuachapan near the wellfield; and La Labor in the Chipilapa region. Chemical analyses of gas samples from Ahuachapan and Chipilapa show similar gas composition indicating a common geothermal source fluid (Sigvaldason and Cuellar, 1970). A marked increase in hydrogen content in fumarole steam toward the southeast suggests that the geothermal upflow zone is located in the area of nearby volcanoes, probably the Laguna Verde volcano. Data from Ahuachapan and Chipilapa wells suggest that the source fluid is highly saline (more than 8000 ppm Cl) and that the upflow temperatures are above 250 °C (Aunzo et al., this volume).

The relationship between Ahuachapan and Chipilapa has been disputed over the years. Early drilling showed identical fluid chemistry and similar reservoir temperatures (Sigvaldason and Cuellar, 1970). Later, a resistivity survey of the area indicated a high-resistivity body (barrier) that separated the two fields. Recent resistivity studies, however, do not show this barrier. The previous interpretation is believed to be in error because of incorrect elevations used in the data analyses (James Fink, personal communication, 1988). The data seem therefore to indicate that the two fields are connected and fed by the same geothermal source. The ultimate proof of this connection would be pressure interference between the wells drilled in the two areas. The simple reservoir model used to match the drawdown history of Ahuachapan (Aunzo et al., 1989) predicts a drawdown in Chipilapa of a few bars due to fluid extraction in Ahuachapan that began in 1968. However, as the wells in Chipilapa are plugged at shallow depth this cannot be confirmed.

The hot springs on the plain north of Ahuachapán are at elevations below 580 masl, generally producing fluids from the Regional Saturated Aquifer (Sigvaldason and Cuellar, 1970; Cuellar et al. 1981). The maximum elevation of these springs matches with the pressure potential of the Regional Saturated Aquifer in Ahuachapán where 600-660 masl water levels are found. An exception to this is the main hot spring area, El Salitre, about 7 km north of Ahuachapán where more than 1000 L/s of 68-70 °C water used to be discharged. The fluid of these springs was, prior to exploitation at Ahuachapán, higher in dissolved solids (especially chloride) than that of the Regional Saturated Aquifer. The original chemistry of El Salitre has been explained to be due to mixing of the fluid from the Regional Saturated Aquifer with 10-20 percent of geothermal fluids with considerable steam heating (Glover, 1970; Sigvaldason and Cuellar, 1970).

The hydrologic model discussed above is summarized in the simplified illustrations shown in Figure 9. It is thought that an upflow of saline, high temperature (above 250 °C) fluid occurs underneath the volcanoes (probably Laguna Verde), southeast of Ahuachapan. From the upflow zone, fluid channels toward the north. A fraction of it flows toward the northwest and enters Ahuachapan near the southeast corner of the wellfield, as suggested by the shape of isotherms and increasing temperatures in AH-18 (Steingrimsson et al., this volume). Another fraction flows toward the east to Chipilapa, however the main stream mixes with fluids from the Saturated Aquifer and is discharged through several hot springs at the El Salitre area.

SUMMARY

Our present understanding of Ahuachapan suggests that the field is only an outflow of a deeper and much larger system and that the reservoir extends much farther to the east and southeast (Fig. 9). The main characteristics of the system are:

1) The Ahuachapan-Chipilapa system is recharged by an upflow zone southeast of the Ahuachapan wellfield, probably beneath the Laguna Verde volcanic complex. The temperature of this upwelling fluid is believed to be 250 °C or higher, as suggested by geochemical temperatures of the discharged fluid (Truesdell et al., this volume).

2) Most of the upwelling fluids flow to the north with the main outflow for this system being in the El Salitre springs area, located about 7 km north of the wellfield. The discharge is a mixture of geothermal and Regional Saturated Aquifer fluids, the mixing believed to occur in the vicinity of the springs rather than close to the geothermal field.

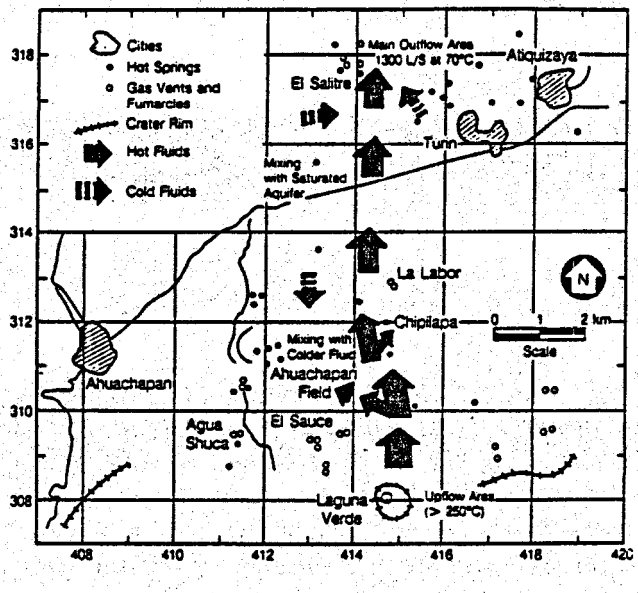

Figure 9. Fluid flow in the Ahuachapan/Chipilapa geothermal system.

3) Colder fluids recharge the Ahuachapán reservoir as evidenced by variations in chloride concentrations in the field. The cold water inflow is either laterally from the north or vertically downwards from the Regional Saturated Aquifer, which overlies the main reservoir and has a higher pressure potential.

4) The main reservoir rocks are the Ahuachapan Andesites and the underlying Older Agglomerates. Most of the produced fluids come from the andesites, although the permeability of the Older Agglomerates is significant, as evidenced by several feed zones encountered in this unit.

5) Faults limit the extent of the Ahuachapan reservoir toward the north and the west. The temperature reversal in well AH-32 also suggests that the extent of the field is limited toward the south.

6) The Ahuachapan and Chipilapa fields seem to communicate at depth and to be outflow zones of a large geothermal system.

ACKNOWLEDGEMENTS

This work was supported by a contract from the Los Alamos National Laboratory and by the U. S. Department of Energy under contract No. DE-AC03-76SF00098.

REFERENCES

Aumento, F., Viale, P., Choussy, M. and Santana, A., "Alteration Mineralogy of the Ahuachapan Geothermal Field", Geothermal Resources Council Trans., Vol. 6, pp. 7-10, 1982.

Aunzo, Z., Bodvarsson, G. S., Laky, C., Lippmann, M. J., Steingrimsson, B. and Truesdell, A. H., "The Ahuachapan geothermal field, El Salvador - Reservoir analysis" Lawrence Berkeley Laboratory report LBL-26612, (in preparation) 1989.

Aunzo, Z., Steingrimsson, B., Bodvarsson, G. S., Escobar, C. and Quintanilla, A., "Modeling studies of the Ahuachapan geothermal field, El Salvador" this volume, 1989.

CEL, "Mapa Estructural, Area Ahuachapan-Chipilapa", internal report, 1985.

Cuellar, G., Choussy, M. and Escobar, D., "Extraction-Reinjection at Ahuachapan Geothermal Field, El Salvador," *in* Rybach, L. and Muffler, L. J. P. (eds.) *Geothermal Systems: Principles and Case Histories*, John Wiley and Sons, pp. 321-336, 1981.

Glover, R.B., "Geochemical Investigations of the Ahuachapan Geothermal Field", UN report, October 1970.

Jonsson, J., "Report on Geological Investigation in Ahuachapan", UN report, July 1970.

Romagnoli, P., Cuellar, G., Jimenez, M., and Ghessi, G., "Hydrogeological Characteristics of the Geothermal Field of Ahuachapan", Proceeding 2nd UN Symposium on the Development and Use of Geothermal Resources, San Francisco, CA, pp. 571-574, 1976.

Sigvaldason, G.E. and Cuellar, G., "Geochemistry of the Ahuachapan Thermal Area, El Salvador", Proceedings UN Symposium on the Development and Utilization of Geothermal Resources, Pisa, Italy, pp. 1392-1399, 1970.

Steingrimsson, B., Bodvarsson, G. S., Cuellar, G. and Escobar, C., "Changes in thermodynamic conditions of the Ahuachapan reservoir due to production and injection," this volume, 1989.

Truesdell, A., Aunzo, Z., Bodvarsson, G. S., Alonso, J. and Campos, A., "The use of Ahuachapan fluid chemistry to indicate initial conditions and reservoir processes during exploitation," this volume, 1989.

Weyl, R., "Geology of Central America", 2nd ed., Gebrueder Borntraeger, Berlin, 1980.

Wiesemann, G., "Remarks on the Geologic Structure of the Republic of El Salvador, Central America", Mitt. Geol. Palaent., Inst. Univ. Hamburg, Vol. 44, pp. 557-574, 1975.

PROCEEDINGS, Fourteenth Workshop on Geothermal Reservoir Engineering
Stanford University, Stanford, California, January 24-26, 1989
SGP-TR-122

The Use of Ahuachapan Fluid Chemistry to Indicate Natural State Conditions and Reservoir Processes during Exploitation

A.H. Truesdell[1], Z. Aunzo[2], G. Bodvarsson[2], J. Alonso[3], and A. Campos[3]

[1] U.S. Geological Survey, Menlo Park, Calif. 94025
[2] Lawrence Berkeley Laboratory, Berkeley, Calif. 94720
[3] Comision Ejecutiva Hidroelectrica de Rio Lempa, San Salvador, El Salvador

ABSTRACT

Chemical analyses of production fluids from Ahuachapan, El Salvador, have been used to indicate natural state reservoir fluid temperatures and chloride concentrations and reservoir processes resulting from exploitation. Geothermometer temperatures (Na-K-Ca and SiO_2) and calculated aquifer Cl for early flows show a gradient from about 265°C and 9000 ppm Cl in the western part of the well field to 235°C and 6000 ppm Cl in the eastern part. The geochemical temperatures are 10-20°C higher than early downhole measurements. Since exploitation started, pressures have declined over most of the drilled area with boiling and excess-enthalpy discharges in the eastern and western parts. In the center of the field, a number of wells show mixing with cooler, less-saline water. These wells are nearly coincident with a major NE-SW oriented fault that may be the conduit for downward recharge of cooler fluids from an overlying aquifer.

INTRODUCTION

In 1987-88 a collaborative study of the Ahuachapan, El Salvador, geothermal reservoir was started by the Comision Ejecutiva Hidroelectrica del Rio Lempa (CEL), the Lawrence Berkeley Laboratory (LBL), and the U.S. Geological Survey (USGS) through a subcontract with the Los Alamos National Laboratory (LANL). Part of this study consists of interpretation of the chemical and gas analyses of Ahuachapan well fluids collected and analyzed by CEL. Chemical studies of produced fluids from geothermal wells provide information on the temperature, salinity, physical state, and flow of fluids in the reservoir. Extrapolation to the time of first production provides estimates of initial conditions, and changes in fluid composition indicate reservoir processes, including boiling, entry of different (usually cooler and less saline) fluids, and conductive heat transfer. The initial study of Ahuachapan well discharges concentrated on the interpretation of geothermometer temperatures and aquifer chlorinity as a function of time. These time-series diagrams have been used to indicate initial conditions and identify reservoir processes.

GEOTHERMOMETRY

Fluid geothermometers depend on temperature-sensitive reactions of fluids with rock minerals or fluid components. In a producing field, downhole temperatures may be conveniently estimated through the use of geothermometers applied to analyses of produced fluids, provided the geothermometer reaction is in equilibrium at downhole conditions (Mahon, 1966). Geothermometer reactions differ in kinetic rates, that is in how rapidly they re-equilibrate in response to a change in conditions. If the temperature of the fluid flowing to a well changes by boiling, by passage through hotter or cooler rocks, or by mixing with hotter or cooler fluids, or if the fluid has specific enthalpy higher than that expected for liquid at the prevailing temperature, then comparison of geothermometer temperatures may indicate reservoir processes. A particularly useful set of temperature indicators for this purpose includes the Na-K-Ca cation geothermometer, the quartz-saturation geothermometer, and the calculated "enthalpy temperature."

Cation geothermometers use temperature-dependent cation exchange reactions with rock aluminosilicates to indicate temperature. Some of these reactions are either too slow or too rapid to be of interest in reservoir studies. The most generally useful one is the empirical Na-K-Ca geothermometer developed by Fournier and Truesdell (1973) that depends on the exchange of K^+ ion for Na^+ and Ca^{++} on aluminosilicate minerals. The kinetics of this reaction are strongly dependent on the salinity of the fluid and on the amount and type of mineral surfaces present. With high-salinity fluid a large amount of mineral transformation is required to change fluid compositions. If no aluminosilicate surfaces are available (as might occur if channelways are mantled with quartz) then the cation exchange will not occur. Because of these factors the Na-K-Ca geothermometer is slow to respond to changes in temperature of even moderately saline fluids (e.g., Cl > 2000 ppm) and responds particularly slowly to decreases in temperature accompanied by quartz precipitation. Most changes in fluid temperatures involve cooling so mantling of surfaces by quartz (or other silica minerals) is very common.

Silica geothermometry uses the experimentally determined solubility of quartz and other silica minerals to indicate temperatures. In high-temperature reservoirs (> 200°C), quartz is the stable polymorph of silica. At these temperatures the precipitation and solution of quartz are relatively rapid (hours at > 260°C; days at > 220°C) and dissolved silica remains in equilibrium with quartz through most reservoir processes including mixing and boiling induced by exploitation. Thus the quartz geothermometer indicates temperatures close to those at the well bottom unless mixing occurs in the wellbore. Further discussion of quartz and cation geothermometry may be found in Fournier (1981).

"Enthalpy temperature" is the temperature of liquid water calculated from the enthalpy of the total fluid, assuming that there is no vapor entering the well. If, in fact, the fluid that enters the well is entirely liquid with no vapor, then the enthalpy temperature is the same as the actual inflow temperature. If there is excess steam, the enthalpy temperature will be higher than the actual inflow temperature. The comparison of geothermometer and enthalpy temperatures can indicate excess steam or mixture with cooler water. Enthalpy temperature is calculated from steam tables, using data for temperature and enthalpy of vapor-saturated liquid. For this calculation, both liquid and vapor phases must be present, so there is some inaccuracy for compressed liquid conditions. This error is small because the enthalpy of water is a weak function of pressure. A more serious limitation is that enthalpies exceeding that of water at the critical point (2100 kJ/kg at 374°C for the pure water steam tables used) cannot be represented by enthalpy temperatures since vapor-saturated liquid cannot exist with these enthalpies.

AQUIFER CHLORIDE

Chloride is a conservative element in geothermal fluids. It is not an essential constituent of any minerals normally found in geothermal systems and is not affected by temperature-sensitive reactions with rock. Concentrations of chloride are affected by boiling and mixing and may be used to identify these processes. Changes in aquifer chloride concentration may, for example, provide indications of the chemical breakthrough of less-saline water or of the amount of boiling and steam loss. Chloride concentrations in surface samples are strongly affected by boiling and steam separation, so for quantitative comparisons the aquifer chloride concentration must be calculated.

Water from geothermal wells is usually sampled from the weirbox of the silencer or from the separator through a cooling coil. If the enthalpy of the aquifer liquid is known, the fraction of steam separating and the change in solute concentrations can be calculated. Using enthalpy and chemical balances,

$$Cl,aquifer = Clseparator \times WFsep$$
$$WFsep = (Esteam, sep - Ewater, aqu) / (Esteam, sep - Ewater, sep)$$

for samples collected from the separator through a cooling coil. For weirbox samples there are the additional equations:

$$Clseparator = Clweirbox \times WFsilencer$$
$$WFsilencer = (Esteam, sil - Ewater, sep) / (Esteam, sil - Ewater, sil),$$

in which WF is the water fraction, and the enthalpy of steam and water at separator (sep) and silencer (sil) pressures are obtained from steam tables. For wells with no excess steam, the measured enthalpy is assumed equal to the aquifer liquid enthalpy for calculating aquifer chloride.

For excess-steam wells, the measured total enthalpy is not equal to the enthalpy of the reservoir liquid so another method is used. Because the liquid enthalpy of most interest to us is that at a distance from the well unaffected by near-well boiling, liquid enthalpy based on the Na-K-Ca temperature is used for calculations of aquifer chloride presented in this paper. An advantage of this procedure is that excess enthalpy produced by near-well boiling without reequilibration of Na-K-Ca temperatures does not affect calculation of aquifer chloride concentrations away from the well. A possible disadvantage is that the chloride values do not help to distinguish between sources of excess enthalpy.

TEMPERATURE-CHLORIDE-TIME PLOTS

The chemical indicators discussed above are combined as temperature-time and chloride-time plots that are interpreted to indicate reservoir processes. Na-K-Ca temperatures are assumed to represent the temperature of the fluid at a distance from the well not affected by mixing and boiling near the well. This relatively distant fluid is assumed to have remained at its indicated temperatures long enough to be fully equilibrated. Silica (quartz-saturation) temperatures are assumed to represent near-well temperatures and are usually fully equilibrated. For several wells at Cerro Prieto, calculated well-bottom temperatures (Goyal et al., 1981) have been shown to agree reasonably well with quartz-saturation geothermometer temperatures (Truesdell, 1988 and unpublished data, 1982). Finally, enthalpy temperatures indicate either the actual temperature of the liquid if only liquid enters the well or indicate the relative amount of excess steam. In this second case, the indicated temperature does not correspond to any real reservoir temperature.

INITIAL CONDITIONS

Geothermometer and aquifer chloride versus time plots allow reasonable estimates of initial reservoir fluid temperature and chloride. The drilling and development of

wells disturbs reservoir conditions in various ways. Drilling water may locally dilute reservoir fluids, and pressure decrease from extensive testing may cause boiling or cold-water entry. Analysis of fluids produced at low flow during well development may be affected by cooling from both wellbore heat loss and boiling. These data cannot then be used to calculate quartz-saturation temperatures or aquifer chloride because the amount of steam loss is not known, although Na/K and usually Na-K-Ca geothermometers are applicable.

For these reasons, chemical and enthalpy measurements for the first year or so of full flow production are usually best for estimating initial conditions. The Na-K-Ca geothermometer has a long memory and aquifer chloride is unlikely to change rapidly. Often a trend in data can be extrapolated to the start of major production. Examples of these estimations will be given later.

CHEMICAL PATTERNS

As noted earlier, the different rates of response of the Na-K-Ca and quartz geothermometer combined with the enthalpy temperature provide indications of fluid state and of fluid temperature near and far from wells. Aquifer chloride provides additional indications for dilution and boiling processes. These indicators are most useful when a relatively long history is available with data collected at frequent intervals. These numerous data are needed for the interpretation of certain processes such as cold-water sweep and allow errors to be estimated. This interpretive method has been applied to Cerro Prieto (Truesdell, et al., 1979, 1984; Truesdell, 1988) and is applied here to Ahuachapan. Although only some of the possible sequences have been observed at Ahuachapan, we will for completeness and possible application elsewhere also include those found at Cerro Prieto. The temperatures are abbreviated as TNaKCa, TSil and TE indicating Na-K-Ca, quartz and enthalpy temperatures, respectively.

1. TNaKCa = TSil = TE indicates all-liquid fully equilibrated reservoir fluid.
2. TE > TNaKCa > TSil indicates fluid boiling during flow to the well in response to decrease in well-bottom pressure. Boiling lowers near-well fluid temperatures (and TSil values) and causes heat transfer from hotter rocks. If pressures are controlled by a constant pressure boundary, well-bottom pressures gradually stabilize and expansion of the boiling zone slows and stops. Within the stabilized boiling zone, temperatures equilibrate and heat is no longer transferred so excess enthalpy decreases slowly and disappears. TSil is still depressed because near-well boiling and temperature decrease continues. The order then becomes TE = TNaKCa > TSil.
3. TNaKCa > TE = TSil results from mixing with cooler water and reequilibration of TSil but not TNaKCa.
4. TE > TNaKCa = TSil indicates mixture of equilibrated liquid with steam formed by boiling away from the well. Wells with two inlet zones may show this pattern.
5. TNaKCa > TSil > TE shows mixture in the well of cooler more dilute water with equilibrated liquid. The lower TSil results from mixture without reequilibration with TNaKCa not significantly affected by moderate dilution. Inflow of shallow cooler water into a well with multiple fluid entries could produce this pattern.
6. TE = TSil > TNaKCa indicates chemical breakthrough of cooler water. TNaKCa still partly retains the memory of equilibration at lower temperatures although the fluid has been heated by flow through hot rock. Aquifer chloride will also indicate chemical breakthrough.

Other cases can occur by combination of these processes; for example, boiling in the reservoir could be combined with cool water entry into the well. Some of these combinations produce ambiguous indications. Consideration of changes in aquifer chloride is of value in sorting out these processes.

AHUACHAPAN INDICATORS

Ahuachapan wells usually exhibit either pattern 2 or 5 and less often 3 and 4, with pattern 1 found in the earliest production. Examples of typical behavior are shown in Figures 1-4.

Well AH-23 (Fig. 1) generally shows excess enthalpy and low silica temperature (pattern TE > TNaKCa > TSil). The initial temperature of 245°C is best indicated by Na-K-Ca. Early calculated silica temperatures were probably depressed by the presence of drilling fluid or by wellbore heat loss as indicated also by low enthalpy temperatures.

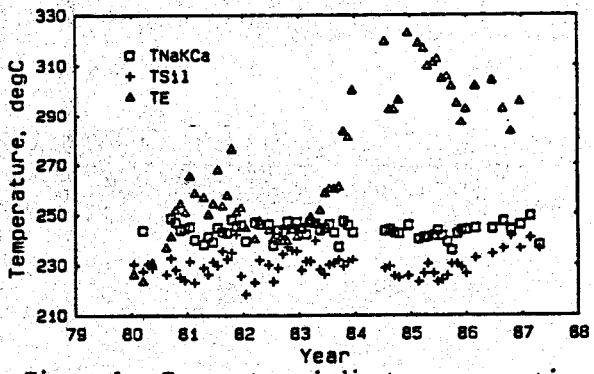

Figure 1. Temperature indicators versus time for Ahuachapan 23 generally showing boiling and excess enthalpy. Symbols: square, TNaKCa; plus, TSil; and triangle, TE.

Well AH-28 (Fig. 2) shows generally low fluid temperatures (shown by enthalpy temperature), but more or less constant Na-K-Ca temperatures and intermediate silica temperatures (TNaKCa > TSil > TE). This pattern is caused by the entry of cooler water into the well,

probably through a shallow feed zone where it mixes with the reservoir fluid. The temperature of the "hot" reservoir fluid is about 245°C, similar to its initial temperature. The temperature of the mixture in the well is about 220°C. If the mixing had occurred away from the well, then the silica temperature would also be near 220°C. The initial Na-K-Ca, silica (except two earliest values affected by conductive cooling), and enthalpy temperatures are all 250 ± 5°C.

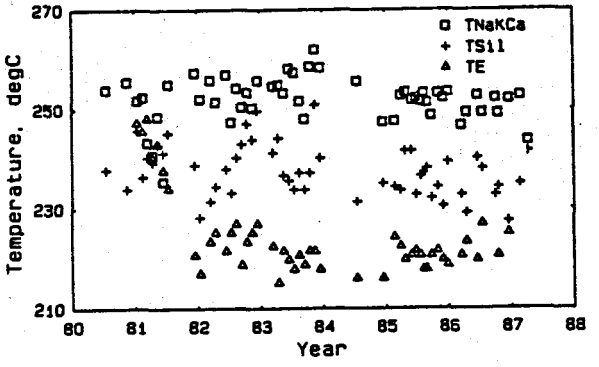

Figure 2. Temperature indicators versus time for Ahuachapan 28 showing mixing with cooler water near the well. Symbols as in Figure 1.

Well 21 (Fig. 3) shows the result of mixing further from the well with mostly TNaKCa > TSil = TE indicating equilibration of silica after mixing. Mixing occurred so early in the history of this well that only TNaKCa can be used to indicate the initial temperature of 260°C.

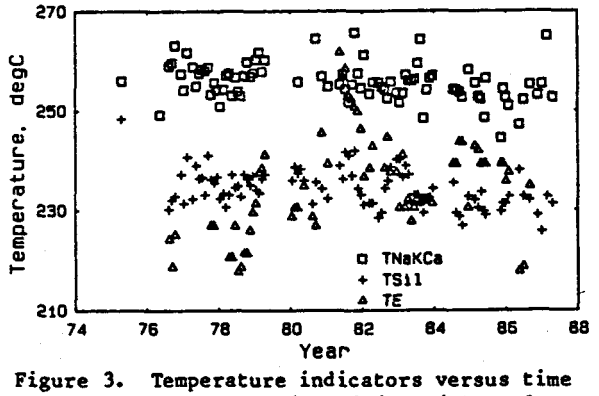

Figure 3. Temperature indicators versus time for Ahuachapan 21 showing mixing with cooler water farther from the well. Symbols as in Figure 1.

The aquifer chloride of well AH-22 (Fig. 4) shows chemical breakthrough in 1981 with aquifer chloride decreasing from about 7000 mg/kg to 6300 mg/kg by 1987. This breakthrough was in response to decreased pressure in the central part of the field, which caused flow from the east where fluids were less saline. Geothermometer temperatures for this well showed immediate (1976) over-all boiling (TE > TNaKCa > TSil) independent of the later chemical breakthrough.

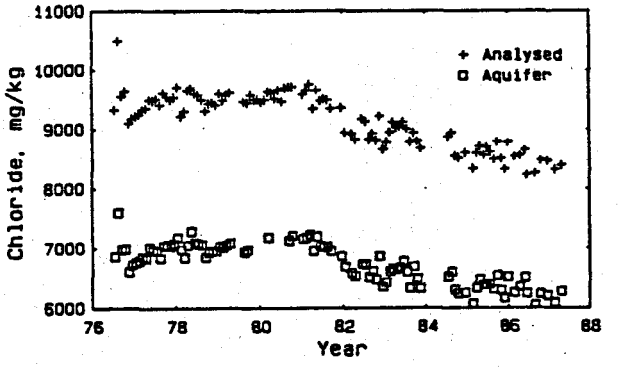

Figure 4. Chloride concentrations versus time for Ahuachapan 22 showing breakthrough of less-saline water. Symbols: plus, Cl concentrations as analyzed; square, aquifer Cl concentrations calculated using TNaKCa for reservoir temperature.

INITIAL TEMPERATURE AND CHLORIDE AT AHUACHAPAN

Using initial geothermometer and aquifer chloride values, or values extrapolated from early production, maps have been prepared with contours of the natural reservoir conditions (Figs. 5 and 6). These maps show a clear increase in both temperature and aquifer chloride concentration from east to west. Liquid enthalpy values (calculated from temperature) are almost linearly related to chloride concentration (Fig. 7), suggesting mixing between a more-saline, hotter water and a more-dilute, cooler water. The low-temperature end member cannot be defined from these data but is not surface water (compare data for Cerro Prieto in Grant et al., 1984).

The Na-K-Ca geothermometer temperatures indicate that fluids produced from the wells were equilibrated with rock minerals at temperatures ranging from above 260°C in the west to below 235°C in the east. These temperatures are uniformly 10-20°C higher than the downhole measured temperatures in the same wells (see Lakey et al., this volume). One possible explanation is that the Na-K-Ca geothermometer is not accurate for Ahuachapan fluids. This is unlikely because the Ahuachapan fluids are in no way chemically unusual and because other geothermometers give similar temperature indications (Table 1). Another possibility is that by the time downhole temperatures were measured, pressure drawdown had already affected temperatures either through boiling with resulting temperature decrease or through cold-water mixing.

RESERVOIR PROCESSES AT AHUACHAPAN

A map can also be drawn showing predominant reservoir processes for each well. A well may show different processes during its history but one process usually predominates. In response to pressure drawdown, high-temperature reservoirs either boil or are flooded with cooler recharge from the top or sides of

the field. In a large reservoir, evidence of boiling or dilution may be delayed unless the well is close to the location of boiling or cold-water entry. In these reservoirs local boiling may occur immediately but evidence of dilution is usually delayed. At Ahuachapan large amounts of fluid were irregularly discharged from wells during extended field development. This discharge may have caused some early drawdown. The relatively early appearance at Ahuachapan of boiling or cold-water mixing may result from extended field development or may indicate that fluid entries are near the top of the reservoir where pressure drawdown effects are first manifest. The response to exploitation at Ahuchapan has either been immediate boiling or immediate dilution. The locations of wells with these behaviors are shown in Figure 8. The wells have been divided into "boilers" (solid circles) and "diluters" (solid squares), simply according to whether TE > TNaKCa or TNaKCa > TE.

The pattern shows a band of diluters running N-S through the center of the field with boilers on both sides. Comparing this map with Figure 9, the fault map of Laky et al. (this volume), we see a remarkable coincidence of the band of diluters with faults 8 and 7. These faults are among the youngest in the field and probably allow hydrologic communication between the reservoir and the overlying Saturated Aquifer, which contains cold water.

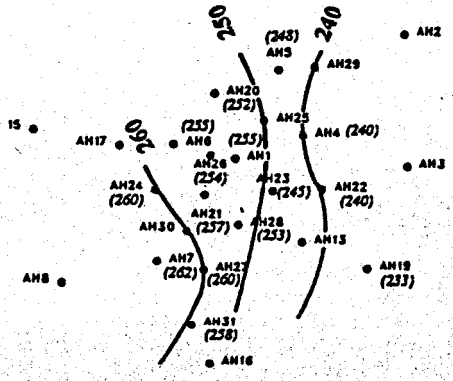

Figure 5. Natural state reservoir temperatures for the Ahuachapan field.

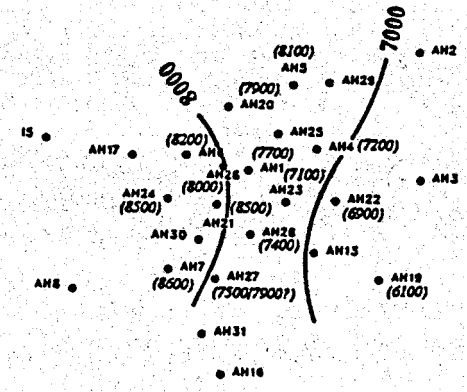

Figure 6. Natural state reservoir chloride concentrations for the Ahuachapan field.

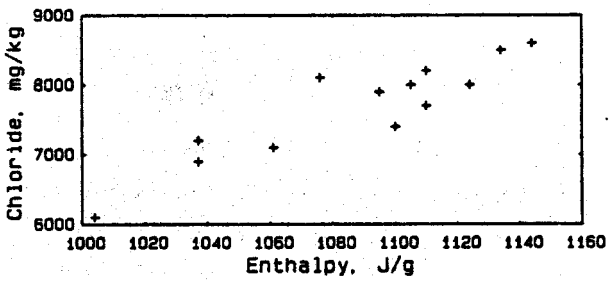

Figure 7. Enthalpy-chloride contents for natural state Ahuachapan reservoir fluids.

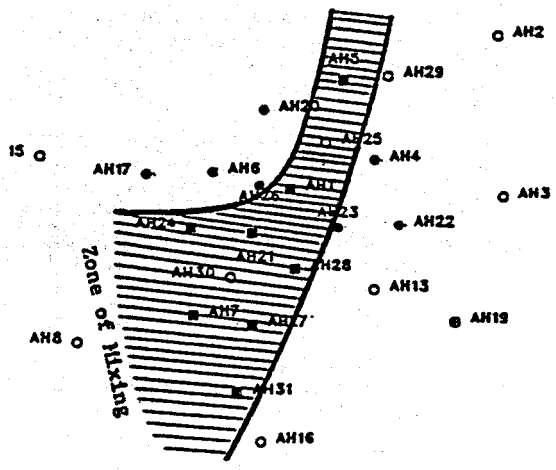

Figure 8. Simplified map of response of Ahuachapan wells to exploitation. See text for explanation.

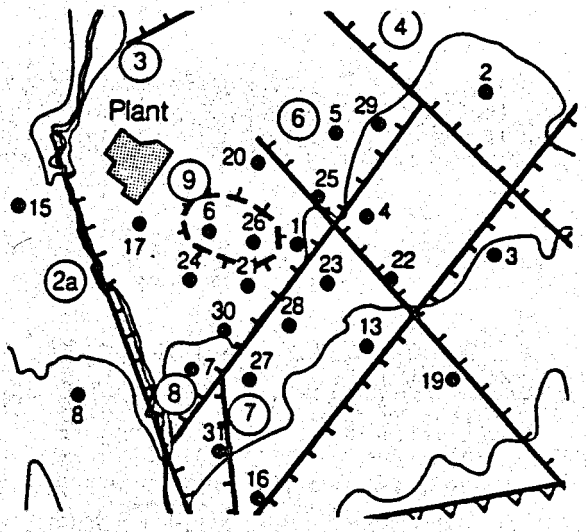

Figure 9. Fault map for the Ahuachapan field from Laky et al. (1989).

IMPLICATIONS FOR THE AHUACHAPAN CONCEPTUAL MODEL

The geochemical interpretations provide major constraints on the natural state model of the field. As described by Laky et al. (this volume) and Steingrimsson et al. (this volume), the behavior of the field is controlled by the major faults (Fig. 9). The main faults believed to feed the Ahuachapan reservoir are faults 6, 2a and 10. In the natural state, mixing of the geothermal fluids with cooler, less-saline fluids occurs in the eastern part of the well field. These cooler fluids probably come from the north via fault 4; another possibility is downward recharge from the overlying Saturated Aquifer, which has a higher hydraulic potential than the main reservoir. This mixing explains the observed gradients in geothermometer temperatures and chloride concentrations across the field.

ACKNOWLEDGMENTS

We wish to thank Robert Fournier, Michael Sorey and Cathy Janik of the U.S. Geological Survey for thoughtful reviews, and Marcelo Lippmann of Lawrence Berkeley Laboratory and Gustavo Cuellar of the Comision Ejecutiva Hidroelectrica de Rio Lempa for stimulating discussions of Ahuachapan reservoir processes and geochemistry. This work has been supported by the U.S. Agency for International Development through a subcontract with the Los Alamos National Laboratory and by the U.S. Department of Energy.

Table 1. Early Geothermometer Temperatures for Ahuachapan Well Discharges in °C.

Well	Date	TNaKCa	TSil	TNaK(1)	TNaK(2)
AH-1	07/74	256	251	247	263
AH-4	06/75	246	237	237	256
AH-5	02/72	248	---	242	259
AH-6	07/74	257	246	252	266
AH-7	04/75	262	256	260	272
AH-16	03/87	240	238	231	251
AH-19	03/85	233	228	218	241
AH-20	07/76	255	234	250	268
AH-21	04/75	256	248	250	265
AH-22	07/76	239	237	226	247
AH-23	09/80	249	233	243	260
AH-24	09/78	262	252	260	273
AH-26	09/76	253	229	246	262
AH-27	10/80	263	246	262	274
AH-28	07/80	254	239	249	264
AH-31	04/85	260	250	257	270

TNaK(1) is the Ellis-White Na-K geothermometer from Truesdell (1976). This usually indicates minimum temperatures.
TNaK(2) is the Na-K geothermometer from Fournier (1979), which usually indicates maximum temperatures.

REFERENCES

Fournier, R.O., 1979, A revised equation for the Na/K geothermometer: Geothermal Resources Council Transactions, v. 3, p. 221-224.

Fournier, R.O., 1981, Application of water geochemistry to geothermal exploration and reservoir engineering, Chap. 4 in Rybach, L. and Muffler, L.J.P. (eds.), Geothermal Systems: Principles and Case Histories: New York, Wiley, p. 109-143.

Fournier, R.O. and Truesdell, A.H., 1973, An empirical Na-K-Ca geothermometer for natural waters: Geochimica et Cosmochimica Acta, v. 37, p. 1255-1275.

Goyal, K.P., Miller, C.W., Lippmann, M.J. and Vonder Haar, S.P., 1981, Analysis of Cerro Prieto production data: Proc. 3rd Symp. Cerro Prieto Geothermal Field, Baja Calif., Mexico, LBL Rept. 11967, p. 496-500.

Grant, M.A., Truesdell, A.H. and Manón, M.A., 1984, Production induced boiling and cold-water entry in the Cerro Prieto geothermal reservoir indicated by chemical and physical measurements: Geothermics, v. 13, p. 117-140.

Laky, C., Lippmann, M., Bodvarsson, G.S., Retana, M. and Cuellar, G., 1989, Hydrogeologic model of the Ahuachapan geothermal field, El Salvador: Proc. 14th Workshop on Geothermal Reservoir Engineering, Stanford, Calif., Jan. 24-26, 1989 (in press).

Mahon, W.A.J., 1966, Silica in hot water discharged from drill holes at Wairakei, New Zealand: New Zealand Journal of Science, v. 9, p. 135-144.

Steingrimsson, B., Bodvarsson, G.S., Cuellar, G. and Escobar, C., 1989, Changes in thermodynamic conditions of the Ahuachapan reservoir due to production and injection: Proc. 14th Workshop on Geothermal Reservoir Engineering, Stanford, Calif., Jan. 24-26, 1989 (in press).

Truesdell, A.H., 1976, Summary of section III - geochemical techniques in exploration: 2nd U.N. Symp. Development and Use of Geother. Resources, San Francisco, Calif., May 1975, v. 1, p. liii-lxiii.

Truesdell, A.H., 1988, Geochemical models for reservoir processes at Cerro Prieto, Mexico: Proc. Int. Symp. Geother. Energy, Kumamoto and Beppu, Japan, Nov. 1988, p. 59-62.

Truesdell, A.H., D'Amore, F. and Nieva, D., 1984, The effects of localized boiling on fluid production at Cerro Prieto: Geother. Resourc. Counc. Trans., v. 8, p. 223-229.

Truesdell, A.H., Manón, A., Jiminéz, M.E., Sánchez, A. and Fausto, J.J., 1979, Geochemical evidence of drawdown in the Cerro Prieto geothermal field: Geothermics, v. 8, p. 257-265.

PROCEEDINGS, Fourteenth Workshop on Geothermal Reservoir Engineering
Stanford University, Stanford, California, January 24-26, 1989
SGP-TR-122

CHANGES IN THERMODYNAMIC CONDITIONS OF THE AHUACHAPAN RESERVOIR DUE TO PRODUCTION AND INJECTION

B. Steingrimsson, G. S. Bodvarsson,* G. Cuellar‡, and C. Escobar‡*

*Earth Sciences Division
Lawrence Berkeley Laboratory
1 Cyclotron Road
Berkeley, California 94720

‡Comision Ejecutiva
Hidroelectrica del Rio Lempa
P.O. Box 01-478
San Salvador, El Salvador

ABSTRACT

Since large-scale exploitation of the Ahuachapán reservoir began in 1975 with the commencement of the first 30 MW_e unit, large changes in the reservoir thermodynamic condition have occurred. Drawdowns up to 15 bars have developed in the production field and significant temperature changes have been observed. In most cases temperatures have declined due to boiling in the reservoir stimulated by the pressure drawdown; cooling due to reinjection of spent geothermal fluids has also been observed. There are indications of a cold fluid recharge to the reservoir from the west and north. Increasing temperatures in the southeast corner of the wellfield show that significant recharge of hot fluids to the wellfield comes from the southeast; they also indicate that the recharge rate has increased with time as the pressure declines in the reservoir.

INTRODUCTION

The Ahuachapán field has been under development and exploitation for more than 20 years. The first production well was drilled in 1968 and presently a total of 32 wells are distributed over a 6 km^2 area, as shown in Figure 1. However, the productive wellfield extends over less than 1 km^2 (Vides-Ramos, 1985). The wells are completed with a cemented casing to about 500 m depth; total depths of the wells vary between 590 and 1600 m.

Exploitation of the Ahuachapán reservoir started in June 1975, when the first 30 MW_e generator went on-line. A second 30 MW_e unit commenced in July 1976, and a third one (35 MW_e) in November 1980. The power plant has never been operated at full capacity due to the lack of sufficient steam. Presently, the total fluid production rate is about 500 kg/s, which is sufficient to generate about 45 MW_e of electrical power.

Ahuachapán was the first geothermal field which utilized large scale reinjection of the waste water (Einarsson et al., 1975). Injection experiments were conducted in 1971, and a reinjection program was initiated in August 1975, shortly after exploitation started. Reinjection stopped in November 1982, and since then the waste water has been gravity-flowed to the Pacific Ocean along a 75 km long concrete channel.

The objective of this paper is to examine the pressure and temperature changes as well as changes in fluid chemistry that have occurred during exploitation of the field. Of primary interest is the evaluation of the temperature decline in producing wells in terms of boiling, reinjection returns and natural recharge.

MASS EXTRACTION HISTORY

Since August 1968, production and reinjection rates for all wells in Ahuachapán have been regularly measured and are available as monthly averages (Vides-Ramos, 1985). The cumulative extraction history of the field is shown in Figure 2. During the development phase (1968-1975), a total of 24 Mtons of fluids were produced from the reservoir, with only 2 Mtons reinjected during the 1971 injection tests. Fluid production increased drastically when the first two generators went on-line and has averaged 17 Mtons/year since 1976. The rate of reinjection has varied considerably. In early 1976 as much as 50% of the produced fluids were reinjected, but on the average some 25-30% of the extracted fluids were injected into the reservoir, until November 1982 when reinjection was stopped. A total of 38 Mtons of waste

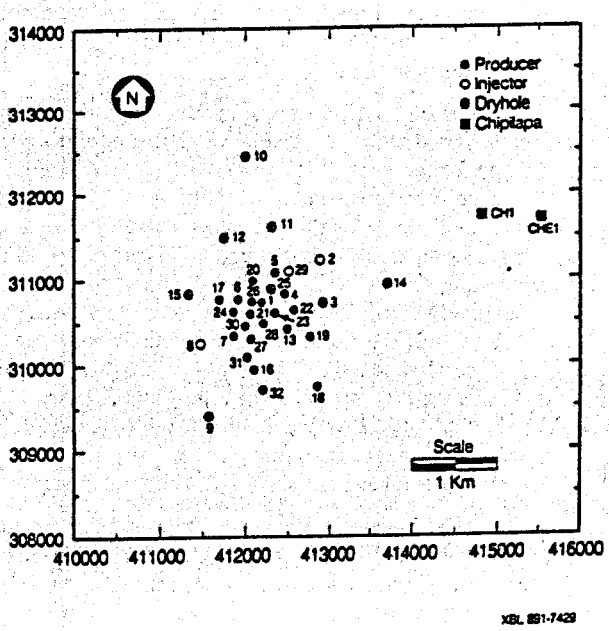

Figure 1. Map of the Ahuachapán wellfield.

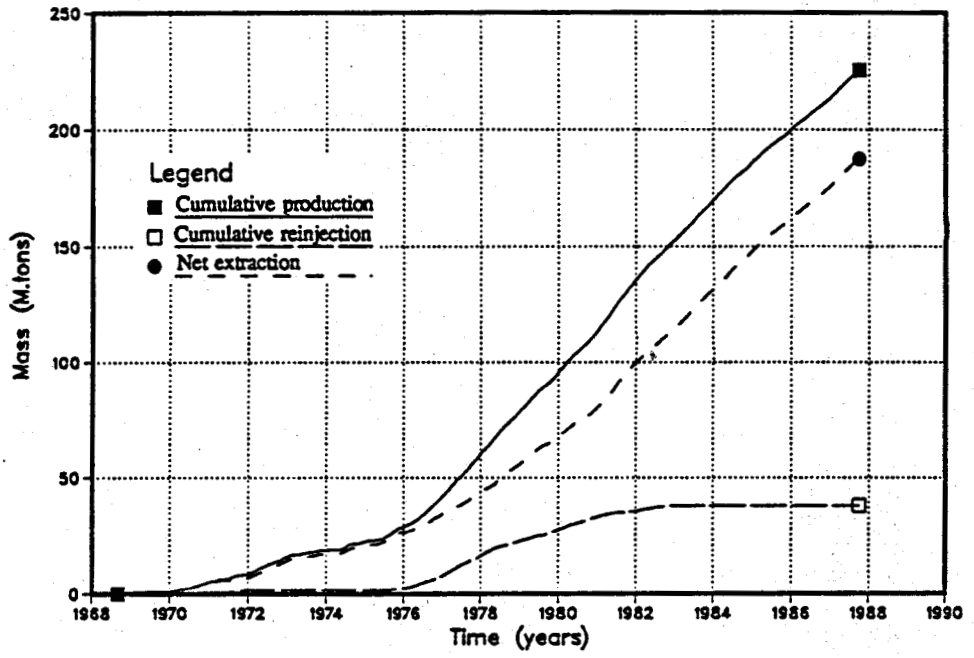

Figure 2. Cumulative fluid production and injection, 1968-1988.

water have been reinjected. In comparison, by the end of September 1988 the net fluid extraction from the field had reached 187 Mtons.

PRESSURE DRAWDOWN

Changes in reservoir pressures have been monitored during the exploitation years by running annual surveys in all wells accessible to logging. Also, daily pressure measurements at 200 masl (approximately 500 m depth) in well AH-25 are available since 1977; this well is located close to the center of the production field (Figure 1). The initial (pre-exploitation) pressures in the Ahuachapán wellfield were fairly uniform corresponding to 36 bar-g at the monitoring elevation of 200 masl (Laky et al., this volume).

Exploitation has caused a significant pressure drawdown in the production area. Figures 3 and 4 show pressure maps for the years 1978 and 1986. Both figures show a near-uniform pressure low engulfing the entire production area. In 1978 the pressures ranged between 28-30 bar-g compared with the initial 36 bar-g; by 1986 the pressures in the wellfield had declined to 20-22 bar-g. Relatively high 1978 pressures in wells AH-8, AH-29, AH-17 and AH-2 are due to reinjection into these wells. Peripheral wells AH-11, AH-14, AH-16 and AH-18 show significant drawdowns indicating natural fluid recharge from the north, east and south. Wells AH-10 and AH-15 are not in pressure communication with the geothermal reservoir and have not shown measurable drawdown.

The AH-25 pressure data have been supplemented with some 1968-1977 average well pressures at 200 masl and converted into drawdown by assuming an initial reservoir pressure of 36 bar-g. These drawdown data are plotted in

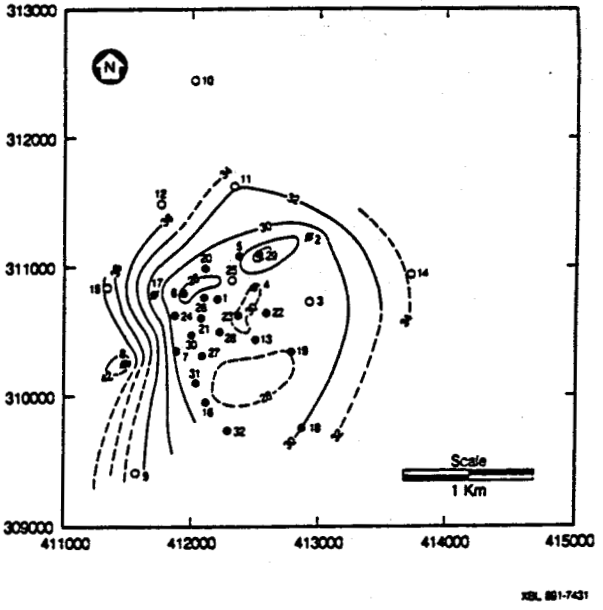

Figure 3. 1978 pressure contours in bar-g at 200 masl.

Figure 5 together with the monthly net extraction rates. The figure illustrates the close relation between the net extraction rate and pressure drawdown. The few data points from the early years show that the fluid production during well testing resulted in a significant drawdown in 1972, but as the production testing was minimal during the next few years, the field had almost recovered to initial pressures when exploitation started in 1975. Figure 5 shows that the pressure drawdown tends to stabilize during long periods of relatively constant net extraction rate,

thus reaching a quasi-steady state. This pressure stabilization and the fast pressure recovery in 1973-1975 indicates that the current production wellfield is only a small part of a much larger system and that recharge into the production area is significant (see Aunzo et al., this volume).

TEMPERATURE CHANGES

Significant reservoir temperature changes have been observed at Ahuachapán due to exploitation. The most dramatic change is a gradual 10-15 °C cooling within the Ahuachapán Andesites in the main production area during the 1975-1986 exploitation period (Figure 6). Some temperature changes are also observed deeper in the reservoir and on the periphery of the wellfield. Careful analysis of the available data shows that there are several processes responsible for the temperature changes including boiling, reinjection returns and natural recharge. In the following sections the observed reservoir temperature changes are discussed in terms of these different processes.

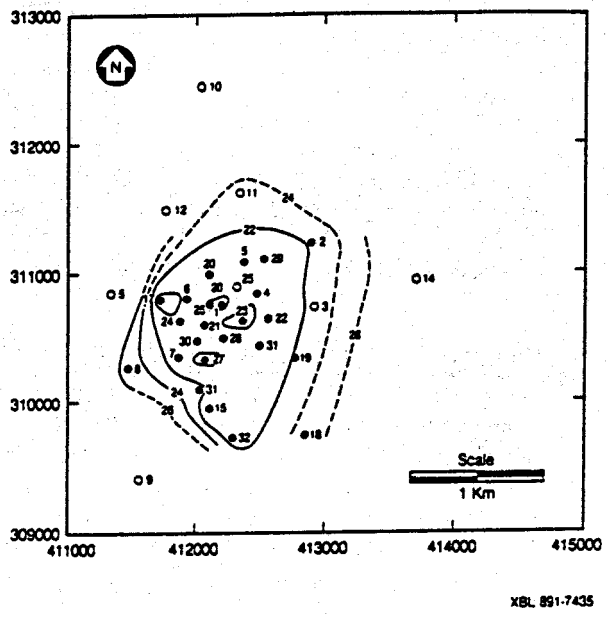

Figure 4. 1986 pressure contours in bar-g at 200 masl.

Temperature changes due to boiling

The upper part of the reservoir was boiling prior to exploitation (Laky et al., this volume). The pressure drawdown in the field has caused the two phase region in the main production area to expand and the boiling zone to cool following the saturation curve. The boiling level, initially found at an elevation of about 300 masl, is currently (1988) at about 250 masl. The cooling of the boiling zone is on the order of 10-15 °C. It can be easily demonstrated that this cooling is primarily caused by boiling either by comparing the temperature and the pressure distribution in the field, or by plotting for each well the temperature and pressure in the two-phase region at different times and comparing the plot with the corresponding saturation values. Example of such a plot is shown in Figure 7.

Temperature changes in the liquid region of the reservoir in the Ahuachapán Andesites

The two phase region resides in the upper region of the Ahuachapán Andesites. The underlying liquid-

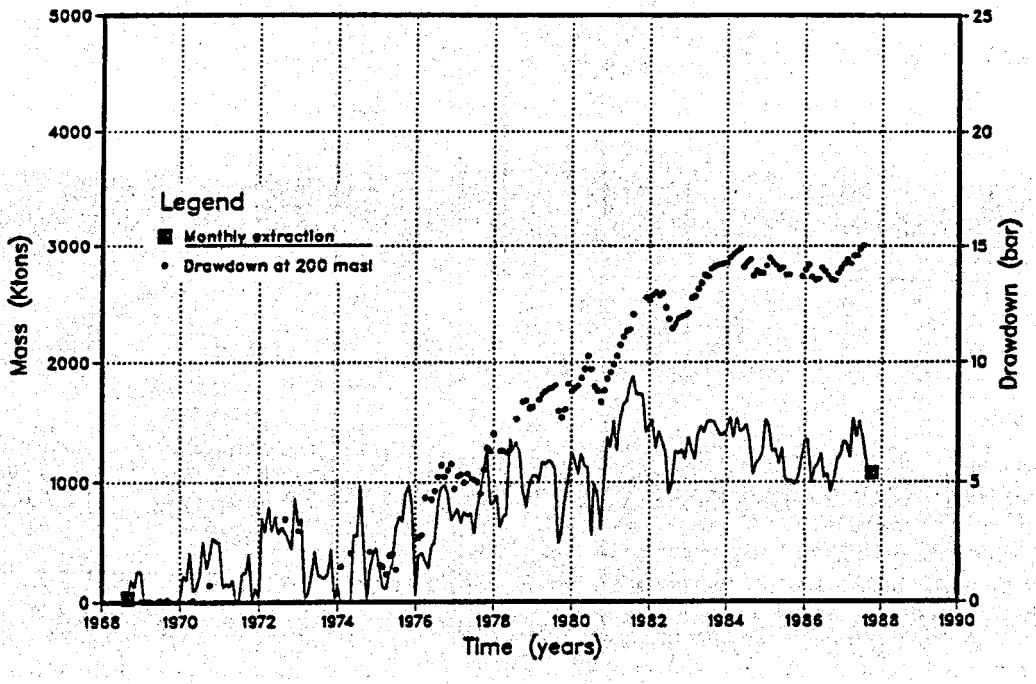

Figure 5. Monthly net extraction rates and the pressure drawdown.

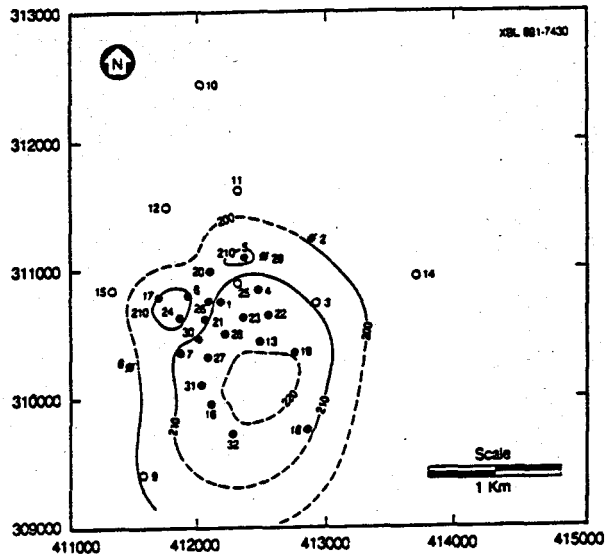

Figure 6. 1986 temperature contour map (in °C) at 200 masl.

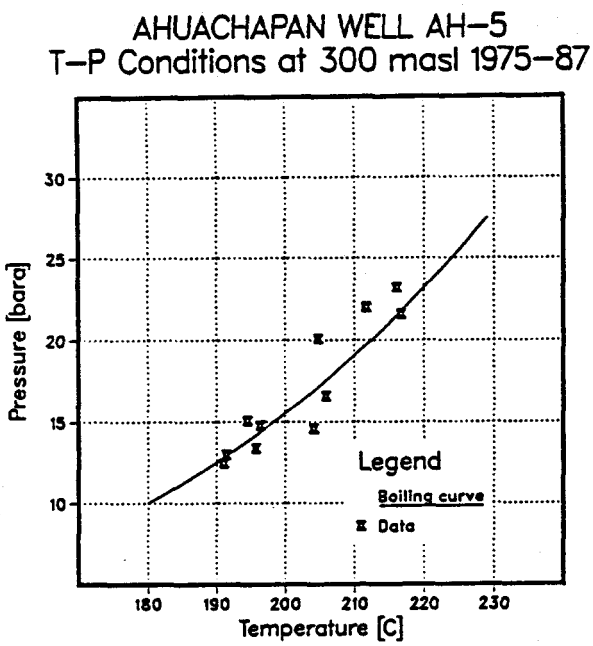

Figure 7. Plot of temperature versus pressure for AH-5 (1975-1987).

dominated zone also experienced considerable cooling during the exploitation years, except in the southwest corner of the wellfield. Early temperature logs show boiling-point-to-depth curves through the two-phase region of the reservoir and a near-isothermal interval below the boiling level to the bottom of the Andesites. These general reservoir characteristics have not changed in the production field. However, the boiling level has fallen some 50 m, as mentioned earlier, and the liquid zone has cooled with time. The best example of this behavior is well AH-21 (Figure 8) but similar behavior is observed in most of the other production wells, with the exception of wells AH-7 and AH-31.

In order to investigate the cooling of the single-phase region of the Andesites, the temperature and the pressure histories of several wells were analyzed. Examples of these plots are shown in Figure 9. In all cases the temperature decline correlates with the pressure drawdown in the reservoir. Such a consistent correlation is highly unusual in a single-phase region. Plots of temperature versus pressure (Figure 10) show that the cooling progresses parallel to the saturation curve indicating that the cooling of the single phase region in the reservoir is actually controlled by boiling. It is believed that the cause of this is recharge of a two-phase mixture of steam and water. This recharge occurs at or above 200 masl, but after entering the field the two phases segregate due to density effects, with liquid occupying the lower portion of the Andesites and steam accumulating in the upper part.

Temperature changes attributed to reinjection

Temperature data have been examined in order to determine reservoir cooling caused by the 1975-1982 reinjection program. The data indicate thermal recovery in few

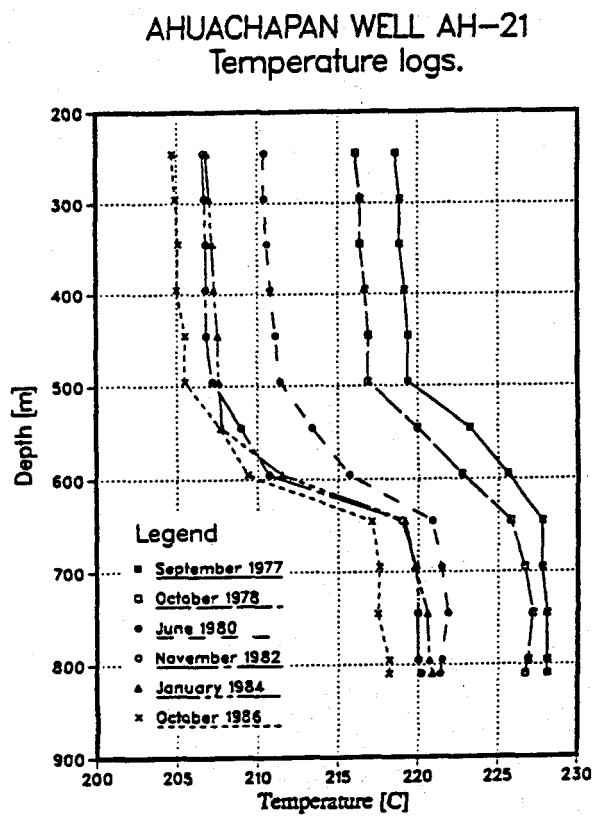

Figure 8. Selected temperature logs for well AH-21.

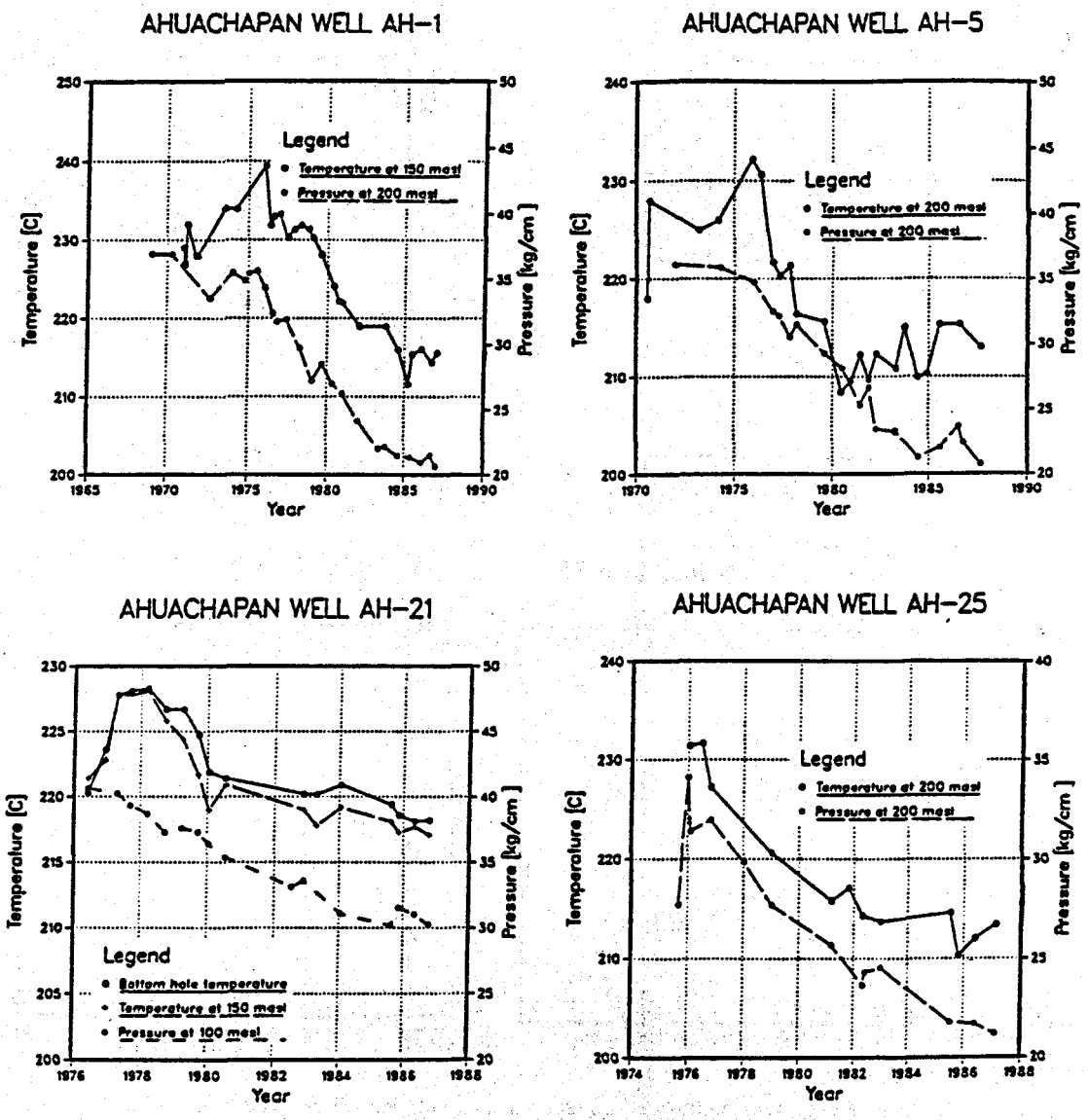

Figure 9. Selected temperature logs for wells AH-1, AH-5, AH-21 and AH-25.

wells after the reinjection was stopped in 1982. All of these wells are relatively close to an injector. Most pronounced is the cooling around injection well AH-8, but some reinjection-related cooling was also observed in the vicinity of AH-29, another injector.

Figure 11 shows temperature data at 100 masl in well AH-7, which is located near the injector AH-8. It shows gradual cooling during the reinjection period and rapid recovery after injection ceased in 1982. The cooling which occurred up to 1982 was on the order of 10-15 °C. By late 1987, the temperature had almost fully recovered. Similar temperature history is found in the vicinity of the injector AH-29 in wells AH-25 and AH-5. In general, however, one can conclude that the substantial reinjection effort did not cause large cooling effects in the producing wells.

Temperature changes due to natural recharge

The drawdown in the reservoir has stimulated natural recharge to the production area of the field. The temperature distribution in the field indicates that in the natural state the geothermal fluid recharged the wellfield from the southeast, close to well AH-18 (Laky et al., this volume). This well has shown increasing temperatures during the exploitation years, as is evident in Figure 12. The early data indicate the thermal recovery of the well after drilling was completed in 1977; the low 1985 temperatures coincide with flow testing of the well (boiling during discharge). Apart from these disturbed readings the plot shows a gradual increase in temperature since 1978. The total temperature rise is about 10 °C, reaching 245 °C in 1987, the highest reservoir temperature measured in Ahuachapán. The increasing temperatures in well AH-18 in response to exploitation support the idea

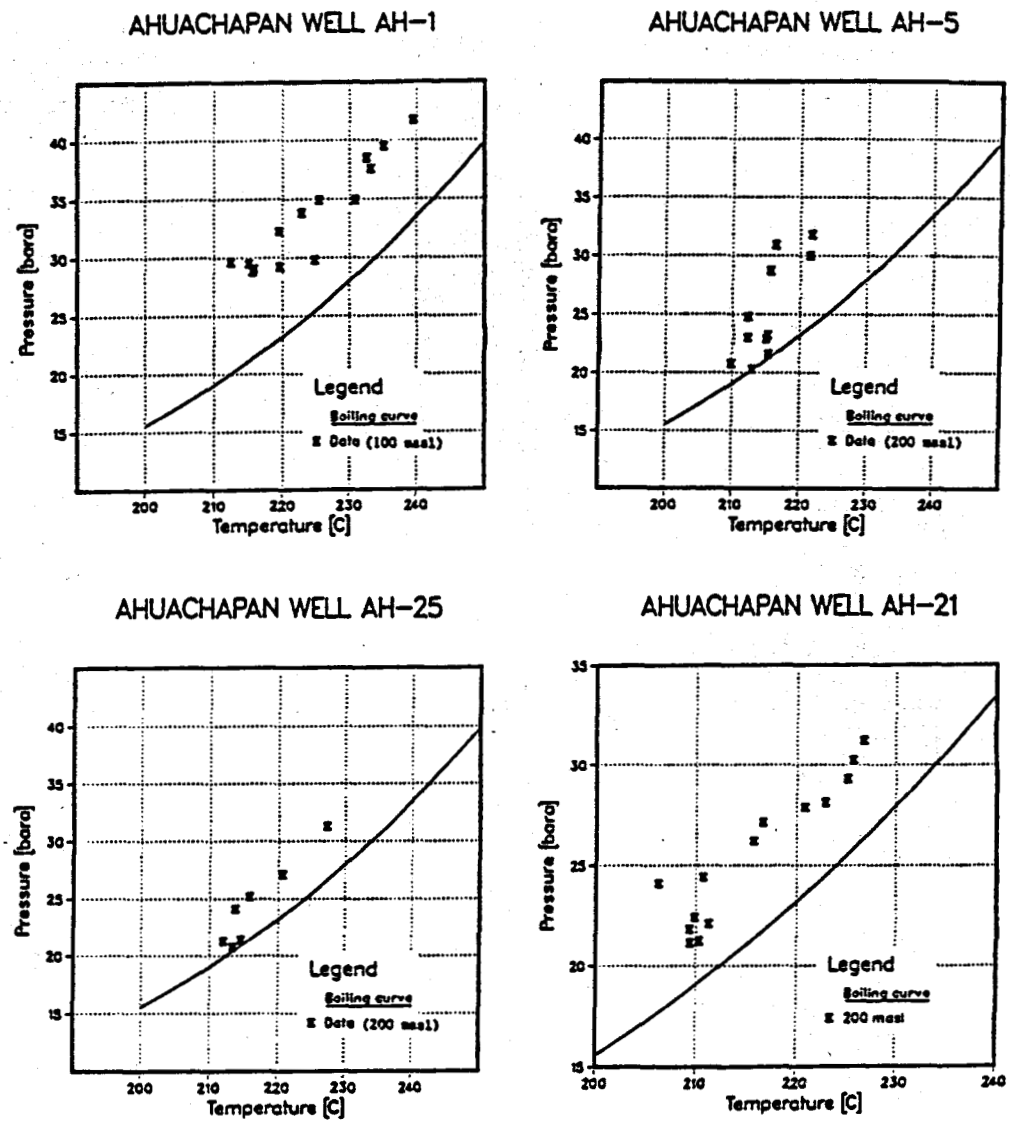

Figure 10. Temperature and pressure histories for wells AH-1, AH-5, AH-21 and AH-25.

of a natural hot fluid recharge in this part of the field and furthermore that the recharge rate has increased due to pressure decline in the reservoir.

Cold water recharge into the wellfield cannot be supported by data from peripheral wells. On the eastern margin of the field no temperature changes have been observed, while at the north and west boundaries no data are available because of obstruction in the wells at shallow depth. However, temperature data from a few wells in the production area indicate deep cold water recharge into the field from the north and west. An example of a well showing this type of cooling is AH-7. This well cooled at shallow depth (100 masl) due to reinjection, as mentioned earlier (see Figure 11). Similar cooling was observed deep in the well during the reinjection years as shown on Figure 13, but in this case little thermal recovery was measured after the reinjection ceased. The reservoir cooling can therefore not be explained by reinjection leaving cold water recharge as the only possible cause for the temperature history deep in well AH-7.

SUMMARY AND DISCUSSION

Exploitation has greatly changed the pressure and temperature conditions in the Ahuachapán reservoir. In the wellfield, pressure has declined some 15 bars and cooling of up to 15 °C has been observed.

As expected the pressure drawdown correlates well with the net extraction rate, with quasi-steady pressure conditions reached after periods of near-constant rates. This suggests that natural recharge is very significant at Ahuachapán and that the system is much larger than the current wellfield.

The temperature history of Ahuachapán is complicated and has been influenced by several factors, including:

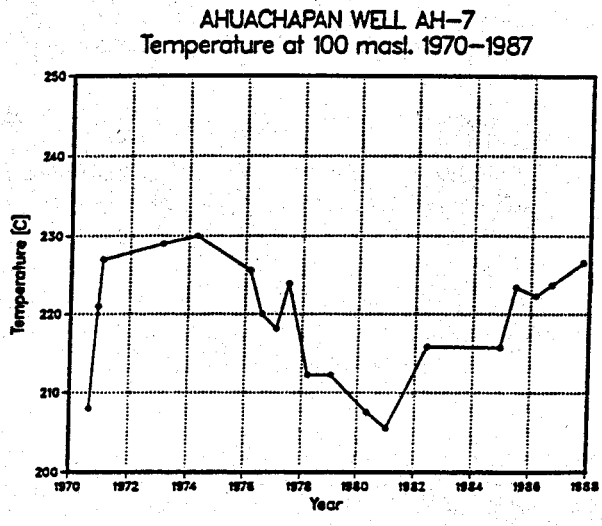

Figure 11. 1970-1987 temperature history of well AH-7 (100 masl).

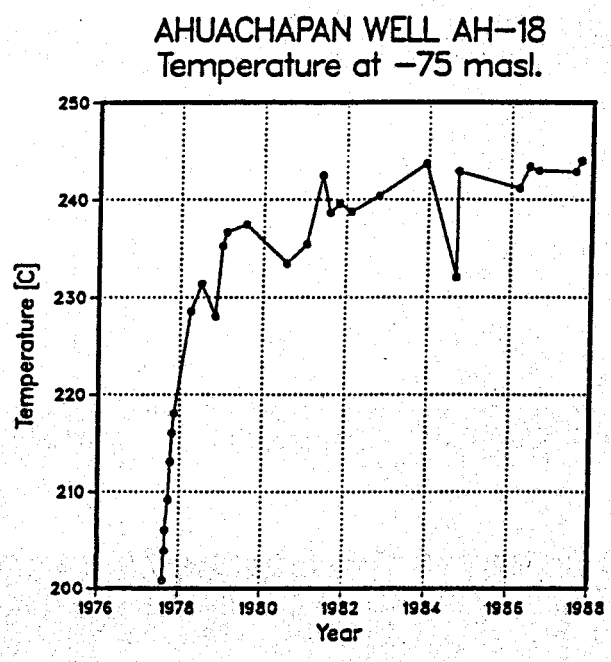

Figure 12. 1977-1988 temperature history of well AH-18 (-75 masl).

(1) Gradual cooling of the upper part of the reservoir due to boiling resulting from pressure decline.

(2) Progressive cooling of the liquid region of the reservoir in the Ahuachapán Andesite at the main production area. This cooling is due to recharge of boiling (two-phase) fluid to the production area.

(3) Temporal cooling in the vicinity of injectors during the reinjection period. This cooling, however, did not cause significant detrimental temperature decline in producing wells.

(4) Cooling in the northern and the western part of the field due to increasing cold water recharge in response to reservoir drawdown.

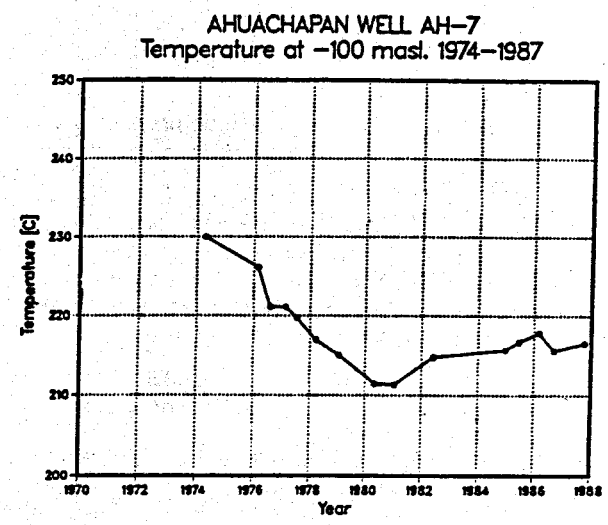

Figure 13. 1974-1987 temperature history of well AH-7 (-100 masl).

(5) Heating-up in the southeastern part of the field due to increasing geothermal (hot) fluid recharge to the production area.

The temperature history to the conceptual model of the field are presented by Laky et al. (this volume). The following statements are made with reference to Figure 2 in Laky et al., which shows major faults and flow directions. The geothermal fluid recharge enters the field from southeast and feeds the main production area through two separate "channels". The main recharge is through Fault #6 where the fluid undergoes boiling before it enters the production area. This boiling zone is believed to be in the vicinity of AH-19, may be at the intersection of Faults #5 and #6 where the Andesites are found at relatively shallow depth. The second recharge channel (Fault #10 and Fault #2a or #7) feeds the area around wells AH-7 and AH-31. Cold water seeps deep into the reservoir from the north through Fault #4 and maybe into the western portion of the field through Fault #8, but the main inflow of cold water occurs through the top of the reservoir probably through fault #6.

ACKNOWLEDGEMENT

The authors appreciate technical review of this paper by M. J. Lippmann and K. Pruess. The first author appreciates the leave of absence granted by the National Energy Authority in Iceland while working on this study at Lawrence Berkeley Laboratory. This work was supported by a contract from the Los Alamos National Laboratory and by the U.S. Department of Energy, under Contract No. DE-AC03-76SF00098.

REFERENCES

Aunzo, Z., Bodvarsson, G. S., Laky, C., Lippmann, M. J., Steingrimsson, B., Truesdell, A. H. and Witherspoon, P. A., (1989a). "The Ahuachapán geothermal field, El Salvador - Reservoir analysis," Lawrence Berkeley Laboratory report LBL-26612, Berkeley, CA.

Aunzo, Z., Steingrimsson, B., Bodvarsson, G. S., Escobar, C., Quintanilla, A. (1989b). "Modeling studies of the Ahuachapán geothermal field, El Salvador," Proc. 14th Workshop on Geothermal Reservoir Engineering, Stanford, CA, Jan 24-26, 1989.

EG&G Idaho, Inc. and Lawrence Berkeley Laboratory (1982). "Low-to-moderate temperature hydrothermal reservoir engineering handbook," Report IDO-10099.

Einarsson, S., Vides, R. A. and Cuellar, G. (1975). "Disposal of geothermal waste water by reinjection," Second United Nations Symposium on the Development and Use of Geothermal Resources, U.S. Government Printing Office, Vol. 2, pp. 1349-1363.

Grant, M. A., (1980). "Simple modeling of production and reinjection at Ahuachapán," DSIR Report, New Zealand, February 1980.

Laky, C., Lippmann, M. J., Bodvarsson, G. S., Retana, M. and Cuellar, G. (1989). "Hydrogeologic model of the Ahuachapán geothermal field, El Salvador," Proc. 14th Workshop on Geothermal Reservoir Engineering, Stanford, CA, Jan. 24-26, 1989.

Truesdell, A. H., Aunzo, Z., Bodvarsson, G. S., Alonso, J. and Campos, A., (1989). "The use of Ahuachapán fluid chemistry to indicate natural state conditions and reservoir processes during exploitation," Proc. 14th Workshop on Geothermal Reservoir Engineering, Stanford, CA, Jan. 24-26, 1989.

Vides-Ramos, A. (1975). "Ahuachapán, El Salvador field management," Trans. Geothermal Resources Council, International Volume, pp. 397-404.

PROCEEDINGS, Fourteenth Workshop on Geothermal Reservoir Engineering
Stanford University, Stanford, California, January 24-26, 1989
SGP-TR-122

MODELING STUDIES OF THE AHUACHAPAN GEOTHERMAL FIELD, EL SALVADOR

Z. Aunzo, B. Steingrimsson,* G. S. Bodvarsson,* C. Escobar† and A. Quintanilla†*

*Earth Sciences Division
Lawrence Berkeley Laboratory
1 Cyclotron Road
Berkeley, California 94720

†Comision Ejecutiva Hidroelectrica del Rio Lempa
P.O. Box 01-478
San Salvador, El Salvador

ABSTRACT

Modeling studies of Ahuachapan include analyses of interference test data, modeling of the fieldwide pressure decline and the development of a three-dimensional natural state model of the field. The main objective of this work is to obtain reasonable estimates for the transmissivity and storativity of the reservoir and to investigate fluid and heat flow patterns in the system.

The analyses of the interference test data and the long term pressure decline data indicate that the average reservoir transmissivity is about 30 Dm and the storativity about 3.5×10^{-6} m/Pa. The natural state modeling supports an overall average transmissivity of 25-35 Dm and indicates that the system is recharged with 255 °C hot water at a rate of about 225 kg/s. The total thermal throughflow for the Ahuachapan system is estimated to be about 250 MW_t.

INTRODUCTION

The Ahuachapan geothermal field in El Salvador has been producing electrical power since 1975. A total of 32 wells have been drilled in the area. The installed plant capacity is 95 MWe, but because of limited replacement well drilling and significant reservoir pressure drawdown a total of about 45 MWe is currently being generated. Lawrence Berkeley Laboratory (LBL), in cooperation with Los Alamos National Laboratory (LANL) and Comision Ejecutiva Hidroelectrica del Rio Lempa (CEL), is performing reservoir evaluation studies of Ahuachapan. The main objective of this work is to evaluate the available data and conduct mathematical modeling studies aimed towards increasing the steam production and the power generation of the field. Three other papers in this volume summarize related work, including a hydrogeological model of Ahuachapan (Laky et al., 1989), geochemical analysis (Truesdell et al., 1989), and evaluation of exploitation effects (Steingrimsson et al., 1989). Some of their important findings in relation to the modeling studies are summarized below.

Hydrogeology

Four major Lithologic units are present at Ahuachapan. From top to bottom, they are the Elluvials (EL), Young Agglomerates (YA), Ahuachapan Andesites (AA) and Older Agglomerates (OA). The Elluvials are composed of colluvium and a series of altered pyroclastics and lavas. The Young Agglomerates, found below the EL, are composed of pyroclastics and andesites ranging in thickness from 300 to 800 m. The bottom of this unit is highly hydrothermally altered, forming a permeability barrier between the YA and the underlying Ahuachapan Andesites, a highly fractured unit that presents the most permeable horizons. The thickness of the AA ranges from 200 to 600m. The underlying Older Agglomerates are a combination of dense breccias and andesites, with low matrix permeability but some fracturing. Three aquifers identified in the field appear to coincide with the different lithological units. These aquifers are the Shallow Aquifer (found in EL), the Saturated Aquifer (found in YA) and the Saline Aquifer, the geothermal reservoir, (found in AA and OA). The geologic structure of the Ahuachapan field appears to be dominated by seven major and four minor faults. These faults control the heat and fluid recharge and the flow within the reservoir (Laky et. al., this volume).

Geochemistry

Analyses of the Ahuachapan well discharges yield valuable data on the initial reservoir condition and processes. The chloride distribution, with a range from 6100 ppm to 8600 ppm, shows increasing chloride from east to west. The geochemical temperatures show the same trends and range from 233 °C to 262 °C. This suggests mixing of cooler, low-salinity fluid in the east; these cooler fluids may recharge the field from the north or downward from the overlying Saturated Aquifer in the eastern part of the wellfield (Truesdell et al., this volume).

Initial Temperature and Pressure Distribution

The pre-exploitaton pressure distribution in the reservoir was near-uniform with values in the range of 32-36 barg at 200 masl. The overlying Saturated Aquifer has a pressure potential about 4-8 bars higher than the geothermal reservoir.

Temperatures exceeding 240 °C are found in the AA and temperature inversions are observed in most wells when entering the OA. All productive wells show similar profiles, with the top of the convective gradient coinciding with the top of the AA. Increasing temperatures are observed toward the southeast, where the highest reservoir temperature (245 °C) has been measured. This suggests hot fluid recharge from the southeast into the field.

Fluid Movement

It is believed that upflow of saline, high temperature (above 250 °C) fluids occurs underneath the nearby volcanic complex (probably Laguna Verde), southeast of Ahuachapan. Only a small fraction (approximately 10%) of the upwelling fluids feed the production area at Ahuachapan. Some of the fluids feed the nearby Chipilapa field, but the majority discharges 10 km to the north at El Salitre Springs. Faults restrict fluid flow to the north and west of the Ahuachapan field (See Figure 7 in Laky et al., this volume).

INTERFERENCE TESTING

Several interference tests have been conducted at Ahuachapan. One such test was carried out during the period from May 6 to August 19, 1982, to obtain data for determining the reservoir transmissivity and storativity.

During the test period the produced fluids were reinjected into wells AH-2, AH-8, and AH-29. Well AH-25 was used as an observation well; its pressure response is shown in Figure 1. Because most of the Ahuachapan wells were flowing for an adequately long time prior to the test, the wellfield pressures were in a state of quasi-equilibrium. Thus, those wells with no changes in flow rates during the test were not considered in the analysis. Table 1 gives the flow rates of the producers and injectors that affected the pressure response in AH-25 during the test period.

In the analysis the computer model VARFLOW, developed at the Lawrence Berkeley Laboratory (EG&G and LBL, 1982), was used. The program calculates pressures at each observation point by superimposing the pressure transients, calculated using the Theis solution, of all producers/injectors. The program can handle variable flowrates, an anisotropic medium and a single linear hydrologic boundary. The reservoir transmissivity and the storativity were varied until a reasonable match to observed pressures at well AH-25 was obtained. The best match between the observed and computed pressure is shown in Figure 1. For this calculation, a reservoir

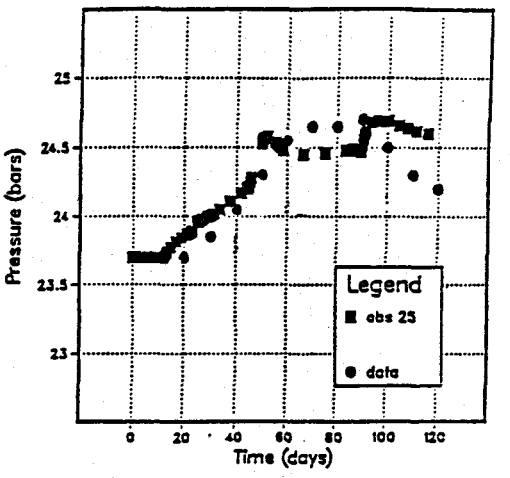

Figure 1. Match between observed and computed pressures at well AH-25 for the May-August 1982 interference test.

transmissivity of 25 Dm and a storativity of 2.5×10^{-6} m/Pa were used.

If one assumes an effective reservoir thickness of 300 m and a porosity of 10%, a total compressibility of about 1×10^{-7} Pa^{-1} can be computed from the storativity. This compressibility value is about two orders of magnitude higher than that of water at 240 °C and about two orders of magnitude lower than two-phase compressibility at 240 °C, which is reasonable given the partial two-phase conditions of the reservoir.

PRESSURE DRAWDOWN HISTORY MATCH

Pressures in Ahuachapan wells were fairly uniform prior to exploitation; production has caused significant drawdown (approximately 15 bars). Drawdown has been monitored by annual pressure surveys in all wells accessible to logging, and by daily pressure measurement at 200 masl in well AH-25.

The pressure history of Ahuachapan has been simulated using simplified models of the field. Grant (1980) did modeling studies in an attempt to match the 1975-1978 pressure changes resulting from fluid extraction. The results did coarsely match the observed pressure history, and both a high storativity coefficient and permeability were necessary to achieve reasonable matches.

In the present study, a simple model was used to match the pressure history of Ahuachapan. The main objective of this work was to obtain coarse estimates of the average reservoir transmissivity and storativity, to be used as initial input parameters for the natural state model. The model assumes an isothermal, horizontal, homogeneous, fully-saturated porous medium reservoir of constant thickness and of infinite areal extent. The system is closed above and below by impermeable boundaries and all wells were assumed to fully penetrate the reservoir. The data were analyzed using the VARFLOW code.

Table 1

Ahuachapan Flow Rates of Reinjection (R) and Producing (P) Wells in (kg/sec) 1982 Interference Test									
Date	AH-2 R	AH-4 P	AH-8 R	AH-20 P	AH-21 P	AH-22 P	AH-23 P	AH-24 P	AH-26 P
May 6	-19.8	45.1	-33.9	37.8	72.9	56.6	31.3	37.5	23.1
May 15	-19.8	45.1	0.0	37.8	72.9	56.6	31.3	37.5	23.1
May 17	-19.8	45.1	0.0	0.0	72.9	56.6	31.3	37.5	23.1
May 26	-19.8	45.1	0.0	0.0	0.0	56.6	31.3	37.5	23.1
June 1	-28.3	50.8	0.0	0.0	0.0	57.7	49.0	35.9	22.5
June 3	-28.3	50.8	0.0	0.0	0.0	57.7	49.0	0.0	22.5
June 19	-28.3	50.8	0.0	0.0	0.0	0.0	0.0	0.0	0.0
June 25	-28.3	50.8	0.0	0.0	0.0	57.7	49.0	0.0	22.5
July 1	-42.2	63.2	0.0	0.0	0.0	58.5	49.8	0.0	21.5
Aug. 1	-53.4	74.2	0.0	0.0	0.0	57.7	50.1	0.0	40.0
Aug. 2	-53.4	74.2	0.0	0.0	82.5	57.7	50.1	40.0	40.0
Aug. 3	0.0	74.2	0.0	0.0	82.5	57.7	50.1	40.0	40.0
Aug. 29	0.0	74.2	0.0	0.0	82.5	57.7	50.1	40.0	40.0

Figure 2 shows the best match of the pressure history in observation well AH-25, obtained for a medium with a transmissivity of 35 Dm and a storativity of 3.5×10^{-6} m/Pa. The model was assumed to have an impermeable N-S boundary near well AH-15, as suggested by field data. The calculated drawdown matches reasonably well the observed pressures, especially for the period up to 1969-1983. The disagreement in later years could be explained by a change in field production pattern. Other possible causes are the effects of a two-phase zone in the reservoir, and the fact that a model using a uniform permeability value is not likely to match well the behavior of this complex heterogeneous fractured system. However, the reservoir parameters obtained are consistent with those inferred from the interference test analysis.

In order to estimate the effects of reinjection that occurred from 1976 to 1982 on the pressure drawdown at Ahuachapan, the pressure history was simulated without considering any reinjection. The results are shown in Figure 3 for well AH-25. The figure shows that reinjection provided significant pressure support, with about 4 bars less pressure drawdown at the end of the reinjection period than if no injection had occurred. The figure also shows that with continued production the effects of the reinjection period became gradually smaller.

NATURAL STATE MODEL

The simulation work was carried out using the numerical model MULKOM (Pruess, 1983) with the following objectives:

1. to verify the conceptual model of the system.
2. to quantify the natural mass and heat flow in the reservoir.
3. to better understand the hydrology of the field.
4. to obtain a coarse estimate of the permeability structure of the field.
5. to obtain proper initial conditions for the exploitation modeling.

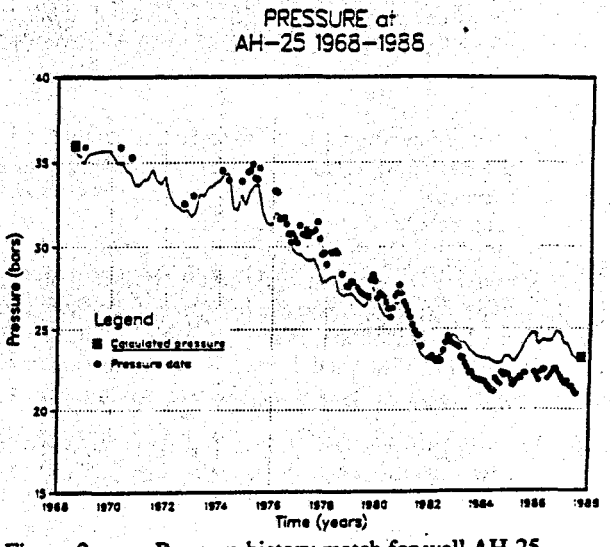

Figure 2. Pressure history match for well AH-25.

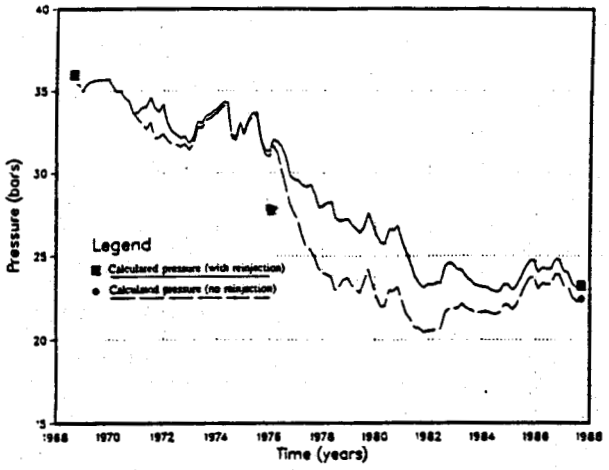

Figure 3. Comparison of pressure decline with or without reinjection.

Approach

The natural state model of Ahuachapan should represent all important features of the conceptual hydrogeological model of the field as defined by Laky et al. (this volume):

1. Hot fluid recharge into the production site occurs southeast of well AH-18. The temperature of the recharge fluids must exceed 250 °C. (See Figure 7 in Laky et al., this volume).
2. The bulk of the hot fluids flow towards the north, with only small fractions of the total flow recharging the Ahuachapan and the nearby Chipilapa reservoirs. The main outflow for the system is at El Salitre, some 7 km north of the Ahuachapan field.
3. The Ahuachapan Andesite unit is highly permeable and serves as the main conduit for lateral fluid flow.
4. The reservoir is bounded by low permeability barriers in the west (close to well AH-15) and in the north (towards well AH-10).
5. Relatively cold, low-salinity waters from the north recharge the system in the eastern part of the field.
6. Reservoir fluids are also discharged at various surface manifestations in the Ahuachapan/Chipilapa area.

The computational mesh used in this study consists of a three-dimensional, three layer grid containing 46 elements per layer, covering an area of some 50 km^2. The grid includes the inferred upflow zone, Ahuachapan, Chipilapa, and the outflow area of El Salitre. The thicknesses of the layers were determined based on lithologic and feed zone data. The top of the model is at 350 masl, which approximately coincides with the top of the AA unit. The model extends down to -600 masl. The areal dimensions of the grid are shown in Figure 4.

Few data are available regarding the fluid and heat flow at surface manifestations except for the El Salitre area, which had an estimated flow of 1300 l/s (≈ 1300 kg/s) at

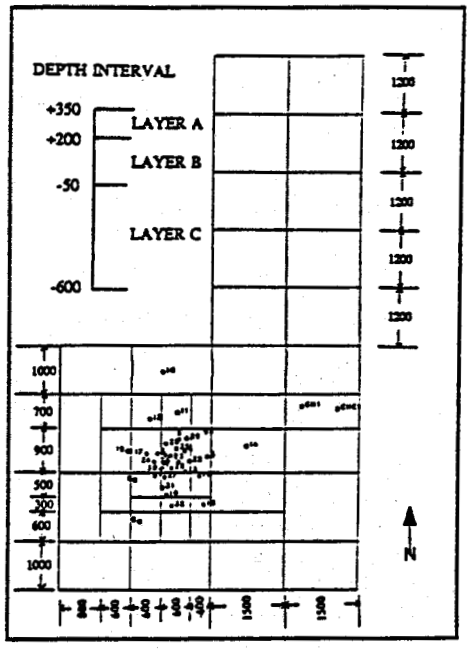

Figure 4. Grid blocks and well locations.

70 °C, with an unknown amount of mixing between geothermal and colder waters (Sigvaldason, et al., 1970). The total energy output from the other surface manifestations was coarsely estimated based on visual observations.

In the model, the surface springs are represented by pressure dependent sinks that were designed so that proper spring outflows would be simulated when the correct pressure distribution was obtained. This feature of the model will be useful in the exploitation simulations to evaluate the spring outputs as a function of reservoir pressure. The conductive heat losses to the surface are computed using an analytical algorithm developed by Vinsome and Westerfeld (1980).

In the simulations, we used a procedure similar to that employed for the Krafla geothermal field (Bodvarsson, et. al., 1984). The adjustable parameters during the modeling iterations were the flowrate and temperature of the upflow zone, spring flowrates and the global permeability distribution. The measured temperatures and pressures in the field were the main constraining parameters. A process of trial and error was carried out until a set of parameters was found that gave reasonable matches with the three-dimensional temperature and pressure distributions. The procedure employed was as follows:

1. Assign sources and sinks to the appropriate nodes,
2. Assign thermodynamic conditions to the cold and hot recharge fluids,
3. Assign rock properties and the permeability distribution,
4. Perform simulation until steady-state thermodynamic conditions are reached,

5. Evaluate the results and return to step 1 if computed temperature and pressure distributions do not fit those observed.

Best Model

A natural state model was developed that reproduces reasonably well the pre-exploitation temperature and pressure in the field. The matches between observed and simulated temperatures and pressures are shown in Figures 5-9. The model, however did not reproduce well the temperatures observed in well CH-1, especially in the lower two layers (Figure 9). The temperature profile used for comparison with the simulated results was obtained in 1969. This is the only log available that penetrates to this depth, and may not show the stabilized temperature conditions in this well.

The simulated results show somewhat colder temperatures than those observed for well AH-15 (Figure 7), which is due to the fact that the well is not in the center of the gridblock, but farther to the east. As temperatures are believed to decrease rapidly west of well AH-15, the temperature profile of this gridblock seems reasonable.

The slight difference between the simulated and observed pressures (simulated pressure are slightly higher; Figure 5) is due to the pressure drawdown caused by well testing during the field development phase (1972-1973). A considerable pressure decline was observed during that period. Although the pressure recovered during the last one and a half years prior to exploitation, the 1974-1975 data (initial pressures) indicate about 1-2 bar lower pressures than in 1968.

The results from the best model indicate that a total flow of 225 kg/s of 255 °C water recharges the system southeast of the wellfield (in the area of the Laguna Verde volcanic complex). The total thermal throughflow for the entire system is estimated to be 250 MW_t. About 60 MW_t are lost through the surface manifestations in the Ahuachapan and Chipilapa areas. Conductive heat losses to the surface are estimated to be about 20 MW_t with the remainder exiting the system by fluid discharge at El Salitre Springs.

Lithology and Permeability Distribution

Four rock types are used in the best model to represent the different lithologic units found in Ahuachapan area (see Figure 10). The material properties used are given in Table 2 and are partly based on data from Larios (1985). Description of these rock types are given below,

Rock Type 1 corresponds to the Young Agglomerates the caprock of geothermal system. The Saturated Aquifer is found in this unit.

Rock Type 2 represents the Ahuachapan Andesites, the main geothermal reservoir.

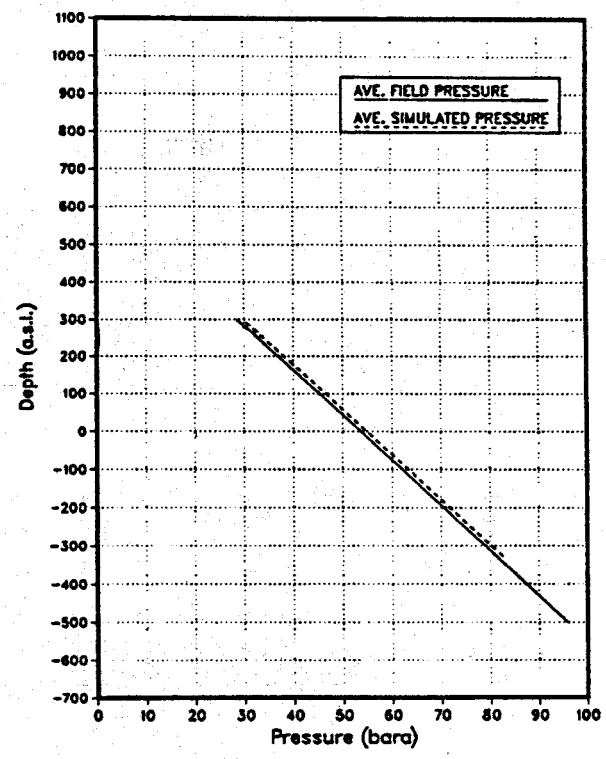

Figure 5. Match between observed and computed pressures for the best model.

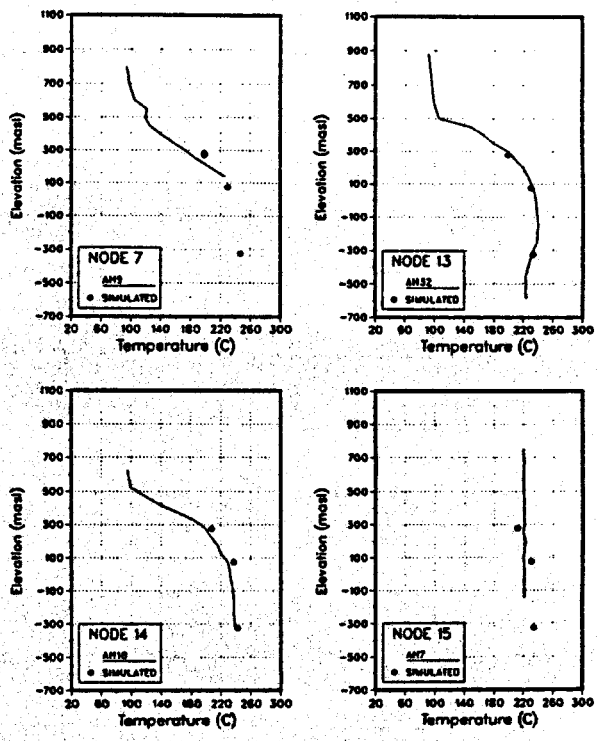

Figure 6. Match between observed and computed temperature profiles for wells AH-9, AH-32, AH-18 and AH-7.

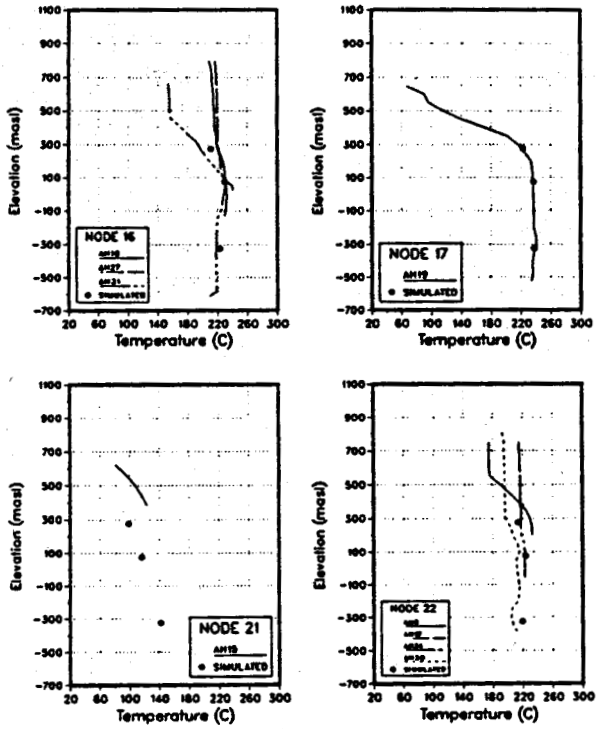

Figure 7. Match between observed and computed temperature profiles for the best model (other wells).

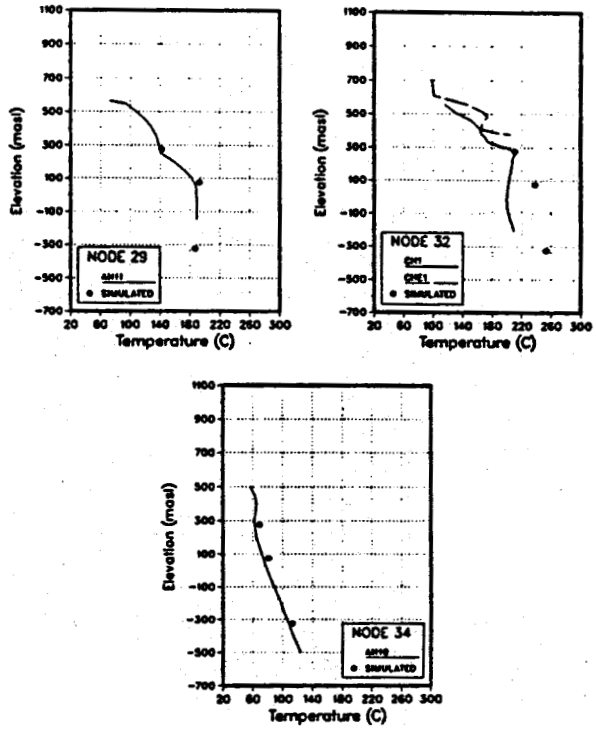

Figure 9. Match between observed and computed temperature profiles for the best model (other wells).

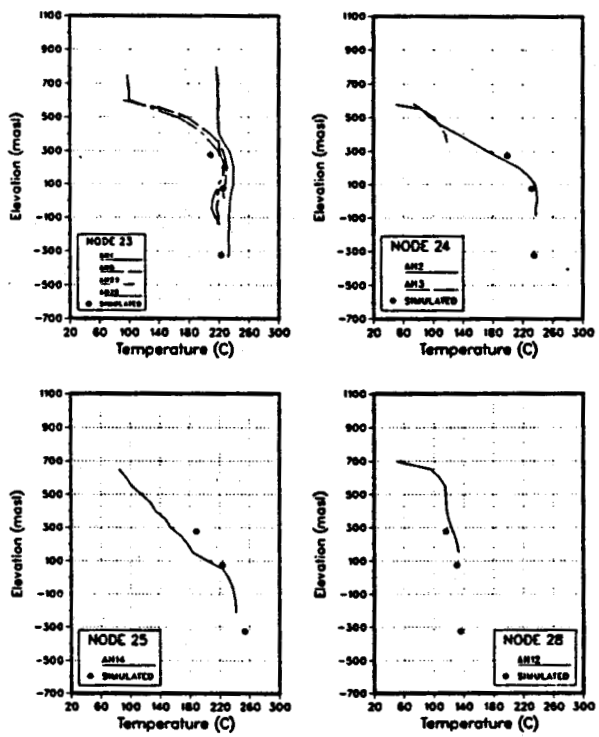

Figure 8. Match between observed and computed temperature profiles for the best model (other wells).

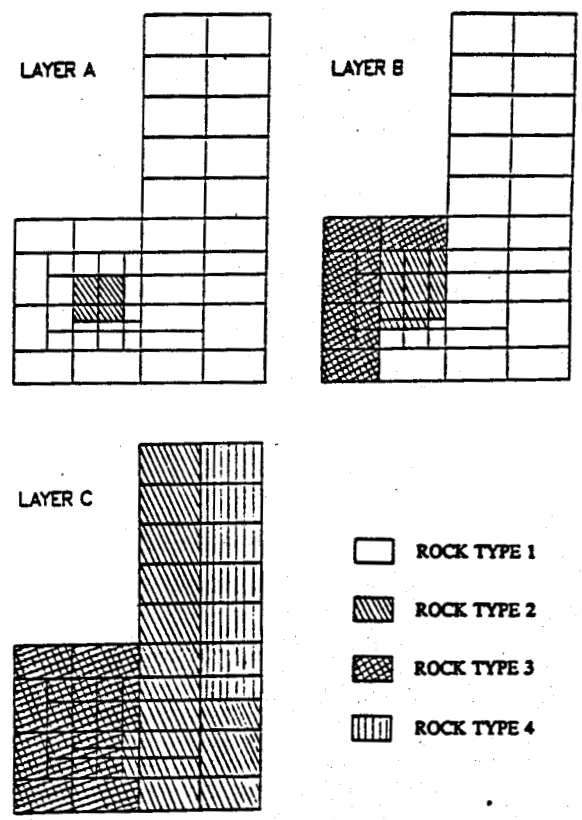

Figure 10. Distribution of rock types for the different layers in the natural state model.

Table 2

Rock Properties Used in the Natural State Model				
	Rock Type 1	Rock Type 2	Rock type 3	Rock Type 4
Density, kg/m^3	2680	2890	2800	2650
Porosity	0.10	0.10	0.05	0.10
Heat Conductivity W/m- °C	2.3	2.3	2.3	2.3
Permeability, md				
horizontal	10	80	20	20
vertical	0.2	16	4	2
Heat Capacity J/kg- °C	1000	1000	1000	1000

Rock Type 3 represents the Older Agglomerates. In previous studies this unit was considered impermeable, but we believe that this rock unit has a significant permeability, although much lower than the overlying Ahuachapan Andesites. Several wells (e.g. AH-28 and 29) encountered permeable zones in this unit.

Rock Type 4 was used only in Layer C (Figure 10) and corresponds to an agglomerate unit, similar to the YA unit but with higher permeability. This material type was necessary to simulate the inferred high flow from the upflow zone toward El Salitre Springs.

The permeability was used as one of the adjustable parameter in the iteration procedure discussed earlier. Table 2 shows the final permeability values used in the best model; other assumed rock properties are also given. The model results indicate a horizontal permeability for the AA unit (Rock Type 2) of 80 md. Given an average thickness of this unit between 300-400 m, a transmissivity of 24-32 Dm is obtained, which agrees well with the value of 25 Dm obtained from the interference test analysis and 35 Dm estimated from the production history. The low vertical permeability of the YA (0.2 md) agrees well with the assumption that the YA unit acts as a caprock to the system. The low permeability barriers to the north and west were modeled using very low interface permeabilities between appropriate gridblocks.

Sources and Sinks

The locations of sources and sinks in the mesh are shown in Figure 11. The estimated flowrates for the surface manifestation are given in Table 3. The computed flowrate value feeding El Salitre Springs, given in Table 3 (170 kg/s) does not consider any mixing with local groundwater. Assuming local mixing to occur with a 40 °C water at shallower depths, the total flowrate of a 70 °C fluid to that area would be approximately 1290 kg/s, which agrees well with the estimate by Sigvaldason et al. (1970).

Small heat sinks were specified in the blocks with wells AH-32, AH-18, AH-31 and AH-19 in order to match the observed temperature inversions. The strengths of these sinks were 3, 6, 1.5 and 3.75 W/m^2, respectively.

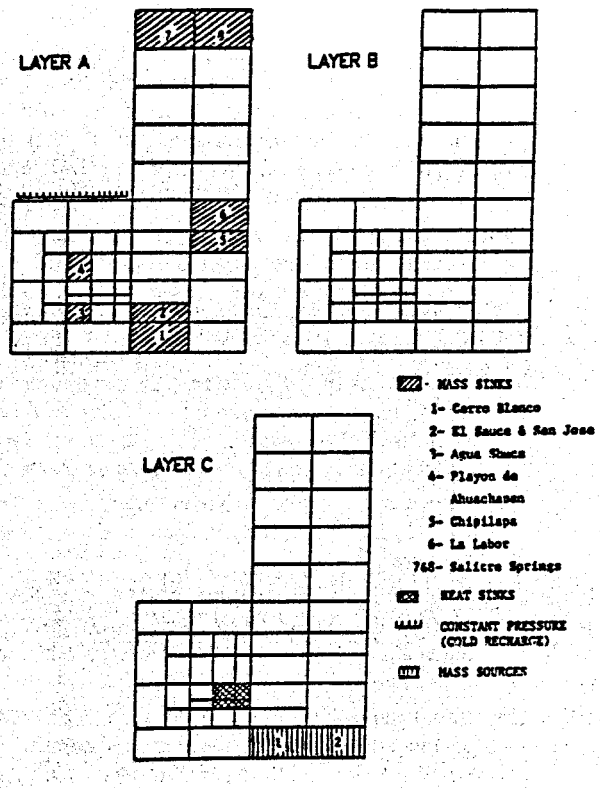

Figure 11. Location of specified sources and sinks in the natural state model.

Table 3

Flow Rates and Heat Outputs of the Different Surface Manifestations		
	Flow (kg/s)	MW_t
Cerro Blanco	5.0	5.1
El Sauce & San Jose	3.4	3.4
Playon de Ahuachapan	20.0	19.0
Agua Shuca	2.2	1.9
Chipilapa	3.5	3.2
La Labor	29.0	28.0
El Salitre	170.0	169.0

Only the outputs associated with geothermal fluids are given (see text).

A source of 60 °C fluid was specified north of AH-10. This was found necessary to match the temperature profile of well AH-10. The cold recharge was modeled using a constant pressure boundary of 42 bars in the uppermost layer (see Figure 11). The pressure at the boundary was specified so that the pressures in the adjacent blocks would be about 5 bars higher than in the rest of the wellfield, which is the observed pressure difference.

CONCLUSIONS

Various modeling studies have been conducted on the Ahuachapan field data including the analysis of interference test data, analysis of the average reservoir drawdown history and the development of a natural state model. The main conclusions of these studies are as follows:

(1) The analysis of the interference test data yields an average transmissivity of about 25 Dm and a storativity of 2.5×10^{-6} m/Pa. This storativity value is consistent with the presence of a two-phase zone in the system.

(2) The analysis of the pressure drawdown data (1969-1988) yields a transmissivity of 35 Dm and a storativity of 3.5×10^{-6} m/Pa. both of these values agree well with the results of the interference test analysis.

(3) Reinjection at Ahuachapan during the period 1976-1982 significantly helped maintain reservoir pressures.

(4) A natural state model of Ahuachapan has been developed that agrees well with the three-dimensional temperature and pressure conditions in the reservoir.

(5) Based upon the model, the horizontal permeability of the Ahuachapan Andesites is estimated to be about 80 md, yielding a transmissivity of about 30 Dm for this unit. This transmissivity is consistent with the results of the interference test analysis and the analysis of the pressure drawdown history. The vertical permeability of the Andesites is estimated to be about 16 md.

(6) The permeability of the Older Agglomerates is estimated to be 20 md horizontally and 4 md vertically.

(7) The total recharge to the Ahuachapan/Chipilapa geothermal systems is estimated to be 225 kg/s of 250 °C water, yielding a total thermal throughflow of 250 MW_t. Most of these fluids discharge in El Salitre Springs (170 kg/s), but significant energy is lost through surface springs in the Ahuachapan/Chipilapa areas (60 MW_t) and through conduction to the ground surface (20 MW_t).

ACKNOWLEDGEMENTS

The authors appreciate technical review of this paper by M. J. Lippmann and C. Doughty. This work was sponsored through a contract from Los Alamos National Laboratory and supported by the Geothermal Technology Division, U.S. Department of Energy, under Contract No. DE-AC03-76SF00098.

REFERENCES

Bodvarsson, G. S., Pruess, K., Stefansson, V. and Eliasson, E. T. (1984). "The Krafla Geothermal Field, Iceland. 2. The Natural State of the System," *Water Resources Research, 20,* 11, 1531-1544.

EG&G Idaho, Inc. and Lawrence Berkeley Laboratory (1982). "Low-to-Moderate Temperature Hydrothermal Reservoir Engineering Handbook" Report IDO-10099.

Grant, M. (1980). "Simple Modeling of Production and Reinjection at Ahuachapan," DSIR report, New Zealand, February 1980.

Larios, D. (1985). "Estudio de la Permeabilidad, Porosidad y Densidad de las Rocas del Campo Geotermico de Ahuachapan," CEL report, El Salvador, February 1985.

Laky, C., Lippmann, M. J., Bodvarsson, G. S., Retana, M. and Cuellar, G. (1989). "A Hydrologic Model of Ahuachapan Geothermal Field, El Salvador," this volume.

Pruess, K. (1983). "Development of the General Purpose Simulator MULKOM," 1982 Earth Sciences Division Annual Report, Lawrence Berkeley Laboratory report LBL-15500, Berkeley, CA.

Sigvaldason, G.E. and Cuellar, G. (1970). "Geochemistry of the Ahuachapan Thermal Area, El Salvador," UN Symposium on the Development and Utilization of Geothermal Resources, Pisa, Italy, Vol. 2, pp. 1392-1399.

Steingrimsson, B., Bodvarsson, G. S., Cuellar, G. and Escobar, C. (1989). "Changes in Thermodynamic Conditions of the Ahuachapan Reservoir Due to Production and Injection," this volume.

Truesdell, A., Aunzo, Z., Bodvarsson, G. S., Alonso, J. and Campos, A. (1989). "The Use of Ahuachapan Fluid Chemistry to Indicate Initial Conditions and Reservoir Processes During Exploitation," this volume.

Vinsome, P. K. W., and Westerfeld, J. (1980). "A Simple Method for Predicting Cap and Base Rock Heat Losses in Thermal Reservoir Simulations," *Journal of Canadian Petroleum Technology*, July-September.

PROCEEDINGS, Fourteenth Workshop on Geothermal Reservoir Engineering
Stanford University, Stanford, California, January 24-26, 1989
SGP-TR-122

A SOLUTION TO PROPPANT DISSOLUTION IN HYDROTHERMAL ENVIRONMENTS

J. A. Knox and J. D. Weaver

Halliburton Services
P. O. Drawer 1431
Duncan, OK 73536

INTRODUCTION

The chemistry of silica may be one of the most widely studied subjects in the world. In Ilers[1] "The Chemistry of Silica" there are over 3000 references. Perhaps it has been so widely studied partially because it is one of the most abundant materials on earth and partially because its behavior is so enigmatic.

The concern with silica in this paper relates to its use as a gravel packing material in wells which produce from an unconsolidated formation or as a proppant used to provide a high permeability fracture path to the wellbore in lower permeability consolidated formations.

In gravel packed wells which produce heavy oil from incompetent formations the practice of injecting steam to enhance production is widespread. It has been found that under the conditions at which steam is injected, that is, pH 11 or higher and at temperatures up to 600°F, quartz sand dissolves fairly rapidly.[2] Attempts to alleviate this problem by substituting other materials for sand have been described.[3,4]

High alumina sintered bauxite has been suggested by one author;[3] a second author obtained contradictory results.[4] Additional studies show that siliceous formations also dissolve but at a lower rate because of impurities in the system[1,5].

Present studies agree with the work of the second author showing that bauxite is not only soluble to a considerable extent in high pH water, but that it also reprecipitates and fills in void spaces, decreasing the permeability of the pack.

Specially graded quartz sand is the primary proppant used in fracturing operations to stimulate production in lower permeability, competent formations. Bauxite type materials are used in deeper, harder formations to provide long term, high fracture permeability. Fracturing techniques using both sand and bauxite[6-8] to stimulate production in geothermal formations have been described.

There is no reason to assume that successful fracture treatments in geothermal wells cannot be accomplished. There may be no reason to be concerned that the quartz proppant should dissolve because one would assume that formation water from a sandstone formation would be saturated with silica. There is evidence that high temperature decreases the strength of quartz proppants.[6]

A review of "Compilation of Data on Fluids from Geothermal Resources in the US" showed silica contents from 4 ppm to 1416 ppm in water samples from different formations and fields.[9] The average concentration was in the range of 200 to 300 ppm. There appeared to be no correlation between pH of the water or total dissolved solids and the silica content. Analytical methods were not described, sampling procedures varied widely, and there was no description of formation composition.

Reprecipitation of silica from highly saturated formation water on to new silica surfaces is a real possibility.[1] Also it is unlikely that the formation water would be saturated with alumina in most instances so the possibility of dissolving bauxite exists.

A description of a new proppant which avoids the shortcoming of both sand and bauxite will be described in the following sections.

EXPERIMENTAL

A schematic of the test equipment used in this study is shown in Figure 1. Equipment includes a reservoir of deionized water which has been adjusted to pH 11 with reagent grade sodium carbonate. Carbon dioxide was excluded by utilizing a trap containing ASCARITE carbon dioxide absorbent. Upstream and downstream backpressure regulators were used to maintain a differential pressure of 60 PSI across the system,

with an absolute system pressure of about 1200 PSI. The regulation equipment was protected by the cold water heat exchangers both up and down stream.

Test samples were contained in a section of 0.375 in. diameter tubing. Both the sample holder and the heat exchange coil were submerged in a thermostatically controlled fluidized sand bath. The entire system was initially constructed of wetted 316 stainless steel parts. Later studies utilized high temperature wetted parts made of monel.

Weight loss data were obtained by weighing oven-dried, loaded test cells before and after the tests. Note that this method does not account for any fines which are generated during the test and retained in the test cell, but only material which is actually produced from the cell.

A computer data acquisition system was used to determine permeability of the packs and to obtain 20 ml eluent samples on an hourly schedule. Fluids were analyzed for Si, Al, and Zr.

DISCUSSION

The initial objective of this study was the evaluation of commercially available proppants (Table I) useful as gravel packing materials for cyclic steam injection wells. These proppants were also to be considered for fracturing geothermal wells. This evaluation was to determine, under realistic conditions, the life expectancy of the packing material.

Laboratory screening conditions were selected to be representative. Most of the initial testing utilized a fluid temperature of 550°F and pH of 11. A fluid velocity of about 4 cm/min was generally used, however, this varied during the tests since a constant pressure differential was maintained. Three days of injection proved to be sufficient duration for the evaluation of most materials.

The weight loss results of some of the materials evaluated are shown in Table II. Sand gave the highest weight loss value, losing 77% of its weight in three days. It was found that this weight loss is proportional to fluid pH, temperature, and throughput volume, Figure 3 is a scanning electron micrograph of the sand sample after the three day test. Notice the smooth surfaces and the absence of any fines, indicating complete and uniform surface dissolution.

Several alumina based proppants, which are reported to have superior crush resistance at high temperatures are available for fracturing operations. These were evaluated and found to indeed be more stable than sand under the harsh conditions of cyclic steam treatments. Results of stability tests on five popular, high performance proppants which have been used for gravel packing cyclic steam injection wells are reported in Table II. The analyses of these materials are given in Table I. Weight loss results after three days of flowing hot water ranged from 37-60%. While this is an improvement over sand, it was considered unsatisfactory for two additional reasons. First, the material cost is very high (10-15 times) when compared to sand, and second, it was observed that pack permeability decreased dramatically. This is shown for IMS-2 in Figure 2.

The unexpected loss in permeability has also been observed in field operations using these type proppants. Figure 4 is a photograph of the sample as it was removed from the flow cell after a three day test. Copious quantities of fines were evident. Some actual consolidation of the pack can be observed. Figure 5 is a micrograph of this material showing an amorphus material being partially responsible for the consolidation of the pack. A crystalline overgrowth is also evident. The crystalline material shown in Figure 6 was identified as analcite ($NaAlSi_2O_6 \cdot H_2O$).

The unexpected occurrence of fines was observed with all the alumina and zirconia based materials. Some of these are shown in Figure 7-10. These results suggested that the use of high strength proppants for gravel packing cyclic steam injection wells or for use in geothermal applications may not be desirable. It has not been determined yet whether the fines formed during degradation of the packing material invade the formation and do permeability damage, nor how deep this damage may occur.

The poor performance of these high strength proppants led to the study of noncommercial materials as possible gravel packing solids. Many materials were evaluated and several were found to possess thermal stability properties. Most of these were eliminated because of poor control over particle size distribution and/or cost considerations. For example, nickel plated sand (Table II) proved to be highly resistant to the test conditions, however cost is prohibitive.

One material emerged as a product of choice. It is low cost, can be sieved to meet most any required size distribution, and is highly resistant to dissolution and fine formation under the test conditions. This material is identified in this paper as SRG

(Steam Resistant Gravel) in Table II. Photomicrographs in Figures 11-13 show the effect of 3 and 14 days of flowing 550°F water. There were no visible fines generated from this treatment as shown by (1) the micrographs and (2) the effect on permeability (Figure 2). Weight loss data show 8% decrease in weight. This occurs rapidly, and no additional loss was observed. This corresponds to a 5-10% silica contamination in the material. It is believed that silica contamination exists as small inclusions since small craters are apparently formed by the dissolution of this silica as shown in Figures 11-13.

This material is somewhat more angular than sand, but usually can meet the API minimum recommended sphericity and angularity requirements for gravel packing. Its acid solubility is very similar to that of sand, which permits performance of HCl and HF acid stimulation treatments through gravel packs of this material.

CONCLUSIONS

1. Sand dissolves rapidly in pH 11, 550°F water but fines formation was not observed and permeability damage did not occur in the pack.
2. High strength, alumina and zirconia based proppants are not stable under test conditions used, losing 37-60% of their weight in three days. They also formed copious quantities of fines and showed severe permeability damage to the pack.
3. A new material (SRG) has been found to have a low loss of weight even after long exposure. There was no evidence of fines formation nor permeability damage. This material is 30-50% the cost of the high strength proppants.

ACKNOWLEDGMENT

The authors wish to thank Halliburton Services for allowing this data to be published. Special thanks go to Mr. David Brown and Mr. William Smith for the collection of laboratory data.

REFERENCES

1. Iler, Ralph K.: "The Chemistry of Silica" A Wiley-Interscience Publication, 1979.
2. Reed, M.G.: "Gravel Pack and Formation Sandstone Dissolution During Steam Injection," J. Pet. Tech (June 1980) pp. 941-949.
3. Underdown, D.R. and Das, K.: "Stability of Gravel Packing Material for Thermal Wells," J. Pet. Tech (Nov. 1985) pp. 2006-2012.
4. Sacuta, A., Nguyen, D.M. and Kissel, G.A.: "Stability of Nickel-Coated Sands as Gravel Pack Material," presented at the 56th SPE California Regional Meeting, Oakland, CA, April 2-4, 1986, SPE Paper 15058.
5. McCorriston, L.L., Denby, R.A., and Peace, E.C.: "Study of Reservoir Damage Produced in Heavy Oil Formations Due to Steam Injection," presented at 56th SPE Annual Fall Tech. Conf. and Exhibition, San Antonio, TX, Oct. 5-7, 1981, SPE Paper 10077.
6. Campbell, D.A., Sinclair, A.R., Harold, R.J., and Vetter, O.J.: "Review of the Geothermal Reservoir Well Stimulation Program," presented at The International Conference on Geothermal Drilling And Completion Technology, Albuquerque, NM, Jan. 21-23, 1981.
7. Campbell, D.A., Morris, C.W., and Verity, R.V.: "Geothermal Well Stimulations Experiments and Evaluation," presented at 56th SPE Annual Fall Tech Conf. and Exhibition, San Antonio, TX, Oct. 5-7, 1981, SPE Paper 10316.
8. Morris, C.W. and Sinclair, A.R.: "Evaluation of Bottomhole Treatment for Geothermal Well Hydraulic Fracture Stimulation," presented at 57th SPE Annual Fall Tech Conf. and Exhibition, New Orleans, LA, September 26-29, 1982, SPE 11157.
9. Cosner, S.R. and Apps, J.A.: "A Compilation of Data on Fluids from Geothermal Resources in the United States," May 1978, Lawrence Berkley Lab., University of California, DOE Contract W-7405-ENG-48.

TABLE I

Typical Analysis for Gravel Packing Materials Tested

Typical Analysis	Ottawa Sand	IMS-1	IMS-2	IMS-3	HS-1	HS-2	SRG
Al_2O_3	0	55-60	39	75	-	77	0
$Al_6Si_2O_{13}$	0	40-45	54	24	-	22	0
$Al(OH)_3$	0	<1	<1	1.4	-	1	0
Amorphous	0	0	7	0	60	0	0
Spinnel	-	-	-	-	-	-	90-95
SiO_2	>98	-	-	-	-	-	5-10
ZrO_2	-	-	-	-	40	-	-

IMS = Intermediate strength proppant.
HS = High strength proppant.
SRG = Steam resistant gravel.

TABLE II

Weight Loss of some Evaluated Gravel Packing Materials

Test Material	Injection Volume (Liters)	Weight Loss (%)
Ottawa Sand	13.6	77
IMS-1	13.1	60
IMS-2	11.6	56
IMS-3	14.5	41
HS-1	14.3	37
HS-2	13.1	48
Nickel Plated Sand	15.1	3
SRG	15.1	8
SRG	70.6	8

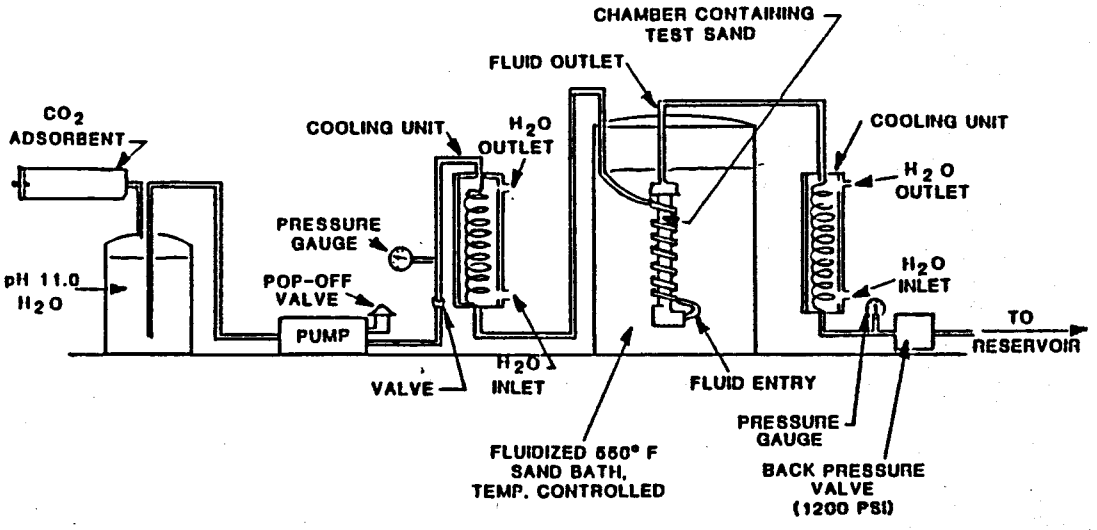

Figure 1: Schematic of Test Equipment for Injecting pH 11, 550°F Water Through a Pack of Test Solids.

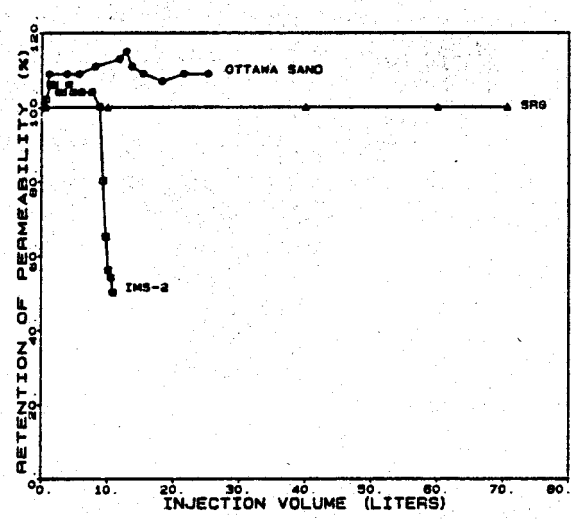

Figure 2: The Effect of Injection Volume of pH 11, 550°F Water on Pack Permeability

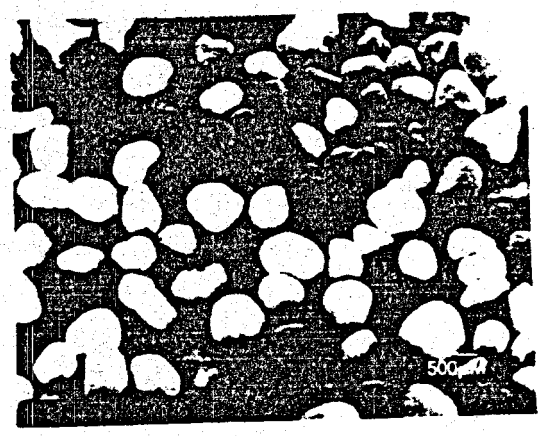

Figure 3: Ottawa Sand After Flowing 550°F Water for 3 Days.

Figure 4: IMS-2 Sample as Removed from Test Cell After 3 Day Exposure to 550°F Water

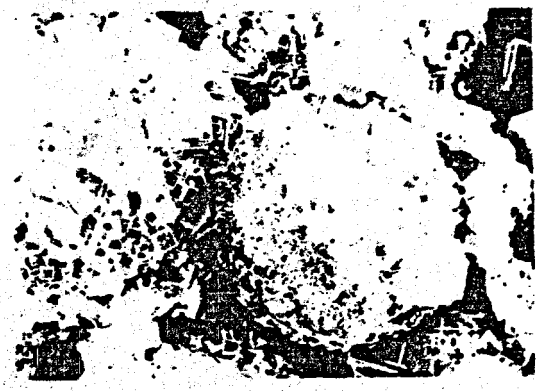

Figure 5: SEM of IMS-2 From Figure 4.

Figure 6: Crystalline Overgrowth From Figure 5 Identified as Analcite.

Figure 7: IMS-1 After 3 Day Exposure to 550°F Water.

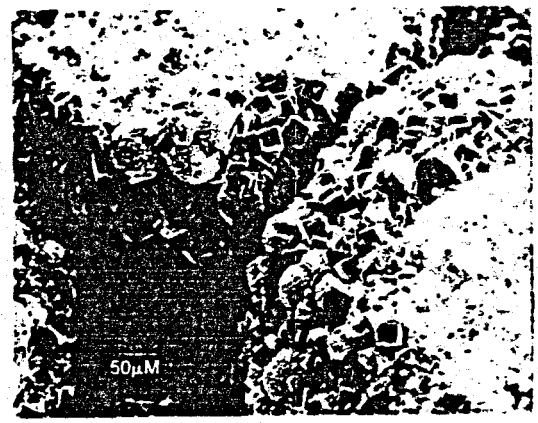

Figure 8: IMS-1 After 3 Day Exposure to 550°F Water. Higher Magnification.

Figure 9: HS-1 After 3 Day Explosure to 550°F Water.

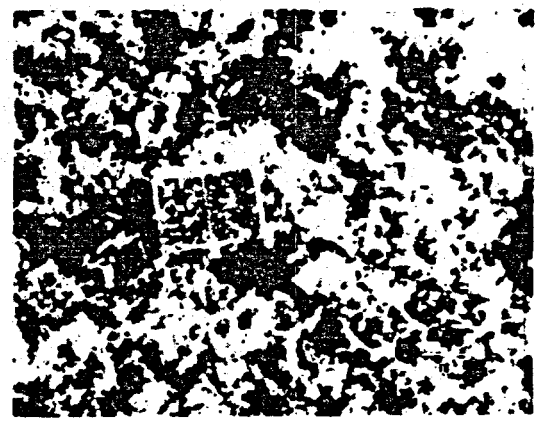

Figure 10: High magnification of Fines From 3 Day Exposure to HS-2.

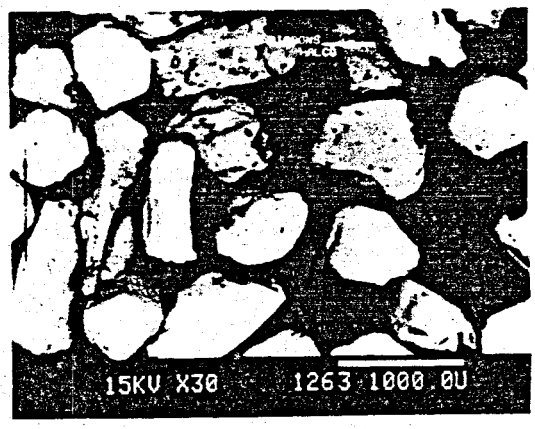

Figure 11: SRG Before Exposure to Hot Water.

Figure 12: SRG After 3 Day Exposure to 550°F Water.

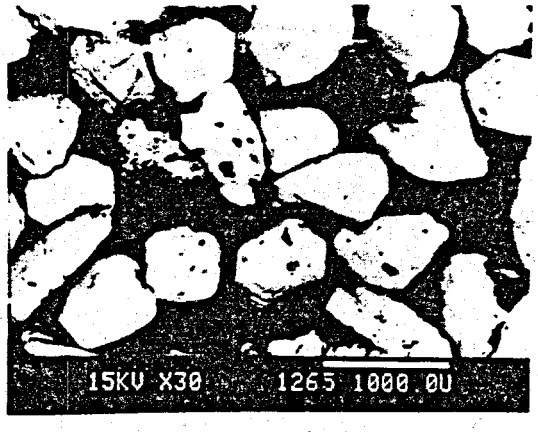

Figure 13: SRG After 14 Day Exposure to 550°F Water.

PROCEEDINGS, Fourteenth Workshop on Geothermal Reservoir Engineering
Stanford University, Stanford, California, January 24-26, 1989
SGP-TR-122

RESERVOIR COMPRESSIBILITY FROM WATER-INFLUX MODELING OF LIQUID-DOMINATED SYSTEMS

D.C. Brock and J.S. Gudmundsson*

Petroleum Engineering Department, Stanford University, Stanford, California
* Geothermal Division, National Energy Authority, Reykjavik, Iceland

ABSTRACT

A water influx model was used to history match the pressure drawdown behavior of three liquid-dominated geothermal reservoirs. The compressibilities of confined and unconfined liquid-only reservoir systems were shown to differ by one to two orders of magnitude in the temperature range 300°C to 100°C. History matching of production data from three high temperature fields (Ahuachapan, Svartsengi and Wairakei) yielded reservoir compressibility values similar to what would be expected for unconfined (free liquid level) systems.

INTRODUCTION

The success of reservoir modeling depends largely on what information is available concerning production history, reservoir shape and size, and the properties of rock and fluid. Many different methods have been used to model the behavior of geothermal reservoirs (Grant, 1983; Bodvarsson et al. 1986). The Hurst simplified model was formulated for use in lumped parameter modeling of petroleum reservoirs with edge-water drive (Hurst, 1958). It is easily modified to describe a liquid-dominated geothermal reservoir with aquifer support.

Examples of water influx modeling of geothermal reservoirs are those of Whiting and Ramey (1969), Olsen (1984), Marcou (1985) and Brock (1986); also Gudmundsson and Olsen (1987). Because liquid-dominated geothermal reservoirs have compressibilities much higher and more highly variable than petroleum reservoirs, the model was formulated to output the compressibility by history matching in the present work.

PHYSICAL PROPERTIES

The compressibility of geothermal reservoirs depends on many factors, including the fluid state and production mechanism. Considering liquid-dominated reservoirs only, two extreme, idealized conditions can be identified: confined and unconfined (free liquid surface). The storage coefficients (m/kPa) for the two types of reservoirs are

$$S_c = \phi c h \qquad (1)$$

and

$$S_u = \frac{\phi}{\rho g} \qquad (2)$$

where the subscripts c and u refer to confined and unconfined conditions (Grant et al., 1982). Other symbols are formation porosity ϕ, fluid compressibility c, formation thickness h, fluid density ρ and the gravity constant g.

Sample values of the storage coefficients with temperature are plotted in Fig. 1, assuming 10 percent porosity ($\phi = 0.1$) and a reservoir thickness $h = 1000$ m. The confined storage coefficient S_c ranges from about 5×10^{-5} to 3×10^{-4} (m/kPa) from 100°C to 300°C. In this temperature range water density decreases from 958 to 712 (kg/m^3), its viscosity decreases from 283×10^{-6} to 91×10^{-6} (Pa.s) and the compressibility (liquid water only) increases from about 0.50 to 3.22 (1/GPa). In other words, the density changes 1.3 times, viscosity 3.1 times and compressibility 6.4 times for liquid water. For the same temperature range the unconfined storage coefficient S_u increases from 1×10^{-2} to 1.4×10^{-2} (m/kPa). Sveinsson (1987) has presented values for the compressibility of liquid water.

For ideal conditions, therefore, an unconfined reservoir is 200 times more compressible than a confined reservoir at 100°C and 40 times more compressible at a temperature of 300°C. These findings agree with Zais and Bodvarsson (1980) who state that the compressibility of unconfined (free liquid surface) systems is 100 to 1000 times greater than that of confined systems.

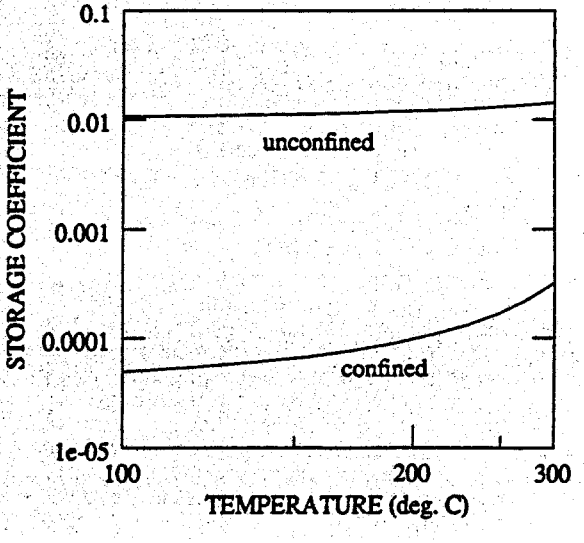

Fig. 1. Sample values of storage coefficients.

HURST'S SIMPLIFIED METHOD

It was reported by Gudmundsson and Olsen (1987) that the Hurst (1958) simplified water influx method gives a satisfactory match to production data from the Svartsengi high temperature, liquid-dominated geothermal field. Likewise, Marcou and Gudmundsson (1986) found the Hurst method satisfactory in the modeling of the Ahuachapan and Wairakei liquid-dominated reservoirs.

In the Hurst (1958) water influx method the reservoir and aquifer compressibility are assumed different and constant. See Olsen (1984) and Brock (1986) for complete derivation of the method for liquid-dominated reservoirs. For a radial reservoir/aquifer system, Hurst (1958) introduced the ratio

$$\sigma = 2\frac{c_a\rho_a}{c\rho} \tag{3}$$

where the numerator refers to aquifer properties and the denominator to that of the reservoir. Hurst (1958) gave the following drawdown solution for an infinite radial aquifer

$$\Delta p = \frac{\mu_a\sigma}{2\pi(kh)_a\rho_a}\sum_{j=0}^{n}\Delta w_{pj}N(\sigma,t_D - t_{Dj}) \tag{4}$$

written in superposition form. The Hurst function N is in Laplace space and is expressed as

$$N(\sigma,t_D) = L^{-1}\left\{\frac{K_0(\sqrt{s})}{s^{3/2}[\sigma K_1(\sqrt{s}) + \sqrt{s}K_0(\sqrt{s})]}\right\} \tag{5}$$

The function is not analytically invertible to real space. Therefore, a numerical inversion method must be used; The Stehfest (1970) algorithm was used in the present work.

Consider two limiting solutions of the pressure drawdown in Equation 4: σ small and σ large. When $c \gg c_a$ the reservoir will dominate the overall system pressure behaviour; surrounding aquifers will not affect drawdown in reservoir pressure with time. In this case, the reservoir responds to fluid production as a confined system (Gudmundsson and Olsen, 1987).

When $c \ll c_a$ the aquifer will dominate the overall system pressure response. In effect, the aquifer is the reservoir. Hurst (1958) showed that in this case the pressure drawdown solution is the same as the general radial system solution; the line source solution applies.

HISTORY MATCHING

In history matching the production data of a reservoir is fitted to a model. The fitting consists of adjusting one or more parameters of the model to find the best match; permeability and permeability-thickness product are commonly used. Compressibility is the parameter that exhibits the greatest range in values; it is also likely to be the least known parameter in reservoir modeling. It follows, that compressibility should be a good parameter to use in history matching for liquid-dominated reservoirs. In the Hurst water influx model the compressibility ratio σ in Equation 3 was used.

The history matching method used in the present work has been detailed by Brock (1986), Marcou (1985) and Olsen (1984). The matching procedure consisted of plotting the drawdown in terms of water head

$$y_n = \frac{\Delta p_n}{\rho g} = \Delta h_n \tag{6}$$

against the Hurst function term

$$x_n = \sum_{j=0}^{n}\Delta w_{pj}\sigma N(\sigma,t_D - t_{Dj}) \tag{7}$$

A liquid-dominated reservoir system conforming to the Hurst water influx model assumptions will exhibit a straight line having the slope

$$m = \frac{\mu_a}{2\pi(kh)_a\rho_a g} \tag{8}$$

The fitting procedure was the following:

(1) Select a value for σ
(2) Calculate x_n and y_n
(3) Find slope m using least squares fit on $y_n = mx_n$
(4) Calculate standard deviation of fit
(5) Select a new σ value and repeat above steps
(6) Plot standard deviation versus σ values
(7) Select σ value giving minimum standard deviation
(8) Select corresponding slope m

Fortran 77 computer programs were written for history matching and forecasting (Brock, 1986). Because the Hurst function in Equation 5 cannot be expressed analytically in real space, numerical inversion had to be used; the Stehfest (1970) algorithm was used. Although this algorithm is well behaved in the Hurst function application, it is slow in execution. In the history matching method x_n and y_n are calculated several times for each data point (often in the hundreds); the Hurst function is inside a doubly nested loop. For a data history of 200 points, say, the Hurst function is evaluated over twenty thousand times. Therefore, a table lookup method was devised to speed up the execution time. For a given σ value a table of $N(t_D)$ was calculated. A table lookup subroutine was then used to obtain by interpolation the appropriate Hurst function value, rather than repeatedly performing the Stehfest algorithm inversion. On a data set of 66 points (time, flowrate, drawdown) the execution time on a VAX 11/750 was more than 1100 seconds of CPU-time while the table lookup method took only 45 seconds. By using the table lookup method it seems model calculations can even be carried out on a typical microcomputer.

FIELD DATA

The production histories of two liquid-dominated fields have been compiled by Marcou (1985): Ahuachapan in El Salvador and Wairakei in New Zealand. The production history of the Svartsengi liquid-dominated field in Iceland has been reported by Olsen (1984). These data were readily available for the purpose of the present study (Brock, 1986; Gudmundsson et al., 1985) report the data also. The

Ahuachapan, Svartsengi and Wairakei fields are all high-temperature: 240°C, 240°C and 260°C, respectively. Grant et al. (1982) provide general information about these fields.

In addition to temperature (both in reservoir and aquifer) and production history (flow rate and drawdown with time), three reservoir parameters are required for the Hurst (1958) water influx model: reservoir radius, porosity and permeability. These parameters were guesstimated for the three liquid-dominated reservoirs and used in the present study. The parameters are shown in Table 1, where reservoir radius is expressed in terms of surface area.

RESULTS AND DISCUSSION

The first step in the history matching procedure was the selection of the σ value, which gave the minimum standard deviation (optimum match) between field data and water influx model. The standard deviations vs. σ values for the three fields are shown in Fig. 2. A minimum was observed for the three fields (Ahuachapan, Svartsengi, Wairakei). The optimum σ value and the corresponding slope m are shown in Table 2 for the three fields.

History matches for the three liquid-dominated fields are shown in Figs. 3, 4 and 5.

Table 1. Reservoir parameters input to history matching.

Field Name	Temperature T (°C)	Area (km^2)	Porosity ϕ	Permeability k (mD)
Ahuachapan	240	15	0.20	50
Svartsengi	240	4	0.05	500
Wairakei	260	15	0.20	30

Table 2. Hurst-model parameters output from history matching.

Field Name	Ratio $\sigma \times 10^{-3}$	Slope m	Standard Deviation
Ahuachapan	37.3	0.133	5.69
Svartsengi	1.6	0.087	1.77
Wairakei	72	0.072	6.56

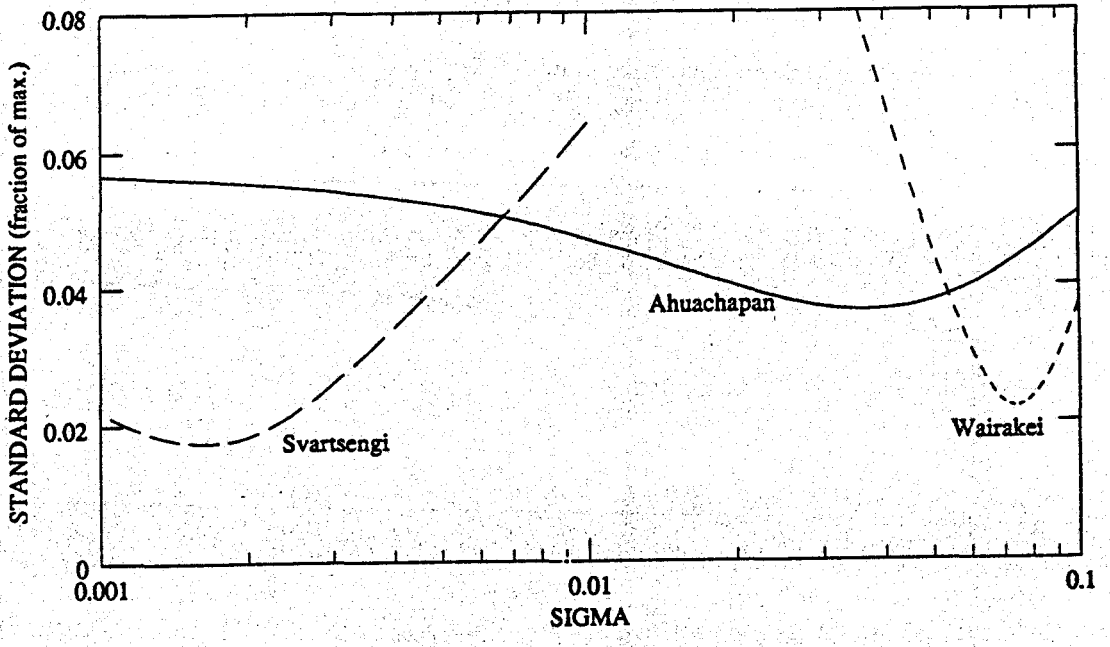

Fig. 2. Choosing the best fit: Standard Deviation vs. σ for the three fields.

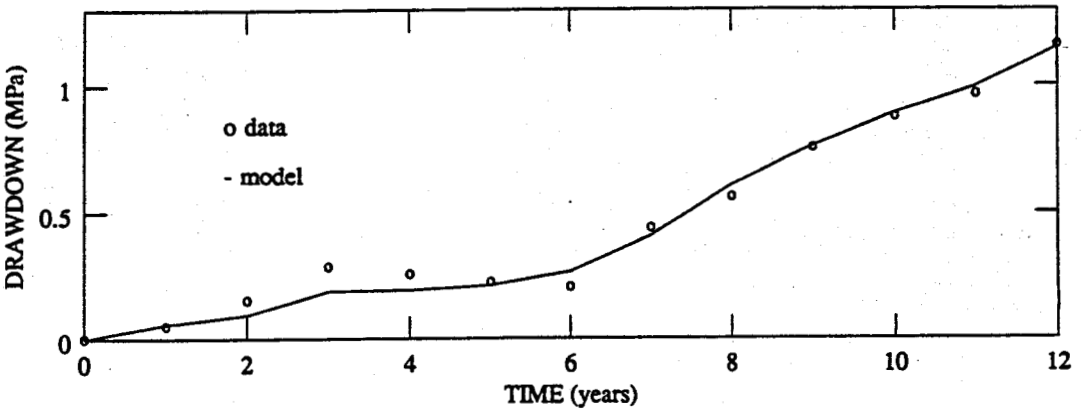

Fig. 3. Drawdown match to the Ahuachapan field data.

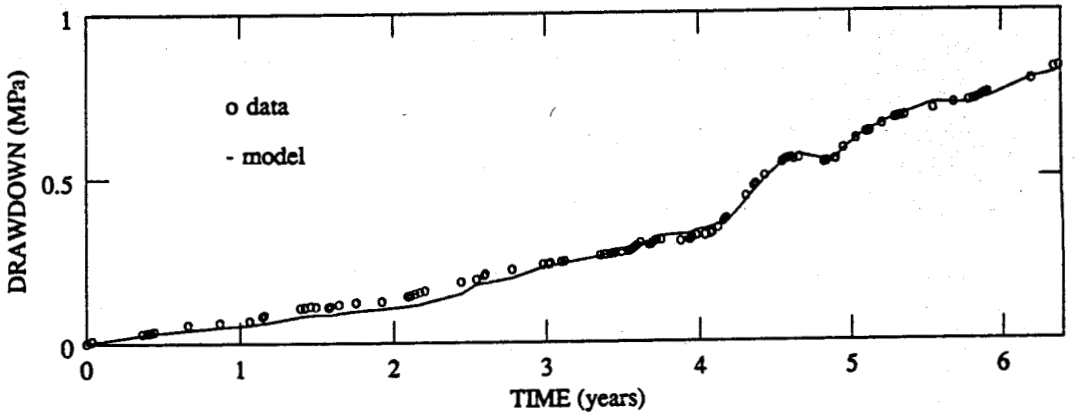

Fig. 4. Drawdown match to the Svartsengi field data.

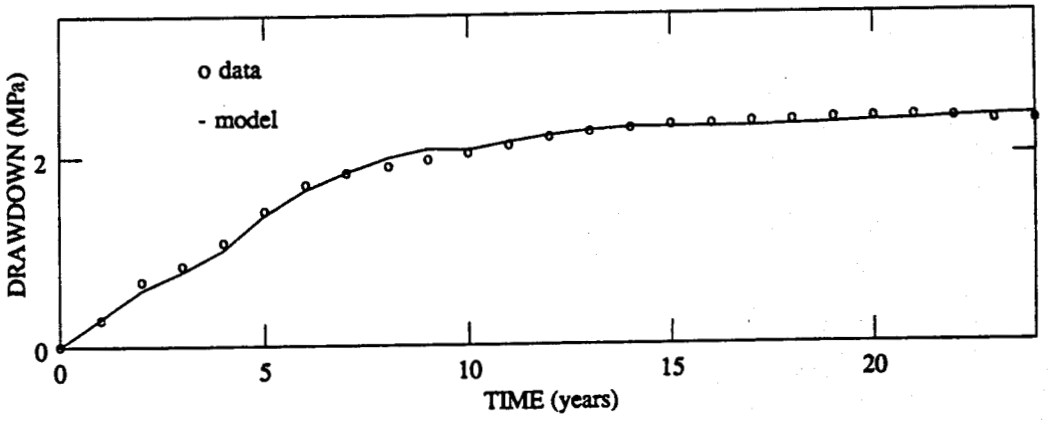

Fig. 5. Drawdown match to the Wairakei field data.

To estimate the reservoir compressibility, c, of the high- temperature fields from their optimum σ value, the aquifer compressibility must first be estimated. However, should the aquifer be assumed confined or unconfined? The density of the reservoir and aquifer fluids must also be estimated - the aquifer temperature was assumed 100°C in the present work. In Table 3 are shown the calculated compressibility values for the Ahuachapan, Svartsengi and Wairakei high-temperature, liquid-dominated reservoirs, for both confined and unconfined aquifer conditions. Also shown are the aquifer permeability-thickness product, $(kh)_a$, derived from the slope, m, obtained by history matching.

The reservoir compressibility values in Table 3 are rather high, particularly when unconfined aquifer conditions are assumed. The storage coefficients for each of the three reservoirs are given in Table 4 and plotted in Fig. 6. They were calculated using the porosity values in Table 1, the compressibility values in Table 3, and for an assumed reservoir thickness of 1000 m. Two values are shown for each reservoir, confined (lower) and unconfined (higher).

Grant et al. (1982) presented a numerical approximation for the compressibility of two-phase reservoir zones. At 240°C this approximation gives the porosity-compressibility product, ϕc, a value of 1400 (1/GPa). For a reservoir thickness of 1000 m, therefore, it corresponds to a storage coefficient of 1.4 (m/kPa). This value exceeds that of an unconfined reservoir by two to three orders of magnitude when the aquifer is confined, and by one to two orders when the aquifer is unconfined.

The results show that the Svartsengi reservoir is more compressible, by one order of magnitude, than both Ahuachapan and Wairakei. The compressibility of the

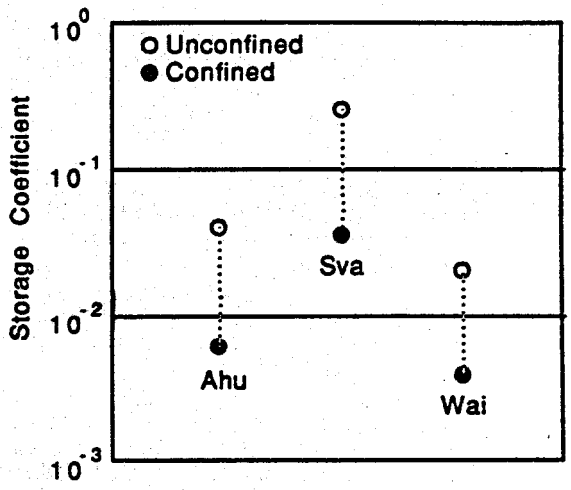

Fig. 6. Storage coefficients for the three fields.

Table 3. Reservoir compressibility and aquifer permeability-thickness product calculated from history matching.

Field Name	Confined Compressibility $(GPa)^{-1}$	Unconfined Compressibility $(GPa)^{-1}$	Permeability-Thickness $(kh)_a$ (Dm)
Ahuachapan	32	206	44
Svartsengi	736	4740	68
Wairakei	17	110	85

Table 4. Reservoir storage coefficients.

Field Name	Confined Aquifer (m/kPa)	Unconfined Aquifer (m/kPa)
Ahuchapan	6.4×10^{-3}	4.1×10^{-2}
Svartsengi	36.8×10^{-3}	23.7×10^{-2}
Wairakei	3.4×10^{-3}	2.2×10^{-2}

Svartsengi reservoir is well above that of an idealized, unconfined system (free liquid surface), no matter what the confinement of the aquifer. This suggests that the two-phase zone, known to exist near the top of the Svartsengi reservoir (Gudmundsson and Thorhallsson, 1986), may to some extent affect the overall pressure response of the system.

CONCLUSIONS

(1) For idealized conditions, an unconfined reservoir is 200 times more compressible at 100°C than a confined reservoir and 40 times more compressible at 300°C.

(2) The Hurst (1958) simplified water influx method gave a satisfactory match to production data from the high-temperature Ahuachapan, Svartsengi and Wairakei fields.

(3) Compressibility is a highly variable parameter in liquid-dominated reservoirs, much more so than porosity and permeability. In water influx and other lumped-parameter modeling, therefore, compressibility should be an output rather than an input parameter.

(4) The effective compressibility of high-temperature liquid-dominated reservoirs is similar to that shown by unconfined (free liquid surface) systems.

REFERENCES

Bodvarsson, G.S., Pruess, K. and Lippmann, M.J. (1986) "Modeling of Geothermal Systems," J. Pet. Tech., Vol. 38, No. 10, (Sept.), 1007-1021.

Brock, D.C. (1986): Compressibility Effects in Modeling Two-Phase Liquid-Dominated Geothermal Reservoirs," M.S. Report, Petroleum Engineering Department, Stanford University, Stanford, California.

Grant, M.A. (1983): "Geothermal Reservoir Modeling," Geothermics, Vol. 12, 251-263.

Grant, M.A., Donaldson, I.G. and Bixley, P.F. (1982): Geothermal Reservoir Engineering, Academic Press, New York.

Gudmundsson, J.S. and Olsen, G., (1987) "Water Influx Modeling of Svartsengi Geothermal Field, Iceland," SPE Reservoir Engineering, Vol. 2, No. 1, (Feb. 1987), 77-84.

Gudmundsson, J.S. and Thorhallsson, S. (1986). "The Svartsengi Reservoir in Iceland," Geothermics, Vol. 15, No. 1, 3-15.

Gudmundsson, J.S., Olsen, G. and Thorhallsson, S. (1985): "Svartsengi Field Production Data and Depletion Analysis," Proc., 10th Workshop Geothermal Reservoir Engineering, Report SGP-TR-84, Stanford University, Stanford, California, 45-51.

Hurst, W. (1958): "The Simplification of the Material Balance Formulas by the Laplace Transformation," Trans. AIME, 213, 292-303.

Marcou, J.A. (1985). Optimizing Development Strategy for Liquid Dominated Geothermal Reservoirs, Stanford Geothermal Program, Report SGP-TR-90, Stanford University, Stanford, CA.

Marcou, J.A. and Gudmundsson, J.S. (1986): "Development Model for Geothermal Resources," Paper SPE 15119, Society of Petroleum Engineers, 56th California Regional Meeting, Oakland, California.

Olsen, G. (1984): Depletion Modeling of Liquid-Dominated Geothermal Reservoirs, MS Report, Pet. Eng. Dept., Stanford U., Stanford, California.

Stehfest, H. (1970): "Algorithm 368, Numerical Inversion of Laplace Transforms," D-5 Communications ACM, Vol. 13, No. 1, 47-49.

Sveinsson, S. (1987): Compressibility and Pressure Drop in Steam Wells, BS Project Report, Mech. Eng. Dept., University of Iceland, 138 pp., (in Icelandic).

Whiting, R.L. and Ramey, H.J. Jr. (1969): "Application of Material and Energy Balances to Geothermal Steam Production," J. Pet. Tech., (July), 893-900.

Zais, E.J. and Bodvarsson, G. (1980): Analysis of Production Decline in Geothermal Reservoirs, Report LBL-11215, Lawrence Berkeley Laboratory, Berkeley, California.

PROCEEDINGS, Fourteenth Workshop on Geothermal Reservoir Engineering
Stanford University, Stanford, California, January 24-26, 1989
SGP-TR-122

CURRENT STATUS AND FUTURE RESEARCH OBJECTIVES FOR THE HGP-A GENERATOR FACILITY

Donald M. Thomas and Harry J. Olson

Hawaii Institute of Geophysics
2525 Correa Road
Honolulu, Hawaii 96822

INTRODUCTION

The HGP-A Geothermal Generator Facility began operation in June 1981 and has been continuously producing electrical power since March 1982. Changes in the chemical composition of the fluids during the operational life of the well have not only presented a number of engineering challenges to the continued production of power but have also provided a number of very valuable insights into the dynamics of the geothermal reservoir associated with the Kilauea East Rift Zone. This paper will review the evolution of the reservoir characteristics and summarize the engineering developments that have made at the HGP-A facility during the last seven years of operation.

BACKGROUND

In 1976 the HGP-A well was drilled into the Lower East Rift Zone of Kilauea volcano to a depth of 1966 meters. Testing showed that the well had a bottom hole temperature of approximately 358°C and was capable of producing approximately 50 metric tonnes of fluid per hour with a steam quality of approximately 44%. In 1981 a 3MWe wellhead generator facility was installed at HGP-A to demonstrate the feasibility of electrical power generation from this geothermal resource. After an extended start-up and shake-down period the generator facility began continuous operation in December, 1981 and has been producing electrical power on a commercial basis since March 1982. The availability factor for the facility has been approximately 95% since the beginning of commercial operation.

RESERVOIR CHARACTERISTICS

During the initial testing of the HGP-A well, the fluids were found to have a total dissolved solids content of approximately 4000 mg/kg in the brine phase. Major dissolved constituents consisted of sodium chloride (~2200 mg/kg) and silica (~850 mg/kg) with lesser amounts of lithium, potassium, magnesium, and calcium. Non-condensable gases in the steam phase had a total concentration of less than 0.25% but had a higher hydrogen sulfide content (~900 mg/kg), relative to carbon dioxide (~1100 mg/kg), than is typically found in geothermal fluids. The balance of the NC gases consisted of nitrogen (~125 mg/kg) and hydrogen (~11 mg/kg) with traces of methane (~1 mg/kg) and inert gases.

During the seven years of operation of the well the most important chemical change observed in the production fluids has been a progressive increase in the total dissolved solids concentrations: sodium chloride concentrations are now about 15,000 mg/kg in the brine phase. This represents a seven-fold increase since the start-up of the well (Figure 1). Both the chloride and the dissolved cation concentrations (Figure 2) showed a rapid initial increase but, after approximately four years of production, they peaked and then began a slow decline. The sodium to chloride ratio of the fluids indicates that the source of the intruding fluids is seawater (Thomas, 1987) but, comparison of the other ion concentrations with seawater of equal chlorinity (Figure 3), shows that lithium and potassium have been highly enriched in the thermal fluids whereas magnesium has been nearly quantitatively removed and calcium has moved from depletion to enrichment during the production period.

The changing fluid chemistry suggests that seawater has infiltrated across the southern boundary of the Kilauea East Rift Zone and into the high-temperature reservoir (Thomas, 1987). As seawater continues to enter the geothermal system, reactions with reservoir basalts can modify the fluid compositions substantially. Other possible consequences of continued seawater intrusion into the reservoir include both a gradually falling fluid temperature and, as indicated by laboratory studies of SW/basalt reactions (Mottl and Holland, 1978), a substantial decline in fluid pH. The former result is supported by Na-K-Ca geothermometer calculated temperatures (Figure 4) that indicate an apparent decline in the source fluid temperatures. Silica concentrations have, however, remained nearly constant suggesting that reservoir temperatures within the silica equilibration path-length have declined only slightly, if at all. The

FIGURE 1

Chloride Ion Concentration versus Time

In HGP–A Geothermal Brine

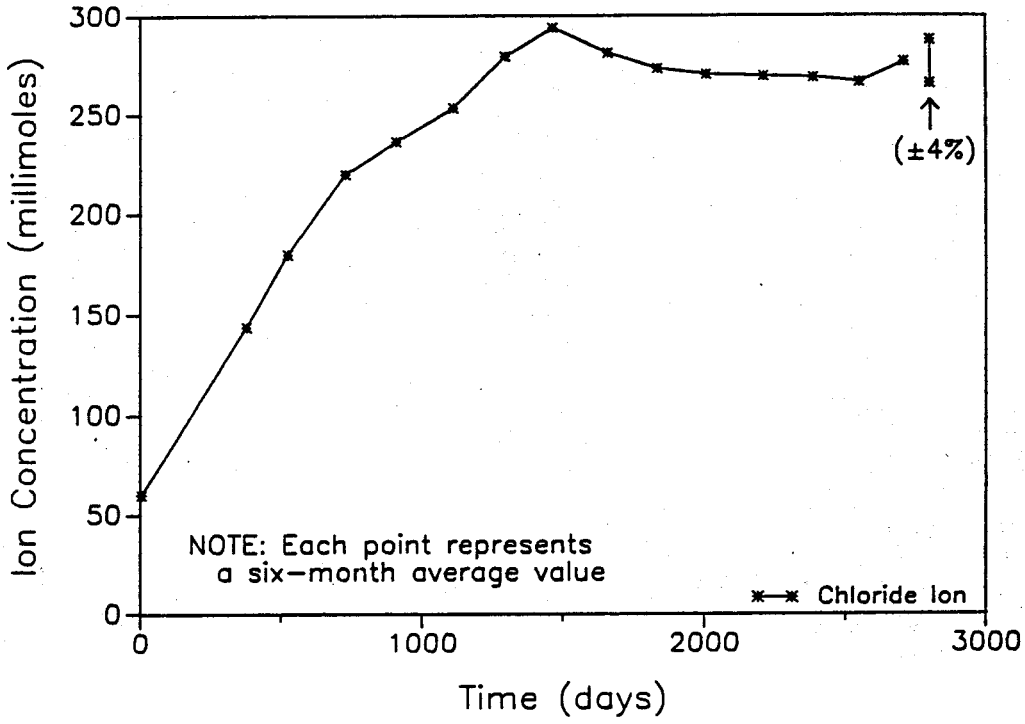

FIGURE 2

Major Cation Concentrations versus Time

In HGP–A Geothermal Brine

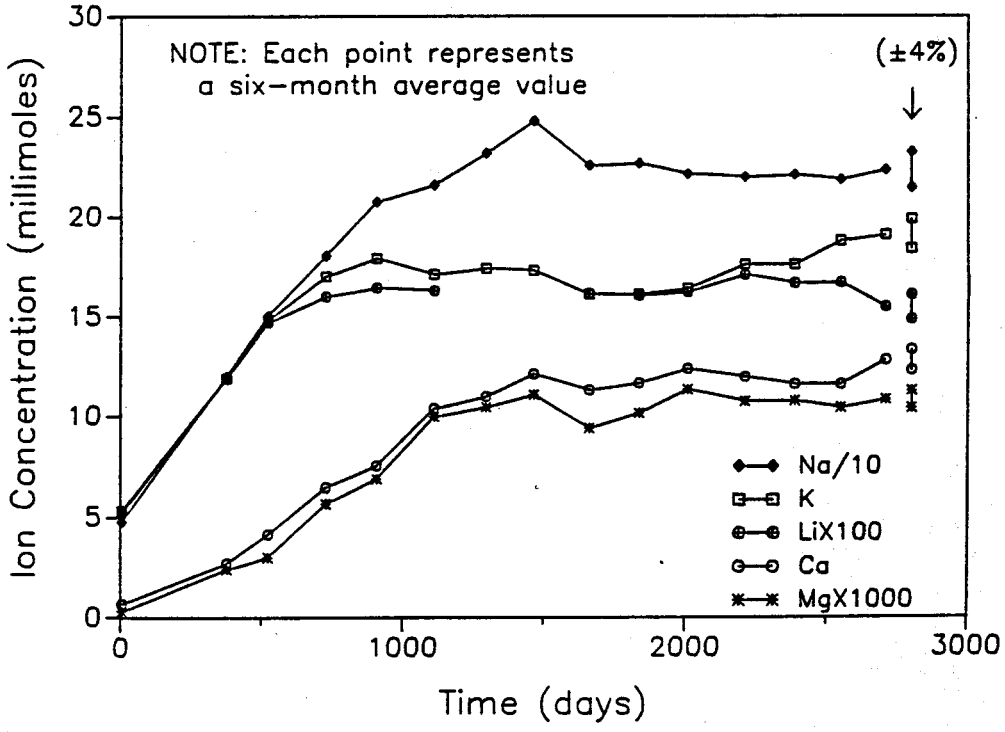

FIGURE 3

Enrichment/Depletion of Cation Concentrations

Relative to Seawater of Equal Chlorinity

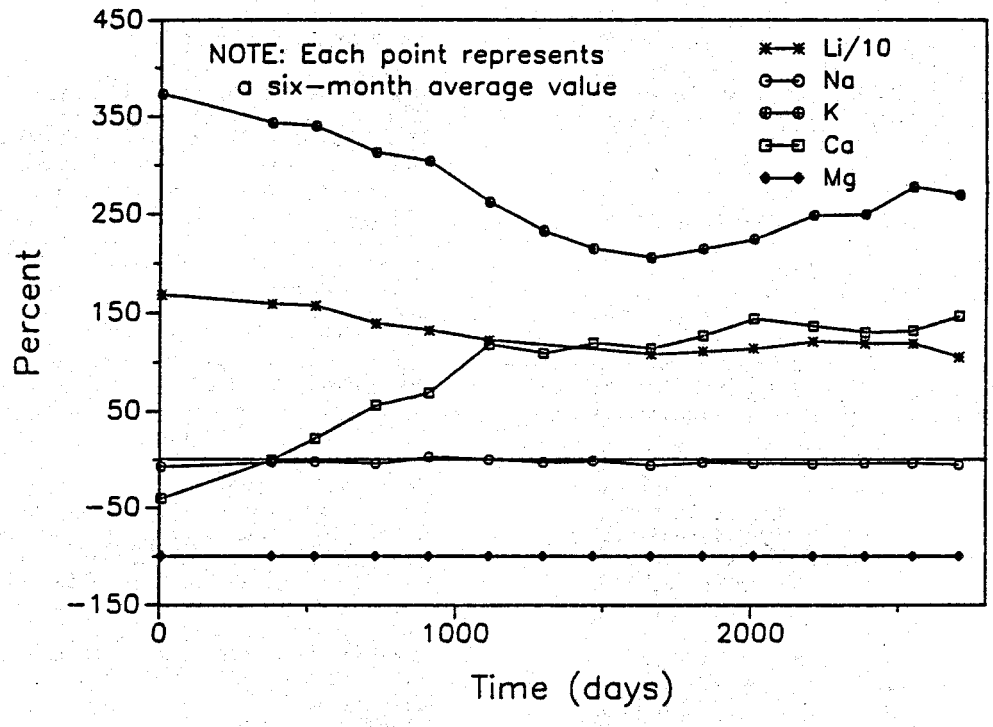

FIGURE 4

Calculated Na-K-Ca Geothermometer Temperature

For HGP-A Brine Composition

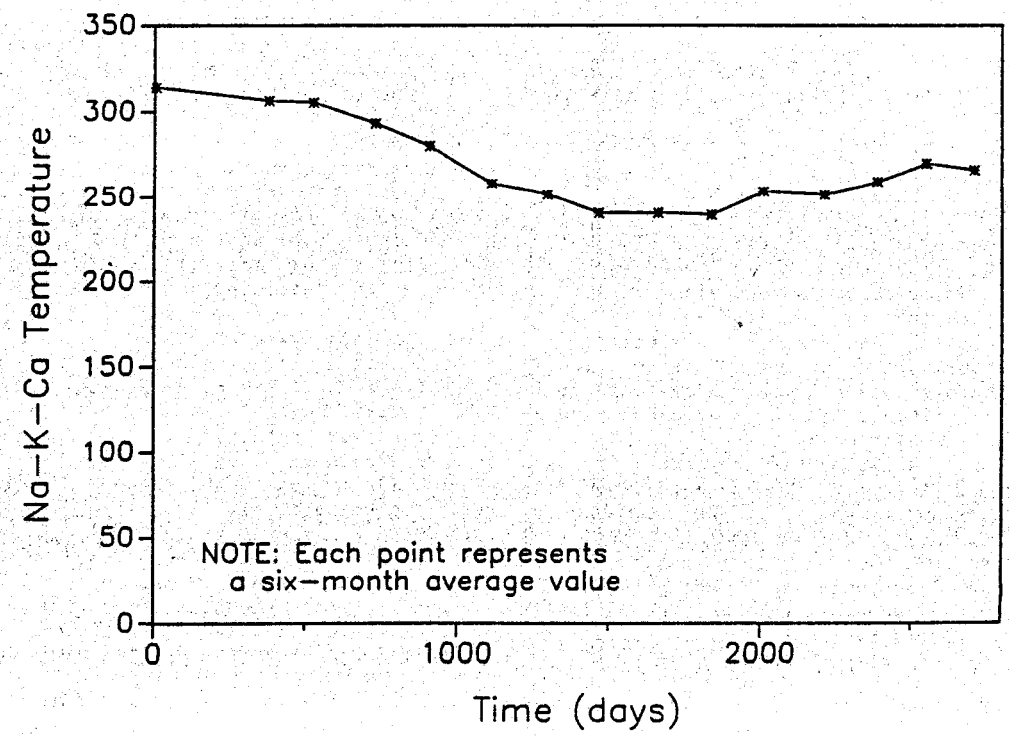

second projected outcome, a decline in fluid pH is also substantiated by measured brine pH values which have declined from a value of approximately 7.6 to about 6.5 during the operational life of the well. This change represents an increase in hydrogen ion concentration in the fluid of more than a factor of ten. Further declines in fluid pH, if continued for an extended duration, could pose corrosion problems for surface equipment as well as downhole casings.

A third possible outcome of seawater infiltration into the reservoir is a direct result of the SW/basalt reactions that modify the fluid chemistry. These reactions also modify the reservoir basalt composition by depositing secondary mineral assemblages that includes anhydrite, calcite, chlorite, and mixed-layer smectite clays. Deposition of these secondary minerals, which have been found in Kilauea East Rift drill cores, can hinder seawater infiltration and may be able to entirely seal off the intrusion zones. This process may may account for the decline in the dissolved solids concentrations that have been observed during the last three years of well production. If deposition of secondary minerals continues, further restriction of fluid intrusion may slow the rate of decline of fluid temperature and pH.

The loss of fluid entry into the reservoir is, however, cause for concern with regard to the future productivity of the well. Steam flow rates measured during the first few months of operation of the well are estimated to have been approximately 20 to 22 metric tonnes per hour (mtph), whereas those measured more recently have shown steam production rates of about 18 mtph reflecting a decline of 10% to 20% over seven years of operation. Although this decline is only an approximation because of uncertainties in the original measurements, it is consistent with changes in gross electrical output of the generator, which has fallen from about 2.9 MWe to its current value of 2.4 MWe.

It should be noted, however, that the decline in production has not been monotonic: on at least two occasions steam production from the well increased by about 10% to 15% and remained at these higher levels for periods of a few days to a few weeks before gradually returning to their original values. Although we do not have a well-substantiated explanation for this behavior, the absence of any corresponding seismic activity or any change in fluid chemistry during these episodes suggests that the increased flow rates may have resulted from the removal of an obstruction in the wellbore that was impeding flow. This in turn suggests that well productivity may be limited by the deposition of silica scale in the wellbore rather than by the productivity of the reservoir itself. (Because the well has been in continuous operation since 1981, we have been unable to test this hypothesis by inspection of the well casing or by conducting caliper logs of the well.)

POWER PLANT ENGINEERING

The wellhead generator steam system consists of a single-stage flash separator, operating at a pressure of 175 psia, followed by a moisture separator, turbine inlet manifold, a six-stage condensing turbine, and a shell and tube condenser. Steam condensate is cycled to the cooling tower as make-up water, and non-condensable gases are removed using steam ejectors and treated with an incinerator scrubber system to remove hydrogen sulfide. The brine system, downstream of the separator, consists of redundant pressurized piping and level control valves that dump the brine to an atmospheric flash system and percolation ponds.

Maintenance problems that have been encountered during the operational life of the facility can be categorized as follows: general maintenance, hydrogen sulfide abatement, surface and internal corrosion, and solids deposition. The general maintenance requirements of the facility have been much greater than might otherwise have been expected because the original design-life stipulated for the facility by the funding agency, was only two years. As a result, chemical pumps, compressors, air blowers, and control systems have required more frequent maintenance, and in some cases eventual replacement, than might have been required if the plant had been designed for a 20- to 30-year life. In most cases, the cost of manpower and lost generation time incurred during the life of the plant have substantially exceeded the cost of equipment appropriate for the conditions present.

The design of the primary hydrogen sulfide abatement system has generated similar problems as well. The short design-life dictated the choice of an incinerator and single-stage scrubber system for hydrogen sulfide abatement which had a lower capital cost. The hydrogen sulfide load (0.5 t/d) for this system resulted in operating costs for chemicals of approximately $1000/day to treat the incinerated gases. In order to reduce chemical costs, a two-stage scrubber unit was installed that reduced the caustic use rate by about 40%. Although the primary abatement system has been highly reliable, the toxicity of the raw condenser gas has required the installation of an emergency back-up column to scrub hydrogen sulfide from the condenser gases when the primary unit fails. Consisting of a packed column with a caustic feed, this system is able to alleviate both personnel hazards associated

with condenser gas discharge as well as nuisance odors in the adjacent community during periods of incinerator upset.

Hydrogen sulfide abatement during periods of turbine standby (atmospheric steam release) is accomplished by injection of sodium hydroxide into the steam phase up-stream of a rock muffler. Although a number of abatement problems were encountered during the initial start-up phase of generator operation, abatement efficiencies of about 95% were found using a caustic to sulfide mole ratio of approximately three to one. Earlier tests of this system using both caustic and peroxide injection showed that the addition of the latter reagent gave only minimal improvement in abatement efficiency; in light of this fact and the increased personnel hazards associated with peroxide transport and on-site storage, the plant design did not use peroxide injection.

Corrosion in the steam and brine systems has not been a major problem at the power plant. Substantial rates of surface corrosion have, however, been observed on mild steel as well as in the interior of the cooling water system. Several factors that are somewhat unique to the HGP-A power plant and to the local environment are responsible for this corrosion: high rainfall rates (>100 in/yr), high ambient levels of sulfur dioxide (produced by an active volcanic vent uprift of HGP-A and by leakage of gases from the hydrogen sulfide abatement system), and high ambient concentrations of saline aerosols from atmospheric discharge of the separated brine phase. All of these factors contribute to the corrosion at the site that has been controlled to only a modest degree by normal maintenance procedures.

The ambient levels of sulfur dioxide and salt aerosols may also contribute to the extreme corrosion observed in the mild steel cooling water piping system. Degradation of the circulation lines is, however, believed to have been caused by the loss of automated pH control of the cooling water system. Even though an effort was made to control fluid pH manually after the original control system failed, periodic treatments of the cooling water with caustic resulted in wide pH swings that produced both acid corrosion of the mild steel and caustic attack of the interior wood framing of the cooling tower. Restoration of automatic control during the last several months has largely alleviated these problems.

Deposition of silica from the flashed geothermal fluids has been one of the most difficult engineering problems encountered during operation of the generator facility. The brine handling system has required frequent maintenance to remove accumulations of amorphous-silica scale deposits from the interior of the flash vessel, the pipelines, and the brine level control valves. Silica deposition in the latter equipment has been especially troublesome because changes in the temperature and pH associated with boiling substantially accelerate silica deposition rates. Even greater problems have been encountered downstream of the brine release system: after the brine flashes to atmospheric pressure the temperature and fluid volume losses increase the concentration of silica in the brine to a factor of about five times its equilibrium solubility. Although silica polymerization and deposition is an inevitable result of this supersaturation, the chemistry and kinetics of these processes result in the formation, over a period of several hours, of a gelatinous precipitate composed of about 5% silica and 95% water. As a result, disposal of the geothermal brines by percolation has required frequent cleaning of the disposal ponds as well as their progressive expansion during the life of the plant.

We do not currently have a satisfactory solution to the scale deposition problems at the HGP-A facility. In order to maintain system reliability, a redundant brine handling systems has been installed that allows continuous operation during system maintenance. In order to minimize the formation of scale on valve seats and stems, the plant operator is required to exercise the level control valves on a frequent basis. The fluid disposal ponds, as noted above, have been expanded from approximately 75 m^2 as originally constructed (and which functioned adequately for the first several months of operation) to 8500 m^2 currently in use for approximately the same volume of brine discharge. Removal of silica has not only become very time consuming and expensive, the material generated has become a solid waste disposal problem. Although this system has allowed us to continue operating the HGP-A facility, improvements in the brine handling system are required for any future commercial-scale geothermal generation stations. The land use and solid waste problems associated with brine disposal on a commercial scale suggest that future generation facilities will have to institute a brine reinjection process which may also require brine pretreatment to reduce silica supersaturation prior to reinjection.

FUTURE RESEARCH OBJECTIVES

During the coming year of operation our research efforts will be focussed on developing solutions for the current operational problems faced by the HGP-A facility. The two most significant issues will be improvements in the hydrogen sulfide abatement technology and development of a process for brine disposal. Although two

separate projects are currently underway to improve these processes, it is hoped that the ultimate solution will be able to combine the disposal of the non-condensable gases and the brine phase. The first set of investigations, conducted by Ormat Energy Systems, is evaluating the engineering conditions under which non-condensable gases from the condenser system can be combined with either the excess cooling water/ condensate or with the waste brine stream and reinjected into a disposal well. The objectives of this study are to determine the optimal conditions for recombining the waste streams while still minimizing corrosion and scaling in the disposal system.

A separate study is also underway on the chemistry of silica polymerization and precipitation in the geothermal fluids produced by the HGP-A. This investigation will determine the polymerization rate of silica in the geothermal fluids under natural conditions and as well as the effects of varying solution pH and dissolved ion concentrations on the rate of polymerization and precipitation. As data becomes available on different types of reagents that might accelerate the precipitation rate of silica, a pilot system for continuously treating a side-stream of brine will be designed. The results of the latter study will be applied to the preparation of a preliminary design of a full-scale brine treatment system capable of reducing silica supersaturation in the geothermal waste fluids. If reagents are identified that retard silica precipitation, then the pilot system will be used to determine whether the retardation times are sufficient to allow commercial volumes of brine to be reinjected on a long-term basis.

The pilot system will also be used to determine whether recombination of the non-condensable gases with the brine phase will affect the polymerization rate of dissolved silica in the brine or whether the gases have a significant effect on the action of other reagents used in the silica removal process.

SUMMARY AND CONCLUSIONS

The seven years of operation of the HGP-A geothermal generator has successfully demonstrated that production of electrical power from Hawaii's geothermal resources is technically feasible. This period of study has also enabled us to characterize the chemistry and reservoir dynamics of a high-temperature hydrothermal system on the Kilauea East Rift Zone and its response to exploitation for power generation.

Operation of this facility has enabled us to test and refine engineering designs appropriate to the reservoir conditions found in Hawaii and to identify economically viable and environmentally acceptable means of producing geothermal power on the island of Hawaii. If the currently planned studies of hydrogen sulfide and silica control are successful, then two of the most important environmental and economic impediments to the development of Hawaii's geothermal resources will have been resolved.

ACKNOWLEDGEMENTS

The authors gratefully acknowledge funding support for the above research from Hawaii Electric Light Company and the State of Hawaii, Department of Business and Economic Development. We also thank R. Schneider for assistance in preparation of the figures and C. Koyanagi for typing the manuscript. This is HIG Contribution No. 2152.

REFERENCES

Mottl, M.J. and Holland, H.D. (1978), "Chemical exchange during hydrothermal alteration of basalt by seawater - I: Experimental results for major and minor components of seawater," Geochimica et Cosmochimica Acta, v. 42, pp. 1103-1115.

Thomas, D.M. (1987), "A geochemical model of the Kilauea East Rift Zone," in Decker, R.W., Wright, T.L., and Stauffer, P.H., eds., U.S. Geological Survey Paper No. 1350: Volcanism in Hawaii, Chapter 56, pp. 1507-1525.

PROCEEDINGS, Fourteenth Workshop on Geothermal Reservoir Engineering
Stanford University, Stanford, California, January 24-26, 1989
SGP-TR-122

A CONCEPTUAL AND MATHEMATICAL MODEL OF THE LARDERELLO PRODUCTION HISTORY

GIUSEPPE NERI

ENEL U.N.G. PISA ITALY

ABSTRACT
The Larderello production history has been interpreted by the author(1987) as the consequence of an initial depletion-type production regime followed by a diffusive type one. At the moment a diffusive flow is developing vertically all over the northern part of the field. This paper presents a mathematical model of the Larderello production history which incorporates the above mentioned concepts. Such a model has been validated calculating the measured reservoir pressure drop caused by the actual production history.

1. INTRODUCTION

In a previous paper (Neri, 1987), the Larderello production history has been interpreted by the author as the consequence of an initial depletion-type production regime followed by a diffusive-type one. At the moment a diffusive flow is developing vertically all over the northern part of the field, as is shown by the wells shut-in tests described in Ref. 1. The depletion regime could have been caused by the uniform boiling of liquid water (White et al.,1971) stored in the uppermost part of the reservoir where a carbonatic formation is present. The diffusion regime starts when the boiling process becomes dominated by a boiling front which propagates down the reservoir giving origin to a process of pressure diffusion. With such a concept in mind,the reservoir can be therefore conceived as made by two different regions as illustrated in Fig.1. Region 1 represents the volume corresponding to the top of the reservoir where evaporation develops uniformly before spreading to the underlying Region 2.

2. THE MATHEMATICAL MODEL

In order to treat in mathematical terms the conceptual reservoir model, it has seemed useful to start out with a few simplifying hypotheses, to make easier the mathematical treatment of the problem.

Hypotheses:

a) All processes occurring within the reservoir are more or less isothermal.
b) The pressure gradient is negligible in Region 1 of Fig. 1, whereas in Region 2 it is small enough to allow the use of the diffusion equation to describe the pressure field.
c) Rock porosity and volumetric saturation of liquid water are homogeneous,rock permeability is homogeneous and isotropic throughout the reservoir.

With these hypotheses,and in reference to the scheme of Fig. 1,the pressure field within the reservoir can be described by the following equations:

$$(1)\quad C^* \frac{dP_1(t)}{dt} = Q_{z1} - Q \qquad \text{Region 1}$$

$$(2)\quad (\text{Grad}^* \text{Grad})P_2(x,t) = (1/n)\,\delta P_2(x,t)/\delta t \qquad \text{Region 2}$$

where $C = c * V * \Phi$

$$Q_{z1} = (K/\mu) * A^* (\delta P_2/\delta x)_{x=o}$$

The initial and the boundary conditions under which equations 1 and 2 must be resolved are:

$$P_1\ (t>o) = P_2\ (x = o, t>o)$$
$$Q\ (t \geq o) \quad \text{Constant}$$

It is convenient to introduce the following dimensionless variables into equations 1 and 2;

$$C_D = \frac{C}{\phi c A \sqrt{A}}$$

$$t_D = \frac{n}{A} t$$

$$P_{1,2,D} = \frac{K\sqrt{A}}{Q\mu} (P_{1,1,2} - P_{1,2})$$

$$x_D = \frac{x}{\sqrt{A}}$$

$P_{1,\ 1,2}$ = Initial pressure in regions 1 or 2.

P_1 depends on time only, whilst P_2 depends on depth too.

Equations 1 and 2 therefore assume the following form:

$$(1)' \quad C_D \frac{dP_{1D}}{dt_D} - \left.\frac{dP_{2D}}{d x_d}\right|_{x_d=0} = 1$$

$$(2)' \quad (\text{Grad} * \text{Grad}) P_{2D} = \frac{dP_{2D}}{dt_D}$$

The resolution of equations (1)' and (2)' in consequence of hypothesis b), which gives us

$$P_{1D} = P_{2D} \ (x_D = o), \ t \geq o$$

is analogous to that of a problem of heat conduction in a semiinfinite medium whose surface is in contact with a well stirred fluid supplied with a constant amount of heat per unit of time .

H. S. Carslaw and J. C. Jaeger report (Ref. 2) a solution to this problem which, adapted to our case, acquires the form:

(3)

$$P_D (t_D, C_D, x_D = o) = 2\sqrt{(t_D/\pi)} + C_D [e^{t_D/C_D^2} * \text{erfc}(\sqrt{t_D/C_D}) - 1]$$

Such a solution is valid for a constant Q and hypothesizing that for

$X_D = 0$, then $P_{1D} = P_{2D} = P_D$ for $t_D > 0$

In eq. (3) appears the parameter C_D, which is an index of the storage capacity of region 1 of the reservoir.

The greater C_D is, longer the depletion production regime will last.

The parameter C_D, may not appear explicitly in the solution of P_D if we define an dimensionless time $t_D"$ given by

$$t_D" = t_D/C_D^2$$

and at the same time define a dimensionless pressure $P_D"$ as

$$P_D" = \frac{P_D}{C_D} = \frac{KA^2}{V} * \frac{(P_i^2 - P^2)}{Q\mu}$$

With these new definitions, solution (3) can be written as

$$(4) \quad P_D" (t_D", x_D = 0) = 2\sqrt{(t_D"/\pi)} + e^{t_D"} * \text{erfc}(\sqrt{t_D"}) - 1$$

Solution (4) is represented in Fig. 2 in the form of a bilogarithmic graph of $P_D"$ as a function of $t_D"$.

From Fig. 4 it can be noted that for "small" $t_D"$ values, $P_D"$ is proportional to $t_D"$, whereas for "large" $t_D"$, $P_D"$ is proportional to $\sqrt{t_D"}$. This is indicating that the pressure is initially controlled by the reservoir storage, then by a diffusion equation for linear flow.

3. THE RESERVOIR PRESSURE DROP AS CALCULATED WITH THE MATHEMATICAL MODEL

The solution $P_D"$ given by (4) constitutes an dimensionless influence function for $X_D = 0$, that is at the top of the reservoir.

If we wish to calculate the pressure drop at the top of the Larderello reservoir, we must solve the system of equations 1 and 2 in the case of variable flow Q, as the flow produced by the field has been variable over time.

Using $\pi_D (t_D", X_D=0)$ to indicate the solution of equations 1 and 2 in the case of variable Q over time, we will get

$$(5) \quad \pi_D(t_D", X_D = 0) = \int_o^{t_D} Q(\tau_D) (dP_D"(t-\tau)_D/dt_D) d\tau_D$$

The integral (5) can be approximated as a finite sum of terms subdividing the time-span t_D into n intervals within each of which flow Q can be assumed to be constant.

With this approximation, (5) becomes

$$(6) \quad \pi_D(t_{Dn}*, X_D=0) = \sum_{j=1}^{n} P_D* (t_n - t_{j-1})_D (Q_j - Q_{j-1}) / Q_1$$

with $Q_o = 0$ for $t_o = 0$

In the place of the volumetric flow Q, the mass flow G can be introduced into (6), and at the same time we can define the dimensionless pressure π_D as:

$$\pi_D = \frac{K[P_i^2 - P^2]A^2}{2G_i \bar{R} Tz\mu V}$$

In the calculation of π_D using (6), flow G actually produced in Larderello north area (Valle Secolo) was approximated with the formula

(7) $G = G_\infty + (G_o - G_\infty) \exp(-t/\tau)$
$G_o = 1981$ t/h
$G_\infty = 625$ t/h
$\tau = 97$ months

which interpolates the measurements taken since August 1956 . The flow G, in the j-th time-period, was calculated as an arithmetical average of the G readings given by (7) at the extreme ends of the period.

In order to use eq. (7) for calculating π_D given by (6),it was necessary to match the physical time t with the dimensionless time t_D. To this purpose various values of the parameter $\tilde{N} = \eta A^2/V^2$,which relates t_D to t by the relation $t_D = \tilde{N}t$,have been used and a family of curves of π_D as a function of time t has been generated.These curves are represented in Fig.3

Using the pressure readings of the shut-in well No. 111, which is peripheral to the group of wells drilled in the Valle Secolo area and can be considered a monitoring well of the reservoir-top pressure, we find that the theoretical curve with $\tilde{N} = 10^{-9}$ s^{-1} interpolates the experimental data of the first 200 months of production, (cf Fig. 4 where the time-scale starts in August 1956), whereas the curve with $\tilde{N} = 10^{-8}$ s^{-1} interpolates better the experimental data after the 50th month from start-up of production (Fig. 5).

The interpolation is acceptable with both values of the parameter $\tilde{N}$, but not outside this range.

Unfortunately well No. 111 is the only well which has been closed for some thirty years and which has shown interference with the producing wells during the field production period.

For shorter time-periods other records exist for shut-in wells which may be indicative of the reservoir's pressure.

These are the pressure-readings for wells 159, Gabbro 4, Gabbro 8, S. Dalmazio 2 and S. Dalmazio 4.

The readings for well 159, which is also located in the Valle Secolo area, follow the trend of the well 111 readings, whereas those of the wells in the Gabbro area (Gabbro 4 and Gabbro 8, S. Dalmazio 2 and 4) have a trend which seems to be that of well No.111 but delayed by some ten years, i. e.the time-lapse which separated the exploiting of the two areas. (Fig. 6)

Graphing the pressure drop of the wells belonging to the Gabbro area in bilogarithmic paper as in the Fig. 7 and 8,it may be observed that the graphs show a trend qualitatively similar to the one calculated with the mathematical model in the case of production at constant flow.Thus the physical assumptions of the mathematical model seem to hold for the various producing area of the Larderello reservoir.

4. ESTIMATES OF DIFFUSIVITY, COMPRESSIBILITY AND PERMEABILITY

By interpolating the pressure reading from well No.111 with the set of theoretical curves, we get two possible values for the following groups of parameters:

i $P_D/C_D = 0.4$; $\delta(P^2) = 100$ (bar^2); $\tilde{N} = 10^{-8}$ s^{-1}

ii $P_D/C_D = 0.07$; $\delta(P^2) = 100$ (bar^2); $\tilde{N} = 10^{-9}$ s^{-1}

depending on whether the interpolation is done with one or the other value for $\tilde{N}$.
From the definition of P_D/C_D and putting:

$G_i = 2000$ t/h $\approx$ 550 Kg/s
$\bar{R} = 460$ J/ (Kg * °K)
$T = 500$°K
$z = 1$
$\mu = 2*10^{-5}$ P_a * s

we get $K (A^2/V) = (200 - 1000) * 10^{-12}$ m^3

Writing $V = A*h$ and assuming :
$A = 5$ Km^2 , the surface area occupied by wells
$h = 500$ m , the thickness of region 1 of the reservoir

It follows $(20 \leq K \leq 100)*10^{-3}$ Darcy

From the definitions of $\tilde{N}$ we get

$$.25*10^{-3} \leq \eta \leq 2.5 * 10^{-3} \text{ m}^2/\text{s}$$

Finally, dividing P_D/C_D by $\tilde{N}$ we can get the total compressibility ΦcV which depends weakly on the parameters of the fit, because, being $\delta(P^2)$ the same for both the groups of parameters, the value of ΦVc depends only on the ratio between P_D/C_D and $\tilde{N}$ which is $0.4*10^6$ s or $0.7*10^6$ s. Adopting the previous assumed values for A and h, we can get Φc from ΦcV. It results:

$$2 *10^{-6} < \Phi c \leq 4 * 10^{-6} \quad P_a^{-1}$$

These values for Φc are strongly affected by the assumed values of A and h. The uncertainty of V is mostly due to the doubts on h, as the surface area of the reservoir, drained by the wells, is known.

The height h should correspond to the thickness of the upper formation of the reservoir, the one known as the anhydritic formation, which does not have a homogeneous thickness, yet is around a few hundred metres. The estimated value for Φc should therefore be in the proper order of magnitude and is, according to Grant et al. (1982), typical of a two phase fluid.

5. PRESSURE DISTRIBUTION ALONG THE RESERVOIR VERTICAL AXIS

The proposed model has been so far used to fit the pressure drop, measured at reservoir top, caused by some 30 years of production. The fit allowed the evaluation of the parameter $\tilde{N}$ which is proportional to the diffusivity η. It now becomes possible to calculate by the model equations the pressure distribution at various reservoir depths caused by the past field exploitation.

The solution of equations 1' and 2' has been still derived by Carslaw and Jaeger. Posing P_D instead of P_D/C_D and introducing the dimensionless depth $X_D^* = X_D/C_D$, the following equation holds:

$$(8)\quad \frac{P_D}{C_D}(t_D^*, X_D^*) = 2\sqrt{\left(\frac{t_D^*}{\pi}\right)} \exp(-X_D^{*2}/4t_D^*) - (1+X_D^*)\,\mathrm{erfc}(X_D^*/2\sqrt{t_D^*}) + \exp(X_D^* + t_D^*) * \mathrm{erfc}[X_D/2\sqrt{t_D^*} + \sqrt{t_D^*}]$$

$$X_D = X/\sqrt{A}$$

$$X_D^* = X_D/C_D = X^* A/V$$

$$t_D^* = t_D/C_D^2 = \eta^*(A^2/V^2)^*t$$

The dimensionless depth X_D^* is the ratio between real depth, measured from the plane separating regions 1 and 2 in the reservoir, and the thickness of region 1.

Having estimated that the parameter $\tilde{N}$ is within the range 10^{-6} and 10^{-8} sec^{-1}, the same method of approach, which adopts the principle of superposition and which was taken to figure out the pressure decline over time at the reservoir top, can be used to calculate the current pressure at various depths of the reservoir.

The results of the calculations, represented in graphic form in Fig. 9, show that the pressure drop is negligible for $X_D^* \approx 2$. This allows us to affirm that the depressurization of the reservoir is limited to a depth of 3h. Being h probably a few hundred meters, it follows that depressurization should not have involved the part of the reservoir at depths over 2000 m.

6. CONCLUSIONS

The model described in this paper has been successfully used to calculate the reservoir pressure drop in the Valle Secolo area of the Larderello field, caused by the field exploitation. The fitting of the field data by the model's results has also allowed us to estimate the hydraulic diffusivity η, the fluid compressibility Φc and the vertical pressure distribution in the reservoir. Such a distribution has been calculated after 30 years of exploitation and therefore is that should exist at present.

It shows that the depressurization of the reservoir turns out to be restricted to a depth of some 2000 m. Recent results obtained by deepening old wells (S. Martino 2, Campo ai Peri, VC8, 156, 119) reveal indeed the existence of a vertical pressure gradient in the reservoir much higher than that due to static steam, consequently reveal a substantial pressure increase with depth in agreement with the model.

The calculations have been restricted to the Valle Secolo area, but it has been verified however that the shut-in wells in the Gabbro area, area exploited some ten years after the Valle Secolo, possess a pressure history qualitatively similar to that foreseen by the model.

This observation shows also that the drainage on the Gabbro area, due to the Valle Secolo wells, is rather weak.

If this low interference (in a horizontal direction) is generalizable for the different producing areas of the whole geothermal field, then we can think that significant reserves of fluid might well still be located at modest depths in the areas where density of production is low.

This consideration seems to be actually confirmed by the drilling of new wells in areas of the Larderello field which are weakly exploited (Val di Cornia, Monteverdi).

ACKNOWLEDGEMENTS

I wish to thank G.Allegrini, who promoted and encouraged this work and A.Barelli for useful suggestions in writing of this paper.

REFERENCES

[1] NERI G. Flow Rate Decline and Pressure Transients in the Larderello Geothermal Field.Proc.13th Workshop on Geothermal Reservoir Engineering.Stanford 1987.

[2] CARSLAW H.S., JAEGER J.C. - Conduction of Heat in Solids - Oxford University Press,2nd Ed.,p.306, London 1959.

[3] WHITE D.E.,MUFFLER L.J.P. and TRUESDELL A.H.-Vapor dominated Hydrotermal Systems Compared with Hot Water Systems.Econ.Geol. 66,1971.

[4] GRANT M.A.,DONALDSON I.A.,BIXLEY P.F. Geothermal Reservoir Engineering.Academic Press 1982.

KEY TO SYMBOLS

P Pressure
G Mass flow-rate
Q Flow-rate in volume
V Volume
A Surface area of flow
$\bar{R}$ = R/Mw where R is the perfect gases constant and Mw is the molecular weight of water
K Permeability
μ Dynamic viscosity
ζ Compressibility factor for steam
η Diffusivity
ϕ Porosity
c Fluid compressibility
r Density
x Position coordinate
t Time

Grad Gradient operator
erf Error function
erfc Complementary error function
e or exp Exponential function

Subscripts

$_{1,2}$ Region indices
$_i$ Time index
$_{21}$ Used in Q_{12} to indicate flow from Region 2 to Region 1
$_D$ Indicates a dimensionless entity

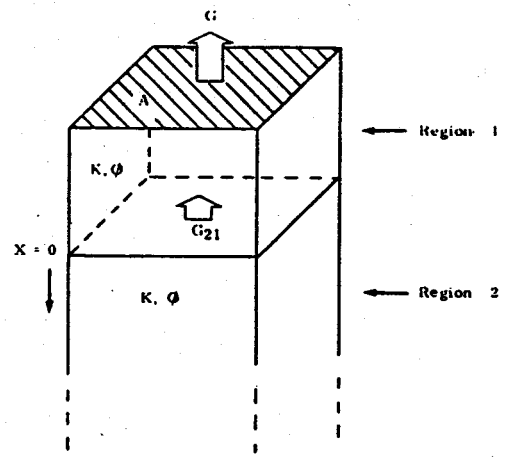

FIG. 1
- Scheme of the reservoir as used for the formulation of the mathematical model.

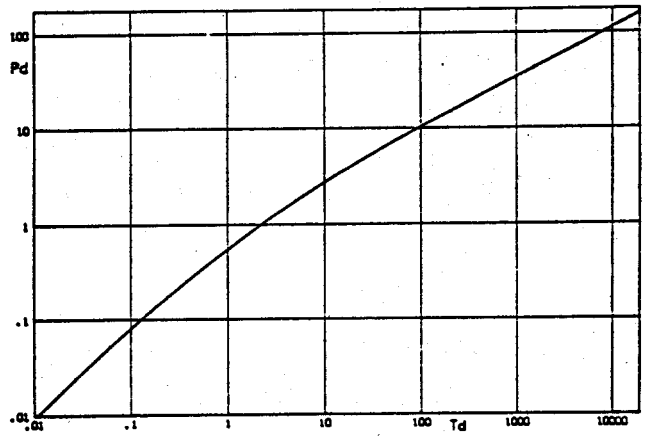

FIG. 2
- Graph of the influence function P_D^* as a function of t_D^*

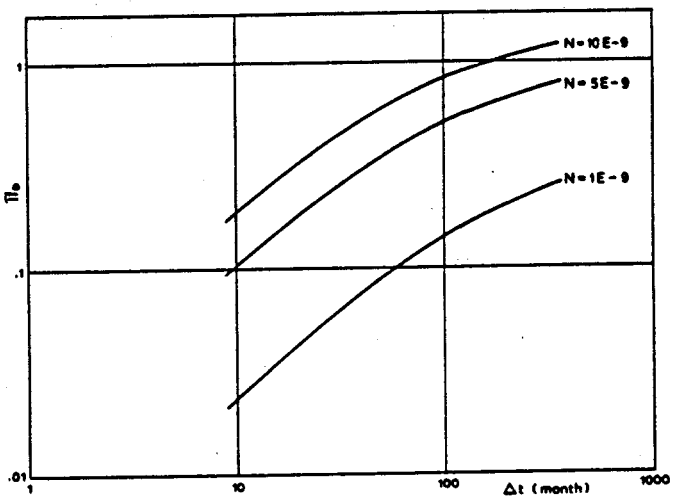

FIG. 3
- Graph of the dimensionless pressure π_D as a function of time and for various values of the parameter $N^{\sim}$.

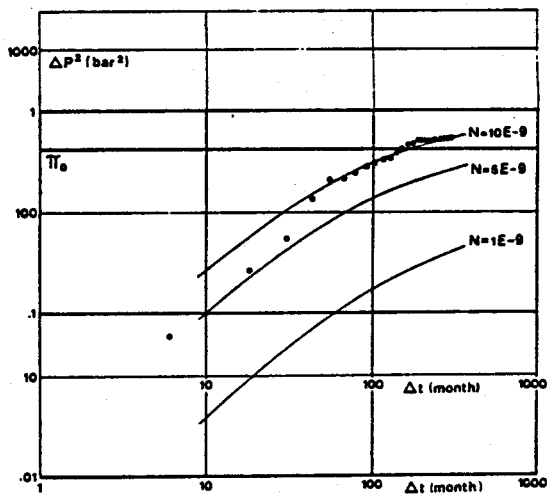

FIG. 4

FIG . 4
- Graph of $\delta\ (P^{\approx}) = P_i^{\approx} - P^{\approx}(t)$ of well 111 in Larderello, as a function of time, interpolated with the function calculated with the mathematical model.

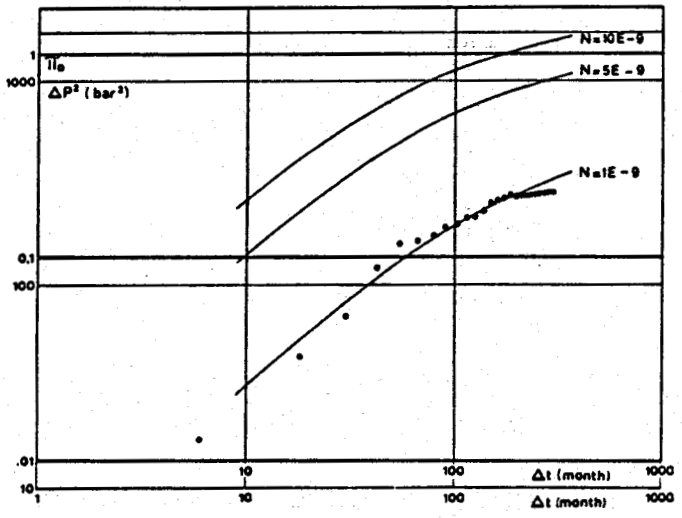

FIG. 5
- Graph of $\delta (P^2) = P_i^2 - P^2(t)$ of well 111 in Larderello, as a function of time, interpolated with the function calculated with the mathematical model.

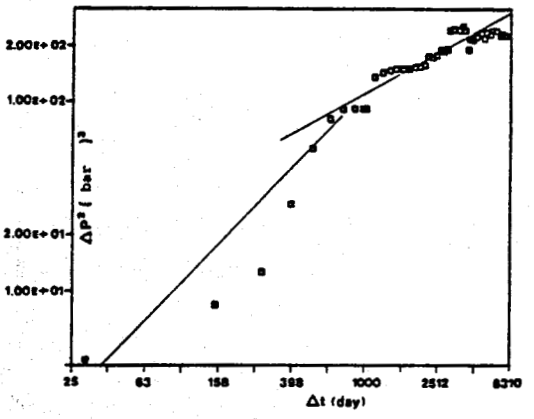

FIG. 7
Graph of $\delta(P^2) = P_i^2 - P^2(t)$ of well Gabbro 8 as a function of time.

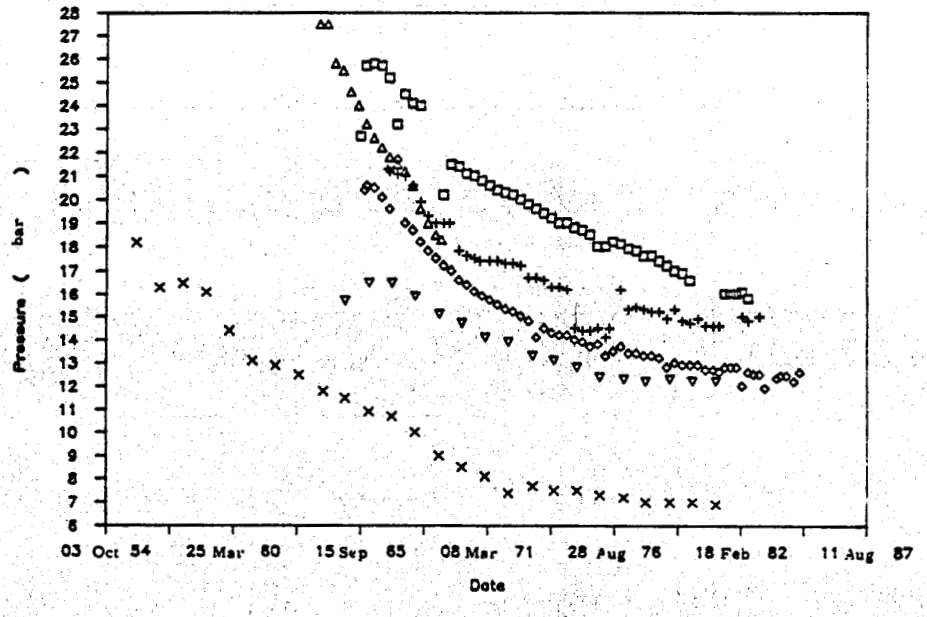

FIG. 6
- Pressure decline of some closed wells in the Valle Secolo and Gabbro areas.

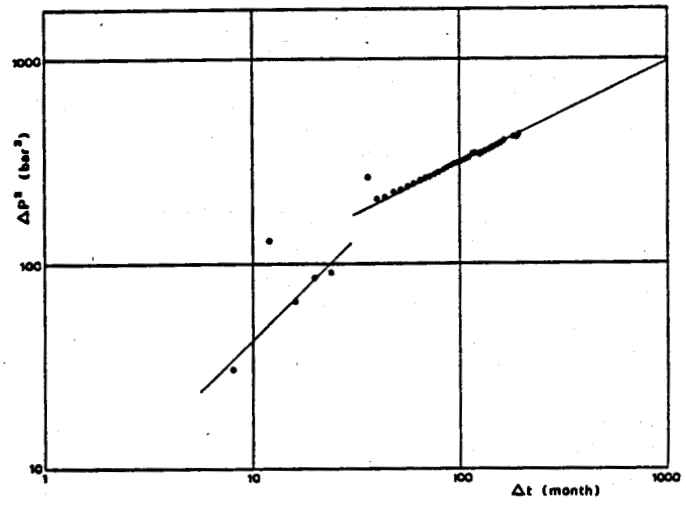

FIG. 8
- Bilogarithmic graph of $\delta (P^2) = P_i^2 - P^2(t)$ of well S. Dalmazio 4 as a function of time.

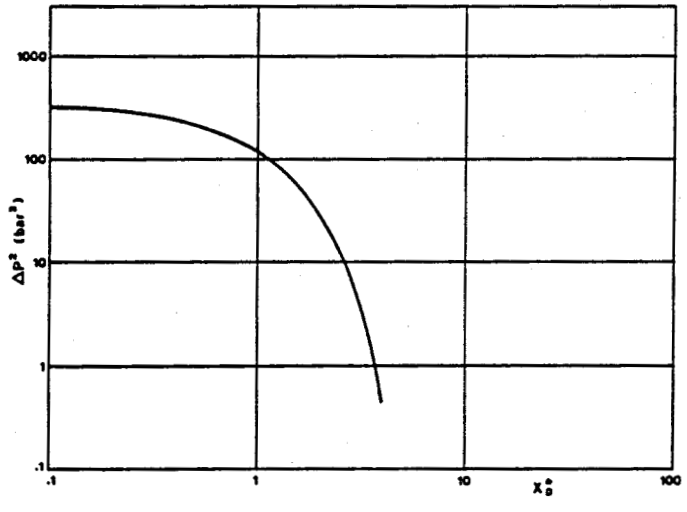

FIG. 9
- Graph of $\delta(P^2) = P_i^2 - P^2(t)$ as a function of dimensionless depth X_D^*, calculated with the mathematical model for $N^- = 10^{-9}\ s^{-1}$ and t = 360 months.

PROCEEDINGS, Fourteenth Workshop on Geothermal Reservoir Engineering
Stanford University, Stanford, California, January 24-26, 1989
SGP-TR-122

THREE-DIMENSIONAL TEMPERATURE FIELD RECONSTRUCTION IN GEOTHERMAL RESERVOIRS BASED ON THE SPLINE APPROXIMATION OF GREEN'S FORMULA

Aleksei V.Kiryukhin*, Dmitrii M.Fage**, Sergei L.Perveev*** and Dmitrii N.Gusev*

*Institute of Volcanology, Petropavlovsk-Kamchatsky, 683006 USSR
**Computer Center, the Siberia Division, USSR Academy of Sciences, Novosibirsk, Lavrentiev Str.,6
***Kamchatkan Hydrogeological Expedition, PGO Sakhalingeologia, USSR

ABSTRACT

The basic idea of the method of three-dimensional temperature field reconstruction is to express the observable temperature field as a superposition of source functions and a core of "Δ^2"-operator (background temperature plane) in accordance with Green's formula.The technical realization of this method was provided on the basis of computer program LIDA-3 (Library of Data Approximation). It has been demonstrated that the method of three-dimensional temperature field reconstruction can be applied to convective geothermal reservoirs. The reconstruction of three-dimensional temperature fields of the Mutnovsky geothermal reservoir is shown as an example.

INTRODUCTION

The three-dimensional temperature field reconstruction based on the temperature logging data is of practical importance for
(a) establishing the temperature anomaly geometry and its genesis;
(b) assessing the heat energy storage (exploitational reserves of geothermal fields);
(c) determining the most favourable sites for geothermal drill holes;
(d) forecasting temperatures at different depths and in adjacent areas;
(e) identifying the high-temperature flows.

Until nowadays the temperature field reconstruction has been made "by hand" in vertical or horizontal (two-dimensional) cross sections on the basis of linear interpolation (extrapolation) taking into account the intuitive notions of an investigator. The attempt to solve reverse boundary problems for elliptic type equation is also inefficient because of the lack of real physical conditions for boundary conditions and geometry determinations. Therefore it is necessary to improve our methods of temperature field reconstruction to satisfy some energetic principles in a three-dimensional field.

METHOD OF TEMPERATURE FIELD RECONSTRUCTION

The stationary temperature field in convective geothermal reservoirs satisfies heat and mass transfer equations

$$\lambda \Delta T - C_0 V \nabla T = 0 \qquad (1)$$

where T is the temperature; λ, the heat conductivity coefficient, C_0, the specific heat capacity of fluid; V, the mass filtration velocity; Δ, Laplas operator and ∇, nabla operator. The mass filtration velocity distribution V depends mainly on geometry of permeable channels in geothermal reservoirs. Then the second term in equation (1) expressed with the help of the heat source function $f(x,y,z)$ can be rewritten as

$$\lambda \Delta T + f(x,y,z) = 0 \qquad (2)$$

Equation (2) can be solved by finding the unknown sources $f(x,y,z)$ in the three-dimensional field. However, the Green's functions for harmonic operator are not continuous. Therefore we transform equation (2) to biharmonic view by applying Δ-operator

$$\Delta^2 T + \Delta f = 0 \qquad (3)$$

Thus, the problem of three-dimensional temperature field reconstruction can be reduced to selection of the Green's functions (sources) for biharmonic operator which can be expressed as

$$T(x,y,z) = \mu_0 + \mu_1 x + \mu_2 y + \mu_3 z + \int_{\Omega} \Delta f(x,y,z) \cdot \sqrt{(x-x_1)^2+(y-y_1)^2+(z-z_1)^2}\, dx_1 dy_1 dz_1 \qquad (4)$$

where the first four right-hand terms are the core of "Δ^2" (Δ) operator and the last term is the source function (the Green's function). When the character of heat transfer is quasi-stationary, the approach based on formula (4) seems to be also possible; in this case the

nonstationary term is also taken into account in function f(x,y,z). It follows also from equation (4) that the temperature field reconstruction is made based on the piece-linear functions for which the mean square error of approximation is 0 (h^2), where h is the distance between observational points. If the temperature data "T_i" in N points ($x_i y_i z_i$) of the geothermal field are known, the Green's function which provides the observable temperature field can be expressed as

$$\sum_{i=1}^{N} \lambda_i \sqrt{(x-x_i)^2+(y-y_i)^2+(z-z_i)^2} \qquad (5)$$

where X_i is the intensity of sources (of convective nature, in our case) in points (x_i, y_i, z_i) which provide the achievement of "T_i" in observational points. The coefficients λ_i (i=1,N) and M_j (j=0.3) can be determined from a system of equations

$$\begin{pmatrix} T \\ 0 \end{pmatrix} = \begin{pmatrix} A & B \\ B^T & 0 \end{pmatrix} \begin{pmatrix} \lambda \\ M \end{pmatrix} \qquad (6)$$

where $T=(T_1 \dots T_N)^T$, $\lambda=(\lambda_1 \dots \lambda_N)^T$, $M=(M_0, M_1, M_2, M_3)^T$. A is the symmetrical matrix with N*N dimension and components $((x_i-x_j)^2+(y_i-y_j)^2+(z_i-z_j)^2)^{1/2}$, B- matrix with N*4 dimension, which consists of $(1, x_i, y_i, z_i)$ vectors; T is the sign of transpose of a matrix (vector). The last four equations in system (6) indicate that the background temperature plane $M_0+M_1x+M_2y+M_3z$ is the average in terms of energy and balances positive and negative anomalies of the temperature field.

After the λ and M determination, the three-dimensional temperature field reconstruction is realized by basis functions (4) using the coefficients λ and M

$$T = M_0+M_1x+M_2y+M_3z + \sum_{i=1}^{N} \lambda_i \sqrt{(x-x_i)^2+(y-y_i)^2+(z-z_i)^2} \qquad (7)$$

In reality, temperature logging in boreholes is made with some error "δ"

$$\delta = \sqrt{\frac{1}{N}\sum_{i=1}^{N} (T-T_i)^2} \qquad (8)$$

In order to assess this error in a system of equations (6) it is necessary to disturb somewhat matrix A

$$A \rightarrow A + \alpha E \qquad (9)$$

Then the contrasting effect of sources and sinks is decreasing. As a result, reconstructions based on formula (7) give an imitation of deviation from erroneous data owing to greater smoothing of the sought temperature field. The problem of searching for the spline functions to equation (6) taking into account equation (8) is solved by using "LIDA-3" computer program (Vasilenko,1987).

THREE-DIMENSIONAL TEMPERATURE FIELD RECONSTRUCTION OF THE MUTNOVSKY GEOTHERMAL RESERVOIR

Data base. The following data were used as a data base for temperature field reconstruction:
(1) bottom hole temperature logging data during drilling after several days of temperature build-up;
(2) data from flow tests (enthalpy, discharge) after penetrating the productive zone.

RESULTS OF CALCULATIONS AND THEIR DISCUSSION

The data base is in accordance with the state as of April 1988; the three-dimensional temperature field reconstructions were made for volume ($x \in 0,4000$ m, $y \in 2500$, 6750 m, $z \in -1300$, +400 m); the horizontal coordinates were arbitrary. The mean square deviation of the calculated temperature field from the actual data was 2°C (AL=1.0). Figures 1,2 and 3 show the temperature distribution in lateral (z=0m a.s.l.)(Fig.1), meridional (Fig.2) and latitudinal (Fig.3) sections. In the lateral section the main thermal anomaly has a center near well B-1 (the whole area of this anomaly is approximately 4 km², the temperature above 200°C). The temperature anomaly here has sharp boundaries with high temperature gradients in the west, north and south which point to the presence of hydrodynamically impermeable boundaries. In the north-east the temperature gradients are very low and the temperature field is more homogeneous which apparently point to large horizontal spread of thermal water flows in this direction.

In the meridional section (Fig.2) there is a prominent ascending flow in the region of well 01, which rises at an angle of 30-45° from the south. There is a descending fluid flow between wells 24 and 012 (descending at an angle of 45° to the south). Apparently, those are elements of semiconfined convective mesh. A subvertical steam tube feeding the natural steam jets (Dachnye fumaroles) is shot off from the upper part of the ascending fluid flow.

In the latitudinal section (Fig.3) the ascending flow can be identified by relatively symmetrical temperature anomaly in a section between wells 7 and 10. The forecasted maximum temperature in the area of the temperature field reconstruction, 200 m to the south of well 01 at an elevation of -1300 m, was 320°C. This flow is probably confined to the superposed submeridional fracture zone and contacts with Miocene intrusions.

Analysis of the temperature field distribution in other sections also shows the existence of ascending hot water flow in the region of

well 013; this flow rises at an angle of 75-80° from the east and it is also confined to the fracture zone of submeridional trend. A descending hot and cold water flow is present in the region of well 011-012 (it descends at an angle of ~45° to the south). This flow is confined to the fracture zone of north-west trend. Unfortunately, the volume of the paper does not allow us to present all corresponding sections of the temperature field.

CONCLUSIONS

The new method of three-dimensional temperature field reconstruction in geothermal reservoirs was suggested. This method is based on the spline approximation of the unknown field using Green's formula.

The three-dimensional temperature field reconstruction was made within the Mutnovsky

Fig.1. The temperature distribution within the Mutnovsky geothermal reservoir as a result of three-dimensional temperature field reconstruction in the lateral section, z=0 m a.s.l., scale 1:25000.

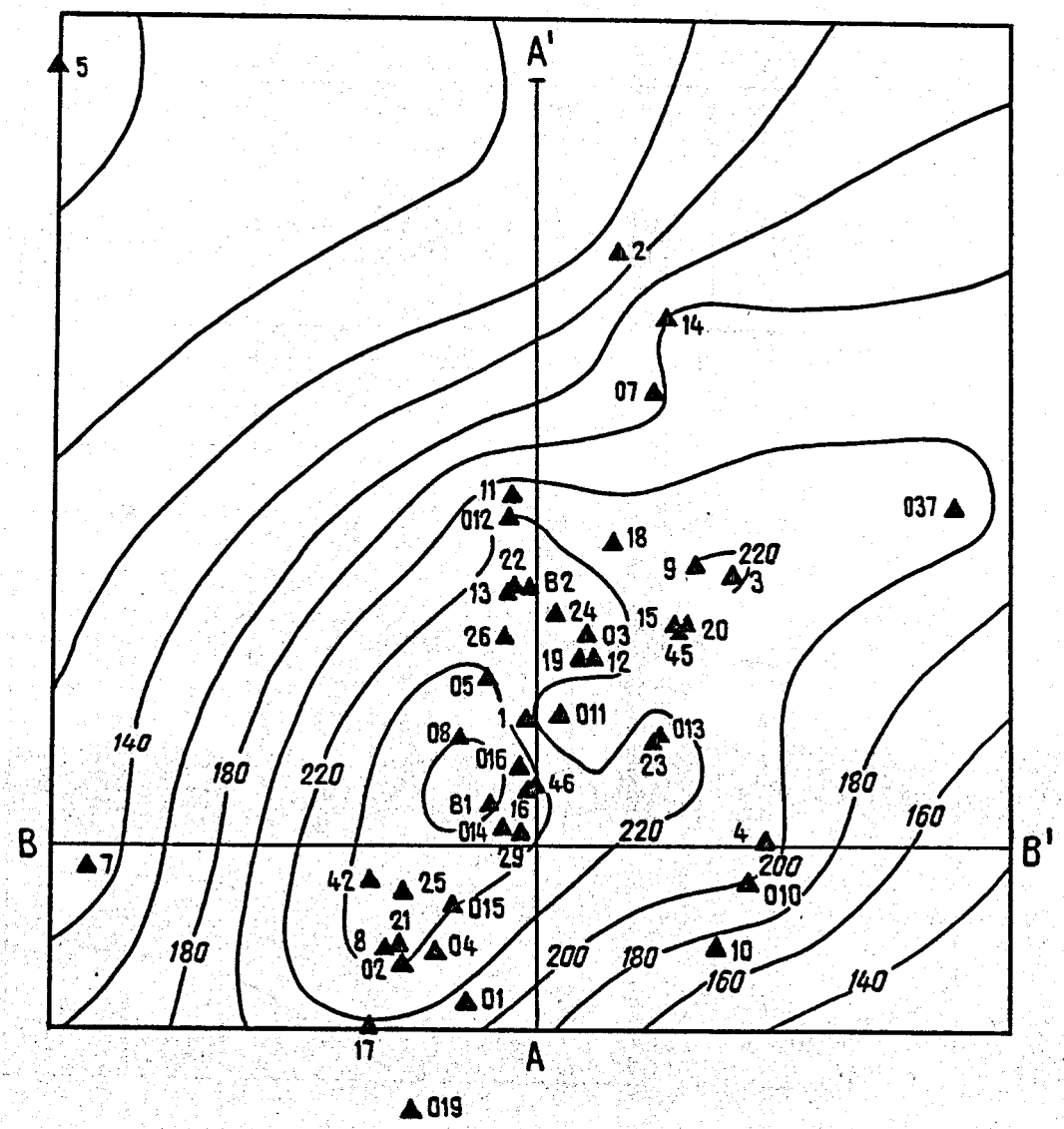

geothermal reservoir (Dachnye Site). The high-temperature flows were identified on the basis of temperature distribution. The forecasted maximum temperature at an elevation of-1300 m was 320°C.

The suggested method of temperature field reconstruction can also be applied to geothermal reservoir monitoring for the purpose of its exploration and exploitation.

REFERENCE

Vasilenko,V.A.(ed.)(1987),"Library of Data Approximation: Functions and Numerical Signal and Image Filtration", Part 1, Novosibirsk, 169 pp.(in Russian).

Fig.2. The temperature distribution within the Mutnovsky geothermal reservoir as a result of three-dimensional temperature field reconstruction in the meridional section AA', scale 1:25000 (horizontal), 1:10000 (vertical).

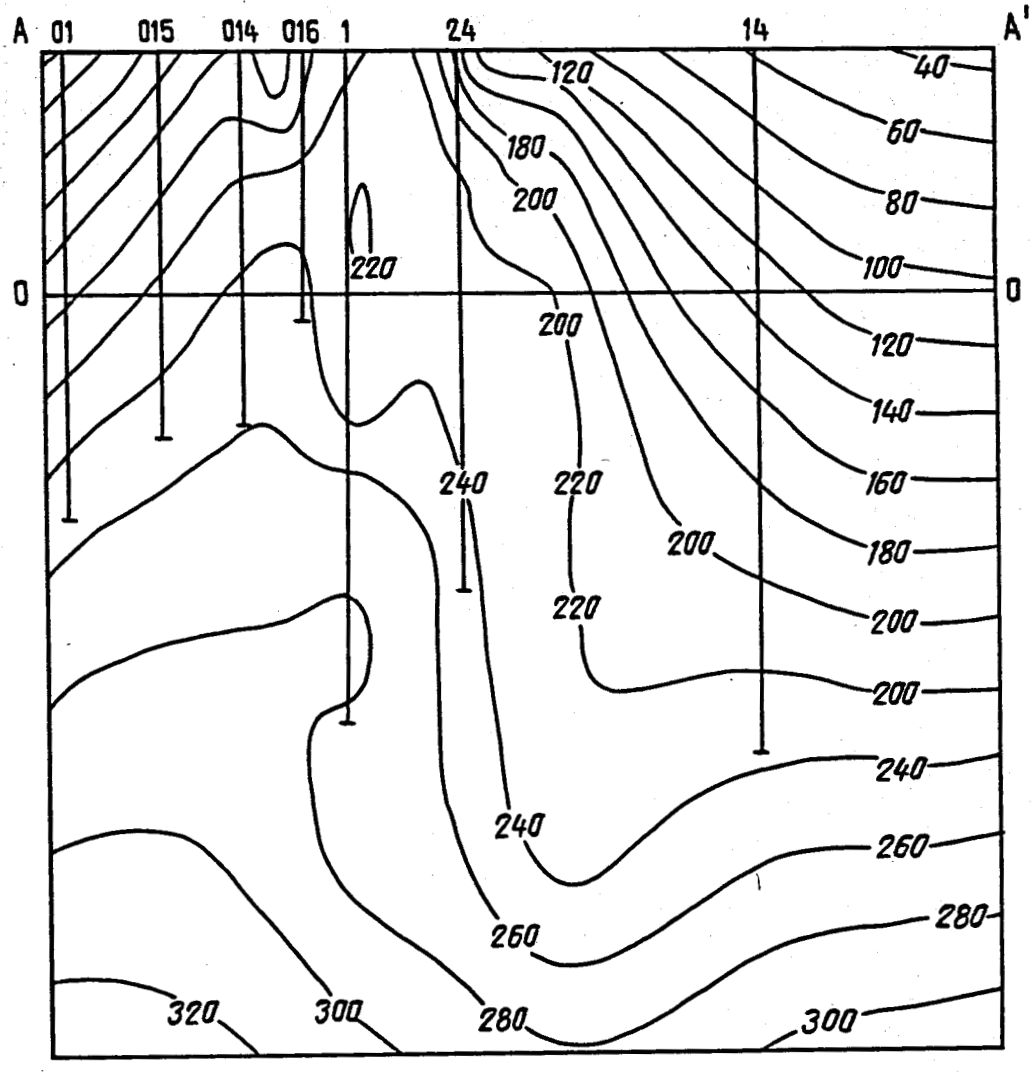

Fig.3. The temperature distribution within the Mutnovsky geothermal reservoir as a result of three-dimensional temperature field reconstruction in the latitudinal section BB^1, scale 1:25000 (horizontal); 1:10000 (vertical).

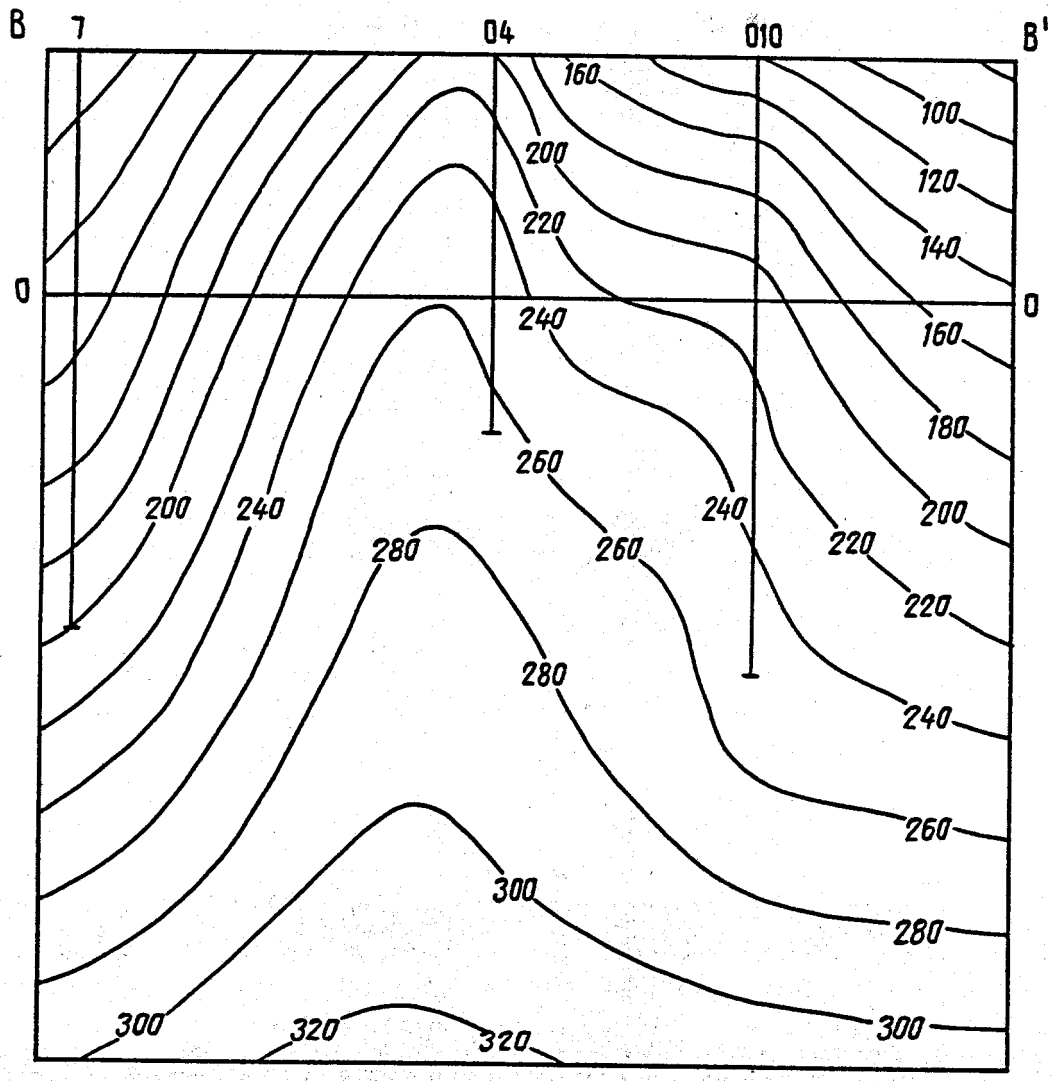

PROCEEDINGS, Fourteenth Workshop on Geothermal Reservoir Engineering
Stanford University, Stanford, California, January 24-26, 1989
SGP-TR-122

ONE CURVE FITS ALL

RUSSELL JAMES

GEOTHERMAL RESEARCH CENTRE,
WAIRAKEI, TAUPO, NEW ZEALAND

ABSTRACT

Characteristic curves of geothermal wells co-ordinate mass flow with wellhead pressure, and although differing from one another, plots of good commercial producers are roughly elliptical in appearance. This occurs whether the flow originates as dry saturated steam or as pressurized hot water.

All ellipses when tilted can be changed to a circle, hence by plotting (W/W_{max}) versus (P/P_{max}) where W is flowrate and P is wellhead pressure, we can obtain a circle when: $(W/W_{max})^2 + (P/P_{max})^2 = 1.0$

Ten geothermal wells - of which half emit dry saturated steam - are plotted employing the above parameters and give surprisingly close approximations to a circle considering the variety of wells tested.

The relationship permits optimization of turbine entry pressures which are found to be proportional to maximum operating wellhead pressures for both dry-steam and wet-steam wells.

Besides giving a sense of unity, this approach can be used to predict the whole output curve for differing discharge pipe diameters from limited field results; an example of this ability is presented with useful economic consequences for a new well under test.

INTRODUCTION

One of the fundamentals of geothermal power is the characteristic curve (also known as the output curve) which correlates wellhead pressure and mass flow-rate. Although there are numerous exceptions, the shape of the curve is elliptical in appearance and this applies both for dry steam wells (saturated steam or slightly superheated) and also for wells discharging mixtures of steam-water. These latter usually derive their flows from a feed of hot water either at boiling point or pressurized above it.

Six examples of the characteristic curves of wells discharging steam-water mixtures from the Cerro Prieto field in Mexico are given in a recent work by Lippman and Manon (1987).

An earlier seminal study by Rumi (1972) compares six dry steam wells of the Larderello field of Italy with modified ellipse equations to give good agreement with the experimentally plotted output curves.

A powerful steam-water well of New Zealand was studied by James (1984) and a similar equation gave good agreement with later output measurements.

No two geothermal wells have the same output characteristics with identical flows and wellhead pressures, hence all such curves are highly individualistic and generally are plotted on their own test result sheets. Under production discharge, both flow and wellhead pressure also decline with time although usually they remain geometrically similar and elliptical in shape. The relationship between flow and wellhead pressure in which both decline in harmony when the well discharges against a constant resistance such as is exerted by a fixed choke or an untouched control valve setting, is an important one and can permit future flow estimates when wellhead pressure trends are known, James (1983).

Various attempts have been made in the past to transform the well output relationship into a visually linear one by means of plotting versions on different types of graph paper, such as log-log and log-linear. As this has not been successful, the present attempt is to plot directly on the quadrant of a circle which should be suitable for all geothermal well outputs including ones taken from the same well at different periods under production discharge. To implement this approach, it is necessary to be aware that ellipses when tilted become circles.

Quadrant Plot

To plot well discharge parameters so that they fall on a circle, the following equation is employed:

$$(W/W_{max})^2 + (P/P_{max})^2 = 1.0 \qquad (1)$$

As this is a non-dimensional formula, consistent units can be used in which discharge ratios can be plotted against pressure ratios

where W and P are spot values; W_{max} and P_{max} are theoretical maximum values taken where P = 0 and W = 0 respectively.

The reason for the term 'theoretical' is because even when a commercially sized well is discharging wide-open, there is a significant wellhead pressure for steam-water wells and to a lesser extent for wells discharging dry saturated or superheated steam. Also for steam-water wells the discharge is usually not zero but a substantial quantity at the highest operating wellhead pressure (known as the MDP or Maximum Discharge-Pressure). For example, at Wairakei flows do not fall much below about 100 t/h for 0.2 m diameter wells when the wellhead pressure is at a maximum (originally about 26 bar). Closing completely the wellhead valve results in the flow dropping to zero while the wellhead pressure can remain at MDP or start slowly to vary from this as explained in James (1980a) taking days or weeks to stabilise. In the case of dry steam wells, the phenomenon of MDP does not exist and hence the discharge truly is zero at the maximum wellhead pressure.

With bleeding of steam-water wells, a change of the relationship between wellhead pressure and flow-rate often takes place in which these parameters now increase (and decrease) together, but this is for non-commercial flows of the order of 1 t/h and has been pursued elsewhere, James and Gould (1987), and is not applicable here.

Plotting Procedure Examples

Taking data from the steam-water well M-102 described by Lippman and Manon (1987) where a wide-open flow of 225 t/h is obtained at a wellhead pressure of 11.5 bar, together with a flow of 75 t/h at 81 bar, we may calculate the theoretical maximum flow and maximum wellhead pressure as follows:

From equation (1), $W_{max} = \dfrac{W}{\sqrt{1 - \left(\frac{P}{P_{max}}\right)^2}}$ (2)

Hence $W_{max} = \dfrac{225}{\sqrt{1 - \left(\frac{11.5}{P_{max}}\right)^2}} = \dfrac{75}{\sqrt{1 - \left(\frac{81}{P_{max}}\right)^2}}$ (3)

Solving gives P_{max} = 85.817 and W_{max} = 227.047

Discharges may now be calculated for various values of wellhead pressure from the following equation and compared with test results on Table 1.

$$W = 227.047 \sqrt{1 - \left(\frac{P}{85.817}\right)^2} \quad (4)$$

Table 1. Calculated discharges from equation (4) compared with test results on well M-102 from Lippman and Manon (1987).

P bar	$\frac{P}{P_{max}}$	W(calculated) t/h	W_t(test)	$\frac{W_t}{W_{max}}$
11.5	0.134	225	225	0.991
21	0.245	220.1	220	0.969
31	0.361	211.7	215	0.947
41	0.478	199.5	200	0.881
51	0.594	182.6	180	0.793
61	0.711	159.7	165	0.727
71	0.827	127.5	130	0.573
81	0.944	75	75	0.330

Taking as a further example a dry steam well of Larderello, Gabbo 1 as described by Rumi (1972) where a wide-open flow of 116 t/h is obtained at a wellhead pressure of 4 bar together with a flow of 20 t/h at 29.8 bar, we determine maximum theoretical flow and maximum wellhead pressure from the following relationship :

$$W_{max} = \frac{116}{\sqrt{1 - \left(\frac{4}{P_{max}}\right)^2}} = \frac{20}{\sqrt{1 - \left(\frac{29.8}{P_{max}}\right)^2}} \quad (5)$$

Solving gives P_{max} = 30.245 and W_{max} = 117.028

Discharges may now be calculated as before at different wellhead pressures from equation (6) following, and compared with test results shown on Table 2.

$$W = 117.028 \sqrt{1 - \left(\frac{P}{30.245}\right)^2} \quad (6)$$

Table 2. Calculated discharges from equation (6) compared with test results on well Gabbro 1 from Rumi (1972).

P bar	$\frac{P}{P_{max}}$	W(calculated) t/h	W_t (test)	$\frac{W_t}{W_{max}}$
4	0.132	116	116	0.991
6.9	0.228	113.94	112	0.957
9.9	0.327	110.58	108.1	0.924
12.8	0.423	106.03	102.5	0.876
15.9	0.526	99.55	97	0.829
18.2	0.602	93.47	89	0.761
25.6	0.846	62.32	56.5	0.483
29.8	0.985	20	20	0.171

Values of $\frac{P}{P_{max}}$ are plotted against $\frac{W}{W_{max}}$ on Figure 1 and taken from Tables 1 and 2. Three other dry steam wells are also plotted, namely VC-10, Scarzai 3 and La Selvaccia with two plots for the latter taken for the years 1958 and 1964 during which severe decline in discharge had occurred. Also plotted is a 'typical' steam well for the Geysers field as presented by Budd (1973).

In the case of steam-water wells, a total of 5 are plotted (including M-102) which are, E-2 and M-110 of Mexico, with MK-5 and KA-21 of New Zealand. It should be mentioned that for wells which have outputs which should not be divulged for commercial reasons, the plots of Figure 1 give no information in the way of enthalpy, discharge or wellhead pressure. The importance of these plots is the significance of the relationship between the parameters, and the result indicates a reasonably good correlation with the arc of a circle. Although any one test measurement point may be unreliable due to a variety of causes, overall there seems little difference attributable to the type of well, powerful or moderate, wet or dry. Causes of unreliability may be lack of stabilizing time, discharge fluctuations or errors caused by instrument fatigue, especially due to vibration inherent in two-phase flow.

Optimization of turbine entry pressure

As the output curves of geothermal wells approximate to the quadrant of a circle as shown in Figure 1, it should not be difficult to determine the turbine entry pressure which generates the maximum amount of electric energy both for steam-water and dry steam wells.
To obtain a practical grasp of the procedure, the quadrant of Figure 2 has the arbitrary values of 30 bar maximum wellhead pressure and 100 t/h maximum discharge. Although the latter figure is low for a commercial steam-water well (but realistic for a dry steam well), the power developed can be factored upwards in proportion to the actual maximum discharge.

Steam-Water well optimum

Assuming that Figure 2 is for a well which is fed from an all-liquid reservoir with Boiling-Point-with Depth applying, we may calculate the feed temperature from the Maximum Discharge-Pressure which in this case is considered as effectively 30 bar. The formula from James (1988) is:

$$C = 99.75\ P_m^{0.283} \quad \text{for } 8 < P_m < 80 \qquad (7)$$

where C is the feed temperature in degrees Celcius, and P_m is the Maximum Discharge-Pressure in bar. For the present example where $P_m = 30$, the feed water temperature is 261.2° which from steam tables gives a liquid water enthalpy of 1140 J/kg and taken here as constant over the whole output curve. Hence at any selected wellhead pressure, the steam fraction can be estimated (and the water fraction if secondary flash is considered). Taking a condenser pressure of 0.15 bar and steam rates from James and Meidav (1977), the power in megawatts of electricity can be estimated for both single-stage flash and double flash (respectively one and two separators).

The case is also considered where single-stage flash is associated with an atomospheric-exhaust turbine venting to a pressure of 1 bar. The results are shown on figure 3 where curves 'A', 'B' and 'C' are for double flash, single-stage flash and atmospheric-exhaust with power potentials of 3, 2.5 and 1.3 MWe at optimum pressures of 1/3, 1/6 and 1/4 of the maximum wellhead pressure. Identical fractions were also found where the maximum wellhead pressure was raised to 60 bar and also when reduced to 15 bar so that if a steam-water well is considered with a maximum wellhead pressure of, say, 42 bar for exploitation by single-stage flash, then the optimum pressure would be 42/6 = 7 bar. It should be noted, however, that this value does not distinguish between wellhead pressure, separator pressure and turbine entry pressure which in this study are considered the same but which in an actual field development would not necessarily be identical. Also, of course, all fields under exploitation result in a shrinkage of the curve of Figure 2 towards the origin whatever the original values of discharge and wellhead pressure. Hence the maximum discharge-pressure diminishes with time and so does the value of $P_m/6$ in the case of single-stage flash, for example.

The optimum values should therefore be considered as maxima and it would be preferable to reduce them somewhat in the initial design when account is taken of discharge and wellhead pressures simultaneously reducing over years of exploitation. With reinjection of separated brine an inherent part of modern geothermal fields where hot water reservoirs are developed, design is moving in the direction of single-stage flash in order to avoid mineral scaling of overland pipes and disposal wells.

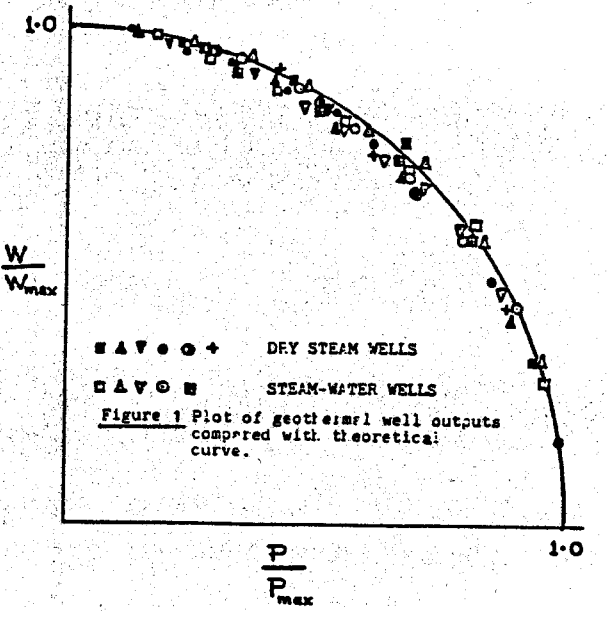

Figure 1 Plot of geothermal well outputs compared with theoretical curve.

Dry Steam Wells

Taking Figure 2 as the curve of a dry steam well, the discharge is known for each value of wellhead pressure and may be used to determine the electric power potential when using turbine steam rates as presented by James and Meidav (1977). This has been accomplished both for condensing sets with a back-pressure of 0.15 bar and for atmospheric -exhaust sets with a back-pressure of 1 bar. The results are shown on Figure 4 where it is seen that condensing sets generate about 50% more power than atmospheric-exhaust sets when designed at their optimum pressures of 12 bar and 15 bar respectively.

These optima are equal to 0.4 P_m and 0.5 P_m and are therefore higher ratios than those for steam-water wells. However, the same caveat applies with both discharge and maximum wellhead pressure declining with exploitation, so that they represent maximum values which would have to be reduced in practice to take into account an estimated maximum wellhead pressure at the end of the economic field-life.

The same ratios are found to apply when a curve similar to Figure 2 for dry saturated steam is considered but where the maximum wellhead pressure is 15 bar instead of 30 bar so can be considered as widely applicable. For theoretical reasons, James (1968), an exploitable steam reservoir with a pressure significantly in excess of 30 to 40 bar is not to be expected, hence calculations based on a maximum wellhead pressure of 60 bar (as for steam-water wells) is not undertaken here.

Predicting whole output curve

A geothermal well which produced large flows of dry saturated steam was tested in New Zealand. Employing a 12 inch production casing, it had a closed-in wellhead pressure of 24.5 bar and when discharged vertically wide-open produced a flow of 174.8 t/h at a wellhead pressure of 19.3 bar. The discharge pipe erected at the wellhead was rather small in diameter at 0.1524 m compared with the internal casing diameter of 0.315 m and was obviously restricting the discharge to a value much smaller than what the well was capable. With no restriction at the wellhead, the characteristic well curve was calculated as follows:

From equation (1), $\left(\frac{174.8}{W_{max}}\right)^2 + \left(\frac{19.3}{24.5}\right)^2 = 1$

Hence $W_{max} = 283.77$ t/h

Discharges may now be determined from various substituted values of wellhead pressure in the following formula:-

$$\left(\frac{W}{283.77}\right)^2 + \left(\frac{P}{24.5}\right)^2 = 1$$

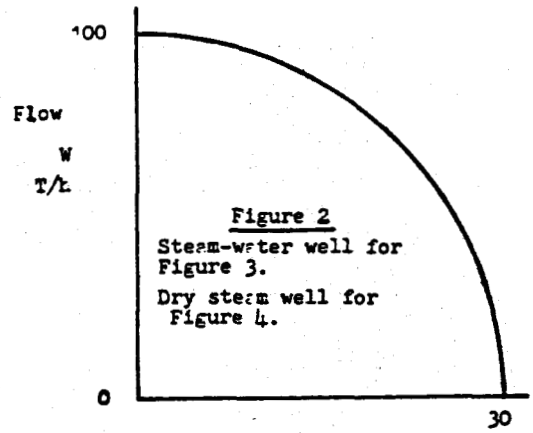

Figure 2
Steam-water well for Figure 3.
Dry steam well for Figure 4.

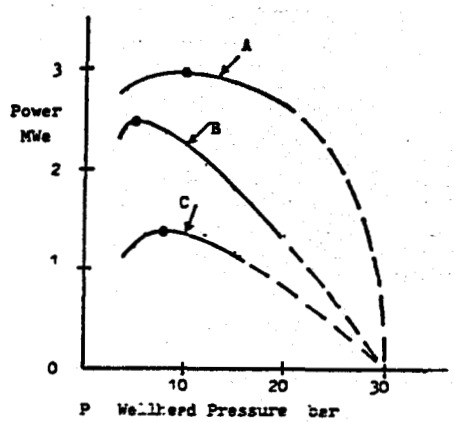

Curve A Double flash } Condenser pressure
Curve B Single flash } = 0.15 bar
Curve C Atmospheric exhaust at 1 bar

Figure 3 Power output of steam-water well of Figure 2

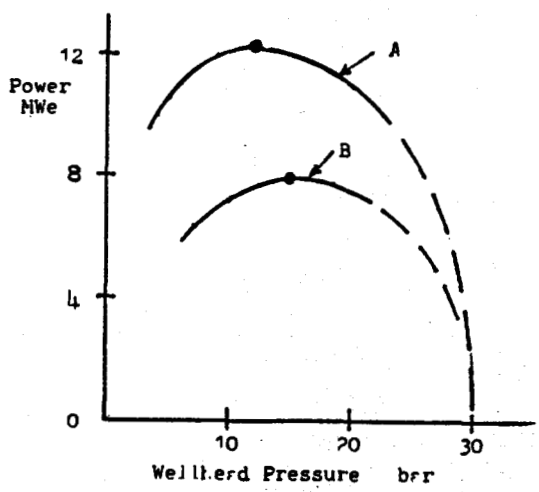

Curve A Condenser set at 0.15 bar
Curve B Atmospheric exhaust at 1.0 bar

Figure 4 Power output of dry steam well of Figure 2

The theoretical curve is shown on Figure 5 together with a few test results employing the 0.1524m diameter discharge pipe which could only cover a limited range of wellhead pressures from 24.5 to 19.3 bar. The line 'A' crosses the location where the minimum wellhead pressure is attained with the 0.1524m diameter discharge pipe. Lines 'B', 'C' and 'D' are shown intercepting the curve at the lowest wellhead pressures attainable when discharging wide-open vertically through 0.2032 m, 0.254 m and 0.3048 m diameter discharge pipes. It was only possible to confirm these estimates by replacing the 0.1524 m dia. by a 0.2032 m pipe and re-testing the well from closed-in to wide-open vertically. The results shown on Figure 5 follow the theoretical curve and nearly reach the estimated lower limit of wellhead pressure crossed by line 'B', hence the calculated curve is considered as a realistic first estimate of discharges attainable at lower wellhead pressures. With suitably large branch lines, it is believed that this well should be capable of a steam flow of 260 t/h at a wellhead pressure of 10.0 bar which is equivalent to an electric power output of about 30 MWe.

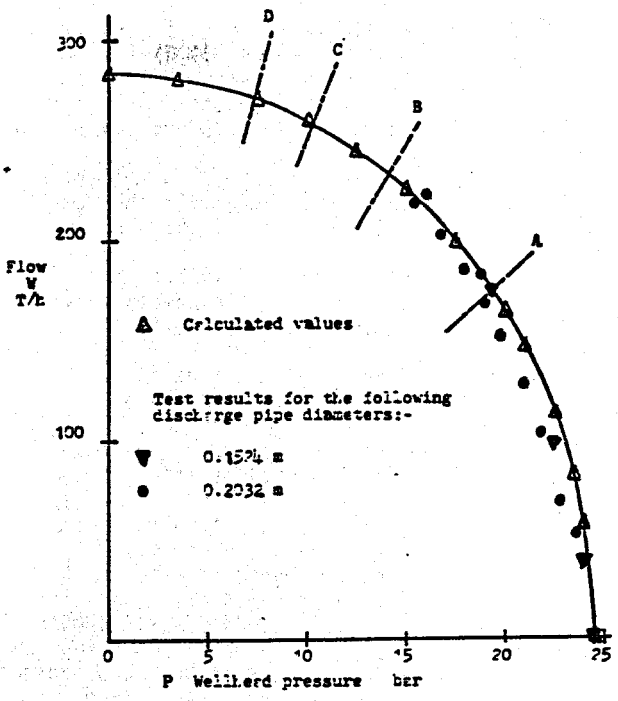

Figure 5 Output curve of powerful dry steam well for different discharge pipe diameters.

Measurement of the mass flow from geothermal wells under conditions of maximum vertical discharge employing the lip pressure technique (critical discharge pressure at sonic velocity) has been described elsewhere, James (1980b) and will not be followed here.

CONCLUSIONS

The power generated by geothermal wells is of course, dependant on discharge. However, the optimum turbine entry pressure is independent of flow and is proportional only to the instantaneous closed-in wellhead pressure for dry saturated steam wells and to the Maximum Discharge-Pressure (MDP) of steam-water wells. The elliptical-shaped characteristic curve which correlates discharge with wellhead pressure is an integral part of such optimizations and is basic to all such studies. As such curves shrink towards the origin with exploitation of a geothermal field, the MDP similarly declines with time (also the closed-in wellhead pressure of dry steam wells). Hence the optimum turbine entry pressure declines pro rata; because of this fact, such optima should emphatically be considered as maximum values and should be reduced somewhat in the original design of a project. Capital costs increase with low turbine pressures, however, and to ameliorate this effect a condenser pressure of 0.15 bar is assumed in the present study to provide a balanced trade-off between such costs and the overall thermal efficiency of utilization.

Although double-flash has been in vogue up to the present, it seems likely that single-stage flash will be increasingly common with re-injection becoming an intrinsic part of future projects. The spread of deeper drilling to 2km or more has also resulted in higher temperature wells with concomitant higher mineral content of the water phase; this requires water at increased temperatures (and pressures) to be transmitted to disposal wells, in order to avoid chemical scaling of plant.

A well's characteristic curve can be estimated (with reasonable approximation to reality) by taking only two sets of test values. Preferably these should be at maximum Discharging-Pressure (MDP) and at Maximum Vertical discharge (MVD) which provide the widest attainable difference of wellhead pressures and lip pressures. Interpolation between these points and extrapolation beyond, permits the full sweep of the output curve to be plotted.

REFERENCES

Budd, C.F. (1973:Steam Production at the Geysers Geothermal Field. In Geothermal Energy, Edited by Kruger, P and Otte, C. Stanford Univ. Press, Stanford, Calif. USA

James, R. (1968): Wairakei and Larderello: Geothermal Power Systems Compared. N.Z.J.Sc., 11,4, 706

James, R. and Meidav, T. (1977): Thermal Efficiency of Geothermal Power. Geo.Energy, 5, 4, 8.

James, R. (1980a): Deductions of the Character of Steam-Water Wells from the shape of the Output Curve. Proc.N.Z.Workshop, Univ.of Auckland, New Zealand

James, R. (1980b): Estimating Maximum Discharge of Geothermal Wells. Proc.6th Workshop Geothermal Reservoir Engineering, Stanford Univ., Stanford, Calif. USA

James, R. (1983): Locus of Wellhead Pressure with Time under Production Discharge. Proc.N.Z.Workshop, Univ. of Auckland, New Zealand

James, R. (1984): Successful Prediction of Mokai 5 Discharge. Geo.Energy, 12, 2, 7.

James, R. and Gould, T, (1987): Bleeding Characteristics of Geothermal Wells. Proc. NZ Workshop, Univ. of Auckland, New Zealand

James, R. (1988): Depth of Feed Water Influences Maximum Discharge-Pressure of Hot Water Geothermal Wells. Proc. 13th workshop Geothermal Reservoir Engineering, Stanford Univ. Calif. USA

Lippman, M.J. and Manon, A (1987): The Cerro Prieto Geothermal Field. Geo.Sc. and Techn. 1, 1, 1.

Rumi, O. 91972): Some Considerations on the Flow-rate/Pressure Curve of the Steam Wells of Larderello. Geothermics 1, 1, 13.

FOURTEENTH ANNUAL WORKSHOP ON GEOTHERMAL RESERVOIR ENGINEERING STANFORD UNIVERSITY JANUARY 24-26, 1989

PARTICIPANTS LIST

Jeff Adams
State Lands Commission
245 West Broadway, Suite #425
Long Beach, CA 90802
213-590-5201

Michael Adams
UURI
391 A Chipeta Way, Suite C
SLC, UT 84108
801-524-3435

Greg Anderson
UNOCAL Geothermal Division
Union Oil Science & Tech. Center
376 S. Valencia, Brea, CA 92631
714-528-7201

Gudni Axelsson
Nat. Energy Authority
Grensasvegur 9
108 Reykjavik, Iceland
0354-1-83600

Elwood L. Baldwin
Baldwin Engineering, Inc.
13604 Midway Road, #178
Dallas, Texas 75244
214-980-0784

Daniel B. Ballantine
PG&E
West Geysers Power Plant
P.O. Box 456
Healdsburg, CA 95448
707-431-3844

Ben Barker
UNOCAL Geothermal Division
P.O. Box 6854
Santa Rosa, CA 95406
707-545-7600

Tony Batchelor
Geoscience Limited
Falmouth Business Park
Bickland Water Rd.
Falmouth, Cornwall UK
011-44-326-211070

Seth Bayer
PG&E
2228 Fremont Dr.
Santa Rosa, CA 95405
707-538-2821

Pascal Bidaux
Lawrence Berkeley Laboratory
1 Cyclotron Road
Berkeley, CA 94720
415-486-6760

Gudmundur Bodvarsson
Lawrence Berkeley Laboratory
1 Cyclotron Rd.
Berkeley, CA 94720
415-486-6760

Tom Box
Geysers Geothermal Co.
P.O. Box 11279
Santa Rosa, CA 95406
707-578-2724

David Brock
Stanford University
Mitchell Bldg. Rm 360
Stanford, CA 94305
415-723-0691

Donald Brown
Los Alamos National Laboratory
Group ESS-4, MS-D446
Los Alamos, NM 87545

Myron Burr
UNOCAL Geothermal Division
3576 Unocal Place
P.O. Box 6854
Santa Rosa, CA 95406
707-545-7600

Dave Camille
UNOCAL Geothermal Division
P.O. Box 6854
Santa Rosa, CA 95406
707-545-7600

Dan J. Cash
Los Alamos National Laboratory
MS-D447, Geophysics Group
Los Alamos, NM 87545
505-667-1866

Raffaele Cataldi
ENEL-ITALY
Via Cesare Battisti, M47
56100-PISA-ITALY

Chieh Chu
Texaco Inc.
P.O. Box 770070
Houston, TX 77215-0070
713-954-6000

Jim Combs
GRI
1825 S. Grant St. Suite #900
San Mateo, CA 94402
415-349-3232

Jean Cook
Stanford University
Mitchell Bldg. Rm 360
Stanford, CA 94305
415-723-4745

Tyler Coplen
U.S.G.S.
431 National Center
Reston, VA 22092
703-648-5862

John R. Counsil
Consultant
1148 Shadyoak Place
Santa Rosa, CA 95404
707-538-2288

Christy Craig
St. Cal. Dept. Conservation D.O.G.
485-B Broadway
El Centro, CA 92243
619-353-9900

Gustavo Cuellar
CEL
P.O. Box 01-478
San Salvador/El Salvador
503-284586

Bert Dennis
Los Alamos National Laboratory
ESS-11 MS D448
P.O. Box 1663
Los Alamos, NM 87545
505-665-0624

Dick Dondanville
UNOCAL Geothermal Division
3576 Unocal Place
P.O. Box 6854
Santa Rosa, CA 95404
707-545-7600

Andy Drenick
GEO Operator Corp.
1330 N. Dutton, Suite A
Santa Rosa, CA 95401
707-523-4272

Herman Dykstra
Petroleum Engineering Consultant
4180 Treat Blvd., Suite I
Concord, CA 94518
415-689-9142

Derek Elsworth
Waterloo Centre for Groundwater Res.
Univ. of Waterloo, Waterloo
Ontario, N2L 391 Canada
519-885-1211

Kathy Enedy
Geysers Geothermal Company
1160 N. Dutton Ave., Suite #200
Santa Rosa, CA 95401
707-578-2710

Steve Enedy
NCPA
P.O. Box 663
Middletown, CA 95492
907-978-3101

Carlos Escobar
CEL- Av. Las Americas y PJE
San Anto-Nio. Col.
Isidro Menendez C.P. 01161
San Salvador, El Salvador
503-25-3898

David D. Faulder
EG&G
P.O. Box 1625
Idaho Falls, ID 83415
208-526-0881

James Fink
Geophynque International
5865 South Old Spanish Trail
Tucson, Arizona 85747
602-721-2390

Robert O. Fournier
U.S.G.S.
345 Middlefield Road
Menlo Park, CA 94025
415-325-5205

Ralph Frick
PG&E
2228 Fremont Dr.
Santa Rosa, CA 95405
707-538-2821

Dr. Sabodh Garg
S-Cubed
P.O. Box 1620
La Jolla, CA 92038-1620
619-453-0060

Norman Goldstein
Lawrence Berkeley Laboratory
1 Cyclotron Road
Berkeley, CA 94720
415-486-6760

David L. Gouveia
PG&E
West Geysers Power Plant
P.O. Box 456
Healdsburg, CA 95448
707-431-3847

Keshav Goyal
Geysers Geothermal Company
P.O. Box 11279
Santa Rosa, CA 95406-1279
707-578-2739

Mohinder Gulati
UNOCAL Geothermal Division
P.O. Box 6854
Santa Rosa, CA 95406
707-545-7600

Arni Gunnarsson
Reykjavik District Heating Corp.
Grensasvegur
108 Reykjavik, ICELAND

Hector Gutierrez
CFE
Ap Postal 31-C
Morelia S8260 Mich.
Mexico
451-4-36-49

Kenneth Henderson
Division of Oil and Gas
1416 Ninth St. Rm. 1310
Sacramento, CA 95814
916-323-1777

R.H. Hendron
Los Alamos National Laboratory
MS D446
Los Alamos, NM 87545
505-667-3644

Dr. Seiichi Hirakawa
Emeritus Professor
University of Tokyo
Kitazawa 2-37-4 Setagaya-ku
Tokyo 155 JAPAN

Paul Hirtz
Thermochem
5347 Skylane Blvd.
Santa Rosa, CA 95403
707-575-1310

Dr. Manfred Hockstein
Geothermal Inst.
Univ. of Auckland
Auckland, New Zealand

Annette Hope
PG&E
P.O. Box 1310
Middletown, CA 95461
707-431-6070

Roland Horne
Stanford University
Mitchell Bldg. Rm 360
Stanford, CA 94305
415-723-9595

Glen Horton
PG&E
P.O. Box 1310
Middletown, CA 95461
707-431-6070

Eduardo Iglesias
Instituto de Investigaciones
Electricas Apartado
P.O. Box 475
Cuernavaca, MEXICO

Joe Iovanetti
Consultant
310 Cortsen Rd.
Pleasant Hill CA 94523
415-944-5544

Tsuneo Ishido
Geological Survey of Japan
1-1-3 Higashi, Tsukuba
Ibaraki, 305 Japan
0298-54-3736

Younes Jalali-Y
Stanford University
Mitchell Bldg. Rm. 360
Stanford, CA 94305
415-723-9476

Cathy J. Janik
U.S.G.S.
345 Middlefield Road, MS-910
Menlo Park, CA 94025
415-329-5213

Jim Jardine
Berkeley Group Technologies
1330 Broadway, Suite #1450
Oakland, CA 94612
415-465-1744

Russell Johns
Stanford University
Lloyd Noble Bldg. Rm 117
Stanford, CA 94305
415-723-0691

Elizabeth Johnson
California Division of Oil & Gas
50 D Street Rm. 300
Santa Rosa, CA 95404
707-576-2385

Steve Johnson
GEO Operator Corp.
1330 N. Dutton, Suite A
Santa Rosa, CA 95401

Oliver T. Jordan
PNOC-EDC
Lawrence Berkeley Lab
1 Cyclotron Rd.
Berkeley, CA 94720
415-486-6167

Dennis Kaspereit
California Energy
P.O. Box 1420
Inyokern, CA 93527
619-764-2551

Yoshiyuki Kawano
Geoth. Survey Dept. New Energy and
Indust. Tech. Dev. Organ.
Sunshine 60, 1-1 Higashi-Ikebukuro
3-chome, Toshima-ku, Tokyo 170
JAPAN
03-987-9451

Sharad Kelkar
Los Alamos National Laboratory
MS J981
Los Alamos, NM 87545
505-665-3054

Jitendra Kikani
Stanford University
Lloyd Noble Bldg. Rm 117
Stanford, CA 94305
415-723-0691

Christopher W. Klein
GeothermEx, Inc.
5221 Central Ave. Suite #201
Richmond, CA 94804
415-527-9876

John A. Knox
Halliburton Services
P.O. Box 1431
Duncan, OK 73536
405-251-3755

Brian A. Koenig
UNOCAL Geothermal Division
P.O. Box 6854
Santa Rosa, CA 95406
707-545-7600

Mark K. Kumataka
Santa Fe Geothermal Inc.
P.O. Box 1009
Middletown, CA 95461
707-987-2335

Cathy Laky
654 Jefferson St.
Red Hill, PA 18076
415-486-6760

G.W. Lanyon
Geoscience Ltd.
Falmouth Business Park
Bickland Water Rd. Falmouth
Cornwall, TR 11 4S2 UK
011-44-326-211070

Pete Ledingham
Geoscience Ltd.
Falmouth Business Park
Bickland Water Rd., Falmouth
Cornwall, TR 11 4S2 UK
011-44-326-211070

Marcelo Lippmann
Lawrence Berkeley Laboratory
1 Cyclotron Rd.
Berkeley, CA 94720
415-486-5035

Jim Lovekin
California Energy Company
P.O. Box 1420
Inyokern, CA 93527
619-764-2551

Dennis A. Lynch
Atlas Wireline Services
3530 Arundell Circle
Ventura, CA 93003
805-656-4841

Steven J. Malone
UNOCAL Geothermal Division
3576 Unocal Place
P.O. Box 6854
Santa Rosa, CA 95406
707-545-7600

John Maney
UNOCAL Geothermal Division
P.O. Box 6854
Santa Rosa, CA 94506
707-545-7600

Sully Marsden
Mitchell Bldg. Rm 360
Stanford University
Stanford, CA 94305
415-723-3570

Dr. Ross McCartney
Geoscience Ltd.
Falmouth Business Park
Bickland Water Rd.
Falmouth, Cornwall U.K.
011-44-326-211070

James R. McNitt
GeothermEx
5221 Central Ave., Suite 201
Richmond, CA 94804
415-527-9876

Tsvi Meidav
Trans-Pacific Geothermal Corp.
1330 Broadway, Suite #1525
Oakland, CA 94612
415-763-7812

Frank Miller
Stanford University
Mitchell Bldg. Rm. 360
Stanford, CA 94305
415-723-2938

Dr. John E. Mock
Director, Geothermal Technology
Div. U.S. Department of Energy
1000 Independence Ave.
Washington, DC 20585
202-586-5340

Phil Mogen
UNOCAL Geothermal Division
P.O. Box 1805
Indio, CA 92202
619-347-8488

George Moore
PG&E
77 Beale St. Rm. 3033
San Francisco, CA 94105
415-972-6642

Joseph N. Moore
Univ. of Utah Res. Inst./Earth
Science Laboratory
391 Chipeta Way, Suite C
Salt Lake City, Utah 84108
801-524-3428

Paul Mount II
State Lands Commission
245 W. Broadway, Suite #425
Long Beach, CA 90802-4471
213-590-5995

Patrick Muffler
U.S.G.S.
345 Middlefield Rd., MS-910
Menlo Park, CA 94025
415-329-5239

Shinsuke Nakao
Geoth. Survey Dept. New Energy and
Indust. Tech. Dev. Organ. Sunshine 60,
1-1 Higashi-Ikebukuro 3-chome,
Toshima-ku, Tokyo 170
JAPAN
03-987-9451

Manuel Natheson
U.S.G.S.
345 Middlefield Road, MS-910
Menlo Park, CA 94025
415-329-5292

Michael Nazroo
Camborne School of Mines
Geothermal Project
Rosemanowes Quarry, Herniss
Penryn Cornwall TR10 9DV, ENGLAND
0209-360141

David Nieva
IIE
Cuernavaca, Mexico
73-12-86-97

Ryohzo Nogami
Geoth. Survey Dept. New Energy and
Indust. Tech. Dev. Organ. Sunshine 60
1-1 Higashi-Ikebukuro 3-chome,
Toshima-ku, Tokyo 170
JAPAN
03-987-9451

Warren (Doug) Noteware
Commissioner
California Energy Commission
1516 Ninth Street, MS-35
Sacramento, CA 95814
916-324-3259

Will Osborn
GEO Operator Corp.
P.O. Box 748
Holtville, CA 92250
619-356-4613

John Pacheco
Calif. Dept. of Water Res.
1416 Ninth Street
P.O. Box 942836
Sacramento, CA 94236-0001
916-323-0103

John W. Pritchett
S-Cubed
P.O. Box 1620
La Jolla, CA 92038-1620
619-453-0060

Karsten Pruess
Lawrence Berkeley Laboratory
1 Cyclotron Rd.
Berkeley, CA 94720
415-486-6732

Stephen Pye
UNOCAL Geothermal Division
1201 West Fifth Street
Los Angeles, CA 90017
213-977-6262

Peter M. Pyle
BGI
1330 Broadway, Suite #1450
Oakland, CA 94612
415-465-1744

Gregory D. Raasch
Philippine Geothermal, Inc.
c/o UNOCAL
P.O. Box 7600 Rm. M-20
Los Angeles, CA 90051
63-2-817-88-76

Henry J. Ramey Jr.
Stanford University
Mitchell Bldg. Rm. 360
Stanford, CA 94305
415-723-1774

Marshall Reed
U.S. Department of Energy
DOE, CE-342
Washington, DC 20585
202-586-8076

Larry F. Rice
577 27th St. #1
San Francisco, CA 94131
415-826-6699

Dr. David Riney
S-Cubed
P.O. Box 1620
La Jolla, CA 92038-1620
619-453-0060

Vasel W. Roberts
EPRI
3412 Hillview Ave.
Palo Alto, CA 94304
415-855-2160

Bruce Robinson
Los Alamos National Laboratory
P.O. Box 1663, MS J981
Los Alamos, NM 87545
505-667-4318

David Rohrs
UNOCAL Geothermal Division
P.O. Box 1805
Indio, CA 92202
619-347-8488

Fernando Samaniego
UNAM and Pemex
Facultad de Ingenieria
UNAM, 04510 Mexico D.F., MEXICO
905-550-8712

Subir Sanyal
GeothermEx
5221 Central Ave., Suite #201
Richmond, CA 94804
57-527-9876

Jim Sexton
PG&E
P.O. Box 1310
Middletown, CA 95461
707-431-6070

Benedilet Steingrimsson
Lawrence Berkeley Laboratory
1 Cyclotron Rd.
Berkeley, CA 94720
415-486-6760

Jeffrey Sternfeld
GEO Operator Corp.
1330 N. Dutton Ave., Suite A
Santa Rosa, CA 95401
707-523-4272

Cal Strobel
UNOCAL Geothermal Division
P.O. Box 6854
Santa Rosa, CA 95406
707-545-7600

Cesar Suarez
CFE
A. Vocta G55, Col. Electricistas
Merelia, Michoacan, Mexico
A.P.31-C
451-4-80-50-164

Jefferson W. Tester
Mass. Institute of Technology
66-305 Chemical Engineering Dept.
Cambridge, MA 02139
617-253-4598

Richard P. Thomas
California Division of Oil & Gas
1416 9th St. Rm. 1310
Sacramento, CA 95814
916-323-1787

Donald M. Thomas
Hawaii Institute of Geophysics
2525 Correa Rd.
Honolulu, HI 96822
808-948-6482

Randy Thompson
UNOCAL Geothermal Division
3576 Unocal Pl.
P.O. Box 6854
Santa Rosa, CA 95406
707-545-7600

Wilbur M. Thompson
California State Lands Commission
245 West Broadway, Suite #425
Long Beach, CA 90802
213-590-5243

Alfred H. Truesdell
U.S.G.S.
345 Middlefield Rd. MS-910
Menlo Park, CA 94025
415-329-5212

Ed Van Eekhout
Los Alamos National Laboratory
MS D446
Los Alamos, NM 87545
505-667-1916

Ed Voge
UNOCAL Geothermal Division
P.O. Box 6854
Santa Rosa, CA 95406
707-545-7600

Mark A. Walters
GEO Operator Corp.
1330 N. Dutton Ave.
Santa Rosa, CA 95401
707-523-4272

Mark Wieszczyk
PG&E

Kenneth H. Williamson
UNOCAL Geothermal Division
3576 Unocal Pl.
Santa Rosa, CA 95401
707-545-7600

Ted Wilmsen
Thermal Power Company
520 Mendocino Ave., Suite #200
Santa Rosa, CA 95401
707-527-8947

Phillip M. Wright
Univ. of Utah Reserch Inst.
Earth Science Laboratory
391 Chipeta Way, Suite C
Salt Lake City, Utah 84108
801-524-3439

Yusaku Yano
Geological Survey of Japan
1-1-3, Higashi, Tsukuba, 305
JAPAN
0298-54-3735

SUBJECT INDEX

AUTHOR INDEX